Uniwersytet Łódzki

Wydział Chemii

Katedra Chemii Organicznej

Rozprawa doktorska

mgr Karolina Kowalczyk

Synteza i aktywność biologiczna metaloorganicznych koniugatów inhibitorów kinezyny-5

Promotor: dr hab. Damian Plażuk, prof. UŁ

Łódź, wrzesień 2024

Podziękowania

Składam serdeczne podziękowania mojemu promotorowi ***Panu dr. hab. Damianowi Plażukowi, prof. UŁ,*** *za przekazaną wiedzę, nieocenione wsparcie merytoryczne, cenne wskazówki, poświęcony czas i wyrozumiałość w trakcie realizacji niniejszej pracy*

Koleżankom i kolegom dziękuję za przyjacielskie wsparcie i tworzenie wspaniałej atmosfery w trakcie całych studiów doktoranckich, a wszystkim pracownikom Katedry Chemii Organicznej Wydziału Chemii UŁ za pomoc w codziennej pracy laboratoryjnej

oraz Moim Najbliższym za wiarę we mnie, wsparcie, wyrozumiałość i pomoc w trudnych chwilach.

Badania wchodzące w skład przedłożonej rozprawy doktorskiej prowadzono pod opieką naukową dr. hab. Damiana Plażuka, prof. UŁ, w okresie od października 2017 do września 2024 w Katedrze Chemii Organicznej Wydziału Chemii Uniwersytetu Łódzkiego.

Przedstawiona rozprawa doktorska została zrealizowana w ramach projektu badawczego finansowanego ze środków Narodowego Centrum Nauki przyznanego na podstawie decyzji o numerze DEC-2015/17/B/ST5/02331

NARODOWE CENTRUM NAUKI

Spis publikacji oryginalnych stanowiących podstawę niniejszej rozprawy doktorskiej:

[P1] Anna Wieczorek-Błauż, Karolina Kowalczyk, Andrzej Błauż, Anna Makal, Sylwia Pawlędzio, Chatchakorn Eurtivong, Homayon J. Arabshahi, Jóhannes Reynisson, Christian G. Hartinger, Błażej Rychlik, Damian Plażuk

Impact of the ferrocenyl group on cytotoxicity and KSP inhibitory activity of ferrocenyl monastrol conjugates

Dalton Trans., **2022**, 51, 491-508

IF=4,569, punkty MNISW=140

DOI: 10.1039/D1DT03553C

Mój udział w publikacji polegał na zsyntezowaniu ferrocenylowych analogów monastrolu oraz niezbędnych substratów, analizie widm NMR. Brałam również udział w analizie uzyskanych wyników oraz w powstawaniu końcowej wersji publikacji.

[P2] Karolina Kowalczyk, Andrzej Błauż, Daniel Moscoh Ayine -Tora, Christian G. Hartinger, Błażej Rychlik, Damian Plażuk

Design, Synthesis, and Evaluation of Biological Activity of Ferrocene-Ispinesib Hybrids: Impact of a Ferrocenyl Group on the Antiproliferative and Kinesin Spindle Protein Inhibitory Activity

Chem.Eur. J., **2023**, 29, e202300813

IF=4,3, punkty MNISW=140

DOI: 10.1002/chem.202300813

Mój udział w publikacji polegał na zsyntezowaniu ferrocenylowych koniugatów ispinesibu oraz niezbędnych substratów, analizie widm NMR. Brałam również udział w analizie uzyskanych wyników oraz w powstawaniu końcowej wersji publikacji.

[P3] Karolina Kowalczyk, Andrzej Błauż, Krzysztof Krawczyk, Błażej Rychlik, Damian Plażuk

Design and Synthesis of Ferrocenyl 1,4-Dihydropyridines and Their Evaluation as Kinesin-5 Inhibitors

Dalton Trans., **2024**, Advance Article

DOI: 10.1039/D4DT01853B

IF=4,569, punkty MNISW=140

Mój udział w publikacji polegał na zsyntezowaniu ferrocenylowych analogów CPUYL064 oraz niezbędnych substratów, analizie widm NMR. Brałam również udział w analizie uzyskanych wyników oraz w powstawaniu końcowej wersji publikacji.

Spis publikacji niestanowiących podstawy niniejszej rozprawy doktorskiej:

[P4] Karolina Kowalczyk, Andrzej Błauż, Wojciech M. Ciszewski, Anna Wieczorek, Błażej Rychlik, Damian Plażuk

Colchicine metallocenyl bioconjugates showing high antiproliferative activities against cancer cell lines

Dalton Trans., **2017**, 46, 17041-17052

IF=4,569, punkty MNISW=140

DOI: 10.1039/C7DT03229C

[P5] Damian Plażuk, Anna Wieczorek, Wojciech M. Ciszewski, Karolina Kowalczyk, Andrzej Błauż, Sylwia Pawlędzio, Anna Makal, Chatchakorn Eurtivong, Homayon J. Arabshahi, Jóhannes Reynisson, Christian G. Hartinger, Błażej Rychlik

Synthesis and in vitro Biological Evaluation of Ferrocenyl Side-Chain-Functionalized Paclitaxel Derivatives

ChemMedChem **2017**, 22, 1882-1892

IF=3,4, punkty MNISW=100

DOI: 10.1002/cmdc.201700576

Spis treści

1. Streszczenie w języku polskim

Modyfikacja związków biologicznie aktywnych za pomocą podstawników metaloorganicznych może znacząco zmienić ich aktywność biologiczną. Aktualnie prowadzone są badania nad syntezą oraz oceną antyproliferacyjnego potencjału związków metaloorganicznych, które mogą znaleźć zastosowanie jako chemioterapeutyki charakteryzujące się wyższą selektywnością, lepszą biodostępnością i mniejszą toksycznością. Metaloorganiczne analogi związków antymitotycznych mogą wykazywać wyższą aktywność przeciwnowotworową, a także przezwyciężyć oporność na leki, którą komórki nowotworowe nabywają w trakcie leczenia.

W niniejszej rozprawie doktorskiej opisano syntezę i oceniono aktywność biologiczną metaloorganicznych analogów monastrolu, CPUYL064 i ispinesibu, będących inhibitorami kinezyny-5.

2. Streszczenie w języku angielskim

The modification of biologically active compounds using organometallic substituents can significantly alter their biological activity. Currently, research is being conducted on the synthesis and evaluation of the antiproliferative potential of organometallic compounds, which may have applications as chemotherapeutic agents with higher selectivity, better bioavailability, and lower toxicity. Organometallic analogs of antimitotic compounds may exhibit enhanced anticancer activity and potentially overcome drug resistance that cancer cells develop during treatment.

This doctoral dissertation describes the synthesis and evaluates the biological activity of organometallic analogs of monastrol, CPUYL064, and ispinesib, which are inhibitors of kinesin-5.

3. Wykaz stosowanych skrótów

ATP - adenozyno-5′-trifosforan

DCE - (ang. *1,2-dichloroethane*) – 1,2-dichloroetan

DCM - (ang. *dichloromethane*) - dichlorometan

DIPEA - (ang. *diisopropylethylamine*) - diizopropyloetyloamina

DMF - (ang. *N,N-dimethylformamide*) - *N,N*-dimetyloformamid

EtOH - etanol

GTP - Guanozyno-5′-trifosforan

IC_{50} - stężenie powodujące 50% inhibicji

MAP - (ang. *microtubule-associated proteins*) - białka związane z mikrotubulami

MDR - (ang. *multi drug resistance*) - oporność wielolekowa

MeOH - metanol

MS - (ang. *mass spectrometry*) - spektrometria mas

MW - (ang. *microwave*) - mikrofale

NMR - (ang. *nuclear magnetic resonance spectroscopy*) - spektroskopia magnetycznego rezonansu jądrowego

RT - (ang. *room temperature)* – temperatura pokojowa

SAR - (ang. *structure activity relationship*) - badania zależności struktura-aktywność

TfOH - (ang. *trifluoromethanesulfonic acid*) kwas trifluorometanosulfonowy

TFA – (ang. *trifluoroacetic acid*) - kwas trifluorooctowy

THF - tetrahydrofuran

^{t}*Bu* - *tert*-butyl

^{t}*BuOK* – *tert*-butanolan potasu

4. Komentarz do rozprawy doktorskiej

4.1 Wprowadzenie

Choroby nowotworowe są jedną z głównych przyczyn zgonów w krajach rozwiniętych, odpowiadając za około 8,2 miliona przypadków śmiertelnych na całym świecie w 2020 roku.[1,2] W 2022 roku odnotowano 1,8 miliona zgonów z powodu nowotworów, z czego najwięcej przypadków dotyczyło nowotworów płuc (18,7%) oraz jelita grubego (9,3%). Prognozy wskazują, że liczba zgonów spowodowanych chorobami nowotworowymi może wzrosnąć dwukrotnie w ciągu najbliższych 15 lat (Rysunek 1).

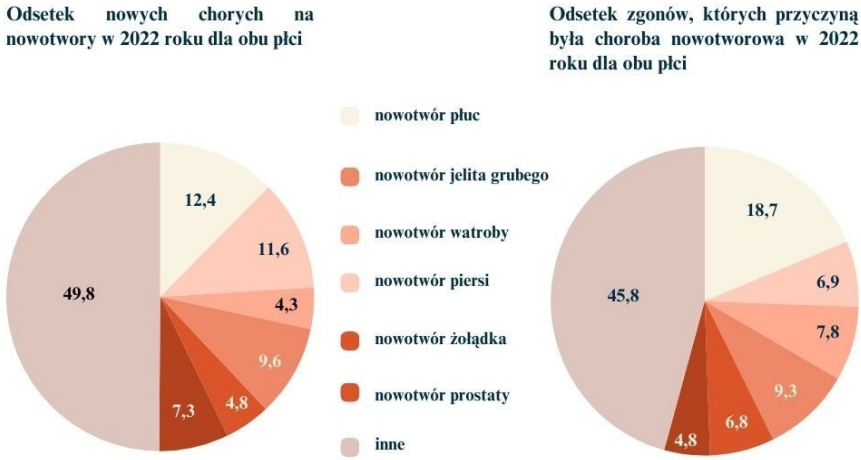

Rysunek 1. *Odsetek nowych zachorowań na nowotwory oraz zgonów z powodu chorób nowotworowych w 2022 r.*

Postęp medycyny umożliwił rozwój szerokiego wachlarza terapii przeciwnowotworowych, takich jak chemioterapia, radioterapia, chirurgia, immunoterapia, hormonoterapia, terapie oparte na przeciwciałach oraz terapie genowe. Mimo dostępności różnych metod leczenia, chemioterapia nadal pełni kluczową rolę w terapii chorób nowotworowych i często jest stosowana w połączeniu z radioterapią czy chirurgią.[3] W zaawansowanych stadiach choroby, gdy inne metody są niedostępne lub nieskuteczne, chemioterapia może być jedyną dostępną opcją leczenia, zwłaszcza w przypadku nowotworów o wysokim stopniu złośliwości. Powszechnie stosowane leki przeciwnowotworowe, w tym leki alkilujące[4], antymetabolity[5], antybiotyki przeciwnowotworowe[6], inhibitory topoizomerazy[7], inhibitory mitozy[8] i kortykosteroidy,[9] często wywołują liczne działania niepożądane i mogą generować oporność wielolekową, co prowadzi do niepowodzenia terapii. Aby przezwyciężyć efekty uboczne i pokonać niedogodności związane ze stosowaniem chemioterapeutyków, niezbędne jest doskonalenie stosowanych leków przeciwnowotworowych. Celem tych działań

jest zwiększenie aktywności lub selektywności leków przy jednoczesnym zmniejszeniu skutków ubocznych, co można osiągnąć poprzez modyfikację chemiczną ich cząsteczek lub opracowanie terapii ukierunkowanych na nowe cele terapeutyczne.

4.2 Związki antymitotyczne

Związki antymitotyczne, takie jak taksany i alkaloidy Vinca (Barwinka różowatego), należą do najważniejszych chemioterapeutyków przeciwnowotworowych. Zakłócają one dynamikę układu tubulina–mikrotubule, prowadząc do zaburzenia funkcji wrzeciona mitotycznego, co skutkuje zahamowaniem podziału komórkowego i śmiercią komórek nowotworowych.[10, 11] Związki antymitotyczne działające na mikrotubule wykazują stosunkowo niską selektywność, co przekłada się na wysoką toksyczność ogólnoustrojową.[12] Mikrotubule, będące kluczowym elementem cytoszkieletu komórek eukariotycznych, powstają w wyniku polimeryzacji cząsteczek tubuliny. Te cylindryczne, sztywne struktury, mają średnicę zewnętrzną wynoszącą 25 nm oraz grubość ściany wynoszącą 5 nm. Mikrotubule są zbudowane z protofilamentów, które składają się z heterodimerów α- i β-tubuliny połączonych wiązaniami niekowalencyjnymi.[13] Struktura mikrotubul wyróżnia się dwoma końcami, dodatnim (+) i ujemnym (-), oraz miejscem wiązania GTP.[14] Związki zaburzające dynamikę mikrotubul klasyfikuje się według miejsca wiązania z białkami oraz ich wpływu na stabilizację mikrotubul. Dotychczas zidentyfikowano sześć miejsc wiążących (domen) w mikrotubulach, z czego pięć wiąże się z β-tubuliną, a jedno z α-tubuliną w dimerach mikrotubul. Wśród tych miejsc wiążących wyróżnia się: domenę Vinca, kolchicynową, paklitakselową, laulimalidową, majtansynową i pironetynową[15] (Rysunek 2).

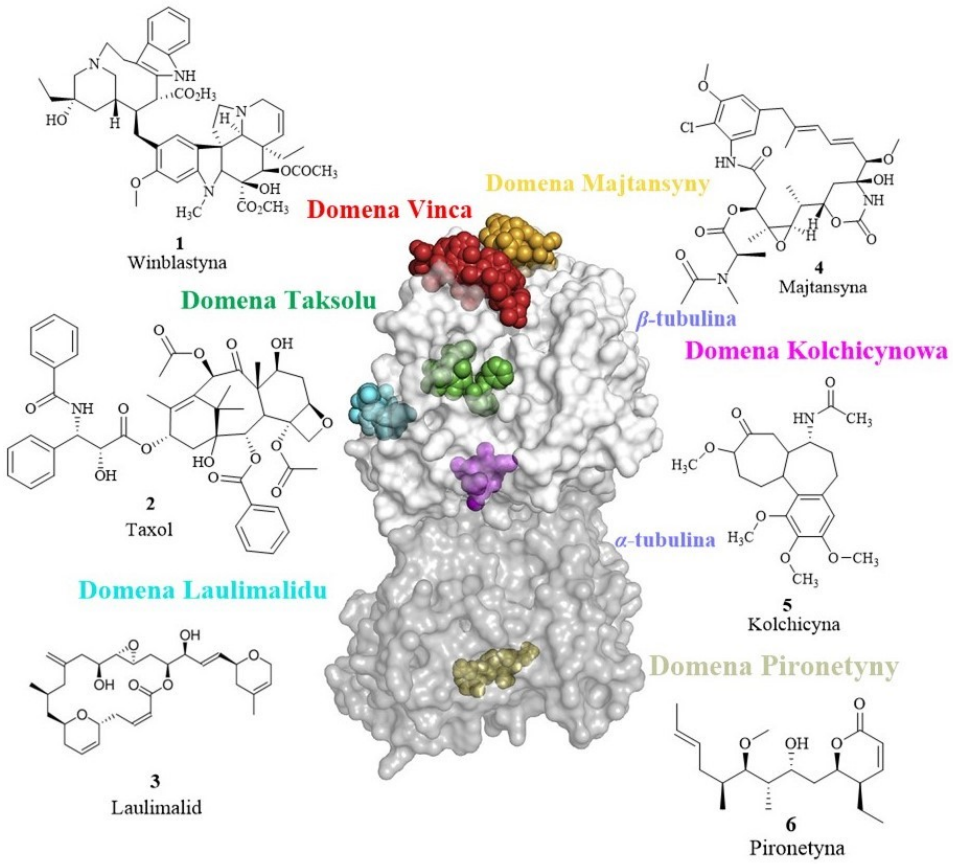

Rysunek 2. *Miejsca wiązania związków ukierunkowanych na mikrotubule (licencja CC BY 4.0[16])*

Związki wpływające na stabilność mikrotubul można podzielić na substancje stabilizujące (aktywatory polimeryzacji) i destabilizujące (inhibitory polimeryzacji) mikrotubule. Do aktywatorów polimeryzacji tubuliny zalicza się związki wiążące się do domeny paklitakselowej takie jak taksany, epotilony oraz do domeny laulimalidu. Do związków destabilizujących mikrotubule zalicza się związki wiążące się do domeny Vinca takie jak winblastyna, winkrystyna oraz związki wiążące się z domeną kolchicynową, domeną majtansyny i domeną pironetyny.[17] Oprócz wymienionych związków odkryto szereg strukturalnie różnych inhibitorów i aktywatorów polimeryzacji tubuliny,[18] a niektóre z nich są stosowane w terapii przeciwnowotworowej (Tabela 1).[19]

Związek	Miejsce wiązania	Zastosowanie terapeutyczne	Status kliniczny
Winblastyna	Domena Vinca	Rak piersi, chłoniak, mięsaki	W zastosowaniu klinicznym[20]
Winkrystyna	Domena Vinca	Rak piersi, chłoniak, mięsaki	W zastosowaniu klinicznym[20]
Winorelbina	Domena Vinca	Rak piersi, rak płuc, mięsaki	W zastosowaniu klinicznym[20]
Winflunina	Domena Vinca	Rak błony śluzowej układu moczowego	W zastosowaniu klinicznym[20]
Kolchicyna	Domena Kolchicynowa	Choroby nienowotworowe (dna moczanowa)	Badania zakończyły się niepowodzeniem z powodu dużej toksyczności[20]
Plinabulina	Domena Kolchicynowa	Rak płuc	Faza II[21]
Paklitaxel	Domena Taxolu	Rak piersi, rak jajnika, wiele innych	W zastosowaniu klinicznym[22]
Docetaxel	Domena Taxolu	Rak piersi, rak płuc, wiele innych	W zastosowaniu klinicznym[23]
Cabazitaxel	Domena Taxolu	hormonooporny rak gruczołu krokowego	W zastosowaniu klinicznym[24]
Epotilon B	Domena Taxolu	Rak płuc	Faza II[25]
Ixabepilon	Domena Taxolu	Rak piersi, rak endometrium	Faza III[26]

Tabela 1. *Przykłady związków antymitotycznych i ich status kliniczny*

Stabilizatory mikrotubul, takie jak taksany (Rysunek 3), są szeroko stosowane w chemioterapii nowotworów piersi, jajnika, pęcherza moczowego, niedrobnokomórkowego raka płuc, nowotworach głowy i szyi, często w połączeniu z radioterapią i innymi chemioterapeutykami, takimi jak cisplatyna.[23,27]

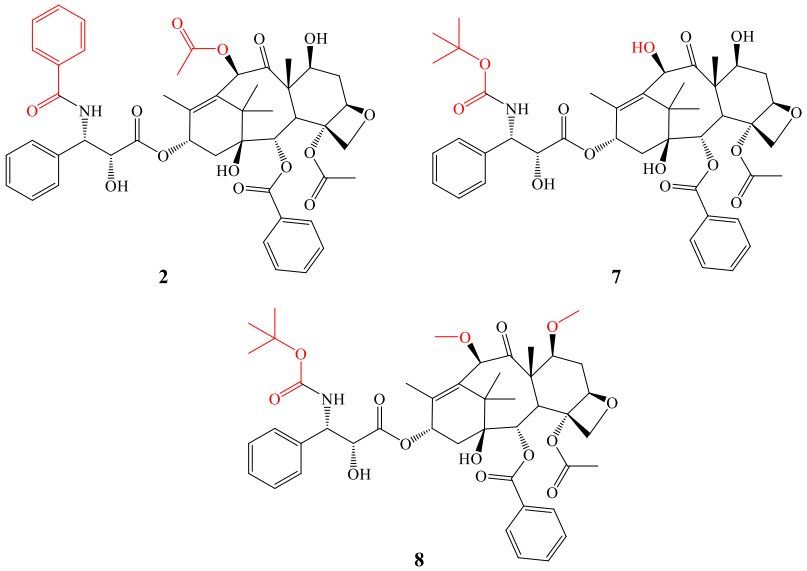

Rysunek 3*. Struktury paklitakselu* ***2****, docetakselu 7 i cabazitakselu* ***8***

Paklitaksel **2**, wyizolowany z kory cisu zachodniego (*Taxus brevifolia*) w 1967 roku[28], jak i jego półsyntetyczny analog docetaksel **7**, hamują depolimeryzację (stabilizują) mikrotubul, zaburzając w ten sposób ich normalną dynamikę wymaganą do mitozy i proliferacji komórek, co ostatecznie skutkuje zatrzymaniem komórek w fazie G_2/M cyklu komórkowego.[29] Taksany mimo podobnej budowy różnią się znacznie pod względem aktywności przeciwnowotworowej oraz toksyczności. Docetaksel **7** ma większe powinowactwo do tubuliny niż **2**, co zwiększa jego cytotoksyczność.[30] W badaniach *in vitro* wykazano, że **7** jest 1,3–12 razy bardziej cytotoksyczny niż paklitaksel w stosunku do różnych linii komórkowych.[31] Obecnie taksany stosowane są w monoterapii oraz w leczeniu skojarzonym z innymi lekami przeciwnowotworowymi w chemioterapii m.in. raka piersi, płuc, żołądka igłowy.[27] Stosowanie taksanów wiąże się z szeregiem skutków ubocznych, a także może prowadzić do wystąpienia oporności wielolekowej (MDR), co skutkuje niepowodzeniem terapii.[32] Konieczność przezwyciężenia tych problemów doprowadziła do opracowania szeregu analogów **2**. Przykładowo, cabazitaksel **8** wykazuje aktywność przeciwko liniom komórkowym opornym na **2** i **7**. Cechą odróżniającą **8** od innych taksanów jest jego zdolność do przekraczania bariery krew-mózg, a zatem może być skuteczny w leczeniu nowotworów znajdujących się w trudno dostępnych miejscach, takich jak mózg.[33] Obecnie **8** został zatwierdzony do terapii raka gruczołu krokowego, który nie reaguje na standardowe leczenie hormonalne.[24]

Poszukiwanie nowych związków antymitotycznych doprowadziło do odkrycia epotilonów będących stabilizatorami mikrotubul.[34] Epotilon B **9** przeszedł fazę II badań klinicznych w leczeniu raka płuc,[25] zaś ixabepilon **10** (Ixempra™) został zatwierdzony do leczenia przerzutowego raka piersi oraz nawracających raków endometrium,[35] i jest obecnie badany m.in. w terapii raka jelita grubego, szyjki macicy, piersi, nerki, raka płuc z nadekspresją βIII-tubuliny oraz potrójnie negatywnego raka piersi (ang. TNBC – triple negative breast cancer)[34] (Rysunek 4).

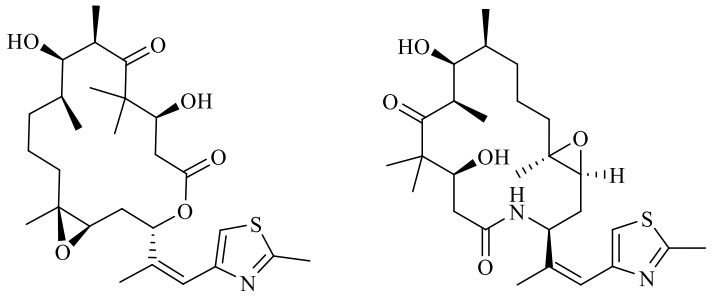

9 **10**

Rysunek 4. *Struktury epotilonu B **9** i ixabepilonu **10***

Inhibitorami polimeryzacji tubuliny o znaczeniu klinicznym są także alkaloidy Vinca, takie jak winblastyna **1**, winkrystyna **11**, winorelbina **12** i winflunina **13** (Rysunek 5).

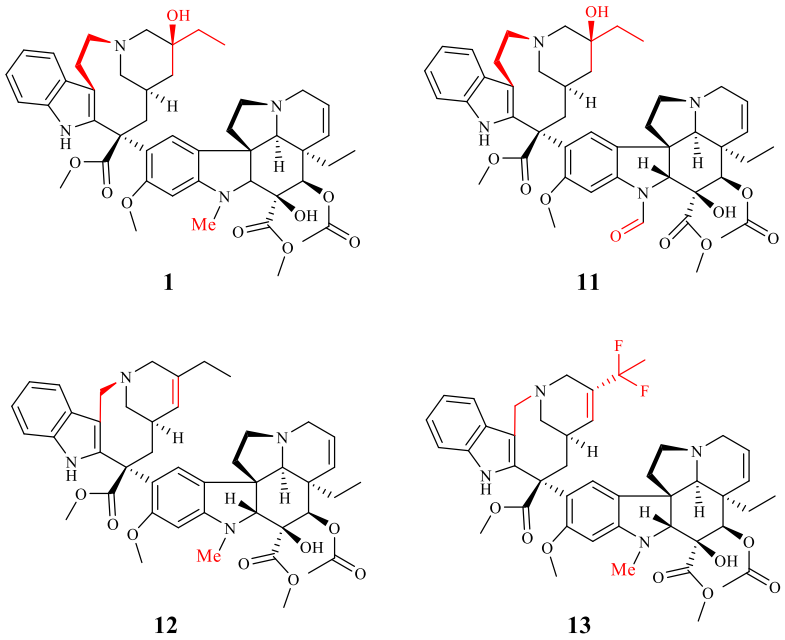

Rysunek 5. *Struktury winblastyny **1**, winkrystyny **11**, winorelbiny **12** i winfluniny **13***

Związki te działają poprzez wiązanie się z *β*-tubuliną w domenie Vinca. Winblastyna **1**, stosowana od kilkudziesięciu lat w monoterapii oraz w terapii skojarzonej, ma znaczenie w hamowaniu angiogenezy i regresji nowotworów[36], w tym raka pęcherza, piersi, chłoniaka złośliwego, mięsaka Kaposiego, raka kosmówki, ziarniniaka, choroby Abta-Letterera-Siwego oraz złośliwej histiocytozy i innych.[37, 38] Winkrystyna **11**, wykazująca szersze spektrum działania niż **1**, jest używana przede wszystkim w leczeniu białaczek limfoblastycznych i szpikowych, również u dzieci, a także w terapii chłoniaków, mięsaków, czerniaka złośliwego, nowotworów ośrodkowego układu nerwowego (OUN) oraz raka piersi.[39, 40] Winorelbina **12**, charakteryzująca się większą skutecznością i mniejszą toksycznością niż **1**, jest stosowana w monoterapii raka piersi, a także w terapiach skojarzeniowych, w leczeniu raka jajnika, chłoniaków, raka przełyku i prostaty.[41] Ponadto, **12** jest jednym z leków używanych w terapii drobnokomórkowego raka płuca (ang. NSCLC – non-small-cell lung carcinoma).[42] Wprowadzenie nowych alkaloidów Vinca, takich jak winflunina **13**, umożliwiło częściowe przezwyciężenie niektórych skutków ubocznych wywołanych przez naturalne alkaloidy Vinca, takie jak odwracalna neuropatia obwodowa, neuropatia autonomicznego układu nerwowego inerwów czaszkowych[43], neutropenia, anemia, nudności i wymioty[41]. Winflunina **13**, wykazuje mniejszą neurotoksyczność w porównaniu do **11**, i jest stosowana w leczeniu zaawansowanego raka urotelialnego (rak błony śluzowej układu moczowego).[44] Najczęściej występującymi działaniami niepożądanymi związanymi ze stosowaniem **13** są zahamowanie czynności szpiku

kostnego oraz zaparcia[45] (Rysunek 5). Kolejnymi inhibitorami polimeryzacji tubuliny wiążącymi się z domeną Vinca są halichondryny, wyizolowane z gąbki morskiej *Halichondria* w 1986 roku (Rysunek 6).[46] Najważniejszym przedstawicielem tych związków jest halichondryn B **14**, polieterowy makrolid, którego właściwości przeciwnowotworowe po raz pierwszy zostały wykazane na mysich liniach komórkowych białaczki (L1210, P-388) i czerniaka (B16).[47] Warto podkreślić, że **14** wykazywał również wyraźną aktywność w badaniach *in vivo* przeciwko różnym rodzajom chemoodpornych ludzkich nowotworów, takich jak czerniak LOX, rak jajnika OVCAR-3, rak płuc NCI H522 oraz rak piersi MDA-MB-435.[48, 49] Badania nad **14** doprowadziły do opracowania związków o wysokiej aktywności biologicznej, takich jak eribulin (E7389) **15**, który wiąże się zarówno z dimerem tubuliny, jak i pojedynczą *β*-tubuliną, hamując wzrost mikrotubul bez ich skracania, co zwiększa skuteczność w pokonywaniu chemiooporności.[38] Aktualnie **15** znajduje się w fazie III badań klinicznych w leczeniu różnych nowotworów, w tym raka prostaty, mięsaka, raka piersi, niedrobnokomórkowego raka płuc (NSCLC), raka pęcherza moczowego, raka jajnika oraz inwazyjnego raka piersi.[50] Jedną z zalet **15** jest jego niższa neurotoksyczność, co pozwoliło na jego wprowadzenie do leczenia tłuszczakomięsaka[19, 51].

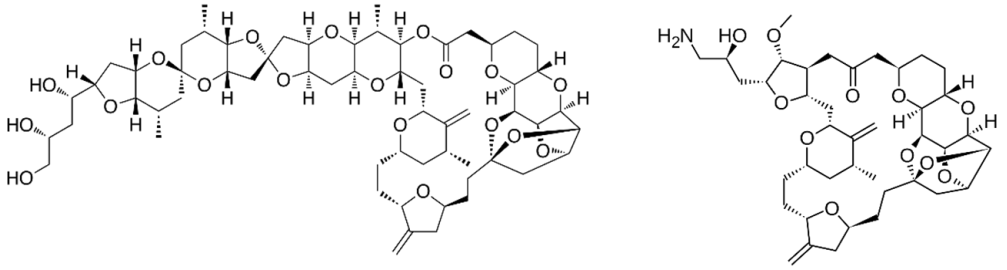

14 **15**

Rysunek 6. *Struktury halichondrynu B **14** i eribulinu **15***

Spośród inhibitorów polimeryzacji tubuliny szczególne znaczenie ma kolchicyna **5**, która jest naturalnym alkaloidem wyizolowanym z Zimowita Jesiennego (*Colchicum autumnale).* Destabilizuje ona mikrotubule, jednakże z uwagi na wysoką toksyczność, nie jest stosowana w terapii przeciwnowotworowej.[52] Kolchicyna **5** jest jednym z najstarszych znanych leków, stosowanym od wieków w leczeniu różnych chorób, aktualnie zaś wykorzystywana jest do leczenia dny moczanowej i choroby Behceta.[53] Najczęstsze skutki uboczne stosowania kolchicyny obejmują biegunkę, nudności i wymioty. Wysokie dawki **5** mogą prowadzić do poważnych problemów żołądkowo-jelitowych. Może ona również powodować mielosupresję (zahamowanie czynności szpiku kostnego), co prowadzi do leukopenii, anemii i trombocytopenii, i jest jednym z głównych ograniczeń jej stosowania w wysokich dawkach.

Przewlekłe stosowanie **5** może prowadzić do toksyczności narządowej, w tym uszkodzenia nerek i wątroby, a także do neuropatii obwodowej objawiającej się drętwieniem i bólem kończyn.[54] W celu zmniejszenia wysokiej toksyczności kolchicyny zsyntezowano i zbadano szereg jej analogów[55-58] (Rysunek 7).

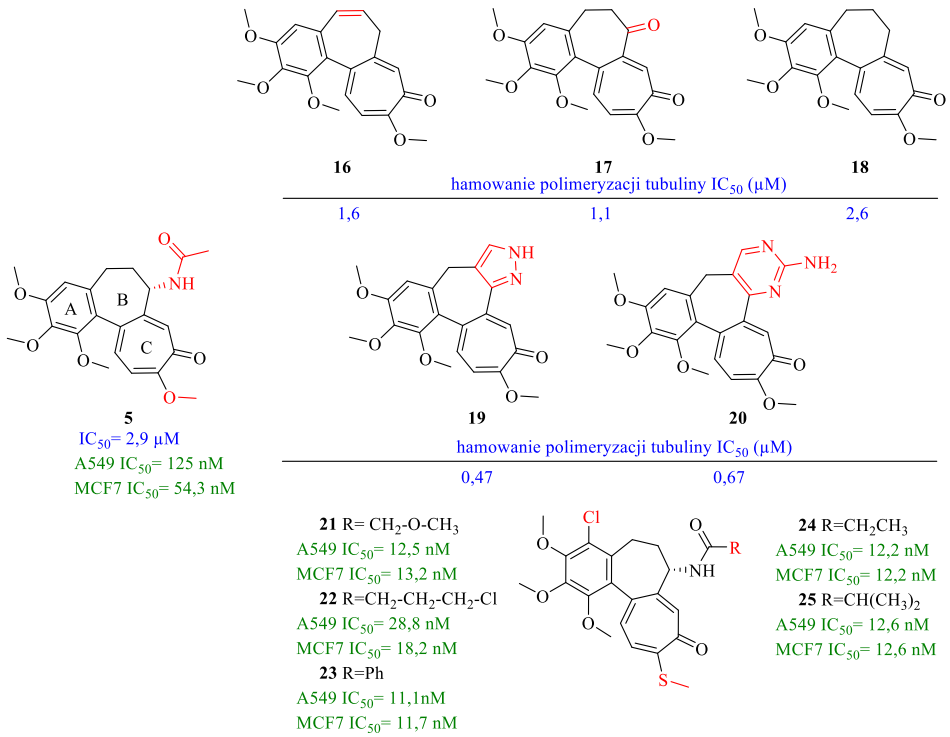

Rysunek 7. *Struktura kolchicyny* ***5*** *i wybranych pochodnych kolchicyny* ***16-25.*** *Wartości* IC_{50} *hamowania polimeryzacji tubuliny (kolor niebieski), wartości* IC_{50} *cytotoksyczności w stosunku do linii A549 i MCF7 (kolor zielony).*

Przykładowo, modyfikacje w pozycji C-7 pierścienia B doprowadziły do powstania aktywnych biologicznie aminowych analogów kolchicyny, z których związek **28** wykazał wyższą toksyczność wobec linii komórkowej HT29 (rak jelita grubego) (IC_{50} = 4,3 nM) i MDA-MB-231 (rak piersi) (IC_{50} = 16,0 nM) niż sama kolchicyna[59] (Rysunek 8).

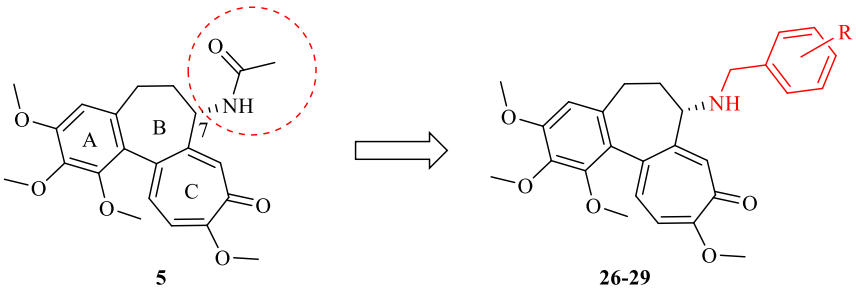

Związek	IC_{50} (nM)				
	5	26 R=3'-F	27 R=2', 3'-F_2	28 R=3', 4'-F_2	29 R=3', 5'-F_2
HT29	69,25	63,4	7,43	4,3	52,0
MDA-MB-231	37,0	89,1	86,0	16,0	523,0

Rysunek 8. *Struktura aminowych analogów kolchicyny* ***26-29***

Niektóre z pochodnych kolchicyny były testowane klinicznie jako potencjalne leki przeciwnowotworowe. Przykładowo, ZD6126 **30** był badany jako środek zaburzający naczynia krwionośne (VDA).Wykazano, że **30** powoduje selektywne zniszczenie naczyń krwionośnych w guzie, co prowadzi do rozległej martwicy nowotworu, szczególnie w dużych guzach.[60] Związek **30** przeszedł badania kliniczne II fazy w leczeniu raka nerkowokomórkowego i jelita grubego[61] (Rysunek 9).

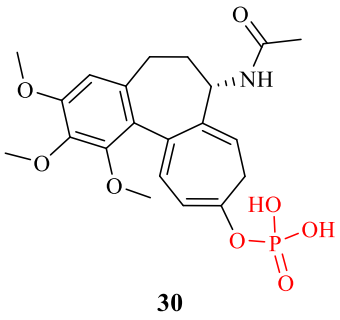

Rysunek 9. *Struktura ZD6126* ***30***

Pomimo, iż sama kolchicyna nie ma znaczenia w terapii przeciwnowotworowej, związki antymitotyczne wiążące się z kolchicynowym miejscem wiązania w tubulinie są intensywnie badane jako potencjalne leki przeciwnowotworowe. Wynika to z faktu, że działają skutecznie już przy niskich stężeniach. Związki te tłumią dynamikę mikrotubul, nie zmieniając znacząco ich masy polimerowej. Oznacza to, że nie powodują one ani całkowitej depolimeryzacji, ani nadmiernej stabilizacji mikrotubul, lecz ograniczają ich zdolność do dynamicznych zmian długości. To wystarcza, aby zakłócić procesy mitotyczne i zatrzymać komórki w fazie mitozy. Przykładem związku antymitotycznego wiążącego do domeny

kolchicynowej jest plinabulina (NPI-2358) **31**, będąca półsyntetycznym analogiem fenylahistyny **32** (Rysunek 10). Wyniki I i II fazy badań klinicznych, wykazały, że związek **31** zwiększał przeżycie, i chronił przed neutropenią wywołaną przez docetaksel, pacjentów z zaawansowanymi nowotworami, w tym z niedrobnokomórkowym rakiem płuca (NSCLC).[21] Profil działań niepożądanych **31** różni się od innych związków wiążących się z domeną kolchicynową zmniejszając ryzyko kardiotoksyczności. Obecnie plinabulina przechodzi badania kliniczne fazy III w łagodzeniu neutropenii wywołanej chemioterapią (CIN).[21]

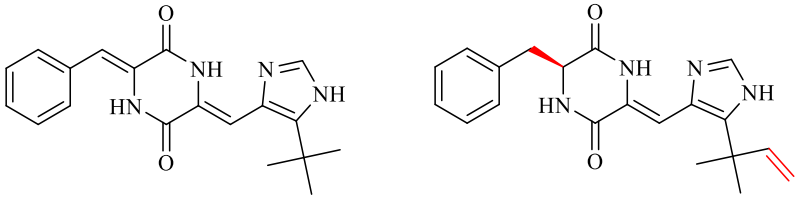

31 **32**

Rysunek 10. *Struktury fenylohistyny **32** i plinabuliny **31***

4.3 Metaloorganiczne związki o właściwościach przeciwnowotworowych ze szczególnym uwzględnieniem związków ferrocenylowych

Pierwszym związkiem metaloorganicznym używanym w medycynie był salwarsan **33** (Rysunek 11), który został wprowadzony do użytku klinicznego w 1910 roku. Lek ten przyczynił się do przełomu w leczeniu kiły, będąc jednym z pierwszych leków, które pozwoliły na skuteczne kontrolowanie tej choroby.[62,63]

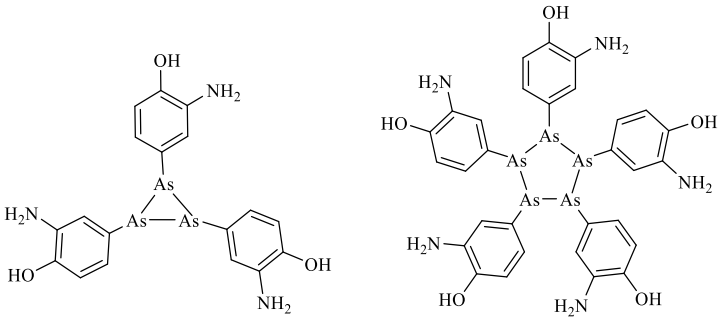

A **B**

33

Rysunek 11. *Struktura salwarsanu **33** jako mieszaniny trimeru **A** i pentameru **B**[63]*

Przełomem w dziedzinie medycyny i chemii było odkrycie właściwości przeciwnowotworowych cisplatyny **34**, nieorganicznego kompleksu platyny znanego od ponad 100 lat.[64] Badania przeprowadzone przez Rosenberga wykazały, że cisplatyna hamuje podział komórek Escherichia coli,[65] a dalsze badania potwierdziły jej aktywność przeciwnowotworową

wobec wielu rodzajów nowotworów, w tym jajnika, głowy oraz szyi.[66] W 1978 roku cisplatyna stała się pierwszym lekiem zawierającym metal ciężki, zatwierdzonym przez FDA do terapii przeciwnowotworowej, i do dziś pozostaje jednym z najskuteczniejszych leków stosowanych w leczeniu raka płuc, jajnika oraz jąder (Rysunek 12).[67]

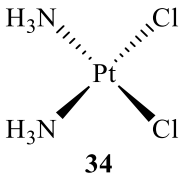

34

Rysunek 12. *Struktura cisplatyny* ***34***

Odkrycie cisplatyny stworzyło nowe możliwości w leczeniu nowotworów, dając początek chemii medycznej opartej na związkach metali, co z kolei znacząco zwiększyło zainteresowanie innymi metalami przejściowymi w medycynie. Szczególne znaczenie miało odkrycie właściwości przeciwnowotworowych pochodnych ferrocenu.[68, 69] Pierwsze doniesienia o aktywności biologicznej związków ferrocenylowych dotyczyły poliamin **35-37** (Rysunek 13), które wykazywały aktywność przeciwnowotworową w stosunku do komórek białaczki limfocytowej P388.[70]

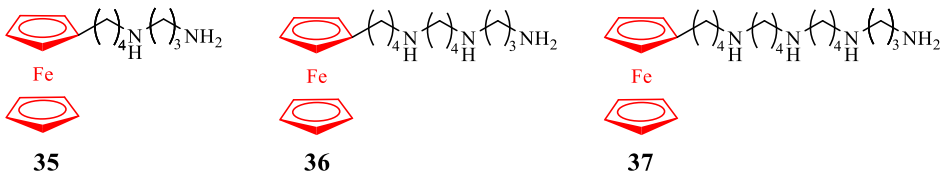

35 **36** **37**

Rysunek 13. *Struktury ferrocenylowych poliamin* ***35-37***

W późniejszych latach dowiedziono, że ferrocen **38** nie jest toksyczny, a właściwości antynowotworowe przypisano kationowi ferroceniowemu **39**. Przykładowo, proste sole ferroceniowe takie jak pikrynian ferroceniowy **40** i trichlorooctan ferroceniowy **41** hamują wzrost nowotworów oskrzeli Ehlricha, czerniaka i raka okrężnicy,[71] z kolei tetrachlorożelazian(III) ferroceniowy **42** jest cytotoksyczny w stosunku do linii komórkowych nowotworu jajnika CHI (IC_{50} = 10 μM).[72] (Rysunek 14).

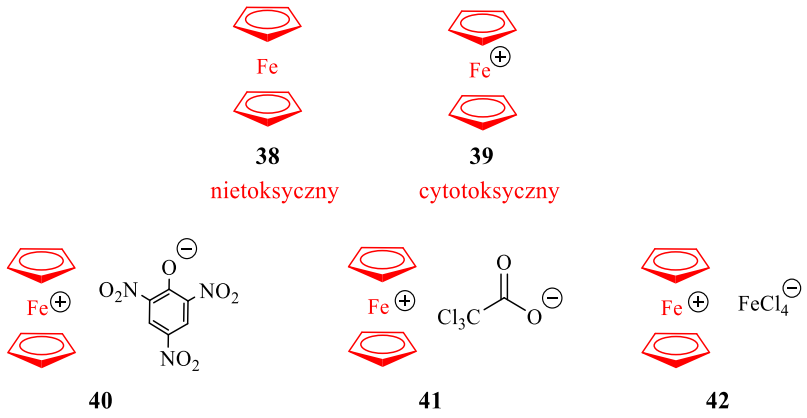

Rysunek 14. *Struktury ferrocenu **38**, kationu ferroceniowego **39**, pikrynianu ferroceniowego **40**, trichlorooctanu ferroceniowego **41** i tetrachlorożelazianu(III) ferroceniowego **42***

W 1996 roku grupa prof. Gérarda Jaouena opisała wyniki badań nad hydroksylową pochodną aktywnego biologicznie chemioterapeutyku stosowanego w leczeniu nowotworów piersi – hydroksytamoksyfenu **43**, będącego aktywnym metabolitem tamoksyfenu **44** (Rysunek 15). Tamoksyfen **44** jest selektywnym modulatorem receptora estrogenowego, stosowanym w leczeniu hormonozależnego raka sutka.[73] Zamiana grupy fenylowej w hydroksytamoksyfenie doprowadziła do związku **45**, wykazującego właściwości antyproliferacyjne zarówno w stosunku do hormonozależnej linii komórek gruczolaka sutka MCF7, jak i hormononiezaleznej MDA-MB-231.[74]

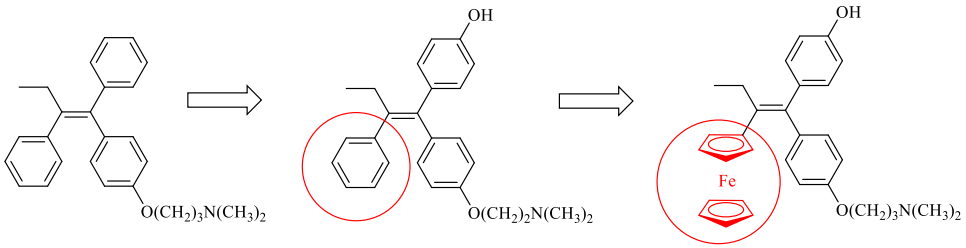

Rysunek 15. *Struktury tamoksyfenu **44**, hydroksytamoksyfenu **43** i hydroksyferrocifenu **45***

Wykazano, że kluczowy mechanizm działania **45** opiera się na reakcji redoks ferrocenu, która zachodzi za pośrednictwem układu π-elektronowego. Proces ten prowadzi do powstania metylidenowego chinonu **49** (Schemat 1), będącego reaktywnym elektrofilem, podatnym na atak nukleofilowy przez biomolekuły, takie jak białka i DNA. Ponadto stwierdzono, że antyproliferacyjne właściwości ferrocifenów są związane z ich zdolnością do generowania reaktywnych form tlenu (ang. reactive oxygen species, ROS) w reakcji Fentona, co prowadzi do uszkodzeń DNA, przyspieszenia starzenia komórek oraz indukcji apoptozy.[75, 76]

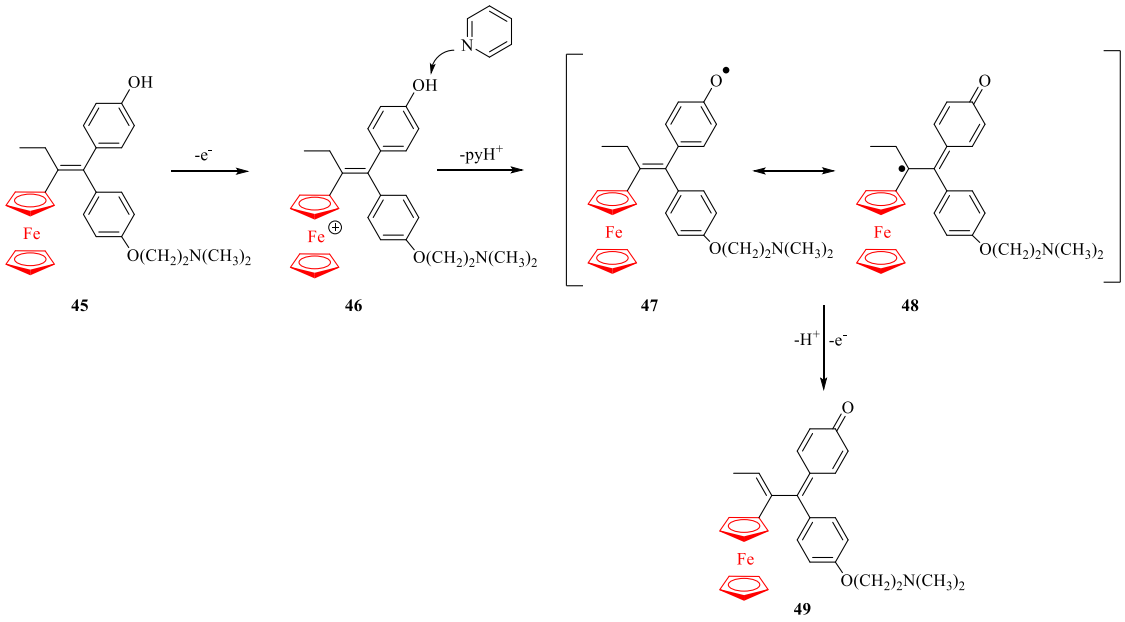

Schemat 1. *Mechanizm powstawania chinonu* ***49*** *z hydroksyferrocifenu* ***45***

Badając analogi tamoksyfenu, zsyntetyzowano nowe analogi ferrocifenu, zarówno sprzężone **50** i **51**[77] jak i niesprzężone **52-54,**[78] spośród których **50** wykazywał najwyższą efektywność w hamowaniu wzrostu komórek MCF7 i MDA-MB-231. Badania SAR wykazały, że umiejscowienie grupy ferrocenylowej znacząco wpływa na aktywność przeciwnowotworową, zaś usunięcie łańcucha dimetyloaminoalkilowego nie wpływa na cytotoksyczność. Ponadto, stwierdzono, iż związki **50** i **51** wykazują większą efektywność w porównaniu do niesprzężonych analogów **52-54**[78] (Rysunek 16).

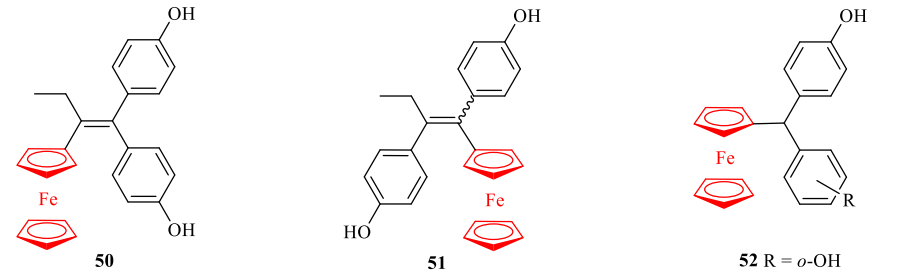

Rysunek 16. *Struktury sprzężonych,* ***50-51****, oraz niesprzężonych pochodnych ferrocifenu* ***52-54***

Spośród szeregu modyfikacji ferrocifenów na szczególną uwagę zasługują pochodne *ansa*-ferrocenu, **55** i **56**. Modyfikacja ta polegała na zahamowaniu rotacji wokół wiązania podwójnego poprzez utworzenie wiązania węgiel-węgiel pomiędzy atomem węgla grupy etylowej ferrocifenu i atomem węgla podstawnika Cp' ferrocifenu. Związek **55** wykazywał

szczególnie wysoką aktywność w stosunku do linii komórkowych nowotworu piersi MDA-MB-231[79] (Rysunek 17). Wysoka cytotoksyczność związku **55** wynika z unikalnego mechanizmu działania, odróżniającego go od innych ferrocifenów. W przeciwieństwie do pozostałych pochodnych, transformacja związku **55** *in situ* do metylidenowego chinonu (QM) zachodzi poprzez klasyczny mechanizm π-delokalizacji, polegający na przemieszczaniu się elektronów w obrębie układu π. Dla związku **56** proces ten może przebiegać poprzez utworzenie pośredniego rodnika *R*-metylenowego, co sugeruje obecność kwaśnych protonów.[79]

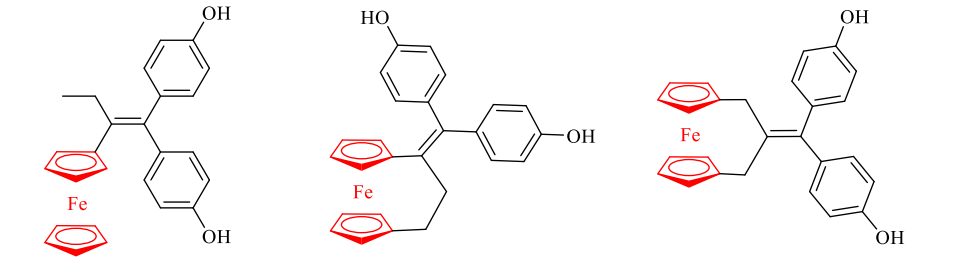

50
MDA-MB-231 IC_{50} = 0,44 µM

55
MDA-MB-231 IC_{50} = 0,09 µM

56
MDA-MB-231 IC_{50} = 0,96 µM

Rysunek 17. *Struktury ansa-ferrocifenów* ***55*** *i* ***56***

Przyłączenie ferrocenu do znanych leków lub zastąpienie grupy fenylowej grupą ferrocenylową pozwoliło na uzyskanie wielu nowych ferrocenylowych analogów związków biologicznie aktywnych. Dobrym przykładem jest ferrochina (związek **58**), analog leku przeciwmalarycznego chlorochiny (związek **57**), która wykazuje skuteczność przeciwko szczepom Plasmodium opornym na chlorochinę[80] (Rysunek 18). Zakłada się, że aktywność ferrochiny wynika z generowania rodników hydroksylowych (•OH) przez grupę ferrocenową. Ponadto, **58** wykazuje wyższą lipofilowość niż **57**, co ułatwia przenikanie przez lipofilową błonę wakuoli, zwiększając jego skuteczność w zwalczaniu infekcji. Obecnie **58** jest w II fazie badań klinicznych w połączeniu z lekiem przeciwpasożytniczym artefenomelem.[81]

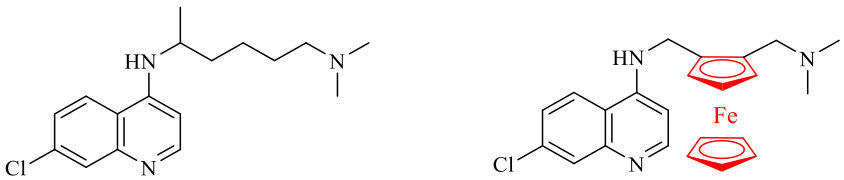

57
IC_{50} = 130 nM

58
IC_{50} = 22 nM

Rysunek 18. *Struktura chlorochiny* ***57*** *i ferrochiny* ***58***

Innym interesującym przykładem wpływu grupy ferrocenylowej na aktywność przeciwnowotworową jest modyfikacja kwasu suberanilohydroksamowego (SAHA) **59**[82], leku zatwierdzonego przez FDA do leczenia chłoniaka T-komórkowego skóry (Rysunek 19).

W wyniku wprowadzenia cząsteczki ferrocenu do **59** otrzymano jego analog **60** (JAHA). Testy *in vitro* potwierdziły, że **60** zachowuje zdolność hamowania deacetylazy histonowej (HDAC) na poziomie porównywalnym z SAHA, jednocześnie wykazując mniejszą skuteczność do hamowania wzrostu komórek raka piersi, zarówno MCF7 (ERα+), jak i wysoce złośliwych, potrójnie negatywnych komórek MDA-MB231 (ERα−).[83, 84]

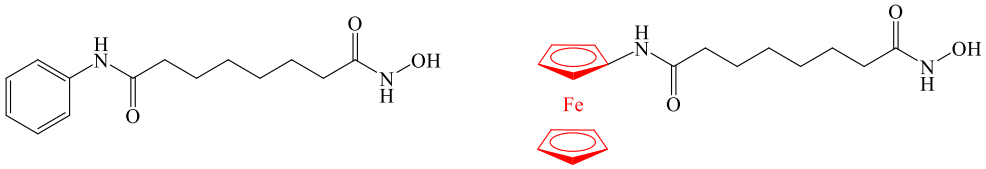

59
MCF IC_{50} = 0,73 μM
MDA-MB-231 IC_{50} = 0,4 μM

60
MCF IC_{50} = 2,44 μM
MDA-MB-231 IC_{50} = 8,45 μM

Rysunek 19. *Struktura SAHA **59** i JAHA **60***

Wprowadzenie grupy ferrocenylowej do paklitakselu zwiększyło cytotoksyczność względem komórek raka okrężnicy SW620: związek **61** był 2,8 razy, a związek **62** 15 razy bardziej aktywny niż **2**. Związek **63** wykazał 13-krotnie wyższą aktywność w stosunku do linii komórkowej SW620D opornej na doksorubicynę i 2,1 razy wyższą wobec docetakselu. Ponadto, związek **64** wykazywał aktywność w stosunku do linii komórek MDR, SW620E, przy stężeniu 1,56 μM [85] (Rysunek 20).

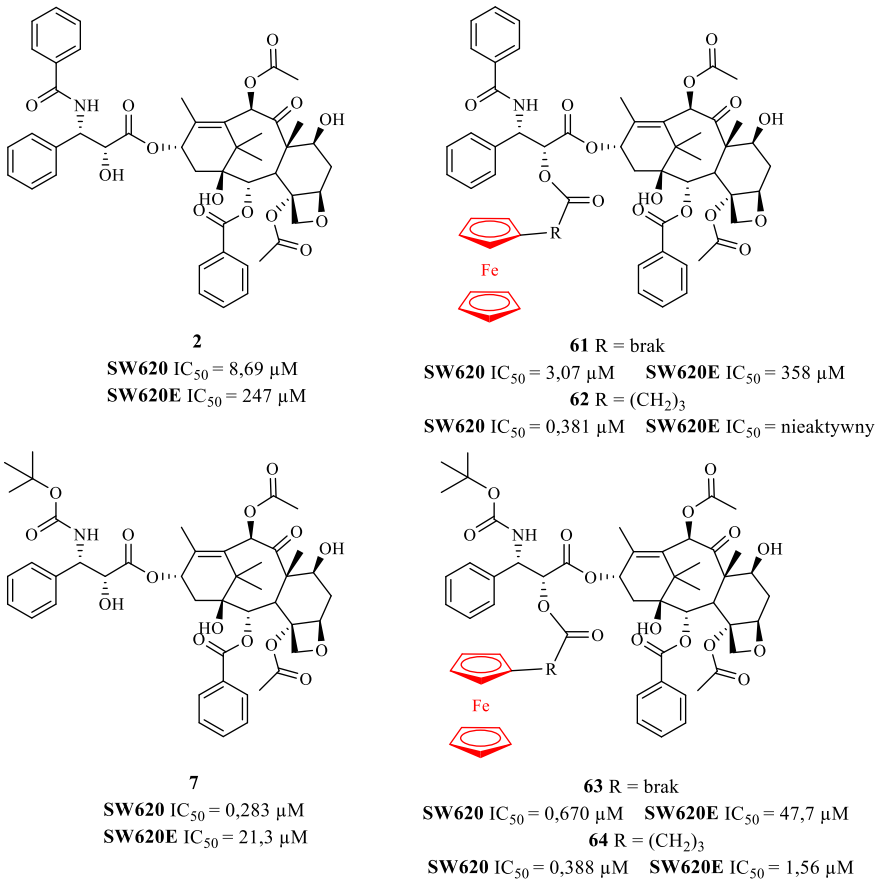

Rysunek 20. *Struktury paklitakselu* ***2****, docetakselu* ***7****, ferrocenylowych pochodnych paklitakselu* ***61*** *i* ***62*** *oraz docetakselu* ***63*** *i* ***64***

Wykazano ponadto, iż zastąpienie grupy *N*-benzoilowej grupą *N*-ferrocenoilową, powoduje 10-krotny wzrost aktywności cytotoksycznej związku **65** w stosunku do linii SW620 w porównaniu z paklitakselem. Wprowadzenie grupy ferrocenylowej w związku **65** skutkowało zwiększeniem zdolności do indukowania polimeryzacji tubuliny oraz wystąpieniem dodatkowych oddziaływań hydrofobowych pomiędzy podstawnikiem ferrocenylowym, a tubuliną[86] (Rysunek 21).

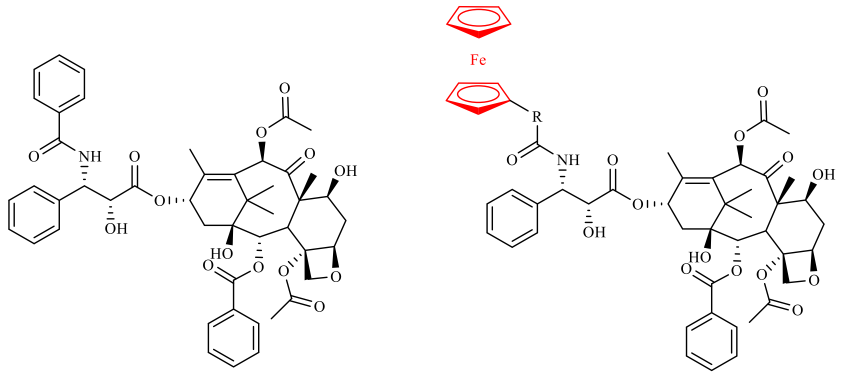

2
SW620 IC_{50} = 1,11 μM

65 R = brak
SW620 IC_{50} = 0,11 μM
66 R = $(CH_2)_3$
SW620 IC_{50} = 5,18 μM

Rysunek 21. *Struktury ferrocenylowych pochodnych paklitakselu* ***65 i 66***

Zbadano również wpływ wprowadzenia podstawnika ferrocenylowego do innych związków antymitotycznych. Przykładowo, zsyntetyzowano i zbadano serię koniugatów ferrocenylowych i rutenocenylowych z kolchicyną, zawierających ugrupowanie 1H-1,2,3-triazolowe.[87] Stwierdzono, że najbardziej aktywne były pochodne rutenocenylowe **70** i **71**, wykazujące 6–7 razy wyższą cytotoksyczność niż **5** w stosunku do komórek HepG2, podczas gdy pochodne ferrocenylowe **68** i **69** wykazywały dwukrotnie wyższą cytotoksyczność niż **5** w stosunku do linii komórkowych HCT116[88] (Rysunek 22).

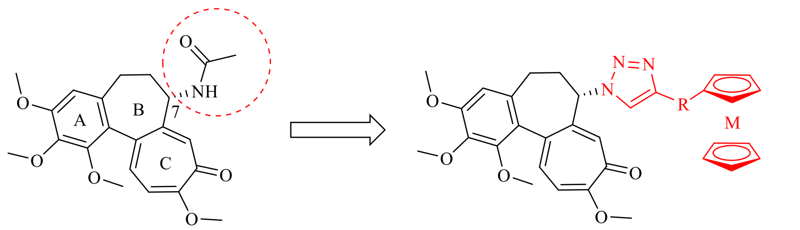

5
HepG2 IC_{50} = 0,023μM
HCT 116 IC_{50} = 0,016μM

67 M = Fe R = nic
HCT 116 IC_{50} = 0,14 μM
68 M = Fe R = $CH_2CH_2CH_2CO$
HCT 116 IC_{50} = 0,006 μM
69 M = Fe R = $CH_2CH_2CH_2CH_2CO$
HCT 116 IC_{50}= 0,009 μM
70 M = Ru R = $CH_2CH_2CH_2CO$
HepG2 IC_{50} = 0,004 μM
71 M = Ru R = $CH_2CH_2CH_2CH_2CO$
HepG2 IC_{50} = 0,003 μM

Rysunek 22. *Struktury 1H-1,2,3-triazolowych analogów kolchicyny* ***67-71***

Interesującym przykładem wpływu wprowadzenia grupy ferrocenylowej do cząsteczki związku biologicznie aktywnego, są ferrocenylowe analogi plinabuliny **72-73**. Zastąpienie grupy fenylowej w cząsteczce plinabuliny grupą ferrocenylową nie zwiększyło cytotoksyczności w stosunku do linii komórkowych MCF7 (rak piersi), HepG2 (rak wątrobowokomórkowy) i SW620 (rak okrężnicy). Wykazano jednak, że otrzymane związki są

aktywne w stosunku do nowotworowych linii komórkowych MDR charakteryzujących się nadekspresją białek ABCB1 i ABCG2. Ponadto, związki te są inhibitorami białek ABCB1 i ABCG2 i podanie ich wraz z lekami przeciwnowotworowymi takimi jak doksorubicyna, etopozyd, metotreksat, winkrystyna prowadzi do śmierci komórek nowotworowych wykazujących oporność wielolekową[89] (Rysunek 23).

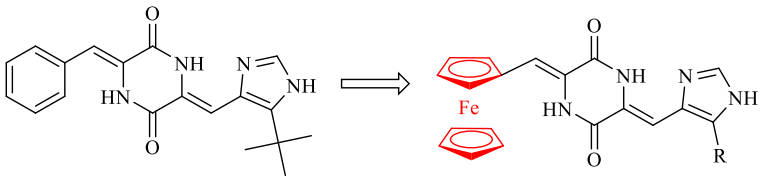

35 **72-73**

Związek	IC_{50} (μM)					
	SW620	**SW620C**	**SW620D**	**SW620E**	**SW620M**	**SW620V**
35	0,034	34.11	>100	52,45	0,132	>100
72 **R= ^{i}Pr**	9,65	31,42	24,23	24,57	23,54	27,95
73 **R= ^{t}Bu**	16,65	19,83	21,77	18,64	32,69	13,68

Rysunek 23. *Struktury plinabuliny* ***35*** *oraz ferrocenylowych analogów plinabuliny* ***72*** *i* ***73***

Ostatnio zsyntetyzowano i zbadano wiele różnorodnych ferrocenylowych analogów i pochodnych związków o interesujących właściwościach przeciwnowotworowych. Przykładowo, pochodne kurkuminy **74** były badane pod kątem aktywności antyproliferacyjnej *in vitro* w stosunku do linii komórkowych B16 (mysi czerniak) oraz NIH3T3 (normalne komórki). Badania SAR wykazały, że wprowadzenie fragmentu zawierającego ferrocen do kurkuminy, prowadzi do związków **75-77** o wyższej aktywności antyproliferacyjnej w porównaniu z kurkuminą, przy czym, **77** wykazał szczególnie wysoką aktywność przeciwnowotworową w stosunku do linii komórkowych B16 i NIH3T3, z wartościami IC_{50} wynoszącymi odpowiednio 2,2 i 6,2 μM. Przyłączanie ferrocenu do **74** zwiększyło zarówno aktywność, jak i selektywność cząsteczek oraz doprowadziło do zwiększonego hamowania polimeryzacji tubuliny[90] (Rysunek 24).

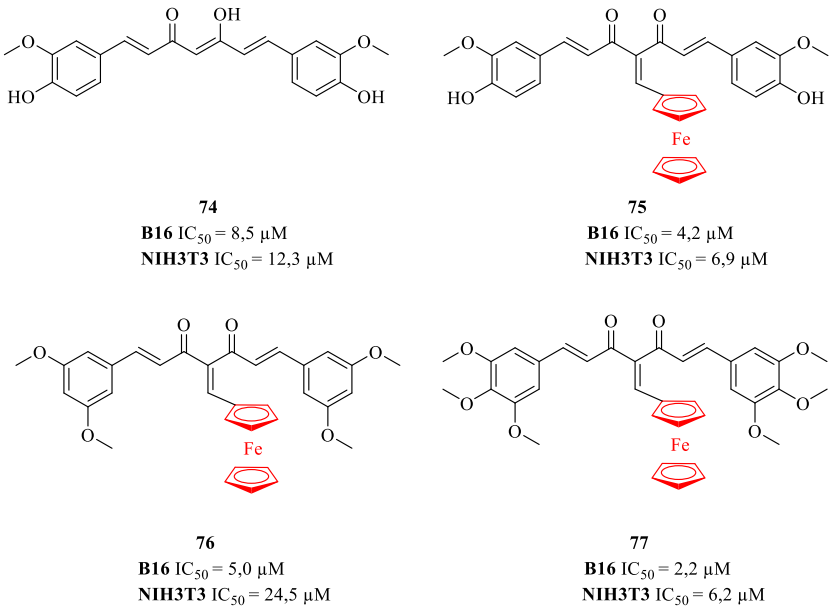

Rysunek 24. *Struktury kurkuminy **74** i pochodnych kurkuminy **75-77***

Kolejnym przykładem są ferrocenylowe pochodne iminocukrów **79a-c**. Wykazano, że zastąpienie grupy fenylowej w **78** ferrocenem, prowadzi do związków **79a-c** cechujących się zwiększoną zdolnością do hamowania aktywności fukozydazy (enzymu odpowiedzialnego za rozkładanie fukozy). Ponadto związki te wykazywały wyższą aktywność antyproliferacyjną w stosunku do komórek raka piersi MDA-MB-231[91] niż **78** (Rysunek 25).

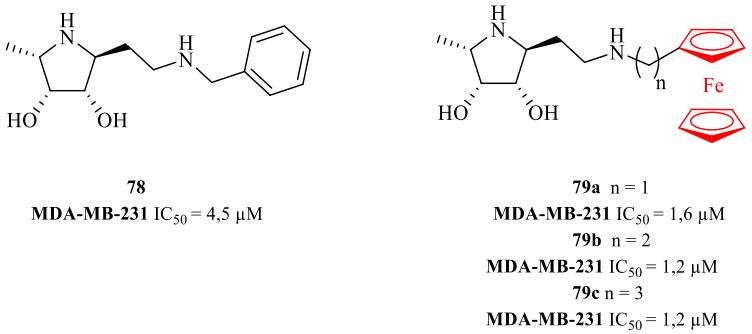

Rysunek 25. *Struktury imonocukru **78** i jego ferrocenylowych analogów **79a-c***

4.4 Białka motoryczne

Leki działające na mikrotubule odniosły sukces kliniczny, jednakże ich stosowanie w chemioterapii wiąże się z poważnymi skutkami ubocznymi, co ogranicza ich kliniczną przydatność. Klasycznie stosowane środki antymitotyczne wpływają zarówno na podział komórek nowotworowych, jak i normalnych komórek, co prowadzi do mielosupresji.[92] Choć mielosupresja jest odwracalna i możliwa do kontrolowania, neuropatia obwodowa u pacjentów leczonych taksanami jest poważniejszym problemem. Jest ona związana z defektem

neuronalnym spowodowanym zaburzeniem dynamiki mikrotubul w niedzielących się komórkach, takich jak neurony obwodowe, i może prowadzić do trwałego uszkodzenia nerwów. W związku z tym istnieje pilna potrzeba opracowania nowych leków przeciwnowotworowych, które zakłócają mitozę bez wpływu na dynamikę mikrotubul w niedzielących się komórkach, co pozwoliłoby uniknąć neuropatii.

Jednym z celów molekularnych, które mogą spełniać powyższe założenia, są kinezyny, w szczególności kinezyna-5. Kinezyny to białka motoryczne związane z mikrotubulami. Odgrywają one rolę w wielu procesach komórkowych, takich jak w transporcie wewnątrzkomórkowym pęcherzyków, organelli, chromosomów i kompleksów białkowych, a także w podziale komórkowym. Do tej pory zidentyfikowano 650 kinezyn, które są obecne u wszystkich organizmów eukariotycznych. Wśród nich około 45 kinezyn mysich i ludzkich zostało podzielone na 14 rodzin. Wszystkie kinezyny posiadają domenę motoryczną zbudowaną z około 340 aminokwasów, która pozwala na przemieszczanie się po mikrotubulach, wykorzystując energię z hydrolizy ATP.[93] Hydroliza ATP do ADP i fosforanu nieorganicznego Pi dostarcza energii kinezynie, co przesuwa ją wzdłuż mikrotubuli. Cykl ten umożliwia kinezynie „kroczenie" po mikrotubulach i transport wewnątrzkomórkowy, zwykle w kierunku plus (+) końca mikrotubuli[94] (Schemat 2). Dzięki temu kinezyny mogą przenosić ładunki na znaczne odległości wewnątrz komórki bez odłączania się od mikrotubuli.

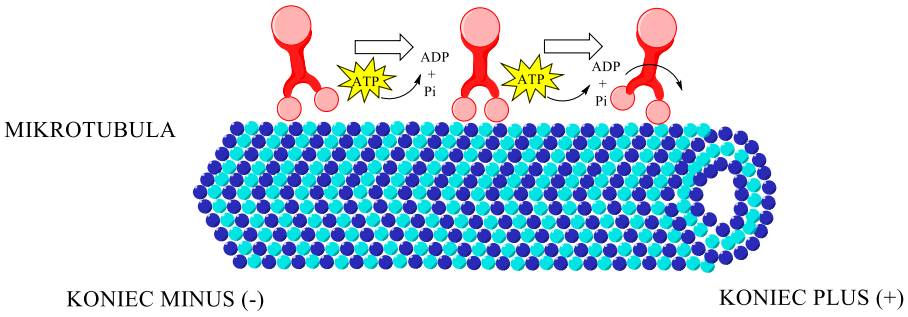

Schemat 2. Mechanizm działania kinezyn

W ostatnich latach jednym z celów farmakologicznych w leczeniu nowotworów jest kinezyna-5 (KSP, Eg5). Białko to ma strukturę homotetrametryczną i pośredniczy w przesuwaniu filamentów mikrotubul. Kinezyna-5 odgrywa kluczową rolę w tworzeniu dwubiegunowego wrzeciona w dzielących się komórkach i jest praktycznie nieobecna w komórkach niedzielących się. KSP jest potrzebna do przejścia z profazy do prometafazy, zaś zablokowanie jej funkcji prowadzi do zaburzenia mitozy i apoptozy komórki.[8, 95]

4.5 Inhibitory KSP

Odkrycie monastrolu **80**, niskocząsteczkowego inhibitora kinezyny-5, zainicjowało poszukiwania innych związków chemicznych wykazujących zdolność do hamowania KSP. Odkryto szereg strukturalnie różnorodnych inhibitorów kinezyny-5, z których część weszła do badań klinicznych (Rysunek 26).[96] Wśród tych związków można wyróżnić pochodne dihydropirymidyny, *β*-karboliny, karbazolu, benzoimidazolu, pirymidyny, chinazoliny, chinolonu, tiadiazoliny, spiropiranu i azobenzenu.

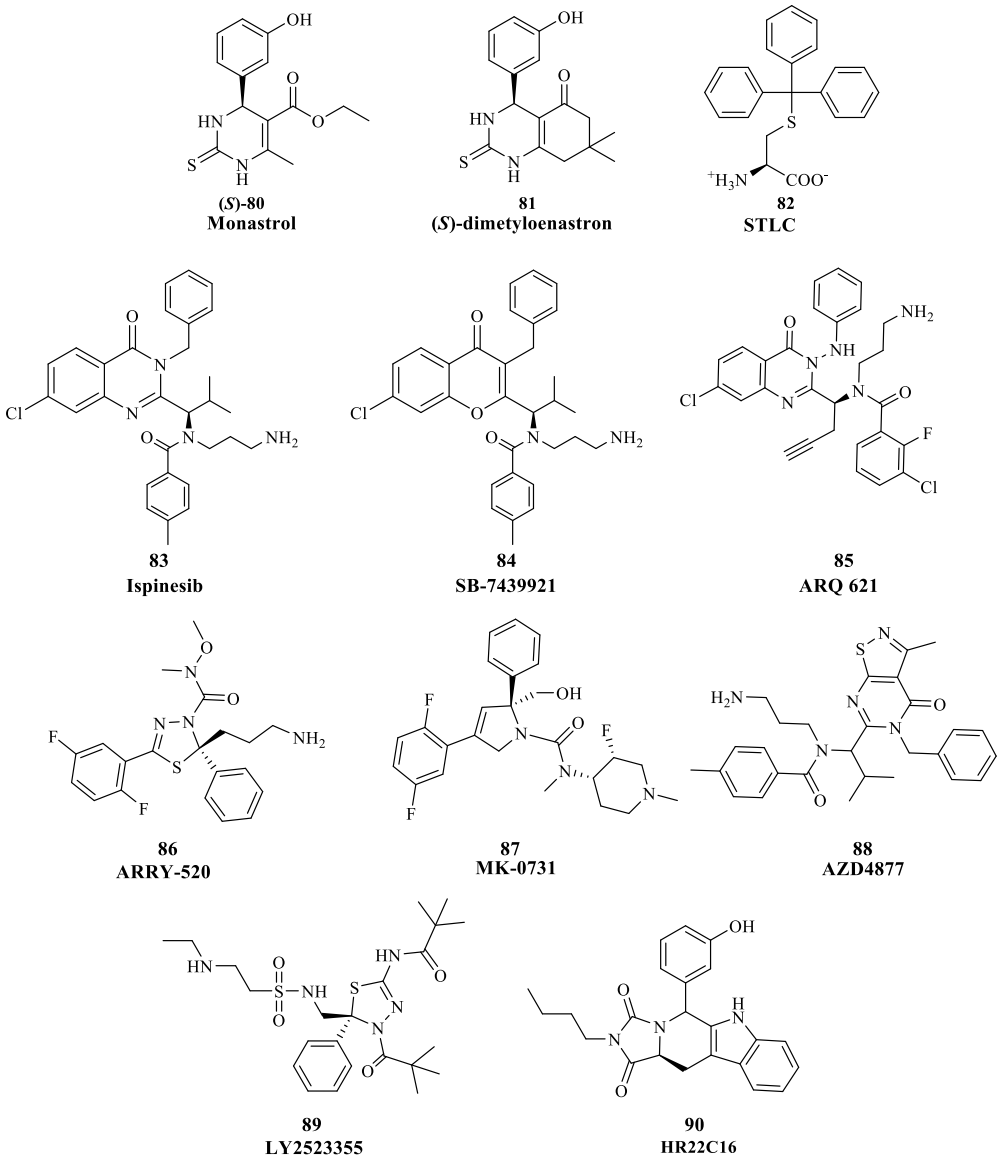

Rysunek 26. *Przykładowe struktury związków hamujących KSP*

Pierwszym odkrytym specyficznym inhibitorem KSP był monastrol.[97] (*S*)-Monastrol **80** jest 15-krotnie silniejszym inhibitorem KSP niż jego (*R*)-enancjomer. (*S*)-**80** hamuje stymulowaną przez mikrotubule aktywność ATPazy KSP (IC_{50} = 30 μM) (Rysunek 27).

Hamowanie aktywności ATPazy w domenie motorycznej KSP przez monastrol zakłóca zdolność tego białka do utworzenia oraz utrzymania wrzeciona dwubiegunowego. Prowadzi to do zatrzymania cyklu komórkowego i indukcji apoptozy.[97] Pomimo, że monastrol **80** wykazuje potencjał w zatrzymywaniu podziału komórek rakowych, nie jest idealnym kandydatem na lek ze względu na swoją niską aktywność oraz brak typowych cech farmakologicznych wymaganych od leków przeciwnowotworowych.

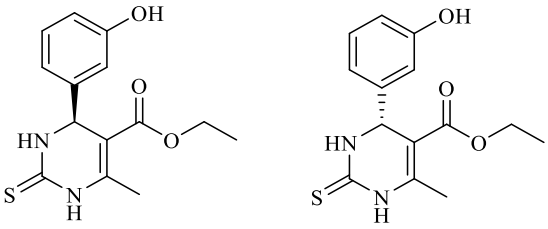

(*S*)-**80**
KSP ATPaza IC_{50} = 30 μM

(*R*)-**80**
KSP ATPaza IC_{50} = 450 μM

Rysunek 27. *Wzór strukturalny (S)-monastrolu* ***80*** *i (R)-monastrolu* ***80***

Odkrycie monastrolu doprowadziło do opracowania jego pochodnych i analogów cechujących się wyższą aktywnością biologiczną oraz mniejszymi efektami ubocznymi. Przykładem takich związków są enastron **91**, dimetylenastron **81** i fluorastrol **92.** Cyklizacja łańcucha bocznego estrowego i grupy metylowej w monastrolu do cyklicznego ketonu w enastronie i dimetylenastronie prowadzi do usztywnienia konformacji, co skutkuje lepszym dopasowaniem tych związków do miejsca wiązania z KSP. Związki **91** i **81** wykazują zdolność do hamowania aktywności ATPazy KSP, z wartościami IC_{50} wynoszącymi odpowiednio 2 μM i 200 nM. Wprowadzenie dwóch grup metylowych w dimetylenastronie zwiększyło zdolność do hamowania aktywności KSP 10-krotnie w stosunku do enastronu[98, 99] (Rysunek 28).

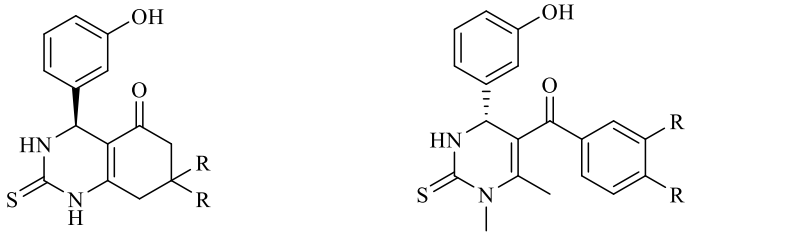

91 R = H (*S*)-enastron
KSP ATPaza IC_{50} = 2 μM
81 R = CH_3 (*S*)- dimetylenastron
KSP ATPaza IC_{50} = 200 nM

92 R = F (*R*)-fluorastrol
KSP komórkowe EC_{50} = 330 nM
93 R = H (*R*)-Mon-97
KSP ATPaza IC_{50} = 2 μM

Rysunek 28. *Wzory strukturalne (S)-enastronu* ***91****, (S)-dimetyloenastronu* ***81****, (R)-fluorastrolu* ***92*** *i (R)-Mon-97* ***93***

Interesującym analogiem monastrolu i dimetylenastronu jest pochodna dihydropiranu CPUYL064 **94**, która jest silnym inhibitorem KSP (ATPaza KSP IC_{50} = 100 nM). Związek ten wykazywał istotną aktywność przeciwnowotworową wobec linii komórkowej HepG2 (rak wątrobowokomórkowy) IC_{50} = 5 μM. Analiza cyklu komórkowego wykazała, iż **94** powoduje zatrzymanie cyklu komórkowego w fazie G_2/M, tak jak ma to miejsce w przypadku monastrolu[100] (Rysunek 29).

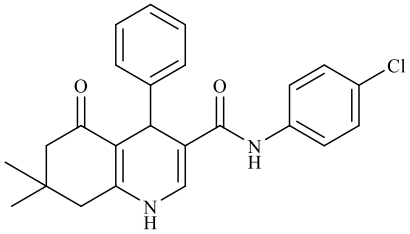

94
KSP ATPaza IC_{50} = 100 nM
HepG2 IC_{50} = 5 μM

Rysunek 29. *Wzór strukturalny CPUYL064* ***94***

Związkiem działającym podobnie do monastrolu jest S-trytylo-L-cysteina (STLC) **82**, która hamuje aktywność ATPazy KSP (IC_{50} = 1,0 μM), w porównaniu do monastrolu (IC_{50} = 9,1 μM), co przekłada się na znacznie wyższą skuteczność przeciwnowotworową wobec komórek raka prostaty opornych na docetaksel.[101] Ograniczenia w stosowaniu **82** w terapii przeciwnowotworowej wynikają z jego nieodpowiednich właściwości fizykochemicznych i niskiej przepuszczalności komórkowej. W odpowiedzi na te wyzwania, zsyntezowano szereg pochodnych **82** poprzez wprowadzenie podstawników do pierścienia fenylowego grupy trytylowej takich jak: grupy alkilowe, alkoksyle lub halogeny w pozycji para, co zwiększa hamowanie aktywności ATPazy KSP.[102, 103] Przykładowo, S-(4-metoksytrytylo)-L-cysteina **95** wykazuje 7-krotny wzrost aktywności hamującej ATPazę KSP w porównaniu do STLC, a przy tym charakteryzuje się wysoką selektywnością wobec KSP oraz niską neurotoksycznością, gdyż nie oddziałuje z tubuliną.[104] Pochodna *p*-trifluorometylowa **96** wykazywała 5-krotny wzrost hamowania aktywności ATPazy KSP w stosunku do STLC.[105] Zastąpienie jednego pierścienia fenylowego grupą benzylową zwiększyło aktywność hamującą ATPazę KSP **97**, a podstawienie jednego z pierścieni fenylowych w **97** chlorem lub grupą hydroksylową prowadzi do związków **98** i **99** o wyższej zdolności do hamowania aktywności KSP[106] (Rysunek 30).

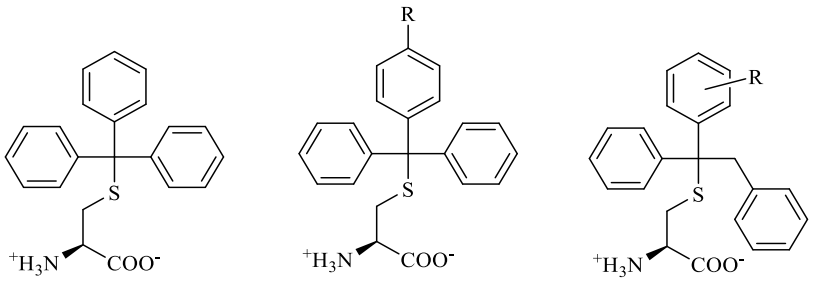

82
KSP ATPaza IC_{50} = 1,0 μM

95 R = OCH
KSP ATPaza IC_{50} = 0,15 μM
96 R = CF_3
KSP ATPaza IC_{50} = 0,22 μM

97 R = H
KSP ATPaza IC_{50} = 138 nM
98 R = 4-Cl
KSP ATPaza IC_{50} = 58 nM
99 R = 3-OH
KSP ATPaza IC_{50} = 67 nM

Rysunek 30. *Wzór strukturalne pochodnych S-trytylo-* L-*cysteiny* ***95-99***

Silnym inhibitorem kinezyny-5 jest filanesib (ARRY-520) **86**, charakteryzujący się wartością IC_{50} na poziomie 6.0 nM (Rysunek 31).[107] Ciekawą cechą **86** jest jego skuteczność w modelach nowotworów opornych na taksany, co sugeruje, że może być on użyteczny w leczeniu pacjentów z nowotworami opornymi na standardowe terapie.[108] Ponadto, w przeciwieństwie do innych terapii przeciwnowotworowych, **86** nie powoduje neuropatii obwodowej, co czyni go obiecującą opcją terapeutyczną z mniejszą toksycznością. Związek ten przeszedł badania kliniczne II fazy i wszystko wskazuje, że wejdzie w fazę III przeciwko szpiczakowi plazmocytowemu.[109]

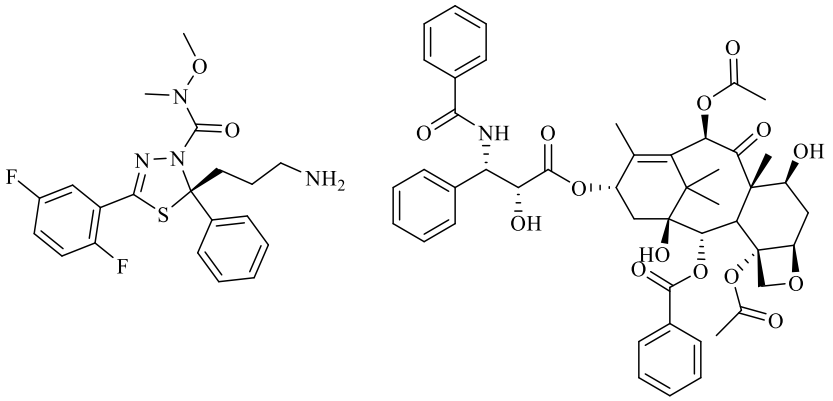

86
KSP ATPaza IC_{50} = 6,0 nM
MCF7 EC_{50} = 0,6 nM
MCF/ADR EC_{50} = 14 nM

2
MCF7 EC_{50} = 1,7 nM
MCF/ADR EC_{50} = 565 nM

Rysunek 31. *Wzór strukturalny filanesibu (ARRY-520)* ***86***

Do innej ważnej klasy inhibitorów KSP należy ispinesib **83**.[110] Ispinesib zaburza wiązanie KSP z mikrotubulami i hamuje jej ruch, co uniemożliwia uwalnianie ATP, ale nie blokuje uwalniania kompleksu KSP-ADP.[111] Ispinesib był pierwszym inhibitorem kinezyny-5,

który przeszedł badania kliniczne, wykazując IC_{50} mniejsze niż 10 nM (KSP ATPaza) i minimalne skutki uboczne. Trzynaście badań klinicznych dotyczących monoterapii ispinesibem w leczeniu guzów litych oraz nowotworów hematologicznych zostało zakończonych lub przerwanych.[111] Dodatkowo, zakończono trzy badania kliniczne fazy I/II, w których stosowano terapię ispinesibem skojarzoną z docetakselem, kapecytabiną oraz karboplatyną w leczeniu guzów litych.[112, 113] We wszystkich badaniach, **83** był dobrze tolerowany przez pacjentów, ale nie zaobserwowano znaczących pozytywnych wyników leczenia, a jedynie kilka przypadków stabilizacji choroby.[112] Wynika z tego, że **83** opóźniał postęp choroby, jednak jego działanie nie było na tyle silne, aby wywołać regresję guza.

Optymalizacja struktury ispinesibu w 2006 roku doprowadziła do odkrycia związku SB-743921 **84** poprzez izosteryczne zastąpienie pierścienia chinazolinowego pierścieniem chromen-4-onu.[114] Związek **84** wykazywał IC_{50} na poziomie 0,1 nM i wszedł do dwóch badań klinicznych fazy I/II, które zostały już zakończone.[115] Badania toksyczności wykazały przewidywalne działania niepożądane, takie jak neutropenia i toksyczność żołądkowo-jelitowa, bez oznak neurotoksyczności.[113]

Kolejnym przykładem analogu ispinesibu jest ARQ621 **85**, który wykazuje aktywność przeciwnowotworową przeciwko szerokiemu spektrum linii komórkowych w badaniach *in vitro.*[116] W 2009 roku **85** wszedł do I fazy badań klinicznych u pacjentów z guzami litymi jako monoterapia, wykazując dobrą tolerancję z najczęstszymi działaniami niepożądanymi w postaci zmęczenia, nudności i niedokrwistości. Jednak **85** nie wykazał zauważalnych efektów terapeutycznych ani postępu jako potencjalny lek przeciwnowotworowy[117] (Rysunek 32).

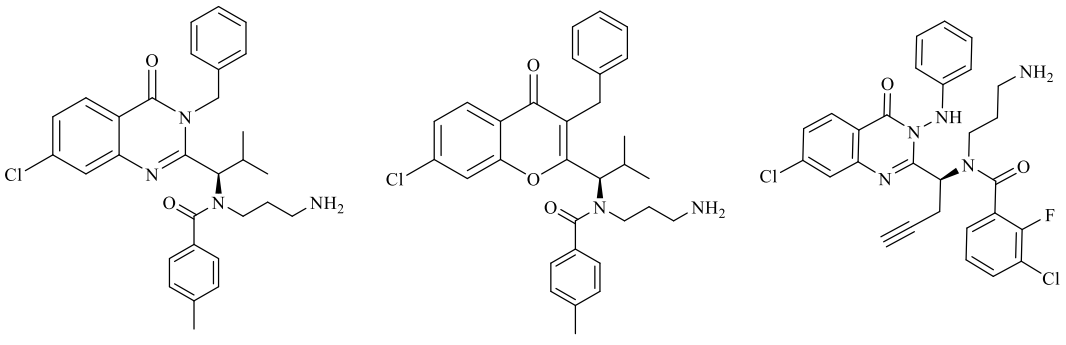

Rysunek 32. Wzór strukturalny ispinesibu **83** i jego analogi **84** i **85**

W ostatnim czasie zsyntezowano półsandwiczowe kompleksy ispinesibu zawierające metale takie jak, ruten (Ru), osm (Os), rod (Rh) i iryd (Ir). Kompleksy z Ir i Rh (**102a**, **103a**,

102b, **103b**) wykazały wyższą aktywność w hamowaniu KSP niż sam ispinesib.[55] Związki z (*R*)-enancjomerycznym ligandem hamowały aktywność ATPazy KSP od 75% (**107a**) do 90% (**108a**) przy stężeniu 100 nM, jednak nie osiągnęły skuteczności ispinesibu, który wykazał 98% inhibicję.[56] Sugeruje to, że kompleksy metaloorganiczne z inhibitorami KSP mogą zwiększać skuteczność leczenia przeciwnowotworowego[118, 119] (Rysunek 33).

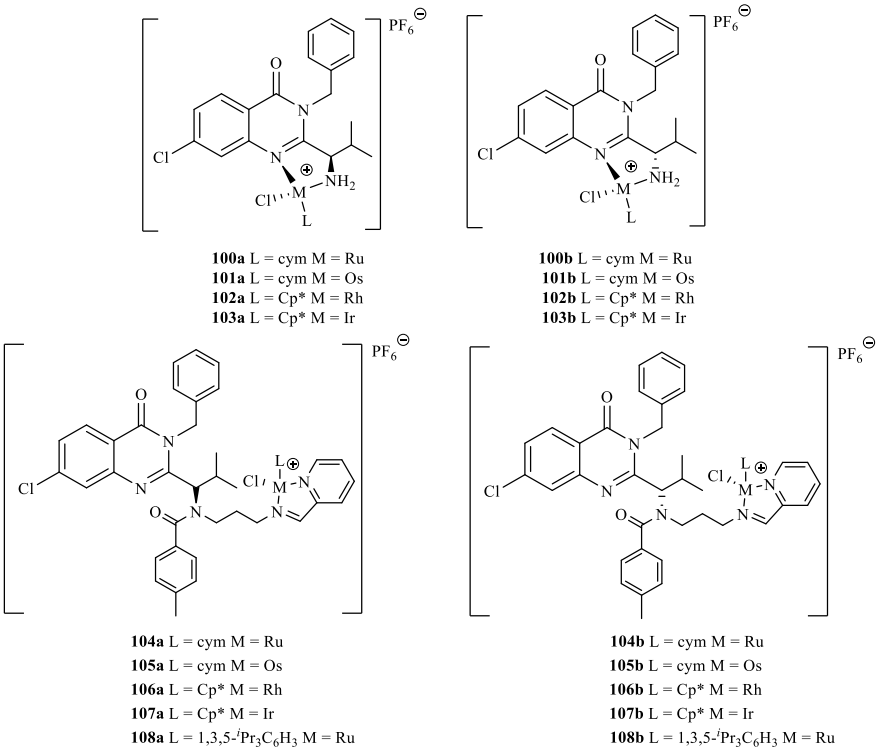

Rysunek 33. *Struktury półsandwiczowych kompleksów ispinesibu* ***100a-108b***

Hipoteza badawcza

Wprowadzenie podstawnika ferrocenylowego do struktury znanych inhibitorów kinezyny-5 może zwiększy aktywność przeciwnowotworową otrzymanych hybryd poprzez połączenie cytotoksycznych właściwości grupy ferrocenylowej z selektywnym hamowaniem aktywności KSP, co doprowadzi do skutecznego zatrzymania mitozy w komórkach nowotworowych.

Obecność ugrupowania ferrocenylowego może przyczynić się do wzrostu cytotoksyczności otrzymanych koniugatów ze względu na zdolność tych ugrupowań do generowania reaktywnych form tlenu oraz wpływania na procesy komórkowe prowadzące do apoptozy. Dodatkowo, fragmenty wiążące się z KSP umożliwią selektywne hamowanie aktywności tego białka, które jest kluczowe dla prawidłowego przebiegu mitozy. Połączenie obu tych strategii w jednej cząsteczce może prowadzić do synergistycznego efektu, zwiększając skuteczność przeciwnowotworową i minimalizując skutki uboczne terapii. Takie koniugaty mogą wykazywać większą selektywność wobec komórek nowotworowych, co pozwoli na ograniczenie wpływu na zdrowe komórki i zmniejszenie potencjalnej toksyczności. Oczekuje się, że otrzymane związki będą w stanie skuteczniej zatrzymywać podział komórek nowotworowych poprzez hamowanie aktywności KSP, jednocześnie wykorzystując cytotoksyczne właściwości ugrupowań metaloorganicznych.

5. Cel badań

Celem mojej pracy doktorskiej była synteza nowych hybrydowych związków chemicznych, w których struktury znanych inhibitorów kinezyny-5 zostały zmodyfikowane poprzez wprowadzenie podstawnika ferrocenylowego. Zamierzałam zbadać wpływ obecności ugrupowania ferrocenylowego na aktywność przeciwnowotworową tych związków, ze szczególnym uwzględnieniem ich zdolności do selektywnego hamowania aktywności kinezyny-5 oraz indukcji apoptozy w komórkach nowotworowych.

Do swoich badań wybrałam trzy znane inhibitory kinezyny-5 jako związki: monastrol, CPUYL064 oraz ispinesib. Poprzez wprowadzenie grupy ferrocenylowej do ich struktur dążyłam do połączenia cytotoksycznych właściwości ugrupowania ferrocenylowego z hamowaniem aktywności KSP.

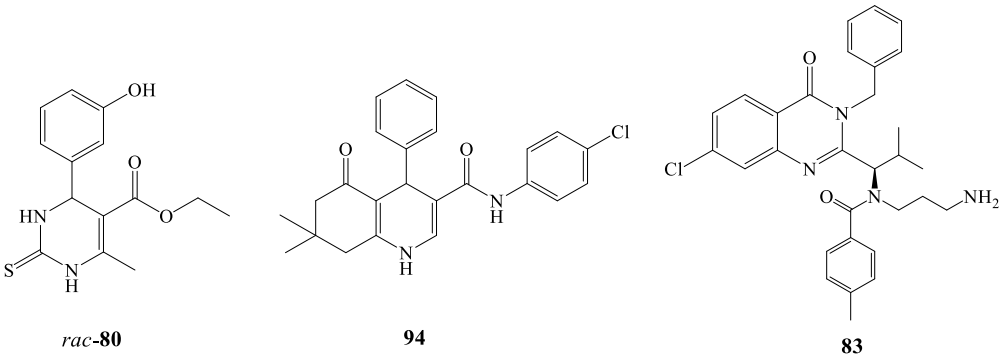

rac-**80** **94** **83**

Rysunek 34. *Struktury monastrolu* ***80*** *CPUYL064* ***94*** *i ispinesibu* ***83***

6. Omówienie wyników badań

6.1 Ferrocenylowe analogi monastrolu

Badania wpływu wprowadzenia podstawnika ferrocenylowego do inhibitorów KSP na ich właściwości biologiczne rozpoczęto od syntezy ferrocenylowych analogów monastrolu. Zaplanowano dwa główne typy modyfikacji cząsteczki monastrolu (Schemat 3). Modyfikacje typu I polegały na zastąpieniu grupy *3*-hydroksyfenylowej podstawnikiem ferrocenylowym oraz *o*-, *m*-, *p*-ferrocenylofenylowym. Modyfikacje typu II polegały na zastąpieniu grupy 4-metylowej w monastrolu grupą ferrocenylową lub *o*-, *m*-, *p*-ferrocenylofenylową. Postanowiono także zbadać wpływ zamiany atomu siarki na atom tlenu w tak otrzymanych koniugatach.

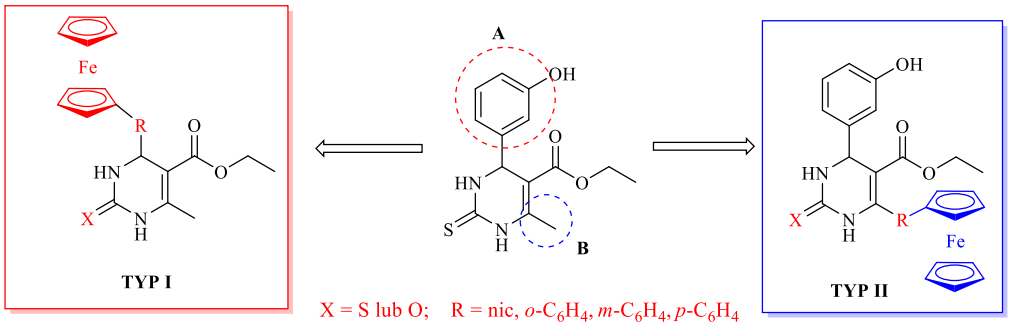

Schemat 3. *Planowane modyfikacje monastrolu*

Ferrocenylowe analogi monastrolu typu I postanowiono zsyntezować w reakcji Biginelliego[120] pomiędzy ferrocenokarboaldehydem lub *o*-, *m*- i *p*-ferrocenylobenzaldehydem, acetylooctanem etylu oraz tiomocznikiem lub mocznikiem. W pierwszym etapie badań zoptymalizowano warunki reakcji ferrocenylokarboaldehydu, acetylooctanu etylu i tiomocznika. W reakcji prowadzonej w obecności katalitycznej ilości kwasu solnego otrzymano związek **111a** z wydajnością 53%. Stwierdzono jednak, że w tych warunkach reakcji, w przypadku zastosowania *o*-, *m*-, *p*-ferrocenylobenzaldehydów, nie powstają oczekiwane produkty. Zaobserwowano, że zastąpienie kwasu solnego chlorkiem antymonu(III) doprowadziło do powstania oczekiwanych produktów **111b-d** z wydajnościami 23-76%, zaś wydajność **111a** była niższa niż przy użyciu kwasu solnego i wynosiła 49%. W przypadku pochodnych mocznika otrzymano produkty **112a-d** z wydajnościami w zakresie 72-80% (Schemat 4).

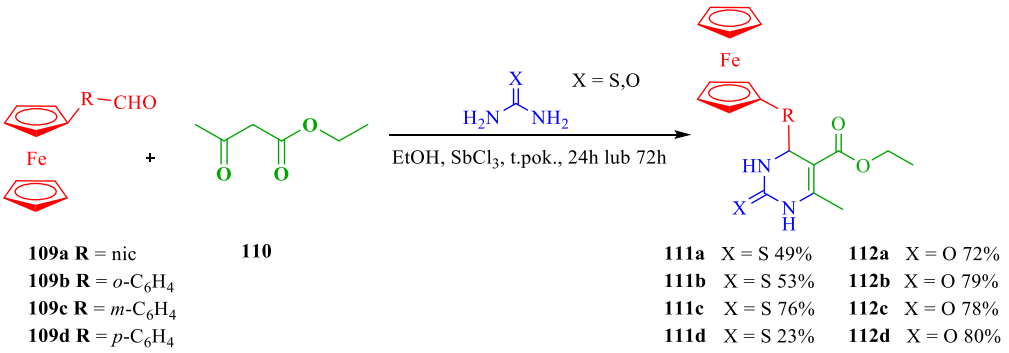

Schemat 4. *Synteza ferrocenylowych pochodnych monastrolu typu I*

Ferrocenylowe analogi monastrolu typu II zsyntezowano w reakcji ferrocenoilooctanu etylu **113a** lub *o*-, *m*- i *p*-ferrocenylobenzoilooctanu etylu **113b-d**, 3-hydroksybenzaldehydu oraz tiomocznika lub mocznika. Ferrocenoilooctan etylu **113a** zsyntezowano w reakcji Friedela-Craftsa ferrocenu z malonianem mono-etylu i bezwodnikiem trifluorooctowym w obecności kwasu trifluorometanosulfonowego z praktycznie ilościową wydajnością (Schemat 5).[79] *o*-, *m*- oraz *p*-ferrocenylobenzoilooctany etylu **113b-d** zsyntetyzowano w reakcji odpowiednich aldehydów **113b-d** z diazooctanem etylu w obecności katalitycznej ilości $NbCl_5$ z wydajnością 11-65% adaptując znaną procedurę[121] (Schemat 6). Strukturę produktów potwierdzono metodami spektroskopii NMR. W widmach ^1H NMR produktów **113a-d** obserwowano sygnały przypisane dla protonów OH enolu przy około 12,3-12,6 ppm, dla związków **113b-d** obserwowano dodatkowo sygnały pochodzące od protonu $CH_{AR\text{-}enol}$ przy ok 7,79-7,30 ppm.

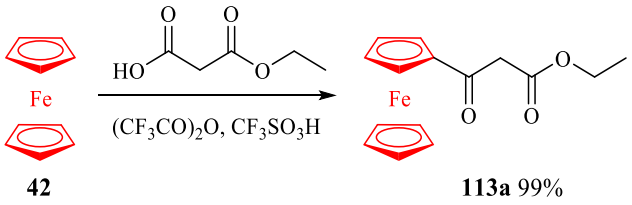

Schemat 5. *Synteza ferrocenylowego β-ketoestru **113a***

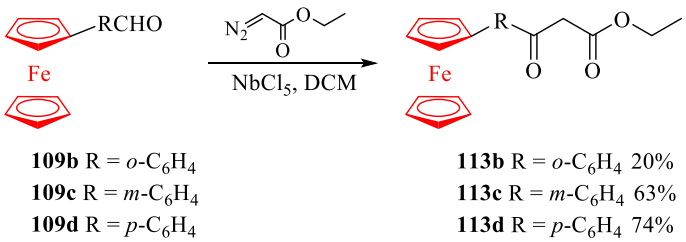

Schemat 6. *Synteza ferrocenylowych β-ketoestrów **113b-d***

W kolejnym etapie otrzymane *β*-ketoestry **113a-d** poddano reakcji Biginelliego. Stwierdzono, że reakcja **113a-d** z 3-hydroksybenzaldehydem i tiomocznikiem w zoptymalizowanych wcześniej warunkach ($SbCl_3$, 24h, temp. pokojowa) prowadzi do mieszaniny związków, których nie dało się rozdzielić żadną dostępną metodą, a oczekiwane produkty były obecne jedynie w niewielkich ilościach. W przypadku użycia mocznika zamiast tiomocznika w powyższych warunkach, wyizolowano z wydajnością 10-34% jedynie związki **117a-d**, które wytrąciły się z mieszaniny reakcyjnej (Schemat 7).

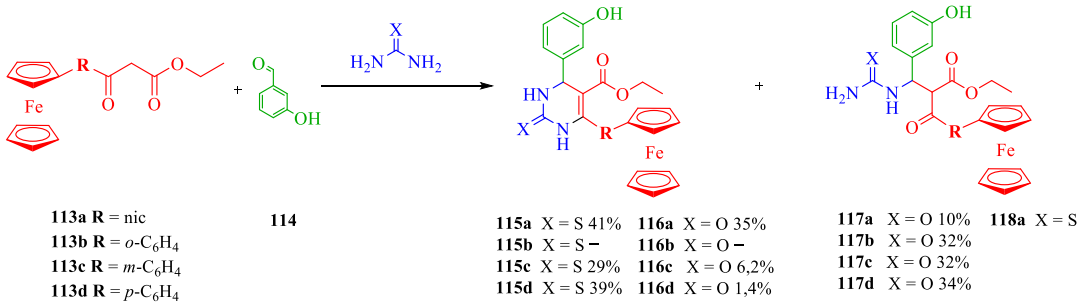

Schemat 7. *Synteza ferrocenylowych pochodnych monastrolu typu II*

W celu optymalizacji powyższej reakcji monitorowano jej postęp za pomocą HPLC-MS. Jako reakcję modelową wybrano reakcję pomiędzy *p*-ferrocenoilooctanem etylu **113a**, 3-hydroksybenzaldehydem **114**, tiomocznikiem i mocznikiem w obecności $SbCl_3$ w temperaturze pokojowej. W przypadku użycia mocznika, analiza HPLC-MS surowej mieszaniny reakcyjnej potwierdziła, że głównym produktem jest **117a** (43,8%), podczas gdy pożądany produkt **116a** powstał z wydajnością 9,4%. W surowej mieszaninie poreakcyjnej stwierdzono obecność niewielkiej ilość nieprzereagowanego substratu **113a** (13,1%). W przypadku użycia tiomocznika stwierdzono także obecność produktu niecyklicznego **118a** w ilości 29,0%, oraz 5.5% oczekiwanego produkt **115a** oraz substratu **113a** w ilości 34,9%. Podwyższenie temperatury reakcji do 40°C spowodowało zmniejszenie zawartości związków niecyklicznych **117a** i **118a** (odpowiednio do 34,2 i 25,5%) przy jednoczesnym zwiększeniu zawartości pożądanych produktów heterocyklicznych **116a** i **117a** (odpowiednio do 25,5 i 29,5%) (Tabela 2). Wydłużenie czasu reakcji do 72h zwiększyło wydajność oczekiwanych produktów do odpowiednio 35 i 41%.

Czas	Temperatura	Katalizator	Rozpuszczalnik	115a (X=S)	116a (X=O)	117a (X=O)	118a (X=S)
24h	21°C	$SbCl_3$	CH_3CH_2OH	5,5%	9,4%	43,8%	29,0%
24h	40°C	$SbCl_3$	CH_3CH_2OH	29,5%	25,5%	34,2%	25,5%

Tabela 2. *Wydajności produktów powstałych w temperaturze pokojowej (lub 40°C) w surowej mieszaninie reakcyjnej, które zostały określone za pomocą HPLC-MS*

W zoptymalizowanych dla **113a** warunkach przeprowadzono reakcję *o*-, *m*- i *p*-ferrocenylobenzoilooctanów etylu **113b-d** z 3-hydroksybenzaldehydem, tiomocznikiem lub mocznikiem oraz $SbCl_3$ w temperaturze 40°C przez 72 godziny. W przypadku zastosowania tiomocznika, otrzymano oczekiwane produkty **115c**, **115d** z wydajnościami 10-54%. Niestety, wszelkie próby syntezy *o*-ferrocenylofenylowej pochodnej **115b** zakończyły się niepowodzeniem. W przypadku użycia mocznika jako substratu próby syntezy tlenowych analogów zawierających grupy *o*-, *m*- lub *p*-ferrocenylofenylowe **116b-d** w powyższych warunkach także zakończyły się niepowodzeniem. W związku z tym, postanowiono przeprowadzić powyższe reakcje w innych warunkach. Prowadząc reakcje w reaktorze mikrofalowym w obecności 10 mol% trifluorometanosulfonianu iterbu (III) w 2,2,2-trifluoroetanolu jako rozpuszczalniku w temperaturze 110°C przez 30 minut otrzymano związki **116c** i **116d** z wydajnością odpowiednio 6,2% i 1,4%. Zaobserwowano także powstawanie śladowych ilości związków **117c** i **117d,** natomiast pochodne **115b** i **116b** nie powstały.

Struktura i czystość wszystkich związków została potwierdzona za pomocą spektroskopii NMR oraz HPLC-MS. W widmach ^{1}H NMR związków **111a-d** i **115c-d** zaobserwowano dwa sygnały przypisane dla protonów H-1 i H-3 odpowiednio przy ok 10,5 i 9,7 ppm, podczas gdy w **112a-d** protony te obserwowano przy ok 9,1 i 7,5 ppm. Natomiast w przypadku **115a** kolejność pików protonowych H-1 i H-3 była odwrócona, a odpowiednie sygnały występowały przy ok 8,7 i 9,9 ppm. W widmach ^{1}H NMR związków **117a-d** sygnały grupy NH_2 występują przy ok 5,6 ppm, a NH przy ok 6,6 ppm jako szerokie singlety lub dublety (Rysunek 36).

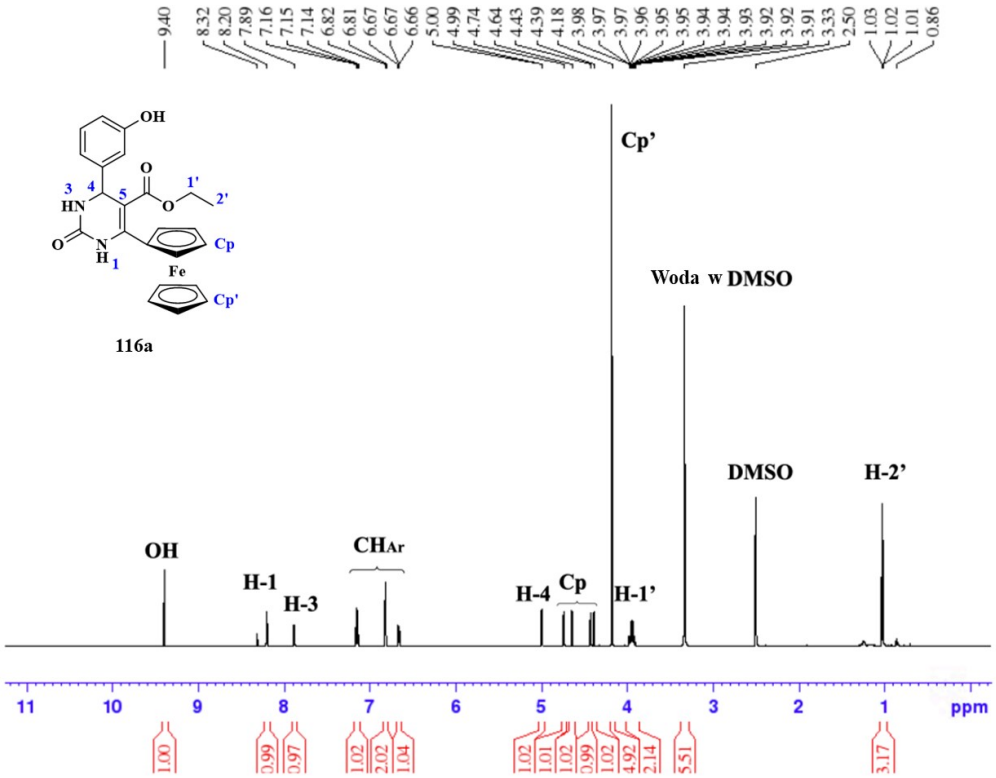

Rysunek 35. *Widmo ^{1}H NMR związku* ***116a***

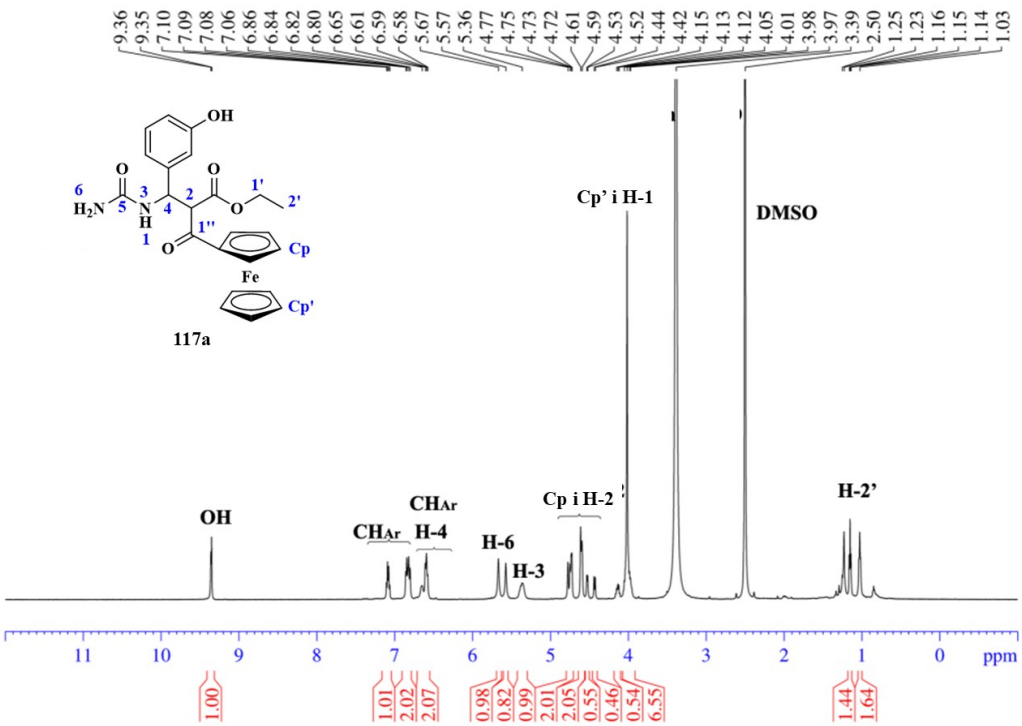

Rysunek 36. *Widmo ^{1}H NMR związku* ***117a***

We współpracy z dr hab. prof. UW Anną Makal z Uniwersytetu Warszawskiego zbadano struktury krystalograficzne **111a** i **115a** (Rysunek 37). Oba związki krystalizują

w centrosymetrycznych grupach przestrzennych: C2/c dla **111a** oraz $P2_1/c$ dla **115a**, jako mieszaniny racemiczne. W obu przypadkach w jednostce asymetrycznej znajduje się pojedyncza cząsteczka związku. Związek **115a** współkrystalizował z jedną cząsteczką dichlorometanu.

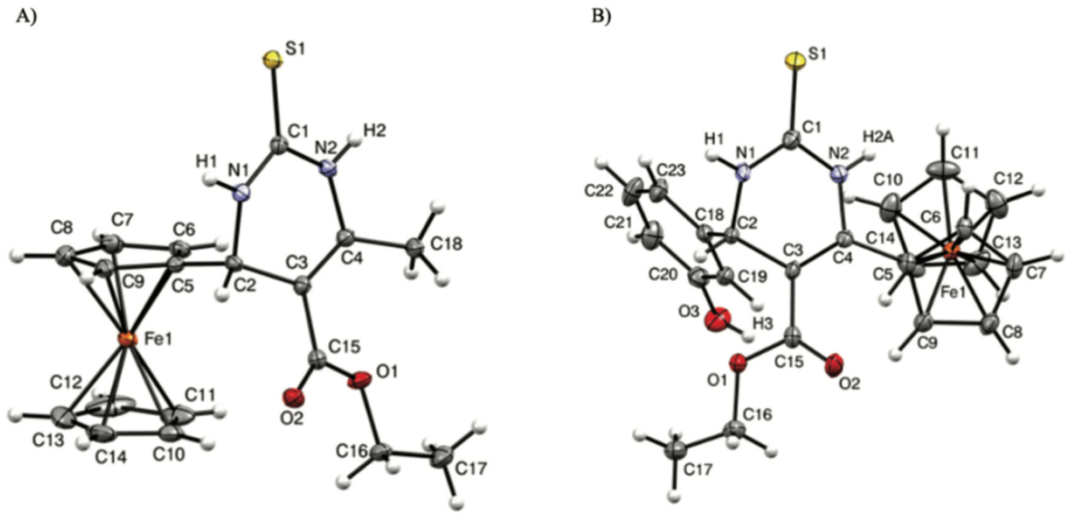

Rysunek 37. *Struktura rentgenograficzna* ***111a*** *(A) i* ***115a*** *(B)*

Geometryczna struktura pierścieni heterocyklicznych w pochodnych monastrolu **111a** i **115a** jest niemal identyczna jak w przypadku monastrolu, co wskazuje, że podstawienie grupy ferrocenylowej w pozycji C2 lub C4 nie wpływa na geometrię farmakoforu. Pomimo wprowadzenia podstawnika ferrocenylowego, wiązania wodorowe w strukturze molekularnej **111a** są zasadniczo takie same jak w monastrolu. Zarówno grupy N1–H, jak i N2–H działają jako donory wiązań wodorowych, a cząsteczki **111a** tworzą dimery połączone parą wiązań N–H···S. Z kolei zastąpienie grupy metylowej w monastrolu przez ferrocen w pozycji C4 w związku **115a** prowadzi do innego układu wiązań wodorowych. W tym przypadku N2–H działa jako donor wiązania wodorowego dla atomu O2, a nowy pierścieniowy układ wiązań N–H···O oraz O–H···S tworzy się z udziałem grupy hydroksylowej podstawnika m-hydroksyfenylowego.

Aktywność antyproliferacyjna zsyntetyzowanych została zbadana we współpracy z dr. Błażejem Rychlikiem i dr. Andrzejem Błaużem (Katedra Biofizyki Molekularnej Uniwersytetu Łódzkiego) wobec komórek nowotworowych: A549 (gruczolakorak komórek nabłonka pęcherzyków płucnych), Colo 205 (gruczolakorak jelita grubego), HCT116 (rak jelita grubego), HepG2 (rak wątrobowokomórkowy), MCF7 (gruczolakorak piersi) i SW620 (gruczolakorak jelita grubego), a także w panelu pięciu lekoopornych (MDR) linii komórkowych

charakteryzujących się nadekspresją różnych białek ABC: ABCG2 (SW620C), ABCC1(SW620M i SW620E), ABCB1(SW620D, SW620E, SW620V).

Początkowo oceniono wpływ zsyntetyzowanych związków na przeżywalność komórek nowotworowych przy stężeniu odpowiadającemu wartości IC_{50} monastrolu dla danej linii komórkowej. Na podstawie uzyskanych danych wybrano dziesięć najbardziej aktywnych związków, dla których określono wartości IC_{50} w badanych liniach komórkowych.

Wprowadzenie grupy ferrocenylowej w miejsce grupy 3-hydroksyfenylowej w monastrolu (związek **111a**) nieznacznie zwiększyło aktywność przeciwnowotworową wobec linii komórkowych Colo 205, HepG2 i SW620. Znaczne zwiększenie aktywności zaobserwowano w przypadku zastąpienia grupy 3-hydroksyfenylowej ugrupowaniem ferrocenylowo-fenylowym. Najbardziej aktywnymi związkami okazały się **111b** i **111d**, zawierające odpowiednio grupy *o*-ferrocenylofenylową i *p*-ferrocenylofenylową. Wymiana atomu siarki na atom tlenu w pierścieniu heterocyklicznym prowadziła do zmniejszenia aktywności antyproliferacyjnej dla związków typu I, z wyjątkiem związku **112b**, który mimo obecności atomu tlenu wykazywał znaczącą aktywność, prawdopodobnie ze względu na obecność grupy *o*-ferrocenylofenylowej.

Zastąpienie grupy 6-metylowej w monastrolu podstawnikami ferrocenylowym lub ferrocenylofenylowymi (związki **112a,c,d**) znacząco zwiększyło aktywność antyproliferacyjną związków typu II. Szczególnie wyróżniał się związek **112c**, zawierający grupę *m*-ferrocenylofenylową, który wykazywał najwyższą aktywność wśród wszystkich badanych związków, z wartościami IC_{50} w zakresie 1–5 μM dla wszystkich linii komórkowych. Badania na liniach komórek opornych (MDR) wykazały, że większość zsyntetyzowanych związków była bardziej aktywna niż monastrol wobec komórek MDR, zaś najwyższą cytotoksyczność wykazywały związki **111b** i **112d**. Otrzymane wyniki pozwoliły na wybranie trzech związki do dalszych badań: ferrocenylowy analog monastrolu **111a** oraz dwa analogi tlenowe **112b** i **115c** (Rysunek 38).

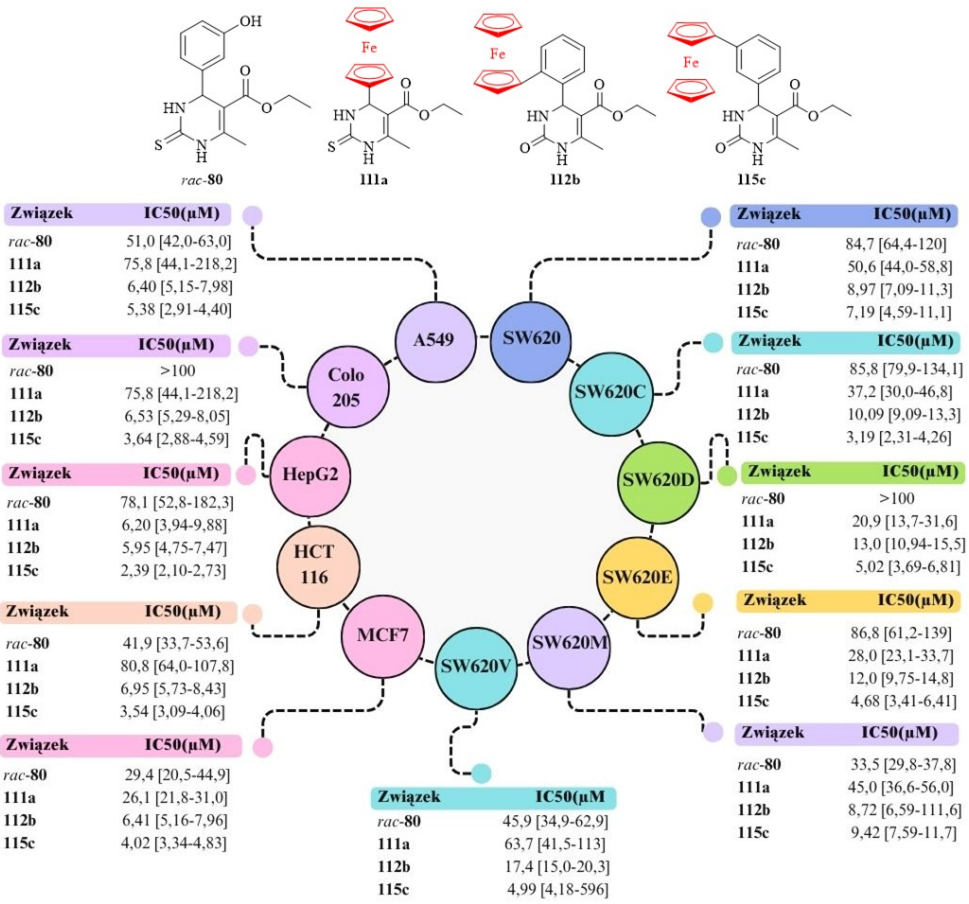

Rysunek 38. *Cytotoksyczność ferrocenylowych analogów monastrolu (**111a, 112b**, **115c**) w liniach komórkowych, 51,0 μM (A549), 112 μM (Colo 205), 41,9 μM (HCT 116), 78,1μM (HepG2), 29,4 μM (MCF7), 84,7 μM (SW620) oraz liniach komórkowych raka MDR. Przedziały ufności (95%) przedstawiono w nawiasach kwadratowych. Zebrane wartości są średnią z trzech niezależnych eksperymentów*

W kolejnym etapie, zbadano efektywność wybranych związków w hamowaniu aktywności kinezyny-5 w porównaniu z monastrolem. Aktywność kinezyny mierzono poprzez ocenę szybkości hydrolizy ATP, korzystając z zestawu Kinesin ATPase Endpoint Biochem Kit, przy stężeniu wynoszącym 10 μM. Wykazano, że resztkowa aktywność ATP-azy KSP była dwukrotnie niższa w przypadku ferrocenylowych analogów w porównaniu z monastrolem: dla związku **111a** wynosiła 7,2%, dla **112b** – 8,8%, a dla **115c** – 9,8%, podczas gdy dla monastrolu była to 18,7%. Stwierdzono także, że żaden z badanych związków nie hamował aktywności innych kinezyn takich jak: KIF4A, KIF23 oraz MCAK. Uzyskane wyniki sugerują, że modyfikacje monastrolu poprzez wprowadzenie ugrupowań ferrocenylowych nie zmieniają specyficzności działania jego analogów. Zwiększona efektywność inhibicji KSP przez badane związki wskazuje, że są one skuteczniejszymi inhibitorami KSP niż monastrol, zachowując przy tym selektywność wobec tego białka.

W dalszej kolejności zbadano wpływ związków ferrocenowych **111a**, **112b**, **115c**, na zdolność generowania ROS w komórkach nowotworowych. Stwierdzono, że wprowadzenie podstawnika ferrocenylowego do monastolu prowadzi do niewielkiego zwiększenia zdolności do generowania ROS w komórkach nowotworowych o ok 25% dla związków **112b** i **115c**.

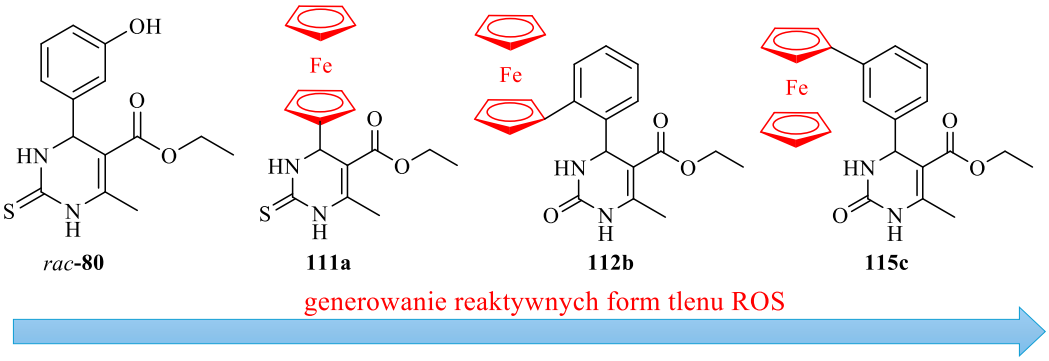

Rysunek 39. *Generowanie ROS w komórkach SW620 po 4h ekspozycji na związki (1 μM)*

Zbadano wpływ związków na cykl komórkowy w komórkach SW620 oraz SW620V. Stwierdzono, że ferrocenylowy analog monastrolu **111a** i monastrol wykazują podobny wpływ na cykl komórkowy. W porównaniu do monastrolu i **111a** analogi **112b** i **115c** prowadziły do zwiększenia liczby komórek apoptycznych (frakcja sub-G_1) i zmniejszenia liczby komórek w fazie G_0/G_1 szczególnie w komórkach SW620.

We współpracy z. prof. Christianem Hartingerem (School of Chemical Sciences, The University of Auckland, New Zealand) przeprowadzono dokowanie molekularne ferrocenylowych pochodnych monastrolu do kinezyny-5. Uzyskane wyniki potwierdziły, że położenie podstawników ferrocenylowych w koniugatach silnie wpływa na ich powinowactwo do kinezyny-5. Najskuteczniejsze wiązanie osiągnięto, gdy grupy ferrocenylowe były rozmieszczone w sposób umożliwiający interakcję związku z miejscami allosterycznymi białka. Analiza wyników dokowania wykazała również kluczowe wiązania wodorowe i hydrofobowe, odpowiadające za stabilizację kompleksu ligand-białko (Rysunek 40).

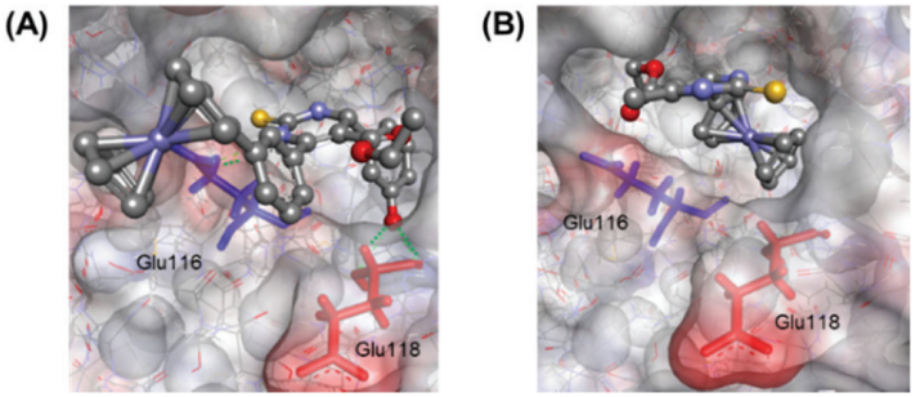

Rysunek 40. Oddziaływania związku **115c** (A) i **111a** (B) z kieszenią wiążącą KSP

Podsumowując, wprowadzenie ugrupowania ferrocenylowego do monastrolu prowadzi do związków wykazujących wyższą cytotoksyczność zarówno w stosunku do nowotworowych linii komórkowych jak i linii wykazujących oporność wielolekową. Wykazano, że wprowadzenie podstawnika ferrocenylowego zwiększa zdolność do hamowania aktywności kinezyny-5 oraz zwiększa zdolność do generowania ROS. Uzyskane wyniki sugerują, że cytotoksyczność tych związków jest związana nie tylko z hamowaniem KSP, ale także z poziomem generowania ROS, co wskazuje na dodatkowy mechanizm działania.

6.2 Ferrocenylowe analogi CPUYL064

Ze względu na znaczący wpływ grupy ferrocenylowej na właściwości cytotoksyczne monastrolu, postanowiono zbadać jej wpływ na aktywność przeciwnowotworową innego inhibitora kinezyny-5, CPUYL064.[122] Modyfikacja typu I polegała na zastąpieniu grupy fenylowej podstawnikiem metalocenowym lub podstawnikiem *o*-, *m*-, *p*-ferrocenylofenylowym z jednoczesnym zachowaniem grup metylowych w pozycji C-7 lub z ich modyfikacją. Dla porównania zsyntetyzowano również analogi estrowe. Modyfikacja typu II polegała na zastąpieniu podstawnika 4-chlorofenylowego grupy amidowej, podstawnikami *o*-, *m*-, *p*-ferrocenylofenylowymi.

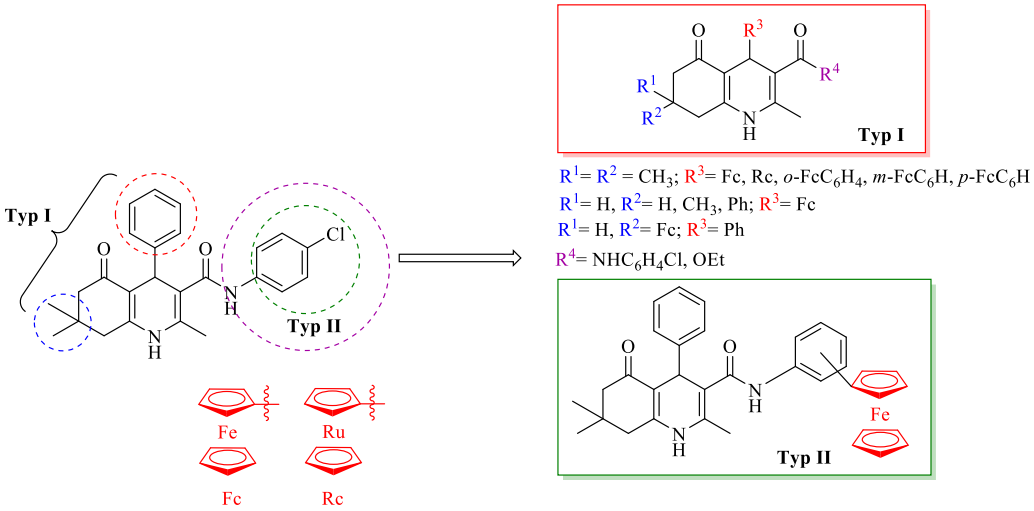

Schemat 8. *Planowane modyfikacje CPUYL064*

Powyższe związki otrzymano z odpowiednich cykloheksano-1,3-dionów **A**, aldehydów aromatycznych **B** i odpowiednich *β*-ketoamidów lub *β*-ketoestrów **C** (Rysunek 41).

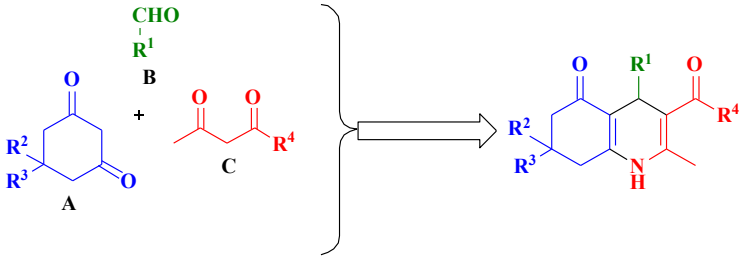

Rysunek 41. *Projekt syntezy ferrocenylowych analogów CPUYL064*

Prace rozpoczęto od zsyntetyzowania niezbędnych substratów. W reakcji arylowania ferrocenu świeżo przygotowanymi chlorkami *o*-, *m*-, *p*-nitrobenzenodiazoniowymi otrzymano odpowiednie *o*-, *m*-, *p*-ferrocenylonitrobenzeny **120a-c** z wydajnościami w zakresie 30-94%. Następnie, związki te poddano redukcji grupy nitrowej do aminowej przy użyciu mrówczanu

amonu w obecności Pd/C (10%), uzyskując *o*-, *m*-, *p*-ferrocenyloaniliny **121a-c** z praktycznie ilościową wydajnością (Schemat 9). Otrzymane *o*-, *m*-, *p*-ferrocenyloaniliny **121a-c** poddano reakcji z acetylooctanem etylu w obecności katalitycznej ilości *tert*-butanolanu potasu w toluenie. Reakcje prowadzono w temperaturze 160°C przez 20-30 minut w reaktorze mikrofalowym, otrzymując odpowiednie *β*-ketoamidy **122a-c** z wydajnościami w zakresie 19-32% (Schemat 9).

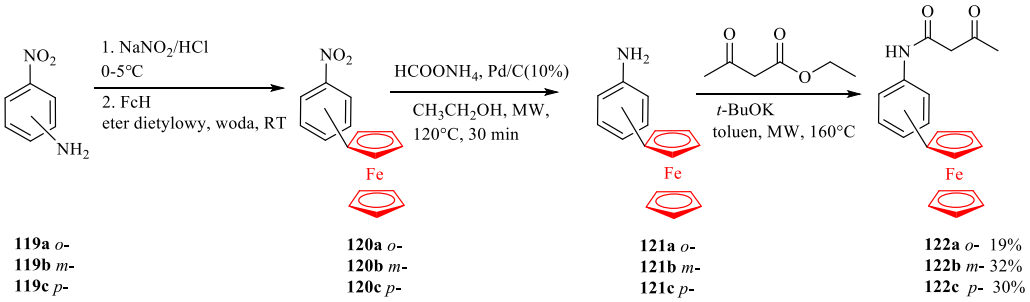

Schemat 9. *Synteza acetoacetanilidów* ***122a-c***

Związek **125e** zsyntetyzowano zgodnie ze Schematem 10. Stosując krzyżową kondensację aldolową z ferrocenokarboksyaldehydu i acetonu w środowisku zasadowym, otrzymano związek **123**.[123] Związek ten poddano reakcji ze świeżo przygotowaną solą sodową malonianu dietylu, otrzymując odpowiedni *β*-ketoester **124**.[124] Następnie przeprowadzono hydrolizę *β*-ketoestru za pomocą roztworu wodorotlenku sodu, uzyskując *β*-ketokwas. Bez wydzielania poddano go dekarboksylacji poprzez ogrzanie z nadmiarem kwasu solnego, otrzymując 5-ferrocenylocykloheksano-1,3-dion **125e** z sumaryczną wydajnością 29%.

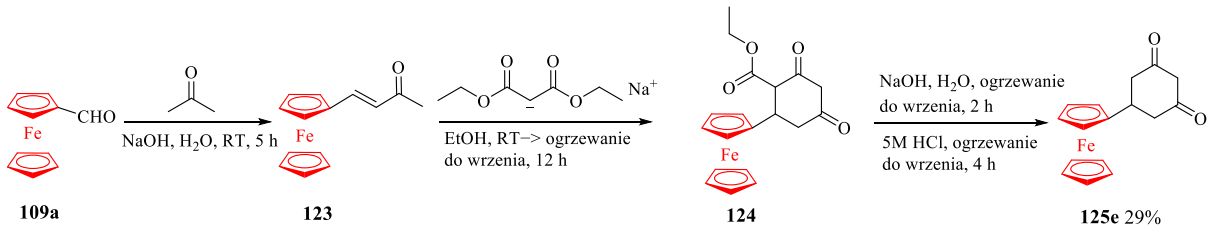

Schemat 10. *Synteza 5-ferrocenylocykloheksano-1,3-dionu* ***125e***

Struktura **125e** została potwierdzona za pomocą analizy NMR i spektrometrii mas (MS). Zaobserwowano, że w roztworze DMSO-d_6 związek **125e** istnieje wyłącznie w formie enolowej. W widmie ^{1}H NMR widoczne są dwa charakterystyczne sygnały: jeden pochodzący od grupy OH przy 11,07 ppm oraz drugi pochodzący od protonu winylowego H-2 przy 5,23 ppm (Rysunek 42). Widmo ^{13}C{^{1}H} NMR wykazało sygnały węgla karbonylowego C-1 przy 197,1 ppm i węgla C-3 przy 176,9 ppm. Stwierdzono, że w roztworze CD_2Cl_2 związek **125e** istnieje wyłącznie w formie diketonowej (Rysunek 43). W widmie ^{13}C{^{1}H} NMR

zarejestrowano sygnał grupy karbonylowej przy 203,9 ppm. Widma ^{1}H NMR potwierdziły obecność sygnałów pochodzących od podstawnika ferrocenylowego oraz protonów cykloheksanu, natomiast nie zaobserwowano sygnałów enolu. Zmiany temperatury próbki miały niewielki wpływ na widma NMR.

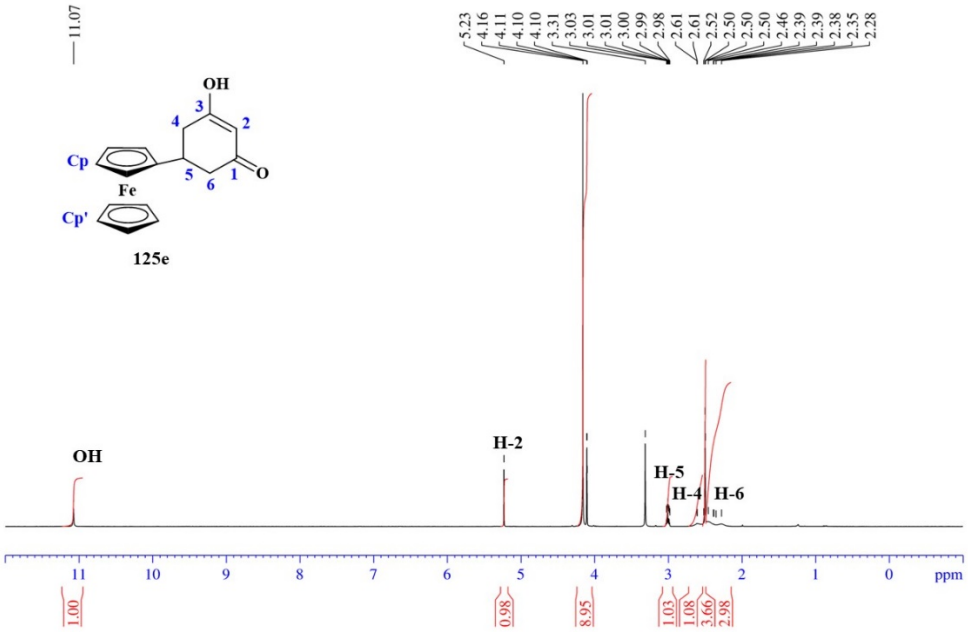

Rysunek 42. *Widmo ^{1}H NMR związku* ***125e*** *w DMSO-d_6*

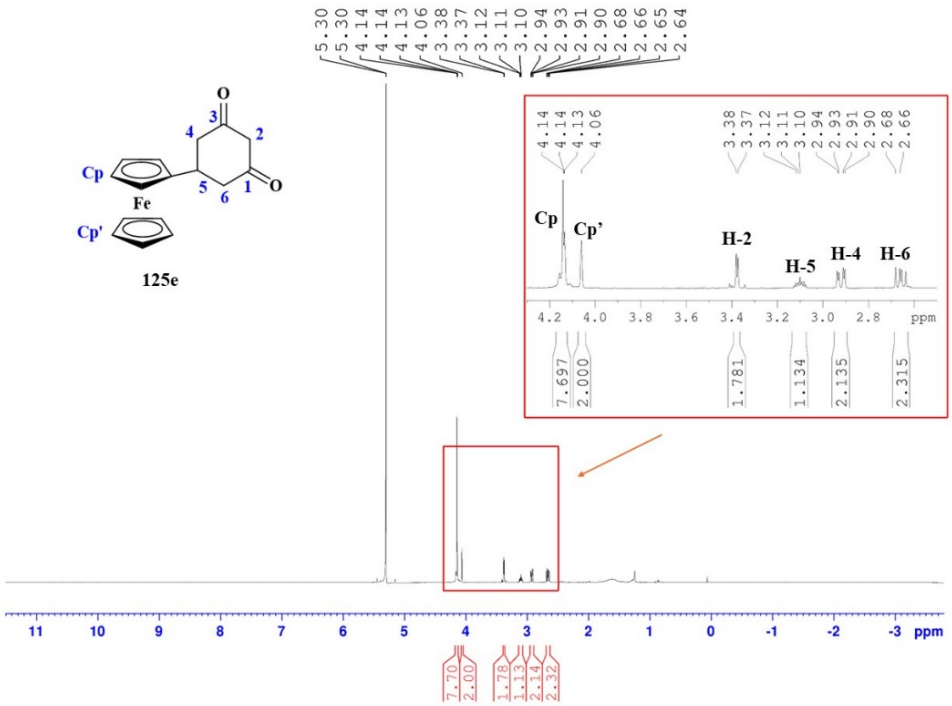

Rysunek 43. *Widmo ^{1}H NMR związku* ***125e*** *w CD_2Cl_2*

Związki typu I **94**, **129b-j** i **130a-j** zsyntetyzowano wykorzystując reaktor mikrofalowy w reakcji cykloheksano-1,3-dionów **125a-e** z odpowiednimi aldehydami **109a-c**, **126**, **127** oraz 4′-chloroacetooacetanilidem **128a** lub acetylooctanem etylu **128b** w obecności octanu amonu w 2,2,2-trifluoroetanolu w temperaturze 110°C w 10 minutowych cyklach, przy czym całkowity czas reakcji różnił się w zależności od związku (Schemat 11).

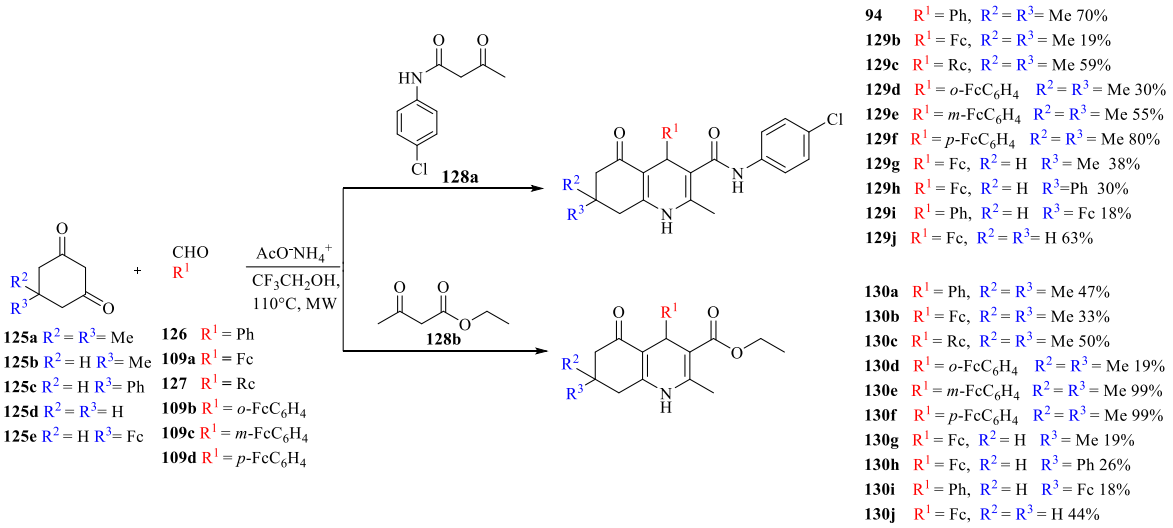

Schemat 11**. Synteza docelowych związków **94**, **129b-j**, **130a-j

Struktury związków **129b-j** i **130a-j** potwierdzono za pomocą analizy NMR. W widmach ^{1}H i $^{13}C\{^{1}H\}$ NMR amidu **129d** obecność dużego podstawnika w pozycji C-4 spowodowała pojawienie się dodatkowych sygnałów, które przypisano rotamerom (Rysunek 44). W przypadku analogu estrowego **130d** obserwowano tylko jeden zestaw sygnałów świadczący o braku rotamerów (Rysunek 45).

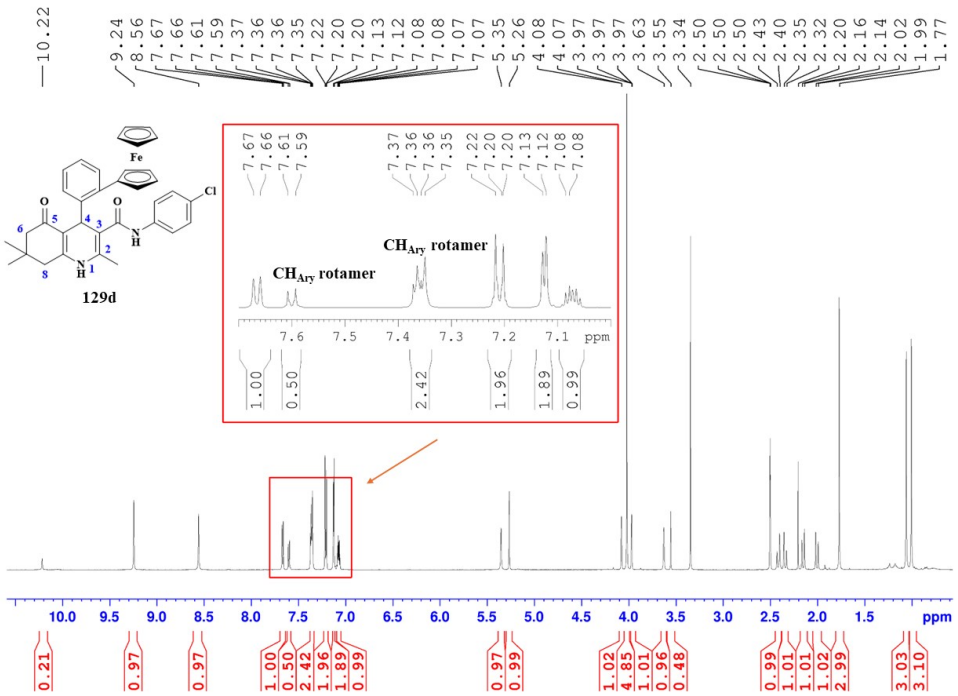

Rysunek 44. *Widmo ^{1}H NMR związku* ***129d***

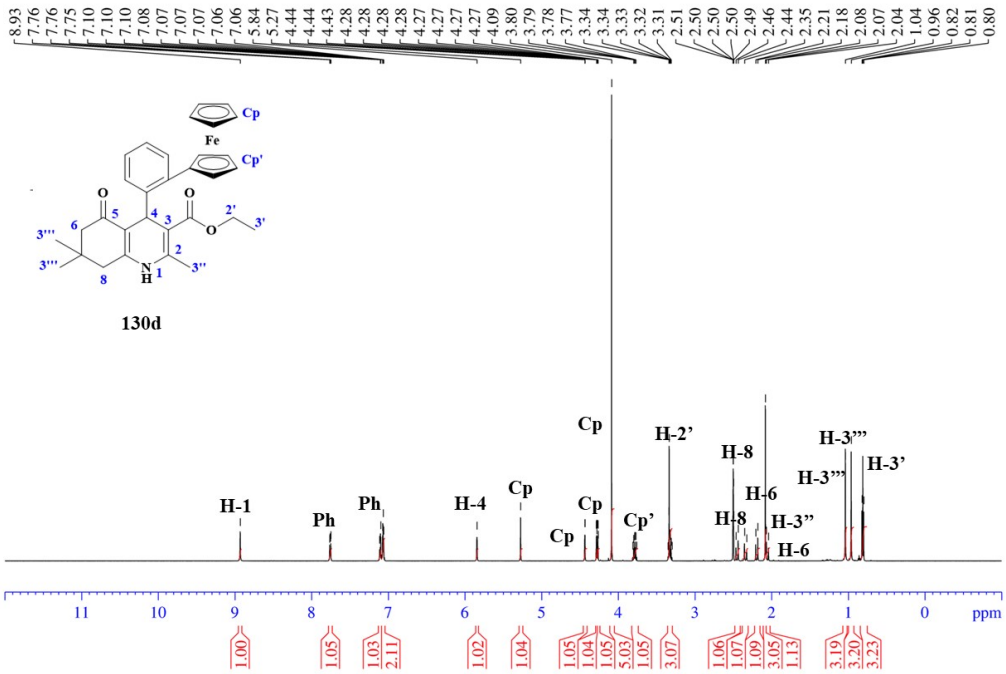

Rysunek 45. *Widmo ^{1}H NMR związku* ***130d***

W widmach ^{1}H i ^{13}C{^{1}H} NMR związków **129g-i** i **130g-i** zawierających po jednym podstawniku w pozycji C-4 i C-7 obserwowano sygnały pochodzące od mieszaniny diastereoizomerów. Przykładowo, dla głównego diastereoizomeru związku **130g** obserwowano sygnał pochodzący od protonu H-1 przy 9,10 ppm, natomiast dla drugiego diastereoizomeru sygnał pochodzący od protonu H-1 występuje przy 9,18 ppm. Obecność diastereoizomerów potwierdzono dodatkowo za pomocą HPLC (Rysunek 47).

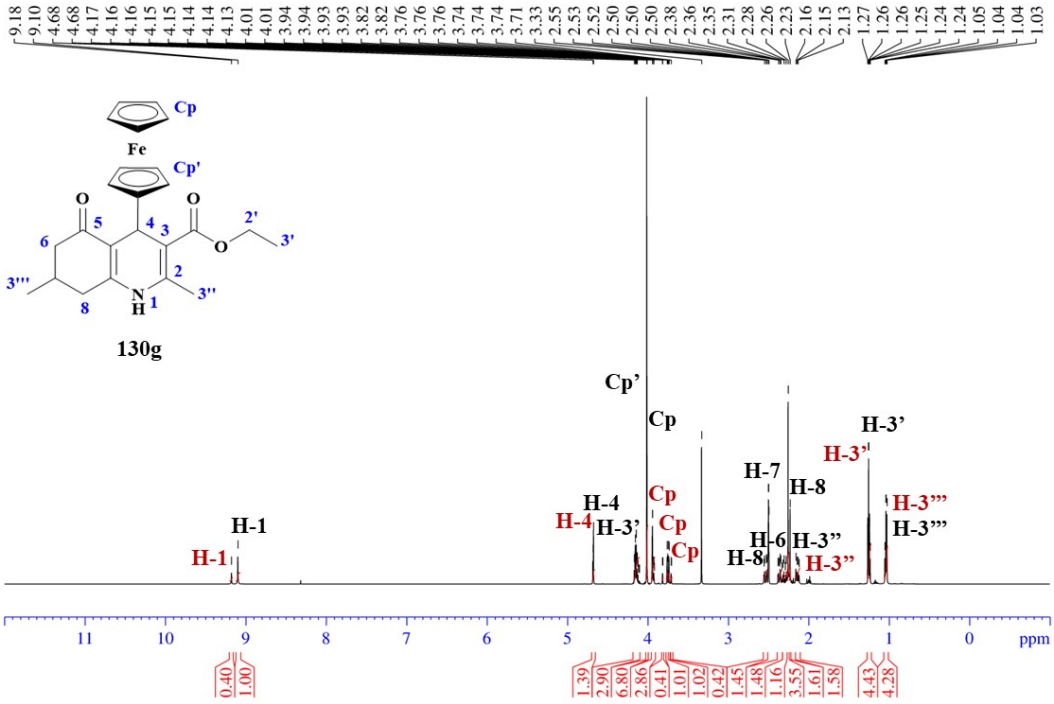

Rysunek 46. *Widmo ^{1}H NMR związku* ***130g***

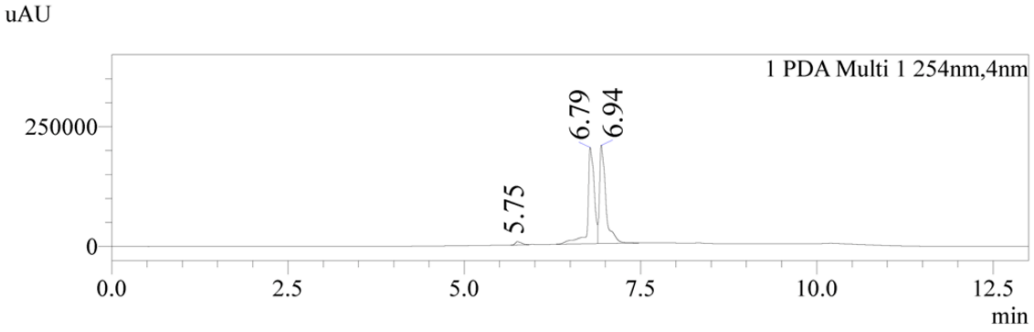

Rysunek 47. *Chromatogram HPLC związku* ***130g***

Stosując tę samą procedurę zsyntetyzowano związki typu II **131a-c** z wydajnościami w zakresie 42-60% (Schemat 12) W przypadku tych związków w widmach ^{1}H i $^{13}C\{^{1}H\}$ NMR nie zaobserwowano obecności sygnałów pochodzących od rotamerów lub diastereoizomerów. W widmach ^{1}H NMR produktów obecne były dodatkowe sygnały w zakresie charakterystycznym dla protonów aromatycznych oraz sygnały pochodzące od podstawionego i niepodstawionego liganda η^5-cyklopentadienylowego, co potwierdza strukturę otrzymanych związków.

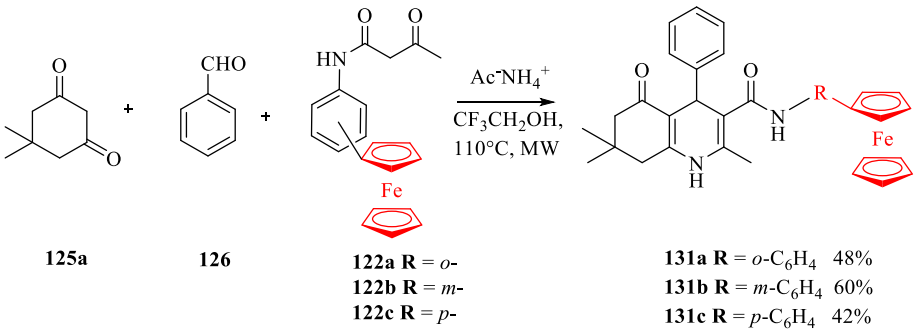

Schemat 12. *Synteza docelowych związków* ***131a-c***

Badania aktywności biologicznej zostały wykonane we współpracy z dr. Błażejem Rychlikiem i dr. Andrzejem Błaużem (Katedra Biofizyki Molekularnej Uniwersytetu Łódzkiego). Rozpoczęto od badań przeżywalności nowotworowych linii komórkowych w obecności zsyntezowanych związków przy stężeniu równym wartość IC_{50} dla związku referencyjnego **94** (Rysunek 48). Badania te wykazały, że zastąpienie grupy 4-fenylowej podstawnikiem ferrocenylowym prowadzi do związku **129b** wykazującego podobną aktywność jak **94**. Wprowadzenie podstawnika rutenocenylowego zamiast ferrocenylowego prowadzi do związku nieaktywnego (przeżywalność powyżej 91%). Stwierdzono jednak, iż wprowadzenie podstawnika *o*-ferrocenylofenylowego zamiast grupy 4-fenylowej w **94** prowadzi do związku **129f** charakteryzującego się wyższą cytotoksycznością niż związek referencyjny. Stwierdzono, że modyfikacja związku **129b** w pozycji C-7 również prowadzi do związków o wysokiej aktywności. Ponadto, zastąpienie podstawnika amidowego grupą estrową spowodowało, iż większość z otrzymanych ferrocenylowych estrowych analogów CPUYL064 wykazywała znaczną cytotoksyczność. Wprowadzenie grupy ferrocenylowej do podstawnika fenylowego grupy amidowej nie prowadziło do zwiększenia cytotoksyczności. Uzyskane wyniki pozwoliły na wybranie czterech związków amidowych oraz sześciu związków estrowych do dalszych badań. Dla wybranych związków wyznaczono wartości IC_{50} w stosunku do nowotworowych linii komórkowych, co umożliwiło wybranie najaktywniejszych związków w tym jednego estru **130f** oraz trzech amidów **129g**,**h**,**j** wykazujących najwyższy wzrost aktywności (do 19 razy) w porównaniu do **94**. Badania aktywności zsyntezowanych związków w stosunku do komórek nienowotworowych MRC-5 wykazały, że za wyjątkiem **129j** wykazują one wysoką toksyczność w stosunku do linii nienowotworowych.

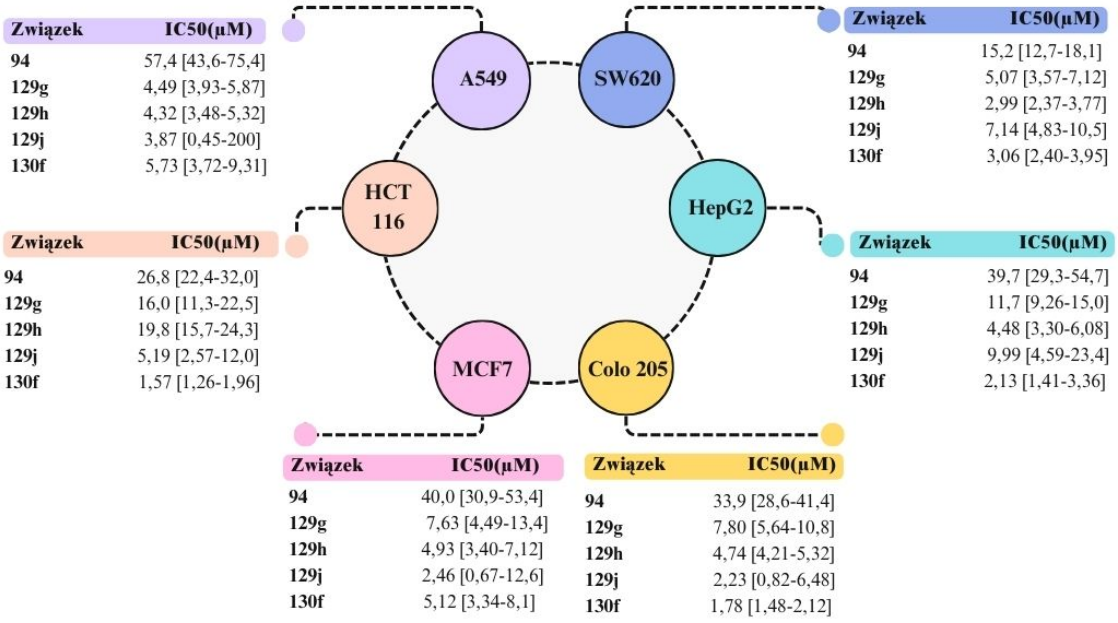

Rysunek 48. *Wartości IC_{50} dla wybranych pochodnych* ***129g,h,j*** *i* ***130f*** *przedziały ufności (95%) przedstawiono w nawiasach kwadratowych, współczynniki oporności podano stosunek wartości IC_{50} dla związku dla linii opornej względem wrażliwej. Zebrane wartości są średnią z trzech niezależnych eksperymentów*

Związek	IC_{50} (μM)				
	94	**129g**	**129h**	**129j**	**130f**
MRC-5	68,3 [43,4-166]	6,43 [5,52-7,46]	4,57 [3,76-5.10]*	20,8 [18,2-23,6]	1,99 [1,66-2,40]

Tabela 3. *Potencjał antyproliferacyjny wybranych pochodnych 1,4-dihydropirydyny w komórkach MRC-5 (czas ekspozycji 72 h). Przedziały ufności 95% (lub 90%, *) przedstawiono w nawiasach kwadratowych. Zebrane wartości są średnią z trzech niezależnych eksperymentów*

Stwierdzono, że związek **94** indukuje zależną od stężenia i czasu blokadę fazy G_2/M w komórkach HepG2, jednak w liniach komórkowych A549 i SW620 obserwowano inne efekty. W obu tych liniach proporcja komórek w fazie G_1 malała, a w fazie S wzrastała wraz z czasem ekspozycji. Blokada w fazie G_2/M była słabo widoczna w komórkach A549, ale wyraźna w SW620. W przypadku innych związków różnice były jeszcze bardziej zauważalne. W linii A549 odsetek komórek w fazie G_1 pozostawał wysoki (ponad 80%), a liczba komórek w fazach S i G_2/M malała, bez obserwacji blokady G_2/M. Natomiast komórki SW620 reagowały przewidywalnie: związki **129g** i **129j** indukowały blokadę G_2/M zależną od czasu,

podczas gdy związki **129h** i **130f** powodowały wzrost liczby komórek w fazie G_1 i spadek w fazie G_2/M, co jest typowe dla związków blokujących przejście do fazy S. Uzyskane wyniki sugerują, że badane związki są silnymi czynnikami antymitotycznymi, hamującymi proliferację komórek przez zatrzymanie ich w różnych fazach cyklu komórkowego. W przeciwieństwie do tradycyjnych środków przeciwmitotycznych, które blokują komórki w fazie G_2/M badane związki indukują także blokadę G_1/S, wskazując na odmienny mechanizm działania w porównaniu do **94**.

Zdolność do inhibicji aktywności KSP przez badane związki oceniono za pomocą testu hydrolizy adenozyno-5'-trifosforanu (ATP). Przy stężeniu 10 nM wszystkie badane związki były w stanie zahamować aktywność KSP o około 45-55%. Przy stężeniu wynoszącym 100 nM amid **129f** oraz ester **130f** wykazywały podobną zdolność do hamowania aktywności KSP jak **94**. Dalsze zwiększanie stężenia związków do 1 µM doprowadziło do całkowitego zahamowania aktywność KSP.

W dalszej kolejności przeprowadzono badania zdolności tych związków do generowania ROS przy stężeniach 1 µM i 10 µM poprzez pomiar szybkości utleniania dihydrorodaminy 123 wewnątrz komórek rakowych (Tabela 4).

Związek	**ROS [% wartości kontrolnej]**			
	A549		**SW620**	
	1 µM	10 µM	1 µM	10 µM
94	89,6±2,6	101,4±3,9	138,9±4,8	169,7±5,8
129g	95,3±2,2	100,1±1,8	106,4±6,3	122,1±7,0
129h	96,6±0,6	106,7±3,1	137,3±0,6	161,1±6,4
129j	91,9±4,1	92,4±1,3	114,4±3,7	150,4±7,0
130f	91,1±1,4	106,3±1,3	116,6±4,6	176,5±9,4

Tabela 4. *Generowanie reaktywnych form tlenu ROS w komórkach A549 i SW620 po 4h ekspozycji na związki przy stężeniu 1 µM i 10 µM. Zebrane dane są średnią z trzech niezależnych eksperymentów*

Badanie zdolności do generowania ROS przez badane związki **129h**, **129j** i **130f** przy 10 µM wykazały, że związki te indukowały generowanie ROS w komórkach SW620, podobnie jak związek **94**. Związek **129g** był mniej aktywny niż **94**, ale nadal zwiększał produkcję ROS o ponad 20% przy 10 µM. Żaden z badanych związków nie zwiększał produkcji ROS

w komórkach A549, co sugeruje specyficzną odpowiedź komórkową i może wynikać z nadregulacji szlaku NRF-2 w tych komórkach. Wyniki wskazują, że modyfikacje związku **94** nie poprawiły jego zdolności do generowania ROS w porównaniu do **94**.

Podsumowując, spośród 22 zsyntezowanych związków wstępnie wyselekcjonowano 10 o najwyższej aktywności przeciwnowotworowej, z których następnie zidentyfikowano cztery najbardziej aktywne. Stwierdzono, że aktywność biologiczna silnie zależy od struktury chemicznej: estry wykazywały wyższą cytotoksyczność niż amidy. Amid **129j**, bez podstawników w pozycji C-7, wykazał znaczącą aktywność jako inhibitor KSP jednakże nie wyższą niż związek referencyjni **94**. Inne cytotoksyczne amidy z grupami metylowymi lub fenylowymi w pozycji C-7 wykazywały mniejszą aktywność inhibitora KSP, ale zachowały wysoki potencjał antyproliferacyjny. Obecność podstawników ferrocenylowych nie zwiększyła zdolności związków do generowania reaktywnych form tlenu. Wszystkie związki były jednak zdolne do indukowania blokady w fazie G_1/S, co jest nietypowe dla tradycyjnych inhibitorów KSP.

6.3 Ferrocenylowe analogi ispinesibu

W kolejnym etapie postanowiono zsyntezować metaloorganiczne analogi i koniugaty ispinesibu, który przeszedł badania kliniczne fazy II jako silny inhibitor KSP. Zaplanowano trzy typy modyfikacji ispinesibu i jego (*S*)-enancjomeru:

- Modyfikacja typu I polegała na usunięciu grupy *p*-toluoilowej oraz 3-aminopropylowej i zastąpieniu ich podstawnikami: benzylowym, *o*-, *m*- i *p*-ferrocenylobenzylowym, ferrocenylometylowym oraz adamantylo-1-metylowym.

- Modyfikacja typu II polegała na zastąpieniu podstawnika 3-aminopropylowego tymi samymi podstawnikami co w modyfikacji typu I.

- Modyfikacja typu III polegała na wprowadzeniu wymienionych podstawników do łańcucha 3-aminopropylowego w ispinesibie.

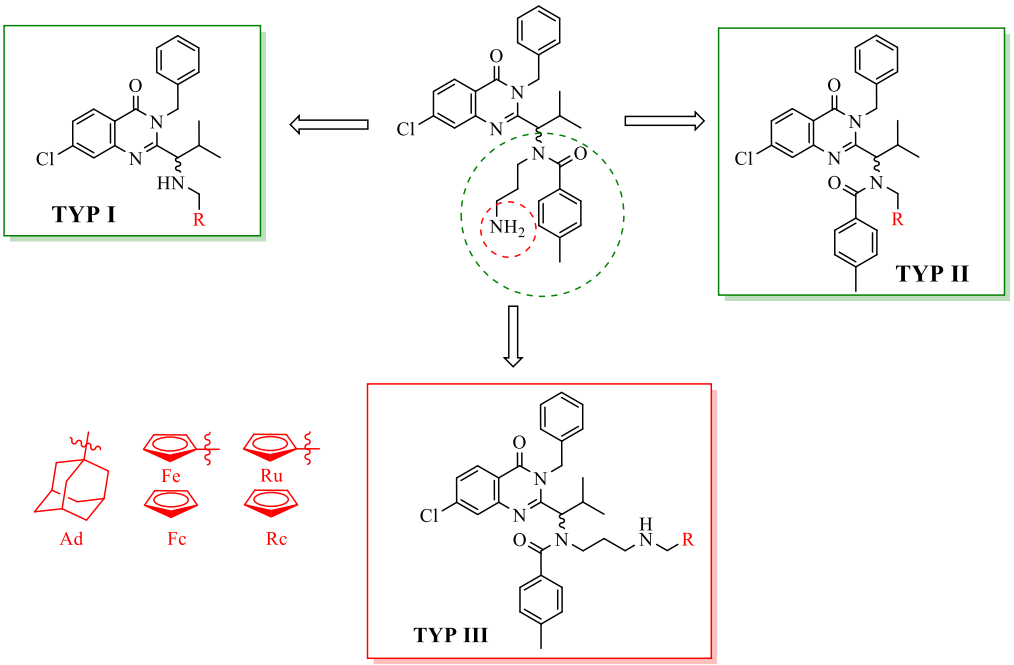

Schemat 13. *Planowane modyfikacje ispinesibu*

Prace rozpoczęto od zsyntetyzowania niezbędnych substratów. Enancjomerycznie czystą aminę (*R*)-**139** i (*S*)-**139** zsyntetyzowano według procedury opisanej w literaturze (Schemat 14).[111] Stwierdzono, że synteza związku **135** nie przebiegała całkowicie, w związku z czym zmodyfikowano procedurę literaturową. Wydłużenie czasu reakcji z 8 godzin do 17 godzin przy jednoczesnym podniesieniu temperatury ze 160°C do 190°C umożliwiło otrzymanie związku **135** z wydajnością 85%. W dalszej kolejności związek **135** przekształcono w ispinesib (*R*)-**83** i jego (*S*)-enancjomer (*S*)-**83** zgodnie z procedurą literaturową.[111]

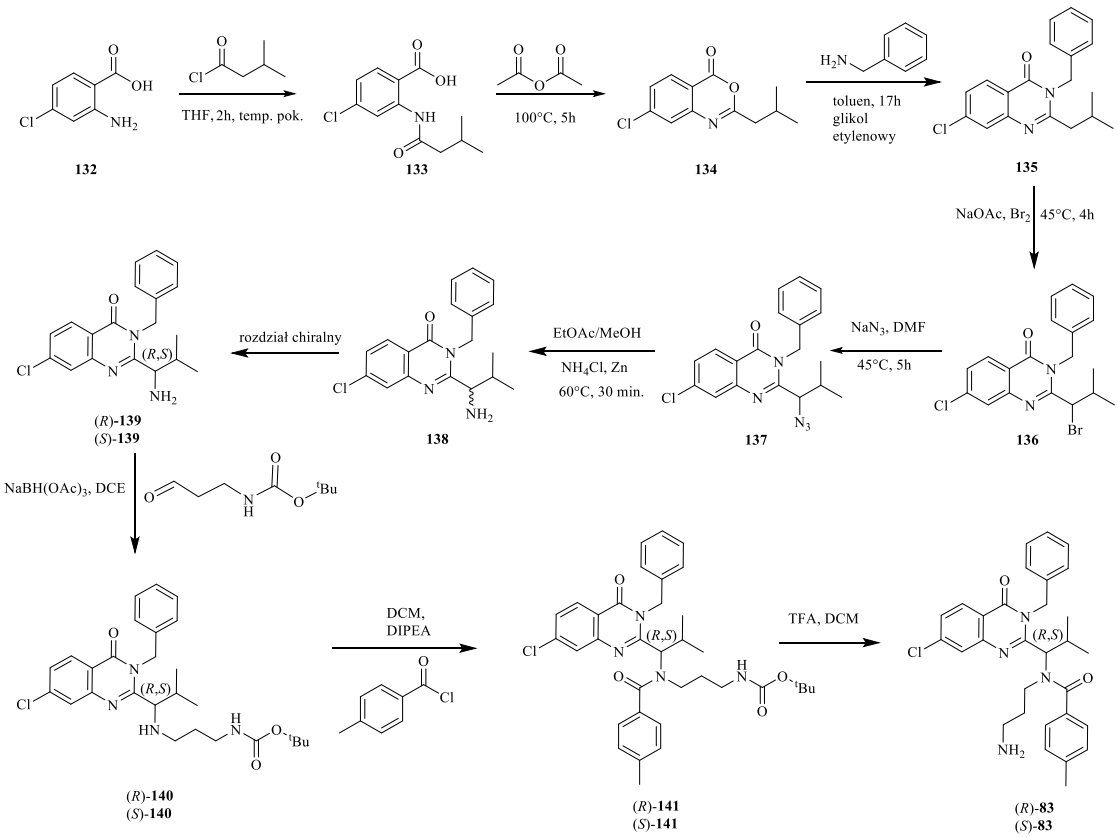

Schemat 14. *Synteza ispinesibu (R)-**83** i jego enancjomeru (S)-**83***

Niezbędny 1-adamantanokarboksyaldehyd **143** zsyntetyzowano w reakcji utleniania 1-adamantanometanolu **142** za pomocą chlorochromianu pirydyny (PCC) w dichlorometanie z wydajnością 98% (Schemat 15). W widmie ^{1}H NMR związku **143** zaobserwowano singlet pochodzący od grupy formylowej przy δ 9,29 ppm.

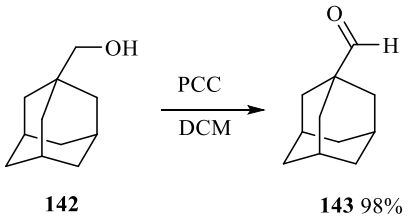

Schemat 15*. Synteza 1-adamantanokarboksyaldehydu **143***

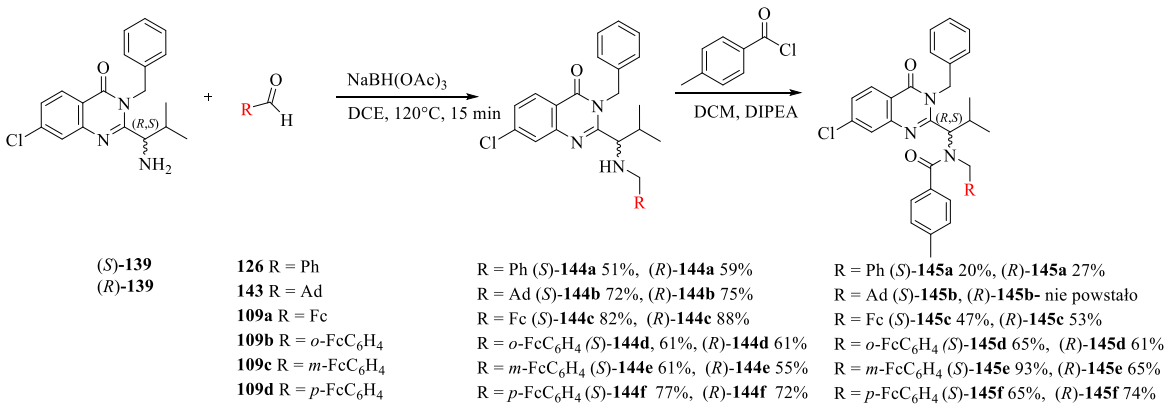

Schemat 16. *Synteza ferrocenylowych analogów ispinesibu typu I i II*

Związki typu I otrzymano w reakcji aminowania redukcyjnego amin (*R*)-**139** i (*S*)-**139**. W pierwszym etapie przeprowadzono reakcje amin (*S*)-**139** i (*R*)-**139** z odpowiednimi aldehydami **72,73a-c**, **92a, 108** w 1,2-dichloroetanie w reaktorze mikrofalowym w temperaturze 120°C przez 15 min w celu wygenerowania odpowiednich imin. Następnie dodano triacetoksyborowodorek sodu i kontynuowano reakcje w reaktorze mikrofalowym przez kolejne 15 min w temperaturze 120°C, otrzymując analogi **142a-f** z wydajnościami w zakresie 51-88%. Analiza HPLC z wykorzystaniem chiralnej kolumny analitycznej Lux Cellulose-2 w układzie faz odwróconych wykazała, że otrzymano mieszaninę enancjomerów **142a-f.** Świadczy to o częściowej racemizacji, która mogła być spowodowana tautomerią iminowo-enaminową. W związku z powyższym postanowiono przeprowadzić reakcję aminowania redukcyjnego amin (*S*)-**139** i (*R*)-**139** w temperaturze pokojowej. Stwierdzono, że w tych warunkach reakcji, racemizacja zachodzi w niewielkim stopniu co potwierdzono analizą HPLC z wykorzystaniem chiralnej kolumny analitycznej Lux Cellulose-2 (Rysunek 49).

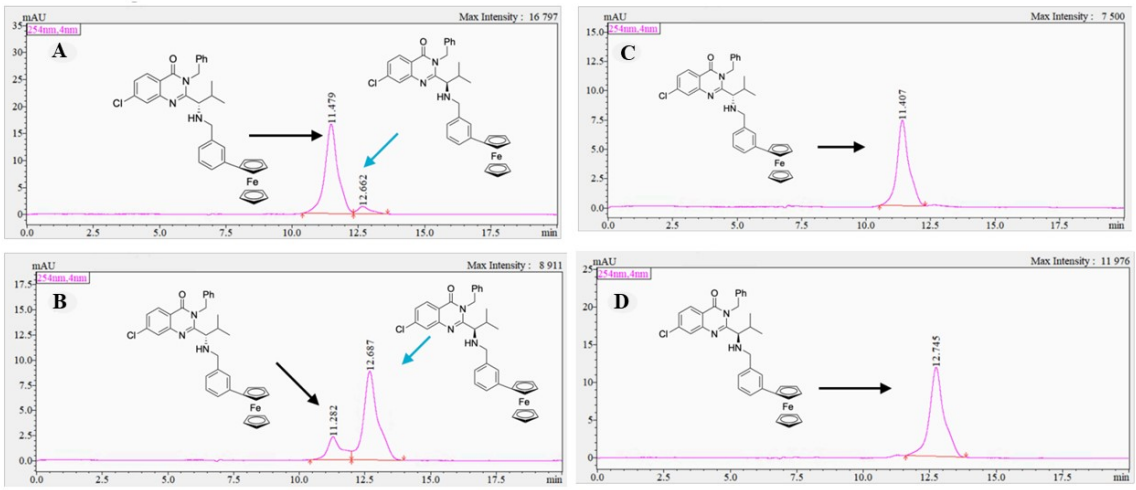

Rysunek 49. *Analiza HPLC z wykorzystaniem chiralnej kolumny Lux Cellulose-2. Reakcja prowadzona w warunkach MW, 120°C, 15 minut* ***A*** *(dla enancjomeru S) i* ***B*** *(dla enancjomeru R); Reakcja prowadzona w temperaturze pokojowej przez 24h* ***C*** *(dla enancjomeru S) i* ***D*** *(dla enancjomeru R)*

W kolejnym etapie otrzymane (*S*)- i (*R*)-**144a-f** poddano reakcji *N*-acylowania chlorkiem *p*-toluoilu w dichlorometanie w obecności DIPEA, uzyskując analogi typu II (*S*)- i (*R*)-**145a-f** z wydajnościami w zakresie 20-99% (Schemat 16). W widmach ^{1}H NMR (*S*)- i (*R*)-**145a-f** obserwowano sygnały w zakresie charakterystycznym dla protonów aromatycznych przy 7,31-7,21 ppm pochodzących od grupy *p*-toluoilowej, sygnał pochodzący od grupy metylowej grupy touloilowej przy 2,28 ppm oraz sygnały pochodzące od dodatkowych protonów metylenowych H-4’ przy 4,74 ppm i 4,0 ppm, jednocześnie nie obserwowano singletu pochodzącego od NH (Rysunek 51). Dodatkowo w widmach ^{13}C{^{1}H} NMR obserwowano dodatkowy sygnał pochodzący od *p*-toluoilowego węgla karbonylowego.

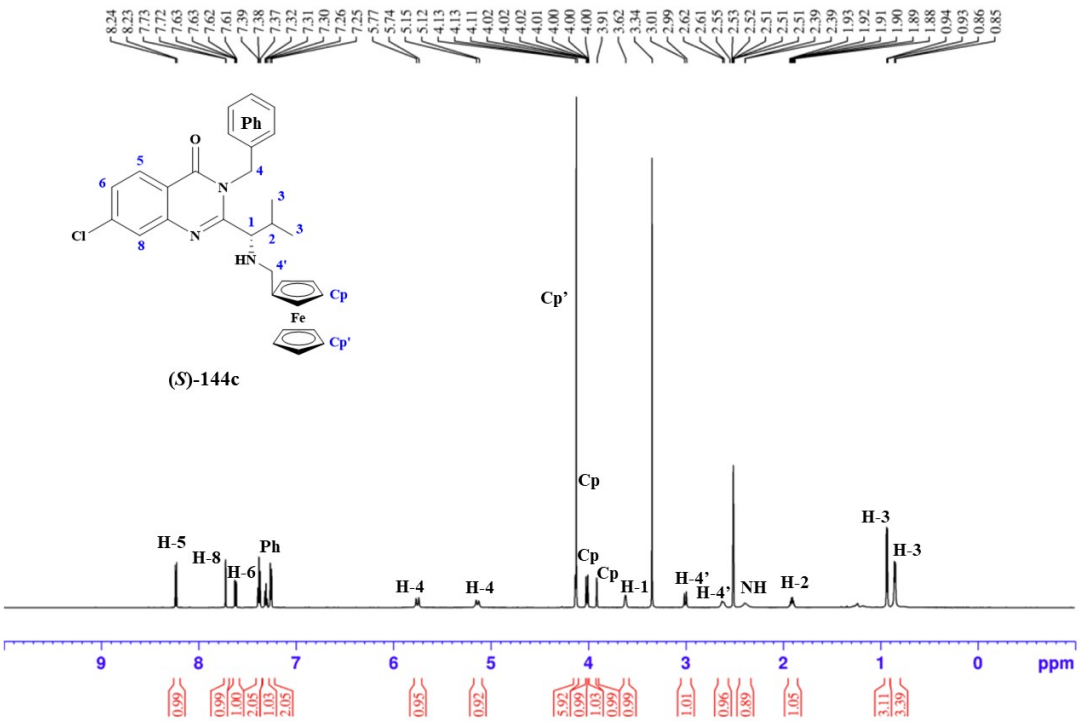

Rysunek 50. *Widmo ^{1}H NMR związku (S)-**144c***

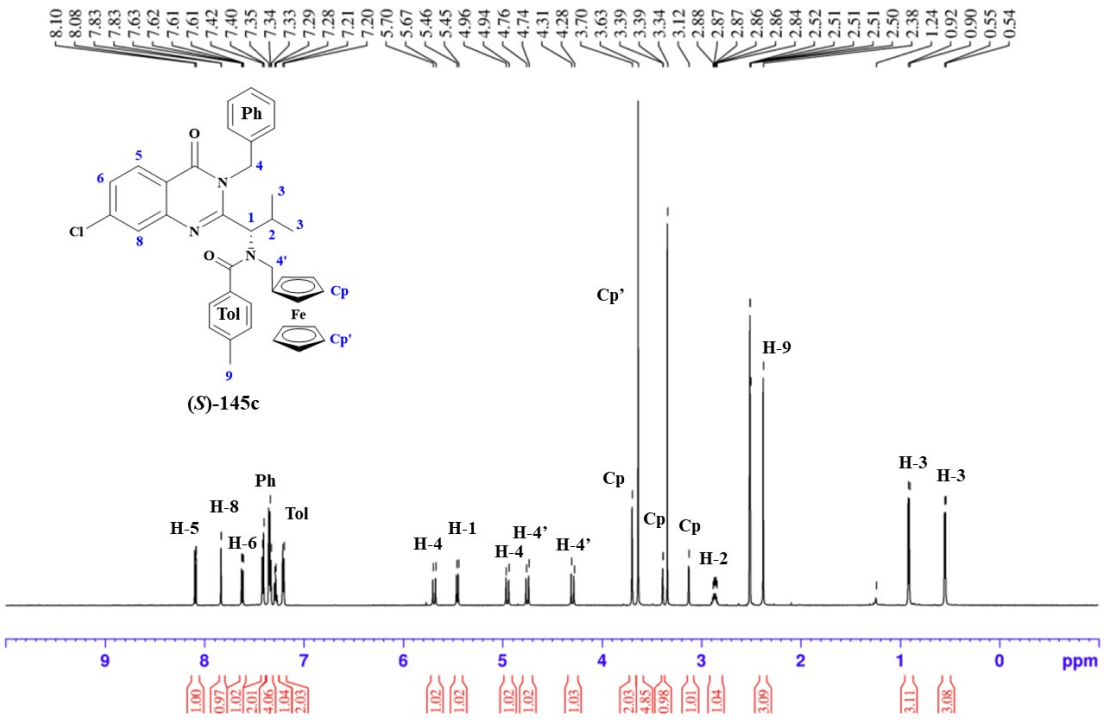

Rysunek 51. *Widmo ^{1}H NMR związku (S)-**145c***

Związki typu III zsyntetyzowano w dwóch etapach w reakcji aminowania redukcyjnego enancjomerycznie czystego ispinesibu (*R*)-**83** i jego (*S*)-enancjomeru (*S*)-**83**. W pierwszym etapie (*R*)-**83** i (*S*)-**83** ogrzewano z odpowiednimi aldehydami **126**, **109a-d**, **143** w 1,2-

dichloroetanie w 120 °C przez 15 min w reaktorze mikrofalowym, a następnie po dodaniu triacetoksyborowodorku sodu kontynuowano ogrzewanie przez kolejne 15 min, uzyskując związki (*S*)- i (*R*)-**146a-f** z wydajnościami w zakresie 23-74% (Schemat 17).

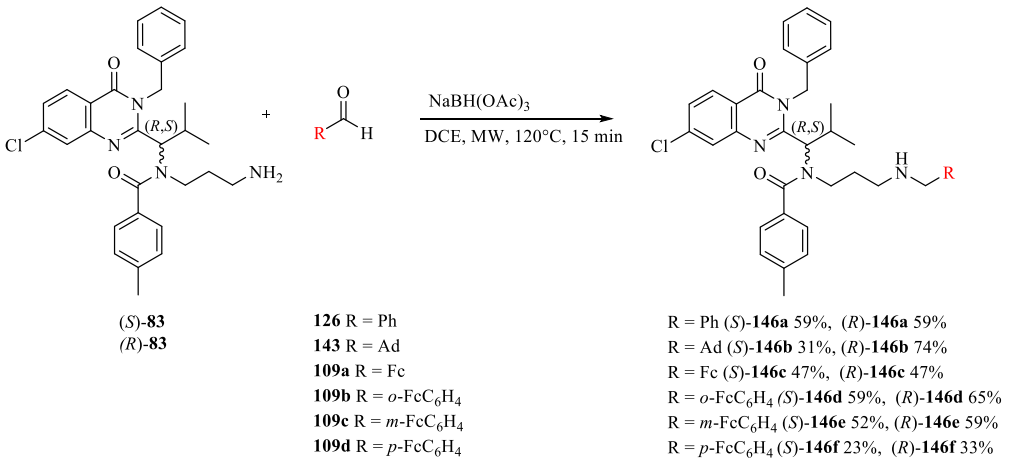

Schemat 17. *Synteza ferrocenylowych analogów ispinesibu typu III*

W widmach ^{1}H NMR związków (*S*)- i (*R*)-**146a-f** obecne były sygnały protonów metylenów pochodzące od dodatkowych grup typu benzylowego H-4’ przy 2,88-2,85 ppm. Dodatkowo w widmach związków ferrocenylowych obecne były sygnały pochodzące od podstawionego i niepodstawionego liganda η^5-cyklopentadienylowego przy 4,02-3,88 ppm, co potwierdziło powstanie oczekiwanych produktów (Rysunek 52).

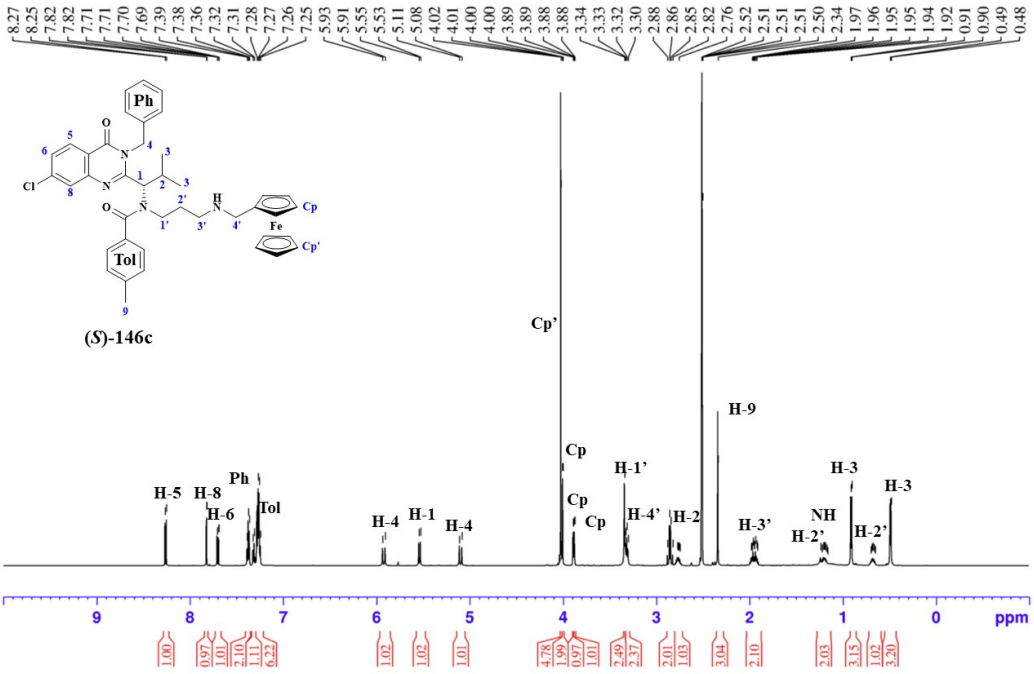

Rysunek 52. *Widmo ^{1}H NMR związku (S)-**146c***

Badania aktywności biologicznej zsyntezowanych związków zostały wykonane we współpracy z dr. Błażejem Rychlikiem i dr. Andrzejem Błaużem (Katedra Biofizyki Molekularnej Uniwersytetu Łódzkiego). Rozpoczęto od badań przeżywalności nowotworowych linii komórkowych w obecności zsyntezowanych związków przy stężeniu równym wartość IC_{50} dla ispinesibu (*R*)-**83** i jego (*S*)-enancjomeru. Spośród związków typu I jedynie związek (*R*)-**144e** zawierający podstawnik *m*-ferrocenylobenzylowy wykazywał znaczną aktywność w stosunku do linii HCT116, MCF7 i SW620. Wprowadzenie podstawnika *p*-toluilowego (związki typu II) prowadziło do zmniejszenia aktywności. W przypadku związków typu III przyłączenie podstawników do terminalnej grupy aminowej ispinesibu prowadziło do zwiększenia cytotoksyczności. Spośród (*S*)-enancjomerów wyższą cytotoksyczność niż związku referencyjnego obserwowano jedynie w przypadku pochodnych typu III zawierających grupę benzylową, ferrocenylometylową lub adamantylo-1-metylową.

Na podstawie uzyskanych wyników wybrano 11 związków, dla których wyznaczono wartości IC_{50} w stosunku do nowotworowych linii komórkowych Colo 205, HCT116, SW620 oraz linii MDR, SW620E wykazującej nadekspresję białka ABCB1 (Rysunek 53). Wykazano, że wszystkie związki (*R*)-**146a-f** wykazują wyższą cytotoksyczność niż ispinesib w stosunku do linii wrażliwych, osiągając wartości IC_{50} w zakresie 43-76 nM (Colo 205), 54-240 nM (HCT116) i 23-136 nM (SW620) w porównaniu do wartości IC_{50} wynoszących odpowiednio 121, 848 i 185 nM dla ispinesibu.

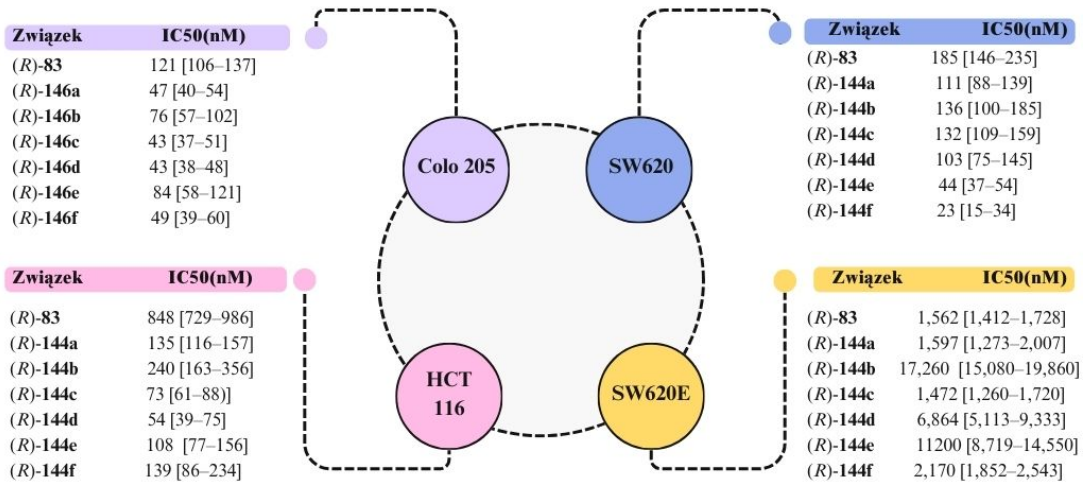

Rysunek 53. *Wartości IC_{50} dla wybranych pochodnych (R)-**144a-f**, w liniach komórkowych ludzkiego raka jelita grubego, przedziały ufności (95%) przedstawiono w nawiasach kwadratowych. Zebrane wartości są średnią z trzech niezależnych eksperymentów*

Badania wpływu zsyntezowanych związków na cykl komórkowy w linii SW620, wykazały, że pochodne ispinesibu typu III, prowadziły do znacznego zmniejszenia liczby komórek w fazie

G_1, przy jednoczesnym zwiększeniu liczby komórek w fazie G_2/M w porównaniu do ispinesibu (Tabela 5). Uzyskane wyniki korelują z aktywnością cytotoksyczną, zaś najaktywniejsze związki indukowały zatrzymanie cyklu w fazie G_2/M.

Związek		**SW620**		
		G_1	S	G_2/M
kontrola	24h	63,4±1,5	18,6±2,623	16,9 ± 0,9
	48h	61,2 ± 0,8	18,1±1,4	18,2 ±1,8
DMSO	24h	63,2±1,6	19,1±3,5	15,9 ±1,0
	48h	63,3±1,2	17,2±2,0	17,1±1,2
***(R)*-83**	24h	43,6±2,5	19,8±0,5	34,1±2,1
	48h	27,8±2,0	32,8±2,3	38,3±1,1
(*R*)-144a	24h	41,7±1,7	25,4±0,3	31,1±0,9
	48h	32,5±2,7	28,3 ±4,1	37,4±1,6
(*R*)-144b	24h	30,7 ±1,0	27,3 ±3,7	39,9±3,3
	48h	16,7±1,4	25,8 ±2,7	56,1 ±1,3
(*R*)-144c	24h	26,1 ±1,9	30,9 ± 2,5	41,1±1,8
	48h	16,7 ±1,8	25,2 ± 3,2	55,6 ± 2,4
(*R*)-144d	24h	42,5 ± 2,2	26,9 ± 3,7	29,5 ± 1,0
	48h	29,7±1,7	31,2 ± 1,8	38,6 ± 1,7
(*R*)-144e	24h	33,1 ±0,9	24,0± 1,8	41,2 ± 16
	48h	19,8 ±1,8	24,7± 3,1	54,3 ± 0,6
(*R*)-144f	24h	30,9±1,5	28,8 ± 2,0	38,6 ± 2,5
	48h	19,3±2,8	26,2 ± 3,1	52,9 ± 2,0

Tabela 5. *Rozkład cyklu komórkowego dla komórek SW620 w obecności związków typu III przez 24h i 48 h (enancjomery (R)- przy stężeniach równych wartościom IC_{75} dla odpowiednich związków). Zebrane wartości są średnią z trzech niezależnych eksperymentów*

Wpływ badanych związków na zdolność do hamowania aktywności KSP zbadano przy stężeniu związków 10 µM. Spośród badanych związków jedynie pochodne typu III wykazywały zdolność do hamowania aktywności KSP, przy czym jedynie związki zawierające podstawnik benzylowy, ferrocenylometylowy lub adamantylo-1-metylowy zachowywały zdolność do hamowania KSP podobnie jak ispinesib, podczas gdy związki zawierające podstawnik *o*-, *m*- lub *p*-ferrocenylobenzylowy hamowały aktywność KSP w niewielkim stopniu (zmniejszenie

aktywności do poziomu ok 80%). Dla najaktywniejszych inhibitorów KSP wyznaczono wartości IC_{50} (Tabela 6). W porównaniu do ispinesibu, otrzymane pochodne wykazywały 2-4 krotnie mniejszą zdolność do hamowania aktywności KSP. Żaden z badanych związków nie hamował aktywności innych niż KSP białek motorycznych w stężeniu 10 μM.

Związek	**IC_{50} (μM)**			
	(*R*)-83	**(*R*)-144a**	**(*R*)-144b**	**(*R*)-144c**
KSP	0,44 [0,33–0,60]	1,53 [0,91–2,65]	1,84 [1,22–2,95]	0,85 [0,54–1,37]

Tabela 6. *Wartości IC_{50} dla najbardziej aktywnych inhibitorów KSP. Przedziały ufności 95% przedstawiono w nawiasach kwadratowych. Zebrane dane są średnią z trzech niezależnych eksperymentów*

Następnie zbadano zdolności do generowania ROS przez zsyntezowane związki przy stężeniu 1 μM. Wykazano, że wprowadzenie podstawnika ferrocenylowego lub adamantylowego, ale nie benzylowego, zwiększa zdolność do generowania ROS o 15-29% w porównaniu do ispinesibu. Uzyskane wyniki sugerują, że wprowadzenie podstawnika ferrocenylowego może indukować stres oksydacyjny w komórce nowotworowej.

We współpracy z. prof. Christianem Hartingerem (School of Chemical Sciences, The University of Auckland, Nowa Zelandia) dokowanie molekularne zsyntezowanych związków do kinezyny-5 wykazało ich wiązanie podobne do ispinesibu. Chociaż niektóre związki osiągnęły wysokie wyniki dokowania, ich zdolność do hamowania aktywności KSP nie zawsze korelowała z wynikami dokowania, co sugeruje wpływ innych mechanizmów, takich jak indukcja stresu oksydacyjnego, na ich działanie przeciwnowotworowe.

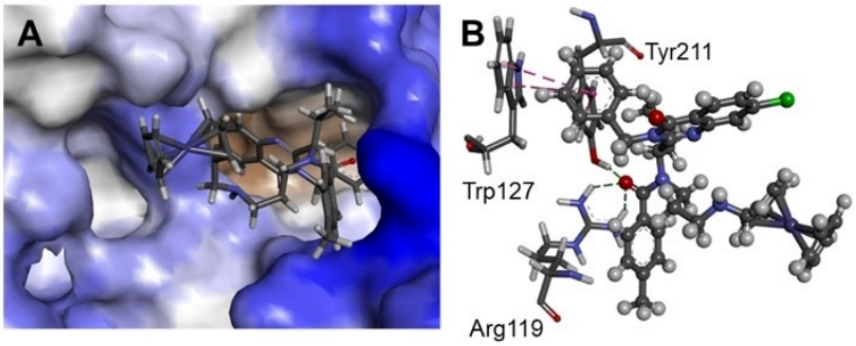

Rysunek 54*. Oddziaływania związku (R)-**146c** z kieszenią wiążącą KSP*

7. Podsumowanie

W ramach niniejszej pracy doktorskiej:

Ferrocenylowe analogi monastrolu: Zsyntezowano dwie serie związków ferrocenylowych będących analogów monastrolu oraz jego tlenowego odpowiednika. Badania aktywności biologicznej potwierdziły, że przeprowadzone modyfikacje chemiczne prowadzą do związków o zwiększonej aktywności przeciwnowotworowej. Analizowane związki zachowały zdolność hamowania aktywności KSP, przy czym najaktywniejsze z nich to pochodne **111a**, **112b** i **115c**. Wykazano, że ich zwiększona cytotoksyczność może wynikać z generowania reaktywnych form tlenu, co sugeruje potencjalny dodatkowy mechanizm działania przeciwnowotworowego.

Ferrocenylowe analogi CPUYL064: Zsyntezowano dwie serie, amidową oraz estrową, ferrocenylowych analogów CPUYL064. Wykazano, że wprowadzenie podstawnika ferrocenylowego zwiększa aktywność przeciwnowotworową w porównaniu do CPUYL064. Pochodne estrowe wykazały się wyższą cytotoksycznością niż odpowiednie amidy. Jeden z analogów amidowych wykazywał wysoką aktywność jako inhibitor KSP, podczas gdy inne cytotoksyczne amidy cechowały się mniejszą zdolność do hamowania tej aktywności. Obecność podstawników ferrocenylowych nie zwiększała zdolności związków do generowania ROS, jednakże badane związki były zdolne do indukowania blokady w fazie G1/S cyklu komórkowego. Z wyjątkiem jednego związku **129j**, wprowadzone modyfikacje zwiększały cytotoksyczność koniugatów względem nienowotworowych linii komórkowych MRC-5.

Ferrocenylowe analogi ispinesibu: Zsyntetyzowano serię metaloorganicznych (ferrocenylowych) i organicznych analogów oraz koniugatów ispinesibu. Przeprowadzone modyfikacje skutkują zwiększoną cytotoksycznością w porównaniu do ispinesibu. Wprowadzone modyfikacje zmniejszały zdolność do hamowania aktywności kinazy KSP, ale zwiększały zdolność do generowania ROS w komórkach, co sugeruje potencjalny dodatkowy mechanizm działania przeciwnowotworowego.

8. Literatura

1. https://ourworldindata.org/grapher/leading-cause-of-death (data dostępu: 24 września 2024, godzina 9.00)
2. Sung, H.; Ferlay, J.; Siegel, R. L.; Laversanne, M.; Soerjomataram, I.; Jemal, A.; Bray, F., Global Cancer Statistics 2020: GLOBOCAN Estimates of Incidence and Mortality Worldwide for 36 Cancers in 185 Countries. *CA. Cancer J. Clin.* **2021,** *71* (3), 209-249.
3. Dickens, E.; Ahmed, S., Principles of cancer treatment by chemotherapy. *Surgery (Oxf)* **2018,** *36* (3), 134-138.
4. Ralhan, R.; Kaur, J., Alkylating agents and cancer therapy. *Expert Opin. Ther. Pat.* **2007,** *17* (9), 1061-1075.
5. Bardos, T. J., Antimetabolites: molecular design and mode of action. *Med. Chem.* **2005**, 63-98.
6. Sioud, M.; Boudabous, A.; Cekaite, L., Transcriptional responses of Bacillus subtillis and thuringiensis to antibiotics and anti-tumour drugs. *Int. J. Mol. Med.* **2009,** *23* (1), 33-39.
7. Miller, K. G.; Liu, L. F.; Englund, P. T., A homogeneous type II DNA topoisomerase from HeLa cell nuclei. *J. Biol. Chem.* **1981,** *256* (17), 9334-9339.
8. Marzo, I.; Naval, J., Antimitotic drugs in cancer chemotherapy: promises and pitfalls. *Biochem. Pharmacol.* **2013,** *86* (6), 703-710.
9. Kumar, S.; Ahmad, M. K.; Waseem, M.; Pandey, A. K., Drug targets for cancer treatment: an overview. *Med. Chem.* **2015,** *5* (3), 115-123.
10. Kastan, M. B.; Bartek, J., Cell-cycle checkpoints and cancer. *Nature* **2004,** *432* (7015), 316-323.
11. Rieder, C. L.; Maiato, H., Stuck in division or passing through: what happens when cells cannot satisfy the spindle assembly checkpoint. *Dev. Cell* **2004,** *7* (5), 637-651.
12. Devi Tangutur, A.; Kumar, D.; Vamsi Krishna, K.; Kantevari, S., Microtubule targeting agents as cancer chemotherapeutics: an overview of molecular hybrids as stabilizing and destabilizing agents. *Curr. Top. Med. Chem.* **2017,** *17* (22), 2523-2537.
13. Wang, L. G.; Liu, X. M.; Kreis, W.; Budman, D. R., The effect of antimicrotubule agents on signal transduction pathways of apoptosis: a review. *Cancer Chemother. Pharmacol.* **1999,** *44*, 355-361.
14. Checchi, P. M.; Nettles, J. H.; Zhou, J.; Snyder, J. P.; Joshi, H. C., Microtubule-interacting drugs for cancer treatment. *Trends Pharmacol. Sci.* **2003,** *24* (7), 361-365.
15. Steinmetz, M. O.; Prota, A. E., Microtubule-targeting agents: strategies to hijack the cytoskeleton. *Trends Cell Biol.* **2018,** *28* (10), 776-792.
16. https://creativecommons.org/licenses/by/4.0/
17. Stanton, R. A.; Gernert, K. M.; Nettles, J. H.; Aneja, R., Drugs that target dynamic microtubules: a new molecular perspective. *Med. Res. Rev.* **2011,** *31* (3), 443-81.
18. Penna, L. S.; Henriques, J. A. P.; Bonatto, D., Anti-mitotic agents: Are they emerging molecules for cancer treatment? *Pharmacol Ther.* **2017,** *173*, 67-82.
19. Čermák, V.; Dostál, V.; Jelínek, M.; Libusová, L.; Kovář, J.; Rösel, D.; Brábek, J., Microtubule-targeting agents and their impact on cancer treatment. *Eur. J. Cell Biol.* **2020,** *99* (4), 151075.
20. Martino, E.; Casamassima, G.; Castiglione, S.; Cellupica, E.; Pantalone, S.; Papagni, F.; Rui, M.; Siciliano, A. M.; Collina, S., Vinca alkaloids and analogues as anti-cancer agents: Looking back, peering ahead. *Bioorg. Med. Chem. Lett.* **2018,** *28* (17), 2816-2826.
21. Gridelli, C.; Rossi, A.; Maione, P.; Rossi, E.; Castaldo, V.; Sacco, P. C.; Colantuoni, G., Vascular disrupting agents: a novel mechanism of action in the battle against non-small cell lung cancer. *Oncol.* **2009,** *14* (6), 612-620.
22. Choy, H., Taxanes in combined modality therapy for solid tumors. *Crit Rev Oncol Hematol* **2001,** *37* (3), 237-247.
23. Engels, F.; Sparreboom, A.; Mathot, R.; Verweij, J., Potential for improvement of docetaxel-based chemotherapy: a pharmacological review. *Br. J. Cancer* **2005,** *93* (2), 173-177.

24. Paller, C. J.; Antonarakis, E. S., Cabazitaxel: a novel second-line treatment for metastatic castration-resistant prostate cancer. *Drug Des. Devel. Ther.* **2011**, 117-124.
25. Larkin, J.; Kaye, S., Potential clinical applications of epothilones: a review of phase II studies. *Ann. Oncol.* **2007,** *18*, v28-v34.
26. Rugo, H. S.; Barry, W. T.; Moreno-Aspitia, A.; Lyss, A. P.; Cirrincione, C.; Leung, E.; Mayer, E. L.; Naughton, M.; Toppmeyer, D.; Carey, L. A., Randomized phase III trial of paclitaxel once per week compared with nanoparticle albumin-bound nab-paclitaxel once per week or ixabepilone with bevacizumab as first-line chemotherapy for locally recurrent or metastatic breast cancer: CALGB 40502/NCCTG N063H (Alliance). *J. Clin. Oncol.* **2015,** *33* (21), 2361-2369.
27. Cortes, J.; Roché, H., Docetaxel combined with targeted therapies in metastatic breast cancer. *Cancer Treat. Rev.* **2012,** *38* (5), 387-396.
28. Schiff, P. B.; Fant, J.; Horwitz, S. B., Promotion of microtubule assembly in vitro by taxol. *Nature* **1979,** *277* (5698), 665-667.
29. Wang, T.-H.; Popp, D. M.; Wang, H.-S.; Saitoh, M.; Mural, J. G.; Henley, D. C.; Ichijo, H.; Wimalasena, J., Microtubule dysfunction induced by paclitaxel initiates apoptosis through both c-Jun N-terminal kinase (JNK)-dependent and-independent pathways in ovarian cancer cells. *J. Biol. Chem.* **1999,** *274* (12), 8208-8216.
30. Verschraegen, C. F.; Sittisomwong, T.; Kudelka, A. P.; Guedes, E. d. P.; Steger, M.; Nelson-Taylor, T.; Vincent, M.; Rogers, R.; Atkinson, E. N.; Kavanagh, J. J., Docetaxel for patients with paclitaxel-resistant Mullerian carcinoma. *J. Clin. Oncol.* **2000,** *18* (14), 2733-2739.
31. Sawaki, M.; Ito, Y.; Hashimoto, D.; Mizunuma, N.; Takahashi, S.; Horikoshi, N.; Tada, K.; Kasumi, F.; Akiyama, F.; Sakamoto, G., Paclitaxel administered weekly in patients with docetaxel-resistant metastatic breast cancer: a single-center study. *Tumori* **2004,** *90* (1), 36-39.
32. Verrills, N.; Kavallaris, M., Improving the targeting of tubulin-binding agents: lessons from drug resistance studies. *Curr. Pharm. Des.* **2005,** *11* (13), 1719-1733.
33. Mita, A. C.; Figlin, R.; Mita, M. M., Cabazitaxel: more than a new taxane for metastatic castrate-resistant prostate cancer? *Clin. Cancer Res.* **2012,** *18* (24), 6574-6579.
34. Forli, S., Epothilones: from discovery to clinical trials. *Curr. Top. Med. Chem.* **2014,** *14* (20), 2312-2321.
35. McMeekin, S.; Dizon, D.; Barter, J.; Scambia, G.; Manzyuk, L.; Lisyanskaya, A.; Oaknin, A.; Ringuette, S.; Mukhopadhyay, P.; Rosenberg, J., Phase III randomized trial of second-line ixabepilone versus paclitaxel or doxorubicin in women with advanced endometrial cancer. *Gynecol. Oncol.* **2015,** *138* (1), 18-23.
36. Jurczyszyn, A.; Wolska-Smoleń, T.; Skotnicki, A., Znaczenie angiogenezy w prawidłowej i nowotworowej hematopoezie. *Adv. Clin. Exp. Med.* **2003,** *12*, 489-496.
37. Smith, N. F.; Mani, S.; Schuetz, E. G.; Yasuda, K.; Sissung, T. M.; Bates, S. E.; Figg, W. D.; Sparreboom, A., Induction of CYP3A4 by vinblastine: role of the nuclear receptor NR1I2. *Ann. Pharmacother.* **2010,** *44* (11), 1709-1717.
38. Kingston, D. G., Tubulin-interactive natural products as anticancer agents. *J. Nat. Prod.* **2009,** *72* (3), 507-515.
39. Risinger, A. L.; Giles, F. J.; Mooberry, S. L., Microtubule dynamics as a target in oncology. *Cancer Treat. Rev.* **2009,** *35* (3), 255-261.
40. Voss, M. E.; Ralph, J. M.; Xie, D.; Manning, D. D.; Chen, X.; Frank, A. J.; Leyhane, A. J.; Liu, L.; Stevens, J. M.; Budde, C., Synthesis and SAR of vinca alkaloid analogues. *Bioorg. Med. Chem. Lett.* **2009,** *19* (4), 1245-1249.
41. Faller, B. A.; Pandit, T. N., Safety and efficacy of vinorelbine in the treatment of non-small cell lung cancer. *Clin. Med. Insights Oncol.* **2011,** *5*, CMO. S5074.
42. Vici, P.; Colucci, G.; Giotta, F.; Sergi, D.; Filippelli, G.; Perri, P.; Botti, C.; Vizza, E.; Carpino, A.; Pizzuti, L., A multicenter prospective phase II randomized trial of

epirubicin/vinorelbine versus pegylated liposomal doxorubicin/vinorelbine as first-line treatment in advanced breast cancer. A GOIM study. *J. Exp. Clin. Cancer Res.* **2011,** *30*, 1-8.
43. Tarlaci, S., Vincristine-induced fatal neuropathy in non-Hodgkin's lymphoma. *Neurotoxicol. Teratol.* **2008,** *29* (4), 748-749.
44. Vallo, S.; Michaelis, M.; Rothweiler, F.; Bartsch, G.; Gust, K. M.; Limbart, D. M.; Rödel, F.; Wezel, F.; Haferkamp, A.; Cinatl Jr, J., Drug-resistant urothelial cancer cell lines display diverse sensitivity profiles to potential second-line therapeutics. *Clin. Transl. Oncol.* **2015,** *8* (3), 210-216.
45. Bachner, M.; De Santis, M., Vinflunine in the treatment of bladder cancer. *The.r Clin. Risk. Manag.* **2008,** *4* (6), 1243-1253.
46. Bai, R.; Edler, M. C.; Bonate, P. L.; Copeland, T. D.; Pettit, G. R.; Luduena, R. F.; Hamel, E., Intracellular activation and deactivation of tasidotin, an analog of dolastatin 15: correlation with cytotoxicity. *Mol. Pharmacol.* **2009,** *75* (1), 218-226.
47. Hirata, Y.; Uemura, D., Halichondrins-antitumor polyether macrolides from a marine sponge. *Pure Appl. Chem.* **1986,** *58* (5), 701-710.
48. Jackson, K. L.; Henderson, J. A.; Phillips, A. J., The halichondrins and E7389. *Chem. Rev.* **2009,** *109* (7), 3044-3079.
49. Towle, M. J.; Salvato, K. A.; Budrow, J.; Wels, B. F.; Kuznetsov, G.; Aalfs, K. K.; Welsh, S.; Zheng, W.; Seletsky, B. M.; Palme, M. H., In vitro and in vivo anticancer activities of synthetic macrocyclic ketone analogues of halichondrin B. *Cancer Res.* **2001,** *61* (3), 1013-1021.
50. Twelves, C.; Cortes, J.; Vahdat, L. T.; Wanders, J.; Akerele, C.; Kaufman, P. A., Phase III trials of eribulin mesylate (E7389) in extensively pretreated patients with locally recurrent or metastatic breast cancer. *Clin. Breast Cancer* **2010,** *10* (2), 160-163.
51. Schöffski, P.; Chawla, S.; Maki, R. G.; Italiano, A.; Gelderblom, H.; Choy, E.; Grignani, G.; Camargo, V.; Bauer, S.; Rha, S. Y., Eribulin versus dacarbazine in previously treated patients with advanced liposarcoma or leiomyosarcoma: a randomised, open-label, multicentre, phase 3 trial. *Lancet* **2016,** *387* (10028), 1629-1637.
52. Hastie, S. B., Interactions of colchicine with tubulin. *Clin. Pharmacol. Ther.* **1991,** *51* (3), 377-401.
53. Yurdakul, S.; Mat, C.; Tüzün, Y.; Özyazgan, Y.; Hamuryudan, V.; Uysal, Ö.; Şenocak, M.; Yazici, H., A double-blind trial of colchicine in Behçet's syndrome. *Arthritis Rheum.* **2001,** *44* (11), 2686-2692.
54. Nagle, A.; Hur, W.; Gray, N. S., Antimitotic agents of natural origin. *Curr. Drug Targets* **2006,** *7* (3), 305-26.
55. Gracheva, I. A.; Shchegravina, E. S.; Schmalz, H. G.; Beletskaya, I. P.; Fedorov, A. Y., Colchicine Alkaloids and Synthetic Analogues: Current Progress and Perspectives. *J. Med. Chem.* **2020,** *63* (19), 10618-10651.
56. Klejborowska, G.; Urbaniak, A.; Maj, E.; Preto, J.; Moshari, M.; Wietrzyk, J.; Tuszynski, J. A.; Chambers, T. C.; Huczyński, A., Synthesis, biological evaluation and molecular docking studies of new amides of 4-chlorothiocolchicine as anticancer agents. *Bioorg. Chem.* **2020,** *97*, 103664.
57. Bergemann, S.; Brecht, R.; Büttner, F.; Guénard, D.; Gust, R.; Seitz, G.; Stubbs, M. T.; Thoret, S., Novel B-ring modified allocolchicinoids of the NCME series: design, synthesis, antimicrotubule activity and cytotoxicity. *Bioorg. Med. Chem.* **2003,** *11* (7), 1269-1281.
58. Roesner, M.; Capraro, H.-G.; Jacobson, A. E.; Atwell, L.; Brossi, A.; Iorio, M. A.; Williams, T. H.; Sik, R. H.; Chignell, C. F., Biological effects of modified colchicines. Improved preparation of 2-demethylcolchicine, 3-demethylcolchicine, and (+)-colchicine and reassignment of the position of the double bond in dehydro-7-deacetamidocolchicines. *J. Med. Chem.* **1981,** *24* (3), 257-261.
59. Cosentino, L.; Redondo-Horcajo, M.; Zhao, Y.; Santos, A. R.; Chowdury, K. F.; Vinader, V.; Abdallah, Q. M.; Abdel-Rahman, H.; Fournier-Dit-Chabert, J.; Shnyder, S. D.,

Synthesis and biological evaluation of colchicine B-ring analogues tethered with halogenated benzyl moieties. *J. Med. Chem.* **2012,** *55* (24), 11062-11066.
60. Siemann, D. W.; Rojiani, A. M., The vascular disrupting agent ZD6126 shows increased antitumor efficacy and enhanced radiation response in large, advanced tumors. *Int. J. Radiat. Oncol. Biol. Phys.* **2005,** *62* (3), 846-853.
61. Soltau, J.; Drevs, J., ZD-6126 AstraZeneca. *Idrugs* **2004,** *7* (4), 380-387.
62. Jones, H. W., Report of a series of cases of syphilis treated by Ehrlich's arsenobenzol at the Walter Reed General Hospital, District of Columbia. *Boston Med. Surg. J.* **1911,** *164* (11), 381-383.
63. Lloyd, N. C.; Morgan, H. W.; Nicholson, B. K.; Ronimus, R. S., The composition of Ehrlich's salvarsan: resolution of a century-old debate. *Angew. Chem.* **2005,** *44* (6), 941-944.
64. Peyrone, M., Ueber die einwirkung des ammoniaks auf platinchlorür. *Justus Liebigs Ann. Chem.* **1844,** *51* (1), 1-29.
65. Rosenberg, B.; Van Camp, L.; Krigas, T., Inhibition of cell division in Escherichia coli by electrolysis products from a platinum electrode. *Nature* **1965,** *205* (4972), 698-699.
66. Oun, R.; Moussa, Y. E.; Wheate, N. J., The side effects of platinum-based chemotherapy drugs: a review for chemists. *Dalton Trans.* **2018,** *47* (19), 6645-6653.
67. Rosenberg, B., Platinum complexes for the treatment of cancer: why the search goes on. *Cisplatin: chemistry and biochemistry of a leading anticancer drug* **1999**, 1-27.
68. Fischer, v. E.; Pfab, W., Cyclopentadien-metallkomplexe, ein neuer Typ metallorganischer verbindungen. *Z. Naturforsch. B* **1952,** *7* (7), 377-379.
69. Woodward, R.; Rosenblum, M.; Whiting, M., A new aromatic system. *J. Am. Chem. Soc.* **1952,** *74* (13), 3458-3459.
70. Fiorina, V. J.; Dubois, R. J.; Brynes, S., Ferrocenyl polyamines as agents for the chemoimmunotherapy of cancer. *J. Med. Chem.* **1978,** *21* (4), 393-395.
71. Harry, A. G. The synthesis, structural characterization and in vitro anticancer activity of novel ferrocenyl bioconjugates. Dublin City University, 2013.
72. Houlton, A.; Roberts, R.; Silver, J., Studies on the anti-tumour activity of some iron sandwich compounds. *J. Organomet. Chem.* **1991,** *418* (1), 107-112.
73. Top, S.; Dauer, B.; Vaissermann, J.; Jaouen, G., Facile route to ferrocifen, 1-[4-(2-dimethylaminoethoxy)]-1-(phenyl-2-ferrocenyl-but-1-ene), first organometallic analogue of tamoxifen, by the McMurry reaction. *J. Organomet. Chem.* **1997,** *541* (1-2), 355-361.
74. Top, S.; Tang, J.; Vessières, A.; Carrez, D.; Provot, C.; Jaouen, G., Ferrocenyl hydroxytamoxifen: a prototype for a new range of oestradiol receptor site-directed cytotoxics. *Chem. Commun.* **1996,** (8), 955-956.
75. Gasser, G.; Ott, I.; Metzler-Nolte, N., Organometallic anticancer compounds. *J. Med. Chem.* **2011,** *54* (1), 3-25.
76. Hillard, E.; Vessières, A.; Thouin, L.; Jaouen, G.; Amatore, C., Ferrocene-mediated proton-coupled electron transfer in a series of ferrocifen-type breast-cancer drug candidates. *Angew. Chem.* **2006,** *118* (2), 291-296.
77. Vessieres, A.; Top, S.; Pigeon, P.; Hillard, E.; Boubeker, L.; Spera, D.; Jaouen, G., Modification of the estrogenic properties of diphenols by the incorporation of ferrocene. Generation of antiproliferative effects in vitro. *J. Med. Chem.* **2005,** *48* (12), 3937-3940.
78. Hillard, E.; Vessieres, A.; Le Bideau, F.; Plażuk, D.; Spera, D.; Huche, M.; Jaouen, G., A series of unconjugated ferrocenyl phenols: prospects as anticancer agents. *ChemMedChem* **2006,** *1* (5), 551-559.
79. Plazuk, D.; Vessieres, A.; Hillard, E. A.; Buriez, O.; Labbe, E.; Pigeon, P.; Plamont, M. A.; Amatore, C.; Zakrzewski, J.; Jaouen, G., A [3]ferrocenophane polyphenol showing a remarkable antiproliferative activity on breast and prostate cancer cell lines. *J. Med. Chem.* **2009,** *52* (15), 4964-7.
80. Domarle, O.; Blampain, G.; Agnaniet, H.; Nzadiyabi, T.; Lebibi, J.; Brocard, J.; Maciejewski, L.; Biot, C.; Georges, A.; Millet, P., In vitro antimalarial activity of a new

organometallic analog, ferrocene-chloroquine. *Antimicrob. Agents Chemother.* **1998,** *42* (3), 540-544.
81. Dubar, F.; Egan, T. J.; Pradines, B.; Kuter, D.; Ncokazi, K. K.; Forge, D.; Paul, J.-F.; Pierrot, C.; Kalamou, H.; Khalife, J., The antimalarial ferroquine: role of the metal and intramolecular hydrogen bond in activity and resistance. *ACS Chem. Biol.* **2011,** *6* (3), 275-287.
82. Richon, V. M.; Zhou, X.; Rifkind, R. A.; Marks, P. A., Histone deacetylase inhibitors: development of suberoylanilide hydroxamic acid (SAHA) for the treatment of cancers. *Blood Cells Mol. Dis.* **2001,** *27* (1), 260-264.
83. Spencer, J.; Amin, J.; Wang, M.; Packham, S.; Alwi, G. S.; Tizzard, S.; Coles, R.; Paranal, J., Bradner, TD Heightman Synthesis and biological evaluation of JAHAs: ferrocene-based histone deacetylase inhibitors ACS Med. *Chem. Lett* **2011,** *2*, 358-362.
84. Librizzi, M.; Longo, A.; Chiarelli, R.; Amin, J.; Spencer, J.; Luparello, C., Cytotoxic effects of Jay Amin hydroxamic acid (JAHA), a ferrocene-based class I histone deacetylase inhibitor, on triple-negative MDA-MB231 breast cancer cells. *Chem. Res. Toxicol.* **2012,** *25* (11), 2608-2616.
85. Plażuk, D.; Wieczorek, A.; Błauż, A.; Rychlik, B., Synthesis and biological activities of ferrocenyl derivatives of paclitaxel. *MedChemComm* **2012,** *3* (4), 498-501.
86. Wieczorek, A.; Błauż, A.; Żal, A.; Arabshahi, H. J.; Reynisson, J.; Hartinger, C. G.; Rychlik, B.; Plażuk, D., Ferrocenyl paclitaxel and docetaxel derivatives: Impact of an organometallic moiety on the mode of action of Taxanes. *Chem. Eur. J.* **2016,** *22* (32), 11413-11421.
87. Nicolaus, N.; Zapke, J.; Riesterer, P.; Neudorfl, J. M.; Prokop, A.; Oschkinat, H.; Schmalz, H. G., Azides derived from colchicine and their use in library synthesis: A practical entry to new bioactive derivatives of an old natural drug. *ChemMedChem* **2010,** *5* (5), 661-5.
88. Kowalczyk, K.; Błauż, A.; Ciszewski, W. M.; Wieczorek, A.; Rychlik, B.; Plażuk, D., Colchicine metallocenyl bioconjugates showing high antiproliferative activities against cancer cell lines. *Dalton Trans.* **2017,** *46* (48), 17041-17052.
89. Wieczorek, A.; Błauż, A.; Zakrzewski, J.; Rychlik, B. e.; Plażuk, D., Ferrocenyl 2, 5-piperazinediones as tubulin-binding organometallic ABCB1 and ABCG2 inhibitors active against MDR cells. *ACS Med. Chem. Lett.* **2016,** *7* (6), 612-617.
90. Arezki, A.; Chabot, G. G.; Quentin, L.; Scherman, D.; Jaouen, G.; Brulé, E., Synthesis and biological evaluation of novel ferrocenyl curcuminoid derivatives. *MedChemComm* **2011,** *2* (3), 190-195.
91. Hottin, A.; Dubar, F.; Steenackers, A.; Delannoy, P.; Biot, C.; Behr, J.-B., Iminosugar–ferrocene conjugates as potential anticancer agents. *Org. Biomol. Chem.* **2012,** *10* (29), 5592-5597.
92. Smith, R. E., Trends in recommendations for myelosuppressive chemotherapy for the treatment of solid tumors. *J. Natl. Compr. Canc. Netw.* **2006,** *4* (7), 649-658.
93. Miki, H.; Okada, Y.; Hirokawa, N., Analysis of the kinesin superfamily: insights into structure and function. *Trends Cell Biol.* **2005,** *15* (9), 467-476.
94. Stock, M. F.; Chu, J.; Hackney, D. D., The kinesin family member BimC contains a second microtubule binding region attached to the N terminus of the motor domain. *J. Biol. Chem.* **2003,** *278* (52), 52315-52322.
95. Shi, J.; Orth, J. D.; Mitchison, T., Cell type variation in responses to antimitotic drugs that target microtubules and kinesin-5. *Cancer Res.* **2008,** *68* (9), 3269-3276.
96. Chamariya, R.; Suvarna, V., Role of KSP inhibitors as anti-cancer therapeutics: an update. *Anticancer Agents Med. Chem.* **2022,** *22* (14), 2517-2538.
97. Mayer, T. U.; Kapoor, T. M.; Haggarty, S. J.; King, R. W.; Schreiber, S. L.; Mitchison, T. J., Small molecule inhibitor of mitotic spindle bipolarity identified in a phenotype-based screen. *Science* **1999,** *286* (5441), 971-974.
98. Kaan, H. Y. K.; Ulaganathan, V.; Rath, O.; Prokopcova, H.; Dallinger, D.; Kappe, C. O.; Kozielski, F., Structural basis for inhibition of Eg5 by dihydropyrimidines:

stereoselectivity of antimitotic inhibitors enastron, dimethylenastron and fluorastrol. *J. Med. Chem.* **2010,** *53* (15), 5676-5683.
99. Gartner, M.; Sunder-Plassmann, N.; Seiler, J.; Utz, M.; Vernos, I.; Surrey, T.; Giannis, A., Development and biological evaluation of potent and specific inhibitors of mitotic Kinesin Eg5. *ChemBioChem* **2005,** *6* (7), 1173-1177.
100. Yang, L.; Jiang, C.; Liu, F.; You, Q.-D.; Wu, W.-T., Cloning, enzyme characterization of recombinant human Eg5 and the development of a new inhibitor. *Biol. Pharm. Bull.* **2008,** *31* (7), 1397-1402.
101. Brier, S.; Lemaire, D.; DeBonis, S.; Forest, E.; Kozielski, F., Identification of the protein binding region of S-trityl-L-cysteine, a new potent inhibitor of the mitotic kinesin Eg5. *Biochem.* **2004,** *43* (41), 13072-13082.
102. El-Nassan, H. B., Advances in the discovery of kinesin spindle protein (Eg5) inhibitors as antitumor agents. *Eur. J. Med. Chem.* **2013,** *62*, 614-631.
103. DeBonis, S.; Skoufias, D. A.; Indorato, R.-L.; Liger, F.; Marquet, B.; Laggner, C.; Joseph, B.; Kozielski, F., Structure–activity relationship of S-trityl-L-cysteine analogues as inhibitors of the human mitotic kinesin Eg5. *J. Med. Chem.* **2008,** *51* (5), 1115-1125.
104. Ogo, N.; Oishi, S.; Matsuno, K.; Sawada, J.-i.; Fujii, N.; Asai, A., Synthesis and biological evaluation of L-cysteine derivatives as mitotic kinesin Eg5 inhibitors. *Bioorg. Med. Chem. Lett.* **2007,** *17* (14), 3921-3924.
105. Shimizu, M.; Ishii, H.; Ogo, N.; Unno, Y.; Matsuno, K.; Sawada, J.-i.; Akiyama, Y.; Asai, A., S-trityl-L-cysteine derivative induces caspase-independent cell death in K562 human chronic myeloid leukemia cell line. *Cancer Lett.* **2010,** *298* (1), 99-106.
106. Abualhasan, M. N.; Good, J. A.; Wittayanarakul, K.; Anthony, N. G.; Berretta, G.; Rath, O.; Kozielski, F.; Sutcliffe, O. B.; Mackay, S. P., Doing the methylene shuffle–Further insights into the inhibition of mitotic kinesin Eg5 with S-trityl l-cysteine. *Eur. J. Med. Chem.* **2012,** *54*, 483-498.
107. Lemieux, C.; DeWolf, W.; Voegtli, W.; DeLisle, R. K.; Laird, E.; Wallace, E.; Woessner, R.; Corrette, C.; Allen, S.; Hans, J. In *ARRY-520, a novel, highly selective KSP inhibitor with potent anti-proliferative activity*, Proc Am Assoc Cancer Res, 2007; p 5590.
108. LoRusso, P. M.; Goncalves, P. H.; Casetta, L.; Carter, J. A.; Litwiler, K.; Roseberry, D.; Rush, S.; Schreiber, J.; Simmons, H. M.; Ptaszynski, M., First-in-human phase 1 study of filanesib (ARRY-520), a kinesin spindle protein inhibitor, in patients with advanced solid tumors. *Invest. New Drugs* **2015,** *33*, 440-449.
109. Ocio, E. M.; Motlló, C.; Rodríguez-Otero, P.; Martínez-López, J.; Cejalvo, M. J.; Martín-Sánchez, J.; Bladé, J.; García-Malo, M. D.; Dourdil, M. V.; García-Mateo, A., Filanesib in combination with pomalidomide and dexamethasone in refractory MM patients: safety and efficacy, and association with alpha 1-acid glycoprotein (AAG) levels. Phase Ib/II Pomdefil clinical trial conducted by the Spanish MM group. *Br. J. Haematol.* **2021,** *192* (3), 522-530.
110. Huszar, D.; Theoclitou, M.-E.; Skolnik, J.; Herbst, R., Kinesin motor proteins as targets for cancer therapy. *Cancer Metastasis Rev.* **2009,** *28*, 197-208.
111. Holland, J. P.; Jones, M. W.; Cohrs, S.; Schibli, R.; Fischer, E., Fluorinated quinazolinones as potential radiotracers for imaging kinesin spindle protein expression. *Bioorg. Chem.* **2013,** *21* (2), 496-507.
112. Blagden, S.; Molife, L.; Seebaran, A.; Payne, M.; Reid, A.; Protheroe, A.; Vasist, L.; Williams, D.; Bowen, C.; Kathman, S., A phase I trial of ispinesib, a kinesin spindle protein inhibitor, with docetaxel in patients with advanced solid tumours. *Br. J. Cancer* **2008,** *98* (5), 894-899.
113. Holen, K. D.; Belani, C. P.; Wilding, G.; Ramalingam, S.; Volkman, J. L.; Ramanathan, R. K.; Vasist, L. S.; Bowen, C. J.; Hodge, J. P.; Dar, M. M., A first in human study of SB-743921, a kinesin spindle protein inhibitor, to determine pharmacokinetics, biologic effects and establish a recommended phase II dose. *Cancer Chemother. Pharmacol.* **2011,** *67*, 447-454.

114. Novais, P.; Silva, P. M.; Amorim, I.; Bousbaa, H., Second-generation antimitotics in cancer clinical trials. *Pharm.* **2021,** *13* (7), 1011.
115. Jackson, J. R.; Gilmartin, A.; Dhanak, D.; Knight, S.; Parrish, C.; Luo, L.; Sutton, D.; Caulder, E.; Diamond, M.; Giardiniere, M., A second generation KSP inhibitor, SB-743921, is a highly potent and active therapeutic in preclinical models of cancer. *Clin. Cancer Res.* **2006,** *12* (19_Supplement), B11-B11.
116. Jeay, S.; Ali, S.; Chen, C.-R.; Uppalapati, U.; Senator, D.; Chan, T.; France, D.; Ashwell, M., Discovery of a novel Eg5 kinesin inhibitor, ARQ 621, with potent antitumor activity while sparing bone marrow-derived cells. *Cancer Res.* **2008,** *68* (9_Supplement), 656-656.
117. Chen, L.; Rosen, L.; Iyengar, T.; Goldman, J.; Savage, R.; Kazakin, J.; Chan, T.; Schwartz, B.; Abbadessa, G.; Von Hoff, D., First-in-human study with ARQ 621, a novel inhibitor of Eg5: Final results from the solid tumors cohort. *J. Clin. Oncol.* **2011,** *29* (15_suppl), 3076-3076.
118. Łomzik, M.; Hanif, M.; Budniok, A.; Błauż, A.; Makal, A.; Tchoń, D. M.; Leśniewska, B.; Tong, K. K.; Movassaghi, S.; Söhnel, T., Metal-dependent cytotoxic and kinesin spindle protein inhibitory activity of Ru, Os, Rh, and Ir half-sandwich complexes of ispinesib-derived ligands. *Inorg. Chem.* **2020,** *59* (20), 14879-14890.
119. Łomzik, M.; Błauż, A.; Głodek, M.; Makal, A.; Tchoń, D.; Ayine-Tora, D. M.; Hartinger, C.; Rychlik, B.; Plażuk, D., Organometallic Ru, Os, Rh and Ir half-sandwich conjugates of ispinesib–impact of the organometallic group on the antimitotic activity. *Dalton Trans.* **2023,** *52* (34), 11859-11874.
120. Russowsky, D.; Canto, R. F.; Sanches, S. A.; D'Oca, M. G.; de Fatima, A.; Pilli, R. A.; Kohn, L. K.; Antonio, M. A.; de Carvalho, J. E., Synthesis and differential antiproliferative activity of Biginelli compounds against cancer cell lines: Monastrol, oxo-monastrol and oxygenated analogues. *Bioorg. Chem.* **2006,** *34* (4), 173-82.
121. Pidathala, C.; Amewu, R.; Pacorel, B.; Nixon, G. L.; Gibbons, P.; Hong, W. D.; Leung, S. C.; Berry, N. G.; Sharma, R.; Stocks, P. A.; Srivastava, A.; Shone, A. E.; Charoensutthivarakul, S.; Taylor, L.; Berger, O.; Mbekeani, A.; Hill, A.; Fisher, N. E.; Warman, A. J.; Biagini, G. A.; Ward, S. A.; O'Neill, P. M., Identification, design and biological evaluation of bisaryl quinolones targeting Plasmodium falciparum type II NADH:quinone oxidoreductase (PfNDH2). *J. Med. Chem.* **2012,** *55* (5), 1831-43.
122. Fu, R. G.; You, Q. D.; Yang, L.; Wu, W. T.; Jiang, C.; Xu, X. L., Design, synthesis and bioevaluation of dihydropyrazolo[3,4-b]pyridine and benzo[4,5]imidazo[1,2-a]pyrimidine compounds as dual KSP and Aurora-A kinase inhibitors for anti-cancer agents. *Bioorg. Chem.* **2010,** *18* (22), 8035-43.
123. Rayar, A.; Veitia, M. S.; Ferroud, C., An efficient and selective microwave-assisted Claisen-Schmidt reaction for the synthesis of functionalized benzalacetones. *Springerplus* **2015,** *4*, 221.
124. Guangfan, H.; Jinjun, W.; Guiji, J., Synthesis of Chroman-4-ono[2,3-b]quinolinone Derivatives. *Chin. J. Chem.* **2003,** *23* (9), 1004-1007.

9. Działalność naukowa

9.1 Udział w projektach badawczych

1. Wykonawca Grantu UMO-2015/17/B/ST5/02331 pt. „Synteza, badania właściwości przeciwnowotworowych oraz powinowactwa do kinezyny wybranych sandwiczowych oraz półsandwiczowych związków metaloorganicznych” (kierownik grantu, dr hab. Damian Plażuk, prof. UŁ)

2. Kierownik Grantu UMO-2018/29/N/ST5/01976 pt. „Synteza i badanie wpływu podstawnika metaloorganicznego na właściwości biologiczne koniugatów kompleksów metaloorganicznych z kolchicyną”

9.2 Spis komunikatów konferencyjnych

Komunikaty posterowe:

1. Karolina Kowalczyk, Wojciech Ciszewski, Andrzej Błauż, Anna Wieczorek, Błażej Rychlik, Damian Plażuk „Ferrocenyl and ruthenocenyl conjugates with colchicinesynthesis and anticancer properties” XX International Symposium „Advences in the chemistry of heteroorganic compounds”, 23-24.11.17, Łódź

2. Karolina Kowalczyk, Anna Wieczorek-Błauż, Andrzej Błauż, Błażej Rychlik, Damian Plażuk „Synteza i aktywność biologiczna wynranych metalocenowych koniugatów ispinezibu” XI Ogólnopolskie Sympozjum Chemii Organicznej, 8-11.04.18, Warszawa

3. Karolina Kowalczyk, Anna Wieczorek-Błauż, Wojciech Ciszewski, Andrzej Błauż, Chatchakorn Eurtivong, Homayon John Arabashahi, Jóhannes Reynisson, Christian G. Hartinger, Błażej Rychlik, Damian Plażuk „Metalocenowe analogi Paklitakselu” VI Łódzkie Sympozjum Doktorantów Chemii, 10-11.05.18, Łódź

4. Karolina Kowalczyk, Anna Wieczorek-Błauż, Andrzej Błauż, Błażej Rychlik, Damian Plażuk „Ferrocenyl and ruthenocenyl monastrol conjugates-synthesis and anticancer activites” 28th International Conference on Organometallic Chemistry, 15-20.07.18, Florencja

5. Karolina Kowalczyk, Anna Wieczorek-Błauż, Andrzej Błauż Błażej Rychlik, Damian Plażuk „Metallocenyl biconjugates of monastrol - synthesis and anticancer activities” XXI International Symposium „Advences in the chemistry of heteroorganic compounds”, 23-24.11.18, Łódź

6. Karolina Kowalczyk, Anna Wieczorek-Błauż, Andrzej Błauż Błażej Rychlik, Damian Plażuk „Synteza i ocena biologiczna nowych koniugatów metaloorganicznych monastrolu" VII Łódzkie Sympozjum Doktorantów Chemii, 9-10.05.19, Łódź

7. Karolina Kowalczyk, Andrzej Błauż, Wojciech Ciszewski, Anna Wieczorek-Błauż, Błażej Rychlik, Damian Plażuk „Organometallic conjugates with colchicine – synthesis and anticancer properties" 15th International Symposium on Applied Bioinorganic Chemistry,2-5.06.19, Nara, Japonia

8. Karolina Kowalczyk, Andrzej Błauż, Wojciech Ciszewski, Anna Wieczorek-Błauż, Błażej Rychlik, Damian Plażuk „Synthesis and evaluation of biological activities of new organometallic conjugates with colchicine" 9th international Symposium on Bioorganometallic Chemistry, 28.07-1.08.2019, York, Wielka Brytania

9. Karolina Kowalczyk, Andrzej Błauż, Błażej Rychlik, Damian Plażuk „Synthesis and anticancer activities organometallic conjugates with colchicine" 16th European Biological Inorganic Chemistry Conference, 17-21.2022, Grenoble, Francja

Komunikaty ustne:

1. Karolina Kowalczyk, Andrzej Błauż, Wojciech Ciszewski, Anna Wieczorek-Błauż, Błażej Rychlik, Damian Plażuk „Synteza i właściwości przeciwnowotworowe koniugatów ferrocenylowych rutenocenylowych z kolchicyną" 62. Zjazd Polskiego Towarzystwa Chemicznego, 2-6.09.19, Warszawa

9.3 Pozostała działalność

1. Zastępca przewodniczącego Wydziałowej Rady Samorządu Doktorantów (rok akademicki 2018/2019; 2019/2020; 2020/2021)

2. Przewodnicząca Wydziałowej Komisji Socjalno-Stypendialnej Doktorantów (rok akademicki 2018/2019; 2019/2020; 2020/2021; 2021/2022: 2022/2023)

3. Członek Komitetu Organizacyjnego V,VI,VII Łódzkiego Sympozjum Doktorantów Chemii

Volume 51
Number 2
14 January 2022
Pages 387-752

Dalton Transactions

An international journal of inorganic chemistry

rsc.li/dalton

ISSN 1477-9226

ROYAL SOCIETY OF CHEMISTRY

PAPER

Damian Plażuk *et al.*

Impact of the ferrocenyl group on cytotoxicity and KSP inhibitory activity of ferrocenyl monastrol conjugates

Dalton Transactions

ROYAL SOCIETY OF CHEMISTRY

PAPER

View Article Online
View Journal | View Issue

Cite this: *Dalton Trans.*, 2022, **51**, 491

Impact of the ferrocenyl group on cytotoxicity and KSP inhibitory activity of ferrocenyl monastrol conjugates†

Anna Wieczorek-Błauż, [a] Karolina Kowalczyk,[a] Andrzej Błauż, [b] Anna Makal,[c] Sylwia Pawlędzio, [c] Chatchakorn Eurtivong, [d,e] Homayon J. Arabshahi,[f] Jóhannes Reynisson, [f,g] Christian G. Hartinger, [f] Błażej Rychlik [b] and Damian Plażuk *[a]

Received 21st October 2021,
Accepted 11th November 2021

DOI: 10.1039/d1dt03553c

rsc.li/dalton

The incorporation of the ferrocenyl moiety into a bioactive molecule may significantly alter the activity of the resulting conjugate. By applying this strategy, we designed ferrocenyl analogs of monastrol – the first low molecular weight kinesin spindle protein (KSP) inhibitor. The obtained compounds showed low micromolar antiproliferative activity towards a panel of sensitive and ABC-overexpressing cancer cells. Most cytotoxic compounds exhibited also higher KSP modulatory activity and ability for ROS generation compared to monastrol. The increased bioactivity of the studied compounds can be attributed to the presence of the ferrocenyl group.

Introduction

Microtubule-targeting drugs, taxanes (*e.g.* paclitaxel, docetaxel, cabazitaxel) and *Vinca* alkaloids (*e.g.* vincristine, vinblastine, vinflunine, vindesine), are widely used in anticancer therapy.[1,2] As microtubules maintain the cell structure and play a crucial role in numerous cellular processes such as cell motility, intracellular transport and cell division[3–5] in all nucleated cells, the use of tubulin-binding drugs results in high systemic toxicity and serious adverse effects.[6–8] Thus, a search for novel inhibitors that affect molecular targets involved in cell division and overexpressed in cancer cells is still highly relevant.[9]

Kinesins, especially kinesin spindle protein (KSP; also known as Eg5 or kinesin-5), are among the most promising targets for novel anticancer agents. There are over 40 human kinesins classified into 14 families, which are important for cell division and intracellular transport.[10] Although hundreds of proteins are associated with mitotic spindle formation,[11] KSP plays an essential role in establishing the bipolar spindle.[12–15] Additionally, this protein is overexpressed only in neoplastic cells, thus KSP inhibitors arrest only dividing cells[16] and are not expected to affect non-proliferating normal cells. Furthermore, it has been reported that overexpression of KSP is correlated with poor clinical outcome in several cancer types.[17–20] This makes KSP a good molecular target for anticancer therapy.[21–25]

The first low molecular weight KSP inhibitor, monastrol **1**, was discovered by Mayer *et al.* in 1999.[26] Despite only moderate anticancer activity of **1**, considerable effort was taken to modify its structure and to design monastrol-derived lead structures as potent KSP inhibitors such as enastron,[26] dimethylenastron,[27] fluorastrol,[28] Mon-97,[29] or CPUYL064.[30] In addition, other natural and synthetic KSP inhibitors were discovered which are structurally different from monastrol.[31,32]

Widespread use of platinum-based anticancer drugs, *e.g.* cisplatin and its analogs,[33,34] led to the growing interest for other metal-based compounds as prospective antineoplastic agents. The conjugation of a metal-containing structural

[a]*Department of Organic Chemistry, Faculty of Chemistry, University of Łódź, Tamka 12, 91-403 Łódź, Poland. E-mail: damian.plazuk@chemia.uni.lodz.pl*
[b]*Cytometry Lab, Department of Molecular Biophysics, Faculty of Biology and Environmental Protection University of Łódź, Pomorska 141/143, 90-236 Łódź, Poland*
[c]*Laboratory for Structural and Biochemical Research, Biological and Chemical Research Centre, Department of Chemistry, University of Warsaw, ul. Żwirki i Wigury 101, 02-089 Warszawa, Poland*
[d]*Program in Chemical Science, Chulabhorn Graduate Institute, Chulabhorn Royal Academy, Bangkok 10210, Thailand*
[e]*Center of Excellence on Environmental Health and Toxicology (EHT), Commission on Higher Education (CHE), Ministry of Education, Bangkok 10400, Thailand*
[f]*School of Chemical Sciences, University of Auckland, Auckland 1142, New Zealand*
[g]*School of Pharmacy and Bioengineering, Keele University, Staffordshire ST5 5BG, UK*

†Electronic supplementary information (ESI) available: Copies of the NMR spectra and HPLC-ESI-MS analysis. CCDC 2010957 and 2010958. For ESI and crystallographic data in CIF or other electronic format see DOI: 10.1039/d1dt03553c

motif, such as a ferrocene moiety, to bioactive molecules often results in increased bioactivity or even altered mode of action in comparison to the organic parent compound.[35] In the last three decades, ferrocene derivatives[36] were extensively investigated as anticancer,[37,38] antimicrobial,[39–42] antiparasitic,[43] including antimalarial, drug candidates.[44–46] Interestingly, organometallic derivatives of KSP inhibitors have only been studied to a minor extent, while much research was focused on half-sandwich complexes. For example, Al-Masoudi and coworkers reported ruthenium complexes of the dihydropyrimidine (DHP) monastrol, however, the obtained compounds possessed lower activity than monastrol.[47,48] Recently, we reported ruthenium, osmium, iridium and rhodium half-sandwich complexes as KSP inhibitors bearing the 2-(1-aminoalkyl)quinazolin-4(3*H*)-one moiety as a bidentate ligand.[49] Although simple ferrocenyl DHP derivatives have been synthesized,[50–53] the biological activity of such compounds has not been investigated in detail, and the impact of the ferrocenyl moiety on KSP activity is unknown.

Continuing our research in organometallic inhibitors of mitosis,[54–59] we have prepared ferrocenyl derivatives of monastrol (X = S) and oxo-monastrol (X = O) (Fig. 1) and evaluated the influence of the organometallic moiety on the bioactivity of the ferrocenyl derivatives.

Results and discussion

Synthesis

The target compounds of type I and II were prepared in Biginelli reactions. The reaction of ferrocenecarboxaldehyde **2a** with ethyl acetoacetate, thiourea and catalytical amounts of HCl at reflux afforded **3a** in 53% yield. Unfortunately, the same procedure led to an inseparable mixture of several products when using aldehydes **2b–2d**. However, we found that the reaction of ferrocenecarboxaldehyde, *o*-, *m*-, or *p*-ferrocenylbenzaldehydes **2a–d** with ethyl acetoacetate and thiourea or urea at RT in anhydrous ethanol in the presence of $SbCl_3$,[60,61] afforded the desired type I compounds **3b–d** and **4a–d** in 23–80% yield (Scheme 1).

To prepare compounds of type II, the corresponding β-ketoesters **5a–d** were required. The Friedel–Crafts acylation

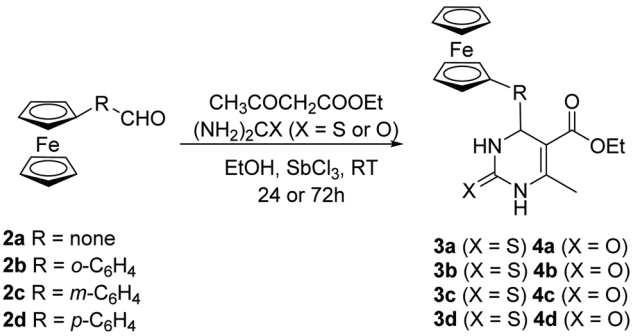

Scheme 1 Synthesis of the type I ferrocenyl monastrol analogs **3a–4d**.

of ferrocene with mono-ethyl malonate and trifluoroacetic anhydride in the presence of trifluoromethanesulfonic acid gave **5a** in almost quantitative yield (Scheme 2).[62] Compounds **5b–d** were prepared in the reaction of **2b–d** with ethyl diazoacetate in the presence of catalytic amounts of $NbCl_5$ in 11–65% yield by adopting a reported procedure (Scheme 2).[63]

The reaction of **5a–d** with 3-hydroxybenzaldehyde and thiourea or urea under optimized conditions ($SbCl_3$ catalyst, 24 h at RT) led to a mixture of undesired and various unidentified products together with small amounts of desired products. When urea was used instead of thiourea, we were able to isolate undesired 2-acyl-3-ureidopropanoates **8a–d** in 10–34% yields which precipitated from the reaction mixture (Scheme 3, condition C). Therefore, to optimize the reaction conditions, we monitored the progress of the reactions of **5a** with urea or thiourea and 3-hydroxybenzaldehyde in the presence of $SbCl_3$ by HPLC-MS. When urea was used, the HPLC-MS analysis of the crude reaction mixture confirmed that **8a** was the major product (43.8%), while the desired **7a** was only formed in 9.4% yield. Besides, a small amount, 13.1%, of unreacted **5a** remained in the reaction mixture after 24 h. Use of thiourea instead of urea resulted in the formation of the ureido derivative **9a** in 29.0%, while **6a** was only formed at 5.5% yield with 34.9% of unreacted **5a** remaining after 24 h at RT. Performing the reaction at 40 °C led to the formation of **6a** or **7a** in 29.5 and 25.5% yield, respectively, while the amounts of ureido derivatives decreased to 25.2 and 34.2%, respectively. Further extension of the reaction time up to 72 h increased the

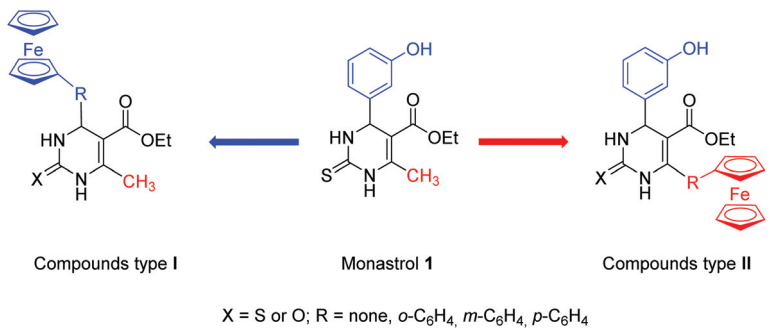

Fig. 1 Structures of monastrol **1** and its ferrocenyl analogs type I and II studied herein.

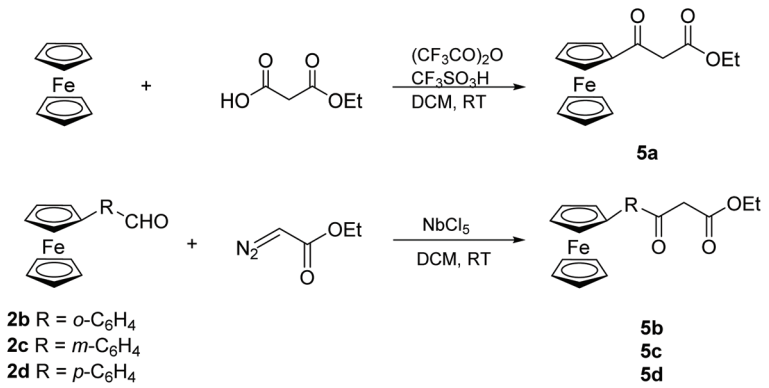

Scheme 2 Synthesis of ethyl ferrocenoyl **5a** and *o*-, *m*-, and *p*-ferrocenylbenzoylacetate **5b–d**.

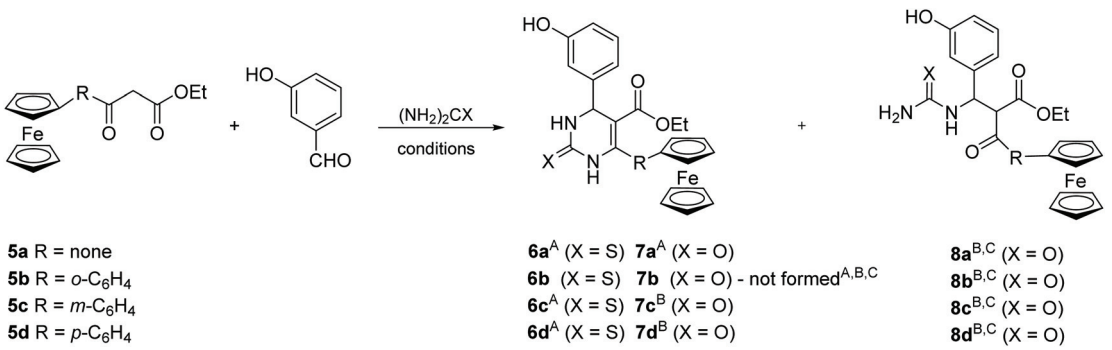

Scheme 3 Synthesis of the type II ferrocenyl monastrol analogs. Conditions: (A) $SbCl_3$ (1 eq.), 40 °C, 72 h; (B) CF_3CH_2OH, $Yb(OTf)_3$ (10% mol), MW, 110 °C, 30 min; (C) $SbCl_3$ (1 eq.), RT, 72 h.

yield of the desired products. In comparison, a similar study performed for the reaction of **2a** with urea or thiourea and ethyl acetoacetate confirmed that the desired products **4a** and **3a** were formed as the major products in yields of 73.8 and 57.7%, respectively within 24 h, together with ethyl 2-ferrocenylmethylideneacetoacetate **13** (12.3–17.3%) and trace amounts of ureido derivatives **12a** and **11a** (1.7 and 2.4%) (Scheme 4).

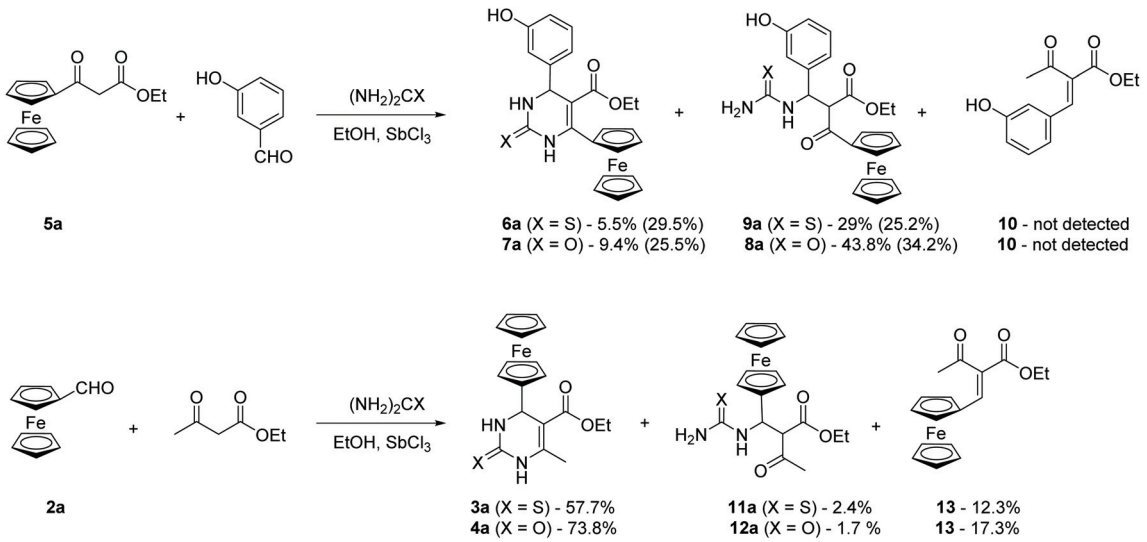

Scheme 4 Biginelli reactions of **5a** with 3-hydroxybenzaldehyde and of **2a** with ethyl acetoacetate, and urea or thiourea catalyzed by $SbCl_3$ for 24 h. Yields of the products formed at RT (or 40 °C) in the crude reaction mixture were determined by HPLC-MS analysis.

Based on the obtained results, we decided to perform the reactions of **5a–d** with 3-hydroxybenzaldehyde, thiourea or urea and $SbCl_3$ at 40 °C for 72 h, which allowed the isolation of **6a**, **6c**, **6d** and **7a** in yields of 10–54% (Scheme 3, condition A). Any further effort to prepare **6b** or **7b–d** under the same conditions failed. Further studies revealed that **7c** and **7d** were formed in 6.2 and 1.4% yield when the reactions were carried out in a microwave reactor in the presence of 10 mol% of Yb $(OTf)_3$ in 2,2,2-trifluoroethanol at 110 °C for 30 min. We also observed the formation of trace amounts of ureido derivatives **8c** and **8d** (1.4–2.5%). Interestingly, under microwave condition, **6a** was formed in only 1.6% yield, while *ortho*-substituted **6b** or **7b** were not found (Scheme 3, condition B).

The structures and purities of all compounds were confirmed by the NMR spectroscopy and HPLC-ESI-MS analysis (ESI†). In the ^{1}H NMR spectra in DMSO-d_6 of **3a–d** and **6b–d**, we observed two signals assigned to the NH-1 and NH-3 protons at *ca*. 10.5 and 9.7 ppm, respectively, while in the oxo-analogs **4a–d** these protons were observed at *ca*. 9.1 and 7.5 ppm. However, in the case of **6a**, the order of the NH-1 and NH-3 proton peaks was inversed, and the corresponding signals were present at *ca*. 8.7 and 9.9 ppm. In comparison to monastrol derivatives, the 2-acyl-3-(ureido)propanoates **8a–d** presented much more complicated spectra as they can exist in both keto and enol forms, as confirmed by NMR spectroscopy. In the ^{1}H NMR spectra of **8a–d** in DMSO-d_6, the signals of the NH_2 group were observed at *ca.* 5.6 ppm while the NH protons resonated at *ca*. 6.6 ppm as broad singlets or doublets. In the $^{13}C\{^1H\}$ NMR spectra of **8a–d**, a set of three carbonyl atom signals was present at *ca*. 195, 168 and 158 ppm, which were assigned to keto CO, ester and 158 ppm urea moieties, correspondingly. The HPLC-ESI-MS analysis of the monastrol derivatives shown the major peaks (with area in a range of 84.1–95.8%) preceded by minor peaks (with area in a range of 3.1–10%) both assigned to cation $[M]^+$ formed by oxidation of studied compound, and only in a case of **6a** we observed molecular ion assigned to $[M + H]^+$ (ESI Fig. S39–S56†). The presence of the major peak together with trace amounts of minor peak observed in the HPLC-ESI-MS spectra of studied compounds can be assigned to the keto–enol forms.

Single crystal X-ray diffraction analysis

The molecular structures of the organometallic analogs of monastrol, *i.e.*, **3a** and **6a**, were determined by single-crystal X-ray diffraction analysis (Fig. 2, 3 and ESI Fig. S1,† Tables 1, 2 and 7). Similarly, to **1**, both **3a** and **6a** crystallized in the centrosymmetric space groups *C*2/*c* (**3a**) and *P*21/*c* (**6a**) as racemic mixtures. In both instances, a single molecule of the compound was found in the asymmetric unit. Compound **6a** co-crystallized with one molecule of CH_2Cl_2 which was found to be severely disordered.

The molecular geometry of the heterocyclic rings in the monastrol derivatives **3a** and **6a** is almost identical to that of **1** (Table 7), demonstrating that ferrocene substitution at either C2 or C4 does not alter the geometry of the pharmacophore.[64] The planar fragments of the aromatic substituents at C2 are oriented perpendicularly to the average plane formed from C1, N1, C3, C4 and N2 in the case of both the *m*-hydroxyphenyl (**3a**) and ferrocenyl (**6a**) substituents. The –C(O)O– fragment does not deviate from planarity with the central ring by more than ±30°, which is again very similar to the case of **1**. The ferrocene moieties in both **3a** and **6a** adopt the common eclipsed conformation (Table 1).

Despite the introduction of the ferrocenyl substituent, the H-bonds formed in the molecular structure of **3a** are essentially the same as the ones observed for **1** (Table 2), with both N1–H and N2–H acting as H-bond donors and molecules of **3a** forming dimers connected by a pair of N–H···S bonds. On the

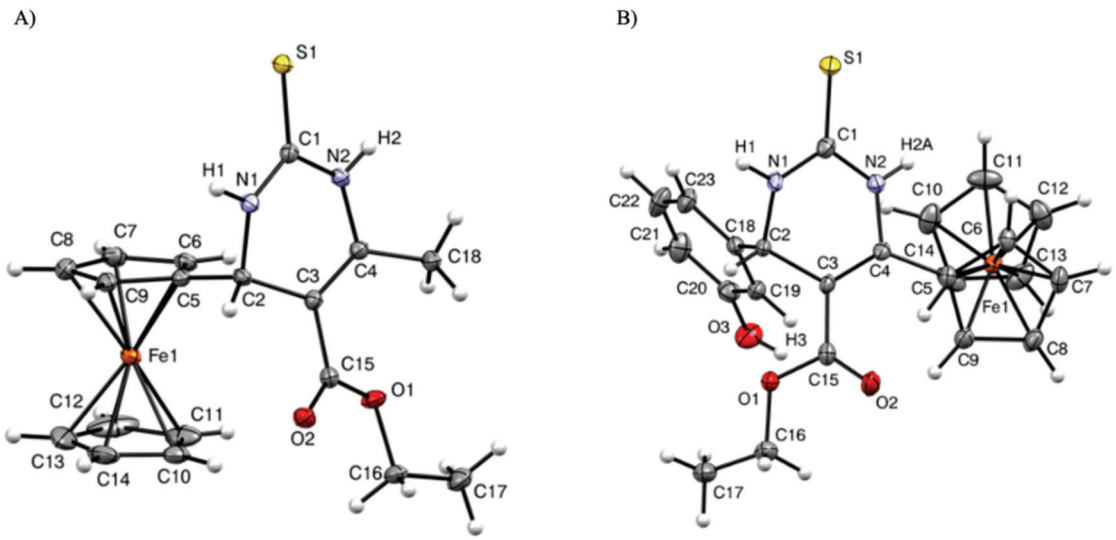

Fig. 2 ORTEP representations of (A) **3a** and (B) **6a**. Labels of H atoms not involved in H-bonding were omitted for clarity. Atomic displacement parameters are presented at 50% probability level.

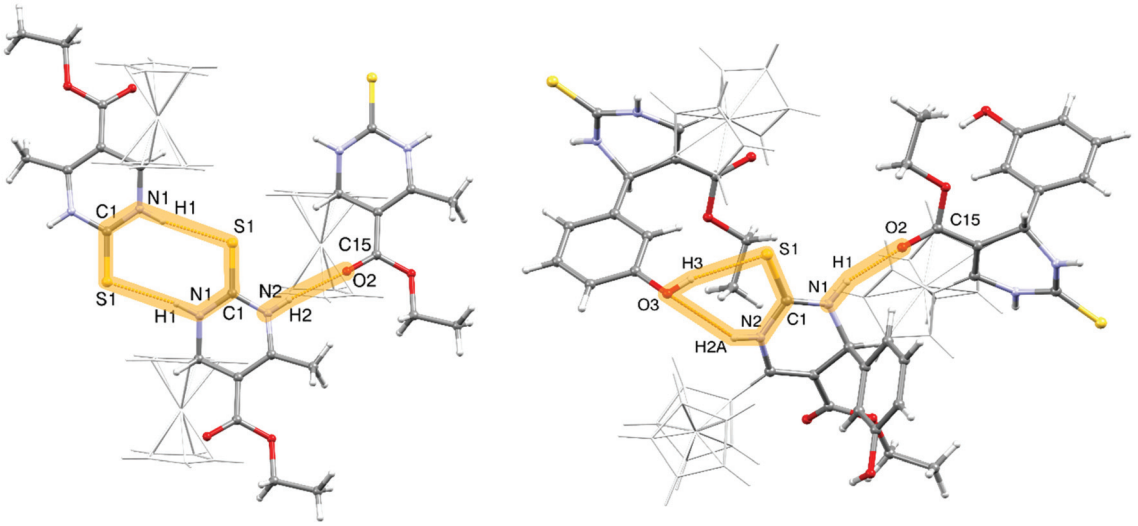

Fig. 3 H-Bond motifs in the structures of **3a** (left) and **6a** (right) highlighted in orange. The ferrocene moieties are represented as light-grey sticks for clarity.

Table 1 Selected geometrical parameters for the molecular structures of **3a** and **6a** compared with the analogous parameters of **1** in Å and °. The original crystal structure data of monastrol **1** can be obtained from the CCDC database (CCDC code QICTIF)

	3a	**1** [11] (QICTIF)	**6a**
Bond lengths/Å			
C1═S1	1.687(2)	1.694(2)	1.689(3)
C1–N1	1.330(2)	1.325(3)	1.327(4)
C1–N2	1.367(2)	1.359(3)	1.370(4)
C2–N1	1.480(2)	1.473(3)	1.465(4)
C2–C3	1.515(2)	1.518(4)	1.523(5)
C2–$C_{substituent@C2}$	1.513(2)	1.514(4)	1.535(6)
C4–C3	1.353(2)	1.349(3)	1.354(4)
C4–N2	1.396(2)	1.400(3)	1.402(4)
C4–$C_{substituent@C4}$	1.497(2)	1.493(4)	1.470(5)
Bond angles/°			
Heterocyclic average plane *vs.* phenyl plane @ C2	81.9(9)	85.4(5)	89.4(6)
C4–C3–C15–O1	−29.7(2)	−10.9(4)	−149.3(6)
Heterocyclic average plane *vs.* Fc plane	n/a	n/a	28.6(6)
Cp1–Fe–Cp2	177(2)	n/a	178.7(9)
Deviation from eclipsed	1.0(9)	n/a	−4.2(6)

Table 2 Geometry of intermolecular H-bonds present in the molecular structures of **3a** and **6a** compared with analogous parameters of monastrol **1**[64] in Å or °

	D···A	D–H	H···A	<DHA	Symmetry code for the A atom
1					
N1–H1···S1	3.354(3)	0.86	2.521	163.5	$-x, 3-y, 1-z$
N2–H2···O2	2.971(3)	0.86	2.13	165.7	$1+x, y, z$
3a					
N1–H1···S1	3.297(1)	0.87(2)	2.44(2)	170(2)	$-x, 1-y, -z$
N2–H2···O2	2.992(2)	0.84(2)	2.16(2)	173(2)	$x, -1+y, z$
6a					
N1–H1···O2	2.789(3)	0.87(3)	1.95(3)	161(4)	$1-x, 1/2+y, 1/2-z$
N2–H2···O3	3.329(4)	0.87(3)	2.56(3)	147(3)	$x, 1.5-y, -1/2+z$
O3–H3···S1	3.204(3)	0.81(3)	2.42(3)	165(4)	$x, 1.5-y, 1/2+z$

other hand, substitution of the methyl group with ferrocene at C4 in **6a** resulted in a different pattern of H-bonds, where N2–H acted as an H-bond donor for O2, and a new ring pattern of N–H···O and O–H···S H-bonds formed involving the hydroxyl group of the *m*-hydroxy-phenyl moiety (Fig. 3 and Table 2).

The difference in the H-bond networks are further reflected in the crystal packing. In the case of **3a**, the H-bonds N–H···S build chains of molecules stretching in [010] direction and layers of ferrocene moieties bound by numerous C–H···π interactions. In **6a**, the H-bonding network is multidirectional, and ferrocene moieties are oriented almost parallel along [010] and contribute to the formation of well-separated double layers of **6a** molecules in the [100] plane (ESI Fig. S1†).

Antiproliferative activity

The antiproliferative activity of the synthesized compounds was studied in a set of human cancer cell lines, namely A549 (alveolar basal epithelial cell adenocarcinoma), Colo 205 (colorectal adenocarcinoma), HCT 116 (colorectal carcinoma), Hep G2 (hepatocellular carcinoma), MCF7 (breast adenocarcinoma), and SW620 (colorectal adenocarcinoma), as well as in a panel of five multidrug-resistant (MDR) cell lines derived from SW620 and characterized by overexpression of various ABC proteins, namely ABCG2 (SW620C), ABCC1 (SW620M and SW620E) and ABCB1 (SW620D, SW620E, and SW620V).[65] As the potential target of our compounds is crucial for cell division, dividing cells would be affected by these anticancer agents and therefore we did not investigate the cytotoxicity of the compounds towards non-cancerous cell lines. Initially, we evaluated the impact of **3a–4d**, **6a**, **6c**, **6d**, **7a**, **7c**, **7d** and **8a–d** on the cell viability at the IC_{50} of **1** of the respective cell line (Fig. 4).

Such screening allowed us to choose 10 of the most active compounds and study them further in a more detailed way. In the next step, we determined the IC_{50} values for selected compounds in the same set of cancer cell lines (Table 3). Analysis of the antiproliferative potential of the synthesized compounds in the A549, Colo 205, Hep G2, HCT 116, SW620 and MCF7 cell lines revealed that ferrocenyl analogs of monastrol **3** and **6** and of its oxo-analogs **4** and **7** were more active than **1**.

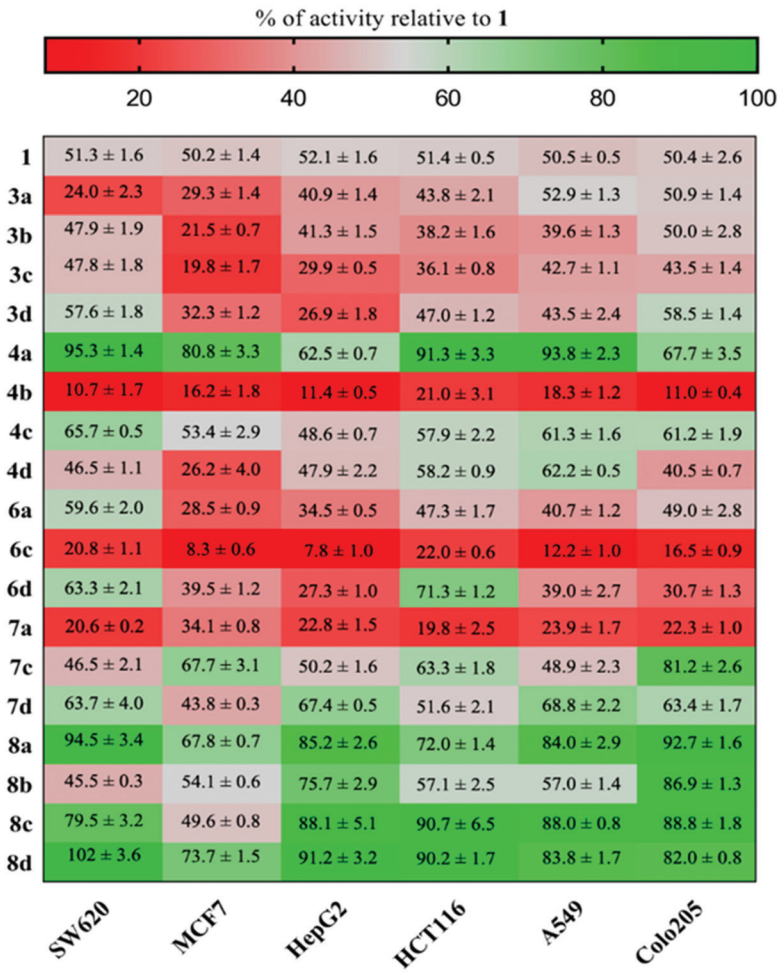

Fig. 4 Antiproliferative activity of the synthesized compounds in comparison to **1**. All compounds were administered at concentrations equal to the IC_{50} values of 1 in the respective cell lines (51.0 μM (A549), 112 μM (Colo 205), 78.1 μM (Hep G2), 41.9 μM (HCT 116), 29.4 μM (MCF7), and 84.7 μM (SW620)). The results are presented as relative viability compared to non-treated controls (mean value ± SD from three independent experiments).

Table 3 Cytotoxicity of the ferrocenyl analogs of monastrol (**3a–d**, **6a**, **6c** and **6d**) and of oxo-monastrol (**4b**, **4d** and **7a**) in cancer cell lines. IC_{50} values are presented with the respective 95% confidence intervals given in brackets. Data presented are derived from three independent experiments

Compound	A549	Colo 205	Hep G2	HCT 116	MCF7	SW620
1	51.0 [42.0–63.4]	>100	78.1 [52.8–182.3]	41.9 [33.7–53.6]	29.4 [20.5–44.9]	84.7 [64.4–120]
3a	**75.8 [44.1–218.2]**	**37.3 [28.9–47.4]**	**6.20 [3.94–9.88]**	**80.8 [64.0–107.8]**	**26.1 [21.8–31.0]**	**50.6 [44.0–58.8]**
3b	11.4 [8.16–16.0]	24.9 [17.5–37.2]	5.38 [4.22–6.84]	17.7 [15.1–20.9]	5.38 [4.35–6.61]	21.3 [16.2–28.7]
3c	16.5 [12.1–23.1]	34.5 [26.3–46.9]	31.5 [24.6–41.8]	32.5 [24.7–44.0]	6.57 [5.62–7.72]	41.5 [36.5–47.4]
3d	6.71 [5.45–8.29]	14.6 [11.5–19.0]	10.2 [9.14–11.5]	23.3 [17.2–32.8]	1.13 [0.81–1.57]	65.1 [50.4–87.2]
4b	**6.40 [5.15–7.94]**	**6.53 [5.29–8.05]**	**5.95 [4.73–7.47]**	**6.95 [5.73–8.43]**	**6.41 [5.16–7.96]**	**8.97 [7.09–11.3]**
4d	>100	72.3 [52.6–187]	52.9 [42.9–67.2]	50.5 [39.2–67.7]	14.8 [11.1–20.0]	54.1 [45.1–66.1]
6a	37.1 [25.9–56.7]	34.6 [20.3–39.9]	12.8 [9.23–17.6]	51.6 [46.1–57.9]	11.2 [9.04–13.9]	38.7 [31.1–18.9]
6c	**3.58 [2.91–4.40]**	**3.64 [2.88–4.59]**	**2.39 [2.10–2.73]**	**3.54 [3.09–4.06]**	**4.02 [3.34–4.83]**	**7.19 [4.59–11.1]**
6d	14.5 [13.2–15.9]	14.9 [11.0–18.8]	11.5 [8.23–15.10]	6.68 [5.69–7.84]	NA	14.2 [12.1–16.6]
7a	24.8[a]	21.9[a]	21.3[a]	23.3[a]	21.7 [18.7–25.5]	25.9 [20.4–34.3]

[a] The 95% confidence intervals were too wide to be precisely calculated by the software.

Notably, their activity strongly depended on the ferrocenyl substituents and the type of heteroatom at C-2. For example, a simple replacement of the 3-hydroxyphenyl moiety in **1** with a ferrocenyl group (**3a**) resulted only in slightly increased antiproliferative potency towards Colo 205, HepG2 and SW620 cells. The biological activity of type I analogs could be further increased by substituting the 3-hydroxyphenyl group in **1** with a ferrocenylphenyl moiety, with the most active representative being the ferrocenylphenyl compounds **3b** and **3d**. Exchanging the sulfur atom for oxygen usually diminished the biological potency of the type I compounds (**3a–d** *vs.* **4a–d**; Fig. 4 and Table 3) with one significant exception being **4b** bearing a 2-ferrocenylphenyl moiety instead of the 3-hydroxyphenyl group. Also, replacing the 6-methyl group in **1** with ferrocenyl or ferrocenylphenyl moieties in compounds **6a**, **6c**, **6d** and **7a** (Table 3) significantly affected the biological activity of type II compounds. The thiones exhibited substantially higher activity than **1**, while only one oxo-analog **7a** exerted moderate activity. It should be noted that the **6c**, bearing a 3-ferrocenylphenyl moiety instead of the 6-methyl group, exhibited the highest antiproliferative potency towards all studied cell lines with IC_{50} values in the low micromolar range. Overall, MCF7 and Hep G2 cells were more sensitive to the investigated compounds while the colorectal and lung cancer cell lines were usually slightly more resistant.

Activity of the multidrug resistance pumps can be an obstacle in delivering a drug into the target cell. Therefore, we studied the biological potency of the compounds in cells overexpressing various ABC transporters responsible for MDR. The synthesized compounds were more active than **1** with the exception of **3a** and **4d** in SW620M and SW620V cells (Table 4). However, no clear effect of MDR pump overexpression on cell sensitivity was observed, neither in case of **1** nor its analogs. The overall pattern of activity in MDR cells was identical to that observed in non-MDR cell lines. Based on these results, we have selected compounds **3a**, **4b** and **6c** for more detailed studies on their biological activity.

KSP inhibition

Kinesins utilize ATP to slide along microtubules and therefore their activity can be assessed by measuring the ATP hydrolysis rate. Since **1** is known to be a specific inhibitor of KSP activity, we tested compounds **3a**, **4b** and **6c** in comparison to **1** for their inhibitory activity on KSP at a concentration of 10 μM. Kinesin inhibition was determined with the Kinesin ATPase Endpoint Biochem kit. The residual KSP ATPase activity was two times

Table 4 Cytotoxicity of the ferrocenyl analogs of monastrol (**3a–d**, **6a**, **6c** and **6d**) and of oxo-monastrol (**4b**, **4d** and **7a**) in MDR cancer cell lines. IC_{50} values are presented with the respective 95% confidence intervals given in brackets. Data presented are derived from three independent experiments

Compound	SW620	SW620C	SW620D	SW620E	SW620M	SW620V
1	84.7 [64.4–120]	85.8 [79.9–134.1]	>100	86.8 [61.2–139]	33.5 [29.8–37.8]	45.9 [34.9–62.9]
3a	**50.6 [44.0–58.8]**	**37.2 [30.0–46.8]**	**20.9 [13.7–31.6]**	**28.0 [23.1–33.7]**	**45.0 [36.6–56.0]**	**63.7 [41.5–113]**
3b	21.3 [16.2–28.7]	24.0 [18.2–32.7]	11.1 [8.53–14.42]	17.1 [11.4–26.1]	19.1 [13.6–27.7]	38.9 [22.8–81.0]
3c	41.5 [36.5–47.4]	68.3 [55.5–87.0]	35.3 [30.3–41.7]	26.5 [22.2–32.0]	32.4 [26.1–40.9]	21.1 [17.3–26.1]
3d	65.1 [50.4–87.2]	34.1 [25.7–46.8]	17.8 [15.1–21.0]	20.4 [15.6–27.3]	12.4 [10.4–14.9]	10.2 [8.28–12.7]
4b	**8.97 [7.09–11.3]**	**10.9 [9.07–13.3]**	**13.0 [10.94–15.5]**	**12.0 [9.75–14.8]**	**8.72 [6.59–11.6]**	**17.4 [15.0–20.3]**
4d	54.1 [45.1–66.1]	46.9 [34.3–68.0]	56.2 [39.3–86.6]	52.9 [41.0–71.0]	48.4 [40.0–59.8]	65.2 [50.2–88.9]
6a	38.7 [31.1–18.9]	29.3 [23.2–36.6]	22.9 [17.7–29.2]	19.3 [14.4–25.4]	18.9 [11.7–31.3]	12.7 [9.95–16.1]
6c	**7.19 [4.59–11.1]**	**3.19 [2.37–4.26]**	**5.02 [3.69–6.81]**	**4.68 [3.41–6.41]**	**9.42 [7.59–11.7]**	**4.99 [4.18–5.96]**
6d	14.2 [12.1–16.6]	8.40 [7.01–10.1]	16.6 [12.2–22.5]	23.0 [18.6–27.9]	14.3 [10.2–19.9]	15.5 [1.98–19.9]
7a	25.9 [20.4–34.3]	19.7 [16.9–23.0]	32.2 [26.5–39.6]	25.4[a]	25.5 [21.1–31.4]	27.3 [23.7–32.0]

[a] The 95% confidence intervals were too wide to be precisely calculated by the software.

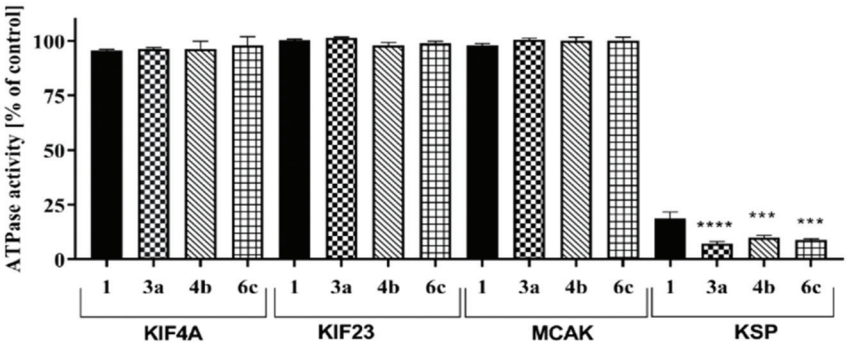

Fig. 5 Relative ATPase activity in presence of 10 μM of **1**, **3a**, **4b** and **6c**. Solvent control activity was referred to as 100%. Data are presented as mean ± SEM, n = 3 or 4 (in case of KSP). Data analyzed by one-way ANOVA and *post hoc* Tukey's test. *** $P < 0.001$, **** $P < 0.0001$.

lower in case of ferrocenyl analogs (**3a** – 7.2%, **4b** – 8.8% and **6c** – 9.8%) than in case of **1** (18.7%) (Fig. 5). To assess whether such effects were selective towards KSP, we used also other motor proteins, kinesin 4 family motor (KIF4A), kinesin-like protein KIF23 and mitotic centromere-associated kinesin (MCAK) but none of the compounds inhibited these proteins. It must be stressed here that the nucleotide binding sequence of all four proteins is highly conserved as revealed by the UniProt alignment tool. It is therefore unlikely that the compounds interact with the ATP-binding domain of KSP in which case they would inhibit all the other proteins too. Thus, it must be implied that the investigated modifications of the core structure do not alter the specificity of the monastrol analogs.

ROS generation

The antiproliferative activity of ferrocenyl compounds is believed to be associated with their increased ability to generate reactive oxygen species (ROS) in target cells.[36] To verify the hypothesis that introducing a ferrocenyl moiety to **1** impacts the mechanism of action, we investigated the ability of **3a**, **4b** and **6c** to induce intracellular ROS formation (Fig. 6). The rate of dihydrorhodamine 123 oxidation was considered the indicator for ROS production in SW620 cells. Compounds **4b** and **6c** were approximately 25% more active in terms of ROS generation than **1**, which supports the hypothesis of ROS involvement in the anticancer activity of such ferrocenyl compounds.

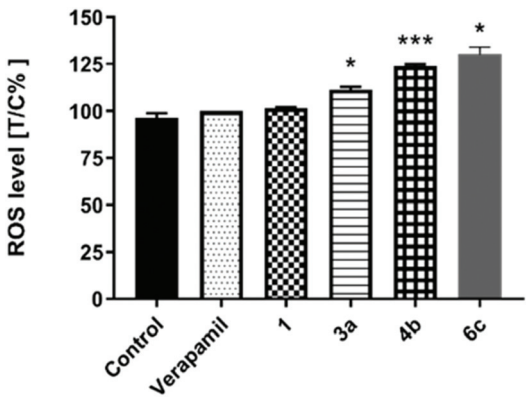

Fig. 6 ROS induction by **3a**, **4b** and **6c** in SW620 cells as compared to verapamil, an ABCB1 inhibitor used to increase rhodamine 123 retention in vulnerable cells, and **1**. Data presented as means ± SEM, n = 3. Data analysed by one-way ANOVA and *post hoc* Tukey's test. * $P < 0.05$, *** $P < 0.001$.

Effect on the cell cycle distribution

As a KSP inhibitor, **1** leads to the formation of monopolar mitotic spindles and chromosome segregation blockade in cancer cells. Flow cytometry was used to assess the cell cycle distribution and in particular to monitor an increase in G_2/M phase cells (Table 5). SW620 and SW620V cells, the latter being twice as sensitive to **1** than the parental SW620 cells were exposed to **4b** and **6c** for 24 h to detect the potential detrimental effects of ROS formation. We did not observe any signs of mitotic arrest in the cells exposed either to **1** or its ferrocenyl analogs. This is not really surprising considering the typical length of human cancer cell cycle ranging between 20 and 24 hours, and the incubation period being relatively short. Indeed, pronounced effects of monastrol are observed after 48-hour exposure – twice the length of the cell cycle duration.[66] However, an increased number of apoptotic cells (sub-G_1 fraction) and a reduced percentage of cells in the G_0/G_1 phase could be clearly seen, especially in SW620 cells exposed to **4b**

Table 5 Cell cycle distribution in SW620 and SW620V cells after treatment with monastrol **1** and its ferrocenyl derivatives **3a**, **4b** and **6c** at a concentration equal to the IC_{90} value of **1** for SW620. Compounds were used at concentrations equal to the respective IC_{90} values. Data presented as means ± SEM, n = 3

Cell line		Sub-G_1	G_0/G_1	S	G_2/M
SW620	ctrl	0.9 ± 0.2	73.7 ± 4.0	13.9 ± 2.6	12.1 ± 1.5
	1	12.4 ± 4.1	63.4 ± 3.4	10.9 ± 3.2	11.1 ± 1.7
	3a	15.7 ± 4.6	65.2 ± 5.7	10.0 ± 3.4	9.8 ± 2.5
	4b	28.2 ± 2.6	50.6 ± 2.8	13.2 ± 4.4	8.0 ± 2.3
	6c	32.1 ± 3.8	45.4 ± 6.7	13.5 ± 1.8	9.3 ± 2.3
SW620V	ctrl	1.1 ± 0.2	75.2 ± 5.0	13.8 ± 2.8	9.0 ± 3.0
	1	5.5 ± 2.2	69.7 ± 7.9	12.3 ± 4,5	10.0 ± 2.1
	3a	6.6 ± 3.2	68.0 ± 6.0	10.9 ± 5.4	11.4 ± 2.8
	4b	11.7 ± 1.9	61.0 ± 5.7	10.4 ± 4.0	11.2 ± 2.3
	6c	12.6 ± 2.2	62.8 ± 8.9	10.3 ± 2.2	13.9 ± 2.6

and **6c**. Such short-term effects support the potential role of ROS formation in the biological activity of the compounds studied.

Docking studies

Molecular modeling was used to investigate the possible binding mode for the ferrocenyl monastrol and oxo-monastrol derivatives. Docking of the (*R*)- and (*S*)-enantiomers of the ferrocenyl derivatives **3a–7d** revealed that the docking is largely independent whether the compound derived of dihydropyrimidin-2(1*H*)-one or a dihydropyrimidin-2(1*H*)-thione (ESI†) and similar predicted binding modes and intermolecular interactions were found.[67] In general, the (*S*)-enantiomers showed higher predicted binding affinities than the (*R*)-isomers (Table 6). The latter have relatively weak pose prediction consistencies between docking runs, *i.e.*, the algorithm predicts many different poses. Several of these configurations were regarded to be implausible, *e.g.*, the 3-hydroxyphenyl ring being predicted to be in the aqueous phase. These results are suggestive of weak binding affinities and biological effects for the (*R*)-isomers. Evidence of this is apparent as Maliga *et al.*[68] demonstrated (*S*)-1 has ~15 times greater potency than its enantiomeric counterpart, (*R*)-1.

Molecular docking revealed that most of the (*S*)-isomers with 6-(ferrocenylphenyl) substituents (**6c**, **6d** and **7d**) retained similar binding poses and intermolecular interactions comparable to (*S*)-monastrol, *e.g.*, the docked configuration of (*S*)-**6c** (Fig. 7A); the 3-hydroxyphenyl moiety remained in the hydrophobic cavity, the thione facing Ile136, and most of the main hydrogen bonding interactions were retained, *i.e.*, the 3-NH tetrahydropyrimidine formed a hydrogen bond with Glu116 and the phenol with Glu118. The introduced 6-(ferrocenylphenyl) moiety is predicted to be outside of the allosteric pocket but is situated close to the hydrophobic regions partly formed by Ala218 and the alkyl side chain of Arg221 where they are expected to form favorable hydrophobic contacts. In contrast to the 4-ferrocenyl or 4-(ferrocenylphenyl) derivatives (**3a–4d**), there is a lack of key predicted hydrogen bonding patterns resulting from the occupation of the ferrocenyl moiety of the hydrophobic cavity and the resulting change in the tetrahydropyrimidine ring orientation, indeed it is pointing out of the binding pocket (Fig. 7B). Additionally, the thione functional group faces away from Ile136 and the ethanoate is directed towards the allosteric cavity. These poses have reversed the position of the ligands as compared to (*S*)-**1**, depriving them of good binding within the allosteric pocket. They lack a favorable mix of hydrogen bonding for specificity and lipophilic contacts for affinity.[69]

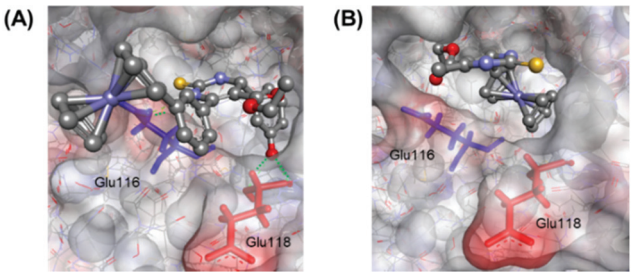

Fig. 7 Docked configurations of (*S*)-**6c** (A) and (*S*)-**3a** (B). The predicted hydrogen bonds are depicted as green dotted lines between the derivative and the residues Glu116 (blue) and Glu118 (red). The protein surface is rendered. Red, blue and grey regions represents partially negative, positive and hydrophobic regions. Hydrogen atoms are hidden for clarity.

Table 6 Docking scores (GS) of ferrocenyl monastrol derivatives

	GS	
Compounds	(*S*)-Isomer	(*R*)-Isomer
Monastrol	60.0	49.9
oxo-monastrol	61.4	55.8
3a	45.2	49.2
3b	59.9	57.2
3c	63.0	57.6
3d	58.5	52.6
4a	45.3	49.5
4b	55.7	52.3
4c	56.0	51.9
4d	53.7	47.3
6a	56.5	52.2
6b	53.3	54.7
6c	56.7	62.2
6d	64.5	32.6
7a	52.0	45.9
7b	58.3	53.6
7c	53.9	59.7
7d	59.5	61.3

The 6-(ferrocenylphenyl) substituted compounds **6c** and **6d** were the most cytotoxic derivatives (Table 3). The molecular modeling results indicate that the substitution of the 3-hydroxyphenyl group with the 4-(ferrocenylphenyl) moiety leads to different orientations of the derivatives thus impairing hydrogen bonding networks within the allosteric cavity. Derivative **4b** contradicts this interpretation as it has good cytotoxic potency (Table 3); it can be speculated that **4b** does not occupy the allosteric pocket but exerts its biological effect by other means.

Conclusion

In conclusion, we report a series of systematically-modified ferrocenyl derivatives of monastrol and oxo-monastrol which were evaluated for their antiproliferative activity and we aimed to rationalize the results by a series of complementary biological studies inspired the biological activity of monastrol. We found that introducing a ferrocenyl moiety leads to a broad spectrum of activity towards all the investigated cells including the MDR panel cell lines. The derivatives **3a**, **4b** and **6c** inhibited KSP with the highest potency. The higher cytotoxic activity of **4b** and **6c** is in agreement with their ability to induce ROS generation, and their pro-apoptotic effects. These data suggest that the cytotoxic potency of the compounds is related also to

the level of ROS generation, not only to KSP inhibition, which suggests an additional mechanism of action. Based on docking studies, we cannot explain the higher activity of oxomonastrol **4b** in relation to monastrol **3b**. Interestingly, we found that the replacement of the 3-hydroxyphenyl group by a 4-ferrocenylphenyl group induces the high antiproliferative activity towards the MCF7 breast cancer cell line, which is currently being further investigated.

Experimental

Synthesis

General information. All reactions were carried out under argon atmosphere using Schlenk line. Compounds **2b–d** [58] and **5a** [62] were prepared as described previously. ^{1}H, ^{13}C{^{1}H} and 2D NMR spectra were recorded on a Bruker ARX 600 MHz NMR spectrometer. Chemical shifts for the ^{1}H NMR spectra are referenced relative to residual protons in the deuterated solvent ($CDCl_3$ δ = 7.27 ppm for ^{1}H and δ = 77.0 ppm for ^{13}C; DMSO-d_6 δ = 2.50 ppm for ^{1}H and δ = 39.5 ppm for ^{13}C). Spectra were recorded at 294 K, chemical shifts are in ppm and coupling constants in Hz. Thin-layer chromatography (TLC) was performed on aluminum sheets pre-coated with Merck 5735 Kieselgel 60 F254. Column chromatography was carried out with SilicaFlash® P60 for flash chromatography (0.040–0.063 mm, 230–400 mesh). The purity of the compounds was confirmed by elemental analysis and HPLC-MS analysis, and it was higher than 95%. HPLC-MS analysis was performed on a Shimadzu UHPLC Nexera XR system equipped with Shimadzu PDA (SPD-M40) and LCMS-2020 detectors on a Phenomenex Kinetex 1.7 μm XB-C18 100 Å column (50 × 2.1 mm) with water containing 0.01% of formic acid (eluent A) and methanol with 0.01% of formic acid (eluent B) as the mobile phase with a gradient of B starting at 10% which increased to 60% of B within 10 min, reached 10% at 11 min and was followed by a hold time at 10% B until 17 min, at a flow rate of 0.4 mL min^{-1}. UV-VIS spectra were recorded in the range of 220–700 nm, and MS data were recorded in ESI+ mode from m/z 100 to 1000 at a scan speed of 15 000 u s^{-1} and with an event time of 0.07 s.

General procedure A – synthesis of ferrocenyl β-ketoesters 5b–d. An aldehyde (1 eq.) and 5% mol of $NbCl_5$ were dissolved in anhydrous dichloromethane (10 mL per 1 mmol of aldehyde) and 1.2 eq. of ethyl diazoacetate was added to the resulting solution. After stirring at RT for 48 h, the reaction was quenched by addition of water, and the product was extracted with dichloromethane. The organic phase was dried over sodium sulfate, evaporated to dryness and the product was isolated by column chromatography on silica using a gradient of ethyl acetate in hexane as the eluent.

General procedure B – synthesis of compounds 3a–d and 4a–d and 8a–d. Aldehydes **2a–d** (2.0 mmol), ethyl acetoacetate (2.2 mmol, 286 mg, 280 μl) and thiourea (3.0 mmol, 228 mg) or urea (3.0 mmol, 180 mg) were placed in a flask containing 10 mL of anhydrous ethanol. After 3 min of stirring, powdered $SbCl_3$ (2.0 mmol, 456 mg) was added and the resulting solution was stirred at RT for 3 days. The volatiles were evaporated and **3a–d** or **8a–d** were isolated by column chromatography on silica gel using a gradient of methanol in dichloromethane starting from 0 to 1% of methanol. Compounds **4a–d** were obtained by dissolving the residue, which was obtained after evaporation of ethanol, in 20 mL of dichloromethane. The organic phase was washed twice with equal amounts of 5% hydrochloric acid, dried over sodium sulfate, and evaporated to dryness. The crude product was purified by column chromatography on silica gel using a gradient of methanol in dichloromethane starting from 0 to 1% of methanol.

General procedure C – synthesis of compounds 6a, 6c, 6d and 7a. Compounds **6a**, **6c**, **6d** and **7a** were synthesized according to a modified version of general procedure B. The reaction mixture was stirred at 40 °C and the products were isolated by column chromatography on silica gel using a gradient of methanol in dichloromethane starting from 0 to 1% of methanol.

General procedure D – synthesis of compounds 7c and 7d. Compound **5c** or **5d** (1.33 mmol, 700 mg), urea (1.33 mmol, 80 mg), 3-hydroxybenzaldehyde (1.33 mmol, 160 mg) and Yb$(OTf)_3$ (80 mg) were placed in a 10 mL reaction vial with a magnetic stir bar. After addition of 2,2,2-trifluoroethanol (3 mL), the reaction vial was closed with a cap and placed in the microwave reactor. The reaction mixture was stirred at 100 °C (temperature control, heating ASAP). After 30 min, the reaction mixture was cooled to 50 °C and the solvent was evaporated to dryness. The residue was dissolved in 25 mL of chloroform, the organic solution was washed with 5% HCl, dried over sodium sulfate and evaporated to dryness. The product was isolated by column chromatography on silica gel using chloroform–methanol. The fractions containing the products were purified on silica gel using 1% methanol in chloroform.

3a. This compound was synthesized in 49% yield (380 mg) starting from 428 mg (2.0 mmol) of **2a** and thiourea according to **general procedure B**. Elemental analysis (%) calculated for $C_{18}H_{20}FeN_2O_2S$ C 56.26, H 5.25, N 7.29, S 8.34% found C 56.26, H 5.33, N 7.35, S 8.24; ^{1}H NMR (DMSO-d_6, 600.3 MHz) δ = 10.35 (s, 1H, H-1), 9.39 (d, J = 4.2 Hz, 1H, H-3), 4.92 (d, J = 4.4 Hz, 1H, H-4), 4.24 (s, 5H, Cp′), 4.15–4.07 (m, 5H, $COCH_2CH_3$ and Cp), 3.92 (br s, 1H, Cp), 2.20 (s, 3H, CH_3), 1.22 (t, J = 7.1 Hz, 3H, $COCH_2CH_3$), ^{13}C{^{1}H} NMR (DMSO-d_6, 150.1 MHz) δ = 174.8 (C-2), 165.3 ($COCH_2CH_3$), 144.3 (C-6), 102.2 (C-5), 92.5 (Cp_{ipso}), 68.6 (Cp′), 67.3 (2×, Cp), 66.2 (Cp), 65.1 (Cp), 59.7 ($COCH_2CH_3$), 49.0 (C-4), 17.0 (CH_3), 14.2 ($COCH_2CH_3$); HPLC-MS τ_1 = 10.8 min m/z calculated for $C_{18}H_{20}FeN_2O_2S$ 384.1 $[M]^+$ found 384.1 $[M]^+$, τ_2 = 11.1 min m/z calculated for $C_{18}H_{20}FeN_2O_2S$ 384.1 $[M]^+$ found 384.1 $[M]^+$.

3b. This compound was synthesized in 53% yield (488 mg) starting from 580 mg (2.0 mmol) of **2b** and thiourea according to **general procedure B**. Elemental analysis calculated (%) for $C_{24}H_{24}FeN_2O_2S$ C 62.62, H 5.25, N 6.09, S 6.96 found C 62.71, H 5.31, N 6.30, S 6.84; ^{1}H NMR (DMSO-d_6, 600.3 MHz) δ = 10.25 (s, 1H, H-1), 9.61 (br s, 1H, H-3), 7.86 (dd, J = 7.7, 1.2 Hz, 1H, CH_{Ar}), 7.30–7.27 (m, 1H, CH_{Ar}), 7.26–7.23 (m, 1H, CH_{Ar}), 7.22–7.20 (m, 1H, CH_{Ar}), 5.56 (d, J = 2.7 Hz, 1H, H-4), 5.04–5.03

(m, 1H, Cp), 4.47–4.45 (m, 1H, Cp), 4.35–4.34 (m, 1H, Cp), 4.32–4.31 (m, 1H, Cp), 4.16 (s, 5H, Cp′), 3.75–3.69 (m, 1H, $COCH_2CH_3$), 3.63–3.58 (m, 1H, $COCH_2CH_3$), 2.23 (s, 3H, CH_3), 0.75 (t, J = 7.1 Hz, 3H, $COCH_2CH_3$); $^{13}C\{^1H\}$ NMR (DMSO-d_6, 150.1 MHz) δ = 173.8 (C-2), 164.7 ($COCH_2CH_3$), 144.0 (C-6), 142.3 (C_{Ar}), 136.4 (C_{Ar}), 131.5 (CH_{Ar}), 127.4 (CH_{Ar}), 127.2 (CH_{Ar}), 127.1 (CH_{Ar}), 102.0 (C-5), 87.2 (Cp_{ipso}), 71.7 (Cp), 69.4 (Cp′), 69.9 (Cp), 67.8 (Cp), 67.7 (Cp), 58.8 ($COCH_2CH_3$), 50.6 (C-4), 16.9 (CH_3), 14.0 ($COCH_2CH_3$); HPLC-MS, τ_1 = 12.6 min, m/z calculated for $C_{24}H_{24}FeN_2O_2S$ 460.1 $[M]^+$ found 460.2 $[M]^+$, τ_2 = 13.4 min, m/z found 460.1 $[M]^+$ (calculated for $C_{18}H_{20}FeN_2O_2S$ 460.1 $[M]^+$).

3c. This compound was synthesized in 76% yield (699 mg) starting from 580 mg (2.0 mmol) of **2c** and thiourea according to **general procedure B**. Elemental analysis calculated (%) for $C_{24}H_{24}FeN_2O_2S$ C 62.62, H 5.25, N 6.09, S 6.96 found C 62.73, H 5.38, N 6.16, S 6.71; ^1H NMR (DMSO-d_6, 600.3 MHz) δ = 10.40 (s, 1H, H-1), 9.71 (d, J = 3.0 Hz, 1H, H-3), 7.41 (br s, 1H, CH_{Ar}), 7.39 (d, J = 7.7 Hz, 1H, CH_{Ar}), 7.25 (t, J = 7.6 Hz, 1H, CH_{Ar}), 7.04 (d, J = 7.7 Hz, 1H, CH_{Ar}), 5.20 (d, J = 3.6 Hz, 1H, H-4), 4.66–4.65 (m, 2H, Cp), 4.34 (br s, 2H, Cp), 4.08–4.03 (m, 2H, $COCH_2CH_3$), 4.02 (s, 5H, Cp′), 2.31 (s, 3H, CH_3), 1.14 (t, J = 7.1 Hz, 3H, $COCH_2CH_3$); $^{13}C\{^1H\}$ NMR (DMSO-d_6, 150.1 MHz) δ = 174.5 (C-2), 165.2 ($COCH_2CH_3$), 145.0 (C-6), 143.6 (C_{Ar}), 139.2 (C_{Ar}), 128.6 (CH_{Ar}), 125.2 (CH_{Ar}), 124.4 (CH_{Ar}), 123.8 (CH_{Ar}), 101.0 (C-5), 84.9 (Cp_{ipso}), 69.5 (Cp′), 68.9 (2×, Cp), 66.5 (Cp), 66.4 (Cp), 59.6 ($COCH_2CH_3$), 53.9 (C-4), 17.2 (CH_3), 14.1 ($COCH_2CH_3$); HPLC-MS, τ_1 = 12.4 min, m/z found 460.1 $[M]^+$, τ_2 = 12.8 min, m/z found 460.0 $[M]^+$ (calculated for $C_{24}H_{24}FeN_2O_2S$ 460.1 $[M]^+$).

3d. This compound was synthesized in 23% (212 mg) yield starting from 580 mg (2.0 mmol) of **2d** and thiourea according to **general procedure B**. Elemental analysis calculated (%) for $C_{24}H_{24}FeN_2O_2S$ C 62.62, H 5.25, N 6.09, S 6.96 found C 63.93, H 5.74, N 6.16, S 6.16; ^1H NMR (DMSO-d_6, 600.3 MHz) δ = 10.34 (s, 1H, H-1), 9.66 (d, J = 2.9 Hz, 1H, H-3), 7.51 (d, J = 8.3 Hz, 2H, CH_{Ar}), 7.13 (d, J = 8.3 Hz, 2H, CH_{Ar}), 5.14 (d, J = 3.6 Hz, 1H, H-4), 4.75 (t, J = 1.8 Hz, 2H, Cp), 4.33 (t, J = 1.8 Hz, 2H, Cp), 4.07–3.97 (m, 2H, $COCH_2CH_3$) overlapped with 4.00 (s, 5H, Cp′), 2.30 (s, 3H, CH_3), 1.10 (t, J = 7.1 Hz, 3H, $COCH_2CH_3$); $^{13}C\{^1H\}$ NMR (DMSO-d_6, 150.1 MHz) δ = 174.1 (C-2), 165.2 ($COCH_2CH_3$), 144.9 (C-6), 141.1 (C_{Ar}), 138.5 (C_{Ar}), 126.5 (CH_{Ar}), 126.1 (CH_{Ar}), 100.7 (C-5), 84.5 (Cp_{ipso}), 69.3 (Cp′), 68.9 (Cp), 66.4 (Cp), 66.3 (Cp), 59.6 ($COCH_2CH_3$), 53.9 (C-4), 17.2 (CH_3), 14.1 ($COCH_2CH_3$); HPLC-MS, τ_1 = 12.4 min, m/z found 460.1 $[M]^+$, τ_2 = 12.8 min, m/z found 460.2 $[M]^+$ (m/z calculated for $C_{24}H_{24}FeN_2O_2S$ 460.1 $[M]^+$).

4a. This compound was synthesized in 72% yield (320 mg) starting from 428 mg (2.0 mmol) of **2a** and urea according to **general procedure B**. The product was isolated as a yellow powder by column chromatography on silica with dichloromethane/methanol 99/1 as the eluent. Elemental analysis calculated (%) for $C_{18}H_{20}FeN_2O_3$ C 58.72, H 5.48, N 7.61 found C 58.43, H 5.55, N 7.61; ^1H NMR (DMSO-d_6, 600.3 MHz) δ = 9.13 (br s, 1H, H-1), 7.50 (br s, 1H, NH, H-3), 4.95 (br s, 1H, H-4), 4.19 (s, 5H, Cp′), 4.09 (br s, 2H, $COCH_2CH_3$), 4.08 (br s, 3H, Cp), 3.94 (s, 1H, Cp), 2.15 (s, 3H, CH_3), 1.23 (br s, 3H, $COCH_2CH_3$); $^{13}C\{^1H\}$ NMR (DMSO-d_6, 150.1 MHz) δ = 165.6 ($COCH_2CH_3$), 153.1 (C-2), 147.5 (C-6), 100.8 (C-5), 93.8 (Cp_{ispo}), 68.5 (Cp′), 67.2 (Cp), 67.0 (Cp), 65.9 (Cp), 65.1 (Cp), 59.4 ($COCH_2CH_3$), 48.7 (C-4), 17.7 (CH_3), 14.3 ($COCH_2CH_3$); HPLC-MS, τ_1 = 9.2 min, m/z found 367.9 $[M]^+$, τ_2 = 9.5 min, m/z found 367.9 $[M]^+$ (m/z calculated for $C_{18}H_{20}FeN_2O$ 368.1 $[M]^+$).

4b. This compound was synthesized in 79% yield (710 mg) starting from 580 mg (2.0 mmol) of **2b** and urea according to **general procedure B**. The product was isolated as a yellow powder by column chromatography on silica with dichloromethane/methanol 99/1 as the eluent. Elemental analysis calculated (%) for $C_{24}H_{24}FeN_2O_3$ C 64.88, H 5.44, N 6.31 found C 64.97, H 5.61, N 6.41; ^1H NMR (DMSO-d_6, 600.3 MHz) δ = 9.14 (s, 1H, H-1), 7.84 (d, J = 7.5 Hz, 1H, CH_{Ar}), 7.55 (br s, 1H, H-3), 7.27–7.21 (m, 3H, CH_{Ar}), 5.49 (d, J = 2.1 Hz, 1H, H-4), 4.85 (br s. 1H, Cp), 4.45–4.44 (m, 1H, Cp), 4.34–4.33 (m, 1H, Cp), 4.31–4.30 (m, 1H, Cp), 4.17 (s, 5H, Cp′), 3.73–3.68 (m, 1H, $COCH_2CH_3$), 3.66–3.60 (m, 1H, $COCH_2CH_3$), 2.22 (s, 3H), 0.75 (t, J = 7.1 Hz, 3H, $COCH_2CH_3$); $^{13}C\{^1H\}$ NMR (DMSO-d_6, 150.1 MHz) δ = 164.9 ($COCH_2CH_3$), 151.6 (C-2), 147.8 (C-6), 143.4 (C_{Ar}), 136.1 (C_{Ar}), 131.4 (CH_{Ar}), 127.0 (CH_{Ar}), 126.8 (CH_{Ar}), 126.7 (CH_{Ar}), 100.1 (C-5), 87.4 (Cp_{ipso}), 71.5 (Cp), 69.4 (Cp′), 68.9 (Cp), 67.7 (Cp), 67.5 (Cp), 58.5 ($COCH_2CH_3$), 50.4 (C-4), 17.6 (CH_3), 14.0 ($COCH_2CH_3$); HPLC-MS, τ_1 = 11.2 min, m/z found 444.1 $[M]^+$, τ_2 = 11.5 min, m/z found 444.1 $[M]^+$ (m/z calculated for $C_{24}H_{24}FeN_2O_3$ 444.1 $[M]^+$).

4c. This compound was synthesized in 78% yield (700 mg) starting from 580 mg (2.0 mmol) of **2c** and urea according to **general procedure B**. The product was isolated as a yellow powder by column chromatography on silica with dichloromethane/methanol 99/1 as the eluent. Elemental analysis calculated (%) for $C_{24}H_{24}FeN_2O_3$ C 64.88, H 5.44, N 6.31 found C 64.73, H 5.50, N 6.50; ^1H NMR (DMSO-d_6, 600.3 MHz) δ = 9.24 (d, J = 1.2 Hz, 1H, H-1), 7.80 (br s. 1H, H-3), 7.42 (br s, 1H, C_{Ar}), 7.37 (d, J = 7.7 Hz, 1H, CH_{Ar}), 7.23 (t, J = 7.6 Hz, 1H, CH_{Ar}), 7.07 (d, J = 7.7 Hz, 1H, CH_{Ar}), 5.17 (d, J = 3.3 Hz, 1H, H-4), 4.65 (t, J = 1.8 Hz, 2H, Cp), 4.34 (t, J = 1.8 Hz, 2H, Cp), 4.03–4.00 (m, 2H, $COCH_2CH_3$) overlapped with 4.01 (s, 5H, Cp′), 2.28 (s, 3H, CH_3), 1.13 (t, J = 7.1 Hz, 3H, $COCH_2CH_3$); $^{13}C\{^1H\}$ NMR (DMSO-d_6, 150.1 MHz) δ = 165.4 ($COCH_2CH_3$), 152.3 (C-2), 148.4 (C-6), 144.9 (C_{Ar}), 138.9 (C_{Ar}), 128.4 (CH_{Ar}), 124.9 (CH_{Ar}), 124.4 (CH_{Ar}), 123.7 (CH_{Ar}), 99.4 (C-5), 85.1 (Cp_{ipso}), 69.4 (Cp′), 68.8 (2×, Cp), 66.5 (Cp), 66.4 (Cp), 59.2 ($COCH_2CH_3$), 53.9 (C-4), 17.8 (CH_3), 14.1 ($COCH_2CH_3$); HPLC-MS, τ_1 = 11.1 min, m/z found 444.1 $[M]^+$, τ_2 = 11.4 min, m/z found 444.1 $[M]^+$ (m/z calculated for $C_{24}H_{24}FeN_2O_3$ 444.1 $[M]^+$).

4d. This compound was synthesized in 80% yield (718 mg) starting from 580 mg (2.0 mmol) of **2d** and urea according to **general procedure B**. The product was isolated as a dark yellow powder by column chromatography on silica with dichloromethane/methanol 99/1 as the eluent. Elemental analysis calculated (%) for $C_{24}H_{24}FeN_2O_3$ C 64.88, H 5.44, N 6.31 found C 64.81, H 5.63, N 6.60; ^1H NMR (DMSO-d_6, 600.3 MHz) δ = 9.20 (d, J = 1.3 Hz, 1H, H-1), 7.74 (s, 1H, H-3), 7.48 (d, J = 8.2 Hz, 2H, CH_{Ar}), 7.16 (d, J = 8.2 Hz, 2H, CH_{Ar}), 5.12 (d, J = 3.2 Hz,

1H, H-4), 4.73 (t, J = 1.8 Hz, 2H, Cp), 4.32 (t, J = 1.7 Hz, 2H, Cp), 4.03–3.96 (m, 2H, COCH_2CH$_3$) overlapped with 4.00 (s, 5H, Cp′), 2.26 (s, 3H, CH$_3$), 1.09 (t, J = 7.1 Hz, 3H, COCH$_2$CH_3); ^{13}C{^{1}H} NMR (DMSO-d$_6$, 150.1 MHz) δ = 165.4 (COCH$_2$CH$_3$), 152.2 (C-2), 148.3 (C-6), 142.4 (C$_{Ar}$), 138.0 (C$_{Ar}$), 126.3 (CH$_{Ar}$), 125.9 (CH$_{Ar}$), 99.2 (C-5), 84.7 (Cp$_{ipso}$), 69.3 (Cp′), 68.8 (2×, Cp), 66.3 (Cp), 66.2 (Cp), 59.2 (COCH$_2$CH$_3$), 53.8 (C-4), 17.9 (CH$_3$), 14.1 (COCH$_2$$CH_3$); HPLC-MS, τ_1 = 11.1 min, m/z found 444.0 [M]$^+$, τ_2 = 11.4 min m/z, found 444.1 [M]$^+$ (m/z calculated for $C_{24}H_{24}FeN_2O_3$ 444.1 [M]$^+$).

5b. This compound was synthesized in 20% yield (150 mg) starting from 580 mg (2.0 mmol) of **2b** according to **general procedure A**. The obtained product was immediately used in the next step. ^{1}H NMR (DMSO-d$_6$, 600.3 MHz) δ = 12.3 (s, OH$_{enol}$), 7.80 (d, J = 7.6 Hz, 1H, CH$_{Ar}$), 7.45 (t, J = 6.9 Hz, 1H, CH$_{Ar}$), 7.33–7.31 (m, 1H, CH$_{Ar}$), 7.29–7.27 (m, 1H, CH$_{Ar}$), 4.48 (br s, 2H, Cp), 4.36 (br s, 2H, Cp), 4.12 (br s, 5H, Cp′), 4.07 (q, J = 7.1 Hz, 2H, COCH_2CH$_3$), 1.28 (t, J = 7.1 Hz, 3H, COCH$_2$CH_3).

5c. This compound was synthesized in 63% yield (664 mg) starting from 812 mg (2.8 mmol) of **2c** according to **general procedure A**. The obtained product was immediately used in the next step. ^{1}H NMR (DMSO-d$_6$, 600.3 MHz) δ = 12.60 (s, 0.2 H, OH, enol), 8.00 (br s, 1H, CH$_{Ar}$), 7.77 (br s, 0.2 H, CH$_{Ar\text{-}enol}$), 7.72 (d, J = 7.4 Hz, 1H, CH$_{Ar}$), 7.65 (d, J = 6.6 Hz, 1H, CH$_{Ar}$), 7.54 (d, J = 7.4 H, 0.2 H, CH$_{Ar\text{-}enol}$), 7.46 (br s, 0.2 H, CH$_{Ar\text{-}enol}$), 7.38 (t, J = 7.0 Hz, 1H, CH$_{Ar}$), 7.30 (br s, 0.2 H, CH$_{Ar\text{-}enol}$), 5.67 (s, 0.2 H, CH$_{enol}$), 4.85 (br s, 0.5 H, Cp$_{enol}$), 4.77 (br s, 2H, Cp), 4.50 (br s, 0.5 H, Cp$_{enol}$), 4.44 (br s, 2H, Cp), 4.29 (q, J = 7.2 Hz, 0.7 H, COCH_2CH$_{3\text{-}enol}$), 4.24 (q, J = 7.0 Hz, 2H, CH_2CH$_3$), 4.19 (br s, 1H, Cp′$_{enol}$), 4.11 (br s., 5H, Cp′), 4.00 (s, 2H, COCH_2CO), 1.35 (t, J = 7.1 Hz, 0.6 H, COCH$_2$C$H_{3\text{-}enol}$), 1.28 (t, J = 7.1 Hz, 3H, COCH$_2$CH_3).

5d. This compound was synthesized in 74% yield (664 mg) starting from 709 mg (2.4 mmol) of **2d** according to **general procedure A**. The obtained product was immediately used in the next step. ^{1}H NMR (DMSO-d$_6$, 600.3 MHz) δ = 12.69 (s, 0.1 H, OH, enol), 7.87 (d, J = 8.5 Hz, 2 H, CH$_{Ar}$), 7.79 (d, J = 8.5 Hz, 0.4 H, CH$_{Ar\text{-}enol}$), 7.68 (d, J = 8.4 Hz, 2 H, CH$_{Ar}$), 7.63 (d, J = 8.5 Hz, 0.4 H, CH$_{Ar\text{-}enol}$), 5.97 (s, 0.2 H, =CH-$_{enol}$), 4.94 (t, J = 1.8 Hz, 2 H, Cp), 4.89 (t, J = 1.8 Hz, 0.4 H, Cp$_{enol}$), 4.46 (t, J = 1.8 Hz, 2 H, Cp), 4.43 (t, J = 1.8 Hz, 0.4 H, Cp$_{enol}$), 4.24 (q, J = 7.1 Hz, 0.4 H, CH_2CH$_{3\text{-}enol}$), 4.16 (s, 2 H, COCH_2COO), 4.12 (q, J = 7.1 Hz, 2 H, COCH_2CH$_3$), 4.03 (s, 5H, Cp′) 1.28 (t, J = 7.1 Hz, 0.6 H, COCH$_2$C$H_{3\text{-}enol}$), 1.18 (t, J = 7.1 Hz, 3 H, COCH$_2$CH_3).

6a. This compound was synthesized in 41% yield (380 mg) starting from 423 mg (2.0 mmol) of **2a** and thiourea according to **general procedure C**. Elemental analysis calculated (%) for $C_{23}H_{22}FeN_2O_3S$ C 59.75, H 4.80, N 6.06, S 6.93 found C 59.80, H 5.04, N 6.15, S 6.87; ^{1}H NMR (DMSO-d$_6$, 600.3 MHz) δ = 9.88 (d, J = 2.3 Hz, 1H, H-3), 9.50 (s, 1H, OH), 8.74 (br s, H-1), 7.16 (t, J = 7.8 Hz, 1H, CH$_{Ar}$), 6.74–6.73 (m, 2H, CH$_{Ar}$), 6.69 (dd, J = 8.0, 1.4 Hz, 1H, CH$_{Ar}$), 5.12 (d, J = 4.0 Hz, 1H, H-4), 4.80 (br s, 1H, Cp), 4.67 (br s, 1H, Cp), 4.44–4.43 (m, 2H, Cp), 4.26 (s, 5H, Cp′), 3.95 (q, J = 7.1 Hz, 2H, COCH_2CH$_3$), 1.01 (t, J = 7.1 Hz, 3H, COCH$_2$CH_3); ^{13}C{^{1}H} NMR (DMSO-d$_6$, 150.1 MHz) δ = 173.9 (C-2), 165.7 (COCH$_2$CH$_3$), 157.6 (C$_{Ar}$), 143.5 (C$_{Ar}$), 142.7 (C-6), 129.6 (CH$_{Ar}$), 116.9 (CH$_{Ar}$), 114.8 (CH$_{Ar}$), 113.3 (CH$_{Ar}$), 102.2 (C-5), 77.4 (Cp$_{ipso}$), 69.9 (Cp), 69.6 (Cp′), 69.5 (Cp), 69.4 (Cp), 69.3 (Cp), 59.9 (COCH$_2$CH$_3$), 54.7 (C-4), 13.8 (COCH$_2$$CH_3$); HPLC-MS, τ_1 = 10.7 min, m/z found 462.3 [M]$^+$, τ_2 = 10.9 min m/z found 463.0 [M + H]$^+$ (m/z calculated for $C_{23}H_{22}FeN_2O_3S$ 462.1 [M]$^+$, $C_{23}H_{22}FeN_2O_3$ + H$^+$ 463.1 [M + H]$^+$).

6c. This compound was synthesized in 29% yield (233 mg) starting from 664 mg (1.76 mmol) of **5c** and thiourea according to **general procedure C**. Elemental analysis calculated (%) for $C_{29}H_{26}FeN_2O_3S$ C 64.69, H 4.87, N 5.20, S 5.95 found C 65.41, H 5.44, N 5.18, S 5.60; ^{1}H NMR (DMSO-d$_6$, 600.3 MHz) δ = 10.50 (br s, 1H, H-1), 9.72 (br s, 1H, H-3), 9.56 (br s, 1H, OH), 7.61 (d, J = 7.7 Hz, 1H, CH$_{Ar}$), 7.39 (br s, 1H, CH$_{Ar}$), 7.33 (t, J = 7.6 Hz, 1H, CH$_{Ar}$), 7.20 (t, J = 7.9 Hz, 1H, CH$_{Ar}$), 7.11 (d, J = 7.5 Hz, 1H, CH$_{Ar}$), 6.83–6.82 (m, 2H, CH$_{Ar}$), 6.71 (d, J = 7.9 Hz, 1H, CH$_{Ar}$), 5.21 (d, J = 3.5 Hz, 1H, H-4), 4.81 (br s, 1H, Cp), 4.80 (br s, 1H, Cp), 4.36 (s, 2H, Cp), 4.07 (s, 5H, Cp′), 3.79–3.75 (m, 2H, COCH_2CH$_3$), 0.78 (t, J = 7.0 Hz, 3H, COCH$_2$CH_3); ^{13}C{^{1}H} NMR (DMSO-d$_6$, 150.1 MHz) δ = 174.3 (C-2), 164.9 (COCH$_2$CH$_3$), 157.6 (C$_{Ar}$), 145.7 (C-6), 144.4 (C$_{Ar}$), 138.7 (C$_{Ar}$), 134.3 (C$_{Ar}$), 129.7 (CH$_{Ar}$), 127.8 (CH$_{Ar}$), 126.6 (CH$_{Ar}$), 126.2 (CH$_{Ar}$), 125.6 (CH$_{Ar}$), 117.2 (CH$_{Ar}$), 114.8 (CH$_{Ar}$), 113.3 (CH$_{Ar}$), 101.9 (C-5), 84.4 (Cp$_{ipso}$), 69.5 (Cp′), 69.0 (Cp), 66.4 (2×, Cp), 59.5 (COCH$_2$CH$_3$), 54.1 (C-4), 13.5 (COCH$_2$$CH_3$); HPLC-MS, τ_1 = 12.4 min, m/z found 538.1 [M]$^+$, τ_2 = 12.6 min, m/z found 538.0 [M]$^+$ (m/z calculated for $C_{29}H_{26}FeN_2O_3S$ 538.1 [M]$^+$).

6d. This compound was synthesized in 39% yield (240 mg) starting from 526 mg (1.4 mmol) of **5d** and thiourea according to **general procedure C**. Elemental analysis calculated (%) for $C_{29}H_{26}FeN_2O_3S$ C 64.69, H 4.87, N 5.20, S 5.95 found C 64.59, H 4.90, N 5.14, S 5.89; ^{1}H NMR (DMSO-d$_6$, 600.3 MHz) δ = 10.44 (s, 1H, H-1), 9.73 (d, J = 3.9 Hz, 1H, H-3), 9.54 (s, 1H, OH), 7.56 (d, J = 8.3 Hz, 2H, CH$_{Ar}$), 7.22 (d, J = 8.3 Hz, 2H, CH$_{Ar}$), 7.18 (t, J = 8.0 Hz, 1H, CH$_{Ar}$), 6.81–6.80 (m, 2H, CH$_{Ar}$), 6.69 (ddd, J = 8.1, 2.2, 1.0 Hz, 1H, CH$_{Ar}$), 5.18 (d, J = 4.0 Hz, 1H, H-4), 4.86–4.85 (m, 2H, Cp), 3.39 (t, J = 1.8 Hz, 2H, Cp), 4.03 (s, 5H, Cp′), 3.82–3.78 (m, 2H, COCH_2CH$_3$), 0.81 (t, J = 7.1 Hz, 3H, COCH$_2$CH_3); ^{13}C{^{1}H} NMR (DMSO-d$_6$, 150.1 MHz) δ = 174.5 (C-2), 165.2 (COCH$_2$CH$_3$), 157.6 (C$_{Ar}$), 145.8 (C-6), 144.4 (C$_{Ar}$), 140.4 (C$_{Ar}$), 131.2 (C$_{Ar}$), 129.7 (CH$_{Ar}$), 128.9 (CH$_{Ar}$), 124.9 (CH$_{Ar}$), 117.1 (CH$_{Ar}$), 114.7 (CH$_{Ar}$), 113.3 (CH$_{Ar}$), 101.3 (C-5), 83.8 (Cp$_{ipso}$), 69.5 (Cp′), 69.3 (Cp), 66.5 (Cp), 66.4 (Cp), 59.6 (COCH$_2$CH$_3$), 54.0 (C-4), 13.5 (COCH$_2$$CH_3$); HPLC-MS, τ_1 = 12.4 min, m/z found 538.3 [M]$^+$, τ_2 = 12.7 min, m/z found 538.1 [M]$^+$ (m/z calculated for $C_{29}H_{26}FeN_2O_3S$ 538.1 [M]$^+$).

7a. This compound was prepared in 35% yield (194 mg) starting from 360 mg (1.2 mmol) of **5a** and 60 mg (1 mmol) of urea according to **general procedure C**. Elemental analysis calculated (%) for $C_{23}H_{22}FeN_2O_4$ C 61.90, H 4.97, N 6.28 found C 61.88, H 5.06, N 6.34; ^{1}H NMR (DMSO-d$_6$) δ = 9.40 (s, 1H, OH), 8.20 (br s, 1H, H-1), 7.88 (br s, 1H, H-3), 7.15 (t, J = 8.0 Hz, 1H, CH$_{Ar}$), 6.82–6.81 (m, 2H, CH$_{Ar}$), 6.67–6.66 (m, 1H, CH$_{Ar}$), 5.00 (d, J = 3.8 Hz, 1H, H-4), 4.74 (br s, 1H, Cp), 4.64 (br s, 1H, Cp), 4.43 (br s, 1H, Cp), 4.39 (br s, 1H, Cp), 4.92 (s, 5H, Cp′), 3.98–3.91 (m, 2H, COCH_2CH$_3$), 1.02 (t, J = 7.1 Hz, 3H, COCH$_2$CH_3); ^{13}C{^{1}H} (DMSO-d$_6$) δ = 166.4 (COCH$_2$CH$_3$), 157.4

(C-2), 152.4 (C-6), 146.6 (C_{Ar}), 145.2 (C_{Ar}), 129.2 (CH_{Ar}), 116.9 (CH_{Ar}), 114.2 (CH_{Ar}), 113.3 (CH_{Ar}), 99.9 (C-5), 76.8 (Cp_{ipso}), 69.9 (Cp′), 69.7 (Cp), 69.5 (Cp), 69.3 (Cp), 69.1 (Cp), 59.4 ($COCH_2CH_3$), 54.0 (C-4), 13.8 ($COCH_2CH_3$); HPLC-MS, τ_1 = 9.2 min, *m*/*z* found 446.1 $[M]^+$, τ_2 = 9.4 min, *m*/*z* found 446.1 $[M]^+$ (*m*/*z* calculated for $C_{23}H_{22}FeN_2O_4$ 446.1 $[M]^+$).

7c. This compound was prepared in 6.2% yield (60 mg) together with 2.5% yield (25 mg) of **8c** starting from **5c** according to **general procedure D**. **7c**: Elemental analysis calculated (%) for $C_{29}H_{26}FeN_2O_4$ C 66.68, H 5.02, N 5.18 found C 66.69, H 5.14, N 5.28; ^{1}H NMR (DMSO-d_6) δ = 9.47 (s, 1H, OH), 9.32 (d, *J* = 1.7 Hz, 1H, H-1), 7.81 (dd, *J* = 2.0, 3.2 Hz, 1H, H-3), 7.59 (d, *J* = 7.8 Hz, 1H, CH_{Ar}), 7.40 (br s. 1H, CH_{Ar}), 7.32 (t, *J* = 7.7 Hz, 1H, CH_{Ar}), 7.17 (t, *J* = 7.8 Hz, 1H, CH_{Ar}), 7.11 (d, *J* = 7.7 Hz, 1H, CH_{Ar}), 6.85–6.83 (m, 2H, CH_{Ar}), 6.68–6.66 (m, 1H, CH_{Ar}), 5.17 (d, *J* = 3.5 Hz, 1H, H-4), 4.81 (s, 1H, Cp), 4.80 (s, 1H, Cp), 4.36 (br s, 2H, Cp), 4.06 (s, 5H, Cp′), 3.74 (q, *J* = 7.0 Hz, 2H, $COCH_2CH_3$), 0.77 (t, *J* = 7.1 Hz, 3H, $COCH_2CH_3$); $^{13}C\{^1H\}$ (DMSO-d_6) δ = 165.1 ($COCH_2CH_3$), 157.5 (C-2), 152.2 (C-6), 148.9 (C_{Ar}), 145.8 (C_{Ar}), 138.6 (C_{Ar}), 135.3 (C_{Ar}), 129.5 (CH_{Ar}), 127.8 (CH_{Ar}), 126.4 (CH_{Ar}), 125.9 (CH_{Ar}), 125.3 (CH_{Ar}), 117.0 (CH_{Ar}), 114.3 (CH_{Ar}), 113.2 (CH_{Ar}), 100.5 (C-5), 84.5 (Cp_{ipso}), 69.4 (Cp′), 69.0 (Cp), 66.4 (Cp), 59.1 ($COCH_2CH_3$), 54.1 (C-4), 13.5 ($COCH_2CH_3$); HPLC-MS, τ_1 = 11.2 min, *m*/*z* found 522.2 $[M]^+$, τ_2 = 11.5 min, *m*/*z* found 522.2 $[M]^+$ (*m*/*z* calculated for $C_{29}H_{26}FeN_2O_4$ 522.1 $[M]^+$). **8c**: Elemental analysis calculated (%) for $C_{29}H_{28}FeN_2O_5$ C 64.46, H 5.22, N 5.18 found C 64.82, H 5.68, N 4.96; ^{1}H NMR (DMSO-d_6, 600.3 MHz) of a mixture of diastereoisomers δ = 9.35 (s, 1H, OH), 8.05 (s, 1H, CH_{Ar}), 7.81–7.76 (m, 1.5 H, CH_{Ar}), 7.71 (d, *J* = 7.8 Hz, 0.5 H, CH_{Ar}), 7.45 (t, *J* = 7.8 HZ, 0.5 H, CH_{Ar}), 7.43 (t, *J* = 7.7 Hz, 0.5 H, CH_{Ar}), 7.08–7.04 (m, 1H, CH_{Ar}), 6.86–6.83 (m, 1H, CH_{Ar}), 6.81–6.79 (m, 1H, CH_{Ar}), 6.67 (d, *J* = 9.2 Hz, 0.5 H, H-4), 6.59–6.53 (m, 1.5 H, CH_{Ar} and H-4), 5.65 (br s, 2H, H-6), 5.49–5.45 (m, 1H, H-3), 5.35 (d, *J* = 6.5 Hz, 0.5 H, H-2), 5.32 (d, *J* = 8.1 Hz, 0.5 H, H-2), 4.91 (br s, 1H, Cp), 4.89 (m, 1H, Cp), 4.41–4.39 (m, 2H, Cp), 4.11–4.07 (m, 0.5 H, $COCH_2CH_3$), 4.06–4.01 (m, 0.5 H, $COCH_2CH_3$), 4.03 and 4.02 (s, 5H, Cp′), 3.96–3.93 (m, 1H, $COCH_2CH_3$), 1.10 (t, *J* = 7.1 H, 1.5 H, $COCH_2CH_3$), 0.94 (t, *J* = 7.0 Hz, 1.5 H, $COCH_2CH_3$); $^{13}C\{^1H\}$ NMR (DMSO-d_6, 150.1 MHz) δ = 193.0 (CO), 168.0 and 167.6 (CO), 157.8 and 157.6 (CO), 157.1, 143.2, 140.1 (2×), 136.7 and 135.8 (C_{Ar}), 131.0 and 130.9 (CH_{Ar}), 129.2 and 129.0 (CH_{Ar}), 125.7 and 125.6 (CH_{Ar}), 117.3 (CH_{Ar}), 114.2 and 114.1 (CH_{Ar}), 113.8 (CH_{Ar}), 83.6 and 83.5 (Cp_{ipso}), 69.5 (Cp), 69.4 (Cp′), 66.8 and 66.6 (Cp′), 66.5 (2 × Cp′), 61.0 and 60.9 ($COCH_2CH_3$), 59.1 (C-2), 52.6 (C-3, based on ^{1}H–^{13}C HSQC), 13.9 and 13.7 ($COCH_2CH_3$); HPLC-MS, τ_1 = 10.9 min, *m*/*z* found 540.2 $[M]^+$, τ_2 = 11.0 min, *m*/*z* found 540.2 $[M]^+$ (*m*/*z* calculated for $C_{29}H_{28}FeN_2O_5$ 540.1 $[M]^+$).

7d. This compound was prepared in 1.4% yield (10 mg) starting from **5d** according to **general procedure D**. Elemental analysis calculated (%) for $C_{29}H_{26}FeN_2O_4$ C 66.68, H 5.02, N 5.36 found C 66.81, H 5.14, N 5.32; ^{1}H NMR (DMSO-d_6) δ = 9.47 (s, 1H, OH), 9.26 (d, *J* = 1.7 Hz, 1H, H-1), 7.82 (d, *J* = 3.3, 2.0 Hz, 1H, H-3), 7.57 (d, *J* = 8.4 Hz, 2H, CH_{Ar}), 7.24 (d, *J* = 8.3, 2H, CH_{Ar}), 7.17 (t, *J* = 7.8 Hz, 1H, CH_{Ar}), 6.82–6.83 (m, 2H, CH_{Ar}), 6.69–6.67 (m, 1H, CH_{Ar}), 5.15 (d, *J* = 3.5 Hz, 1H, H-4), 4.85 (t, *J* = 1.9 Hz, 2H, Cp), 4.40 (t, *J* = 1.8 Hz, 2H, Cp), 4.04 (s, 5H, Cp′), 3.79 (q, *J* = 6.9 Hz, 2H, $COCH_2CH_3$) 0.82 (t, *J* = 7.1 Hz, 3H, $COCH_2CH_3$); $^{13}C\{^1H\}$ NMR (DMSO-d_6) δ = 165.4 ($COCH_2CH_3$), 157.7 (C-2), 152.3 (C_{Ar}), 148.8 (C_{Ar}), 145.7 (C-6), 140.0 (C_{Ar}), 132.3 (C_{Ar}), 129.4 (CH_{Ar}), 128.6 (CH_{Ar}), 125.0 (CH_{Ar}), 116.7 (CH_{Ar}), 114.4 (CH_{Ar}), 113.2 (CH_{Ar}), 100.1 (C-5), 84.0 (Cp_{ipso}), 69.4 (Cp′), 69.2 (Cp), 66.4 (2×, Cp) 59.1 ($COCH_2CH_3$), 54.0 (C-4), 13.6 ($COCH_2CH_3$); HPLC-MS, τ_1 = 11.2 min, *m*/*z* found 522.2 $[M]^+$, τ_2 = 11.5 min, *m*/*z* found 522.2 $[M]^+$ (*m*/*z* calculated for $C_{29}H_{26}FeN_2O_4$ 522.1 $[M]^+$).

8a. This compound was isolated in 10% yield (90 mg) starting from 660 mg (2.2 mmol) of **5a** according to **general procedure B**. Elemental analysis calculated (%) for $C_{23}H_{24}FeN_2O_5$ C 59.50, H 5.21, N 6.03 found C 60.92, H 5.80, N 6.07; ^{1}H NMR (DMSO-d_6, 600.3 MHz) δ = 9.36 (br s, 0.4 H, OH, minor), 9.35 (br s, 0.6 H, OH, major), 7.10–7.06 (m, 1H, CH_{Ar}), 6.86–6.80 (m, 2H, CH_{Ar}), 6.65 (br s, 0.5 H, H-4), 6.60–6.58 (m, 1.5 H, CH_{Ar} and H-4), 5.67 (br s, 1H, H-6), 5.57 (br s, 1H, H-6), 5.36 (br s, 1H, H-3), 4.77–4.72 (m, 2H, Cp), 4.61–4.60 (m, 2H, Cp), 4.53 (d, *J* = 6.5 Hz, 0.5 H, H-2), 4.43 (d, *J* = 9.1 Hz, 0.5 H, H-2), 4.15–4.12 (m, 0.5 H, $COCH_2CH_3$), 4.05–3.97 (m, 1.5 H, $COCH_2CH_3$) overlapped with 4.01 (s, 5H, Cp′), 1.16 (t, *J* = 7.0 Hz, 1.8 H, $COCH_2CH_3$), 1.02 (t, *J* = 6.5 Hz, 2H, $COCH_2CH_3$); $^{13}C\{^1H\}$ NMR (DMSO-d_6, 150.1 MHz) δ = 197.0 and 195.0 (CO), 167.5 (CO), 157.7 and 157.5 (CO), 157.1 (C_{Ar}), 143.5 and 143.1 (C_{Ar}), 129.1 and 128.9 (CH_{Ar}), 117.8 (2 × CH_{Ar}), 114.6 and 114.3 (CH_{Ar}), 114.1 and 113.9 (CH_{Ar}), 79.4 and 78.1 (Cp_{ipso}), 72.9 (2×), 72.7 (Cp), 72.6 (Cp), 69.7 (2×, Cp′), 69.4 (Cp), 69.3 (Cp), 69.2 (Cp), 61.4 (Cp), 60.9 (Cp), 60.8 ($COCH_2CH_3$), 59.2 (C-2 based on ^{1}H–^{13}C HSQC), 52.6 (C-3 based on ^{1}H–^{13}C HSQC), 14.0 and 13.8 ($COCH_2CH_3$); HPLC-MS, τ = 8.0 min, *m*/*z* found 465.1 $[M + H]^+$, 487.1 $[M + Na]^+$, τ_2 = 8.2 min, *m*/*z* found 464.3 $[M]^+$, 487.1 $[M + Na]^+$ (*m*/*z* calculated for $C_{23}H_{24}FeN_2O_5$ 464.1 $[M]^+$, $C_{23}H_{24}FeN_2O_5$ + H 465.1 $[M + H]^+$, $C_{23}H_{24}FeN_2O_5$ + Na 487.1 $[M + Na]^+$).

8b. This compound was isolated in 32% yield (70 mg) starting from 150 mg (0.40 mmol) of **5b** according to **general procedure B**. Elemental analysis calculated (%) for $C_{29}H_{28}FeN_2O_5$ C 64.46, H 5.22, N 5.18 found C 64.94, H 5.52, N 5.36; ^{1}H NMR (DMSO-d_6, 600.3 MHz) of a mixture of diastereoisomers δ = 9.33 (s, 1H, OH), 7.91 (d, *J* = 7.8 Hz, 0.7 H, CH_{Ar}), 7.89 (d, *J* = 7.7 Hz, 0.3 H, CH_{Ar}), 7.52–7.48 (m, 1H, CH_{Ar}), 7.39 (br s, 0.3 H, CH_{Ar}), 7.30–7.26 (m, 1H, CH_{Ar}), 7.16 (d, *J* = 7.0 Hz, 0.7 H, CH_{Ar}), 7.04 (t, *J* = 7.8 Hz, 0.3 H, CH_{Ar}), 7.00 (t, *J* = 7.8 Hz, 0.7 H, CH_{Ar}), 6.67–6.65 (m, 0.6 H, CH_{Ar}), 6.59–6.43 (m, 3.5 H, CH_{Ar}, and H-4), 5.74 (br s, 1.5 H, H-6), 5.61 (br s, 0.5 H, H-6), 5.25 (br s, 0.2 H, H-3), 4.93 (dd, *J* = 9.8, 6.4 Hz, 0.7 H, H-3), 4.49 (d, *J* = 8.1 Hz, 0.3 H, H-2), 4.44 (br s, 0.7 H, Cp), 4.36 (br s, 0.7 H, Cp), 4.33 (br s, 0.8 H, Cp), 4.30 (br s, 1.3 H, Cp), 4.28–4.27 (m, 0.3 H, Cp), 4.27–4.26 (m, 0.3 H, Cp), 4.16 (d, *J* = 6.3 Hz, 0.7 H, H-2), 4.10 (s, 3.5 H, Cp′), 4.05 (s, 1.5 H, Cp′), 3.97–3.93 (m, 0.8 H, $COCH_2CH_3$), 3.90–3.85 (m, 0.7 H, $COCH_2CH_3$), 3.82–3.78 (m, 0.5 H, $COCH_2CH_3$), 1.00 (t, *J* = 7.1 H, 2 H, $COCH_2CH_3$), 0.89 (t, *J* = 7.1 H, 1H, $COCH_2CH_3$); $^{13}C\{^1H\}$ NMR (DMSO-d_6,

150.1 MHz) δ = 199.7 (CO), 167.8 (CO), 157.6 and 157.5 (CO), 157.0 (C_{Ar}), 142.8 and 142.6 (C_{Ar}), 138.6 and 137.6 (C_{Ar}), 137.7, 136.8 (C_{Ar}), 132.1 and 131.6 (CH_{Ar}), 130.7 and 130.6 (CH_{Ar}), 129.0 (CH_{Ar}), 128.0 and 127.7 (CH_{Ar}), 126.2 and 125.9 (CH_{Ar}), 117.6 and 117.0 (CH_{Ar}), 114.3 and 113.9 (CH_{Ar}), 113.7 (CH_{Ar}), 85.4 and 85.3 (Cp_{ipso}), 70.0 and 69.9 (Cp′), 69.8 and 69.7 (Cp), 69.4 (Cp), 69.2 (Cp), 68.9 (Cp), 68.7 (Cp), 68.4 (Cp), 62.8 (C-2), 60.7 and 60.6 ($COCH_2CH_3$), 51.7 (C-3), 13.8 and 13.6 ($COCH_2CH_3$); HPLC-MS, τ_1 = 10.4 min, *m*/*z* found 540.3 $[M]^+$, τ_2 = 10.6 min, *m*/*z* found 540.2 $[M]^+$, τ_3 = 11.2 min, *m*/*z* found 540.2 $[M]^+$ (*m*/*z* calculated for $C_{29}H_{28}FeN_2O_5$ 540.1 $[M]^+$).

8c. This compound was synthesized in 32% yield (140 mg) starting from 300 mg (0.80 mmol) of **2c** according to **general procedure B**.

8d. This compound was isolated in 34% yield (100 mg) starting from 210 mg (0.558 mmol) of **5d** according to **general procedure B**. Elemental analysis calculated (%) for $C_{29}H_{28}FeN_2O_5$ C 64.46, H 5.22, N 5.18 found C 64.93, H 5.80, N 5.18; ^{1}H NMR (DMSO-d_6, 600.3 MHz) δ = 9.32 (s, 1H, OH), 7.89 (d, *J* = 8.4 Hz, 1H, CH_{Ar}), 7.85 (d, *J* = 8.3 Hz, 1H, CH_{Ar}), 7.66 (t, *J* = 7.6 Hz, 1H, CH_{Ar}), CH_{Ar}, 7.07–7.02 (m, 1H, CH_{Ar}), 6.82–6.77 (m, 2H, CH_{Ar}), 6.63 (d, *J* = 9.2 Hz, 0.5 H, H-4), 6.59–6.53 (m, 1.5 H, H-4 and CH_{Ar}), 5.64 (br s, 1H, H-6), 5.62 (br s, 1H, H-6), 5.47–5.44 (m, 1H, H-3), 5.23 (d, *J* = 7.4 Hz, 0.5H, H-2), 5.16 (d, *J* = 8.5 Hz, 0.5 H, H-2), 4.92 (t, *J* = 1.7 Hz, 2H, Cp), 4.46–4.45 (m, 2H, Cp), 4.12–4.07 (m, 0.5, $COCH_2CH_3$), 4.05–4.00 (m, 0.5 H, $COCH_2CH_3$) overlapped with 4.03–4.02 (m, 5H, Cp′), 3.95–3.88 (m, 1H, $COCH_2CH_3$), 1.09 (t, *J* = 7.1 Hz, 1.8 H, $COCH_2CH_3$), 0.97 (t, *J* = 6.9 Hz, 1.2 H, $COCH_2CH_3$); $^{13}C\{^1H\}$ NMR (DMSO-d_6, 150.1 MHz) δ = 192.4 (CO), 167.9 (CO), 157.8 and 157.6 (C), 157.1 (C), 146.1 (C_{Ar}), 143.3 (C_{Ar}), 133.7 (C_{Ar}), 132.7 (C_{Ar}), 129.0 and 128.9 (CH_{Ar}), 128.7 (CH_{Ar}), 125.8 (CH_{Ar}), 117.4 (CH_{Ar}), 114.3 and 114.1 (CH_{Ar}), 113.8 (CH_{Ar}), 82.4 (Cp_{ipso}), 70.1 (Cp), 69.7 (Cp′), 67.1 and 67.0 (Cp), 67.0 (Cp), 60.9 ($COCH_2CH_3$), 58.7 and 57.9 (C-2), 52.8 (C-3, based on ^{1}H–^{13}C HSQC), 13.9 and 13.7 ($COCH_2CH_3$); HPLC-MS, τ_1 = 10.6 min, *m*/*z* found 540.2 $[M]^+$, τ_2 = 10.7 min, *m*/*z* found 540.2 $[M]^+$ (*m*/*z* calculated for $C_{29}H_{28}FeN_2O_5$ 540.1 $[M]^+$).

Cell lines

The A549 (alveolar basal epithelial cell adenocarcinoma), Colo 205 (colorectal adenocarcinoma), HCT 116 (colorectal carcinoma), Hep G2 (hepatocellular carcinoma), MCF7 (breast adenocarcinoma), and SW620 (colorectal adenocarcinoma) cell lines were purchased from American Type Culture Collection (USA) *via* LGC Standards. Multidrug resistant SW620 variants were derived and characterized as described previously.[65] All cell lines were cultured in standard conditions (37 °C, 5% CO_2, 100% relative humidity) in high-glucose Dulbecco's modified Eagle medium supplemented with GlutaMAX™, HEPES (ThermoFisher Scientific, USA) and 10% fetal bovine serum (EURx, Poland). Care was taken not to cross-contaminate the cultures and all cell lines were processed separately using filter pipette tips. The cultures were routinely monitored every 3 months for signs of Mycoplasma infection using MycoProbe Myoplasma Detection kit (R&D Systems, USA).

Antiproliferative/cytotoxic activity assay

The drug sensitivity was determined using the neutral red uptake assay.[70] Cells were seeded in 96-well plates at a density of 1×10^4 cells per well. Following an overnight incubation to allow the cells to attach to the surface, they were treated with desired concentrations of the test compounds. Stock solutions of the investigated compounds were freshly prepared in DMSO and used within a maximum of 4 hours since dissolution. The final DMSO concentration in all samples was constant and equal to 0.1% (v/v) as such solvent level was proven to be virtually non-toxic to the cells as determined in pilot experiments. Cells treated with DMSO only were considered fully viable controls. Following 70 h-exposure, neutral red was added to all wells to the final concentration of 1 mM. After further 2 h, the medium was carefully aspirated and wells were washed with phosphate-buffered saline (PBS). Finally, the cells were dissolved in 200 μL of solubilizer (1% HOAc (v/v) in 50% EtOH (v/v)) and shaken on an orbital shaker for 10 min to allow for neutral red extraction. The sample absorbance at 540 nm was measured using an EnVision Multilabel Plate Reader (Perkin Elmer, USA). The results were calculated as a percentage of control and presented either as such or the IC_{50} values were determined by GraphPad Prism 7.03 software (GraphPad Prism Inc.) using a four-parameter non-linear logistic regression model.

Cell cycle analysis

SW620 and its multidrug-resistant variant SW620V (selected by increasing concentration of vincristine, overexpressing ABCB1) were selected for cell cycle analysis. 1×10^5 cells were seeded in a 6-well plate and left to attach for 24 h. Then the cells were treated with the investigated compounds at a concentration corresponding to the IC_{90} of **1** for SW620 (1.5 μM). After further 24-hour incubation, the medium was collected, cells were trypsinized and resuspended in autologous medium, washed twice with ice-cold PBS, and fixed with ice-cold ethanol (70% v/v). After overnight incubation at 4 °C, they were stained with propidium iodide staining solution (75 μM propidium iodide and 50 Kunitz units per mL RNAse A in PBS) for 30 minutes at 37 °C. The samples were analyzed using an LSRII flow cytometer (Becton Dickinson, USA; excitation 488 nm, emission 575/26 nm, PE channel) and cell cycle phase distribution was determined with FlowJo 7.6.1 software (FlowJo, USA) using a built-in cell cycle analysis module (Watson pragmatic algorithm).

Reactive oxygen species formation

The oxidation rate of dihydrorhodamine 123 (DHR123) was considered as the marker of intracellular reactive oxygen species production. Exponentially growing SW620 cells (100 000 cells per well seeded in 6-well plates for 20–24 h before time 0) were exposed to 1 μM of the test compound for 4 h in the presence of 1 μM DHR123. Since this assay is sus-

pected to be influenced by ABCB1 activity,[55] 10 μM verapamil was added as an inhibitor of ABCB1. Cells were then harvested by trypsinization and suspended in a complete growth medium. The samples were then analysed with an LSRII (Becton Dickinson, USA) instrument and median fluorescence (excitation 488 nm, emission 530/30 nm, FITC channel) was analysed. Median fluorescence of cells incubated with DHR123 and DMSO alone was considered 100% in a given experiment. Statistical significance of the differences was assessed by one-way ANOVA and Tukey's *post hoc* test, assuming 0.05 as the significance level.

Kinesin ATPase inhibition assay

Kinesin modulatory activity of the investigated compounds was assayed with the Kinesin ATPase Endpoint Biochem Kit (Cytoskeleton, Inc.). Compounds were dissolved in DMSO (final concentration 0.1%), and then diluted in 100 mM PIPES buffer pH 7.0 to obtain final concentrations of 10, 100 and 1000 nM. The experiment was performed according to the manufacturer's instructions and phosphate release was measured as the absorbance at 650 nm using EnVision Multilabel Plate Reader (Perkin Elmer, USA).

Molecular structure determination

Single crystals of **3a** and **6a** were obtained by solvent evaporation from CH_2Cl_2/*n*-hexane solution. Suitable single crystals were placed on an Agilent Supernova 4 circle diffractometer system equipped with a copper (CuKα) microsource and molybdenum (MoKα) microsource and Atlas CCD detector. The data were collected and integrated with CrysAlis171[71] software and corrected for absorption effects using the multi-scan method (SCALE3 ABSPACK[41]). The sample was cooled by keeping it in a cold nitrogen stream, using Oxford Cryosystems cooling device. The copper source was selected for **3a** as the crystals of both compounds were very thin plates, expected to yield a relatively weak X-ray diffraction signal.

Both structures were solved using Olex2[72] with the olex2.solve[73] structure solution program using Charge Flipping. The structures were subsequently refined with the SHELXL[74] refinement package using Least Squares minimization. In both instances, the hydrogen atoms were visible in the residual density map but were added geometrically and refined mostly in riding approximation. H atoms involved in H-bonds were refined with only donor-H distance restraint, and isotropic ADP-s derived from the ADP-s of the appropriate donor atom. In the case of **6a**, solvent molecules incorporated in the crystal structure were refined as disordered over two alternative positions. The figures were prepared using Mercury 4.3.[75] Detailed information about the data processing, structure solution and refinement is presented in Table 7.

Docking studies

The derivatives were docked to the crystal structure of tubulin PDB ID 1Q0B with a resolution of 1.9 Å.[76] Scigress v2.6[77] was used to prepare the crystal structure for docking, *i.e.* the hydrogen atoms were added, and the co-crystallized ligands as well as crystallographic water molecules were removed. The Scigress software suite was also used to build the chemical structures which were optimized using the MM2 force field[78] and the PM6 semi-empirical method.[79] The center of the binding was defined in the protein crystal structure as C5 of the co-crystallized monastrol molecule (x = 41.347, y = 15.526, z = 49.897) with a 10 Å radius. Fifty docking runs were allowed for each ligand with default search efficiency (100%). The basic amino acids lysine and arginine were defined as protonated. Furthermore, aspartic and glutamic acid residues were assumed to be deprotonated. The GoldScore (GS)[80] scoring function was implemented to validate the predicted binding modes and relative energies of the ligands using the GOLD v5.4.0 software suite.

Table 7 Crystal data and refinement parameters for **3a** and **6a**

Compound	**3a**	**6a**
CCDC	2010958	2010957
Empirical formula	$C_{18}H_{20}FeN_2O_2S$	$C_{23}H_{22}FeN_2O_3S{\cdot}0.5\,CH_2Cl_2$
Formula weight/g mol^{-1}	384.27	504.80
Temperature/K	100.00(10)	100.00(10)
Crystal system	Monoclinic	Monoclinic
Space group	$C2/c$	$P2_1/c$
a/Å	18.7579(2)	13.9949(10)
b/Å	7.28947(8)	11.5388(5)
c/Å	24.6904(3)	15.5543(8)
α/°	90	90
β/°	97.4762(11)	106.060(7)
γ/°	90	90
Volume/Å3	3347.36(7)	2413.7(3)
Z	8	4
ρ_{calc}/g cm^{-3}	1.525	1.389
μ/mm^{-1}	8.498	0.849
F(000)	1600.0	1044.0
Crystal size/mm^3	0.1389 × 0.08 × 0.0356	0.5468 × 0.1944 × 0.0275
Radiation/Å	CuKα (λ = 1.54184)	MoKα (λ = 0.71073)
2Θ range for data collection/°	7.222 to 142.708	4.460 to 54.206
Index ranges	$-22 \le h \le 22$, $-8 \le k \le 8$, $-30 \le l \le 30$	$-17 \le h \le 17$, $-14 \le k \le 14$, $-19 \le l \le 19$
Reflections collected	16 123	40 306
Independent reflections	3233 [R_{int} = 0.0303, R_{sigma} = 0.0208]	5320 [R_{int} = 0.0987, R_{sigma} = 0.0569]
Data/restraints/parameters	3233/5/262	5320/44/329
Goodness-of-fit on F^2	1.040	1.082
Final R indexes [$I \ge 2\sigma(I)$]	R_1 = 0.0261, wR_2 = 0.0608	R_1 = 0.0639, wR_2 = 0.1478
Final R indexes [all data]	R_1 = 0.0286, wR_2 = 0.0623	R_1 = 0.0843, wR_2 = 0.1584
Largest diff. peak/hole/e Å^{-3}	0.30/−0.31	1.41/−0.49

Author contributions

The manuscript was written through contributions of all authors. All authors have given approval to the final version of the manuscript.

Conflicts of interest

There are no conflicts to declare.

Acknowledgements

This study was financially supported by the National Science Centre Poland (NCN) based on decision UMO-2015/17/B/ST5/02331.

Notes and references

1 C. Dumontet and M. A. Jordan, Microtubule-binding agents: a dynamic field of cancer therapeutics, *Nat. Rev. Drug Discovery*, 2010, **9**(10), 790–803.
2 J. Tischer and F. Gergely, Anti-mitotic therapies in cancer, *J. Cell Biol.*, 2018, **218**(1), 10–11.
3 A. Desai and T. J. Mitchison, Microtubule polymerization dynamics, *Annu. Rev. Cell Dev. Biol.*, 1997, **13**(1), 83–117.
4 H. C. Joshi, Microtubule dynamics in living cells, *Curr. Opin. Cell Biol.*, 1998, **10**(1), 35–44.
5 J. Lane, Microtubule-based membrane movement, *Biochim. Biophys. Acta*, 1998, **1376**, 27–55.
6 A. Canta, A. Chiorazzi and G. Cavaletti, Tubulin: a target for antineoplastic drugs into the cancer cells but also in the peripheral nervous system, *Curr. Med. Chem.*, 2009, **16**(11), 1315–1324.
7 J. Crown, M. O'Leary and W. S. Ooi, Docetaxel and paclitaxel in the treatment of breast cancer: a review of clinical experience, *Oncologist*, 2004, **9**, 24–32.
8 M. Rowinsky and K. Eric, The development and clinical utility of the taxane class of antimicrotubule chemotherapy agents, *Annu. Rev. Med.*, 1997, **48**(1), 353–374.
9 I. Marzo and J. Naval, Antimitotic drugs in cancer chemotherapy: promises and pitfalls, *Biochem. Pharmacol.*, 2013, **86**(6), 703–710.
10 L. S. Goldstein and A. V. Philp, The road less traveled: emerging principles of kinesin motor utilization, *Annu. Rev. Cell Dev. Biol.*, 1999, **15**(1), 141–183.
11 G. Sauer, R. Körner, A. Hanisch, A. Ries, E. A. Nigg and H. H. W. Silljé, Proteome Analysis of the Human Mitotic Spindle*, *Mol. Cell. Proteomics*, 2005, **4**(1), 35–43.
12 J. C. Cochran, J. E. Gatial, T. M. Kapoor and S. P. Gilbert, Monastrol inhibition of the mitotic kinesin Eg5, *J. Biol. Chem.*, 2005, **280**(13), 12658–12667.
13 D. J. Sharp, G. C. Rogers and J. M. Scholey, Microtubule motors in mitosis, *Nature*, 2000, **407**(6800), 41–47.
14 T. Wittmann, A. Hyman and A. Desai, The spindle: A dynamic assembly of microtubules and motors, *Nat. Cell Biol.*, 2001, **3**(1), E28–E34.
15 K. A. Myers and P. W. Baas, Kinesin-5 regulates the growth of the axon by acting as a brake on its microtubule array, *J. Cell Biol.*, 2007, **178**(6), 1081–1091.
16 V. Sarli and A. Giannis, Targeting the Kinesin Spindle Protein: Basic Principles and Clinical Implications, *Clin. Cancer Res.*, 2008, **14**(23), 7583.
17 S. Ding, N. Xing, J. Lu, H. Zhang, K. Nishizawa, S. Liu, X. Yuan, Y. Qin, Y. Liu and O. Ogawa, Overexpression of Eg5 predicts unfavorable prognosis in non–muscle invasive bladder urothelial carcinoma, *Int. J. Urol.*, 2011, **18**(6), 432–438.
18 C. Liu, N. Zhou, J. Li, J. Kong, X. Guan and X. Wang, Eg5 Overexpression Is Predictive of Poor Prognosis in Hepatocellular Carcinoma Patients, *Dis. Markers*, 2017, **2017**, 2176460–2176460.
19 D. Sun, J. Lu, K. Ding, D. Bi, Z. Niu, Q. Cao, J. Zhang and S. Ding, The expression of Eg5 predicts a poor outcome for patients with renal cell carcinoma, *Med. Oncol.*, 2013, **30**(1), 476.
20 M. Liu, X. Wang, Y. Yang, D. Li, H. Ren, Q. Zhu, Q. Chen, S. Han, J. Hao and J. Zhou, Ectopic expression of the microtubule–dependent motor protein Eg5 promotes pancreatic tumourigenesis, *J. Pathol.*, 2010, **221**(2), 221–228.
21 S. DeBonis, D. A. Skoufias, L. Lebeau, R. Lopez, G. Robin, R. L. Margolis, R. H. Wade and F. Kozielski, In vitro screening for inhibitors of the human mitotic kinesin Eg5 with antimitotic and antitumor activities, *Mol. Cancer Ther.*, 2004, **3**(9), 1079–1090.
22 J. A. Good, G. Berretta, N. G. Anthony and S. P. Mackay, *The discovery and development of Eg5 inhibitors for the clinic*, in *Kinesins and Cancer*, Springer, 2015, pp. 27–52.
23 S. M. Myers and I. Collins, Recent findings and future directions for interpolar mitotic kinesin inhibitors in cancer therapy, *Future Med. Chem.*, 2016, **8**(4), 463–489.
24 K. W. Wood, W. D. Cornwell and J. R. Jackson, Past and future of the mitotic spindle as an oncology target, *Curr. Opin. Pharmacol.*, 2001, **1**(4), 370–377.
25 L. Duan, T. Q. Wang, W. Bian, W. Liu, Y. Sun and B. S. Yang, Centrin: Another target of monastrol, an inhibitor of mitotic spindle, *Spectrochim. Acta, Part A*, 2015, **137**, 1086–1091.
26 T. U. Mayer, T. M. Kapoor, S. J. Haggarty, R. W. King, S. L. Schreiber and T. J. Mitchison, Small molecule inhibitor of mitotic spindle bipolarity identified in a phenotype-based screen, *Science*, 1999, **286**(5441), 971–974.
27 M. Gartner, N. Sunder-Plassmann, J. Seiler, M. Utz, I. Vernos, T. Surrey and A. Giannis, Development and Biological Evaluation of Potent and Specific Inhibitors of Mitotic Kinesin Eg5, *ChemBioChem*, 2005, **6**(7), 1173–1177.
28 H. Y. K. Kaan, V. Ulaganathan, O. Rath, H. Prokopcova, D. Dallinger, C. O. Kappe and F. Kozielski, Structural basis for inhibition of Eg5 by dihydropyrimidines: stereoselectivity of antimitotic inhibitors enastron, dimethylenastron and fluorastrol, *J. Med. Chem.*, 2010, **53**(15), 5676–5683.
29 I. Garcia-Saez, S. DeBonis, R. Lopez, F. Trucco, B. Rousseau, P. Thuéry and F. Kozielski, Structure of human Eg5 in complex with a new monastrol-based inhibi-

tor bound in the R configuration, *J. Biol. Chem.*, 2007, **282**(13), 9740–9747.
30 L. Yang, C. Jiang, F. Liu, Q.-D. You and W.-T. Wu, Cloning, Enzyme Characterization of Recombinant Human Eg5 and the Development of a New Inhibitor, *Biol. Pharm. Bull.*, 2008, **31**(7), 1397–1402.
31 H. B. El-Nassan, Advances in the discovery of kinesin spindle protein (Eg5) inhibitors as antitumor agents, *Eur. J. Med. Chem.*, 2013, **62**, 614–631.
32 I. Garcia-Saez and D. A. Skoufias, Eg5 targeting agents: From new anti-mitotic based inhibitor discovery to cancer therapy and resistance, *Biochem. Pharmacol.*, 2021, **184**, 114364.
33 S. Ghosh, Cisplatin: The first metal based anticancer drug, *Bioorg. Chem.*, 2019, **88**, 102925.
34 N. J. Wheate, S. Walker, G. E. Craig and R. Oun, The status of platinum anticancer drugs in the clinic and in clinical trials, *Dalton Trans.*, 2010, **39**(35), 8113–8127.
35 T. R. Steel, F. Walsh, A. Wieczorek-Błauż, M. Hanif and C. G. Hartinger, Monodentately-coordinated bioactive moieties in multimodal half-sandwich organoruthenium anticancer agents, *Coord. Chem. Rev.*, 2021, **439**, 213890.
36 M. Patra and G. Gasser, The medicinal chemistry of ferrocene and its derivatives, *Nat. Rev. Chem.*, 2017, **1**(9), 0066.
37 P. Chellan and P. J. Sadler, Enhancing the Activity of Drugs by Conjugation to Organometallic Fragments, *Chem. – Eur. J.*, 2020, **26**(40), 8676–8688.
38 G. Jaouen, A. Vessières and S. Top, Ferrocifen type anti cancer drugs, *Chem. Soc. Rev.*, 2015, **44**(24), 8802–8817.
39 M. Daniluk, W. Buchowicz, M. Koszytkowska-Stawińska, K. Jarząbek, K. N. Jarzembska, R. Kamiński, M. Piszcz, A. E. Laudy and S. Tyski, Ferrocene Amino Acid Ester Uracil Conjugates: Synthesis, Structure, Electrochemistry and Antimicrobial Evaluation, *ChemistrySelect*, 2019, **4**(37), 11130–11135.
40 N. C. Costa, J. P. Piccoli, N. A. Santos-Filho, L. C. Clementino, A. M. Fusco-Almeida, S. R. De Annunzio, C. R. Fontana, J. B. Verga, S. F. Eto and J. M. Pizauro-Junior, Antimicrobial activity of RP-1 peptide conjugate with ferrocene group, *PLoS One*, 2020, **15**(3), e0228740.
41 M. Wenzel, M. Patra, C. H. R. Senges, I. Ott, J. J. Stepanek, A. Pinto, P. Prochnow, C. Vuong, S. Langklotz, N. Metzler-Nolte and J. E. Bandow, Analysis of the mechanism of action of potent antibacterial hetero-tri-organometallic compounds: A structurally new class of antibiotics, *ACS Chem. Biol.*, 2013, **8**(7), 1442–1450.
42 M. Patra, G. Gasser and N. Metzler-Nolte, Small organometallic compounds as antibacterial agents, *Dalton Trans.*, 2012, **41**(21), 6350–6358.
43 B. S. Ludwig, J. D. G. Correia and F. E. Kühn, Ferrocene derivatives as anti-infective agents, *Coord. Chem. Rev.*, 2019, **396**, 22–48.
44 F. Dubar, C. Slomianny, J. Khalife, D. Dive, H. Kalamou, Y. Guérardel, P. Grellier and C. Biot, The ferroquine antimalarial conundrum: redox activation and reinvasion inhibition, *Angew. Chem., Int. Ed.*, 2013, **52**(30), 7690–7693.
45 D. Dive and C. Biot, Ferroquine as an oxidative shock antimalarial, *Curr. Top. Med. Chem.*, 2014, **14**(14), 1684–1692.
46 T. Wells and R. van Huijsduijnen Hooft, Ferroquine: welcome to the next generation of antimalarials, *Lancet Infect. Dis.*, 2015, **15**(12), 1365–1366.
47 W. A. Al-Masoudi and N. A. Al-Masoudi, A ruthenium complexes of monastrol and its pyrimidine analogues: Synthesis and biological properties, *Phosphorus, Sulfur Silicon Relat. Elem.*, 2019, **194**(11), 1020–1027.
48 W. A. Al-Masoudi, N. A. Al-Masoudi, B. Weibert and R. Winter, Synthesis, X-ray structure, in vitro HIV and kinesin Eg5 inhibition activities of new arene ruthenium complexes of pyrimidine analogs, *J. Coord. Chem.*, 2017, **70**(12), 2061–2073.
49 M. Łomzik, M. Hanif, A. Budniok, A. Błauż, A. Makal, D. M. Tchoń, B. Leśniewska, K. K. H. Tong, S. Movassaghi, T. Söhnel, S. M. F. Jamieson, A. Zafar, J. Reynisson, B. Rychlik, C. G. Hartinger and D. Plażuk, Metal-Dependent Cytotoxic and Kinesin Spindle Protein Inhibitory Activity of Ru, Os, Rh, and Ir Half-Sandwich Complexes of Ispinesib-Derived Ligands, *Inorg. Chem.*, 2020, **59**(20), 14879–14890.
50 N.-Y. Fu, Y.-F. Yuan, M.-L. Pang, J.-T. Wang and C. Peppe, Indium(III) halides-catalyzed preparation of ferrocene-dihydropyrimidinones, *J. Organomet. Chem.*, 2003, **672**(1), 52–57.
51 K. Kiss, A. Csámpai and P. Sohár, New ferrocenyl-substituted heterocycles. Formation under Biginelli conditions, DFT modelling, and structure determination, *J. Organomet. Chem.*, 2010, **695**(15–16), 1852–1857.
52 R. Wang and Z.-Q. Liu, Ferrocene as a functional group enhances the inhibitive effect of dihydropyrimidine on radical-induced oxidation of DNA, *Org. Chem. Front.*, 2014, **1**(7), 792–797.
53 A. Csámpai, A. Györfi, G. I. Turos and P. Sohar, Application of Biginelli reaction to the synthesis of ferrocenylpyrimidones and [3]-ferrocenophane-containing pyrimido [4, 5-d] pyrimidinediones, *J. Organomet. Chem.*, 2009, **694**(22), 3667–3673.
54 K. Chrabaszcz, A. Blauz, M. Gruchala, M. Wachulec, B. Rychlik and D. Plazuk, Synthesis and Biological Activity of Ferrocenyl and Ruthenocenyl Analogues of Etoposide: Discovery of a Novel Dual Inhibitor of Topoisomerase II Activity and Tubulin Polymerization, *Chem. – Eur. J.*, 2021, **27**(20), 6254–6262.
55 K. Kowalczyk, A. Blauz, W. M. Ciszewski, A. Wieczorek, B. Rychlik and D. Plazuk, Colchicine metallocenyl bioconjugates showing high antiproliferative activities against cancer cell lines, *Dalton Trans.*, 2017, **46**(48), 17041–17052.
56 A. Wieczorek, A. Blauz, A. Zal, H. J. Arabshahi, J. Reynisson, C. G. Hartinger, B. Rychlik and D. Plazuk, Ferrocenyl Paclitaxel and Docetaxel Derivatives: Impact of an Organometallic Moiety on the Mode of Action of Taxanes, *Chem. – Eur. J.*, 2016, **22**(32), 11413–11421.
57 D. Plażuk, A. Wieczorek, A. Błauż and B. Rychlik, Synthesis and biological activities of ferrocenyl derivatives of paclitaxel, *MedChemComm*, 2012, **3**(4), 498–501.

58 D. Plażuk, A. Wieczorek, W. M. Ciszewski, K. Kowalczyk, A. Błauż, S. Pawlędzio, A. Makal, C. Eurtivong, H. J. Arabshahi, J. Reynisson, C. G. Hartinger and B. Rychlik, Synthesis and in vitro Biological Evaluation of Ferrocenyl Side-Chain-Functionalized Paclitaxel Derivatives, *ChemMedChem*, 2017, **12**(22), 1882–1892.

59 A. Wieczorek, A. Blauz, A. Makal, B. Rychlik and D. Plazuk, Synthesis and evaluation of biological properties of ferrocenyl-podophyllotoxin conjugates, *Dalton Trans.*, 2017, **46**(33), 10847–10858.

60 I. Cepanec, M. Litvić, M. Filipan-Litvić and I. Grüngold, Antimony(III) chloride-catalysed Biginelli reaction: a versatile method for the synthesis of dihydropyrimidinones through a different reaction mechanism, *Tetrahedron*, 2007, **63**(48), 11822–11827.

61 D. Russowsky, R. F. S. Canto, S. A. A. Sanches, M. G. M. D'Oca, A. de Fatima, R. A. Pilli, L. K. Kohn, M. A. Antonio and J. E. de Carvalho, Synthesis and differential antiproliferative activity of Biginelli compounds against cancer cell lines: Monastrol, oxo-monastrol and oxygenated analogues, *Bioorg. Chem.*, 2006, **34**(4), 173–182.

62 D. Plazuk, A. Vessieres, E. A. Hillard, O. Buriez, E. Labbe, P. Pigeon, M. A. Plamont, C. Amatore, J. Zakrzewski and G. Jaouen, A [3]ferrocenophane polyphenol showing a remarkable antiproliferative activity on breast and prostate cancer cell lines, *J. Med. Chem.*, 2009, **52**(15), 4964–4967.

63 C. Pidathala, R. Amewu, B. Pacorel, G. L. Nixon, P. Gibbons, W. D. Hong, S. C. Leung, N. G. Berry, R. Sharma, P. A. Stocks, A. Srivastava, A. E. Shone, S. Charoensutthivarakul, L. Taylor, O. Berger, A. Mbekeani, A. Hill, N. E. Fisher, A. J. Warman, G. A. Biagini, S. A. Ward and P. M. O'Neill, Identification, Design and Biological Evaluation of Bisaryl Quinolones Targeting Plasmodium falciparum Type II NADH:Quinone Oxidoreductase (PfNDH2), *J. Med. Chem.*, 2012, **55**(5), 1831–1843.

64 C. O. Kappe, O. V. Shishkin, G. Uray and P. Verdino, X-Ray Structure, Conformational Analysis, Enantioseparation, and Determination of Absolute Configuration of the Mitotic Kinesin Eg5 Inhibitor Monastrol, *Tetrahedron*, 2000, **56**(13), 1859–1862.

65 A. Blauz and B. Rychlik, Drug-selected cell line panels for evaluation of the pharmacokinetic consequences of multidrug resistance proteins, *J. Pharmacol. Toxicol. Methods*, 2017, **84**, 57–65.

66 H. Asraf, R. Avunie-Masala, M. Hershfinkel and L. Gheber, Mitotic Slippage and Expression of Survivin Are Linked to Differential Sensitivity of Human Cancer Cell-Lines to the Kinesin-5 Inhibitor Monastrol, *PLoS One*, 2015, **10**(6), e0129255.

67 U. Soumyanarayanan, V. G. Bhat, S. S. Kar and J. A. Mathew, Monastrol mimic Biginelli dihydropyrimidinone derivatives: synthesis, cytotoxicity screening against HepG2 and HeLa cell lines and molecular modeling study, *Org. Med. Chem. Lett.*, 2012, **2**(1), 23.

68 Z. Maliga, T. M. Kapoor and T. J. Mitchison, Evidence that Monastrol Is an Allosteric Inhibitor of the Mitotic Kinesin Eg5, *Chem. Biol.*, 2002, **9**(9), 989–996.

69 A. Fersht, *Structure and mechanism in protein science: a guide to enzyme catalysis and protein folding*, Macmillan, 1999.

70 G. Repetto, A. Del Peso and J. L. Zurita, Neutral red uptake assay for the estimation of cell viability/cytotoxicity, *Nat. Protoc.*, 2008, **3**(7), 1125–1131.

71 CrysAlisPro 1.171.38.43d (Rigaku OD, 2015).

72 O. V. Dolomanov, L. J. Bourhis, R. J. Gildea, J. A. Howard and H. Puschmann, OLEX2: a complete structure solution, refinement and analysis program, *J. Appl. Crystallogr.*, 2009, **42**(2), 339–341.

73 L. J. Bourhis, O. V. Dolomanov, R. J. Gildea, J. A. Howard and H. Puschmann, The anatomy of a comprehensive constrained, restrained refinement program for the modern computing environment–Olex2 dissected, *Acta Crystallogr., Sect. A: Found. Crystallogr.*, 2015, **71**(1), 59–75.

74 G. Sheldrick, Crystal structure refinement with SHELXL, *Acta Crystallogr., Sect. C: Struct. Chem.*, 2015, **71**(1), 3–8.

75 C. F. Macrae, P. R. Edgington, P. McCabe, E. Pidcock, G. P. Shields, R. Taylor, M. Towler and J. Streek, Mercury: visualization and analysis of crystal structures, *J. Appl. Crystallogr.*, 2006, **39**(3), 453–457.

76 Y. Yan, V. Sardana, B. Xu, C. Homnick, W. Halczenko, C. A. Buser, M. Schaber, G. D. Hartman, H. E. Huber and L. C. Kuo, Inhibition of a mitotic motor protein: where, how, and conformational consequences, *J. Mol. Biol.*, 2004, **335**(2), 547–554.

77 Fijitsu Limited, 2008–2016.

78 N. L. Allinger, Conformational analysis. 130. MM2. A hydrocarbon force field utilizing V1 and V2 torsional terms, *J. Am. Chem. Soc.*, 1977, **99**, 8127–8134.

79 J. J. Stewart, Optimization of parameters for semiempirical methods V: modification of NDDO approximations and application to 70 elements, *J. Mol. Model.*, 2007, **13**(12), 1173–1213.

80 G. Jones, P. Willet, R. C. Glen, A. R. Leach and R. Taylor, Development and Validation of a Genetic Algorithm for Flexible Docking, *J. Mol. Biol.*, 1997, **267**, 727–748.

Electronic Supplementary Material (ESI) for Dalton Transactions.

Impact of the Ferrocenyl Group on Cytotoxicity and KSP Inhibitory Activity of Ferrocenyl Monastrol Conjugates

Anna Wieczorek-Błauż,[a] Karolina Kowalczyk,[a] Andrzej Błauż,[b] Anna Makal,[c] Sylwia Pawlędzio,[c] Chatchakorn Eurtivong,[d,e] Homayon J. Arabshahi,[f] Jóhannes Reynisson,[f,g] Christian G. Hartinger,[f] Błażej Rychlik,[b] Damian Plażuk[a]*

[a] Department of Organic Chemistry, Faculty of Chemistry, University of Łódź, Tamka 12, 91-403 Łódź, Poland

[b] Cytometry Lab, Department of Molecular Biophysics, Faculty of Biology and Environmental Protection University of Łódź, Pomorska 141/143, 90-236 Łódź, Poland

[c] Laboratory for Structural and Biochemical Research, Biological and Chemical Research Centre, Department of Chemistry, University of Warsaw, ul. Żwirki i Wigury 101, 02-089 Warszawa, Poland

[d] Program in Chemical Science, Chulabhorn Graduate Institute, Chulabhorn Royal Academy, Bangkok 10210, Thailand

[e] Center of Excellence on Environmental Health and Toxicology (EHT), Commission on Higher Education (CHE), Ministry of Education, Bangkok 10400, Thailand

[f] School of Chemical Sciences, University of Auckland, Auckland 1142, New Zealand

[g] School of Pharmacy and Bioengineering, Keele University, Staffordshire ST5 5BG, United Kingdom

Table of Contents

[100]

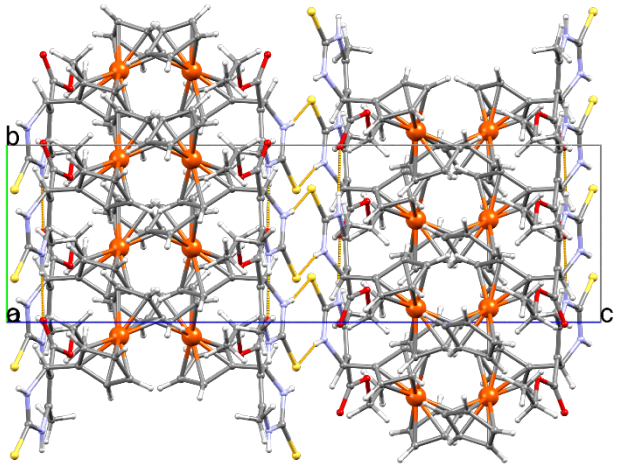

[010]

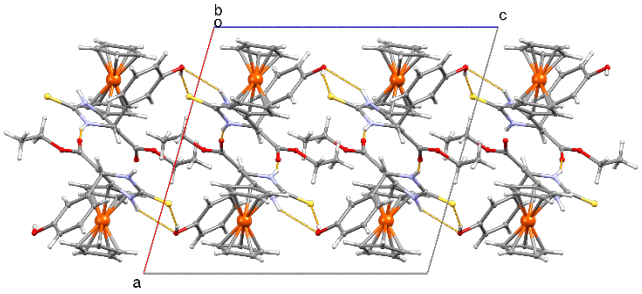

[010]

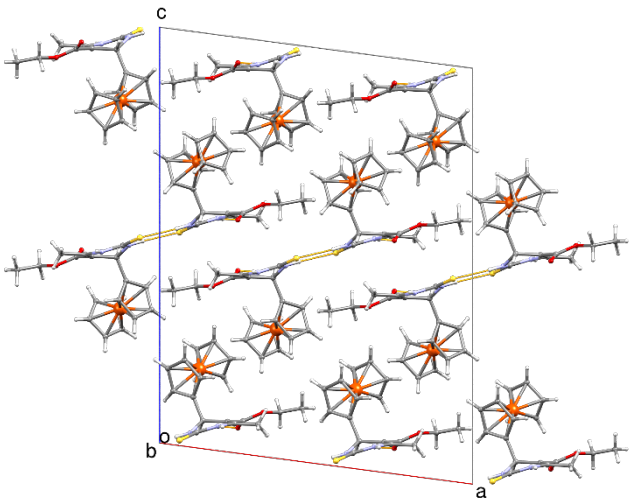

[001]

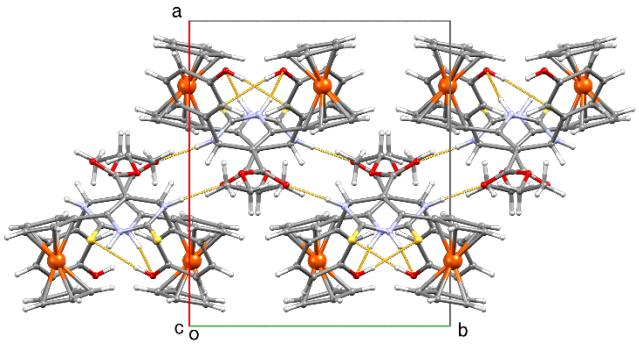

Supporting Figure S1. Selected views of the crystal packing of **4a** (left) and **6a** (right).

Docking studies

The KSP crystal structure derived from Homo sapiens was obtained from the Protein Data Bank (PDB ID: 1Q0B).[1] The co-crystallized ligand (*S*)-**1** was removed and re-docked to the allosteric site with excellent docking overlay (RMSD = 0.532 Å). The co-crystallized ligand, and its re-docked configuration, showed the phenol group deeply buried in the hydrophobic cavity (Supporting Figure S2). The cavity is populated with hydrophobic amino acids Trp127, Ala133, Ile136, Pro137, Tyr211 and Leu214, which form favorable hydrophobic contacts with aromatic phenol and the tetrahydropyrimidine core. Hydrogen bonding were predicted between the phenol and the Arg119 side chain and Glu118 carbonyl backbone. Additionally, the 3-NH forms a hydrogen bond with the Glu116 carbonyl backbone. The thione moiety is oriented towards Ile136 deep within the binding pocket with the ethanoate group facing the water phase. The spatial orientation and intermolecular interactions are in agreement with X-ray crystallographic data reported by Garcia-Saez et al.[2] and molecular modelling studies on monastrol mimics by Soumyanarayanan et al.[3] The similarities in the docked configurations to the one described in the literature and a low RMSD value suggest the reliability and reproducibility of the docking protocol.

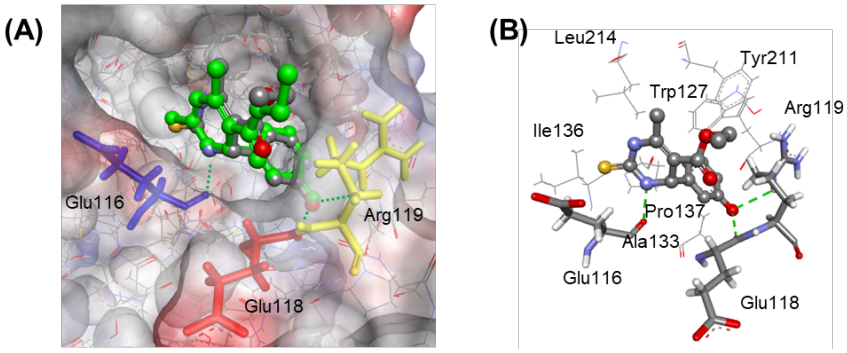

Supporting Figure S2. Docked configuration of (*S*)-monastrol. Hydrogen atoms have been omitted for clarity. H-bonds are depicted as green dotted lines. (A) Overlays between co-crystallized (*S*)-monastrol (green) and re-docked (*S*)-monastrol. Residues involved in hydrogen bonding; Glu116 (blue), Glu118 (red) and Arg119 (yellow) are shown. The surface of the allosteric site is rendered, hydrophobic, partial negative and postive regions are coloured grey, red and blue, respectively. (B) Docked configuration of (*S*)-monastrol surrounded by hydrophobic and hydrogen bonding amino acid residues.

^{1}H and $^{13}C\{^{1}H\}$ NMR spectra

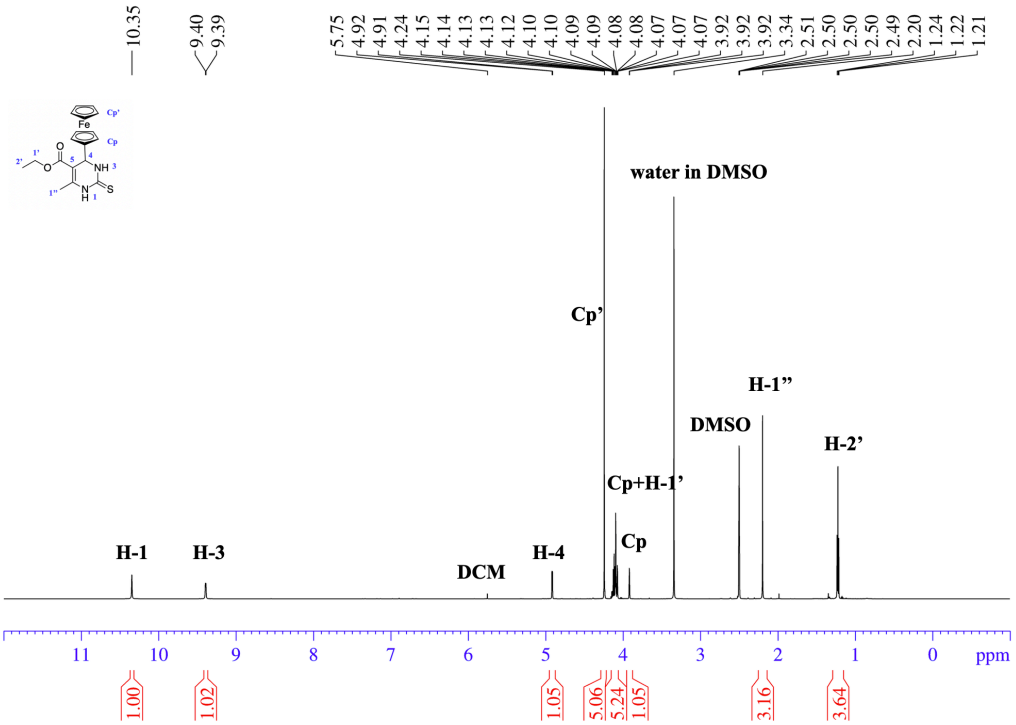

Supporting Figure S3. ^{1}H NMR spectra of 3a in DMSO-d_6.

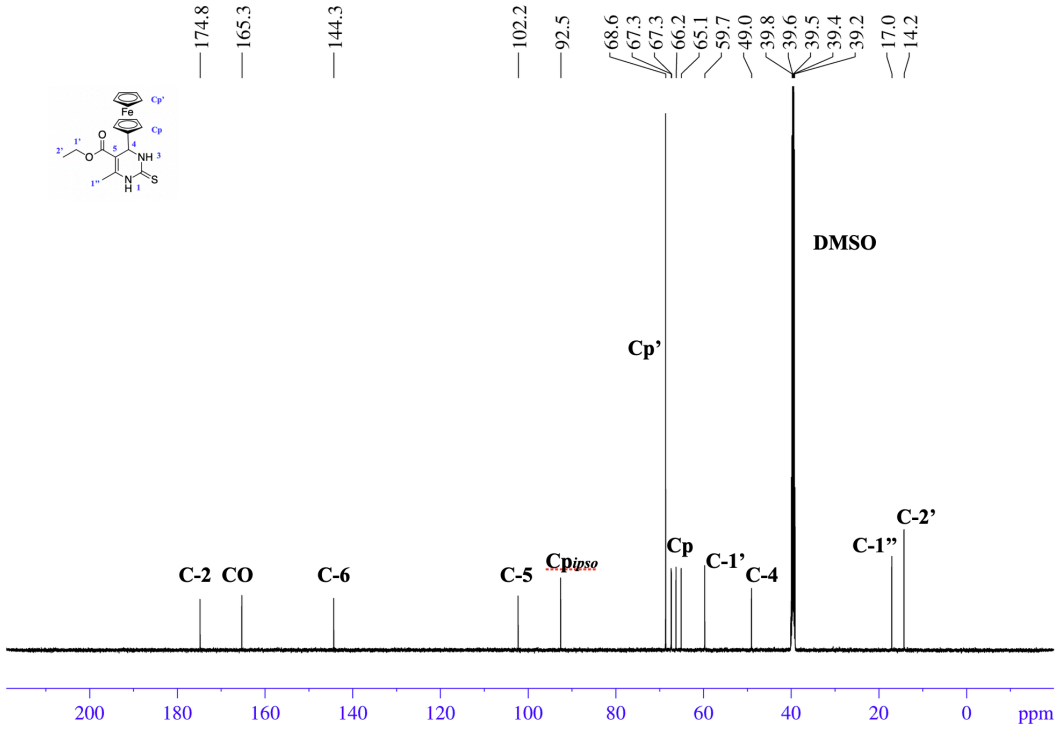

Supporting Figure S4. $^{13}C\{^{1}H\}$ NMR spectra of 3a in DMSO-d_6.

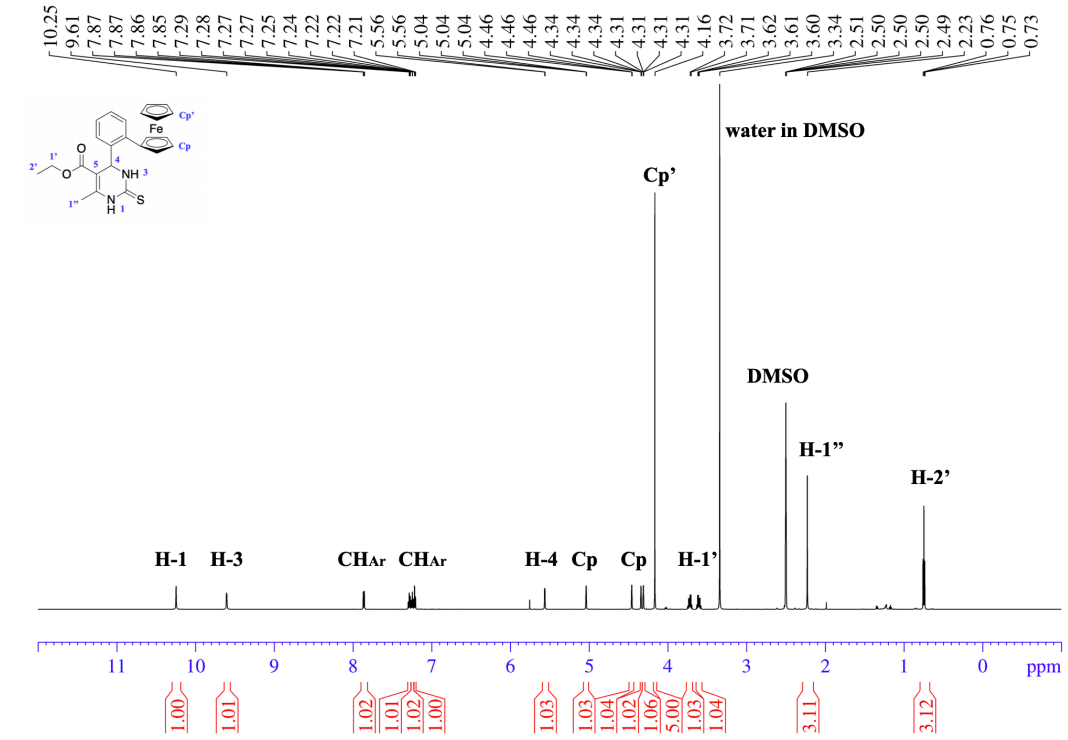

Supporting Figure S5. ^{1}H NMR spectra of 3b in DMSO-d$_6$.

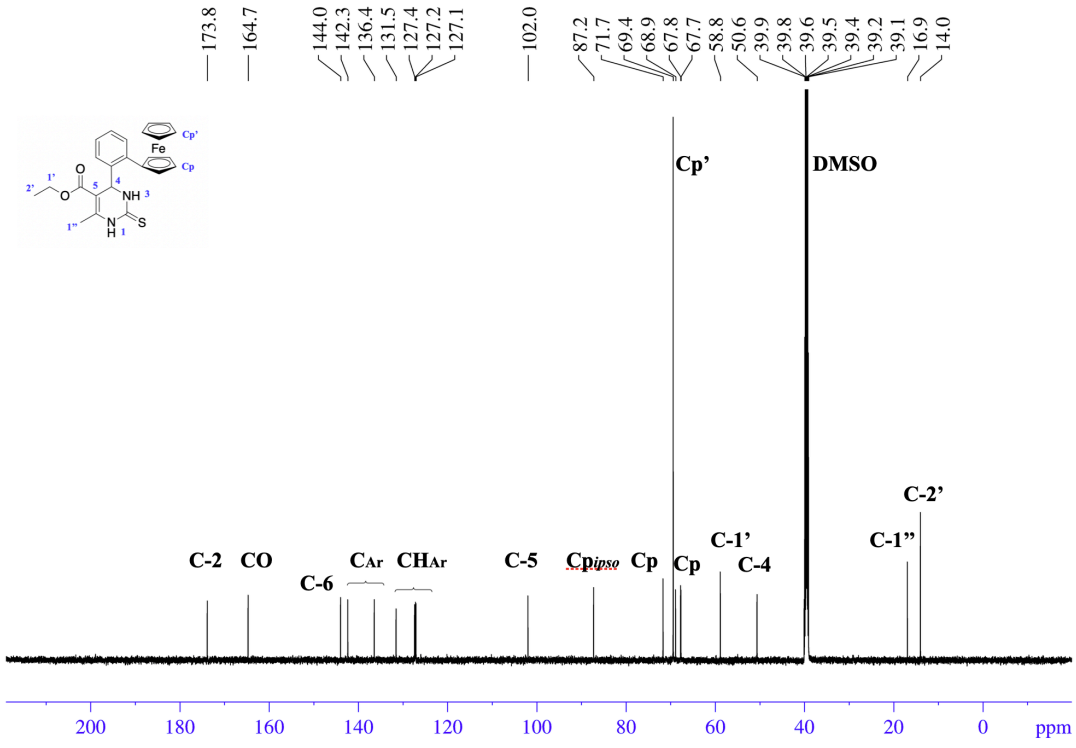

Supporting Figure S6. ^{13}C{^{1}H} NMR spectra of 3b in DMSO-d$_6$.

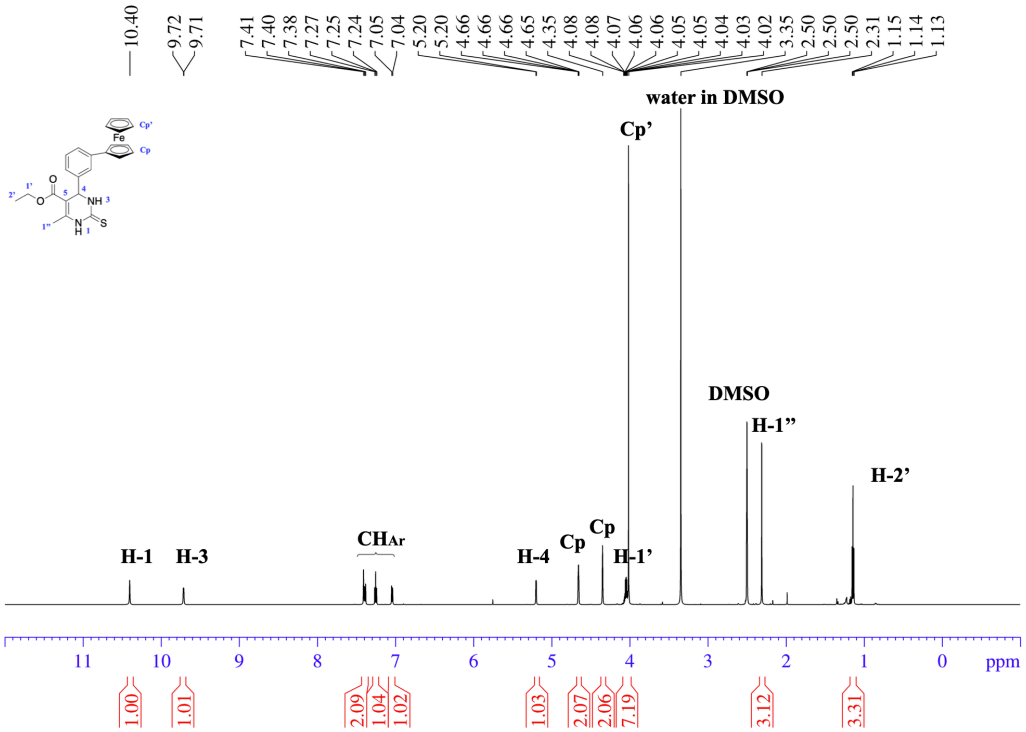

Supporting Figure S7. ^{1}H NMR spectra of 3c in DMSO-d_6.

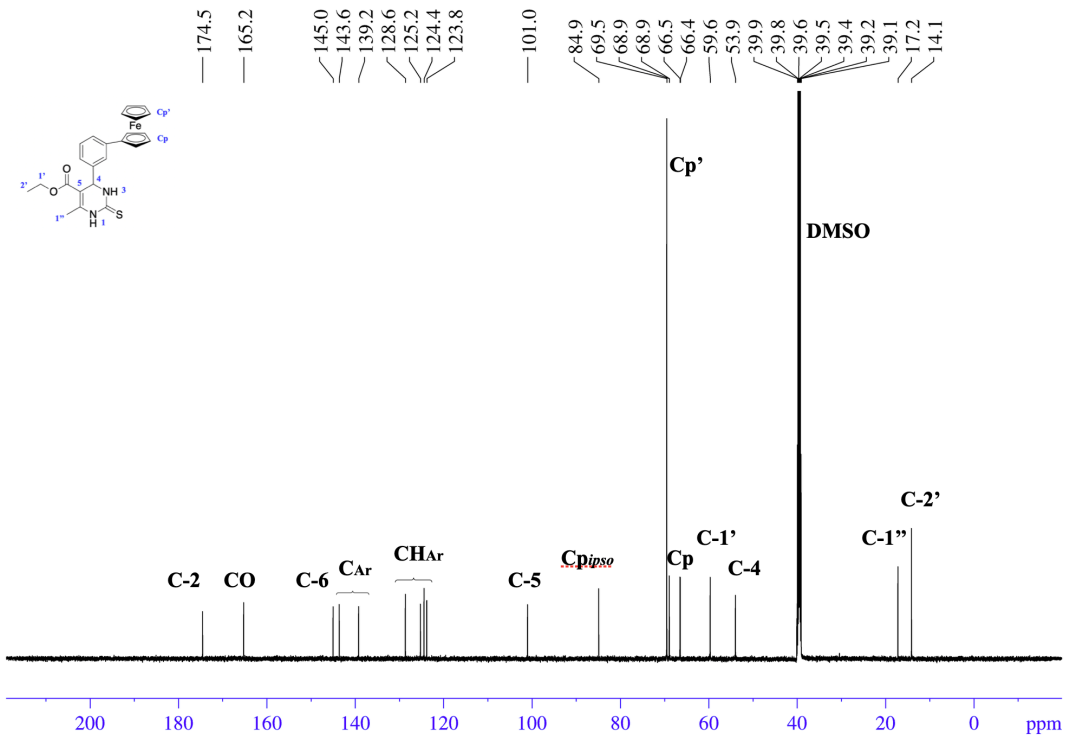

Supporting Figure S8. $^{13}C\{^{1}H\}$ NMR spectra of 3c in DMSO-d_6.

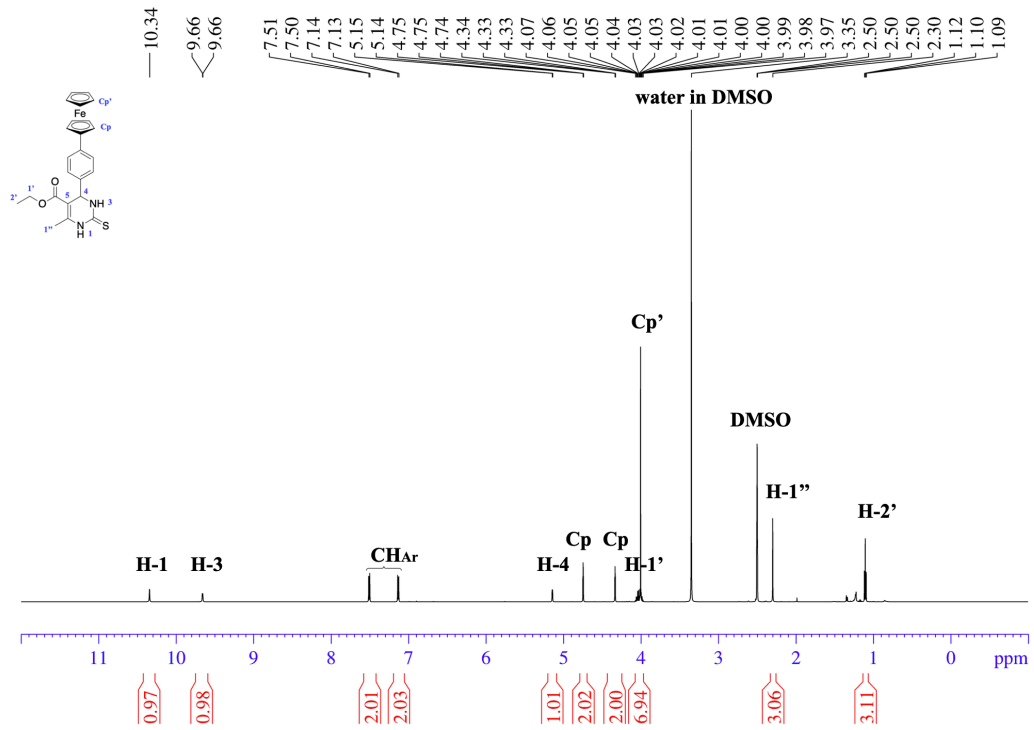

Supporting Figure S9. ^{1}H NMR spectra of 3d in DMSO-d$_6$.

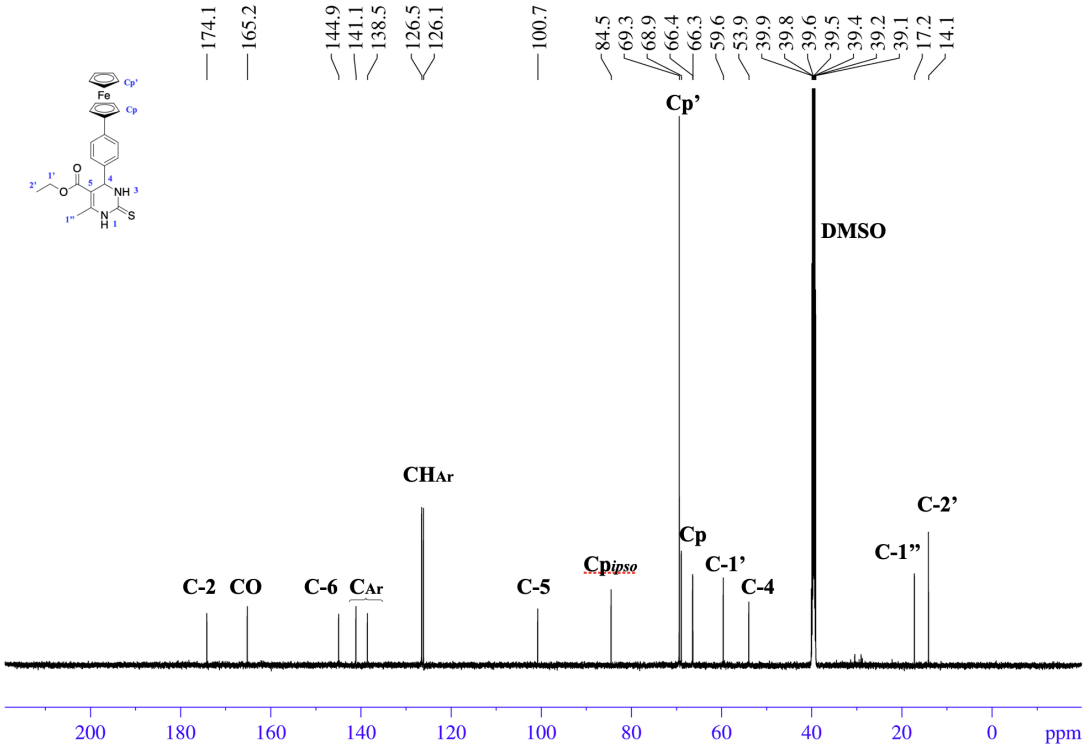

Supporting Figure S10. ^{13}C{^{1}H} NMR spectra of 3d in DMSO-d$_6$.

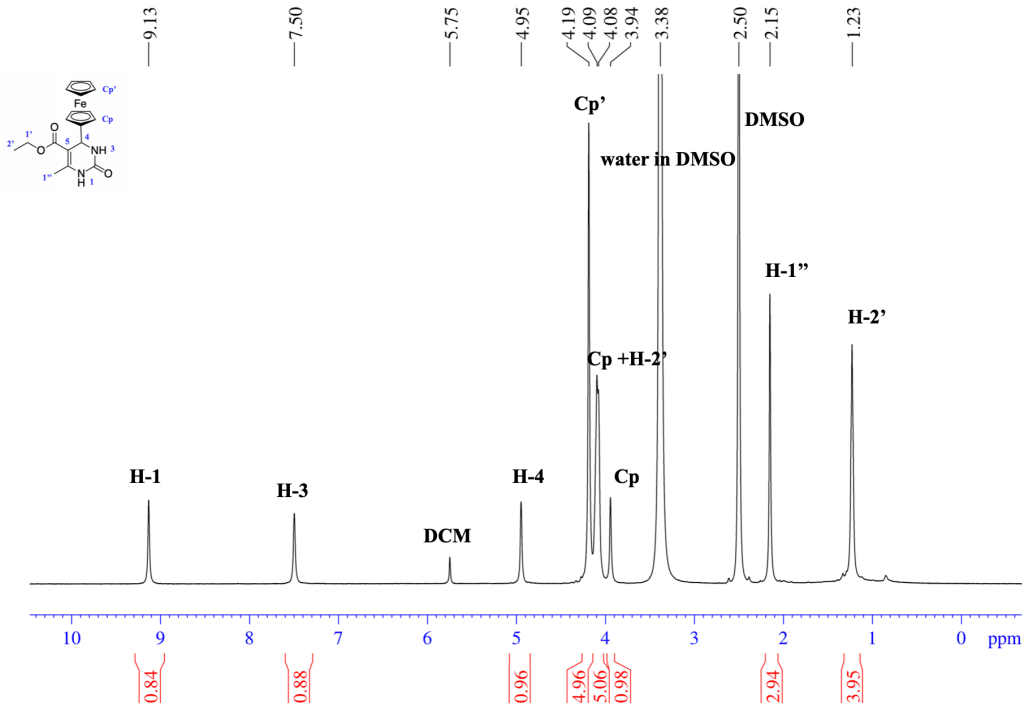

Supporting Figure S11. ^{1}H NMR spectra of 4a in DMSO-d$_6$.

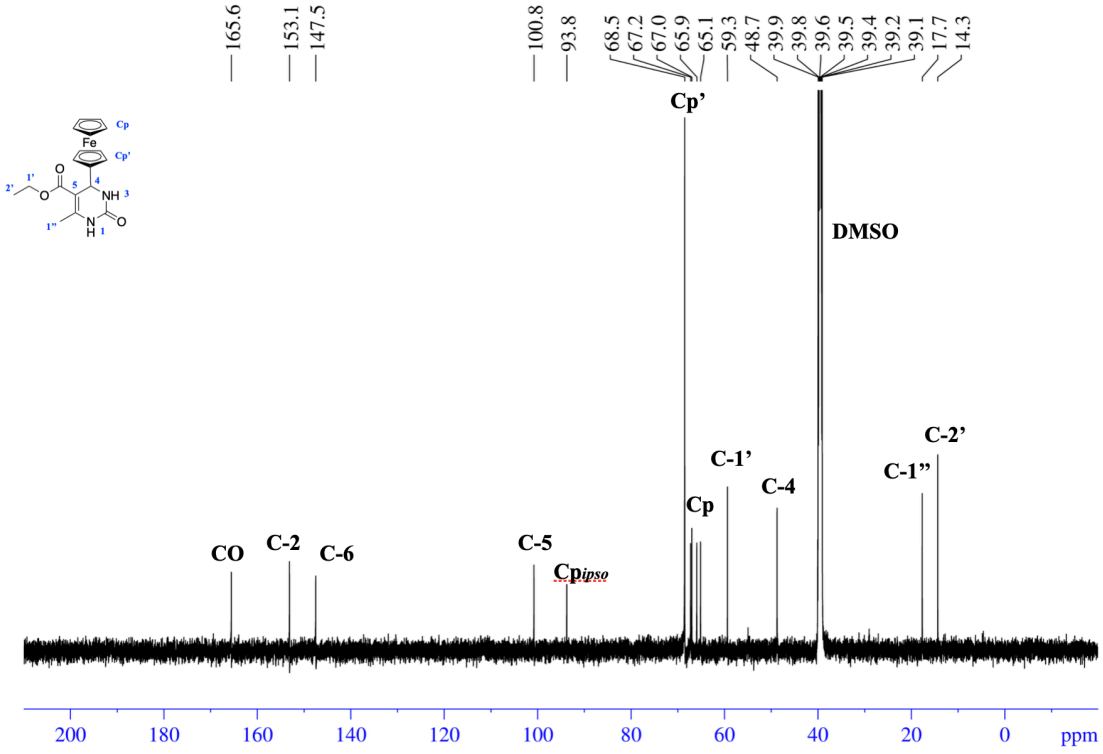

Supporting Figure S12. ^{13}C{^{1}H} NMR spectra of 4a in DMSO-d$_6$.

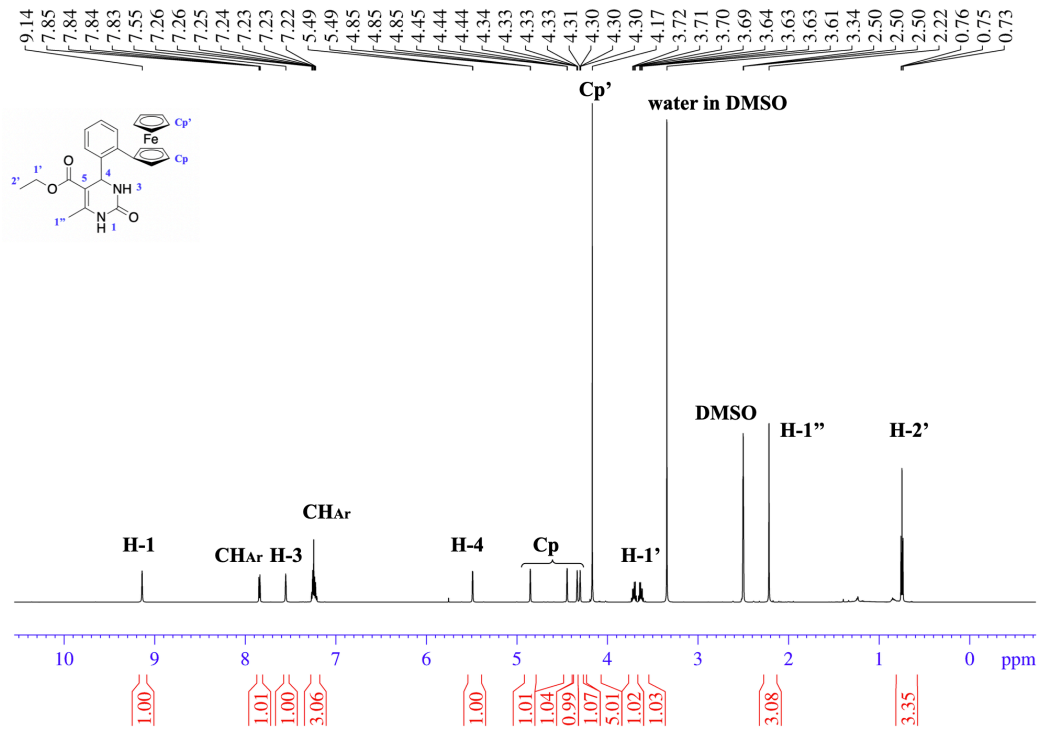

Supporting Figure S13. ^{1}H NMR spectra of 4b in DMSO-d$_6$.

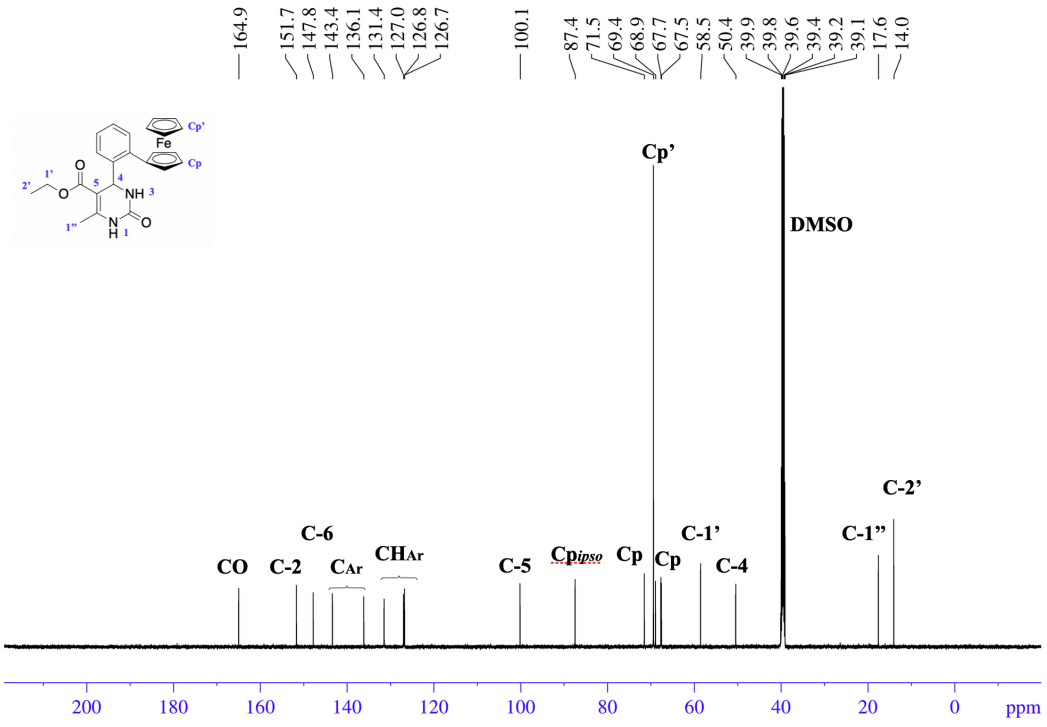

Supporting Figure S14. ^{13}C{^{1}H} NMR spectra of 4b in DMSO-d$_6$.

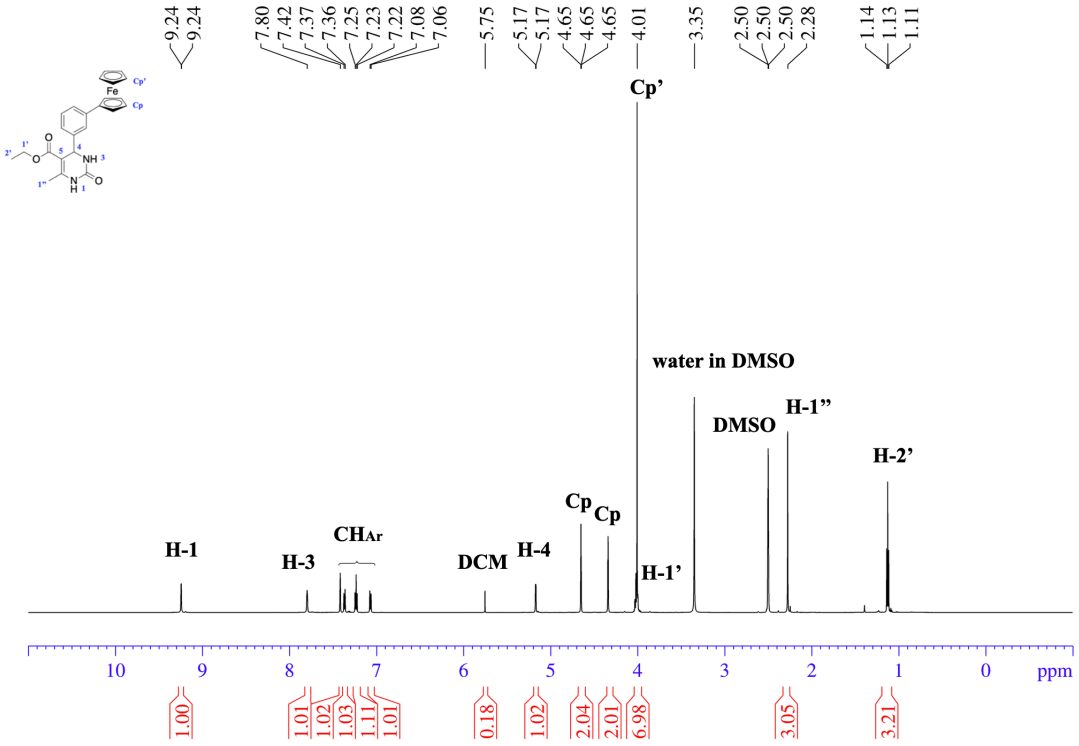

Supporting Figure S15. ^{1}H NMR spectra of 4c in DMSO-d$_6$.

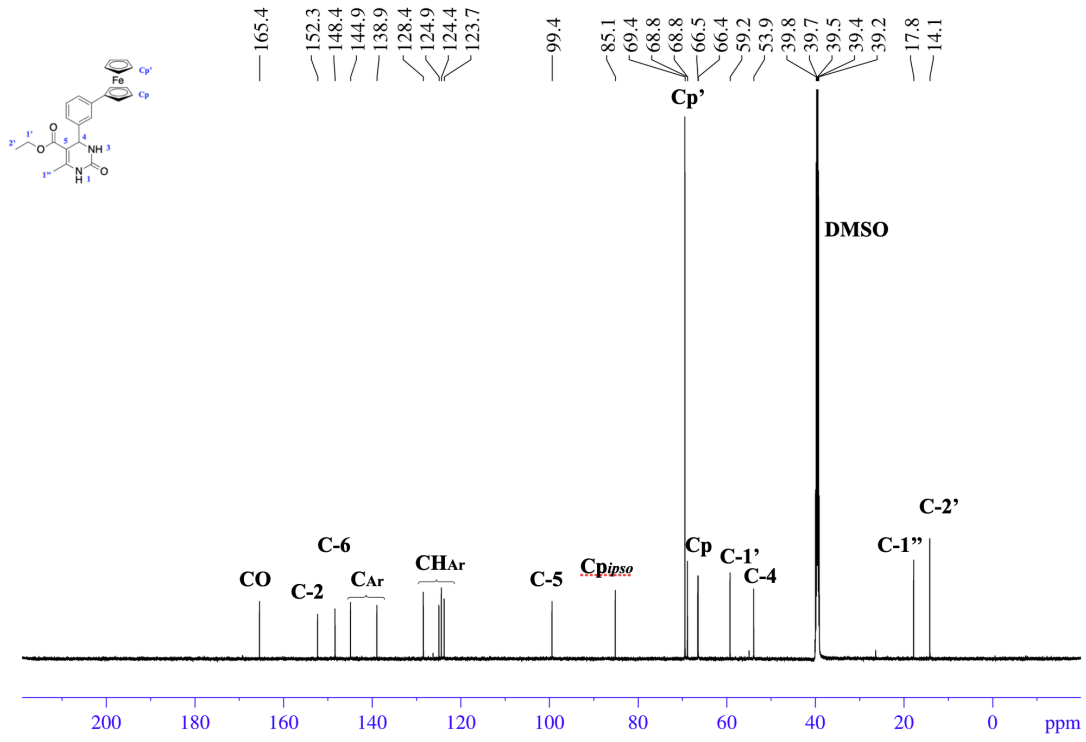

Supporting Figure S16. ^{13}C{^{1}H} NMR spectra of 4c in DMSO-d$_6$.

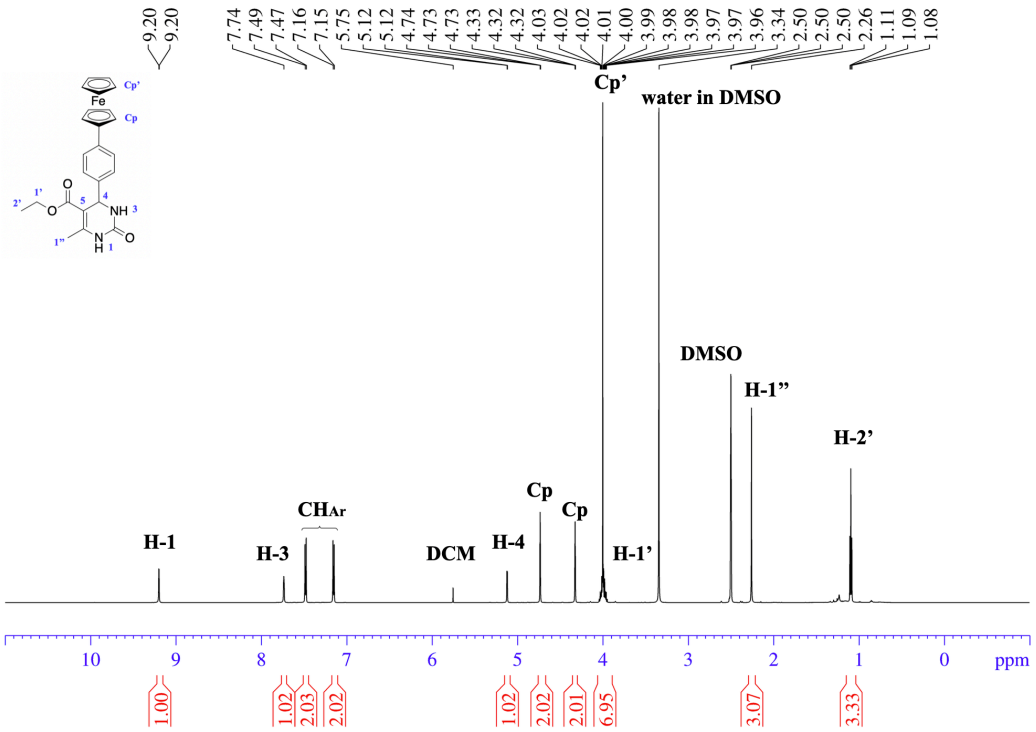

Supporting Figure S17. ^{1}H NMR spectra of 4d in DMSO-d$_6$.

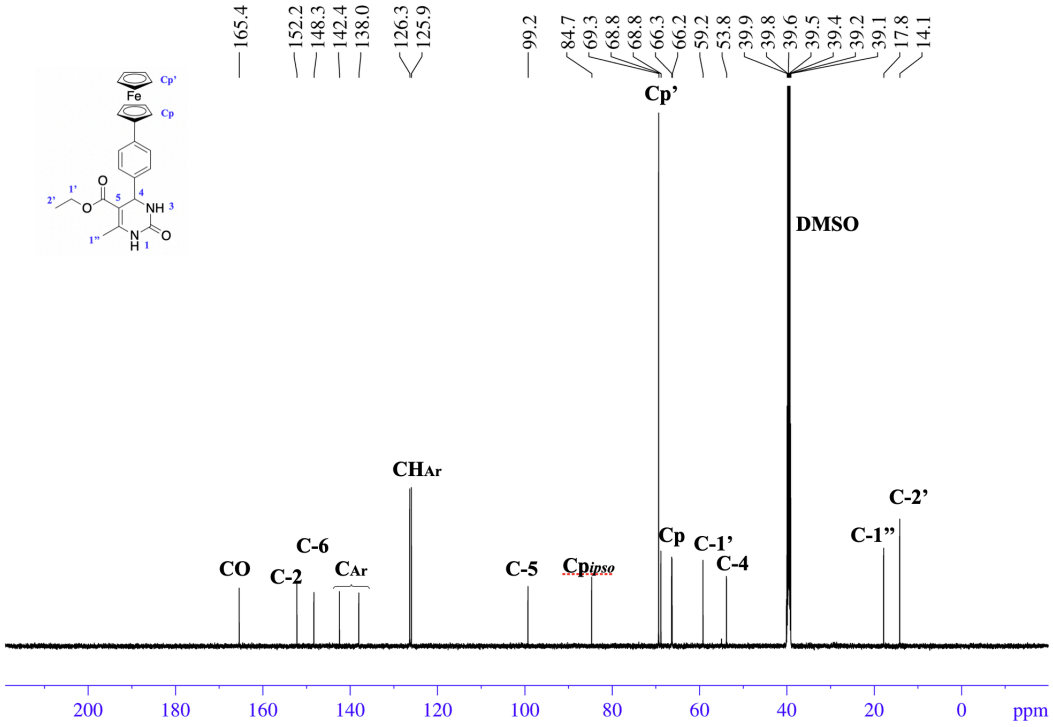

Supporting Figure S18. ^{13}C{^{1}H} NMR spectra of 4d in DMSO-d$_6$.

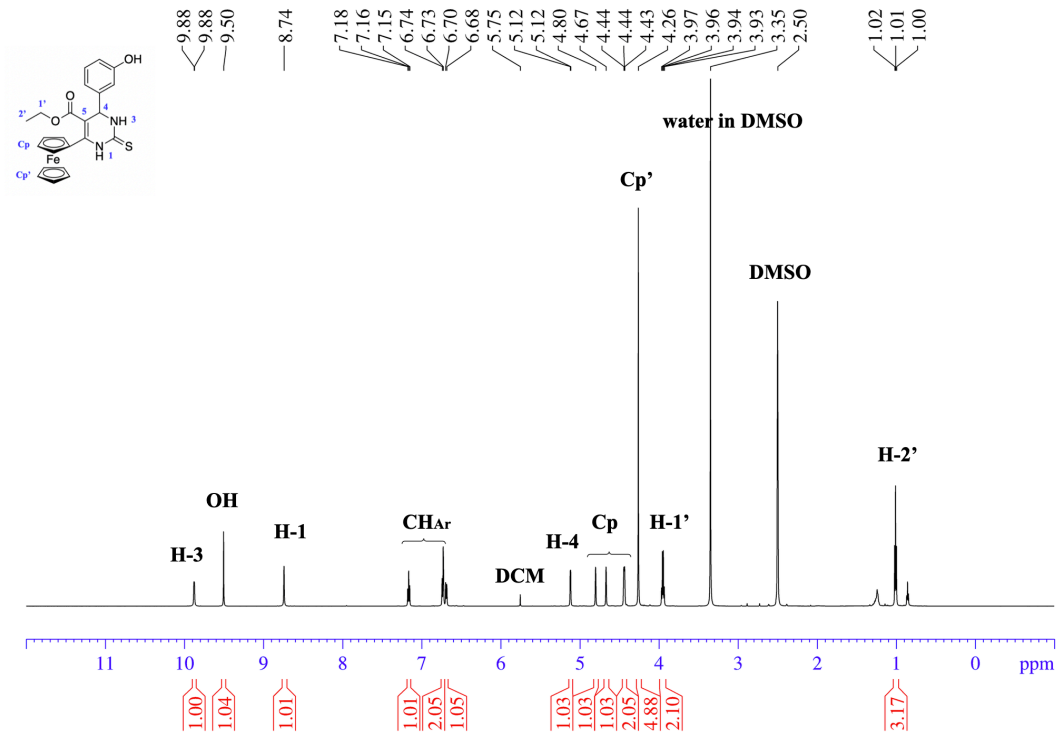

Supporting Figure S19. ^{1}H NMR spectra of 6a in DMSO-d$_6$.

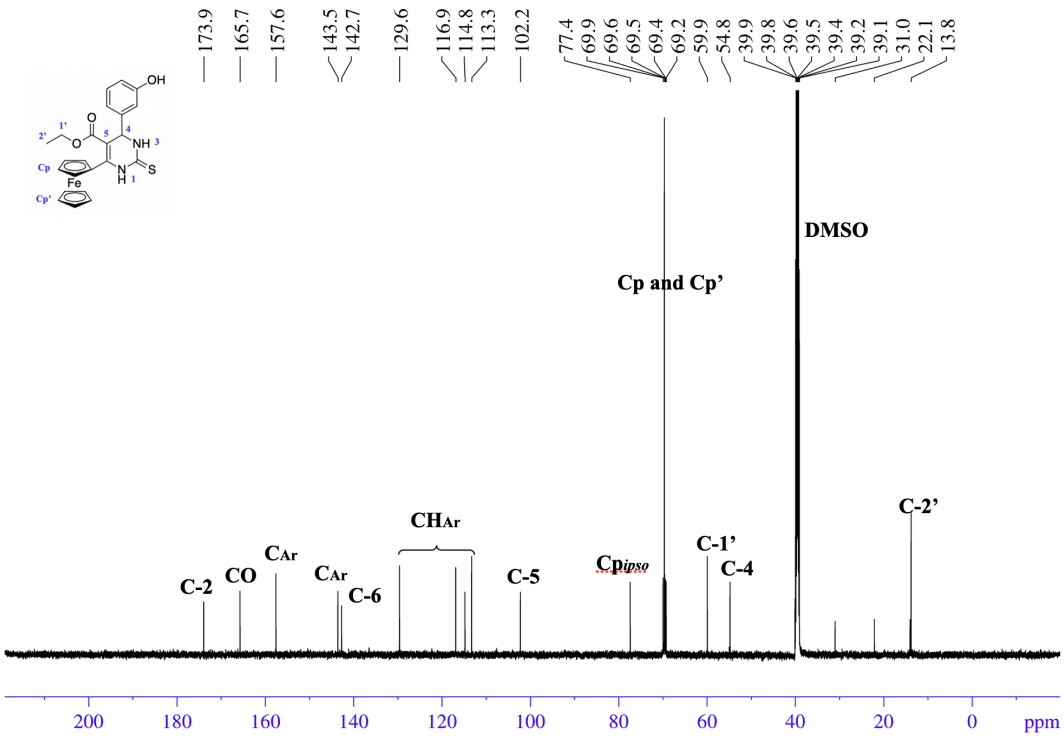

Supporting Figure S20. ^{13}C{^{1}H} NMR spectra of 6a in DMSO-d$_6$.

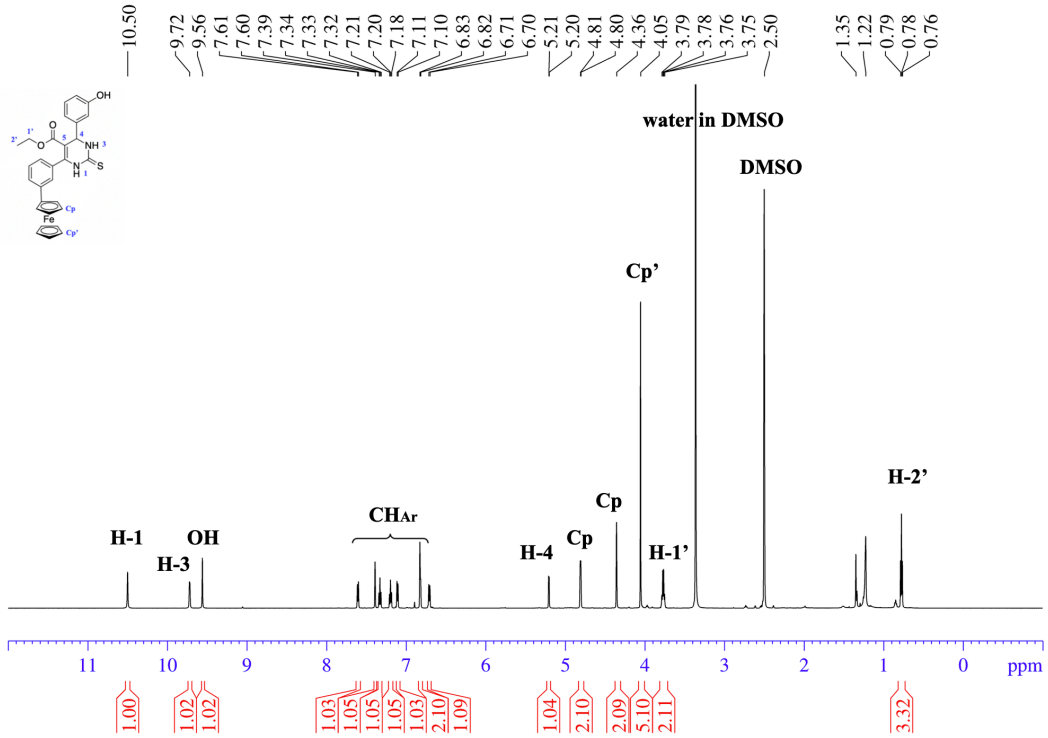

Supporting Figure S21. ^{1}H NMR spectra of 6c in DMSO-d$_6$.

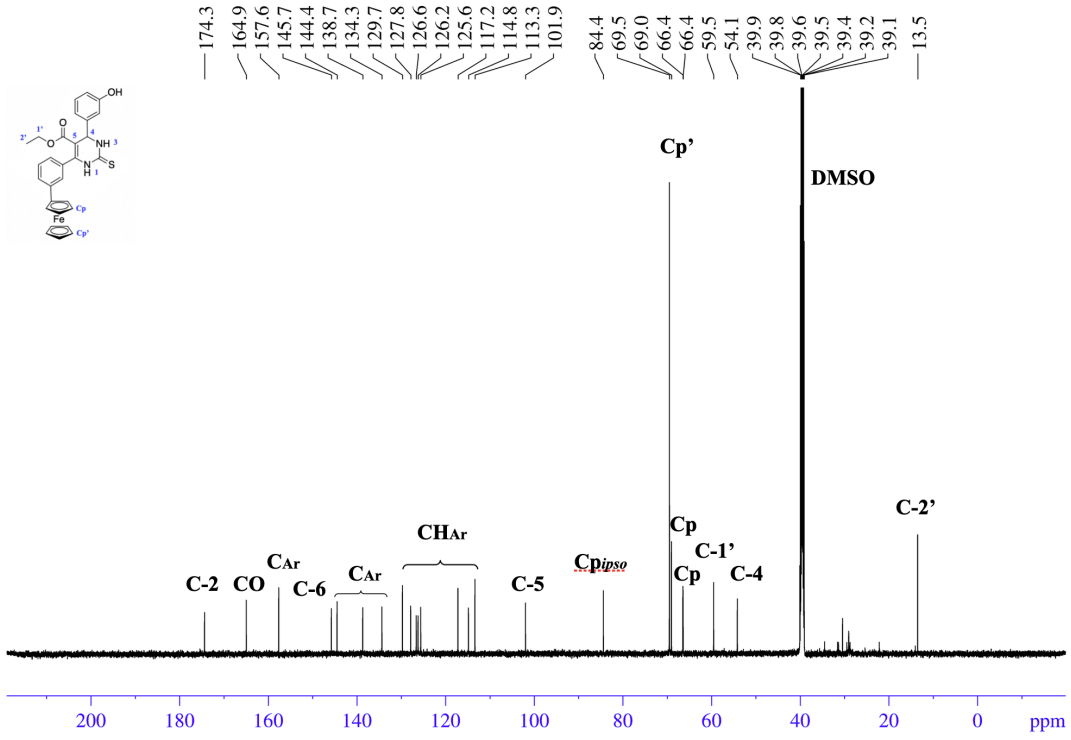

Supporting Figure S22. ^{13}C{^{1}H} NMR spectra of 6c in DMSO-d$_6$.

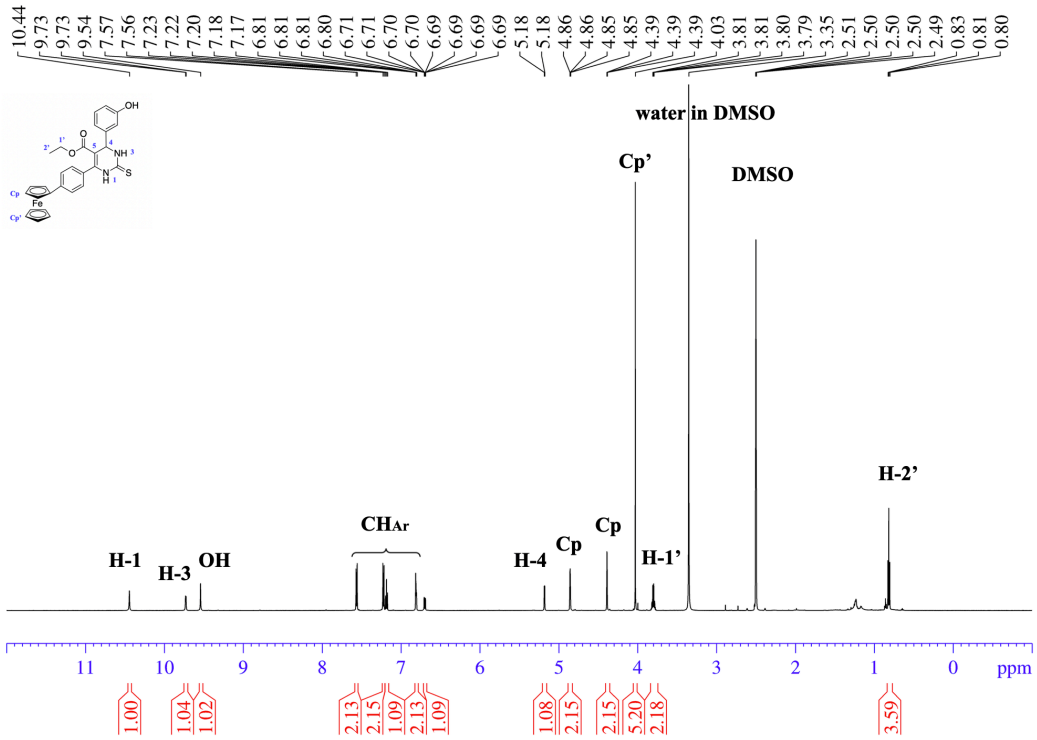

Supporting Figure S23. ^{1}H NMR spectra of 6d in DMSO-d$_6$.

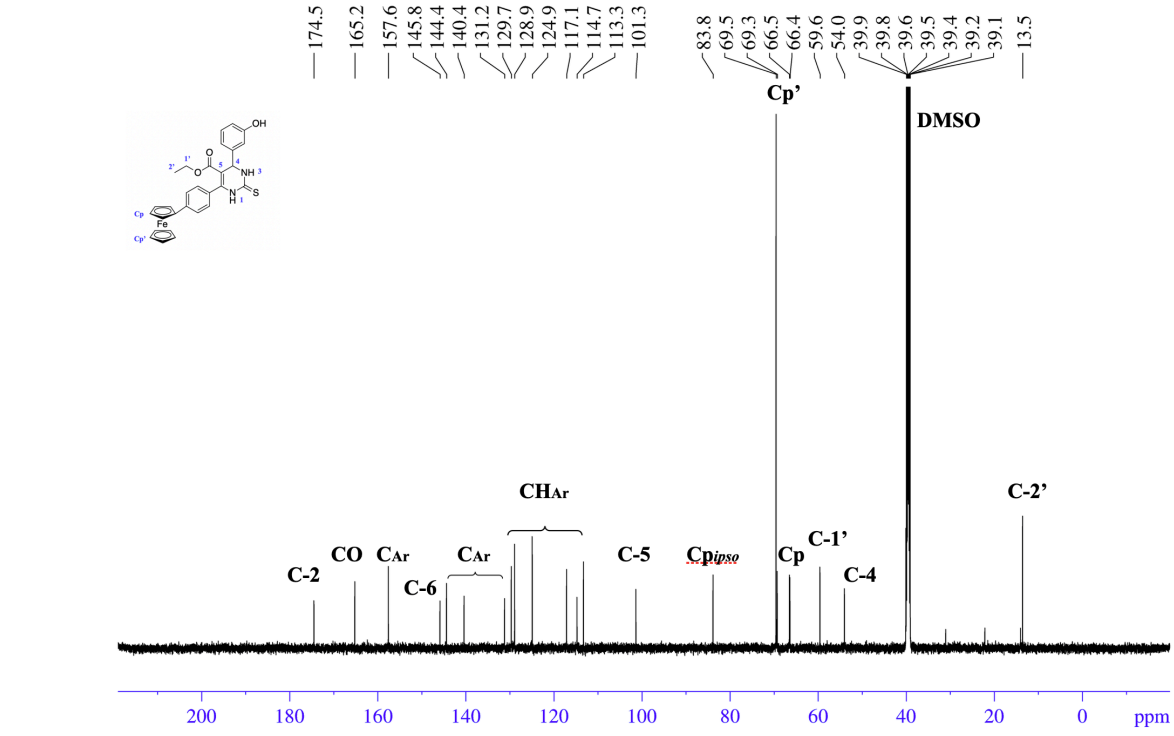

Supporting Figure S24. ^{13}C{^{1}H} NMR spectra of 6d in DMSO-d$_6$.

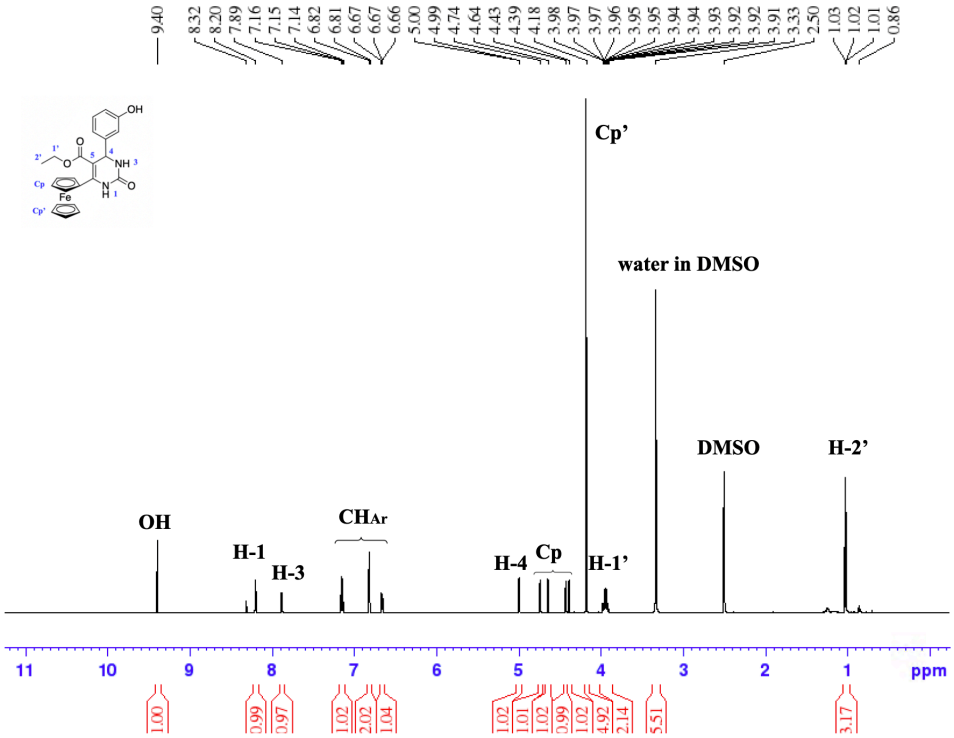

Supporting Figure S25. ^{1}H NMR spectra of 7a in DMSO-d$_6$.

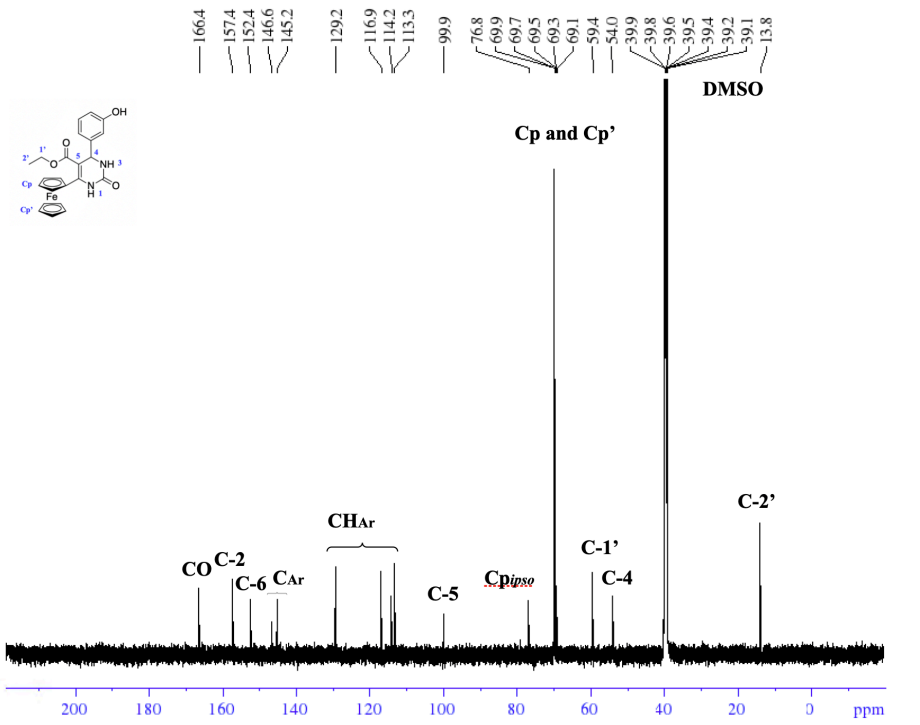

Supporting Figure S26. ^{13}C{^{1}H} NMR spectra of 7a in DMSO-d$_6$.

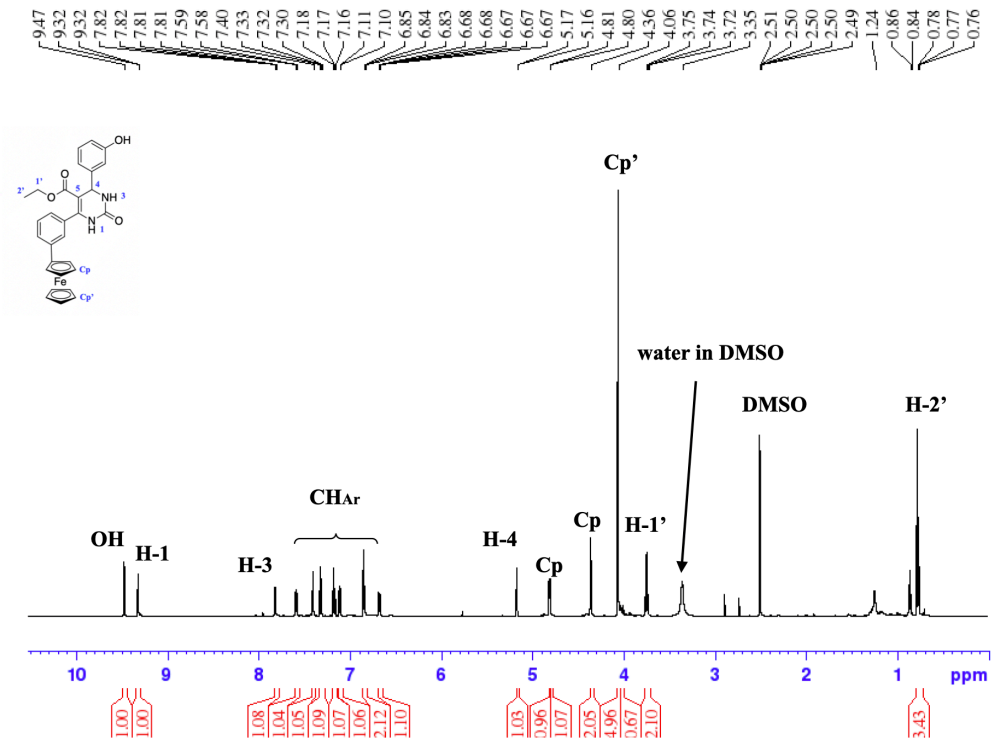

Supporting Figure S27. ^{1}H NMR spectra of 7c in DMSO-d$_6$.

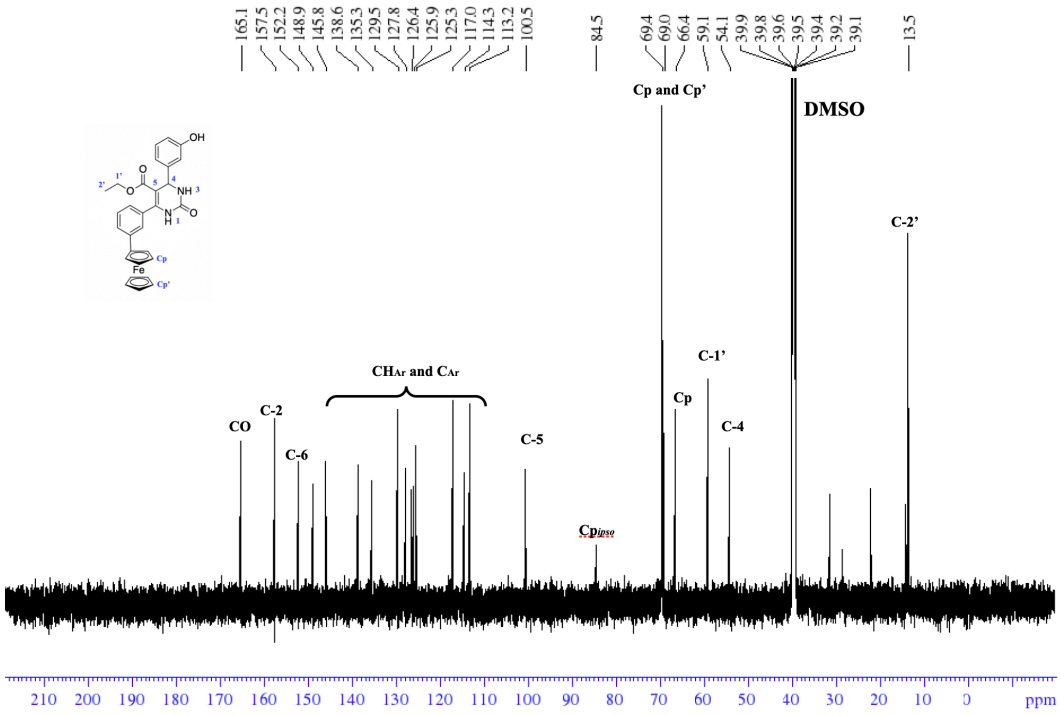

Supporting Figure S28. ^{13}C{^{1}H} NMR spectra of 7c in DMSO-d$_6$.

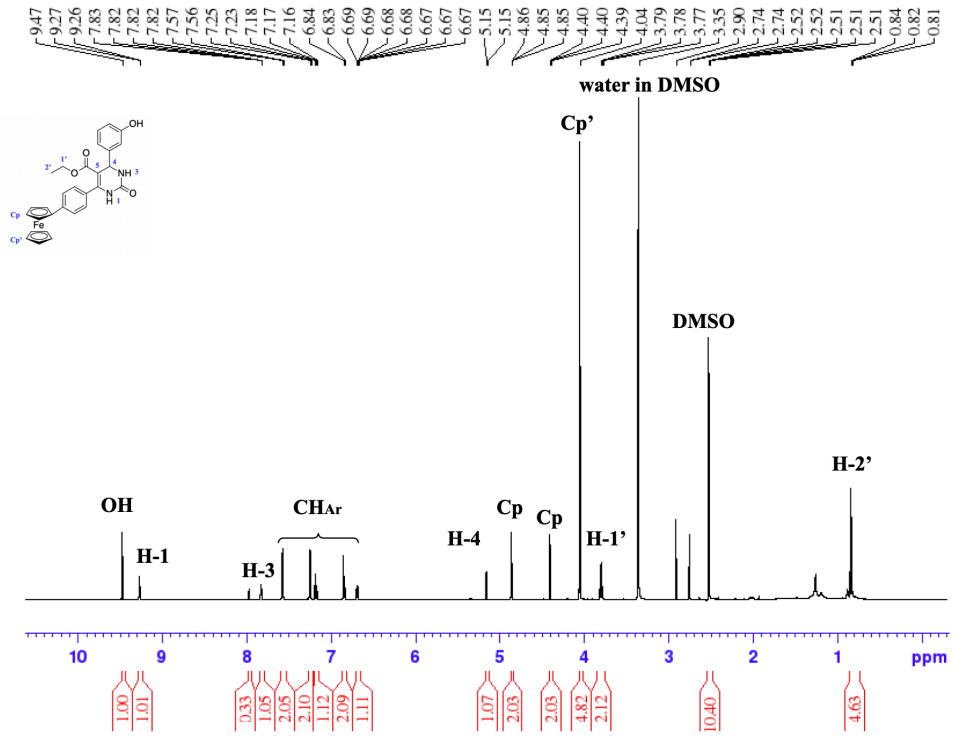

Supporting Figure S29. ^{1}H NMR spectra of 7d in DMSO-d$_6$.

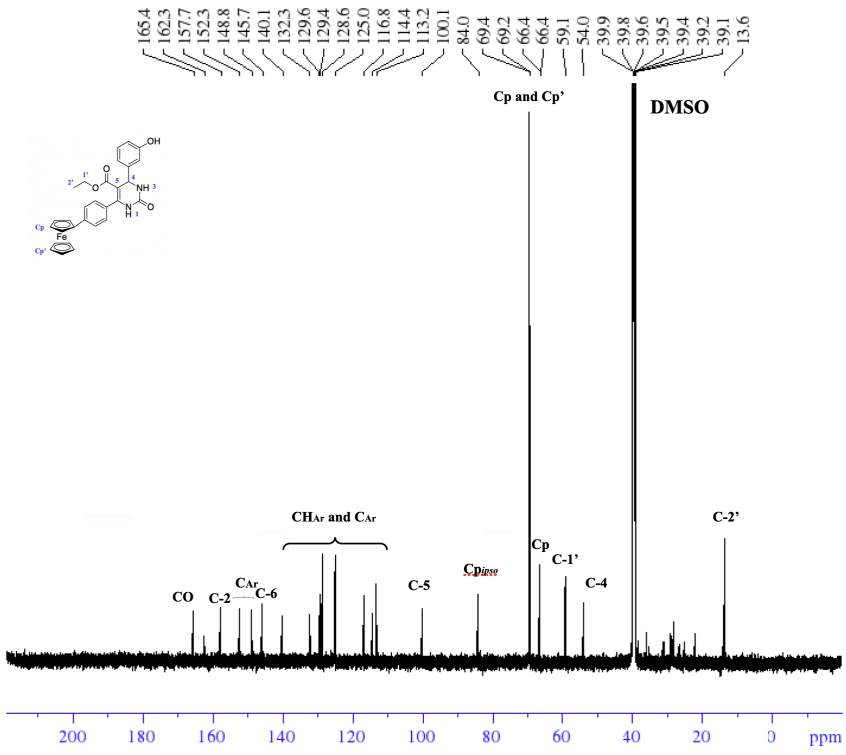

Supporting Figure S30. ^{13}C{^{1}H} NMR spectra of 7d in DMSO-d$_6$.

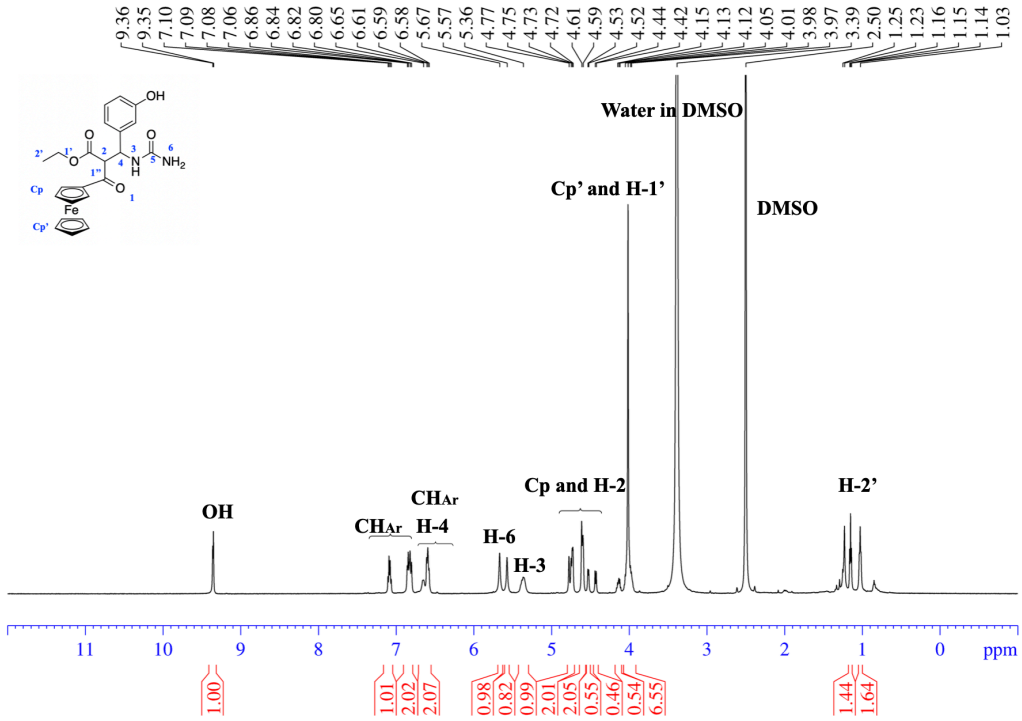

Supporting Figure S31. ^{1}H NMR spectra of 8a in DMSO-d$_6$.

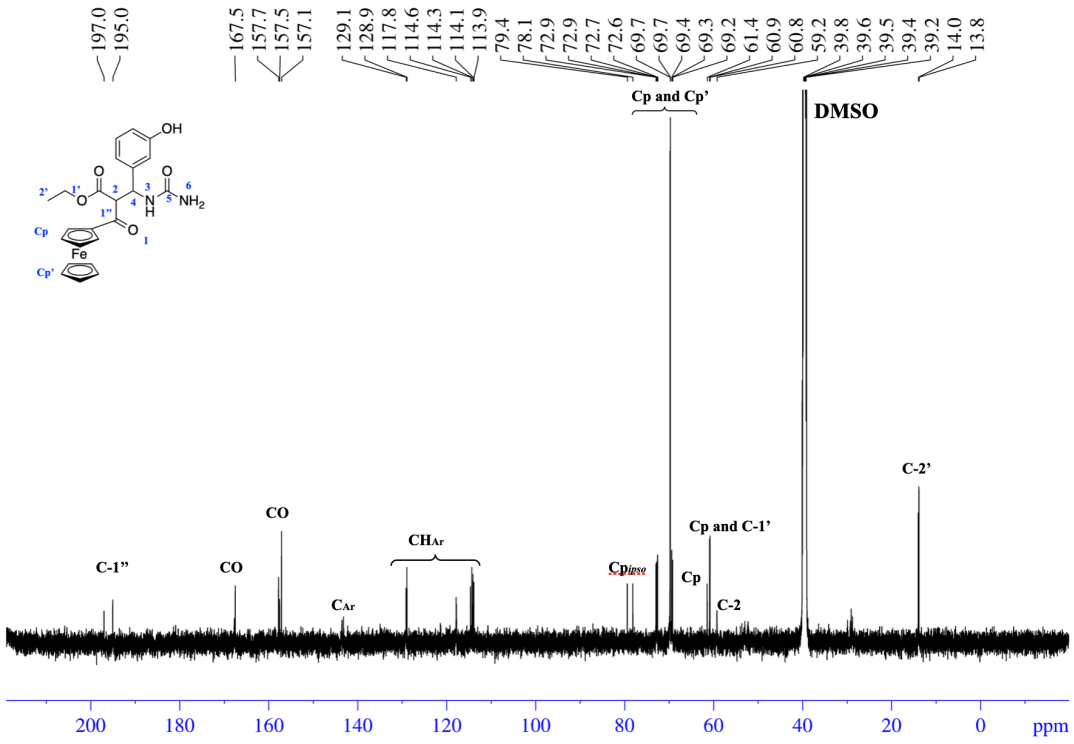

Supporting Figure S32. ^{13}C{^{1}H} NMR spectra of 8a in DMSO-d$_6$.

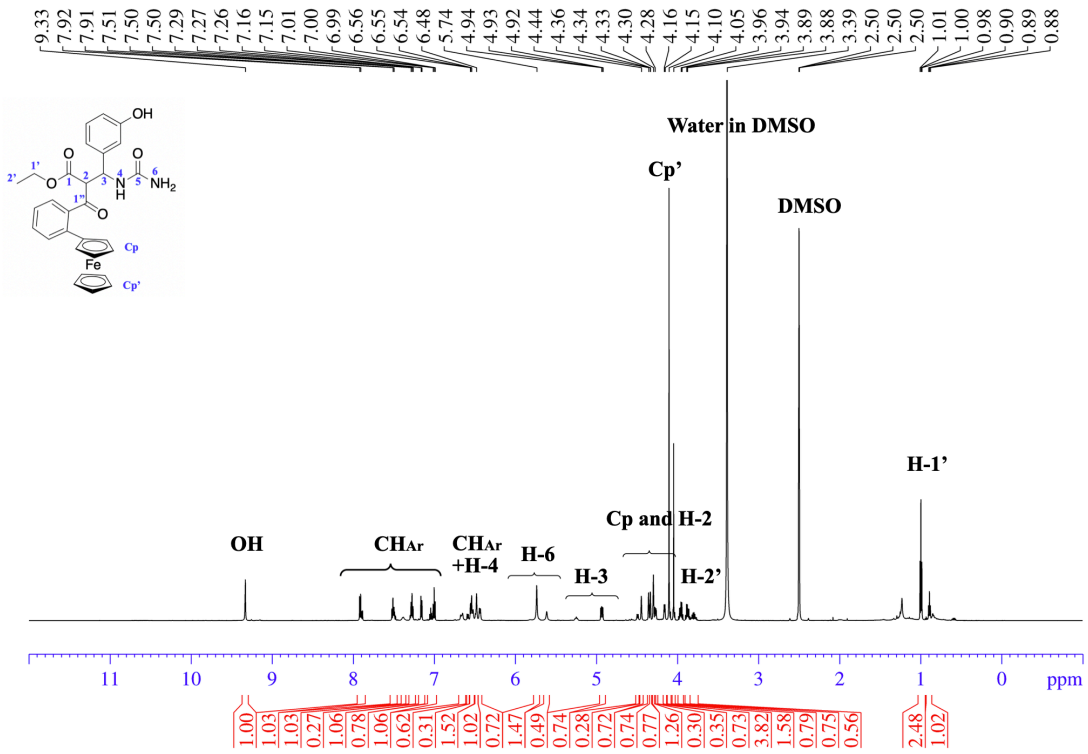

Supporting Figure S33. ^{1}H NMR spectra of 8b in DMSO-d$_6$.

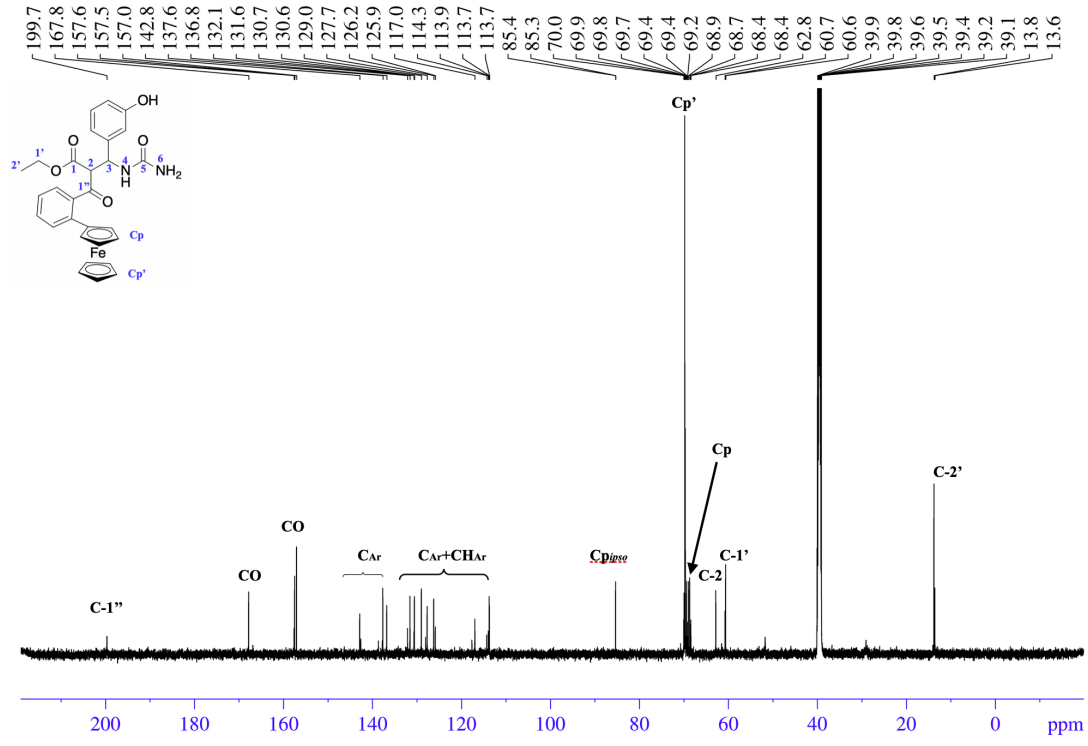

Supporting Figure S34. ^{13}C{^{1}H} NMR spectra of 8b in DMSO-d$_6$.

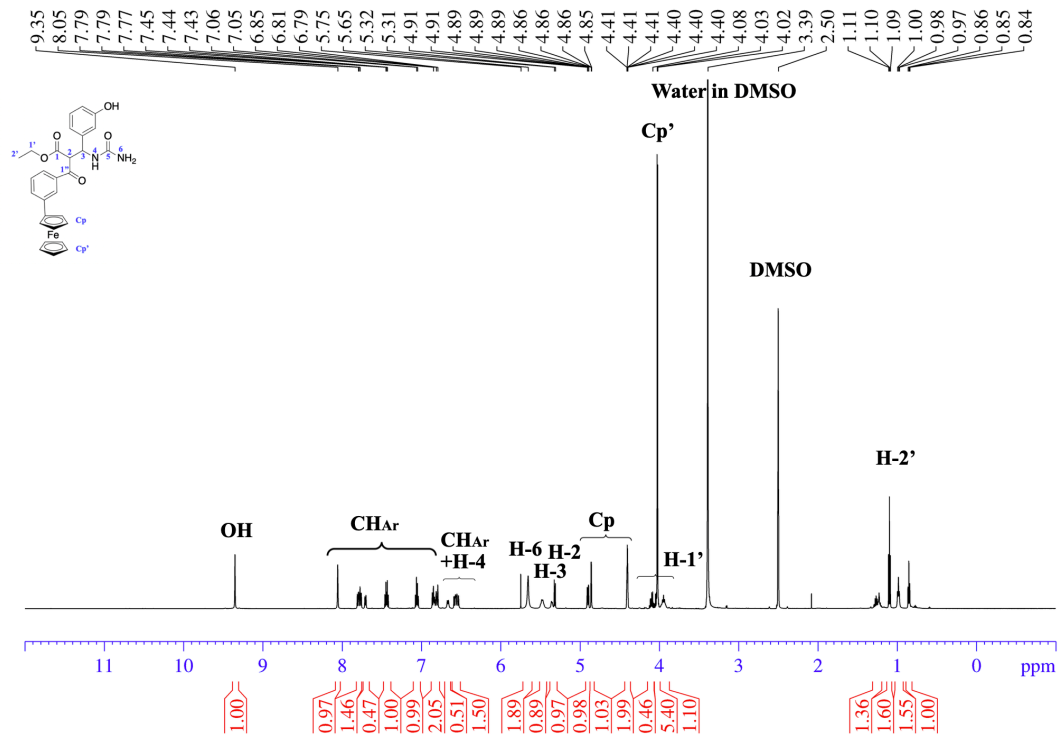

Supporting Figure S35. ^{1}H NMR spectra of 8c in DMSO-d$_6$.

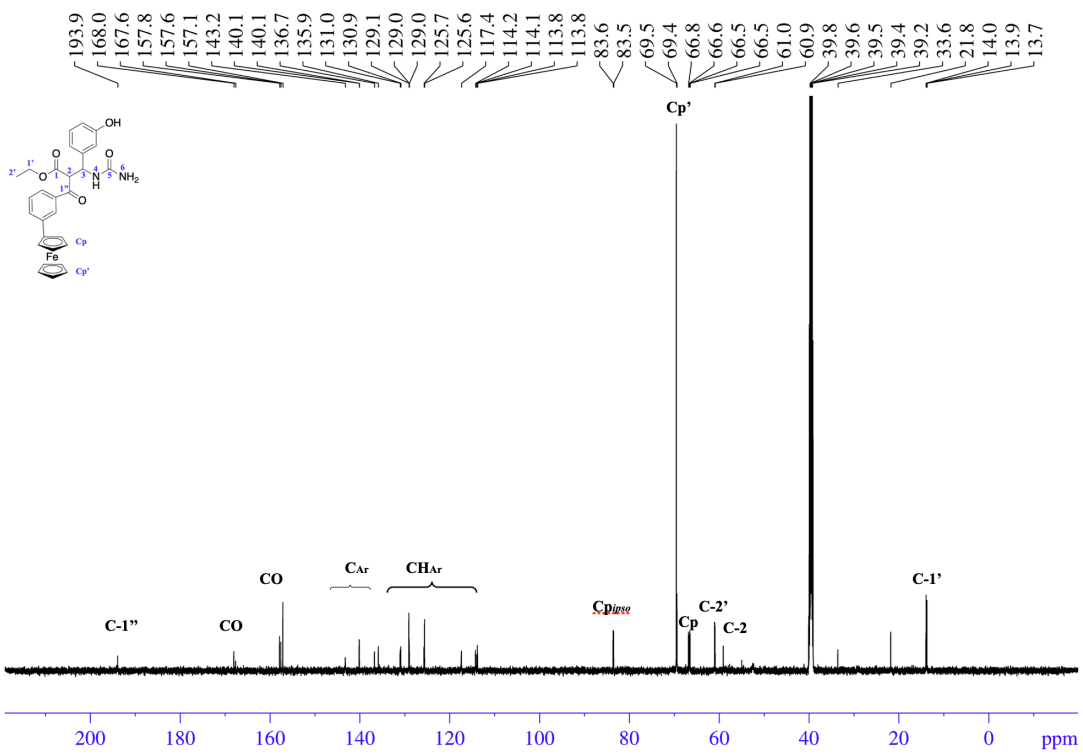

Supporting Figure S36. ^{13}C{^{1}H} NMR spectra of 8c in DMSO-d$_6$.

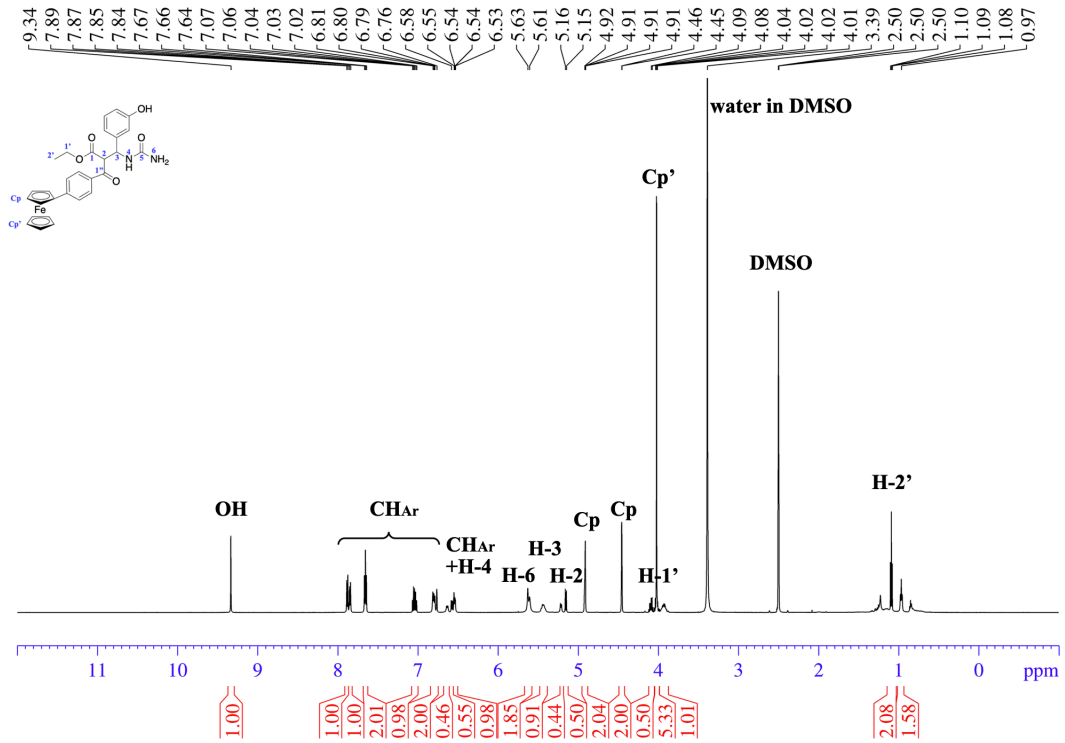

Supporting Figure S37. ^{1}H NMR spectra of 8d in DMSO-d$_6$.

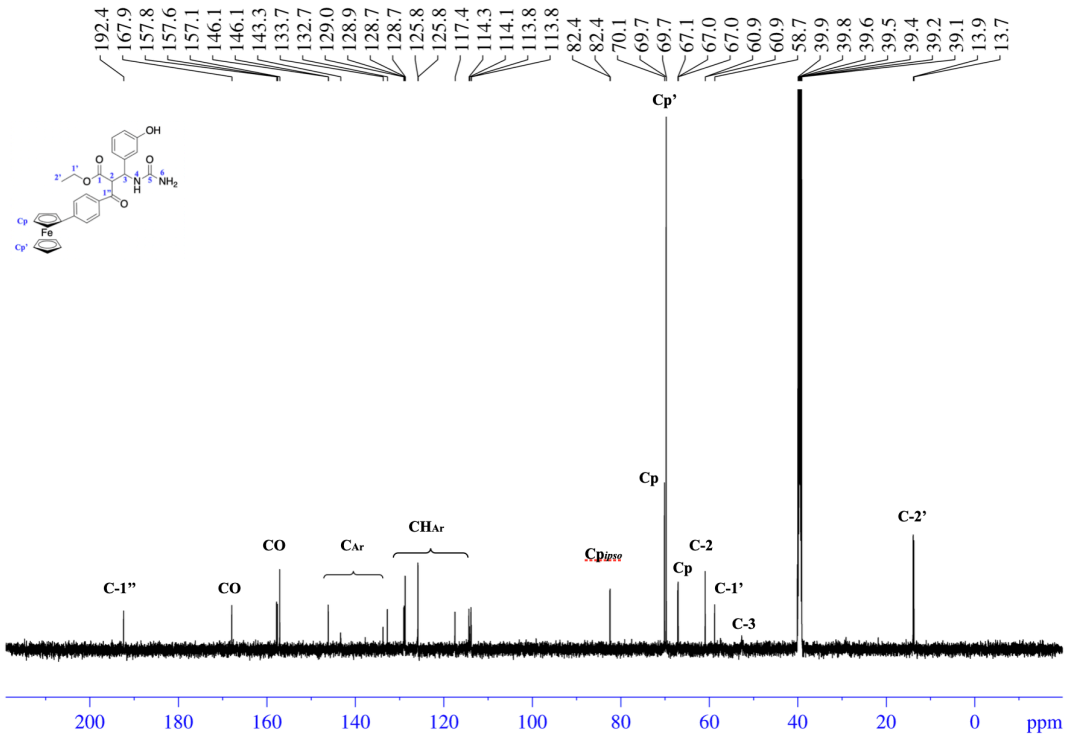

Supporting Figure S38. ^{13}C{^{1}H} NMR spectra of 8d in DMSO-d$_6$.

LC-MS analysis

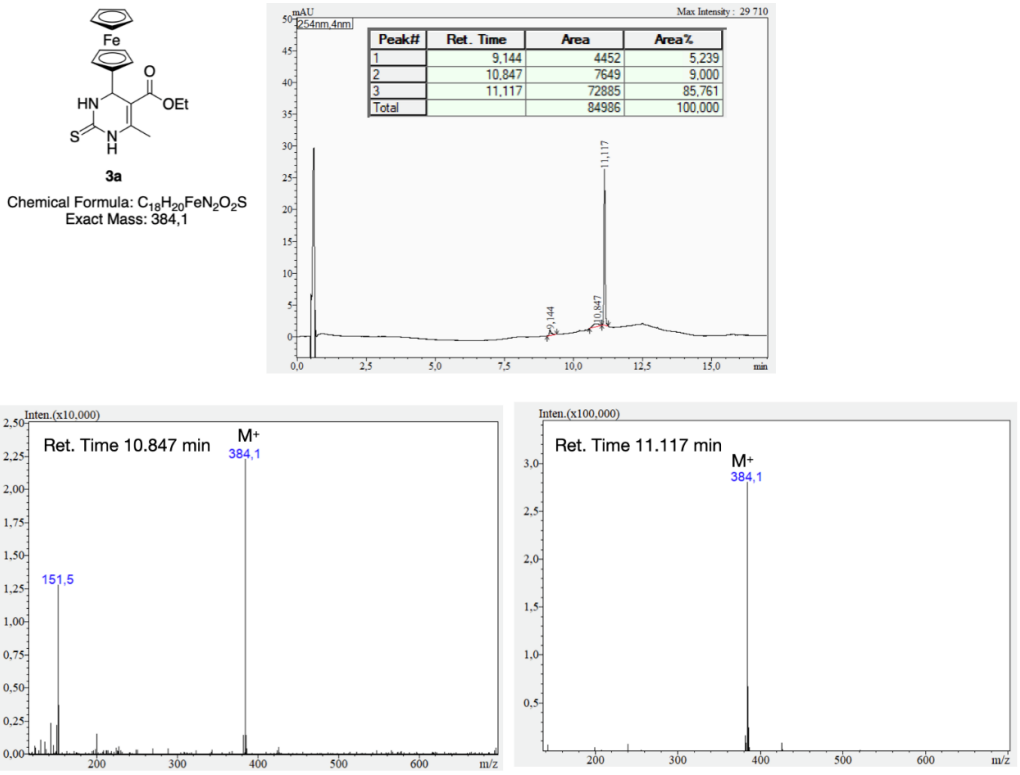

Supporting Figure S39. LC-MS analysis of 3a.

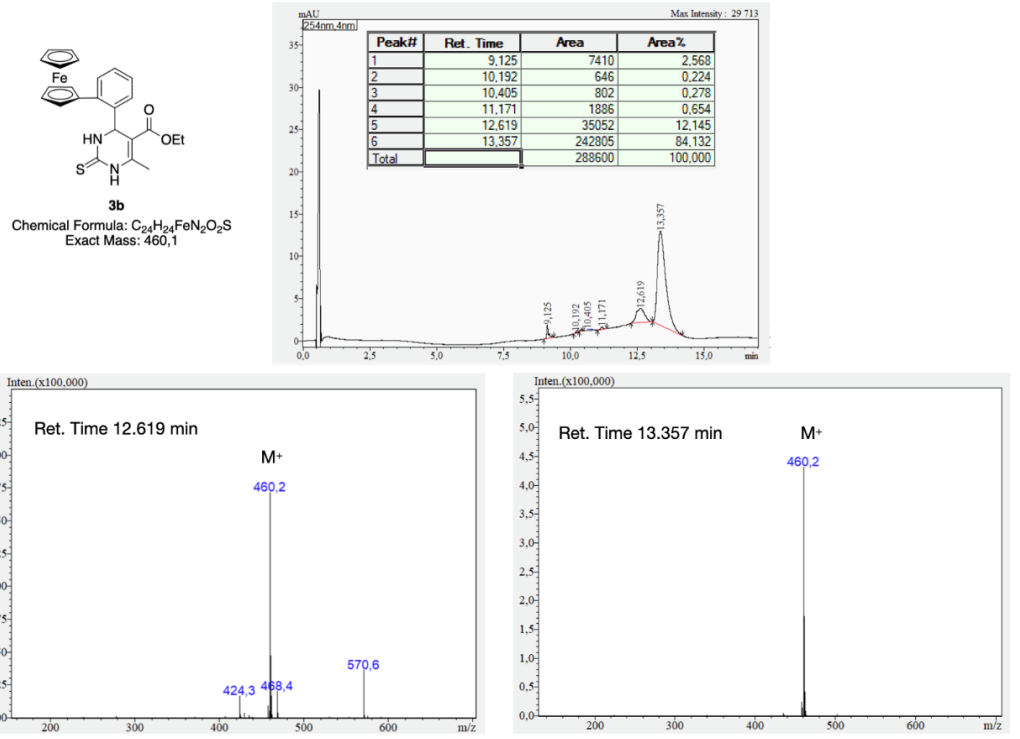

Supporting Figure S40. LC-MS analysis of 3b.

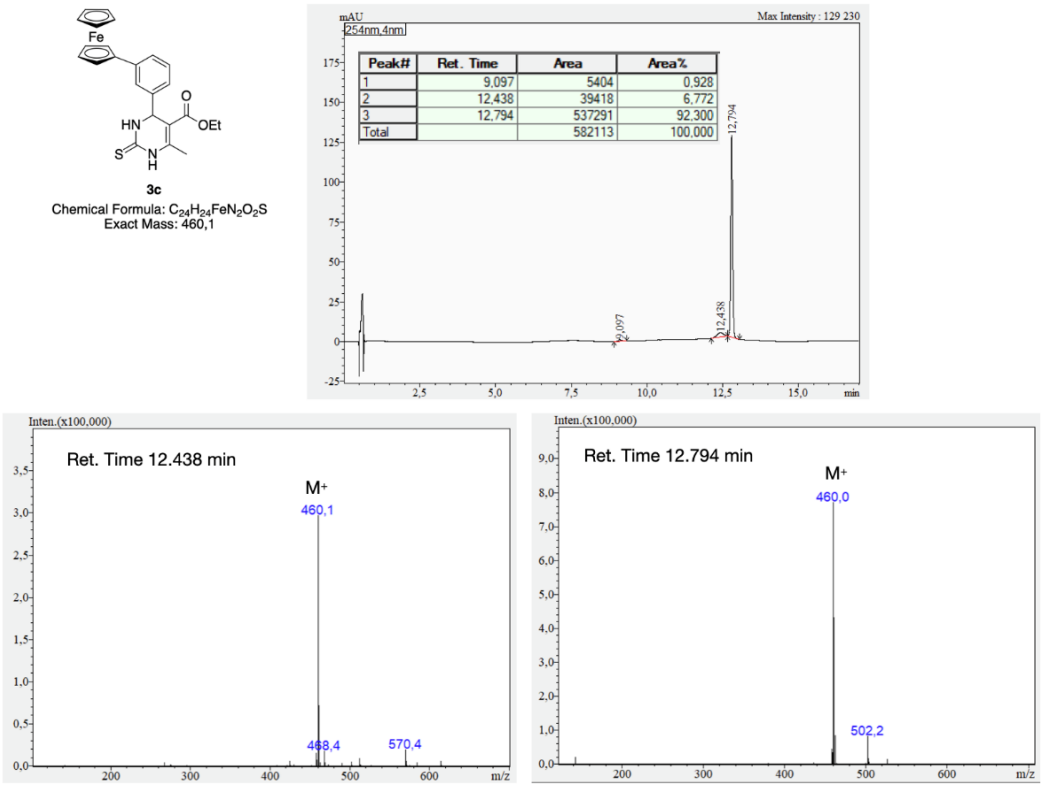

Supporting Figure S41. LC-MS analysis of 3c.

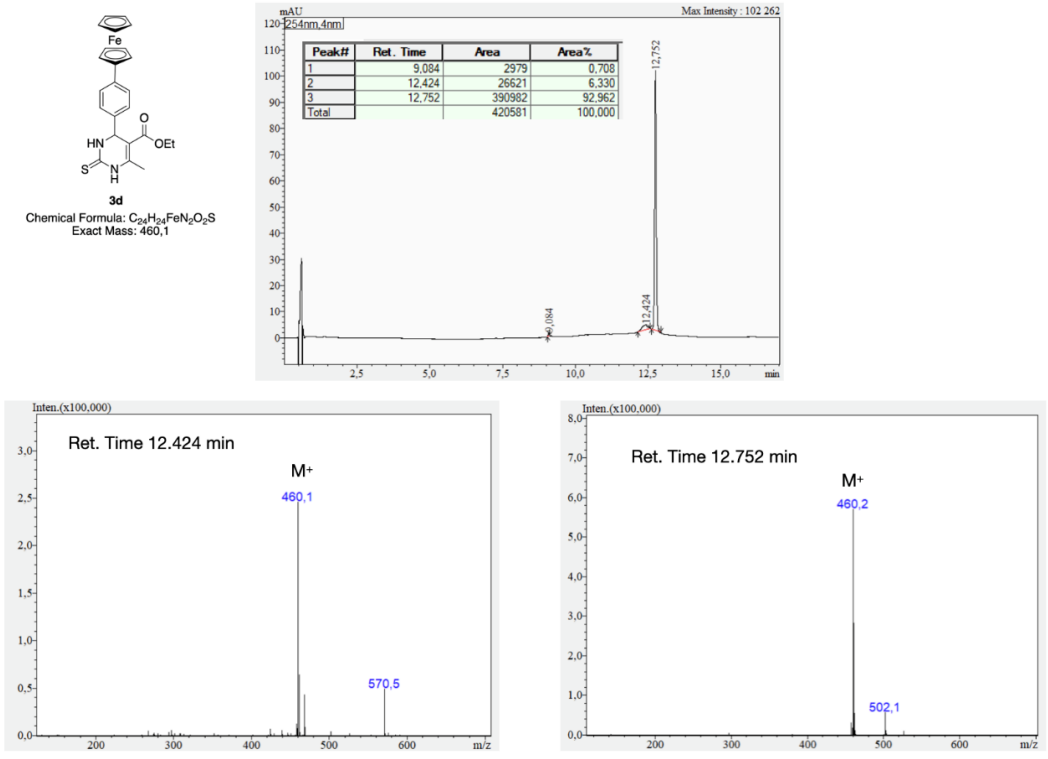

Supporting Figure S42. LC-MS analysis of 3d.

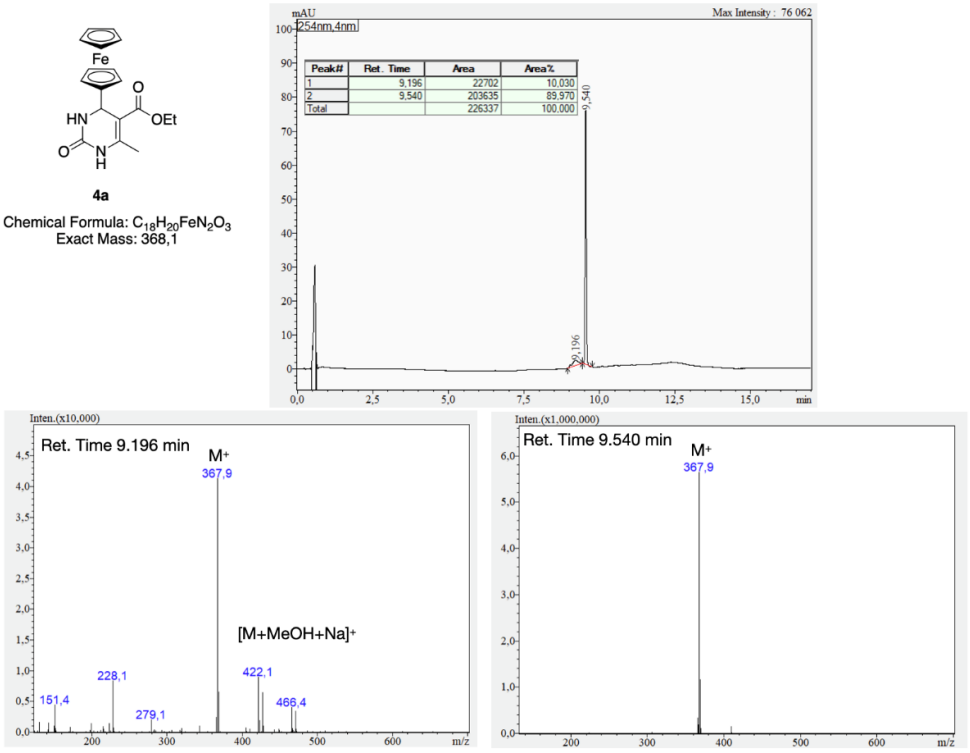

Supporting Figure S43. LC-MS analysis of 4a.

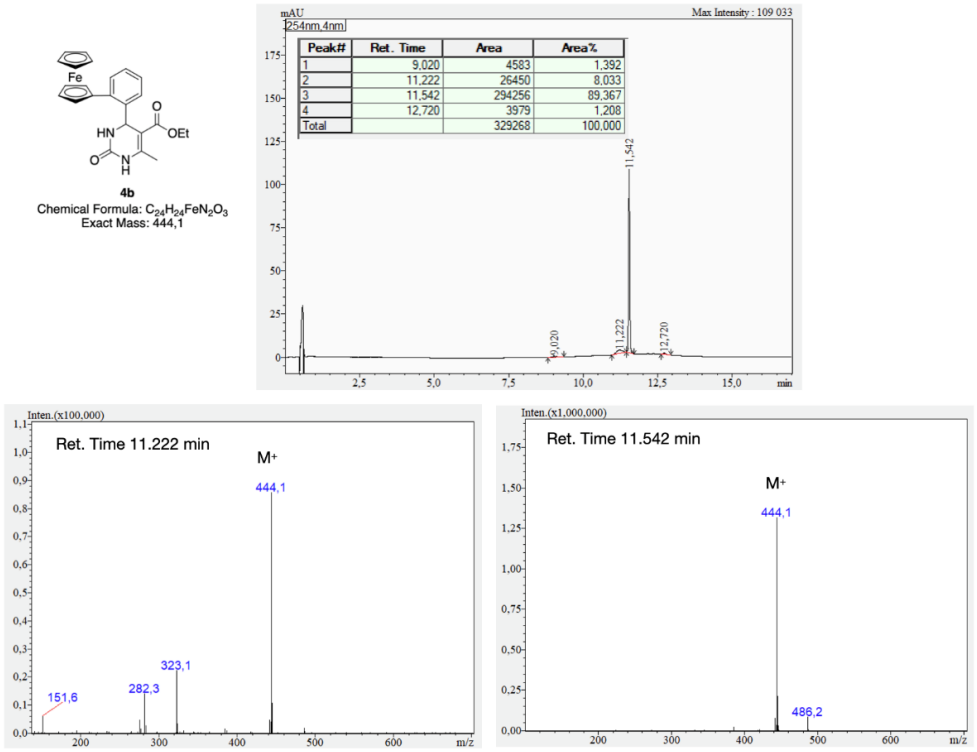

Supporting Figure S44. LC-MS analysis of 4b.

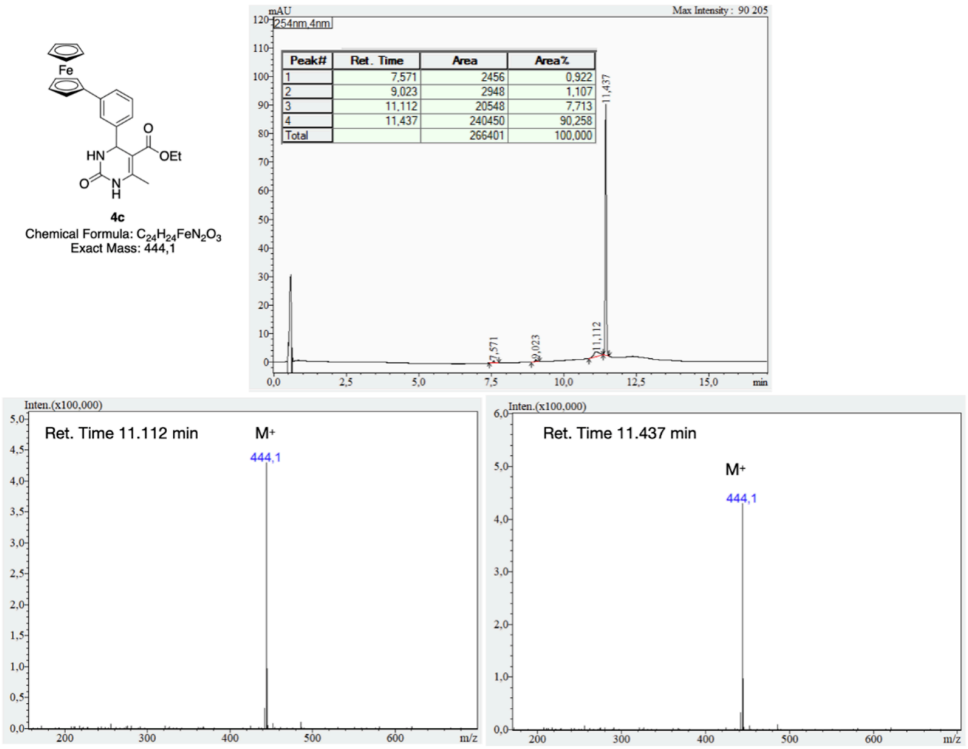

Supporting Figure S45. LC-MS analysis of 4c.

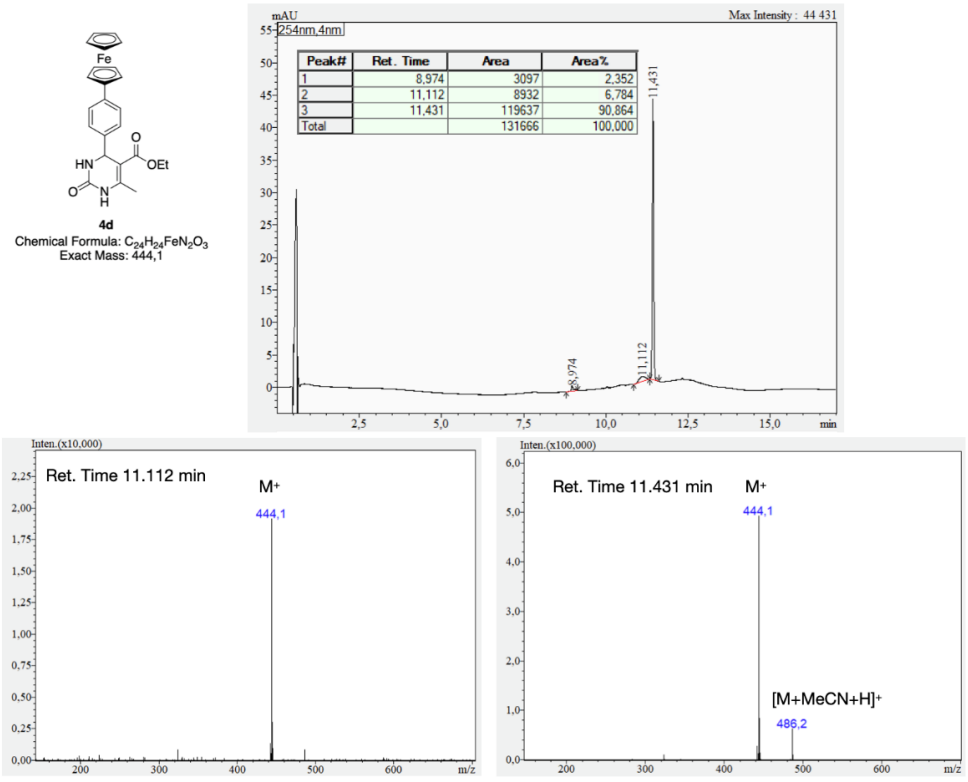

Supporting Figure S46. LC-MS analysis of 4d.

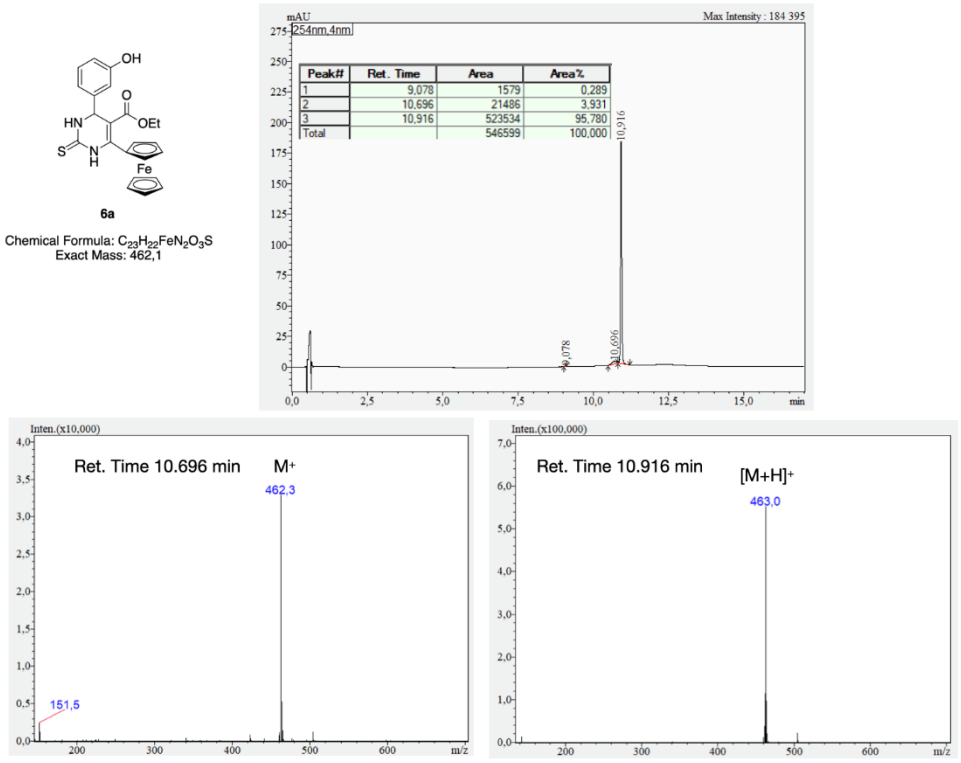

Supporting Figure S47. LC-MS analysis of 6a.

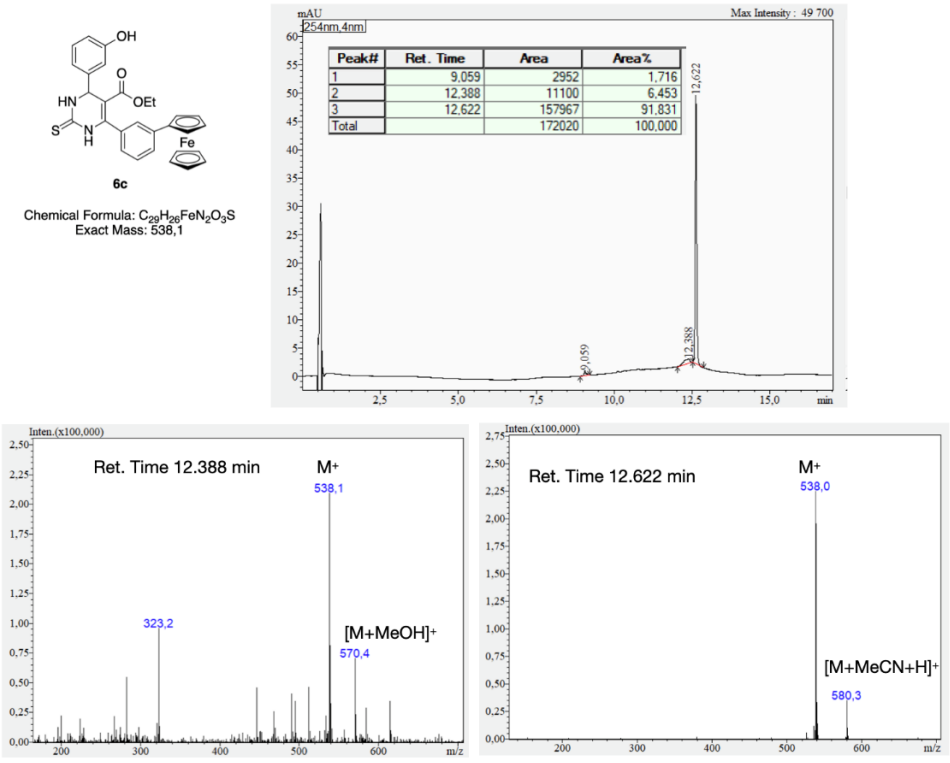

Supporting Figure S48. LC-MS analysis of 6c.

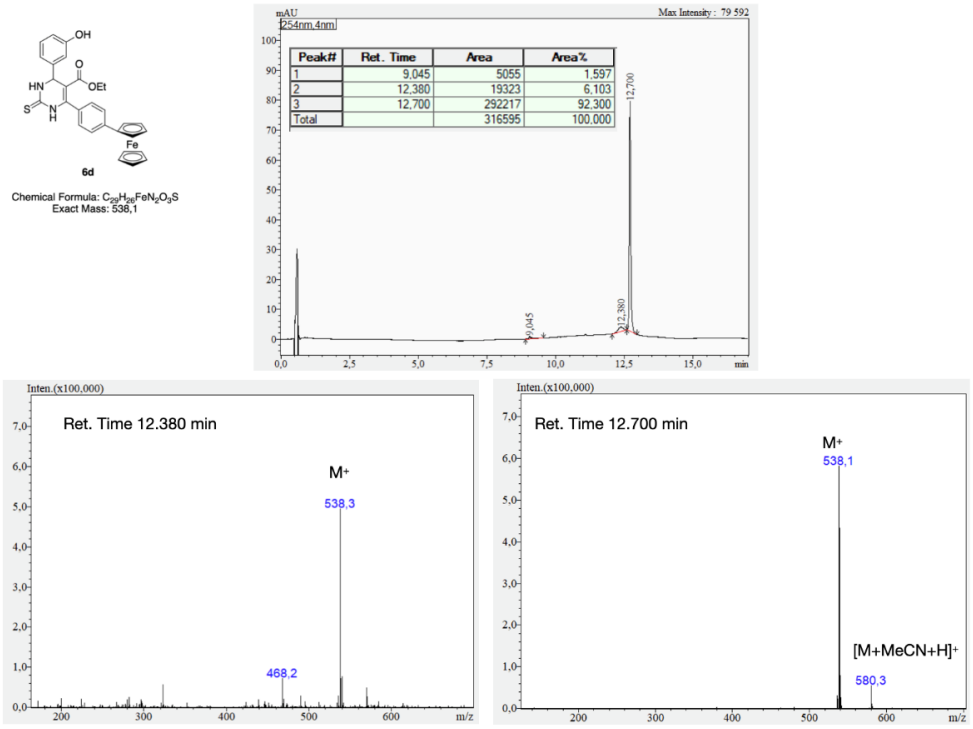

Supporting Figure S49. LC-MS analysis of 6d.

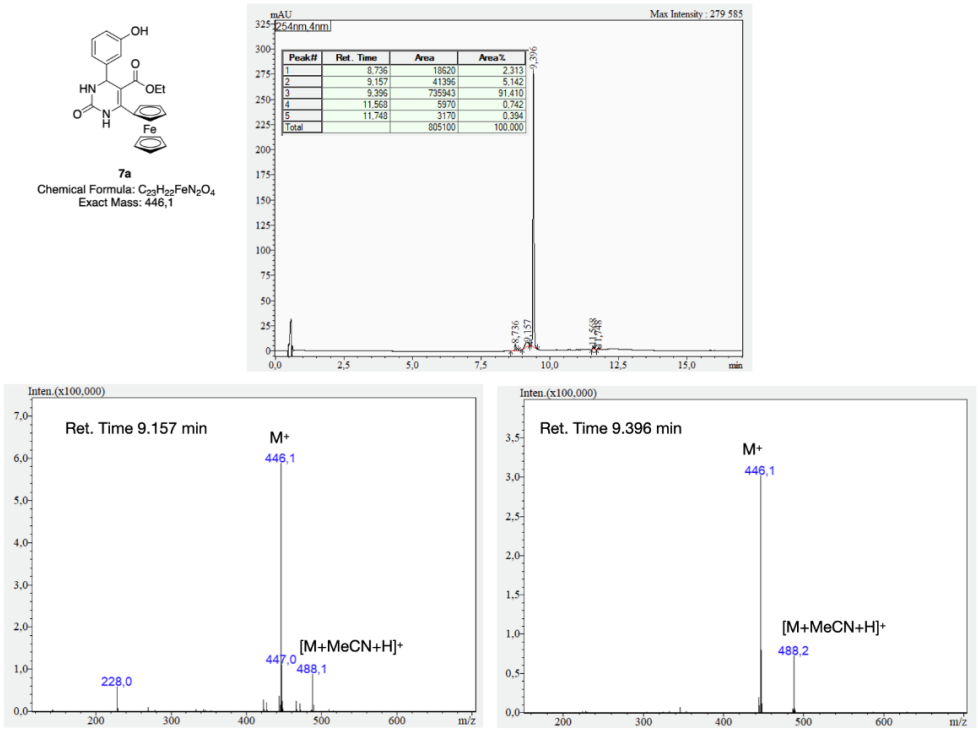

Supporting Figure S50. LC-MS analysis of 7a.

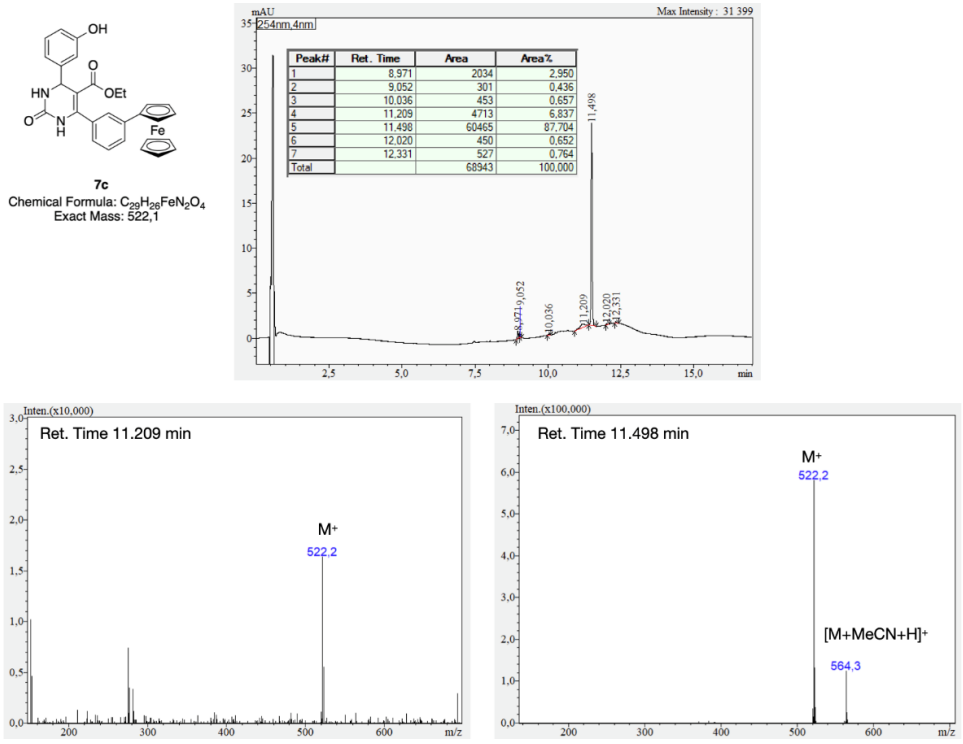

Supporting Figure S51. LC-MS analysis of 7c.

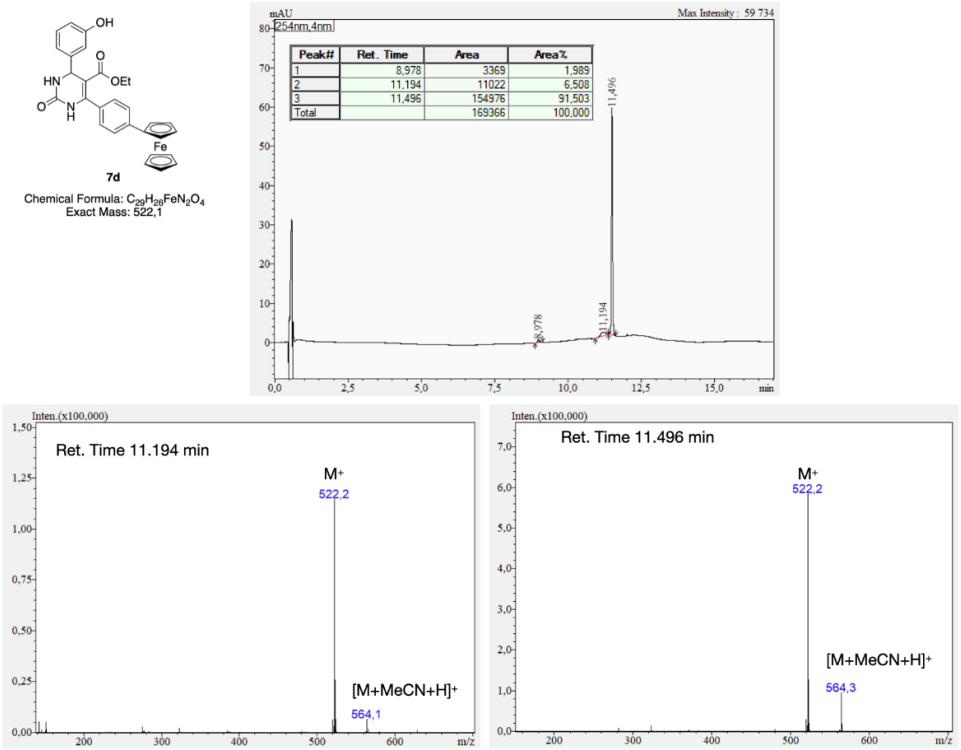

Supporting Figure S52. LC-MS analysis of 7d.

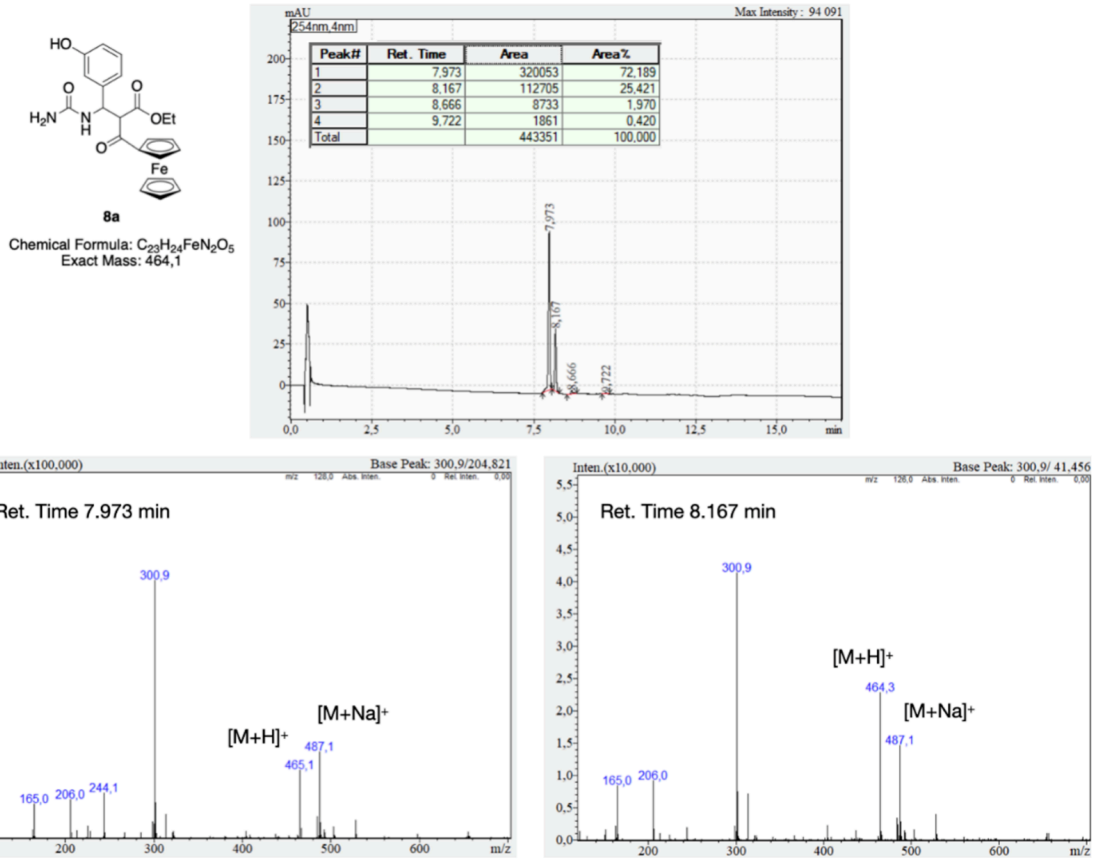

Supporting Figure S53. LC-MS analysis of 8a.

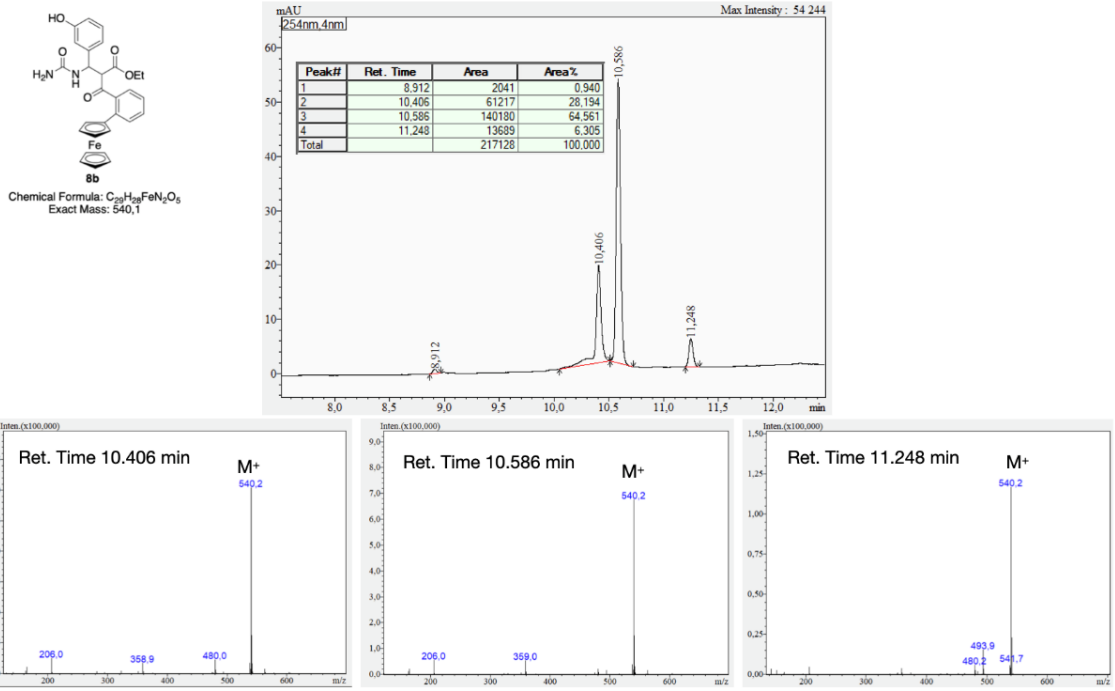

Supporting Figure S54. LC-MS analysis of 8b.

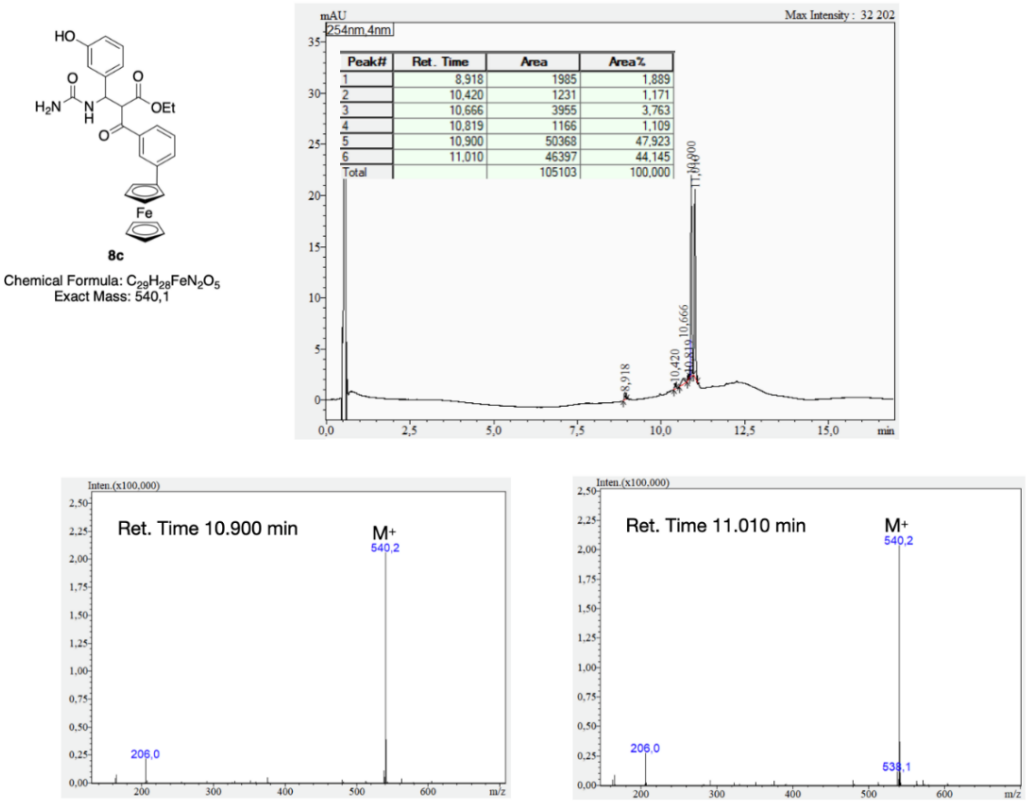

Supporting Figure S55. LC-MS analysis of 8c.

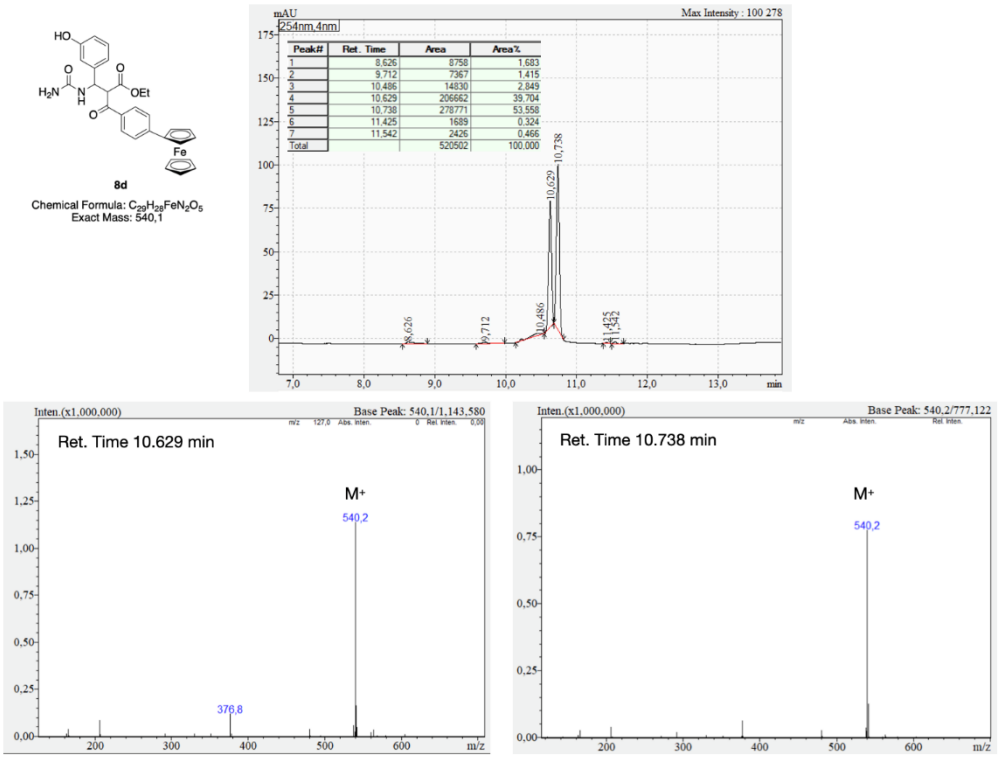

Supporting Figure S56. LC-MS analysis of 8d.

References

1. Yan, Y.; Sardana, V.; Xu, B.; Homnick, C.; Halczenko, W.; Buser, C. A.; Schaber, M.; Hartman, G. D.; Huber, H. E.; Kuo, L. C., Inhibition of a mitotic motor protein: where, how, and conformational consequences. *J. Mol. Biol.* **2004,** *335* (2), 547-54.
2. Garcia-Saez, I.; DeBonis, S.; Lopez, R.; Trucco, F.; Rousseau, B.; Thuéry, P.; Kozielski, F., Structure of human Eg5 in complex with a new monastrol-based inhibitor bound in the R configuration. *J. Biol. Chem.* **2007,** *282* (13), 9740-9747.
3. Soumyanarayanan, U.; Bhat, V. G.; Kar, S. S.; Mathew, J. A., Monastrol mimic Biginelli dihydropyrimidinone derivatives: synthesis, cytotoxicity screening against HepG2 and HeLa cell lines and molecular modeling study. *Org. Med. Chem. Lett.* **2012,** *2* (1), 23.

Dalton Transactions

ROYAL SOCIETY OF CHEMISTRY

PAPER

View Article Online
View Journal

Cite this: DOI: 10.1039/d4dt01853b

Design and synthesis of ferrocenyl 1,4-dihydropyridines and their evaluation as kinesin-5 inhibitors†

Karolina Kowalczyk,[a] Andrzej Błauż,[b] Krzysztof Krawczyk,[b] Błażej Rychlik[b] and Damian Plażuk*[a]

Received 26th June 2024,
Accepted 9th September 2024

DOI: 10.1039/d4dt01853b

rsc.li/dalton

Kinesin-5 inhibitors offer cancer cell-targeted approach, thus securing reduced systemic toxicity compared to other antimitotic agents. By modifying the 1,4-dihydropyridine-based kinesin-5 inhibitor CPUYL064 with a ferrocenyl moiety (Fc), we designed and prepared a series of organometallic hybrids that show high antiproliferative activity, with the best compounds exhibiting up to 19-fold increased activity. This enhanced activity can be attributed to the presence of the ferrocenyl moiety.

Introduction

Conventional antimitotic agents, such as taxanes and *Vinca* alkaloids, disturb microtubule dynamics, eventually leading to cell death.[1–3] However, these drugs are associated with severe side effects resulting from their effects on non-malignant cells. Additionally, the use of antimitotic agents may be inefficient due to the development of multidrug resistance (MDR), leading to cancer relapse and therapy failure.[4] To improve the efficiency of antimitotic agents and alleviate side effects of the therapy, there is a need for targeted treatment that can discriminate between cancerous and normal cells, minimizing systemic toxicity while enhancing antitumor efficacy. Among the targets for such therapies, the kinesin-5 protein (KSP, also known as Eg5) is particularly interesting.[1,5–8] Kinesin-5, a tetrameric plus-end-directed motor protein is essential for spindle bipolarity and thus effective mitosis.[9,10] Inhibition of Eg5 results in the formation of monopolar spindles, an aberrant mitotic arrest, and subsequent cell death of dividing cells. The specificity of Eg5 to mitotic processes provides a therapeutic advantage by primarily affecting proliferating cancer cells rather than non-dividing normal cells. Since the first low-molecular-weight kinesin-5 inhibitor, monastrol[11] **1**, was discovered through screening the library of 16 320 organic molecules, significant efforts have been made to develop more efficient and relatively non-toxic inhibitors.[5,6,12] The discovery of monastrol led to the development of structurally diverse Eg5 inhibitors, such as dimethylenastrone[13] **2**, Mon-97 **3**, fluorastrol[14] **4**, and CPUYL064 **5**.[15–17] Many other structurally different kinesin-5 inhibitors, including organic and organometallic compounds, *i.e.* **6**, have been discovered, with some entering clinical trials.[15,18–24]

Over the past decades, significant efforts have been put to design and evaluate the biological properties of organometallic conjugates and analogs of biologically active compounds. There has been particular interest in sandwich complexes, mainly involving ferrocene,[25–31] as well as half-sandwich complexes,[32–35] for their potential as anticancer,[36] antibacterial,[37] antifungal,[38,39] antiparasitic,[40] and other therapeutic agents[41] with some of them evaluated under clinical trials.[42–45] While organometallic hybrids with natural antimitotic agents that target microtubules—such as taxanes,[46–48] podophyllotoxin,[49,50] colchicine,[51,52] and plinabulin[53]—have been studied, organometallic hybrids showing KSP inhibitory activity have received comparatively less attention. Recently, we and others have reported sandwich and half-sandwich complexes and analogs of monastrol[54–57] and ispinesib.[58–60] Although some of the synthesized hybrids have demonstrated promising anticancer activity compared to purely organic Eg5 inhibitors, the impact of the organometallic moiety on the biological properties of such hybrids is unclear.

Continuing our research on organometallic antimitotic kinesin-5 inhibitors, we have prepared a series of ferrocenyl analogs and hybrids of the 1,4-dihydropyridine KSP inhibitor CPUYL064[61,62] and evaluated the impact of the organometallic moiety on their biological properties (Fig. 1).

[a]*Laboratory of Molecular Spectroscopy, Department of Organic Chemistry, Faculty of Chemistry, University of Lodz, ul. Tamka 12, 91-403 Łódź, Poland.*
E-mail: damian.plazuk@chemia.uni.lodz.pl
[b]*Cytometry Lab, Department of Oncobiology and Epigenetics, Faculty of Biology and Environmental Protection, University of Lodz, ul. Pomorska 141/143, 90-236 Łódź, Poland*

†Electronic supplementary information (ESI) available: Additional figures, copies of ^{1}H and $^{13}C\{^{1}H\}$ NMR spectra and the HPLC-MS analysis of final products. See DOI: https://doi.org/10.1039/d4dt01853b

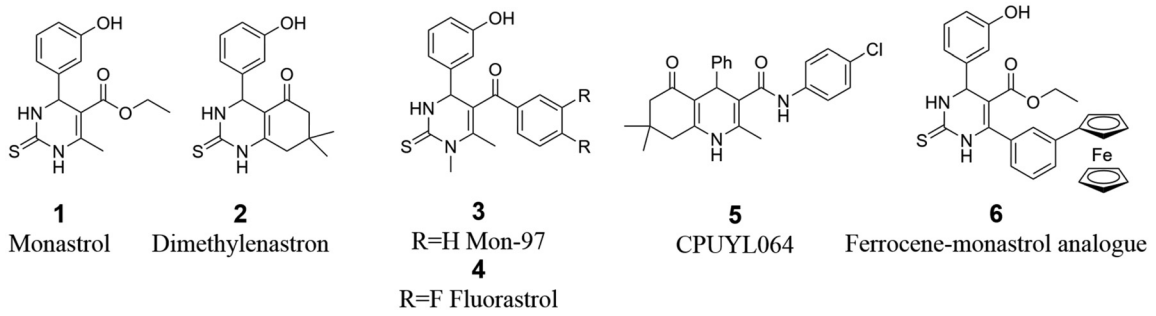

Fig. 1 Structure of monastrol **1**, and an example of organic **2–5** and ferrocenyl analogue **6**.

Results and discussion

Synthesis

All the final 1,4-dihydropyridine derivatives were synthesized in a multicomponent reaction. The required ruthenocenecarboxaldehyde[63] **11c** and *o*-, *m*-, and *p*-ferrocenylbenzaldehydes[46] **11d–f** were prepared from corresponding metallocenes in a few steps following reported procedures. The ferrocene-substituted acetoacetanilides **10a–c** were synthesized from *o*-, *m*- and *p*-nitroanilines as outlined in Scheme 1. First, ferrocene reacted with freshly prepared *o*-, *m*-, and *p*-nitrobenzenediazonium chlorides to yield the corresponding *o*-, *m*-, and *p*-ferrocenylnitrobenzenes **8a–c**, which were isolated in 30–94% yields. Next, the nitroarenes **8a–c** were reduced to anilines **9a–c** using ammonium formate with 10% palladium on carbon in ethanol at 120 °C under microwave conditions, achieving quantitative yields. Subsequently, the resulting anilines **9a–c** reacted with ethyl acetoacetate in the presence of a catalytic amount of potassium *tert*-butoxide in toluene at 160 °C for 20–30 minutes under microwave conditions, producing the desired ferrocene-substituted acetoacetanilides **10a–c** in yields ranging from 19% to 32%. The 5-ferrocenylcyclohexane-1,3-dione **13e** was synthesized as outlined in Scheme 2 by adapting reported procedure.[64] The reaction of ferrocenecarboxaldehyde **11b** with acetone in the presence of sodium hydroxide solution afforded 4-ferrocenylbut-3-en-2-one **12**,[65] which further reacted with the freshly prepared sodium salt of diethyl malonate to yield the corresponding β-ketoester. This β-ketoester was hydrolyzed using a sodium hydroxide to produce the β-ketoacid, which underwent decarboxylation upon refluxing in hydrochloric acid solution to yield **13e** with an overall yield of 29%. The structure of **13e** was confirmed by the NMR analysis and MS spectroscopy. In the DMSO-d_6 solution **13e** exists solely in enol form which was confirmed by the NMR spectroscopy. In the ^{1}H NMR spectrum of **13e** in DMSO-d_6, the singlet at 11.07 ppm assigned to the OH enol group, and singlet of vinyl enol proton CH═C(OH) (H-2) at 5.23 ppm confirmed the formation of enol (Fig. S14†). However, while the metallocene protons were present in the spectrum, the signals of aliphatic cyclohexane ring were only poorly visible. In the ^{13}C{^{1}H} NMR spectrum of **13e** in DMSO-d_6, signals of both the carbonyl carbon at 197.1 ppm (C-1) and the enol carbon atom ═C(OH)– (C-3) at 176.9 ppm were observed which confirmed the enol form (Fig. S15†). Signals assigned to the vinyl enol carbon atom (C-2) at 103.5 ppm and the Cp originated signals and C-5 atom of cyclohexane ring were observed with typical intensity. In comparison, signals of both methylene groups of cyclohexane ring were observed as low-intense singlets at 43.5 and 35.8 ppm. To confirm the structure of **13e**, we performed an additional NMR analysis. In the ^{1}H NMR spectrum of **13e** in CD_2Cl_2 allowed to register the NMR spectrum of **13e** existing as diketone (Fig. S16†). In the ^{1}H NMR spectrum, signals assigned to the ferrocenyl moiety and all the cyclohexane protons including three CH_2 groups and one CH group were present, while no enol signals were detected. In the ^{13}C{^{1}H} NMR spectrum of **13e** in CD_2Cl_2, one signal at 203.9 ppm assigned to the carbonyl groups and signals assigned to the ferrocenyl, three methylene and one CH carbon atoms originating from the cyclohexane ring were present (Fig. S17 and 18†). Both increasing (up to 343 K for DMSO-d_6 solution) and decreasing (down to 243 K for CD_2Cl_2 solution) sample temperatures only slightly affected the NMR spectra. The HPLC-MS analysis of **13e**

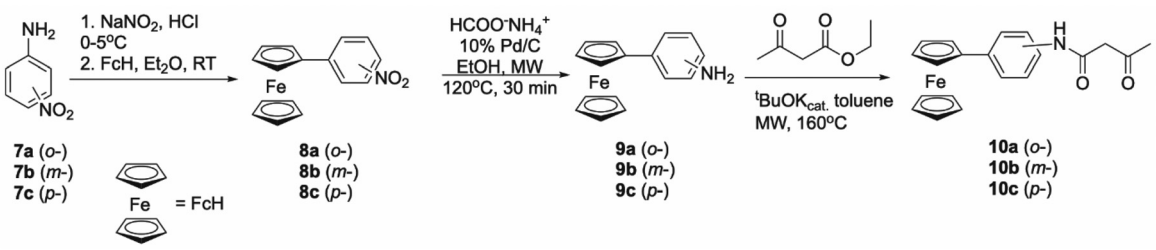

Scheme 1 Synthesis of ferrocenyl acetoacetanilides **10a–c**.

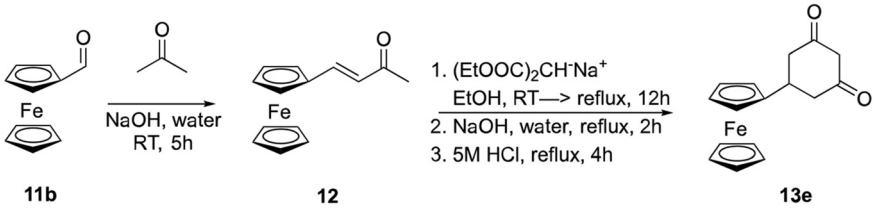

Scheme 2 Synthesis of 5-ferrocenylcyclohexane-1,3-dione **13e**.

showed singly charged peak at 8.77 min with *m*/*z* of 295.9 attributed to $[M]^+$ (positive mode) and *m*/*z* of 294.8 attributed to $[M - H^+]^-$ (negative mode).

All the targeted 1,4-dihydropyridine derivatives were synthesized by a multicomponent reaction involving β-ketoamides **10a–d** or β-ketoester **10e**, aromatic aldehydes **11a–f**, cyclohexane-1,3-diones **13a–e** and ammonium acetate in 2,2,2-trifluoroethanol at 110 °C under microwave conditions (Scheme 3). Using other alcohols, such as ethanol or methanol, resulted in lower yields of the products (the reaction yields were tested for the synthesis of **14b**). According to the optimized conditions, amides **5,14b–j** were synthesized in 17–80% yield, esters **16a–j** were isolated in 18–99% yield, while amides **16a–c** were obtained in 42–60% yield. The structures of the obtained products were confirmed by 1D and 2D NMR spectra. The presence of two substituents at C-4 and C-7 resulted in the formation of diastereoisomer mixtures. The ^{1}H and ^{13}C NMR spectra of C-7 monosubstituted amides **14g–i** and esters **15g–i** confirmed the presence of additional signals, indicating the formation of diastereoisomers (*e.g.*, Fig. S34†). The HPLC-MS analysis also confirmed the presence of diastereoisomers in **14g–i** and **15g–h**. For example, the HPLC-MS analysis of amide **14h** and ester **15h** showed two peaks at 7.61 min and 7.71 min with *m*/*z* of 576.2 attributed to $[M]^+$ of amide (Fig. S39†) and two peaks at 6.79 min and 6.94 min with *m*/*z* of 495.4 assigned to $[M]^+$ of the ester (Fig. S69†). The presence of a bulky substituent, *i.e.*, 2-ferrocenylphenyl at C-4 in amide **14d**, resulted in the appearance of additional signals in ^{1}H and ^{13}C NMR spectra, which were assigned to rotamers (Fig. S25 and 26†). Replacing the amide moiety by the ester group, as in **15d**, results in one set of signals in the ^{1}H and ^{13}C NMR spectra with no signals from rotamers (Fig. S55†). The purity of the synthesized compounds was confirmed by elemental analysis and HPLC-MS analysis. In the MS spectra of most of the ferrocenyl 1,4-dihydropyridine derivatives, only the singly charged ions attributed to $[M]^+$ were observed, with the exception of ester **15i** and the ferrocenyl-substituted amides **16a–c** where singly charged ions attributed to the protonated form $[M + H]^+$ were present. All the ruthenocenyl derivatives also gave singly charged ions assigned to the protonated form $[M + H]^+$.

Structure–activity relationship

In the first step, we screened the synthesized compounds for their antiproliferative activity evaluating survival of 6 cancer cell lines of different tissue origin exposed to a single concentration of a given compound equal to IC_{50} value for reference **5** (Fig. 2). Replacing the 4-phenyl moiety in **5** by a ferrocenyl sub-

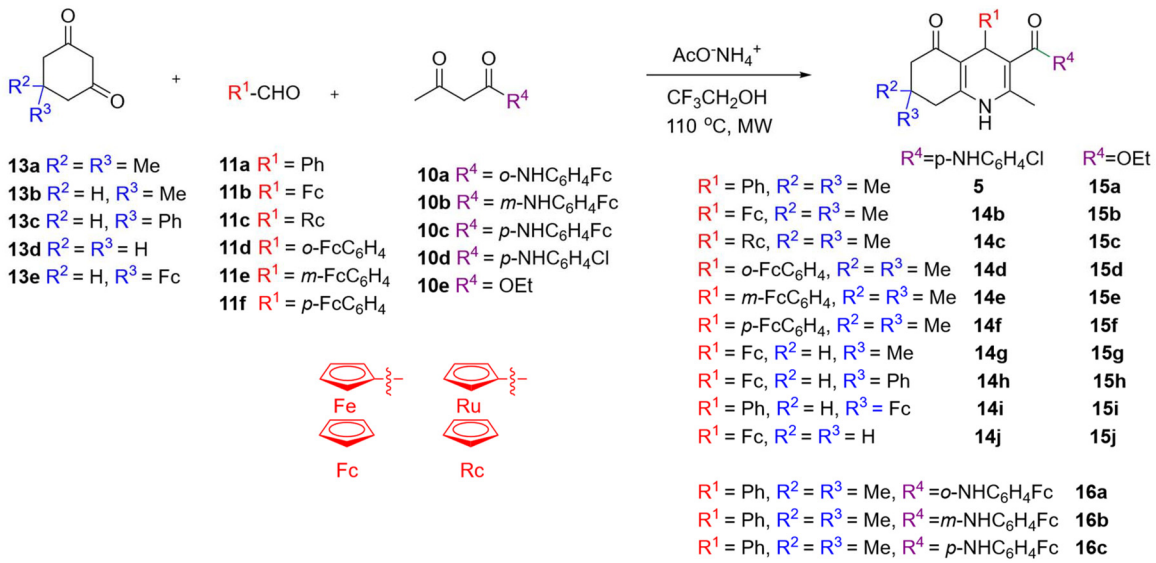

Scheme 3 Synthesis of the targeted 1,4-dihydropyridine amides **5,14b–j**, **16a–c** and esters **15a–j**.

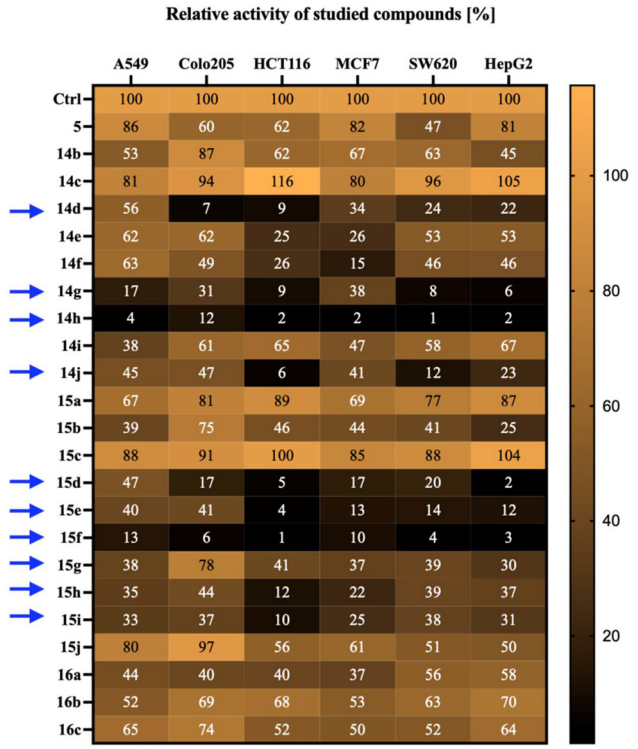

Fig. 2 Antiproliferative activity of the synthesized compounds in comparison to **5** at concentrations equal to IC_{50} values of **5** in the respective cancer cell lines A549 (IC_{50} = 57.4 μM), Colo 205 (IC_{50} = 33.9 μM), HCT116 (IC_{50} = 26.8 μM), MCF7 (IC_{50} = 40.0 μM), SW620 (IC_{50} = 15.2 μM), HepG2 (IC_{50} = 39.7 μM). The results are presented as relative viability compared to non-treated controls (mean values, n = 3).

stituent led to compound **14b**, which possessed similar activity to **5**. Further replacing the ferrocenyl group in **14b** by a ruthenocenyl moiety led to compound **14c**, which exhibited practically no activity (survival rates higher than 91% at the studied concentration). On the other hand, *o*-substituted ferrocenyl decorated **14d** demonstrated significantly higher activity than the parent molecule, with survival rates varying from 7–34% for Colo 205, HCT116, MCF7, SW620 and HepG2 lines. This effect was abolished in *m*- and *p*-ferrocenyl derivatives, **14e** and **14f**, respectively, which demonstrated antiproliferative activity only toward HCT116 and MCF-7 cells. The activity of the ferrocenyl analogue **14b** could be improved by modifying the substituents at C-7. Compounds bearing one methyl substituent (**14g**) or one phenyl moiety (**14h**), or having no substituents (**14j**) at C-7 showed increased antiproliferative activity compared to the dimethyl derivative **14a** (*e.g.* cancer cell viability dropped down to 1–4% for **14h** in A549, HCT116, MCF7, SW620 and HepG2 lines). However, when the ferrocenyl moiety was attached at C-7, *i.e.* **14i**, the biological activity was almost eliminated. Replacing the 4-chloroanilide group in **5** with an ethyl ester moiety, *i.e.* **15a**, led to almost inactive compound. Nonetheless, the ferrocene-substituted esters showed higher activity than the parent compound **5** or its ester analogue **15a**. On the contrary, modifying the 4-chloroanilide moiety by conjugation with the ferrocene substituent led to moderately active compound **16a**. Based on the obtained results, we have selected four the most active amides **14d,g,h,j** and six esters **15d–i** for further studies.

Determination of IC_{50} values (Table 1) confirmed that the selected compounds possess significantly higher activity than the parent molecule **5**. Activity Quotients (AQ) demonstrated the positive impact of the ferrocenyl moiety on antiproliferative activity (Fig. S1B†), although effects of different compounds differed among cell lines. The overall cell susceptibility to the investigated compounds was as follows: HepG2 (most vulnerable) > Colo 205 = SW620 > A549 > MCF7 > HCT116 (least vulnerable) as revealed by rank analysis. Of the compounds, ester **15f** and amides **14h**, **14j** and **14g** were the most active, reaching even 19.0-fold, 13-fold, 16-fold and 12-fold greater antiproliferative potential than reference **5**, respectively. Therefore, these compounds were selected for further studies.

Next, we evaluated the antiproliferative potential of the most active compounds toward the human fetal lung fibroblast line MRC-5 (Table 2). Similarly to cancer cells, normal fibroblasts were more susceptible to ferrocene-substituted compounds than to **5**. Surprisingly, the results observed for **14g**, **14h**, and **15f** were comparable to the ones observed for malignant cells. **14j** was an exclusive exception being 2- to 9-fold less active in MRC-5 cells. These results suggest that the ferrocenyl derivatives of **5** exhibit a distinct mode of action that may involve not only KSP inhibition but also some other biological effects.

Impact on the cell cycle

Analyzing the impact of the investigated compounds on the cell cycle can be a rough measure of their mode of action as kinesin-5 activity is crucial for mitotic spindle formation and cell division. To elucidate the kinetics of cell cycle modulation and the potential mechanistic implications of ferrocenyl substitution of **5**, we utilized flow cytometry to analyze cell cycle distribution at 24, 48, and 72 hours in A549 and SW620 cell lines at concentrations equivalent to the IC_{75} values for **5** (Table 3 and Fig. S2†). **5** was demonstrated to induce concentration- and time-dependent G_2/M block in HepG2 cells,[61] however its effects on A549 and SW620 cells were different. In both cases, the proportion of G_1 cells was decreasing and the proportion of S cells was increasing with exposure time while G_2/M block was faintly visible in A549 and quite evident in SW620 cells. The differences between these two cell lines were even more profound in case of other compounds. In A549 line, the proportion of G_1 cells was consistently high over entire exposure time to ferrocenyl derivatives of **5** reaching over 80% which was further accompanied by time-dependent reduction of S and G_2/M cell counts. In neither case G_2/M block was observed. On the other hand, SW620 cells tended to respond in a more predictable way, with **14g** and **14j** inducing G_2/M block in a time-dependent manner. **14h** and **15f** however, exerted effects similar to those observed in A549 cells (*i.e.* increased number of G_1 cells and reduced number of G_2/M cells) – a behavior expected for agents blocking S phase entry checkpoint. These results suggest the potential of the investi-

Table 1 Antiproliferative activity of studied 1,4-dihydropyridine derivatives in human cancer cell lines (exposure time 72 h). IC_{50} values are presented along with the corresponding 95% confidence intervals (in parentheses), n = 3. The Activity Quotients (AQ) of studied compounds in comparison to cytotoxic activity of **5** were calculated as AQ = $IC_{50(5)}/IC_{50(compound)}$ (in italics)

	IC_{50} (μM)					
Compound	A549	Colo 205	HCT116	MCF7	SW620	HepG2
5	57.4 (43.6–75.4)	33.9 (28.6–41.4)	26.8 (22.4–32.0)	40.0 (30.9–53.4)	15.2 (12.7–18.1)	39.7 (29.3–54.7)
14d	27.5 (22.4–34.1)	5.82 (4.64–7.26)	24.2 (15.6–39.7)	14.5 (11.8–17.9)	15.6 (11.4–21.4)	7.51 (5.75–9.78)
	2.1	*5.8*	*1.1*	*2.8*	*1.0*	*5.3*
14g	4.49 (3.93–5.87)	7.80 (5.64–10.8)	16.0 (11.3–22.5)	7.63 (4.49–13.4)	5.07 (3.57–7.12)	11.7 (9.26–15.0)
	12.8	*4.3*	*1.7*	*5.2*	*3.0*	*3.4*
14h	4.32 (3.48–5.32)	4.74 (4.21–5.32)	19.8 (15.7–24.3)	4.93 (3.40–7.12)	2.99 (2.37–3.77)	4.48 (3.30–6.08)
	13.3	*7.2*	*1.4*	*8.1*	*5.1*	*8.9*
14j	3.87 (0.45–200)	2.23 (0.829–6.48)	5.19 (2.57–12.0)	2.46 (0.670–12.6)	7.14 (4.83–10.5)	9.99 (4.59–23.4)
	14.8	*15.2*	*5.2*	*16.3*	*2.1*	*4.0*
15a	>100	50.9 (41.0–63.0)	91.2 (70.5–139)	>100	89.7 (70.0–151)	63.4 (38.9–120)
		0.7	*0.3*		*0.2*	*0.6*
15d	8.57 (6.70–11.0)	8.14 (7.07–9.32)	21.9 (16.8–29.1)	10.1 (7.47–13.8)	7.54 (5.94–9.74)	6.96 (5.03–9.56)
	6.7	*4.2*	*1.2*	*4.0*	*2.0*	*5.7*
15e	35.5 (16.5–105)	6.06 (4.94–7.42)	14.3 (9.30–23.3)	25.0 (15.0–45.5)	12.7 (8.91–18.7)	5.39 (3.92–7.44)
	1.6	*5.6*	*1.9*	*1.6*	*1.2*	*7.4*
15f	5.73 (3.72–9.31)	1.78 (1.48–2.12)	1.57 (1.26–1.96)	5.12 (3.34–8.14)	3.06 (2.40–3.95)	2.13 (1.41–3.36)
	10.0	*19.0*	*17.1*	*7.8*	*5.0*	*18.6*
15g	6.81 (5.67–8.12)	22.5 (14.9–34.6)	17.6 (14.0–22.2)	19.0 (13.9–26.3)	10.7 (8.05–14.3)	11.7 (7.07–20.3)
	8.4	*1.5*	*1.5*	*2.1*	*1.4*	*3.4*
15h	37.0 (24.0–63.2)	6.66 (5.48–8.15)	18.1 (12.2–28.1)	7.16 (4.73–11.1)	34.4 (24.1–52.5)	13.8 (9.58–20.4)
	1.6	*5.1*	*1.5*	*5.6*	*0.4*	*2.9*
15i	24.5 (15.9–40.9)	4.61 (3.11–6.81)	14.4 (9.09–23.9)	6.01 (4.20–8.71)	20.2 (14.0–30.1)	12.1 (7.68–19.9)
	2.3	*7.4*	*1.9*	*6.7*	*0.8*	*3.3*

Table 2 Antiproliferative potential of selected 1,4-dihydropyridine derivatives in MRC-5 cells (exposure time 72 h). IC_{50} values are presented along with the corresponding 95% (or 90%, *) confidence intervals (in parentheses), n = 3

	IC_{50} (μM)				
Compound	**5**	**14g**	**14h**	**14j**	**15f**
MRC-5	68.3 (43.4–166)	6.43 (5.52–7.46)	4.57 (3.76–5.10)*	20.8 (18.2–23.6)	1.99 (1.66–2.40)

gated compounds as powerful antimitotic agents, inhibiting cell proliferation by preventing cells from advancing through the cell cycle. Traditional antimitotic agents, including microtubule targeting drugs such as taxanes, *Vinca* alkaloids, and kinesin-5 inhibitors, *e.g.*, ispinesib, lead to an accumulation of cells in the G_2/M phase by blocking mitosis.[66–68] The observed G_1/S arrest induced by studied compounds implies a mechanism of action different from the mechanism of action of the parent molecule, potentially involving interactions with cell cycle regulators like cyclins, cyclin-dependent kinases (CDKs), checkpoint proteins, DNA repair proteins or other signaling pathways that control the G_1 to S phase transition.[69] Further studies are necessary to pinpoint the exact pathways and molecular targets involved, which could reveal novel therapeutic approaches distinct from traditional antimitotic strategies.

Kinesin inhibition

The impact of modifying the kinesin-5 inhibitor CPUYL064 with a ferrocenyl moiety on its ability to inhibit KSP activity was evaluated using the adenosine 5′-triphosphate (ATP) hydrolysis assay (Fig. 3). At 10 nM all investigated compounds were able to reduce the kinesin-5 activity by approximately 45–55%. However, further inhibition at 100 nM was observed only in case of the reference compound **5**, amide **14j** and ester **15f**. At 1 μM, all compounds were able to completely abolish enzyme activity. The KSP inhibitory activity of the ferrocenyl amides seems to depend on the substituents at the C-7 position as only non-substituted **14j** exerted significantly enhanced activity at 100 nM contrary to both C-7 monosubstituted derivatives **14g–h**. These results suggest participation of an additional mechanism other than KSP inhibition responsible for the antiproliferative activity of the studied ferrocenyl compounds.

ROS generation

The antiproliferative activity of ferrocenyl compounds is often linked to their capability to enhance the production of reactive oxygen species (ROS) in cells.[27,70] We could expect that introducing the ferrocenyl moiety to **5** would impact its oxidoreductive activity. Therefore, we evaluated the ROS-inducing potential of these compounds at 1 and 10 μM by measuring the rate of intracellular dihydrorhodamine 123 oxidation (Fig. 4). 10 μM **14h**, **14j** and **15f** significantly increased ROS

Table 3 Cell cycle phase distribution in A549 and SW620 cells exposed for 24, 48 and 72 h to **5** and its ferrocenyl analogues at concentrations equal to the IC_{75} values for **5**. Data are presented as mean ± SD, n = 3

		A549			SW620		
Compound		G_1	S	G_2/M	G_1	S	G_2/M
Ctrl	24 h	55.8 ± 1.4	20.4 ± 0.8	20.9 ± 1.3	57.3 ± 1.8	20.4 ± 0.3	21.0 ± 1.3
	48 h	54.4 ± 3.5	25.1 ± 3.5	21.8 ± 0.3	54.3 ± 2.8	23.3 ± 0.9	20.3 ± 0.0
	72 h	54.8 ± 0.6	24.5 ± 1.0	20.1 ± 0.5	53.2 ± 3.0	24.6 ± 2.2	21.1 ± 2.1
5	24 h	59.2 ± 0.9	20.6 ± 0.5	19.2 ± 0.5	54.5 ± 2.4	19.2 ± 0.8	23.9 ± 0.9
	48 h	42.6 ± 2.0	47.1 ± 3.6	9.7 ± 2.2	28.7 ± 2.0	44.7 ± 1.4	25.9 ± 2.9
	72 h	10.2 ± 0.1	62.4 ± 0.8	26.2 ± 0.5	23.5 ± 3.0	43.0 ± 1.7	32.5 ± 2.4
14g	24 h	71.6 ± 1.0	21.2 ± 0.8	6.0 ± 0.8	61.7 ± 1.0	21.0 ± 1.3	15.7 ± 2.2
	48 h	72.9 ± 3.1	17.2 ± 1.0	8.8 ± 1.7	28.4 ± 1.1	27.8 ± 2.2	43.3 ± 2.6
	72 h	80.3 ± 3.0	20.7 ± 0.4	2.6 ± 0.3	23.4 ± 2.8	32.2 ± 2.6	44.2 ± 1.8
14h	24 h	70.4 ± 1.2	19.5 ± 0.4	9.6 ± 1.2	69.3 ± 1.4	20.5 ± 0.7	8.0 ± 0.4
	48 h	66.7 ± 3.8	24.4 ± 1.0	8.3 ± 4.3	64.2 ± 2.2	25.9 ± 1.7	9.8 ± 1.6
	72 h	62.3 ± 2.7	22.2 ± 1.8	14.8 ± 4.0	58.1 ± 1.0	31.3 ± 2.1	10.2 ± 2.0
14j	24 h	70.8 ± 1.0	20.7 ± 0.4	7.8 ± 0.5	58.1 ± 1.2	23.3 ± 0.3	16.2 ± 1.2
	48 h	71.8 ± 1.4	15.6 ± 1.5	12.3 ± 2.8	33.1 ± 1.7	30.4 ± 4.3	34.6 ± 1.8
	72 h	80.3 ± 3.0	16.9 ± 2.9	2.6 ± 0.3	31.7 ± 2.0	43.3 ± 1.3	22.8 ± 2.4
15f	24 h	70.5 ± 0.3	20.9 ± 0.6	7.6 ± 0.3	68.9 ± 1.9	17.4 ± 0.3	11.8 ± 2.0
	48 h	81.9 ± 2.0	14.3 ± 2.1	3.4 ± 1.9	68.9 ± 1.0	16.3 ± 2.7	13.7 ± 2.7
	72 h	82.9 ± 1.1	12.9 ± 2.3	3.6 ± 2.6	79.0 ± 0.7	16.0 ± 1.6	4.7 ± 1.0

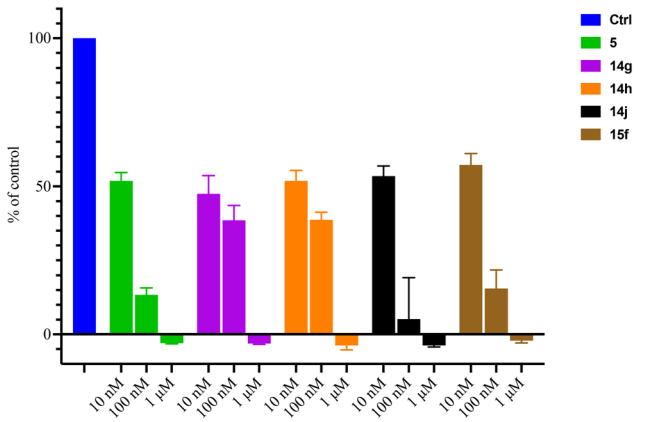

Fig. 3 Impact of the compounds on the KSP activity after treatment at 10 nM, 100 nM and 1 μM. Data are presented as mean ± SD, n = 3. Ctrl denotes KSP activity in absence of any inhibitors.

generation in SW620 cells with the similar efficiency compared to **5**. The effects observed at 1 μM concentrations of the aforementioned compounds were much less pronounced but still higher than in control cells. **14g** was significantly less active than **5**, but still able to increase ROS generation by over 20% compared to control at 10 μM. Interestingly, none of the investigated compounds could elevate ROS production in A549 cells, indicating a cell type-specific response to ferrocenyl compounds. It should be noted here that metabolic and oxidative stress response mechanisms in A549 cells are elevated due to upregulation of NRF-2 signaling pathway, which may mitigate the ROS-inducing effects.[71] The results suggest that replacing the phenyl group in **5** with a ferrocenyl substituent and modifying the C-7 position has did not enhance the ability of investigated compounds to generate ROS in susceptible cells compared to their purely organic counterpart. This effect emphasizes the need for further investigation into the structural

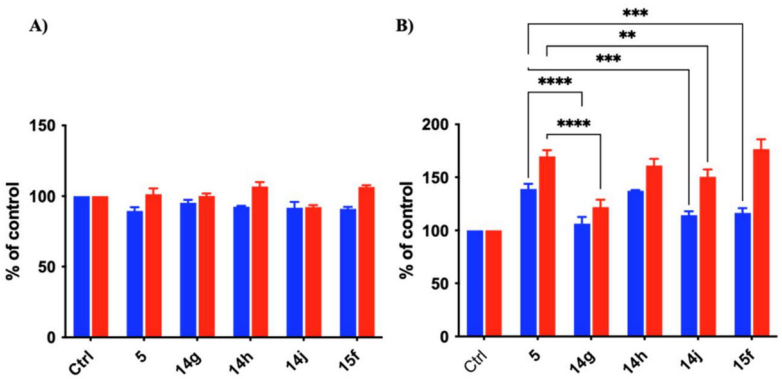

Cmpd.	ROS [% of control]			
	A549		SW620	
	1 μM	10 μM	1 μM	10 μM
5	89.6±2.6	101.4±3.9	138.9±4.8	169.7±5.8
14g	95.3±2.2	100.1±1.8	106.4±6.3	122.1±7.0
14h	92.6±0.6	106.7±3.1	137.3±0.6	161.0±6.4
14j	91.9±4.1	92.4±1.3	114.4±3.7	150.4±7.0
15f	91.1±1.4	106.3±1.3	116.6±4.6	176.5±9.4

Fig. 4 ROS generation in A549 (A) and SW620 (B) cells after 4-hour exposure to 1 (blue) or 10 μM (red) of the investigated compounds. Ctrl denotes cells in a complete DMEM culture medium with 0.1% DMSO. Results are expressed as mean ± SEM, n = 3. Asterisks denoted statistical significance against the reference compound **5** (P < 0.0001 (****), 0.001 (***), 0.01 (**), two-way ANOVA followed by *post-hoc* Tukey test).

factors and cellular contexts that influence the ROS-generating potential and anticancer activity of ferrocenyl compounds.

Conclusions

In conclusion, we have successfully synthesized a series of 22 compounds by microwave-assisted methodology and initially evaluated their antiproliferative potential in a preliminary screening. Then 10 compounds were selected for a detailed antiproliferative activity screening, ultimately identifying the four most active compounds for further studies. The biological activity strongly depends on the chemical structure of the compounds. Notably, esters exhibited higher cytotoxicity compared to amides. Amide **14j** lacking substituents at the C-7 position, demonstrated significant KSP inhibitory activity. In contrast, other highly cytotoxic amides bearing methyl or phenyl groups at C-7 showed lower KSP inhibitory activity but maintained high antiproliferative potential. Furthermore, the presence of ferrocenyl substituent did not increase their ability to generate intracellular reactive oxygen species. Interestingly, all compounds are able to induce G_1/S checkpoint arrest in appropriate conditions, which is unexpected taking into account the mode of action of traditional KSP inhibitors. These results underscore the crucial role of ferrocenyl moiety and structural variations in modulating the biological activities of the studied kinesin-5 inhibitors.

Experimental

General

Except for the reactions performed under microwave conditions, all other reactions were conducted under an argon atmosphere using the Schlenk line. The reactions performed under microwave conditions were carried out using an Anthon Paar Monowave 400 microwave reactor using closed reaction vessels with temperature control. 1D and 2D NMR spectra were recorded on a Bruker Neo 600 MHz spectrometer equipped with Prodigy CryoProbe. Chemical shifts are referenced relatively to residual signals in deuterated solvent (DMSO-d_6 δ = 2.50 ppm for ^{1}H and 39.51 ppm for ^{13}C, CD_2Cl_2 δ = 5.32 ppm for ^{1}H and 53.5 ppm for ^{13}C). Spectra were recorded at 300 K unless otherwise specified; chemical shifts are in ppm and coupling constants in Hz. Compounds were purified on silica gel using column chromatography (SiliaFlash® P60 230–400 mesh). The purity of the compounds was confirmed by HPLC-MS analysis and elemental analysis, which was higher than 95%. HPLC-MS analysis was performed on a Shimadzu UHPLC Nexera XR system equipped with Shimadzu PDA (SPD-M40) and LCMS-2020 detectors on a Phenomenex Kinetex 1.7 μm XB-C18 100 Å column (50 × 2.1 mm).

Synthesis

2-Ferrocenylnitrobenzene 8a. This compound was synthesized according to modified procedure.[72] A solution of 3.0 g (43 mmol) of sodium nitrite in 5 ml of water was added dropwise to a slurry of 6.0 g (43 mmol) of 2-nitroaniline **7a** in a mixture of 15 ml of water and 15 ml of conc. hydrochloric acid at 0–3 °C (temperature was keep below 5 °C). The cold solution (cooled to 0–5 °C by adding an ice) of the obtained diazonium salt was added dropwise to a vigorous stirred solution of 10 g (50 mmol) of ferrocene in 150 ml of diethyl ether contained 1 g of trimethylhexadecylammonium chloride maintaining the temperature below 5 °C. Then colling bath was removed and the resulting mixture was vigorously stirred for an additional 2 h before a slight excess of titanium(III) chloride in hydrochloric acid was added (to reduce ferrocenium cation). The products were extracted with dichloromethane, organic solution was dried, evaporated and purified by chromatography of silica using dichloromethane – cyclohexane (3–2) as eluent. The first fraction contained unreacted ferrocene while the second fraction contained product. The second fraction was evaporated to dryness, the product was gently mixed with *n*-pentane, and the solution was discarded while the solid product was dried under vacuum. The pure product (4.0 g) was obtained in 30% yield. The NMR spectra were identical with the reported spectra.[72]

3-Ferrocenylnitrobenzene 8b. This compound was synthesized in 35% yield (4.7 g of red crystals) according to **8a** starting from 6.0 g (43 mmol) of 3-nitroaniline **7b**. The NMR spectra were identical with the reported spectra.[72]

4-Ferrocenylnitrobenzne 8c. This compound was synthesized in 42% yield (13 g of red crystals) according to **8a** starting from 14 g of 4-nitroaniline **7c**. The NMR spectra were identical with the reported spectra.[72]

2-Ferrocenylaniline 9a. 1.0 g (3.26 mmol) of **8a** was placed in the reaction tube and dissolved in 6.0 ml of ethanol. Next 800 mg (10.4 mmol) of ammonium formate and 17 mg of 10% Pd on carbon were added to the reaction tube the resulted mixture was heated at 120 °C for 30 min under MW. After cooling to RT, the reaction mixture was filtered through the Cellite® pad and evaporated to dryness which afford 900 mg (99% yield) of product which was used in the next step without purification. Elemental analysis (%) calculated for $C_{16}H_{15}FeN$ C – 69.34, H – 5.46, N – 5.05 found C – 69.51, H – 5.45, N – 4.88. ^{1}H NMR (DMSO-d_6): δ 7.22 (dd, J = 7.6, 1.5 Hz, 1H), 6.97 (dt, J = 8.3, 1.6 Hz, 1H), 6.96 (d, J = 1.5 Hz, 1H), 6.71 (dd, J = 8.0, 1.1 Hz, 1H), 6.54 (ddd, J = 7.4, 7.4, 1.1 Hz, 1H), 5.13 (s, 2H), 4.57 (t, J = 1.8 Hz, 2H), 4.35 (t, J = 1.8 Hz, 2H), 4.17 (s, 5H). ^{13}C{^{1}H} NMR (DMSO-d_6): δ 145.3 (C), 129.6 (CH_{Ary}), 127.0 (CH_{Ary}), 120.6 (C), 116.5 (CH_{Ary}), 115.2 (CH_{Ary}), 85.3 (Cp_{ipso}), 68.8 (Cp′), 68.1 (Cp), 67.1 (Cp). MS calculated for $C_{16}H_{15}FeN$ m/z = 277.1 $[M]^+$ found m/z = 278.0 $[M + H]^+$, 277.0 $[M]^+$.

3-Ferrocenylaniline 9b. This compound was synthesized in quantitative yield according to **9a** starting from 1.0 g of **8b**. The NMR spectra were identical with the reported spectra.[73]

4-Ferrocenylaniline 9c. This compound was synthesized in quantitative yield according to **9a** starting from 1.0 g of **8c**. The NMR spectra were identical with the reported spectra.[73]

***N*-(2-Ferrocenylphenyl)-3-oxobutanamide 10a.** 900 mg (3.25 mmol) of **9a** and 0.40 ml (3.25 mmol) of ethyl acetoace-

tate were dissolved in 6.0 ml of toluene. To the resulted solution 10 mg of potassium *t*-butoxide was added and the obtained solution was stirred at 160 °C for total 25 min (15 min + 10 min – the progress of the reaction was monitored by TLC with dichloromethane – ethyl acetate 9–1 as eluent). After the reaction was completed, the volatiles were evaporated and product was isolated by chromatography on silica gel using gradient of methanol in DCM staring from 0 to 1% of methanol. The product was purified again by chromatography on silica using dichloromethane – ethyl acetate (9–1) as eluent which led to obtain pure **10a** isolated in 19% (220 mg) as an orange powder. Elemental analysis (%) calculated for $C_{20}H_{19}FeNO_2$ C – 66.50, H – 5.30, N – 3.88 found C – 55.53, H – 5.14, N – 3.84. ^{1}H NMR (DMSO-d$_6$) δ 9.34 (s, 1H, CON*H*), 7.75–7.74 (m, 1H, C$_6$*H*$_4$Fc), 7.43–7.41 (m, 1H, C$_6$*H*$_4$Fc), 7.21–7.19 (m, 2H, C$_6$*H*$_4$Fc), 4.67 (t, *J* = 1.7 Hz, 2H, Cp), 4.35 (s, 2H, Cp), 4.10 (s, 5H, Cp′), 3.56 (s, 2H, C*H*$_2$), 2.19 (s, 3H, C*H*$_3$). ^{13}C{^{1}H} NMR (DMSO-d$_6$) δ 203.1 (C-3), 165.2 (*C*ONH), 134.2 (C$_{Ar}$), 132.6 (C$_{Ar}$), 130.5 (*C*H$_{C_6H_4Fc}$), 126.3 (*C*H$_{C_6H_4Fc}$), 126.1 (*C*H$_{C_6H_4Fc}$), 125.4 (*C*H$_{C_6H_4Fc}$), 83.3 (Cp$_{ipso}$), 68.4 (Cp′), 69.0 (Cp), 68.4 (Cp), 51.7 (*C*H$_2$), 30.3 (*C*H$_3$). MS calculated for $C_{20}H_{19}FeNO_2$ *m*/*z* = 361.1 [M]$^+$ found *m*/*z* = 361.1 [M]$^+$.

***N*-(3-Ferrocenylphenyl)-3-oxobutanamide 10b.** This compound was synthesized in 32% yield (380 mg of orange powder) according to **10a** starting from 900 mg (3.25 mmol) of **9b** with total reaction time 30 min (2 × 15 min). The product was purified by chromatography on silica using dichloromethane as eluent. Elemental analysis (%) calculated for $C_{20}H_{19}FeNO_2$ C – 66.50, H – 5.30, N – 3.88 found C – 66.57, H – 5.48, N – 3.87. ^{1}H NMR (DMSO-d$_6$) δ 10.1 (CON*H*), 7.70 (br s, 1H, C$_6$*H*$_4$Fc), 7.46–7.44 (m, 1H, C$_6$*H*$_4$Fc), 7.24–7.23 (m, 2H, C$_6$*H*$_4$Fc), 4.68 (t, *J* = 1.8 Hz, 2H, Cp), 4.34 (t, *J* = 1.8 Hz, 2H, Cp), 4.03 (s, 5H, Cp′), 3.57 (s, 2H, C*H*$_2$), 2.23 (s, 3H, C*H*$_3$); ^{13}C{^{1}H} NMR (DMSO-d$_6$) δ 202.9 (C-3), 165.1 (*C*ONH), 139.5 (C$_{Ar}$), 138.9 (C$_{Ar}$), 128.7 (*C*H$_{C_6H_4Fc}$), 121.3 (*C*H$_{C_6H_4Fc}$), 116.8 (*C*H$_{C_6H_4Fc}$), 116.6 (*C*H$_{C_6H_4Fc}$), 84.8 (Cp$_{ipso}$), 69.4 (Cp′), 68.9 (Cp), 66.3 (Cp), 52.4 (*C*H$_2$), 30.3 (*C*H$_3$). MS calculated for $C_{20}H_{19}FeNO_2$ *m*/*z* = 361.1 [M]$^+$ found *m*/*z* = 361.1 [M]$^+$.

***N*-(4-Ferrocenylphenyl)-3-oxobutanamide 10c.** This compound was synthesized in 30% yield (350 mg of orange powder) according to **10a** starting from 900 mg (3.25 mmol) of **9c** with total reaction time 20 min (1 × 20 min). The product was purified by chromatography on silica using dichloromethane as eluent. Elemental analysis (%) calculated for $C_{20}H_{19}FeNO_2$ C – 66.50, H – 5.30, N – 3.88 found C – 66.43, H – 5.33, N – 3.93. ^{1}H NMR (DMSO-d$_6$) δ 10.07 (s, 1H, CON*H*), 7.51–7.47 (m, 4H, C$_6$*H*$_4$Fc), 4.73 (s, 2H, Cp), 4.31 (s, 2H, Cp), 4.01 (s, 5H, Cp′), 3.54 (s, 2H, C*H*$_2$), 2.22 (s, 3H, C*H*$_3$). ^{13}C{^{1}H} NMR (DMSO-d$_6$) δ 202.8 (C-3), 164.8 (*C*ONH), 136.8 (C$_{Ar}$), 133.9 (C$_{Ar}$), 126.1 (*C*H$_{C_6H_4Fc}$), 119.1 (*C*H$_{C_6H_4Fc}$), 84.7 (Cp$_{ipso}$), 69.3 (Cp′), 68.6 (Cp), 65.9 (Cp), 52.3 (*C*H$_2$), 30.2 (*C*H$_3$). MS calculated for $C_{20}H_{19}FeNO_2$ *m*/*z* = 361.1 [M]$^+$ found *m*/*z* = 361.1 [M]$^+$.

5-Ferrocenylcyclohexane-1,3-dione 13e. A solution of 160 mg of sodium hydroxide in 2 ml of water was added to a stirred solution of 4.28 g (20 mmol) of aldehyde **11b** in 100 ml of acetone and the obtained mixture was stirred at RT for 5 h. Next the volatiles were evaporated to dryness, the product was extracted with chloroform, dried and evaporated. The obtained crude **12**, 5 g of dark red solid, was used in the next step without further purification. In a separate flask 600 mg of sodium (26 mmol) was dissolved in 30 ml of ethanol with heating. The obtained solution of sodium ethoxide was cooled to RT and 4.0 g of diethyl malonate (26 mmol) was added in one portion and the obtained solution was stirred at RT for 20 min. Next, a solution of 5.0 g of crude **12** in 10 ml of anhydrous ethanol was added and the obtained solution was refluxed for 16 h. The obtained mixture contained orange solid was cooled to RT and a solution of 2.0 g of sodium hydroxide in 10 ml of water was added and refluxed for 2 h and evaporated to dryness. Then 20 ml of ethanol followed by 60 ml of 18% of hydrochloric acid were added and the resulted mixture was refluxed for 4 h, cooled to RT and the product was extracted with *n*-butyl acetate. The organic solution was dried with sodium sulphate, filtered and evaporated. The crude product was dissolved in a mixture of 100 ml of chloroform and 50 ml of methanol, mixed with 100 g silica gel and evaporated. The product was then eluted from the obtained solid with chloroform – ethyl acetate 2–1 mixture. The obtained product was purified again by chromatography on silica gel using chloroform followed by chloroform – *n*-butyl acetate (1–2) as eluent. The fractions contained product were collected and evaporated. The obtained solid was recrystallized from *n*-butyl acetate by dissolving in boiling *n*-butyl acetate following by cooling to RT and keeping the obtained mixture at −28 °C for 24 h. The product was filtered off and dried under vacuum affording 1.7 g (29% overall yield) of an orange solid. Elemental analysis (%) calculated for $C_{16}H_{16}FeO_2$ C – 64.89, H – 5.45 found C – 64.91, H – 5.61. ^{1}H NMR (CD_2Cl_2) δ 4.164 (s, 5H, Cp,), 4.157 (t, *J* = 1.8 Hz, 2H, Cp), 4.08 (t, *J* = 1.8 Hz, 2H, Cp), 3.41 (d, *J* = 17.5 Hz, 1H, H-2), 3.38 (d, *J* = 17.6 Hz, 1H, H-2), 3.15–3.10 (m, 1H, H-5), 2.96–2.92 (m, 2H, H-4 and H-6), 2.70–2.66 (m, 2H, H-4 and H-6); ^{13}C{^{1}H} NMR (CD_2Cl_2) δ 203.7 (C-1 and C-3), 90.9 (Cp$_{ipso}$), 69.0 (Cp′), 68.3 (Cp), 66.6 (Cp), 58.2 (C-2), 47.9 (C-4 and C-6), 31.1 (C-5). MS calculated for $C_{16}H_{16}FeO_2$ *m*/*z* = 296.0 [M]$^+$ found *m*/*z* = 295.9 [M]$^+$.

***N*-(4-Chlorophenyl)-2,7,7-trimethyl-5-oxo-4-phenyl-1,4,5,6,7,8-hexahydroquinoline-3-carboxamide 5.** A mixture of 212 mg (204 µl, 2.0 mmol) of aldehyde **11a**, 280 mg (2.0 mmol) of 1,3-diketone **13a**, 155 mg (2.0 mmol) of ammonium acetate, 422 mg (2.0 mmol) of 4′-chloroacetoacetanilide **10d** in 3.0 ml of 2,2,2-trifluoroethanol was placed in MW reaction tube and was heated at 110 °C for total 10 min. After cooling to RT volatiles were evaporated and 50 ml of ethyl acetate was added to the residue and sonicated for 2 min. The product was filtered off and purified by chromatography on silica gel using gradient from 0 to 30% of ethyl acetate in chloroform. The product was isolated in 70% yield (590 mg) as white powder. Elemental analysis (%) calculated for $C_{25}H_{25}ClN_2O_2$ C – 71.33, H – 5.99, N – 6.66 found C – 71.25, H – 5.76, N – 6.72. ^{1}H NMR (DMSO-d$_6$) δ 9.69 (s, 1H, NHCO), 8.73 (s, 1H, N*H*), 7.59 (d, *J* = 8.9 Hz, 2H, C$_6$*H*$_4$Cl), 7.29 (d, *J* = 8.9 Hz, 2H, C$_6$*H*$_4$Cl), 7.29–7.28 (m, 4H, C*H*$_{Ph}$), 7.07–7.04 (m, 1H, C*H*$_{Ph}$), 4.97 (s, 1H, H-4), 2.40 (d, *J* =

16.9 Hz, 1H, H-8), 2.32 (d, J = 16.6 Hz, 1H, H-8), 2.15 (d, J = 16.0 Hz, 1H, H-6), 2.04 (s, 3H, 2-CH_3), 1.99 (d, J = 15.9 Hz, 1H, H-6), 1.03 (s, 3H, 7-CH_3), 0.91 (s, 3H, 7-CH_3). ^{13}C{^{1}H} (DMSO-d_6) δ 196.7 (C-5), 167.4 (*C*ONH), 150.4 (C), 147.1 (C), 138.4 (C), 138.4 (C), 135.5 (C), 128.3 (*C*H$_{C_6H_4Cl}$), 127.9 (*C*H$_{Ph}$), 127.4 (*C*H$_{Ph}$), 126.4 (C), 125.7 (*C*H$_{Ph}$), 121.1 (*C*H$_{C_6H_4Cl}$), 110.6 (C), 108.0 (C), 50.4 (C-8), 39.5 (C-5 overlapped with DMSO), 38.0 (C-4), 32.1 (C), 28.0 (7-CH_3), 26.8 (7-*C*H$_3$), 17.1 (2-*C*H$_3$). MS calculated for $C_{25}H_{26}ClN_2O_2$ m/z = 421.2 $[M + H]^+$ found m/z = 421.2 $[M + H]^+$, 443.2 $[M + Na]^+$.

***N*-(4-Chlorophenyl)-4-ferrocenyl-2,7,7-trimethyl-5-oxo-1,4,5,6,7,8-hexahydroquinoline-3-carboxamide 14b.** This compound was synthesized in 19% yield (1.0 g of orange solid) according to **5**, starting from 1.40 g (10 mmol) **13a**, 2.14 g (10 mmol) of **11b**, 2.11 g (10 mmol) of **11d**, 799 mg (10 mmol) of ammonium acetate and 8.0 ml of 2,2,2-trifluoroethanol. Total reaction time 10 min. After evaporation of the volatiles the residue was gently mixed with 50 ml of ethyl acetate (with sonification in ultrasonic bath) and the precipitated product was filtered off, washed with ethyl acetate and diethyl ether and dried. Elemental analysis (%) calculated for $C_{29}H_{29}ClFeN_2O_2$ C – 65.86, H – 5.53, N – 5.30 found C – 65.65, H – 5.26, N – 5.13. ^{1}H NMR (DMSO-d_6) δ 9.86 (s, 1H, H-1), 8.67 (s, 1H, CON*H*), 7.83 (d, J = 8.9 Hz, 2H, C$_6H_4$Cl), 7.36 (d, J = 8.9 Hz, 2H, C$_6H_4$Cl), 4.82 (s, 1H, H-4), 3.98–3.92 (m, 9H, Cp′ and Cp), 2.33 (d, J = 17.0 Hz, H, H-8), 2.16 (d, J = 15.9 Hz, H-6), 2.14 (d, J = 16.9 Hz, 1H, H-8), 2.11 (s, 3H, 2-CH_3), 2.04 (d, J = 15.9 Hz, 1H, H-6), 1.00 (s, 3H, 7-CH_3), 0.81 (s, 3H, 7-CH_3). ^{13}C{^{1}H} (DMSO-d_6) δ 193.9 (C-5), 168.7 (*C*ONH), 150.1 (C), 138.7 (C), 136.2 (C), 128.4 (*C*H$_{C_6H_4Cl}$), 126.3 (C), 121.0 (*C*H$_{C_6H_4Cl}$), 109.1 (C), 109.0 (C), 95.1 (Cp$_{ipso}$), 68.3 (Cp′), 67.0 (Cp), 66.0 (Cp), 65.7 (Cp), 65.6 (Cp), 50.4 (C-6), 40.0 (C-8), 31.9 (C-4), 30.4 (7-*C*H$_3$), 29.4 (C), 25.9 (7-*C*H$_3$), 17.0 (2-*C*H$_3$). MS calculated for $C_{29}H_{29}ClFeN_2O_2$ m/z = 528.1 $[M]^+$ found m/z = 528.1 $[M]^+$.

***N*-(4-Chlorophenyl)-2,7,7-trimethyl-5-oxo-4-ruthenocenyl-1,4,5,6,7,8-hexahydroquinoline-3-carboxamide 14c.** This compound was synthesized in 59% yield (341 mg) as pale yellow solid according to **5**, starting from 140 mg (1.0 mmol) of **13a**, 259 mg (1.0 mmol) of **11c**, 211 mg (1.0 mmol) of **10d**, 77 mg (1.0 mmol) of ammonium acetate and 2.5 ml of 2,2,2-trifluoroethanol. Total reaction time 30 min (1 × 30 min). After evaporation of the volatiles the residue was gently mixed with 50 ml of ethyl acetate (with sonification in ultrasonic bath) and the precipitated product was filtered off, washed with ethyl acetate and diethyl ether and dried. Elemental analysis (%) calculated for $C_{29}H_{29}ClN_2O_2Ru$ C – 60.67, H – 5.09, N – 4.88 found C – 60.79, H – 6.02, N – 4.93. ^{1}H NMR (DMSO-d_6) δ 9.68 (s, 1H, H-1), 8.72 (s, 1H, CON*H*), 7.81 (d, J = 9.0 Hz, 2H, C$_6H_4$Cl), 7.35 (d, J = 9.0 Hz, 2H, C$_6H_4$Cl), 4.61 (s, 1H, H-4), 4.41–4.40 (m, 1H, Cp), 4.36–4.35 (m, 1H, Cp), 4.33 (s, 5H, Cp′), 4.31–4.30 (m, 1H, Cp), 4.28–4.27 (m, 1H, Cp), 2.35 (d, J = 17.0 Hz, 1H, H-8), 2.18 (d, J = 16.7 Hz, 1H, H-8), 2.17 (d, J = 16.0 Hz, 1H, H-6), 2.09 (s, 3H, 2-CH_3), 2.04 (d, J = 16.2 Hz, 1H, H-6), 1.01 (s, 3H, 7-CH_3), 0.86 (s, 3H, 7-CH_3). ^{13}C{^{1}H} NMR (DMSO-d_6) δ 193.9 (C-5), 163.3 (*C*ONH), 150.2 (C), 138.8 (C), 136.4 (C), 128.4 (*C*H$_{C_6H_4Cl}$), 126.2 (C), 120.8 (*C*H$_{C_6H_4Cl}$), 109.0 (C), 108.9 (C), 97.4 (Cp$_{ipso}$), 70.6 (Cp′), 69.3 (Cp), 69.1 (Cp), 68.7 (Cp), 68.3 (Cp), 50.6 (C-6), 39.7 (C-8 overlapped with DMSO residual), 32.0 (C), 30.3 (C-4), 29.5 (7-*C*H$_3$), 25.9 (7-*C*H$_3$), 17.1 (2-*C*H$_3$). MS calculated for $C_{29}H_{30}ClN_2O_2Ru$ m/z = 575.1 $[M + H]^+$ found m/z = 575.1 $[M + H]^+$.

***N*-(4-Chlorophenyl)-4-(2-ferrocenylphenyl)-2,7,7-trimethyl-5-oxo-1,4,5,6,7,8-hexahydroquinoline-3-carboxamide 14d.** This compound was synthesized in 30% yield (180 mg) as orange solid according to **5**, starting from 140 mg (1.0 mmol) of **13a**, 290 mg (1.0 mmol) of **11d**, 211 mg (1.0 mmol) of **10d**, 77 mg (1.0 mmol) of ammonium acetate and 6.0 ml of 2,2,2-trifluoroethanol. Total reaction time 20 min (2 × 10 min). After evaporation of the volatiles the product was isolated by chromatography on silica gen using dichloromethane – ethyl acetate (4–1) as eluent. The obtained product was purified again by chromatography on silica gel using dichloromethane – ethyl acetate (9–1). Elemental analysis (%) calculated for $C_{35}H_{33}ClFeN_2O_2$ C – 69.49, H – 5.50, N – 4.63 found C – 69.21, H – 5.34, N – 4.38. ^{1}H NMR (DMSO-d_6) δ 10.22 (s, 0.2 H, H-1, minor rotamer), 9.24 (s, 1H, H-1), 8.56 (s, 1H, CON*H*), 7.67 (d, J = 7.6 Hz, 1H, C*H*$_{Ary}$), 7.60 (d, J = 8.9 Hz, 0.5H, C*H*$_{Ary}$, minor rotamer), 7.36 (d, J = 8.8 Hz, 0.5H, C*H*$_{Ary}$, minor rotamer), 7.36 (d, J = 8.8 Hz, 2H, C*H*$_{Ary}$), 7.21 (d, J = 8.9 Hz, 2H, C*H*$_{Ary}$), 7.13 (br s, 1H, C*H*$_{Ary}$), 7.12 (br s, 1H, C*H*$_{Ary}$), 7.08–7.06 (m, 1H, C*H*$_{Ary}$), 5.35 (s, 1H, Cp), 5.26 (s, 1H, H-4), 4.08–4.07 (m, 1H, Cp), 4.02 (s, 5H, Cp′), 3.97 (br s, 1H, Cp), 3.63 (br s, 1H, Cp), 2.41 (d, J = 16.9 Hz, 1H, H-8), 2.34 (d, J = 16.8 Hz, 1H, H-8), 2.15 (d, J = 15.9 Hz, 1H, H-6), 2.00 (d, J = 15.8 Hz, 1H, H-6), 1.77 (s, 3H, 2-CH_3), 1.06 (s, 3H, 7-CH_3), 1.00 (s, 3H, 7-CH_3). ^{13}C{^{1}H} NMR (DMSO-d_6) δ 202.7 (C-5, minor rotamer), 193.8 (C-5), 167.0 (*C*ONH), 165.2 (*C*ONH, minor rotamer), 151.3 (C), 146.4 (C), 148.5 (C), 137.8 (C, minor rotamer), 135.2 (C), 131.2 (*C*H$_{Ary}$, minor rotamer), 130.9 (C), 128.7 (*C*H$_{Ary}$), 128.3 (*C*H$_{Ary}$, minor rotamer), 127.4 (*C*H$_{Ary}$), 126.9 (C, minor rotamer), 126.5 (*C*H$_{Ary}$), 125.8 (C), 125.0 (*C*H$_{Ary}$), 120.9 (*C*H$_{Ary}$), 120.6 (*C*H$_{Ary}$), 113.6 (C), 108.6 (C), 88.6 (Cp$_{ipso}$), 77.2 (Cp), 69.7 (Cp), 68.9 (Cp′), 66.9 (Cp), 66.8 (Cp), 50.6 (C-6), 40.0 (C-8 overlapped with DMSO residual signal), 34.4 (C-4), 32.1 (C), 29.3 (7-*C*H$_3$), 26.8 (7-*C*H$_3$), 16.2 (2-*C*H$_3$). MS calculated for $C_{35}H_{33}ClFeN_2O_2$ m/z = 604.2 $[M]^+$ found m/z = 604.5 $[M]^+$.

***N*-(4-Chlorophenyl)-4-(3-ferrocenylphenyl)-2,7,7-trimethyl-5-oxo-1,4,5,6,7,8-hexahydroquinoline-3-carboxamide 14e.** This compound was synthesized in 55% yield (330 mg) as orange solid according to **5**, starting from 140 mg (1.0 mmol) of **13a**, 290 mg (1.0 mmol) of **11e**, 211 mg (1.0 mmol) of **10d**, 77 mg (1.0 mmol) of ammonium acetate and 6.0 ml of 2,2,2-trifluoroethanol. Total reaction time 15 min (10 + 5 min). After evaporation of the volatiles the product was isolated by chromatography on silica gen using dichloromethane – ethyl acetate (4–1) as eluent. The obtained product was purified again by chromatography on silica gel using dichloromethane – ethyl acetate (9–1). Elemental analysis (%) calculated for $C_{35}H_{33}ClFeN_2O_2$ C – 69.49, H – 5.50, N – 4.63 found C – 69.54, H – 5.49, N – 4.44. ^{1}H NMR (DMSO-d_6) δ 9.76 (s, 1H, H-1), 8.79 (s, 1H, CON*H*), 7.65 (d, J = 8.9 Hz, 2H, C$_6H_4$Cl), 7.36 (br s, 1H, C$_6H_4$Fc), 7.29 (d, J = 8.9 Hz, 2H, C$_6H_4$Cl), 7.17 (d, J = 7.7 Hz,

1H, C_6H_4Fc), 7.08 (t, J = 7.6 Hz, 1H, C_6H_4Fc), 6.96 (d, J = 7.7 Hz, 1H, C_6H_4Fc), 5.01 (s, 1H, H-4), 4.55–4.54 (m, 1H, Cp), 4.51–4.50 (m, 1H, Cp), 4.28–4.27 (m, 2H, Cp), 3.92 (s, 5H, Cp′), 2.45 (d, J = 17.0 Hz, 1H, H-8), 2.35 (d, J = 16.5 Hz, 1H, H-8), 2.20 (d, J = 16.0 Hz, 1H, H-6), 2.07 (s, 3H, 2-CH_3), 2.02 (d, J = 15.9 Hz, 1H, H-6), 1.06 (s, 3H, 7-CH_3), 0.98 (s, 3H, 7-CH_3). ^{13}C{^{1}H} NMR (DMSO-d$_6$) δ 193.7 (C-5), 167.4 (*C*ONH), 150.5 (C), 147.0 (C), 138.5 (C), 138.2 (C), 135.8 (C), 128.3 ($CH_{C_6H_4Cl}$), 127.9 ($CH_{C_6H_4Fc}$), 126.4 (C), 125.6 ($CH_{C_6H_4Fc}$), 124.8 ($CH_{C_6H_4Fc}$), 123.4 ($CH_{C_6H_4Fc}$), 121.1 ($CH_{C_6H_4Cl}$), 110.6 (C), 110.1 (C), 85.4 (Cp$_{ipso}$), 69.3 (Cp′), 68.6 (Cp), 68.5 (Cp), 66.7 (Cp), 65.8 (Cp), 50.4 (C-6), 39.6 (C-8 overlapped with DMSO residual signals) 37.9 (C-4), 32.1 (C), 29.2 (7-CH_3), 26.6 (7-CH_3), 17.2 (2-CH_3). MS calculated for $C_{35}H_{33}ClFeN_2O_2$ m/z = 604.2 [M]$^+$, found m/z = 604.3 [M]$^+$.

***N*-(4-Chlorophenyl)-4-(4-ferrocenylphenyl)-2,7,7-trimethyl-5-oxo-1,4,5,6,7,8-hexahydroquinoline-3-carboxamide 14f.** This compound was synthesized in 80% yield (483 mg) as orange solid according to **5**, starting from 140 mg (1.0 mmol) of **13a**, 290 mg (1.0 mmol) of **11f**, 211 mg (1.0 mmol) of **10d**, 77 mg (1.0 mmol) of ammonium acetate and 6.0 ml of 2,2,2-trifluoroethanol. Total reaction time 20 min (2 × 10 min). After evaporation of the volatiles the product was isolated by chromatography on silica gen using dichloromethane – ethyl acetate (4–1) as eluent. The obtained product was purified again by chromatography on silica gel using dichloromethane – ethyl acetate (9–1). Elemental analysis (%) calculated for $C_{35}H_{33}ClFeN_2O_2$ C – 69.49, H – 5.50, N – 4.63 found C – 69.54, H – 5.37, N – 4.34. ^{1}H NMR (DMSO-d$_6$) δ 9.70 (s, 1H, H-1), 8.74 (s, 1H, CON*H*), 7.60 (d, J = 8.9 Hz, 2H, C_6H_4Cl), 7.34 (d, J = 8.2 Hz, 2H, C_6H_4Fc), 7.28 (d, J = 8.9 Hz, 2H, C_6H_4Cl), 7.08 (d, J = 8.2 Hz, 2H, C_6H_4Fc), 4.95 (s, 1H, H-4), 4.65 (t, J = 1.8 Hz, 2H, Cp), 4.27 (t, J = 1.7 Hz, 2H, Cp), 3.96 (s, 5H, Cp′), 2.41 (d, J = 16.9 Hz, 1H, H-8), 2.32 (d, J = 16.8 Hz, 1H, H-8), 2.17 (d, J = 16.0 Hz, 1H, H-6), 2.06 (s, 3H, 2-CH_3), 2.02 (d, J = 15.9 Hz, 1H, H-6), 1.03 (s, 3H, 7-CH_3), 0.92 (s, 3H, 7-CH_3). ^{13}C{^{1}H} NMR (DMSO-d$_6$) δ 193.7 (C-5), 167.5 (*C*ONH), 150.4 (C), 144.7 (C), 138.4 (C), 136.1 (C), 135.4 (C), 128.3 ($CH_{C_6H_4Cl}$), 127.3 ($CH_{C_6H_4Fc}$), 126.4 (C), 125.6 ($CH_{C_6H_4Fc}$), 121.1 ($CH_{C_6H_4Cl}$), 110.5 (C), 108.0 (C), 85.3 (Cp$_{ipso}$), 69.2 (Cp′), 65.5 (Cp), 65.5 Cp (Cp), 66.2 (Cp), 66.1 (Cp), 50.4 (C-6), 39.4 (C-8 overlapped with DMSO residual signals), 37.6 (C-4), 32.1 (C), 29.1 (7-CH_3), 26.7 (7-CH_3), 17.1 (2-CH_3). MS calculated for $C_{35}H_{33}ClFeN_2O_2$ m/z = 604.2 [M]$^+$, found m/z = 604.2 [M]$^+$.

***N*-(4-Chlorophenyl)-4-ferrocenyl-2,7-dimethyl-5-oxo-1,4,5,6,7,8-hexahydroquinoline-3-carboxamide 14g.** This compound was synthesized in 38% yield (393 mg) as orange solid according to **5**, starting from 252 mg (2.0 mmol) of **13b**, 428 mg (2.0 mmol) of **11b**, 422 mg (2.0 mmol) of **10d**, 154 mg (2.0 mmol) of ammonium acetate and 6.0 ml of 2,2,2-trifluoroethanol. Total reaction time 20 min (2 × 10 min). After evaporation of the volatiles the residue was gently mixed with 50 ml of ethyl acetate and 50 ml of cyclohexane was added, the precipitated product was filtered off, washed with 100 ml of ethyl acetate – cyclohexane (2–3) and dried. Elemental analysis (%) calculated for $C_{28}H_{27}ClFeN_2O_2$ C – 65.32, H – 5.29, N – 5.44 found C – 65.18, H – 5.55, N – 5.26. ^{1}H NMR (DMSO-d$_6$) δ 9.87 (s, 1H, H-1), 8.77 (s, 0.3H, CON*H* minor isomer), 8.68 (s, 0.7H, CON*H*), 7.83 (d, J = 8.9 Hz, 2H, C_6H_4Cl), 7.36 (d, J = 8.9 Hz, 2H, C_6H_4Cl), 4.83 (s, 0.3H, H-4, minor isomer), 4.81 (s, 0.7H, H-4). 4.03 (br s, 0.3H, Cp, minor isomer), 4.00 (br s, 1H, Cp), 3.99 (br s, 0.8H, Cp), 3.97 (s, 5H, Cp′), 3.94 (br s, 1H, Cp), 3.91 (br s, 1H, Cp), 2.40 (d, J = 16.2 Hz, 0.5H, H-8), 2.39 (d, J = 16.2 Hz, 0.5H, H-8), 2.30 (d, J = 16.1, 0.5H, H-6), 2.29 (d, J = 16.0 Hz, 0.5, H-6), 2.25 (d, J = 16.1 Hz, 0.4H, H-8), 2.23 (d, J = 16.2, 0.4H, H-8), 2.16 (d, J = 17.1 Hz, 0.2H, H-8), 2.14 (d, J = 17.3, 0.2H, H-8), 2.11–2.07 (m, 3.6H, 2-CH_3 and H-6), 1.99 (d, J = 16.0 Hz, 0.2H, H-6), 1.96 (d, J = 16.0, 0.2H, H-6), 1.59–1.47 (m, 1H, H-7), 0.84 (d, J = 6.7 Hz, 3H, 7-CH_3). ^{13}C{^{1}H} NMR (DMSO-d$_6$) δ 194.4 (minor), 194.2 (C-5), 168.7 (*C*ONH), 151.7 (C_{minor}), 151.6, 138.7, 136.2, 135.9 (minor), 128.5 ($CH_{C_6H_4Cl}$), 126.4 (minor), 126.3 (C), 120.9 ($CH_{C_6H_4Cl}$), 110.2 (C), 110.0 (C_{minor}), 109.4 (C_{minor}), 108.8 (C), 95.6 (Cp$_{ipso\text{-minor}}$), 95.4 (Cp$_{ipso}$), 68.3 (Cp′), 67.0 (Cp), 66.3 (Cp), 66.2 (Cp$_{minor}$), 65.9 (Cp), 65.7 (Cp$_{minor}$), 65.6 (Cp), 41.1 (C-6), 40.4 (C-8), 31.2 (C-7$_{minor}$), 30.9 (C-7), 30.6 (C-7$_{minor}$), 30.1 (C-8$_{minor}$), 29.9 (C-8), 19.7 (7-CH_3), 19.6 (7-$CH_{3\text{-minor}}$), 19.4 (7-$CH_{3\text{-minor}}$), 17.0 (2-CH_3). MS calculated for $C_{28}H_{27}ClFeN_2O_2$ m/z = 514.1 [M]$^+$ found m/z = 514.3 [M]$^+$.

***N*-(4-Chlorophenyl)-4-ferrocenyl-2-methyl-5-oxo-7-phenyl-1,4,5,6,7,8-hexahydroquinoline-3-carboxamide 14h – mixture of diastereomers.** This compound was synthesized in 30% yield (350 mg) as yellow solid according to **5**, starting from 376 mg (2.0 mmol) of **13c**, 428 mg (2.0 mmol) of **11b**, 422 mg (2.0 mmol) of **10d**, 154 mg (2.0 mmol) of ammonium acetate and 6.0 ml of 2,2,2-trifluoroethanol. Total reaction time 20 min (1 × 20 min). After cooling to RT the precipitated product was filtered off, washed with ethyl acetate (50 ml) followed by 20 ml of methanol – ethyl acetate (1–1). Elemental analysis (%) calculated for $C_{33}H_{29}ClFeN_2O_2$ C – 68.71, H – 5.07, N – 4.86 found C – 68.53, H – 5.08, N – 4.72. ^{1}H NMR (DMSO-d$_6$) δ 10.2 (s, 0.12H, H-1 minor), 9.91 (s, 0.88H, H-1), 8.81 (s, 0.42H, CON*H*), 8.72 (s, 0.44H, CON*H*), 8.68 (s, 0.07H, CONH_{minor}), 8.60 (s, 0.06H, CONH_{minor}), 7.86–7.84 (m, 2H, CH_{Ar}), 7.41–7.30 (m, 4H, CH_{Ar}), 7.26–7.16 (m, 3H, CH_{Ar}), 4.91 (s, 0.07H, H-4$_{minor}$), 4.91 (s, 0.4H, H-4), 4.89 (s, 0.07H, H-4$_{minor}$), 4.88 (s, 0.4H, H-4), 4.40–4.39 (m, 0.26 H, Cp$_{minor}$), 4.33 (br s, 0.25H, Cp$_{minor}$), 4.13–3.92 (m, 9H, Cp and Cp′), 3.38–3.34 (m, 0.6H, H-7), 3.32–3.06 (m, 0.4H, H-7), 2.96–2.84 (m, 0.2 H, H-6), 2.69–2.60 (m, 1.7H, H-6 or H-8), 2.57–2.52 (m, 1.8H, H-6 or H-8), 2.41 (br s, 0.25H, H-6 or H-8), 3.38 (br s, 0.25H, H-6 or H-8), 2.31 (s, 1.8H, 2-CH_3), 2.12 (s, 1.8H, 2-CH_3); ^{13}C{^{1}H} NMR (DMSO-d$_6$) δ 193.5 (C-5), 193.1 (C-5), 168.7 (*C*ONH), 151.2 (C), 150.7 (C), 143.8 (C), 143.6 (C), 138.7 (2 × C), 136.0 (C), 135.7 (C), 128.5 (2 × CH_{Ar}), 128.3 (CH_{Ar}), 127.0 (2 × CH_{Ar}), 126.6 ($CH_{Ar\text{-minor}}$) 126.4 ($CH_{Ar\text{-minor}}$), 120.9 (2 × CH_{Ar}), 110.4 (C), 110.0 (C), 109.6 (C), 109.0 (C), 95.5 (Cp$_{ipso}$), 94.8 (Cp$_{ipso}$), 69.2 (Cp), 68.5 (Cp′$_{minor}$), 68.4 (Cp′), 68.3 (Cp′), 67.1 (2 × Cp), 66.3 (2 × Cp), 66.1 (Cp), 66.0 (Cp), 65.7 (Cp), 65.6 (Cp), 44.1 (C-6), 43.5 (C-6), 38.9 (C-7), 38.4 (C-7), 33.9 (C-8), 33.4 (C-8), 30.7 (C-4), 30.6 (C-4), 17.1 (2-CH_3), 17.0 (2-CH_3). MS calculated for $C_{33}H_{29}ClFeN_2O_2$ m/z = 576.1 [M]$^+$ found m/z = 576.2 [M]$^+$.

***N*-(4-Chlorophenyl)-7-ferrocenyl-2-methyl-5-oxo-4-phenyl-1,4,5,6,7,8-hexahydroquinoline-3-carboxamide 14i – mixture of diastereomers.** This compound was synthesized in 18% yield (105 mg) as orange solid according to **5**, starting from 296 mg (1.0 mmol) of **13e**, 106 mg (102 μl, 1.0 mmol) of **11a**, 211 mg of **10d**, 77 mg (1.0 mmol) of ammonium acetate and 6.0 ml of 2,2,2-trifluoroethanol. Total reaction time 20 min (2 × 10 min). Elemental analysis (%) calculated for $C_{33}H_{29}ClFeN_2O_2$ C – 68.71, H – 5.07, N – 4.86 found C – 68.87, H – 4.93, N – 4.57. ^{1}H NMR (DMSO-d$_6$) δ 10.21 (s, 0.6H$_{minor}$), 9.70 (s, 1H, H-1), 8.80 (s, 1H, CONH), 7.60–7.59 (m, 3H, CH$_{Ary}$), 7.36 (d, J = 8.9 Hz, 1.5H, CH$_{Ary\text{-}minor}$), 7.29 (d, J = 8.9 Hz, 2H, CH$_{Ary}$), 7.15–7.09 (m 4H, CH$_{Ary}$), 7.05–7.03 (m, 1H, CH$_{Ary}$), 4.98 (s, 1H, H-4), 4.16–4.14 (m, 1H, Cp), 4.15 (s, 5H, Cp′), 4.07–4.06 (m, 1H, Cp), 4.03–4.02 (m, 1H, Cp), 3.98–3.97 (m, 1H, Cp), 3.14–3.10 (m, 1H, H-7), 2.85 (d, J = 16.5 Hz, 0.5H, H-8), 2.84 (d, J = 16.5 Hz, 0.5H, H-8), 2.68 (d, J = 16.5 Hz, 0.5H, H-8), 2.66 (d, J = 16.4 Hz, 0.5H, H-8), 2.30 (d, J = 16.2 Hz, 0.5H, H-6), 2.28 (d, J = 16.2 Hz, 0.5H, H-6), 2.05 (s, 3H, 2-CH$_3$). ^{13}C{^{1}H} NMR (DMSO-d$_6$) δ 202.7 (C-5$_{minor}$), 193.1 (C-5), 167.4 (CONH), 165.2 (CONH$_{minor}$), 151.4 (C), 146.6 (C), 138.4 (C), 137.8 (C$_{minor}$), 135.2 (C), 128.7 (CH$_{Ary}$), 128.3 (CH$_{Ary}$), 127.8 (CH$_{Ary}$), 127.5 (CH$_{Ary}$), 126.9 (C$_{minor}$), 126.4 (C$_{minor}$), 125.6 (CH$_{Ary\text{-}minor}$), 121.1 (CH$_{Ary}$), 120.6 (CH$_{Ary}$), 110.6 (C), 108.7 (C), 91.8 (Cp$_{ipso}$), 68.3 (Cp′), 67.0 (Cp), 66.9 (Cp), 66.8 (Cp), 66.2 (Cp), 44.4 (C-6), 38.1 (C-4), 33.5 (C-8), 33.2 (C-7), 30.2 (C), 17.1 (2-CH$_3$). MS calculated for $C_{33}H_{29}ClFeN_2O_2$ m/z = 576.1 [M]$^+$ found m/z = 576.0 [M]$^+$.

***N*-(4-Chlorophenyl)-4-ferrocenyl-2-methyl-5-oxo-1,4,5,6,7,8-hexahydroquinoline-3-carboxamide 14j.** This compound was synthesized in 64% yield (635 mg) as pale yellow solid according to **5**, starting from 224 mg (2.0 mmol) of **13d**, 428 mg (2.0 mmol) of **11b**, 422 mg (2.0 mmol) of **10d**, 154 mg (2.0 mmol) of ammonium acetate and 6.0 ml of 2,2,2-trifluoroethanol. Total reaction time 20 min (1 × 20 min). After evaporation of the volatiles the residue was gently mixed with 50 ml of ethyl acetate and 50 ml of cyclohexane (with sonification in ultrasonic bath) and the precipitated product was filtered off, washed with 100 ml of ethyl acetate – cyclohexane (2–3) and dried. Elemental analysis (%) calculated for $C_{27}H_{25}ClFeN_2O_2$ C – 64.76, H – 5.03, N – 5.59 found C – 64.67, H – 5.15, N – 5.48. ^{1}H NMR (DMSO-d$_6$) δ 9.86 (s, 1H, H-1), 8.75 (s, 1H, CONH), 7.82 (d, J = 8.9 Hz, 2H, C$_6$H$_4$Cl), 7.36 (d, J = 8.9 Hz, 2H, C$_6$H$_4$Cl), 4.83 (s, 1H, H-4), 4.03 (br s, 1H, Cp), 4.00 (br s, 1H, Cp), 3.97 (s, 5H, Cp′), 3.95–3.94 (m, 1H, Cp), 3.92 (br s, 1H, Cp), 2.39–2.37 (m, 2H, H-8), 2.28–2.17 (m, 2H, H-6), 2.10 (s, 3H, 2-CH$_3$), 1.89–1.85 (m, 1H, H-7), 1.71–1.67 (m, 1H, H-7). ^{13}C{^{1}H} NMR (DMSO-d$_6$) δ 194.3 (C-5), 168.7 (CONH), 151.9 (C), 138.7 (C), 135.8 (C), 128.5 (CH$_{C_6H_4Cl}$), 126.4 (CH$_{C_6H_4Cl}$), 120.9 (C), 110.3 (C), 109.3 (C), 95.7 (Cp$_{ipso}$), 68.3 (Cp′), 67.0 (Cp), 66.3 (Cp), 65.9 (Cp), 65.7 (Cp), 37.0 (C-7), 30.5 (C), 26.4 (C-8), 20.8 (C-6), 17.0 (2-CH$_3$). MS calculated for $C_{27}H_{25}ClFeN_2O_2$ m/z = 500.1 [M]$^+$ found m/z = 500.4 [M]$^+$.

Ethyl 2,7,7-trimethyl-5-oxo-4-phenyl-1,4,5,6,7,8-hexahydroquinoline-3-carboxylate 15a. This compound was synthesized in 47% yield (160 mg of white powder) as orange solid according to **5**, starting from 140 mg (1.0 mmol) of **13a**, 106 mg (102 μl, 1.0 mmol) of **11a**, 130 mg (1.0 mmol, 126 μl) of **10e**, 77 mg (1.0 mmol) of ammonium acetate and 2.5 ml of 2,2,2-trifluoroethanol. Total reaction time 10 min (1 × 10 min). After evaporation of the volatiles the residue was gently mixed with 50 ml of ethyl acetate (with sonification in ultrasonic bath) and the precipitated product was filtered off, washed with ethyl acetate and diethyl ether and dried. Elemental analysis (%) calculated for $C_{21}H_{25}NO_3$ C – 74.31, H – 7.42, N – 4.13 found C – 74.11, H – 7.26, N – 3.86. ^{1}H NMR (DMSO-d$_6$) δ 9.06 (s, 1H, NH), 7.19–7.14 (m, 4H, CH$_{Ph}$), 7.07–7.05 (m, 1H, CH$_{Ph}$), 4.85 (s, 1H, H-4), 3.97 (q, J = 7.0 Hz, 2H, COOCH$_2$CH$_3$), 2.41 (d, J = 17.0 Hz, 1H, H-8), 2.29 (d, J = 15.9 Hz, 1H, H-8), 2.28 (s, 3H, 2-CH$_3$), 2.16 (d, J = 16.1 Hz, 1H, H-6), 1.97 (d, J = 16.3 Hz, 1H, H-6), 1.12 (t, J = 7.1 Hz, 3H, COOCH$_2$CH$_3$), 1.00 (s, 3H, 7-CH$_3$), 0.84 (s, 3H, 7-CH$_3$); ^{13}C{^{1}H} NMR (DMSO-d$_6$) δ 194.2 (C-5), 166.8 (COOCH$_2$CH$_3$), 149.5 (C), 147.6 (C), 145.0 (C), 127.7 (CH$_{Ph}$), 127.4 (CH$_{Ph}$), 125.7 (CH$_{Ph}$), 109.9 (C), 103.6 (C), 59.0 (COOCH$_2$CH$_3$), 50.2 (C-6), 39.4 (C-8 overlapped with DMSO residual signals), 35.8 (C-4), 32.1 (C), 29.1 (7-CH$_3$), 26.4 (7-CH$_3$), 18.3 (2-CH$_3$), 14.1 (COOCH$_2$CH$_3$). MS calculated for $C_{21}H_{26}NO_3$ m/z = 340.2 [M + H]$^+$ found m/z = 340.2 [M + H]$^+$.

Ethyl 4-ferrocenyl-2,7,7-trimethyl-5-oxo-1,4,5,6,7,8-hexahydroquinoline-3-carboxylate 15b. This compound was synthesized in 36% yield (1.6 g) as orange solid according to **5**, starting from 1.4 g (10 mmol) of **13a**, 2.14 g (10 mmol) of **11b**, 1.30 g (10 mmol, 1.26 ml) of **10e**, 799 mg (10 mmol) of ammonium acetate and 8.0 ml of 2,2,2-trifluoroethanol. Total reaction time 20 min (2 × 10 min). After evaporation of the volatiles the residue was gently mixed with 50 ml of ethyl acetate (with sonification in ultrasonic bath) and the precipitated product was filtered off, washed with ethyl acetate and diethyl ether and dried. Elemental analysis (%) calculated for $C_{25}H_{29}FeNO_3$ C – 67.12, H – 6.53, N – 3.13 found C – 67.30, H – 6.23, N – 2.90. ^{1}H NMR (DMSO-d$_6$) δ 9.11 (s, 1H, H-1), 4.68 (s, 1H, H-4), 4.16 (q, J = 7.0 Hz, 2H, COOCH$_2$CH$_3$), 4.02 (s, 5H, Cp′), 3.96 (br s, 2H, Cp), 3.76 (s, 1H, Cp), 3.72 (s, 1H, Cp), 2.40 (d, J = 17.2 Hz, 1H, H-8), 2.30 (d, J = 17.2 Hz, 1H, H-8), 2.26 (s, 3H, 2-CH$_3$), 2.20 (d, J = 16.1 Hz, 1H, H-6), 2.13 (d, J = 16.0 Hz, 1H, H-6), 1.26 (t, J = 7.1 Hz, 3H, COOCH$_2$CH$_3$), 1.03 (s, 3H, 7-CH$_3$), 1.02 (s, 3H, 7-CH$_3$). ^{13}C{^{1}H} NMR (DMSO) δ 194.5 (C-5), 167.5 (COOCH$_2$CH$_3$), 150.2 (C), 144.6 (C), 109.2 (C), 103.5 (C), 95.9 (Cp$_{ipso}$), 68.3 (Cp′), 66.4 (Cp), 66.2 (Cp), 65.7 (Cp), 65.6 (Cp), 59.2 (COOCH$_2$CH$_3$), 50.5 (C-6), 39.6 (C-8, overlapped with DMSO residual signal), 31.9 (C), 29.4 (7-CH$_3$), 27.9 (C-4), 26.4 (7-CH$_3$), 18.2 (2-CH$_3$), 14.4 (COOCH$_2$CH$_3$). MS calculated for $C_{25}H_{29}FeNO_3$ m/z = 447.1 [M]$^+$ found m/z = 447.4 [M]$^+$.

Ethyl 2,7,7-trimethyl-5-oxo-4-ruthenocenyl-1,4,5,6,7,8-hexahydroquinoline-3-carboxylate 15c. This compound was synthesized in 50% yield (247 mg) as white solid according to **5**, starting from 140 mg (1.0 mmol) of **13a**, 259 mg (1.0 mmol) of **11c**, 130 mg (126 μl, 1.0 mmol) of **10e**, 77 mg (1.0 mmol) of ammonium acetate and 2.5 ml of 2,2,2-trifluoroethanol. Total reaction time 30 min (3 × 10 min). After evaporation of the volatiles the residue was gently mixed with 10 ml of ethyl acetate (with sonification in ultrasonic bath) and the precipitated product was filtered off, washed with ethyl acetate and

diethyl ether and dried. Elemental analysis (%) calculated for $C_{25}H_{29}NO_3Ru$ C – 60.96, H – 5.93, N – 2.84 found C – 60.78, H – 5.69, N – 2.55. ^{1}H NMR (DMSO-d$_6$) δ 9.11 (s, 1H, H-1), 4.56 (s, 1H, H-4), 4.38 (s, 5H, Cp′), 4.31–4.29 (m, 2H, Cp), 4.17–4.11 (m, 4H, Cp and COOCH_2CH$_3$), 2.40 (d, J = 17.3 Hz, 1H, H-8), 2.28 (d, J = 17.0 Hz, 1H, H-8), 2.25 (s, 3H, 2-CH_3), 2.18 (d, J = 16.1 Hz, 1H, H-6), 2.10 (d, J = 16.2 Hz, 1H, H-6), 1.24 (t, J = 7.1 Hz, 3H, COOCH$_2$CH_3), 1.03 (s, 3H, 7-CH_3), 1.02 (s, 3H, 7-CH_3). ^{13}C{^{1}H} NMR (DMSO-d$_6$) δ 194.4 (C-5), 167.4 (*C*OOCH$_2$CH$_3$), 150.0 (C), 144.7 (C), 109.1 (C), 103.4 (C), 99.2 (Cp$_{ipso}$), 70.6 (Cp′), 69.1 (Cp), 68.8 (Cp), 68.7 (Cp), 68.5 (Cp), 59.1 (COO*C*H$_2$CH$_3$), 50.4 (C-6), 39.5 (C-8 overlapped with DMSO residual signal), 31.9 (C), 29.6 (7-*C*H$_3$), 27.8 (C-4), 26.3 (7-*C*H$_3$), 18.2 (2-*C*H$_3$), 14.4 (COOCH$_2$*C*H$_3$). MS calculated for $C_{25}H_{30}NO_3Ru$ m/z = 494.1 [M + H]$^+$ found m/z = 494.3 [M + H]$^+$.

Ethyl 4-(2-ferrocenylphenyl)-2,7,7-trimethyl-5-oxo-1,4,5,6,7,8-hexahydroquinoline-3-carboxylate 15d. This compound was synthesized in 19% yield (100 mg) as orange solid according to **5**, starting from 140 mg (1.0 mmol) of **13a**, 286 mg (1.0 mmol) of **11d** (1.0 mmol), 130 mg (126 µl, 1.0 mmol) of **10e**, 77 mg (1.0 mmol) of ammonium acetate and 8.0 ml of 2,2,2-trifluoroethanol. Total reaction time 20 min (2 × 10 min). Pure product was isolated by chromatography on silica gel using dichloromethane – ethyl acetate (9–1) as eluent. Elemental analysis (%) calculated for $C_{31}H_{33}FeNO_3$ C – 71.13, H – 6.35, N – 2.68 found C – 71.06, H – 6.21, N – 2.44. ^{1}H NMR (DMSO-d$_6$) δ 8.93 (s, 1H, H-1), 7.76–7.75 (m, 1H, C$_6H_4$Fc), 7.11–7.10 (m, 1H, C$_6H_4$Fc), 7.07–7.06 (m, 2H, C$_6H_4$Fc), 5.84 (s, 1H), 5.27 (s, 1H, Cp), 4.44–4.33 (m, 1H, Cp), 4.29–4.28 (m, 1H, Cp), 4.27–4.26 (m, 1H, Cp), 4.09 (s, 5H, Cp′), 3.79 (ddd, J = 14.0, 10.6, 7.0 Hz, 1H, COOCH_2CH$_3$), 3.33 (ddd, J = 14.1, 10.6, 7.0 Hz, 1H, COOCH_2CH$_3$, overlapped with HOD residual signal), 2.45 (d, J = 16.9 Hz, 1H, H-8), 2.34 (d, J = 16.2 Hz, 1H, H-8), 2.19 (d, J = 16.0 Hz, 1H, H-6), 2.08 (s, 3H, 2-CH_3), 2.06 (d, J = 16.0 Hz, 1H, H-6), 1.04 (s, 3H, 7-CH_3), 0.96 (s, 3H, 7-CH_3), 0.81 (t, J = 7.0 Hz, COOCH$_2$CH_3). ^{13}C{^{1}H} NMR (DMSO-d$_6$) δ 194.7 (C-5), 167.0 (*C*OOCH$_2$CH$_3$), 150.5 (C), 146.7 (C), 141.9 (C), 135.6 (C), 131.2 (*C*H$_{C_6H_4Fc}$), 128.5 (*C*H$_{C_6H_4Fc}$), 126.2 (*C*H$_{C_6H_4Fc}$), 125.2 (*C*H$_{C_6H_4Fc}$), 110.7 (C), 106.4 (C), 89.0 (Cp$_{ipso}$), 71.7 (Cp), 69.6 (Cp), 69.2 (Cp′), 67.1 (Cp), 67.0 (Cp), 58.4 (COO*C*H$_2$CH$_3$), 50.6 (C-6), 39.9 (C-8 overlapped with DMSO residual signal), 32.3 (C), 32.1 (C-4), 29.1 (7-*C*H$_3$), 26.8 (7-*C*H$_3$), 17.9 (2-*C*H$_3$), 14.2 (COOCH$_2$*C*H$_3$). MS calculated for $C_{31}H_{33}FeNO_3$ m/z = 523.2 [M]$^+$ found m/z = 523.5 [M]$^+$.

Ethyl 4-(3-ferrocenylphenyl)-2,7,7-trimethyl-5-oxo-1,4,5,6,7,8-hexahydroquinoline-3-carboxylate 15e. This compound was synthesized in 99% yield (930 mg) as orange solid according to **5**, starting from 251 mg (1.79 mmol) of **13a**, 520 mg (1.79 mmol) of **11e**, 233 mg (226 µl, 179 mmol) of **10e**, 138 mg (1.79 mmol) of ammonium acetate and 4.0 ml of 2,2,2-trifluoroethanol. Total reaction time 20 min (2 × 10 min). After evaporation of the volatiles the residue was gently mixed with 50 ml of ethyl acetate (with sonification in ultrasonic bath) and the precipitated product was filtered off, washed with ethyl acetate and diethyl ether and dried. Elemental analysis (%) calculated for $C_{31}H_{33}FeNO_3$ C – 71.16, H – 6.35, N – 2.68 found C – 71.20, H – 6.12, N – 2.44. ^{1}H NMR (DMSO-d$_6$) δ 9.13 (s, 1H, H-1), 7.36 (s, 1H, C$_6H_4$Fc), 7.18 (d, J = 7.6 Hz, 1H, C$_6H_4$Fc), 7.09 (t, J = 7.6 Hz, 1H, C$_6H_4$Fc), 6.98 (d, J = 7.7 Hz, 1H, C$_6H_4$Fc), 4.88 (s, 1H, H-4), 4.58 (br s, 1H, Cp), 4.57 (br s, 1H, Cp), 4.31 (br s, 1H, Cp), 4.30 (br s, 1H, Cp), 4.01 (q, J = 6.9 Hz, 2H, COOCH_2CH$_3$), 3.98 (s, 5H, Cp′), 2.46 (d, J = 17.0 Hz, 1H, H-8), 2.34–2.31 (m, 4H, 2-CH$_3$ and H-8), 2.21 (d, J = 16.1 Hz, 1H, H-6), 2.00 (d, J = 16.0 Hz, 1H, H-6), 1.17 (t, J = 7.1 Hz, 3H, COOCH$_2$CH_3), 1.03 (s, 3H, 7-CH_3), 0.90 (s, 3H, 7-CH_3). ^{13}C{^{1}H} NMR (DMSO-d$_6$) δ 194.3 (C-5), 166.9 (*C*OOCH$_2$CH$_3$), 149.6 (C), 147.5 (C), 145.0 (C), 138.1 (C), 127.7 (*C*H$_{C_6H_4Fc}$), 125.7 (*C*H$_{C_6H_4Fc}$), 125.1 (*C*H$_{C_6H_4Fc}$), 123.5 (*C*H$_{C_6H_4Fc}$), 110.0 (C), 103.7 (C), 85.6 (Cp$_{ipso}$), 69.3 (Cp′), 68.7 (Cp), 68.6 (Cp), 66.7 (Cp), 65.9 (Cp), 59.1 (COO*C*H$_2$CH$_3$), 50.3 (C-6), 39.5 (C-8 overlapped with DMSO residual signal), 35.7 (C-4), 32.2 (C), 29.2 (7-*C*H$_3$), 26.3 (7-*C*H$_3$), 18.3 (2-*C*H$_3$), 14.2 (COOCH$_2$*C*H$_3$). MS calculated for $C_{31}H_{33}FeNO_3$ m/z = 523.2 [M]$^+$ found m/z = 523.6 [M]$^+$.

Ethyl 4-(4-ferrocenylphenyl)-2,7,7-trimethyl-5-oxo-1,4,5,6,7,8-hexahydroquinoline-3-carboxylate 15f. This compound was synthesized in 82% yield (430 mg) as orange solid according to **5**, starting from 140 mg (1.0 mmol) of **13a**, 290 mg (1.0 mmol) of **11f**, 130 mg (126 µl, 1.0 mmol) of **10e**, 77 mg (1.0 mmol) of ammonium acetate and 2.0 ml of 2,2,2-trifluoroethanol. Total reaction time 20 min (2 × 10 min). After evaporation of the volatiles the residue was gently mixed with 50 ml of ethyl acetate (with sonification in ultrasonic bath) and the precipitated product was filtered off, washed with ethyl acetate and diethyl ether and dried. Elemental analysis (%) calculated for $C_{31}H_{33}FeNO_3$ C – 71.13, H – 6.35, N – 2.68 found C – 71.02, H – 6.60, N – 2.44. ^{1}H NMR (DMSO-d$_6$) δ 9.07 (s, 1H, H-1), 7.34 (d, J = 8.3 Hz, 2H, C$_6H_4$Fc), 7.07 (d, J = 8.2 Hz, 2H, C$_6H_4$Fc), 4.84 (s, 1H, H-4), 4.67–4.66 (m, 2H, Cp), 4.29–4.27 (m, 2H, Cp), 4.04–3.96 (m, 7H, Cp′ and COCH_2CH$_3$), 2.42 (d, J = 17.1 Hz, 1H, H-8), 2.30 (s, 3H, 2-CH_3), 2.29 (d, J = 16.9 Hz, 1H, H-8), 2.17 (d, J = 16.1 Hz, 1H, H-6), 1.99 (d, J = 16.2 Hz, 1H, H-6), 1.13 (t, J = 7.1 Hz, 3H, COCH$_2$CH_3), 1.01 (s, 3H, 7-CH_3), 0.84 (s, 3H, 7-CH_3). ^{13}C{^{1}H} NMR (DMSO-d$_6$) δ 194.3 (C-5), 166.9 (*C*OOCH$_2$CH$_3$), 149.4 (C), 145.3 (C), 145.0 (C), 136.1 (C), 127.3 (*C*H$_{C_6H_4Fc}$), 125.5 (*C*H$_{C_6H_4Fc}$), 109.9 (C), 103.4 (C), 85.3 (Cp$_{ipso}$), 69.2 (Cp′), 68.5 (2 × Cp), 66.2 (Cp), 66.0 (Cp), 59.0 (COO*C*H$_2$CH$_3$), 50.3 (C-6), 39.4 (C-8 overlapped with DMSO residual signal), 35.4 (C-4), 32.1 (C), 29.2 (7-*C*H$_3$), 26.3 (7-*C*H$_3$), 18.3 (2-*C*H$_3$). 14.2 (COOCH$_2$*C*H$_3$). MS calculated for $C_{31}H_{33}FeNO_3$ m/z = 523.2 [M]$^+$ found m/z = 523.2 [M]$^+$.

Ethyl 4-ferrocenyl-2,7-dimethyl-5-oxo-1,4,5,6,7,8-hexahydroquinoline-3-carboxylate 15g – mixture of diastereoisomers. This compound was synthesized in 20% yield (170 mg) as orange solid according to **5**, starting from 252 mg (2.0 mmol) of **13b**, 428 mg (2.0 mmol) of **11b**, 260 mg (252 µl, 2.0 mmol) of **10e**, 155 mg (2.0 mmol) of ammonium acetate and 6.0 ml of 2,2,2-trifluoroethanol. Total reaction time 20 min (2 × 10 min). Pure product was isolated by chromatography on silica gel using dichloromethane – ethyl acetate (9–1) as eluent. Elemental analysis (%) calculated for $C_{24}H_{27}FeNO_3$ C – 66.52, H – 6.28, N – 3.23 found C – 66.50, H – 6.24, N – 2.84. ^{1}H NMR (DMSO-d$_6$) δ 9.18 (s, 0.4 H, H-1, minor isomer), 9.10 (s, 1H,

H-1), 4.68 (s, 0.4 H, H-4$_{minor}$), 4.68 (s, 1H, H-4), 4.17–4.12 (m, 3H, COOCH_2CH$_3$), 4.01 (s, 5H, Cp′) and 4.01 (s, 2H, Cp′$_{minor}$), 3.95–3.94 (m, 2H, Cp), 3.93–3.92 (m, 0.5H, Cp$_{minor}$), 3.82–3.81 (m, 0.4H, Cp$_{minor}$), 3.76–3.75 (m, 1H, Cp), 7.74–3.73 (m, 1H, Cp), 3.71–3.70 (m, 0.4 H, Cp$_{minor}$), 2.56–2.52 (m, 1.4H, H-8), 2.38–2.35 (m, 1.4H, H-6), 2.32–2.28 (m, 1.2H, H-8), 2.26 (s, 3.5H, 2-CH_3 and H-7), 2.23 (s, 1.6H, 2-CH_{3minor}), 2.16–2.12 (m, 1.6H, H-6 and H-7), 1.26 (t, J = 7.1 Hz, 3H, COOCH$_2$CH_3), 1.25 (t, J = 7.1 Hz, 1.4H, COOCH$_2$CH_{3minor}), 1.05 (d, J = 6.3 Hz, 1.3 Hz, 7-CH$_{3minor}$), 1.03 (d, J = 6.6 Hz, 3H, 7-CH_3). ^{13}C{^{1}H} NMR (DMSO-d$_6$) δ 194.8 (C-5, minor isomer), 194.4 (C-5), 167.5 (*C*OOCH$_2$CH$_3$), 167.4 (*C*OOCH$_2$CH$_{3minor}$), 151.5 (C$_{minor}$), 150.5 (C), 144.5 (C), 144.4 (C$_{minor}$), 110.0 (C), 109.8 (C$_{minor}$), 104.1 (C$_{minor}$), 103.4 (C), 96.3 (Cp$_{ipso\text{-}minor}$), 96.1 (Cp$_{ipso}$), 68.3 (Cp′$_{minor}$), 68.3 (Cp′), 66.4 (Cp), 66.3 (Cp$_{minor}$), 66.3 (Cp$_{minor}$), 66.2 (Cp), 66.0 (Cp$_{minor}$), 65.8 (Cp), 65.7 (Cp), 65.5 (Cp$_{minor}$), 59.1 (COO*C*H$_2$CH$_3$), 45.2 (C-6$_{minor}$), 44.5 (C-6), 34.3 (C-8$_{minor}$), 33.5 (C-8), 28.3 (C-7), 28.2 (C-7$_{minor}$), 27.9 (C-4), 27.8 (C-4$_{minor}$), 20.6 (7-CH$_{3minor}$), 20.2 (7-*C*H$_3$), 18.1 (2-*C*H$_3$), 14.4 (COOCH$_2$*C*H$_3$). MS calculated for $C_{24}H_{27}FeNO_3$ m/z = 433.1 [M]$^+$ found m/z = 433.1 [M]$^+$.

Ethyl 4-ferrocenyl-2-methyl-7-phenyl-5-oxo-1,4,5,6,7,8-hexahydroquinoline-3-carboxylate 15h. This compound was synthesized in 30% yield (150 mg) as orange solid according to **5**, starting from 188 mg (1.0 mmol) of **13c**, 214 mg (1.0 mmol) of **11b**, 130 mg (126 μl, 1.0 mmol) of **10e**, 77 mg (1.0 mmol) of ammonium acetate and 2.5 ml of 2,2,2-trifluoroethanol. Total reaction time 20 min (2 × 10 min). Pure product was isolated by chromatography on silica gel using dichloromethane – ethyl acetate (9–1) as eluent. Elemental analysis (%) calculated for $C_{29}H_{29}FeNO_3$ C – 70.31, H – 5.90, N – 2.83 found C – 70.12, H – 5.92, N – 2.54. ^{1}H NMR (DMSO-d$_6$) δ 9.23 (s, 0.6H, H-1$_{major}$), 9.13 (s, 0.4H, H-1$_{minor}$), 7.22–7.18 (m, 2H, C*H*$_{Ph}$), 7.15–7.05 (m, 3H, C*H*$_{Ph}$), 4.93 (s, 0.6H, H-4$_{major}$), 4.87 (s, 0.4H, H-4$_{minor}$), 4.18–4.10 (m, 7.5H, Cp′ and Cp), 4.02–3.96 (m, 3.5H, COOCH_2CH$_3$ and Cp), 3.14–3.11 (m, 0.4H, H-7$_{minor}$), 2.85–2.81 (m, 1.6H, H-7 and H-8$_{major}$), 2.64 (d, J = 16.6 Hz, 0.2H, H-8$_{minor}$), 2.63 (d, J = 16.6 Hz, 0.2 Hz, H-8$_{minor}$), 2.59 (d, J = 18.0 Hz, 0.3H, H-8$_{major}$), 2.57 (d, J = 18.0 Hz, 0.3H, H-8$_{major}$), 2.53–2.50 (m, 0.5H, overlapped with DMSO residual signal, H-6), 2.44–2.41 (m, 0.6H, H-6), 2.33–2.25 (m, 4.2H, 2-CH_3 and H-6), 1.13 (t, J = 7.1 Hz, 3H, COOCH$_2$CH_3). ^{13}C{^{1}H} (DMSO-d$_6$) δ 194.0 (C-5), 193.6 (C-5$_{minor}$), 166.9 (*C*OOCH$_2$CH$_3$), 150.9 (C), 150.3 (C$_{minor}$), 147.7 (C), 147.2 (C$_{minor}$), 144.9 (C), 127.9 (*C*H$_{Ph}$), 127.6 (*C*H$_{Ph}$), 127.5 (*C*H$_{Ph}$), 125.7 (*C*H$_{Ph\text{-}minor}$), 125.6 (CH$_{Ph\text{-}minor}$), 110.8 (C), 110.7 (C$_{minor}$), 103.7 (C), 103.5 (C$_{minor}$), 91.8 (Cp$_{ipso}$), 91.7 (Cp$_{ipso\text{-}minor}$), 68.3 (Cp′$_{minor}$), 68.2 (Cp′), 67.1 (Cp), 67.0 (Cp), 66.9 (Cp), 66.8 (Cp), 66.2 (Cp), 65.8 (Cp$_{minor}$), 59.1 (COO*C*H$_2$CH$_3$), 59.0 (COO*C*H$_2$CH$_{3\ minor}$), 44.5 (C-6), 44.2 (C-6$_{minor}$), 35.9 (C-4$_{minor}$), 35.7 (C-4), 33.5 (C-8), 33.2 (C-8), 33.1 (C-7$_{minor}$), 32.4 (C-7), 18.3 (2-*C*H$_3$), 14.1 (COOCH$_2$*C*H$_3$). MS calculated for $C_{29}H_{29}FeNO_3$ m/z = 495.1 [M]$^+$ found m/z = 495.4 [M]$^+$.

Ethyl 7-ferrocenyl-2-methyl-5-oxo-4-phenyl-1,4,5,6,7,8-hexahydroquinoline-3-carboxylate 15i. This compound was synthesized in 18% yield (90 mg) as orange solid according to **5**, starting from 296 mg (1.0 mmol) of **13e**, 106 mg (102 μl, 1.0 mmol) of **11a**, 130 mg (126 μl, 1.0 mmol) of **10e**, 77 mg (1.0 mmol) of ammonium acetate and 3.0 ml of 2,2,2-trifluoroethanol. Total reaction time 20 min (2 × 10 min). Pure product was isolated by chromatography on silica gel using dichloromethane – ethyl acetate (9–1) as eluent. Elemental analysis (%) calculated for $C_{29}H_{29}FeNO_3$ C – 70.31, H – 5.90, N – 2.83 found C – 70.13, H – 5.94, N – 2.54. ^{1}H NMR (DMSO-d$_6$) δ 9.12 (s, 1H, H-1), 7.15–7.10 (m, 4H, C*H*$_{Ph}$), 7.06–7.03 (m, 1H, C*H*$_{Ph}$), 4.87 (s, 1H, H-4), 4.14 (s, 5H, Cp′), 4.10 (br s, Cp), 4.03–4.02 (m, 1H, Cp), 4.10–3.96 (m, 3H, COOCH_2CH$_3$ and Cp), 3.92 (br s, 1H, Cp), 3.15–3.10 (m, 1H, H-7), 2.84 (d, J = 16.6, 0.4H, H-8), 2.83 (d, J = 16.6 Hz, 0.6H, H-8), 2.64 (d, J = 16.6, 0.6H, H-8), 2.63 (d, J = 16.6 Hz, 0.4H, H-8), 2.53–2.49 (m, 1H, H-6, overlapped with DMSO residual signal), 2.30 (s, 3H, 2-CH_3), 2.28 (d, J = 16.5 Hz, 0.6H, H-6), 2.26 (d, J = 16.3 Hz, 0.4H, H-6), 1.12 (t, J = 7.1 Hz, 3H, COOCH$_2$CH_3). ^{13}C{^{1}H} NMR (DMSO-d$_6$) δ 193.6 (C-5), 166.9 (*C*OOCH$_2$CH$_3$), 150.3 (C), 147.2 (C), 144.9 (C), 127.6 (*C*H$_{Ph}$), 125.6 (*C*H$_{Ph}$), 110.7 (C), 103.5 (C), 91.7 (Cp$_{ipso}$), 68.3 (Cp′), 66.9 (2 × Cp), 66.8 (Cp), 66.2 (Cp), 59.0 (COO*C*H$_2$CH$_3$), 44.2 (C-6), 35.9 (C-4), 33.2 (C-8), 33.1 (C-7), 18.3 (2-*C*H$_3$), 14.1 (COOCH$_2$*C*H$_3$). MS calculated for $C_{29}H_{30}FeNO_3$ m/z = 496.2 [M + H]$^+$ found m/z = 496.1 [M + H]$^+$.

Ethyl 4-ferrocenyl-2-methyl-5-oxo-1,4,5,6,7,8-hexahydroquinoline-3-carboxylate 15j. This compound was synthesized in 44% yield (1.83 g) as orange solid according to **5**, starting from 1.12 g (10 mmol) of **13d**, 2.14 g (10 mmol) of **11b**, 1.30 g (1.26 ml, 10 mmol) of **10e**, 799 mg (10 mmol) of ammonium acetate and 8.0 ml of 2,2,2-trifluoroethanol. Total reaction time 20 min (2 × 10 min). Pure product was isolated by chromatography on silica gel using gradient of ethyl acetate in chloroform starting from 0 to 25% of ethyl acetate as eluent. Elemental analysis (%) calculated for $C_{23}H_{25}FeNO_3$ C – 65.88, H – 6.01, N – 3.34 found C – 65.67, H – 5.94, N – 3.05. ^{1}H NMR (DMSO-d$_6$) δ 9.18 (s, 1H, H-1), 4.70 (s, 1H, H-7), 4.17–4.11 (m, 2H, COOCH_2CH$_3$), 4.01 (s, 5H, Cp′), 3.95–3.94 (m, 1H, Cp), 3.94–3.93 (m, 1H, Cp), 3.82–3.81 (m, 1H, Cp), 3.73–3.72 (m, 1H, Cp), 2.54–2.43 (m, 2H, H-8 overlapped with DMSO residual), 2.37–2.32 (m, 1H, H-6), 2.26–2.21 (m, 4H, 2-CH_3 and H-6), 1.98–1.94 (m, 1H, H-7), 1.90–1.83 (m, 1H, H-7), 1.25 (t, J = 7.1 Hz, 3H, COOCH$_2$CH_3). ^{13}C{^{1}H} NMR (DMSO-d$_6$) δ 194.8 (C-5), 167.4 (*C*OOCH$_2$CH$_3$), 151.8 (C), 144.3 (C), 110.2 (C), 104.0 (C), 96.3 (Cp$_{ipso}$), 68.3 (Cp′), 66.3 (2 × Cp), 66.0 (Cp), 65.5 (Cp), 59.1 (COO*C*H$_2$CH$_3$), 36.9 (C-6), 27.7 (C-4), 26.3 (C-8), 20.9 (C-7), 18.1 (2-*C*H$_3$), 14.4 (COOCH$_2$*C*H$_3$). MS calculated for $C_{23}H_{25}FeNO_3$ m/z = 419.1 [M]$^+$ found m/z = 419.2 [M]$^+$.

***N*-(2-Ferrocenylphenyl)-2,7,7-trimethyl-5-oxo-4-phenyl-1,4,5,6,7,8-hexahydroquinoline-3-carboxamide 16a.** This compound was synthesized in 53% yield (150 mg) as orange solid according to **5**, starting from 77 (0.5 mmol) mg of **13a**, 60 mg (51 μl, 0.5 mmol), 181 mg (0.5 mmol) of **10b**, 39 mg (0.5 mmol) of ammonium acetate and 3.0 ml of 2,2,2-trifluoroethanol. Total reaction time 10 min (1 × 10 min). Pure product was isolated by chromatography on silica gel using dichloromethane – ethyl acetate (4–1) as eluent. An orange solid. Elemental analysis (%) calculated for $C_{35}H_{34}FeN_2O_2$ C – 73.69,

H – 6.01, N – 4.91 found C – 73.59, H – 6.27, N – 4.65. ^{1}H NMR (DMSO-d$_6$) δ 8.75 (s, 1H, H-1), 8.41 (s, 1H, CON*H*), 7.52–7.50 (m, 2H, C*H*$_{Ary}$), 7.26 (t, J = 7.6 Hz, 2H, C*H*$_{Ary}$), 7.20–7.16 (m, 4H, C*H*$_{Ary}$), 7.08–7.07 (m, 1H, C*H*$_{Ary}$), 7.91 (s, 1H, H-4), 4.31–4.30 (m, 1H, Cp), 4.28–4.27 (m, 1H, Cp), 4.17–4.16 (m, 1H, Cp), 4.07 (s, 5H, Cp′), 4.84–4.83 (m, 1H, Cp), 2.42 (d, J = 16.9 Hz, 1H, H-8), 2.31 (d, J = 16.2 Hz, 1H, H-8), 2.16 (d, J = 16.1 Hz, 1H, H-6), 2.06 (s, 3H, 2-C*H*$_3$), 1.98 (d, J = 16.0 Hz, 1H, H-6), 1.02 (s, 3H, 7-C*H*$_3$), 0.89 (s, 3H, 7-C*H*$_3$). ^{13}C{^{1}H} MNR (DMSO-d$_6$) δ 193.6 (C-5), 167.4 (*C*ONH), 150.4 (C), 147.0 (C), 134.8 (C), 134.6 (C), 130.2 (C), 130.1 (*C*H$_{Ary}$), 128.2 (*C*H$_{Ary}$), 127.5 (*C*H$_{Ary}$), 125.3 (*C*H$_{Ary}$), 126.1 (*C*H$_{Ary}$), 124.4 (*C*H$_{Ary}$), 111.0 (C), 108.0 (C), 83.1 (Cp$_{ipso}$), 69.1 (Cp′), 69.0 (Cp), 68.7 (Cp), 68.5 (Cp), 67.9 (Cp), 50.3 (C-6), 39.7 (C-8 overlapped with DMSO residual signal), 39.1 (C-4), 29.1 (7-*C*H$_3$), 26.6 (7-*C*H$_3$), 17.0 (2-*C*H$_3$). MS calculated for $C_{35}H_{34}FeN_2O_2$ m/z = 570.2 [M]$^+$ found m/z = 570.3 [M]$^+$.

***N*-(3-Ferrocenylphenyl)-2,7,7-trimethyl-5-oxo-4-phenyl-1,4,5,6,7,8-hexahydroquinoline-3-carboxamide 16b.** This compound was synthesized in 60% yield (340 mg) as orange solid according to **5**, starting from 140 mg (1.0 mmol) of **13a**, 106 mg (102 µl, 1.0 mmol) of **11a**, 361 mg (1.0 mmol) of **10c**, 77 mg (1.0 mmol) of ammonium acetate and 6.0 ml of 2,2,2-trifluoroethanol. Total reaction time 20 min (2 × 10 min). Pure product was isolated by chromatography on silica gel using dichloromethane – ethyl acetate (4–1) as eluent. Elemental analysis (%) calculated for $C_{35}H_{34}FeN_2O_2$ C – 73.69, H – 6.01, N – 4.91 found C – 73.58, H – 5.78, N – 4.63. ^{1}H NMR (DMSO-d$_6$) δ 9.51 (s, 1H, H-1), 8.72 (s, 1H, CON*H*), 7.67 (br s, 1H, C*H*$_{Ary}$), 7.44–7.43 (m, 1H, C*H*$_{Ary}$), 7.21–7.14 (m, 6H, C*H*$_{Ary}$), 7.08–7.05 (m, 1H, C*H*$_{Ary}$), 5.00 (s, 1H, H-4). 4.63–5.62 (m, 2H, Cp), 4.32 (t, J = 1.7 Hz, 2H, Cp), 4.03 (s, 5H, Cp′), 2.41 (d, J = 16.9 Hz, 1H, H-8), 2.33 (d, J = 16.9 Hz, 1H, H-8), 2.16 (d, J = 16.0 Hz, 1H, H-6), 2.08 (s, 3H, 2-C*H*$_3$), 1.04 (s, 3H, 7-C*H*$_3$), 0.91 (s, 3H, 7-C*H*$_3$). ^{13}C{^{1}H} NMR (DMSO-d$_6$) δ 193.6 (C-5), 167.3 (*C*ONH), 150.5 (C), 147.2 (C), 193.4 (C), 193.1 (C), 135.1 (C), 128.4 (*C*H$_{Ary}$), 127.9 (*C*H$_{Ary}$), 127.4 (*C*H$_{Ary}$), 125.7 (*C*H$_{Ary}$), 120.9 (*C*H$_{Ary}$), 117.4 (2 × *C*H$_{Ary}$), 110.9 (C), 108.2 (C), 85.2 (Cp$_{ipso}$), 69.4 (Cp′), 68.8 (Cp), 68.7 (Cp), 66.4 (Cp), 66.3 (Cp), 50.4 (C-6), 38.1 (C-8), 32.1 (C-4), 29.1 (7-*C*H$_3$), 26.8 (7-*C*H$_3$), 17.2 (2-*C*H$_3$). MS calculated for $C_{35}H_{34}FeN_2O_2$ m/z = 570.2 [M]$^+$ found m/z = 570.3 [M]$^+$.

***N*-(4-Ferrocenylphenyl)-2,7,7-trimethyl-5-oxo-4-phenyl-1,4,5,6,7,8-hexahydroquinoline-3-carboxamide 16c.** This compound was synthesized in 42% yield (240 mg) as orange solid according to **5**, starting from 140 mg (1.0 mmol) of **13a**, 106 mg (102 µl, 1.0 mmol) of **11a**, 361 mg (1.0 mmol) of **10d**, 77 mg (1.0 mmol) of ammonium acetate and 6.0 ml of 2,2,2-trifluoroethanol. Total reaction time 10 min (1 × 10 min). Pure product was isolated by chromatography on silica gel using dichloromethane – methanol (99–1) as eluent. Elemental analysis (%) calculated for $C_{35}H_{34}FeN_2O_2$ C – 73.69, H – 6.01, N – 4.91 found C – 73.46, H – 5.74, N – 4.66. ^{1}H NMR (DMSO-d$_6$) δ 9.53 (s, 1H, H-1), 8.70 (s, 1H, CON*H*), 7.49 (d, J = 8.7 Hz, 2H, C$_6$*H*$_4$Fc), 7.41 (d, J = 8.7 Hz, 2H, C$_6$*H*$_4$Fc), 7.19 (s, 2H, C*H*$_{Ph}$), 7.18 (s, 2H, C*H*$_{Ph}$), 7.08–7.05 (m, 1H, C*H*$_{Ph}$), 4.98 (s, 1H, H-4), 4.70 (t, J = 1.8 Hz, 2H, Cp), 4.29 (t, J = 1.8 Hz, 2H, Cp), 4.00 (s, 5H, Cp′), 2.40 (d, J = 16.9 Hz, 1H, H-8), 2.32 (d, J = 16.6 Hz, 1H, H-8), 2.15 (d, J = 16.0 Hz, 1H, H-6), 2.07 (s, 3H, 2-C*H*$_3$), 2.00 (d, J = 16.3 Hz, 1H, H-6), 1.03 (s, 3H, 7-C*H*$_3$), 0.91 (s, 3H, 7-C*H*$_3$). ^{13}C{^{1}H} NMR (DMSO-d$_6$) δ 193.6 (C-5), 167.1 (*C*ONH), 150.5 (C), 147.1 (C), 137.4 (C), 134.9 (C), 133.3 (C), 127.9 (*C*H$_{Ph}$), 127.4 (*C*H$_{Ph}$), 125.8 (*C*H$_{C_6H_4Fc}$), 125.7 (*C*H$_{Ph}$), 119.6 (*C*H$_{C_6H_4Fc}$), 111.0 (C), 108.0 (C), 85.0 (Cp$_{ipso}$), 69.2 (Cp′), 68.5 (Cp), 65.9 (Cp), 50.4 (C-6), 39.8 (C-8), 38.1 (C-4), 32.1 (C-7), 29.1 (7-*C*H$_3$), 26.8 (7-*C*H$_3$), 17.1 (2-*C*H$_3$). MS calculated for $C_{35}H_{34}FeN_2O_2$ m/z = 570.2 [M]$^+$ found m/z = 570.3 [M]$^+$.

Cell lines

All cell lines were purchased in American Type Culture Collection (ATCC) *via* LGC Standards sp. z o.o. The cells were cultured in standard conditions (5% CO_2, 100% relative humidity, 37 °C) in Dulbecco's modified Eagle's medium (DMEM) supplemented with 10% v/v fetal bovine albumin (FBS). Aseptic technique was strictly employed during cell passages to avoid antibiotic use and special care was taken not to cross-contaminate the cultures. All cell lines were routinely monitored for potential *Mycoplasma* infection.

Proliferation assay

The antiproliferative potential of the investigated compounds was determined using the neutral red uptake assay.[74] Cells were seeded on 96-well plates at a predetermined number (HepG2: 4 × 10^3 per well, A549: 5 × 10^3 per well, other cell lines: 10^4 per well) in final volume of 100 µL in a complete medium and allowed to attach for 24 h. The stock solutions of investigated compounds freshly prepared in dimethyl sulfoxide (DMSO) were appropriately diluted in a complete medium to a desired concentration. 100 µL of such solutions were added to the respective wells of the 96-well plate. The final DMSO concentration was equal in all samples, including controls, did not exceed 1% v/v and was determined to be non-toxic to the cells. After 70 h of incubation, neutral red was added to the medium to a final concentration of 1 mM. After another 2 h of incubation, the cells were washed twice with phosphate buffered saline (PBS), de-stained in 200 µL extraction solution (1% acetic acid (v/v) in 50% ethanol (v/v)) and placed on a rotary shaker for 15 min in dark, until the dye was released from the cells. The absorbance was measured at 540 nm with an EnVision Multilabel Plate Reader (PerkinElmer, Waltham, Massachusetts, USA). The results were calculated as the percentage of the controls and the IC_{50} values for each cell line and substance were calculated with GraphPad Prism 10.2.1 software (GraphPad Software, LLC, San Diego, California, USA) using a four-parameter non-linear logistic regression.

Cell cycle

10^5 of SW620 or A549 cells were seeded per well of 6-well plates, and left for 24 h to attach to the substrate. The tested compounds were added at the IC_{75} concentration of **5** calculated from viability curves for the SW620/A549 cells, respectively. After 24, 48 and 72 h, the cells were trypsinized, washed once with ice

cold PBS and fixed using 70% cold ethanol. The cells were then rehydrated with PBS and stained with 75 μM propidium iodide and 50 Kunitz units per mL of RNAse A in PBS for 30 minutes at 37 °C. The samples were analyzed on an Symphony A1 (Becton Dickinson) instrument (excitation 488 nm, emission 575/26 nm) and the cell cycle phase distribution was determined with FlowJo 7.6.1 software (FlowJo, LLC) using a built-in cell cycle analysis module (Watson pragmatic algorithm).

ROS detection

10^5 of A549 or SW620 cells were seeded per well of 6-well plates for 24 h. The cells were treated with the test compounds (1 and 10 μM), dihydrorhodamine 123 (1 μM) and verapamil (10 μM) for 4 h. The cells were then harvested and suspended in a complete medium. The samples were then collected on an Symphony A1 (Becton Dickinson) instrument and median fluorescence (excitation 488 nm, emission 530/30 nm) was analyzed. Results were calculated as a percentage of control.

Kinesin ATPase inhibition assay

The kinesin modulatory activity was determined using Kinesin ATPase Endpoint Biochem Kit (Cytoskeleton Inc.) according to the manufacturer's protocol. Phosphate release was measured at 650 nm (EnVision Plate Reader – PerkinElmer, USA). The DMSO concentration in the samples was 0.1%.

Data availability

The data supporting this article have been included as part of the ESI.†

Conflicts of interest

There are no conflicts to declare.

Acknowledgements

This study was financially supported by the National Science Centre Poland (NCN) based on decision UMO-2015/17/B/ST5/02331.

References

1 J. Tischer and F. Gergely, *J. Cell Biol.*, 2019, **218**, 10–11.
2 I. Marzo and J. Naval, *Biochem. Pharmacol.*, 2013, **86**, 703–710.
3 R. J. van Vuuren, M. H. Visagie, A. E. Theron and A. M. Joubert, *Cancer Chemother. Pharmacol.*, 2015, **76**, 1101–1112.
4 W. Krause, *Cancer Drug Resist.*, 2019, **2**, 82–106.
5 O. Rath and F. Kozielski, *Nat. Rev. Cancer*, 2012, **12**, 527–539.
6 R. Shahin and S. Aljamal, *Future Sci. OA*, 2022, **8**, FSO778.
7 P. Novais, P. M. A. Silva, I. Amorim and H. Bousbaa, *Pharmaceutics*, 2021, **13**, 1011.
8 J.-M. Wang, F.-H. Zhang, Z.-X. Liu, Y.-J. Tang, J.-F. Li and L.-P. Xie, *Biochem. Pharmacol.*, 2024, **224**, 116229.
9 N. Hirokawa, Y. Noda, Y. Tanaka and S. Niwa, *Nat. Rev. Mol. Cell Biol.*, 2009, **10**, 682–696.
10 H. Miki, Y. Okada and N. Hirokawa, *Trends Cell Biol.*, 2005, **15**, 467–476.
11 T. U. Mayer, T. M. Kapoor, S. J. Haggarty, R. W. King, S. L. Schreiber and T. J. Mitchison, *Science*, 1999, **286**, 971–974.
12 M. Nejabat, F. Hadizadeh and A. Sahebkar, *Curr. Rev. Clin. Exp. Pharmacol.*, 2024, **19**, 370–378.
13 X. D. Sun, X. J. Shi, X. O. Sun, Y. G. Luo, X. J. Wu, C. F. Yao, H. Y. Yu, D. W. Li, M. Liu and J. Zhou, *Acta Pharmacol. Sin.*, 2011, **32**, 1543–1548.
14 H. Y. Kaan, V. Ulaganathan, O. Rath, H. Prokopcova, D. Dallinger, C. O. Kappe and F. Kozielski, *J. Med. Chem.*, 2010, **53**, 5676–5683.
15 I. Garcia-Saez and D. A. Skoufias, *Biochem. Pharmacol.*, 2021, **184**, 114364.
16 D. Bongero, L. Paoluzzi, E. Marchi, K. M. Zullo, R. Neisa, Y. Mao, R. Escandon, K. Wood and O. A. O'Connor, *Leuk. Lymphoma*, 2015, **56**, 2945–2952.
17 D. Nikam, P. Chaure, L. Dhindale and P. Bhagat, *J. Mol. Struct.*, 2024, **1308**, 138134.
18 R. Chamariya and V. Suvarna, *Anti-Cancer Agents Med. Chem.*, 2022, **22**, 2517–2538.
19 C. Carbajales, M. A. Prado, H. Gutierrez-de-Teran, A. Cores, J. Azuaje, S. Novio, M. J. Nunez, B. Fernandez-Garcia, E. Sotelo, X. Garcia-Mera, P. Sanchez-Lazo, M. Freire-Garabal and A. Coelho, *ChemBioChem*, 2014, **15**, 1471–1480.
20 S. S. Rosenfeld, in *Kinesins and Cancer*, ed. F. S. B. F. Kozielski, Springer Netherlands, Dordrecht, 2015, ch. 4, pp. 63–76. DOI: 10.1007/978-94-017-9732-0_4.
21 L. Rosen, L. C. Chen, T. Iyengar, J. Goldman, S. Lahr, C. R. Chen, D. S. France, T. C. K. Chan, B. Schwartz, G. Abbadessa and D. D. Von Hoff, *Cancer Res.*, 2010, **70**, 2750–2750.
22 C. W. Lee, K. Belanger, S. C. Rao, T. M. Petrella, R. G. Tozer, L. Wood, K. J. Savage, E. A. Eisenhauer, T. W. Synold, N. Wainman and L. Seymour, *Invest. New Drugs*, 2008, **26**, 249–255.
23 K. D. Holen, C. P. Belani, G. Wilding, S. Ramalingam, J. L. Volkman, R. K. Ramanathan, L. S. Vasist, C. J. Bowen, J. P. Hodge, M. M. Dar and P. T. Ho, *Cancer Chemother. Pharmacol.*, 2011, **67**, 447–454.
24 H. Wakui, N. Yamamoto, S. Kitazono, H. Mizugaki, S. Nakamichi, Y. Fujiwara, H. Nokihara, Y. Yamada, K. Suzuki, H. Kanda, S. Akinaga and T. Tamura, *Cancer Chemother. Pharmacol.*, 2014, **74**, 15–23.
25 A. Vessières, Y. Wang, M. J. McGlinchey and G. Jaouen, *Coord. Chem. Rev.*, 2021, **430**, 213658.
26 M. Patra and G. Gasser, *Nat. Rev. Chem.*, 2017, **1**, 0066.
27 G. Jaouen, A. Vessieres and S. Top, *Chem. Soc. Rev.*, 2015, **44**, 8802–8817.
28 B. Sharma and V. Kumar, *J. Med. Chem.*, 2021, **64**, 16865–16921.

29 B. Diaz de Greñu, D. M. Fernández-Aroca, J. A. Organero, G. Durá, F. A. Jalón, R. Sánchez-Prieto, M. J. Ruiz-Hidalgo, A. M. Rodríguez, L. Santos, J. L. Albasanz and B. R. Manzano, *J. Biol. Inorg. Chem.*, 2023, **28**, 531–547.
30 V. Hamala, K. Ondrášková, L. Červenková Šťastná, A. Krčil, M. Müllerová, M. Kurfiřt, K. Hiršová, J. Holčáková, R. Gyepes, I. Císařová, J. Bernášková, R. Hrstka and J. Karban, *Appl. Organomet. Chem.*, 2024, **38**, e7399.
31 J. M. Aksić, M. S. Genčić, N. S. Radulović, M. V. Dimitrijević, Z. Z. Stojanović-Radić, T. Ilic Tomic and M. V. Rodić, *Bioorg. Chem.*, 2023, **139**, 106708.
32 B. S. Murray and P. J. Dyson, *Curr. Opin. Chem. Biol.*, 2020, **56**, 28–34.
33 S. Swaminathan, J. Haribabu, N. Balakrishnan, P. Vasanthakumar and R. Karvembu, *Coord. Chem. Rev.*, 2022, **459**, 214403.
34 C. Sumithaa and M. Ganeshpandian, *Mol. Pharm.*, 2023, **20**, 1453–1479.
35 M. Shao, X. Liu, Y. Sun, S. Dou, Q. Chen, X.-A. Yuan, L. Tian and Z. Liu, *Dalton Trans.*, 2020, **49**, 12599–12609.
36 W. D. J. Tremlett, D. M. Goodman, T. R. Steel, S. Kumar, A. Wieczorek-Blauz, F. P. Walsh, M. P. Sullivan, M. Hanif and C. G. Hartinger, *Coord. Chem. Rev.*, 2021, **445**, 213950.
37 M. A. Sierra, L. Casarrubios and M. C. de la Torre, *Chem. – Eur. J.*, 2019, **25**, 7232–7242.
38 N. N. Efimov, D. A. Loginov, M. Y. Sharipov, A. A. Nazarov, Y. V. Nelyubina and D. S. Perekalin, *J. Organomet. Chem.*, 2020, **916**, 121272.
39 Z. H. Chohan, H. Pervez, K. M. Khan and C. T. Supuran, *J. Enzyme Inhib. Med. Chem.*, 2005, **20**, 81–88.
40 P. F. Salas, C. Herrmann and C. Orvig, *Chem. Rev.*, 2013, **113**, 3450–3492.
41 Y. C. Ong, S. Roy, P. C. Andrews and G. Gasser, *Chem. Rev.*, 2019, **119**, 730–796.
42 B. S. Ludwig, J. D. G. Correia and F. E. Kühn, *Coord. Chem. Rev.*, 2019, **396**, 22–48.
43 P. Štarha, *Coord. Chem. Rev.*, 2021, **431**, 213690.
44 C. G. Hartinger, N. Metzler-Nolte and P. J. Dyson, *Organometallics*, 2012, **31**, 5677–5685.
45 C. Ornelas and D. Astruc, *Pharmaceutics*, 2023, **15**, 2044.
46 D. Plazuk, A. Wieczorek, W. M. Ciszewski, K. Kowalczyk, A. Blauz, S. Pawledzio, A. Makal, C. Eurtivong, H. J. Arabshahi, J. Reynisson, C. G. Hartinger and B. Rychlik, *ChemMedChem*, 2017, **12**, 1882–1892.
47 A. Wieczorek, A. Blauz, A. Zal, H. J. Arabshahi, J. Reynisson, C. G. Hartinger, B. Rychlik and D. Plazuk, *Chem. – Eur. J.*, 2016, **22**, 11413–11421.
48 D. Plazuk, A. Wieczorek, A. Blauz and B. Rychlik, *MedChemComm*, 2012, **3**, 498–501.
49 K. Chrabąszcz, A. Błauż, M. Gruchała, M. Wachulec, B. Rychlik and D. Plażuk, *Chem. – Eur. J.*, 2021, **27**, 6254–6262.
50 M. Beaupérin, D. Polat, F. Roudesly, S. Top, A. Vessières, J. Oble, G. Jaouen and G. Poli, *J. Organomet. Chem.*, 2017, **839**, 83–90.
51 K. Kowalczyk, A. Blauz, W. M. Ciszewski, A. Wieczorek, B. Rychlik and D. Plazuk, *Dalton Trans.*, 2017, **46**, 17041–17052.
52 N. Nicolaus, J. Zapke, P. Riesterer, J. M. Neudörfl, A. Prokop, H. Oschkinat and H. G. Schmalz, *ChemMedChem*, 2010, **5**, 661–665.
53 A. Wieczorek, A. Blauz, J. Zakrzewski, B. Rychlik and D. Plazuk, *ACS Med. Chem. Lett.*, 2016, **7**, 612–617.
54 A. Wieczorek-Błauż, K. Kowalczyk, A. Błauż, A. Makal, S. Pawlędzio, C. Eurtivong, H. J. Arabshahi, J. Reynisson, C. G. Hartinger, B. Rychlik and D. Plażuk, *Dalton Trans.*, 2022, **51**, 491–508.
55 W. A. Al-Masoudi and N. A. Al-Masoudi, *Phosphorus, Sulfur Silicon Relat. Elem.*, 2019, **194**, 1020–1027.
56 W. A. Al-Masoudi, N. A. Al-Masoudi, B. Weibert and R. Winter, *J. Coord. Chem.*, 2017, **70**, 2061–2073.
57 J. Jadhav, A. Juvekar, R. Kurane, S. Khanapure, R. Salunkhe and G. Rashinkar, *Eur. J. Med. Chem.*, 2013, **65**, 232–239.
58 M. Łomzik, M. Hanif, A. Budniok, A. Błauż, A. Makal, D. M. Tchoń, B. Leśniewska, K. K. H. Tong, S. Movassaghi, T. Söhnel, S. M. F. Jamieson, A. Zafar, J. Reynisson, B. Rychlik, C. G. Hartinger and D. Plażuk, *Inorg. Chem.*, 2020, **59**, 14879–14890.
59 K. Kowalczyk, A. Blauz, D. Moscoh Ayine-Tora, C. G. Hartinger, B. Rychlik and D. Plazuk, *Chem. – Eur. J.*, 2023, **29**, e202300813.
60 M. Łomzik, A. Błauż, M. Głodek, A. Makal, D. Tchoń, D. M. Ayine-Tora, C. Hartinger, B. Rychlik and D. Plażuk, *Dalton Trans.*, 2023, **52**, 11859–11874.
61 L. Yang, C. Jiang, F. Liu, Q. D. You and W. T. Wu, *Biol. Pharm. Bull.*, 2008, **31**, 1397–1402.
62 R. G. Fu, Q. D. You, L. Yang, W. T. Wu, C. Jiang and X. L. Xu, *Bioorg. Med. Chem.*, 2010, **18**, 8035–8043.
63 D. E. Bublitz, W. E. Mcewen and J. Kleinberg, *J. Am. Chem. Soc.*, 1962, **84**, 1845–1849.
64 I. Y. El-Deeb, T. Funakoshi, Y. Shimomoto, R. Matsubara and M. Hayashi, *J. Org. Chem.*, 2017, **82**, 2630–2640.
65 R. Banfeng, G. Weiwei and L. Qingshan, Hefei University of Technology A, N106905380A, 2017, **https://patents.google.com/patent/CN106905380A/zh**.
66 P. B. Schiff, J. Fant and S. B. Horwitz, *Nature*, 1979, **277**, 665–667.
67 P. B. Schiff and S. B. Horwitz, *Proc. Natl. Acad. Sci. U. S. A.*, 1980, **77**, 1561–1565.
68 Y. Murase, H. Ono, K. Ogawa, R. Yoshioka, Y. Ishikawa, H. Ueda, K. Akahoshi, D. Ban, A. Kudo, S. Tanaka and M. Tanabe, *Cancer Sci.*, 2021, **112**, 4641–4654.
69 G. I. Shapiro and J. W. Harper, *J. Clin. Invest.*, 1999, **104**, 1645–1653.
70 R. Wang, H. H. Chen, W. T. Yan, M. W. Zheng, T. S. Zhang and Y. H. Zhang, *Eur. J. Med. Chem.*, 2020, **190**, 112109.
71 V. Ngo and M. L. Duennwald, *Antioxidants*, 2022, **11**, 2345.
72 K. Ochiai and S. Fujii, *Bioorg. Med. Chem. Lett.*, 2021, **46**, 128141.
73 A. A. Altaf, A. Badshah, B. Lal, S. Murtaza, P. B. Chatterjee, K. Akbar and D. C. Crans, *Appl. Organomet. Chem.*, 2018, **32**, e4334.
74 G. Repetto, A. del Peso and J. L. Zurita, *Nat. Protoc.*, 2008, **3**, 1125–1131.

Supporting Information

Design and Synthesis of Ferrocenyl 1,4-Dihydropyridines and Their Evaluation as Kinesin-5 Inhibitors

Karolina Kowalczyk[1], Andrzej Błauż[2], Krzysztof Krawczyk[2], Błażej Rychlik[2], Damian Plażuk[1]

[1] *Laboratory of Molecular Spectroscopy, Department of Organic Chemistry, Faculty of Chemistry, University of Lodz, ul. Tamka 12, 91-403 Łódź, Poland*

[2] *Cytometry Lab, Department of Oncobiology and Epigenetics, Faculty of Biology and Environmental Protection, University of Lodz, ul. Pomorska 141/143, 90-236 Łódź, Poland*

Table of Contents

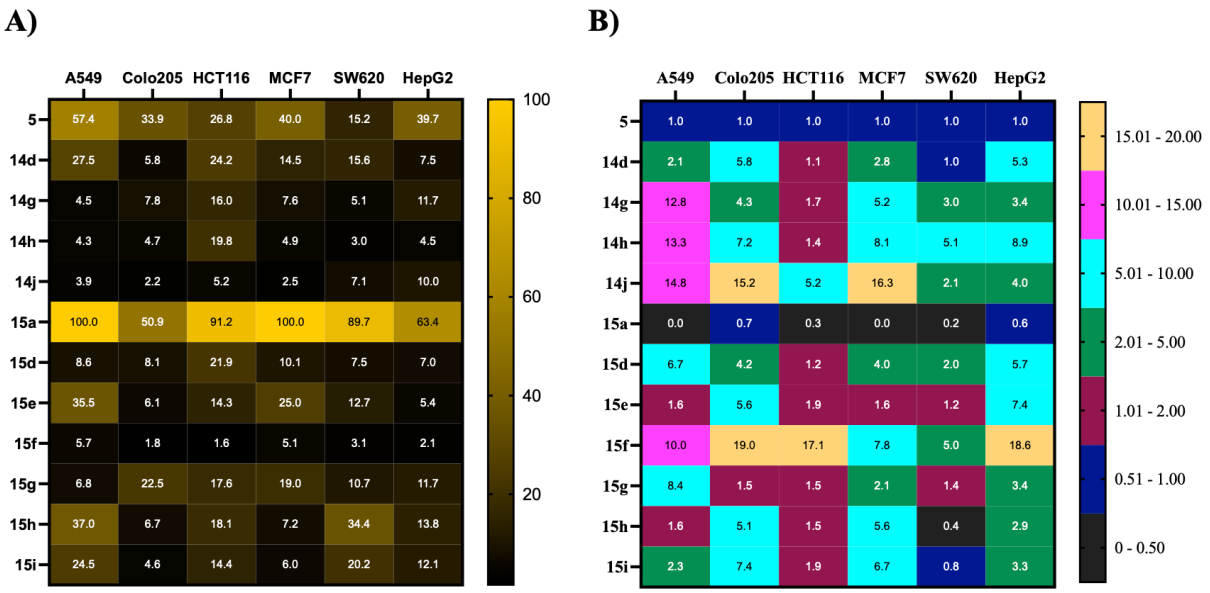

Figure S1. Antiproliferative activity **A**) Cytotoxic activity (IC_{50} values), **B**) The Activity Quotients (AQ) of studied compounds in comparison to cytotoxic activity of **5** were calculated as AQ = $IC_{50(\mathbf{5})}/IC_{50(\mathbf{compound})}$

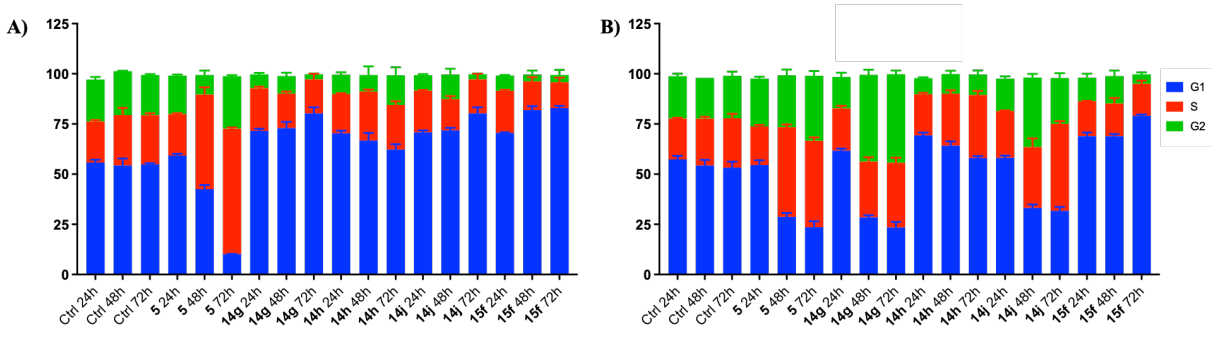

Figure S2. Cell cycle phase distribution for A549 (**A**) and SW620 (**B**) cells exposed for 24, 48 and 72h to **5** and its ferrocenyl analogues at concentration equal to the IC_{75} values for **5**. Data are presented as mean ± SD, n = 3

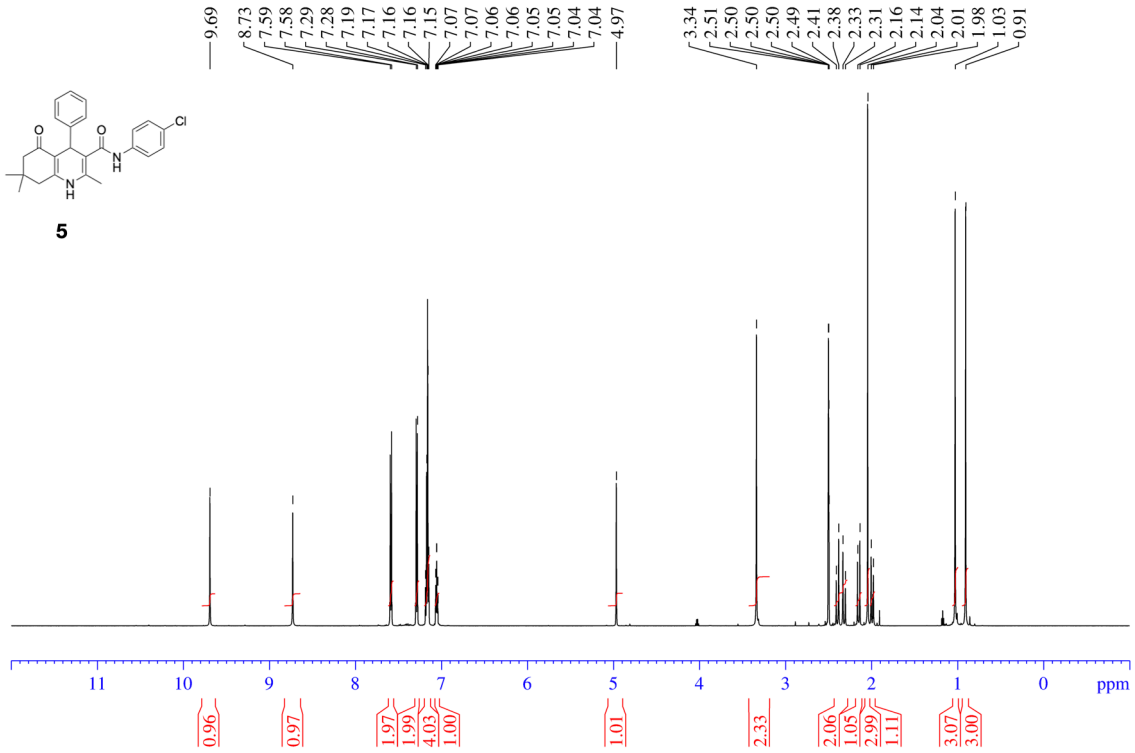

Figure S3. ^{1}H NMR spectrum of **5** in DMSO-d_6

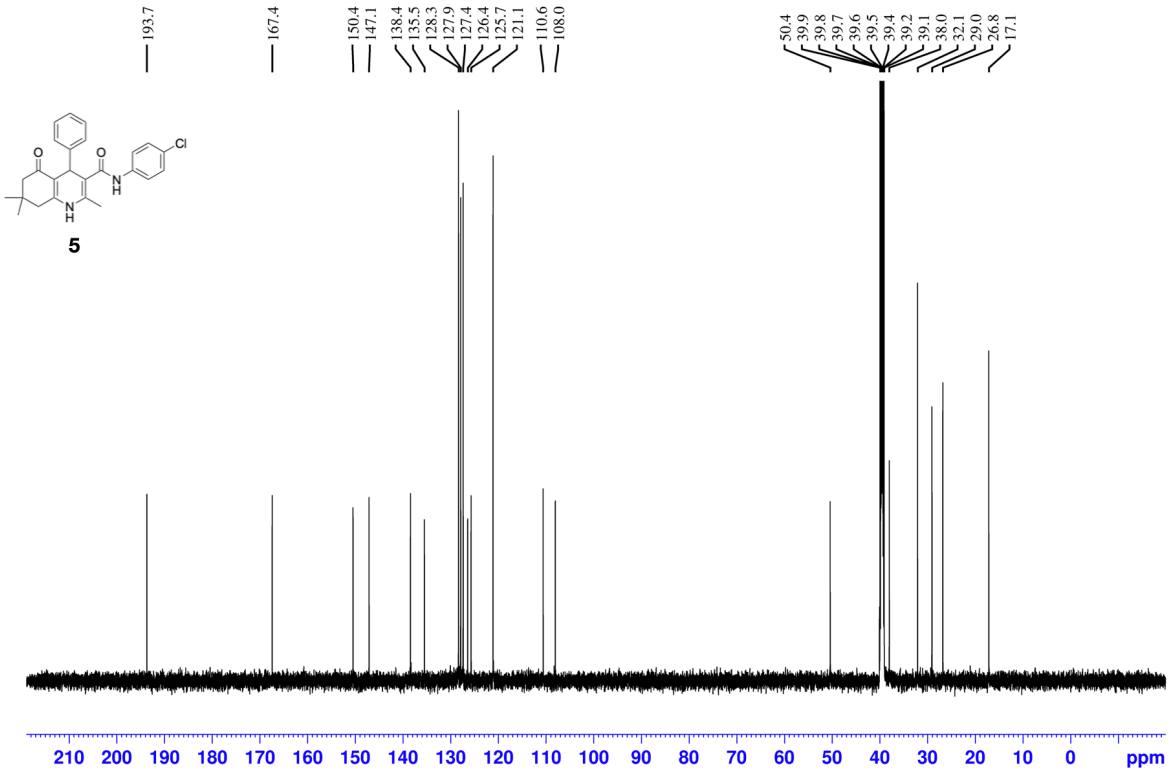

Figure S4. $^{13}C\{^{1}H\}$ NMR spectrum of **5** in DMSO-d_6

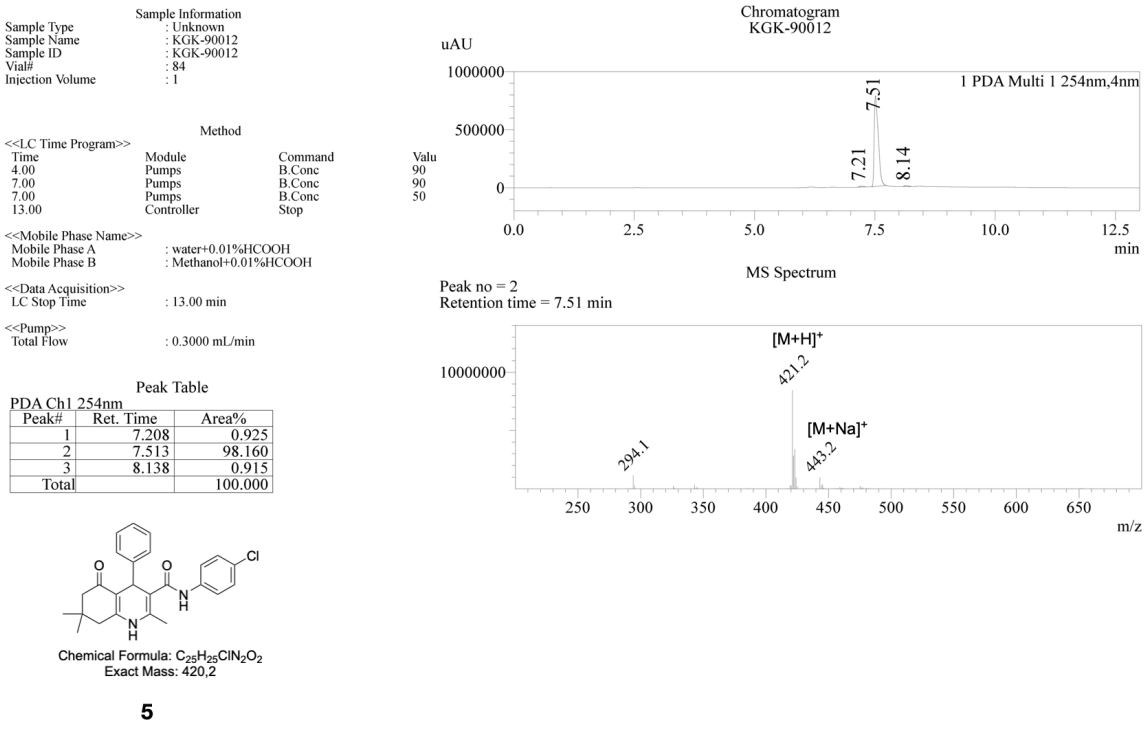

Figure S5. HPLC-MS analysis of **5**

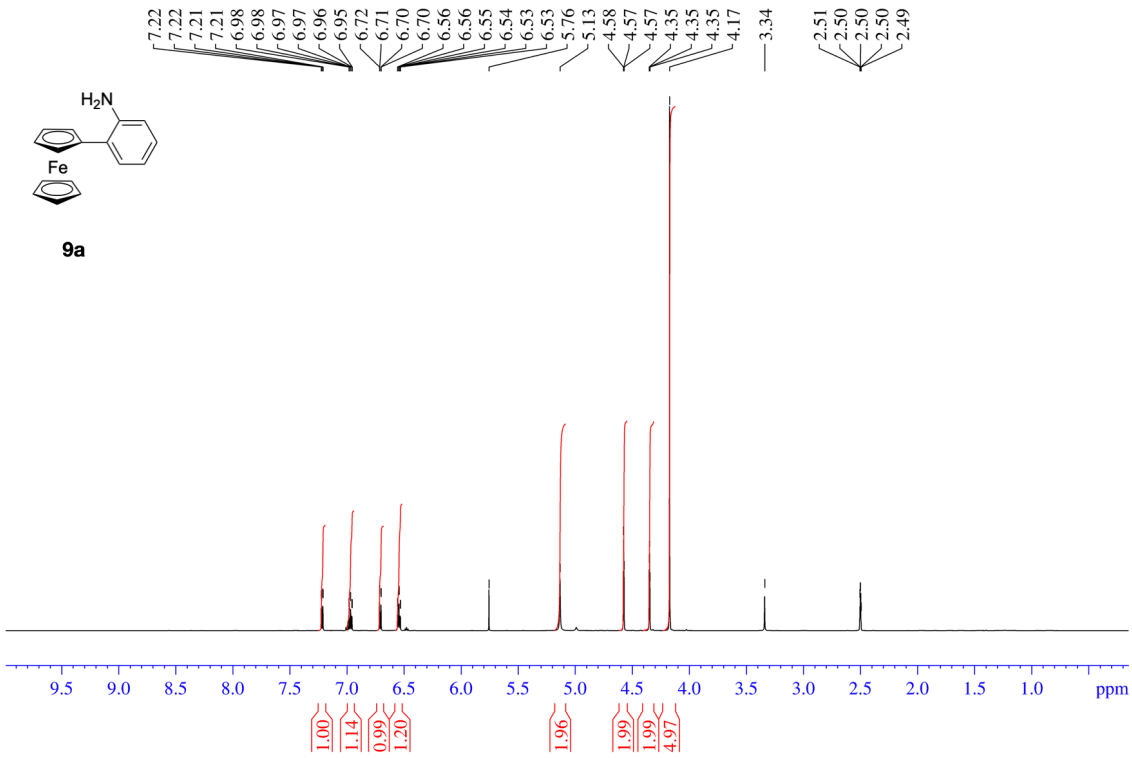

Figure S6. ^{1}H NMR spectrum of **9a** in DMSO-d_6

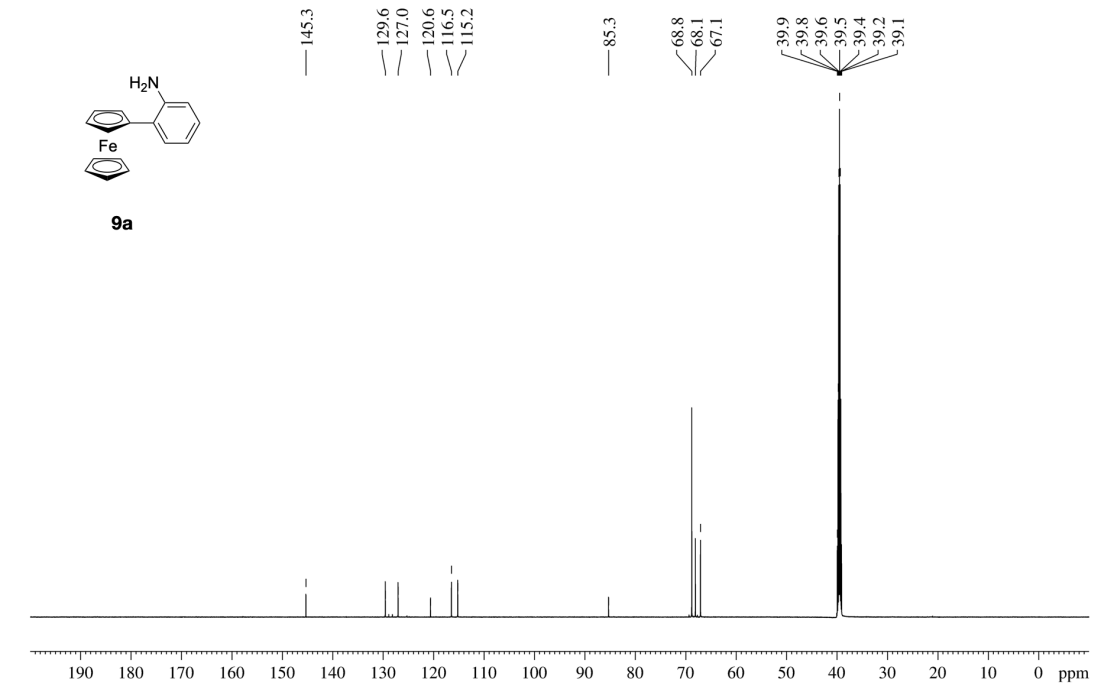

Figure S7. $^{13}C\{^{1}H\}$ NMR spectrum of **9a** in DMSO-d_6

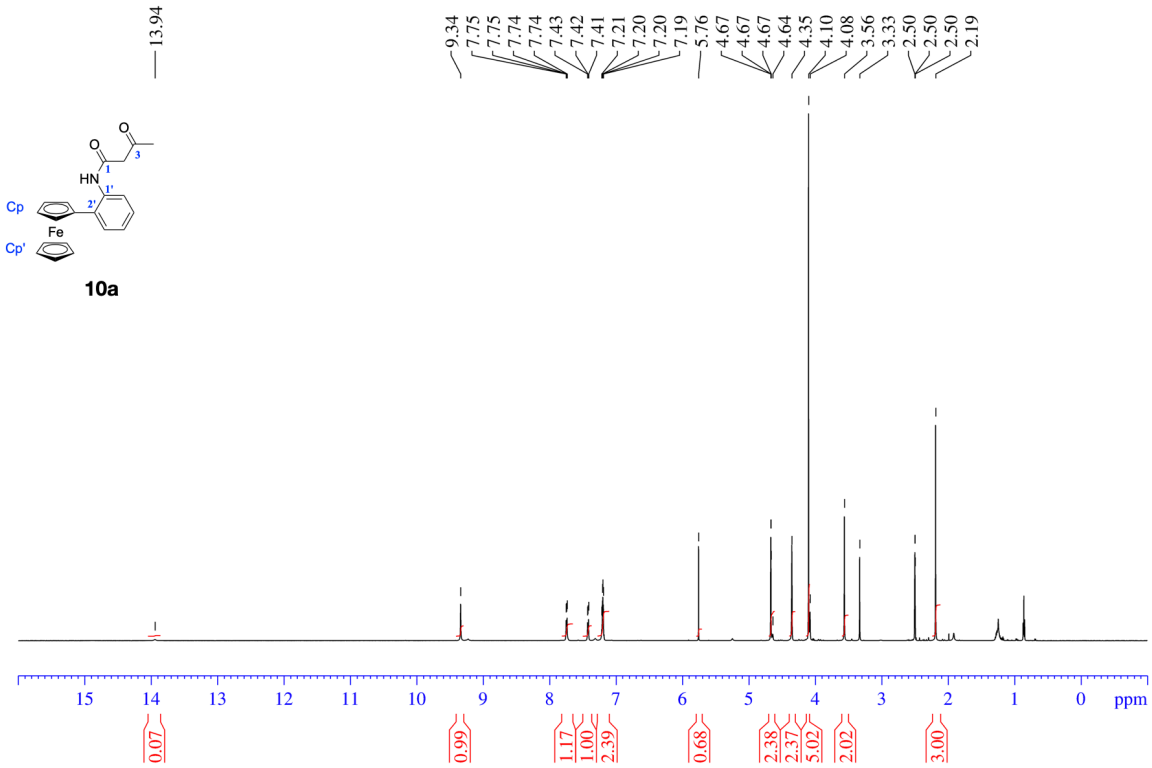

Figure S8. ^{1}H NMR spectrum of **10a** in DMSO-d_6

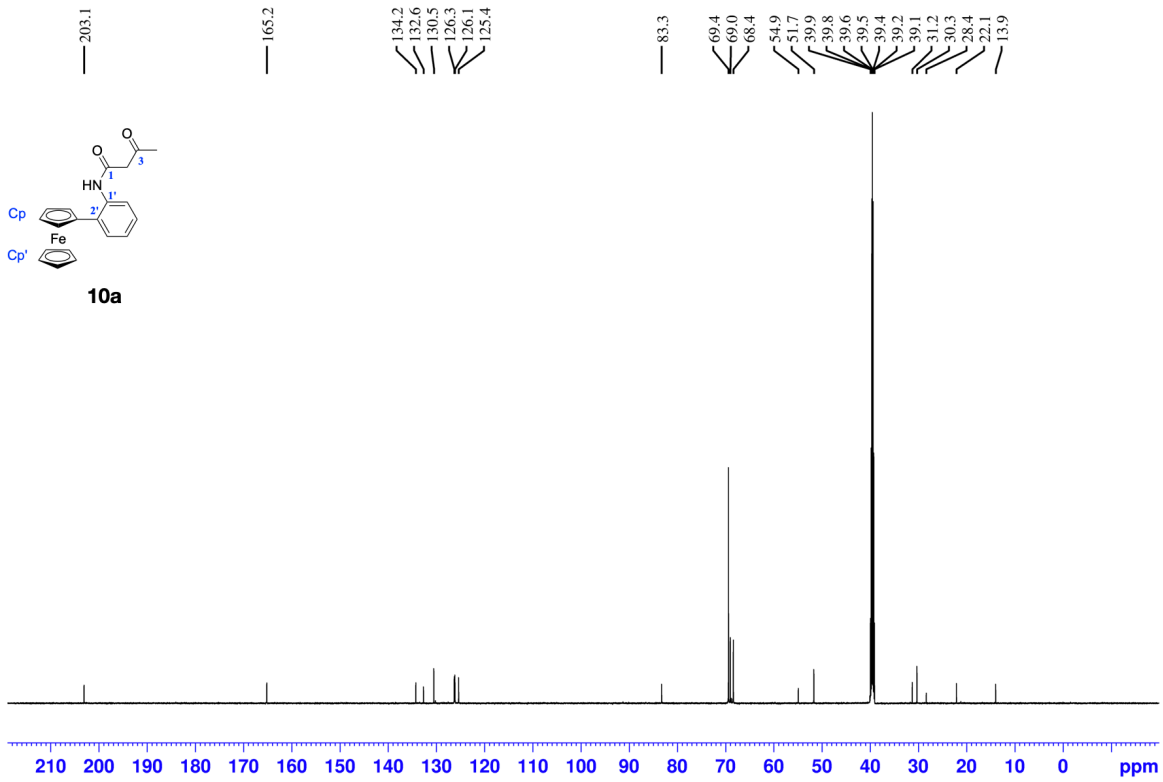

Figure S9. $^{13}C\{^{1}H\}$ NMR spectrum of **10a** in DMSO-d_6

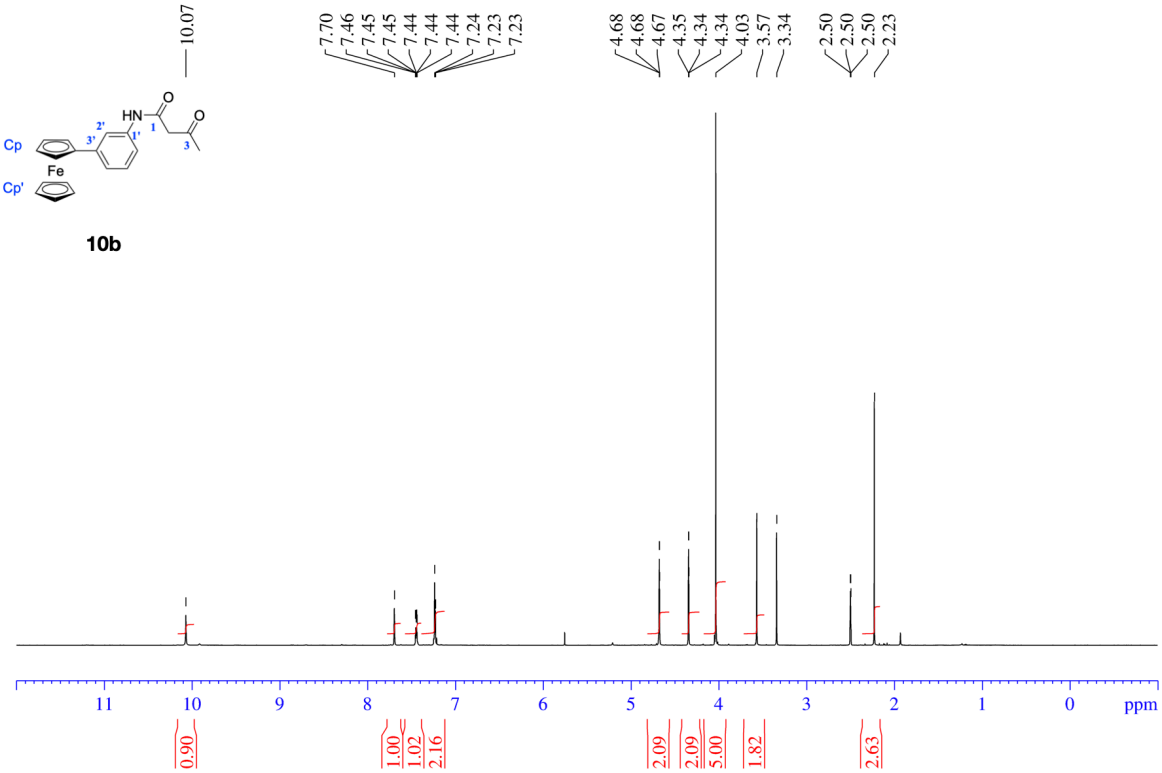

Figure S10. ^{1}H NMR spectrum of **10b** in DMSO-d_6

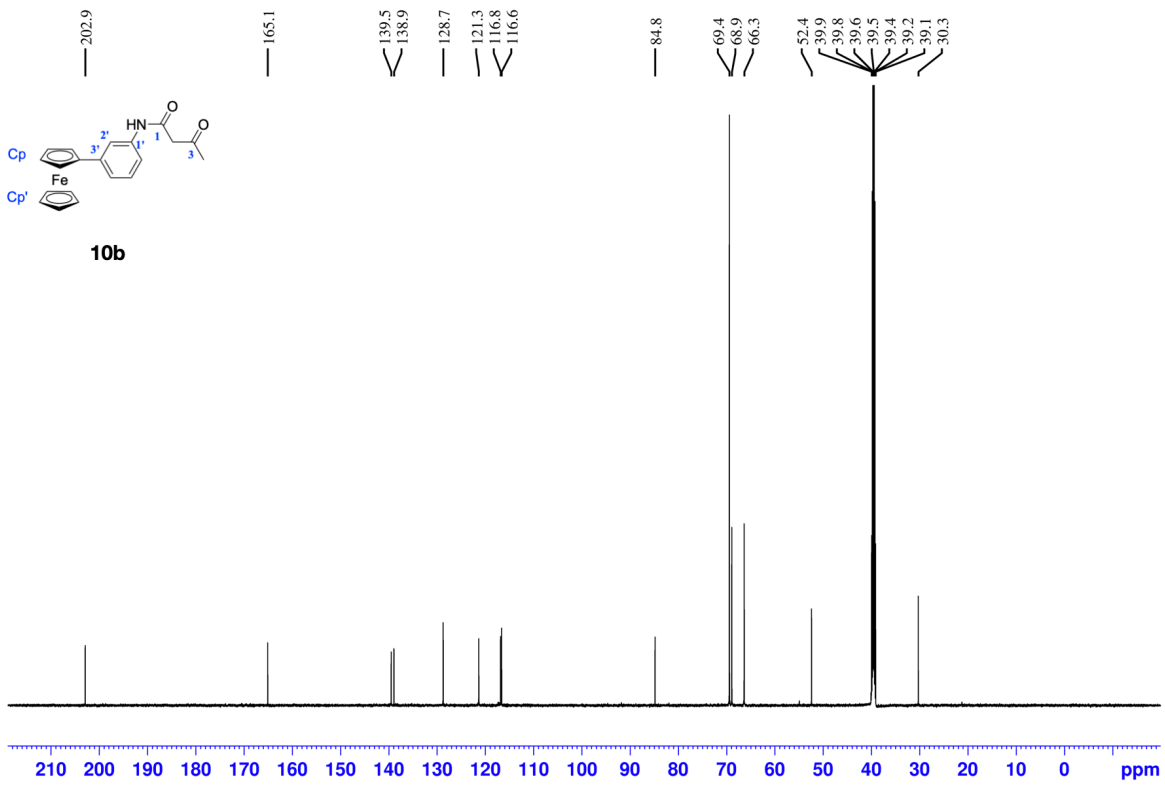

Figure S11. $^{13}C\{^{1}H\}$ NMR spectrum of **10b** in DMSO-d_6

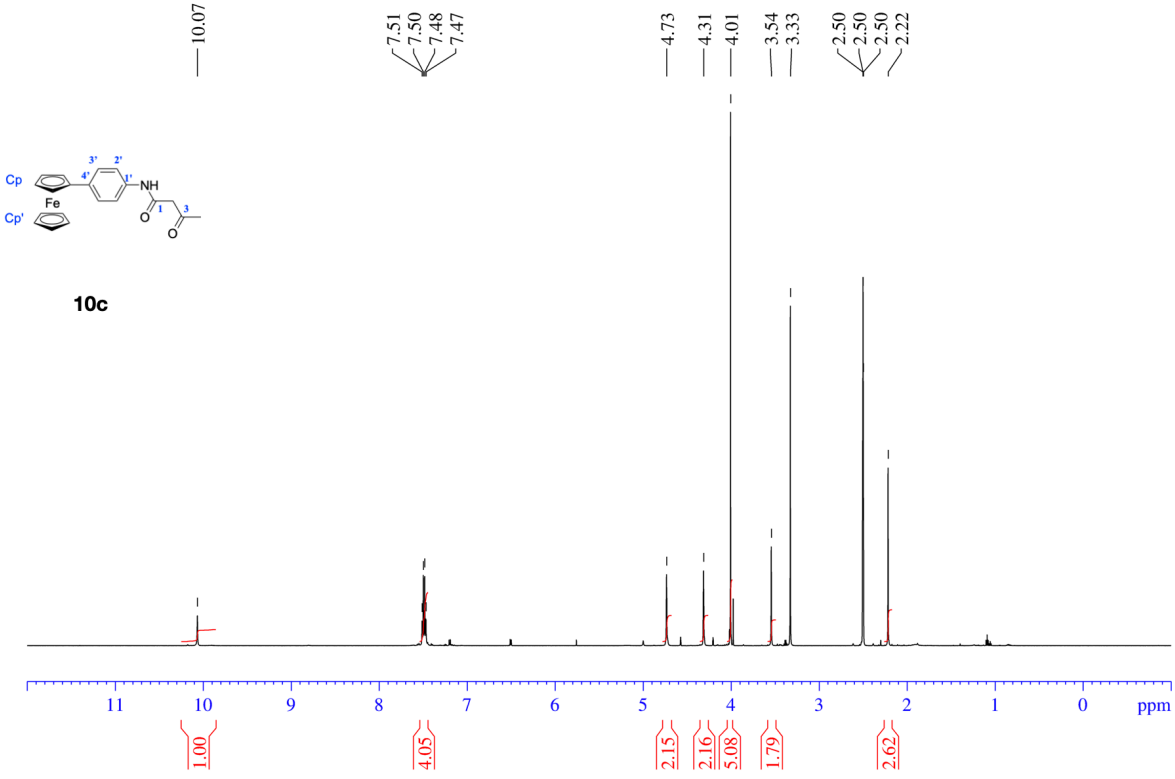

Figure S12. ^{1}H NMR spectrum of **10c** in DMSO-d_6

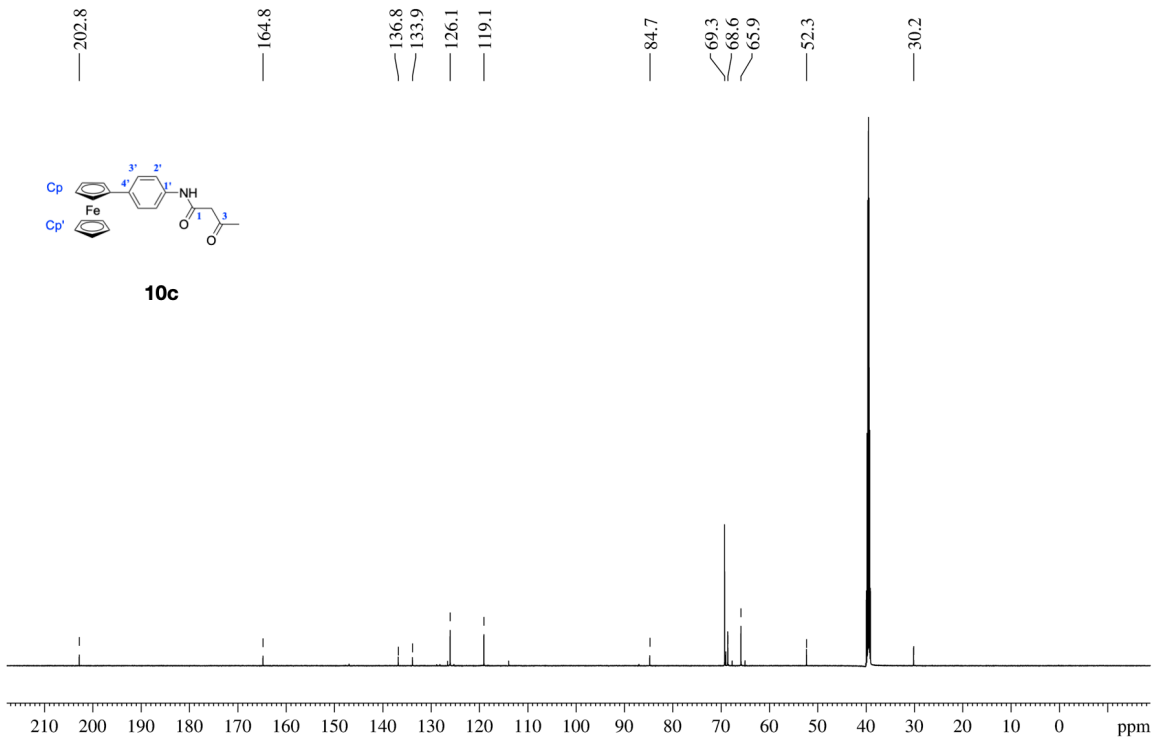

Figure S13. $^{13}C\{^{1}H\}$ NMR spectrum of **10c** in DMSO-d_6

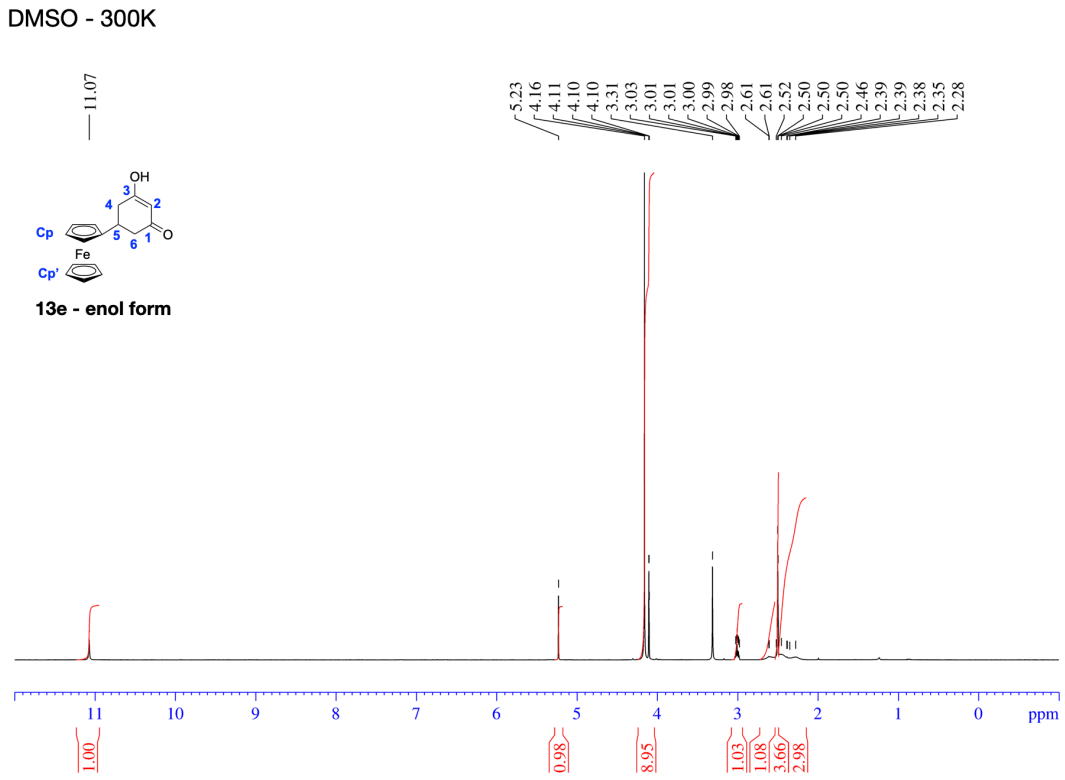

Figure S14. ^{1}H NMR spectrum of **13e** in DMSO-d_6

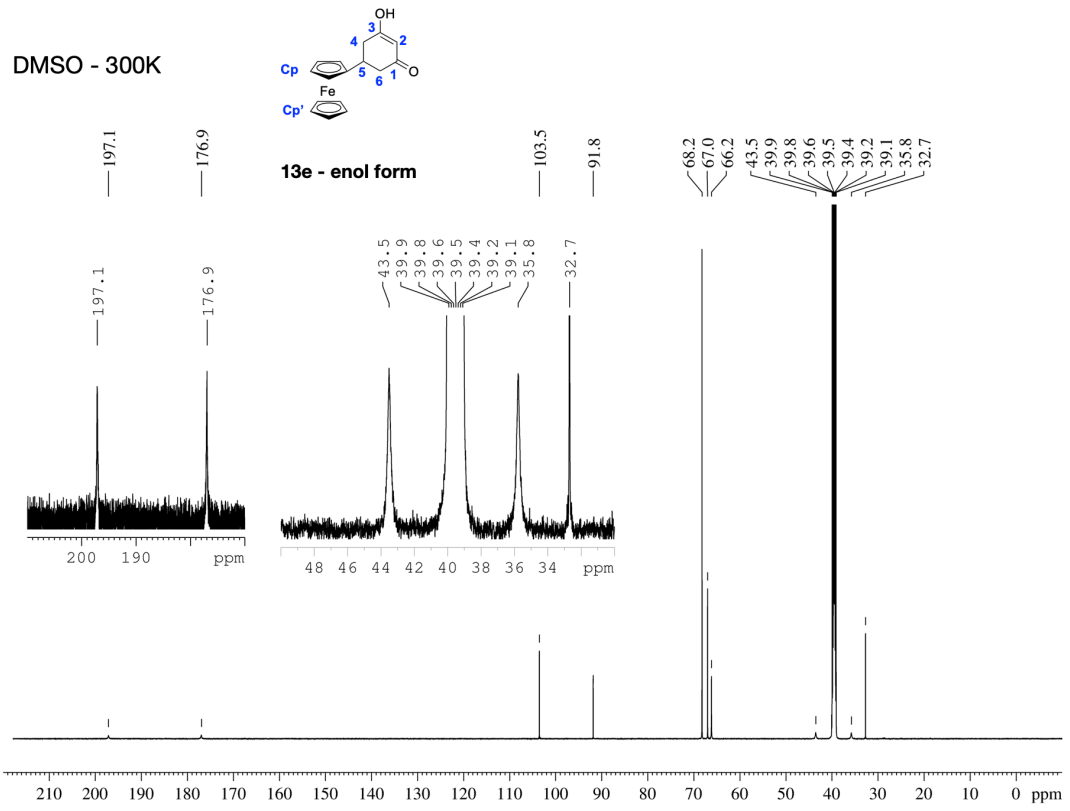

Figure S15. $^{13}C\{^{1}H\}$ NMR spectrum of **13e** in DMSO-d_6

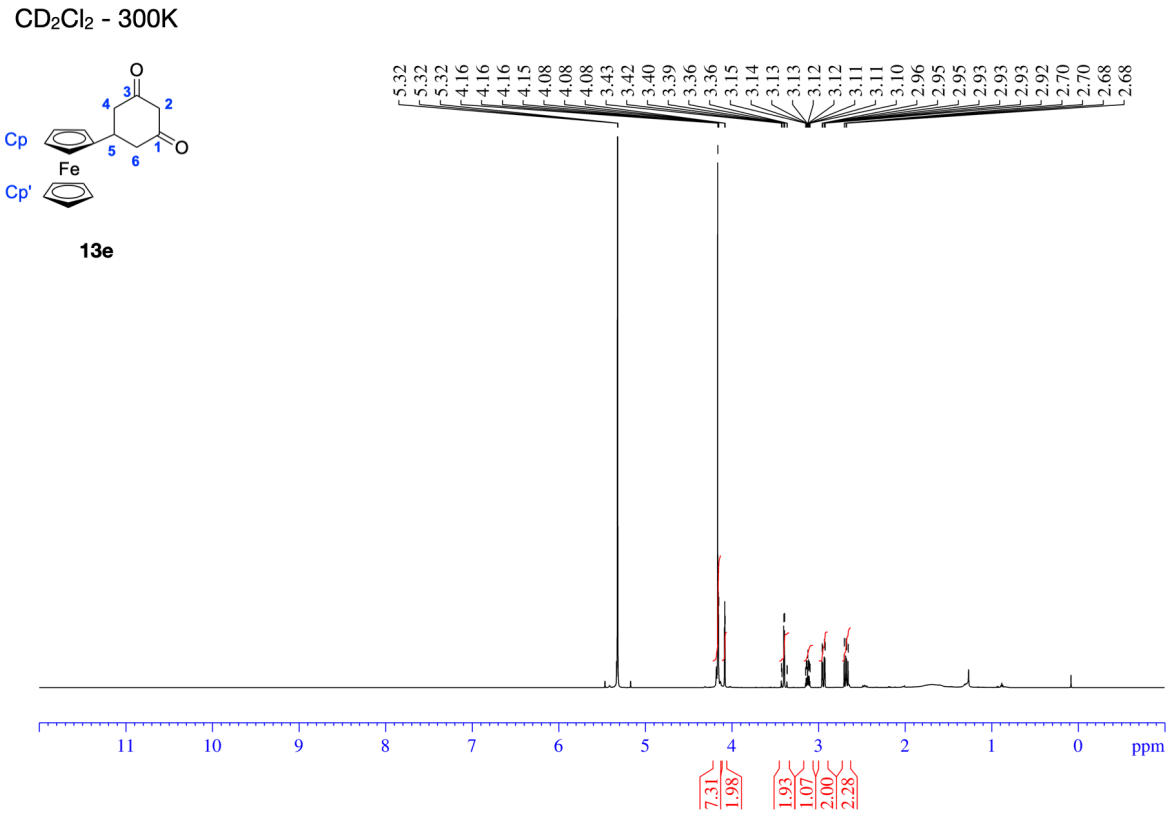

Figure S16. ^{1}H NMR spectrum of **13e** in DMSO-d_6

CD_2Cl_2 - 300K

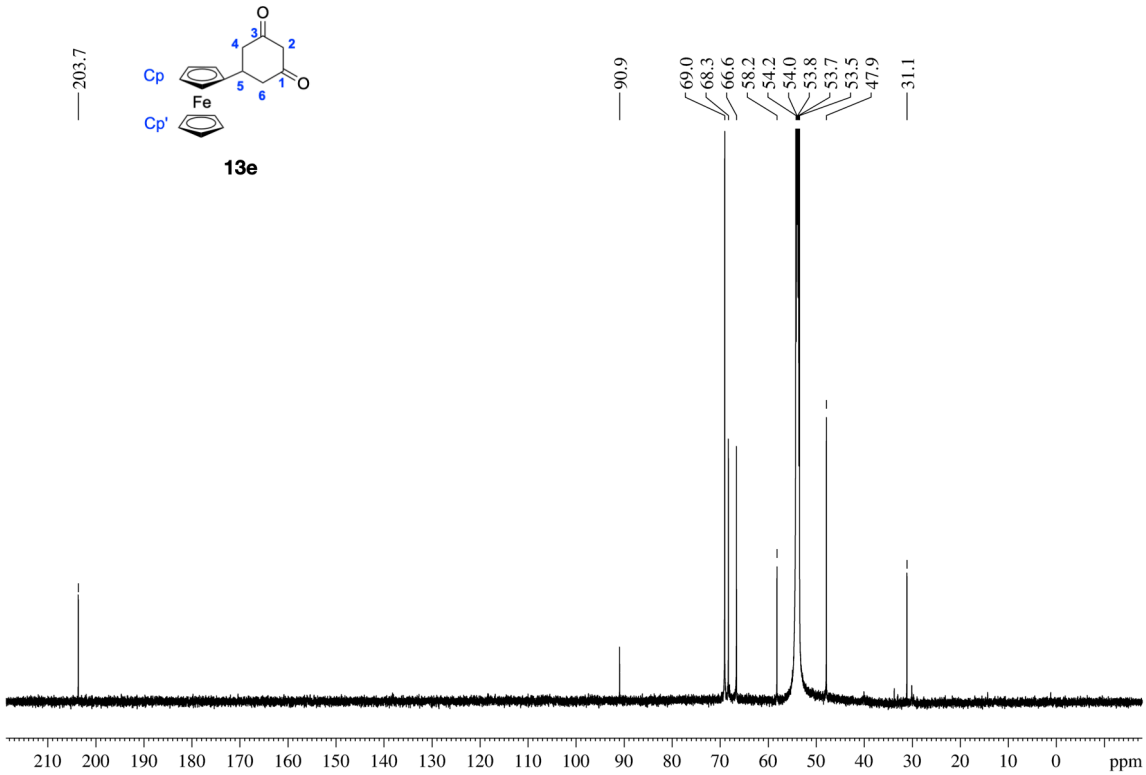

Figure S17. $^{13}C\{^1H\}$ NMR spectrum of **13e** in DMSO-d_6

CD_2Cl_2 - 243K

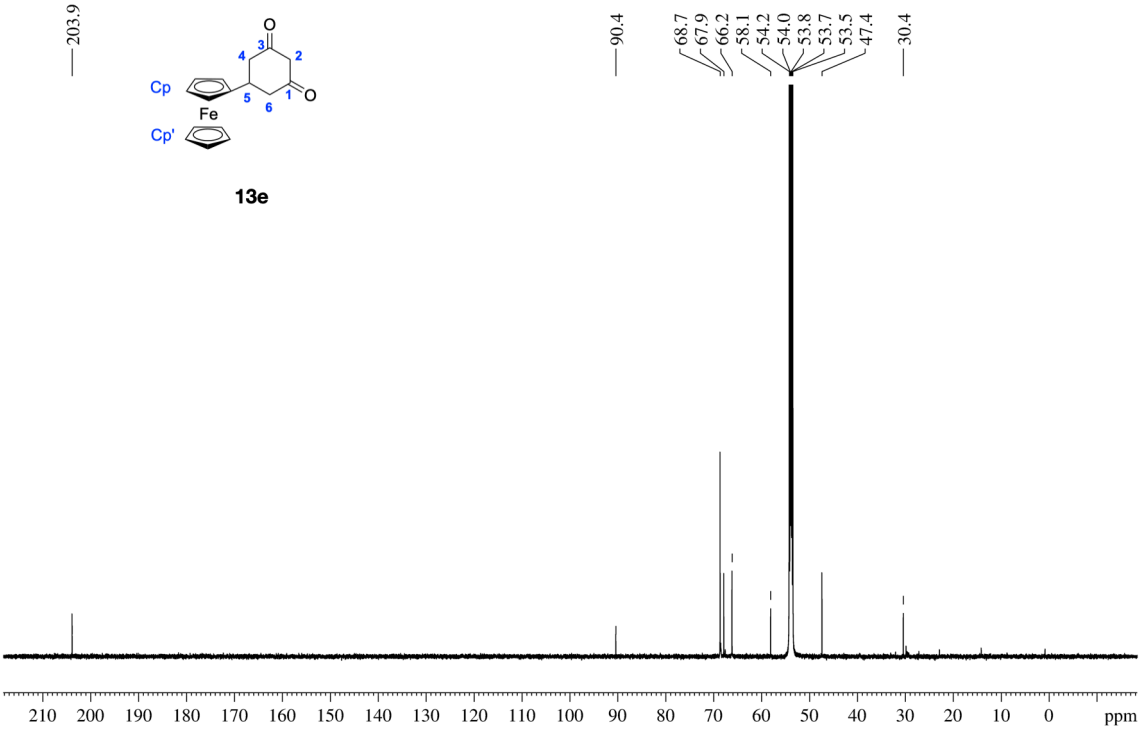

Figure S18. $^{13}C\{^1H\}$ NMR spectrum of **13e** in DMSO-d_6

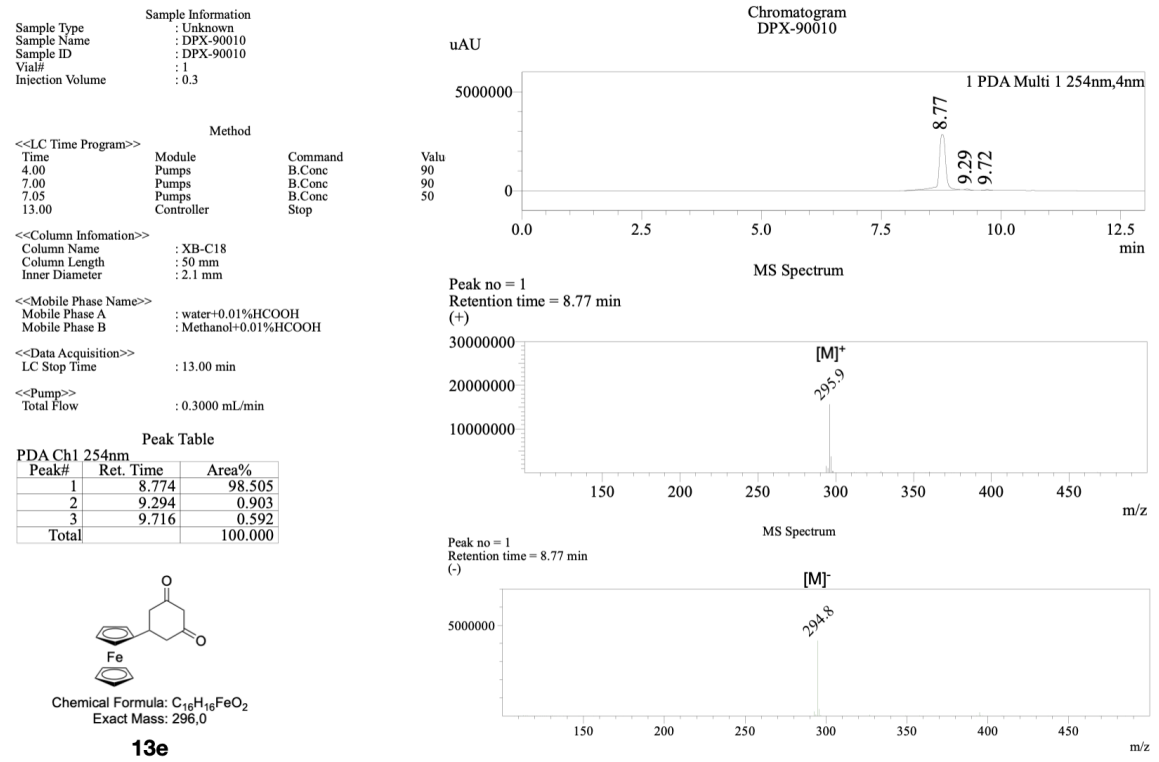

Figure S19. HPLC-MS analysis of **13e**

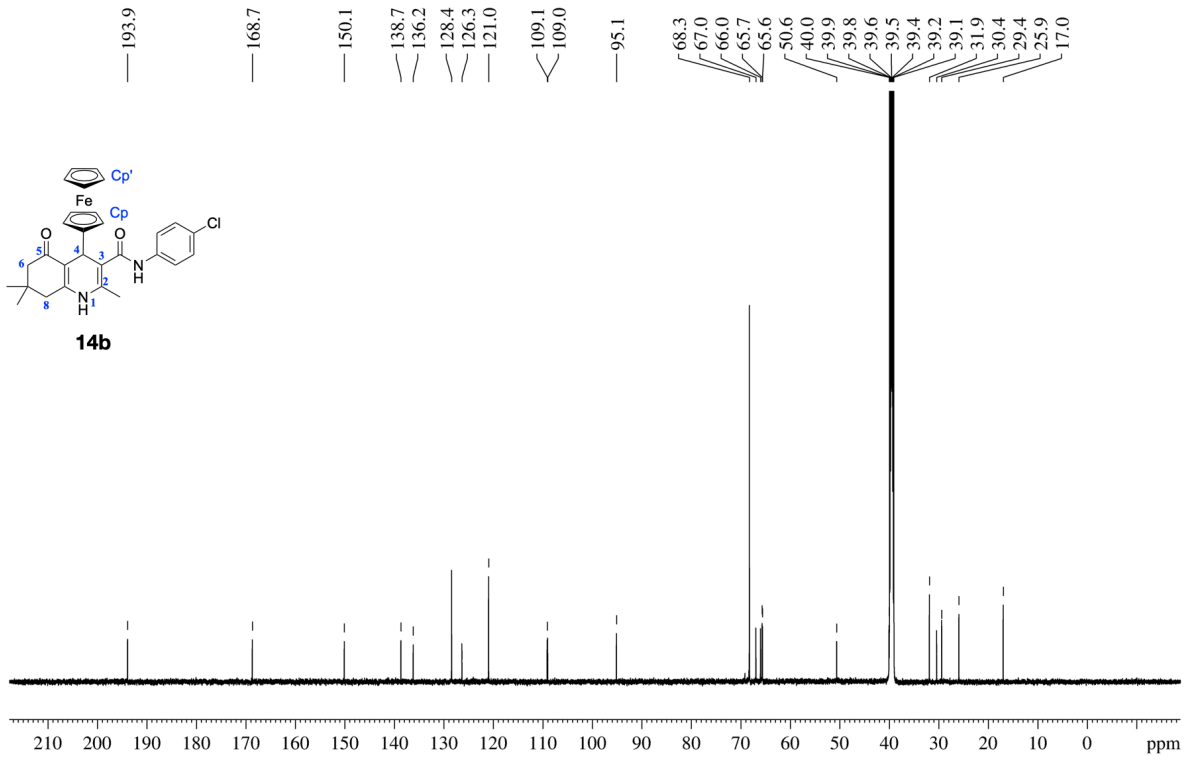

Figure S20. $^{13}C\{^{1}H\}$ NMR spectrum of **14b** in DMSO-d_6

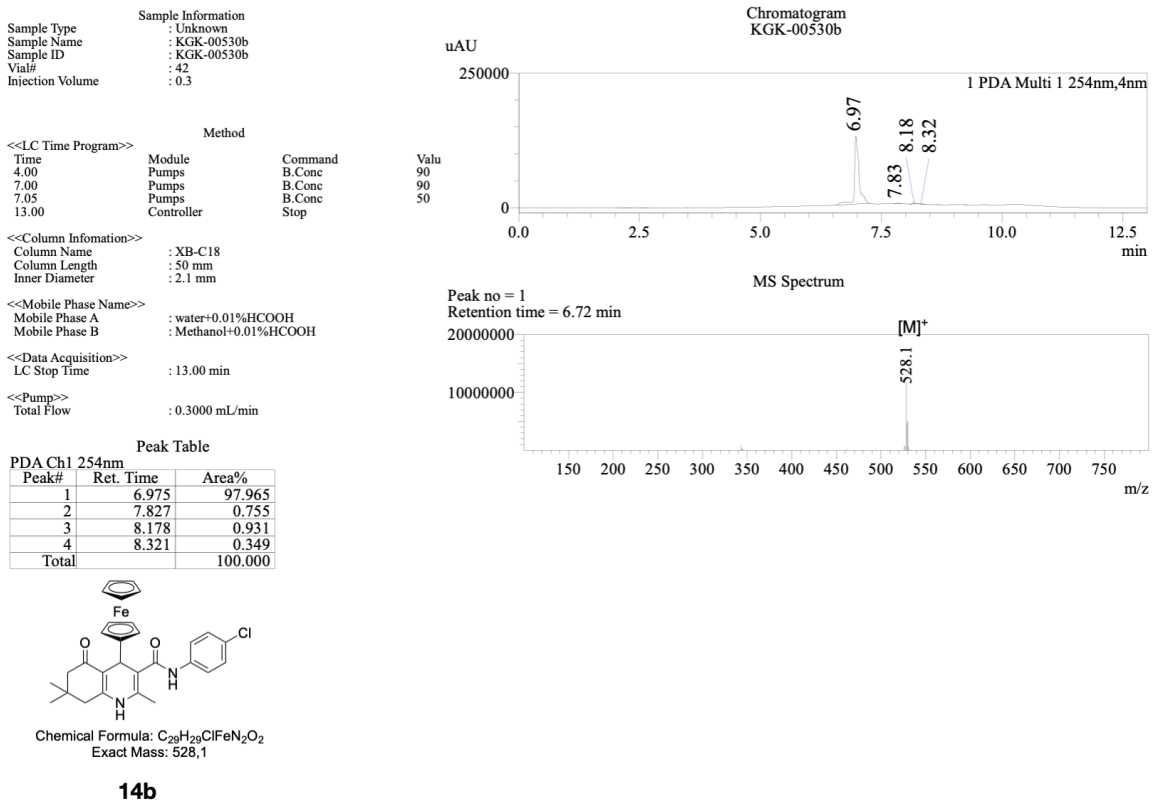

Figure S21. $^{13}C\{^{1}H\}$ NMR spectrum of **14b** in DMSO-d_6

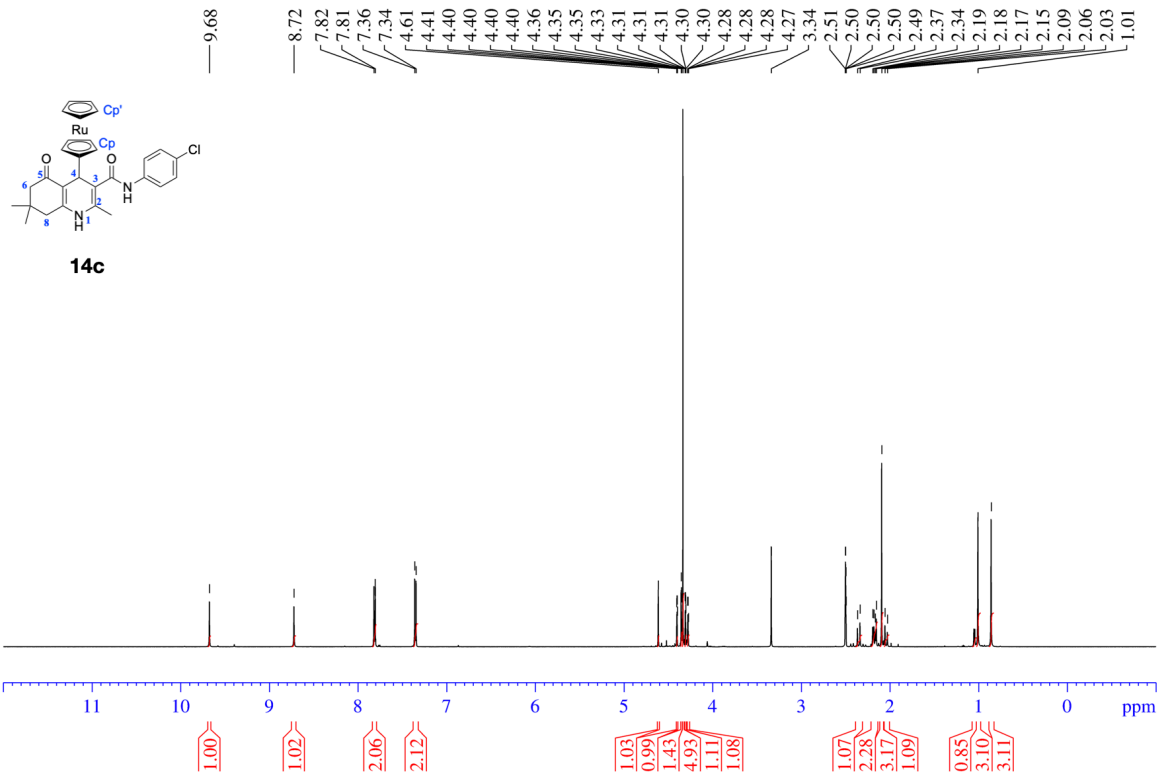

Figure S22. $^{13}C\{^{1}H\}$ NMR spectrum of **14c** in DMSO-d_6

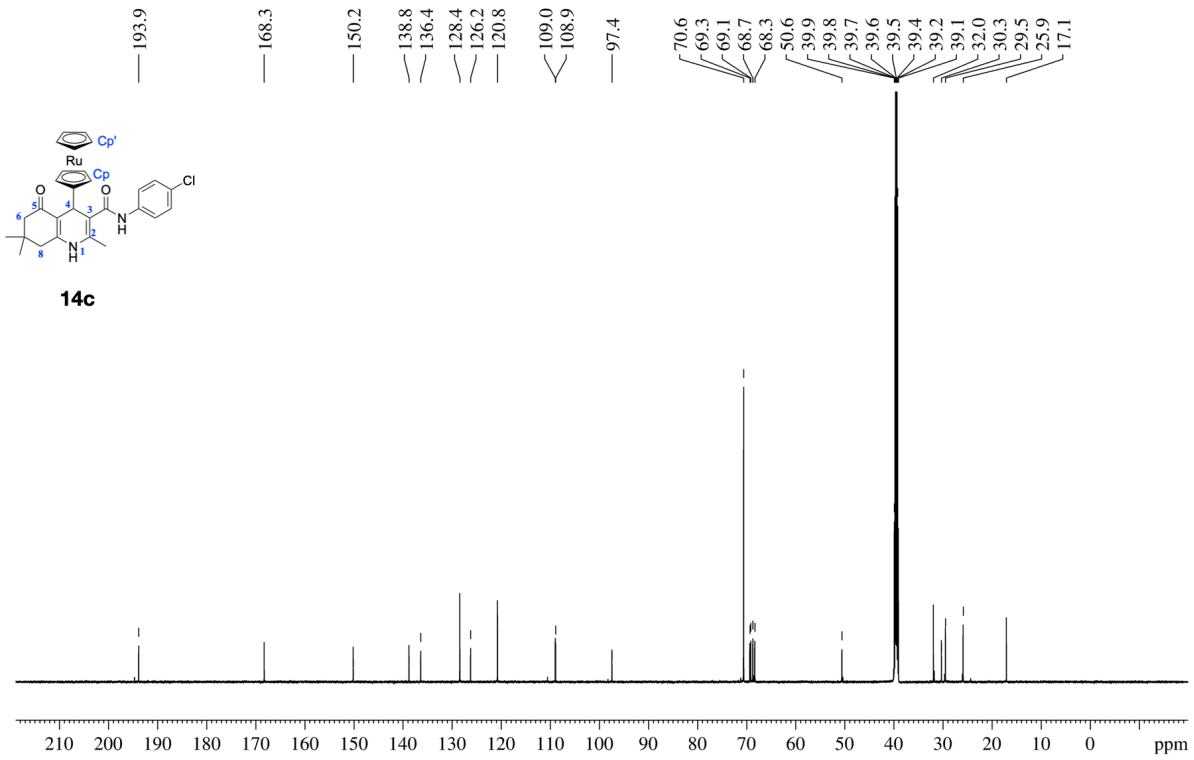

Figure S23. $^{13}C\{^{1}H\}$ NMR spectrum of **14c** in DMSO-d_6

Sample Information

Sample Type	: Unknown
Sample Name	: DPX-90033
Sample ID	: DPX-90033
Vial#	: 40
Injection Volume	: 0.3

Method

<<LC Time Program>>

Time	Module	Command	Valu
4.00	Pumps	B.Conc	90
7.00	Pumps	B.Conc	90
7.05	Pumps	B.Conc	50
13.00	Controller	Stop	

<<Column Infomation>>

Column Name	: XB-C18
Column Length	: 50 mm
Inner Diameter	: 2.1 mm

<<Mobile Phase Name>>

Mobile Phase A	: water+0.01%HCOOH
Mobile Phase B	: Methanol+0.01%HCOOH

<<Data Acquisition>>

LC Stop Time	: 13.00 min

<<Pump>>

Total Flow	: 0.3000 mL/min

Peak Table

PDA Ch1 254nm

Peak#	Ret. Time	Area%
1	6.215	3.913
2	7.016	96.087
Total		100.000

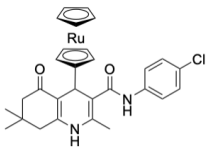

Chemical Formula: $C_{29}H_{29}ClN_2O_2Ru$
Exact Mass: 574,1

14c

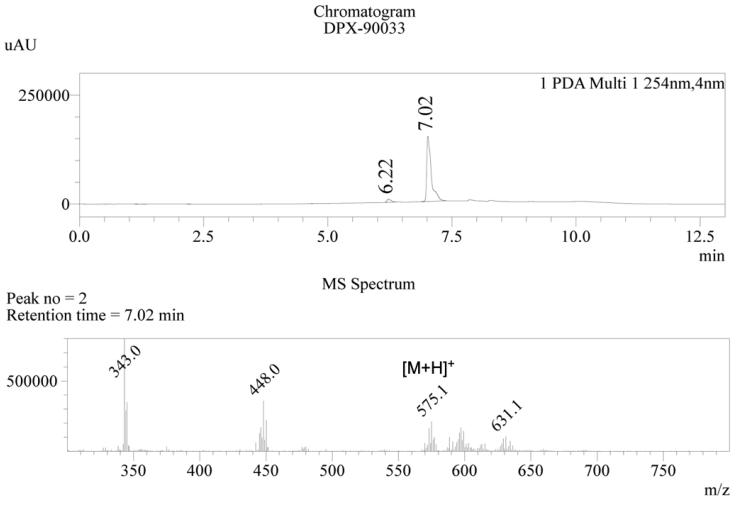

Figure S24. $^{13}C\{^{1}H\}$ NMR spectrum of **14c** in DMSO-d_6

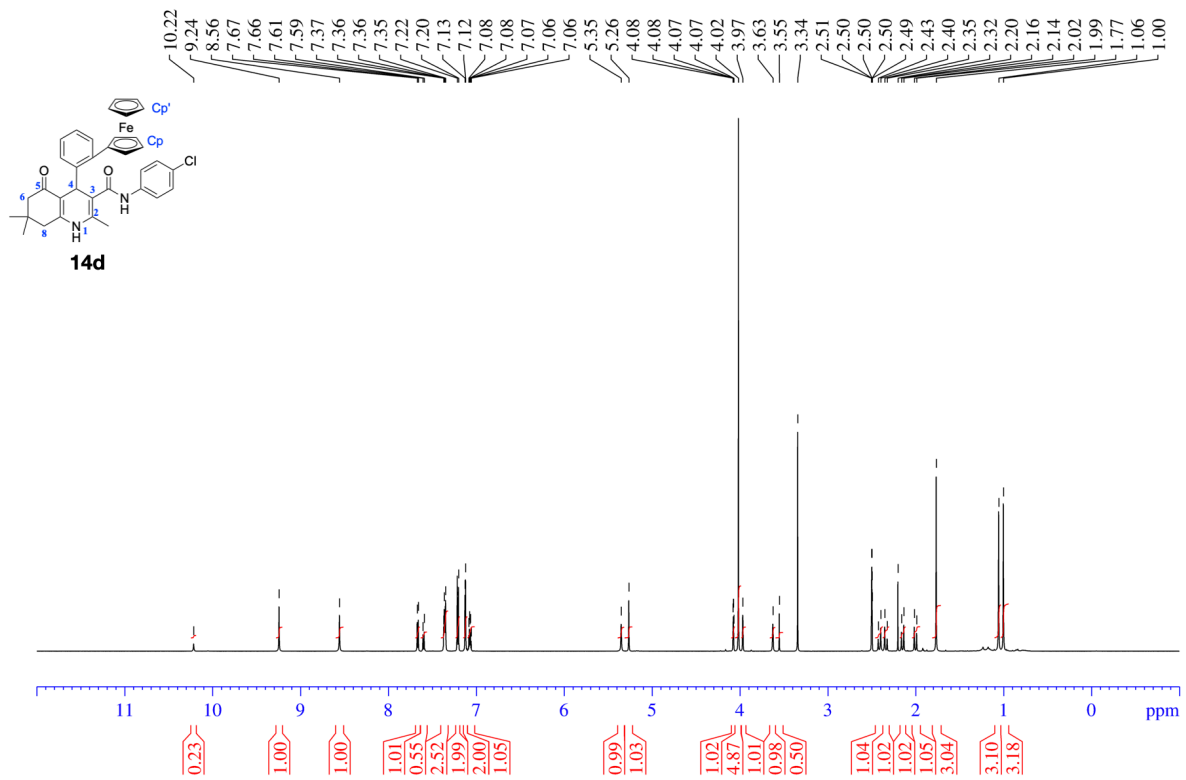

Figure S25. $^{13}C\{^{1}H\}$ NMR spectrum of **14d** in DMSO-d_6

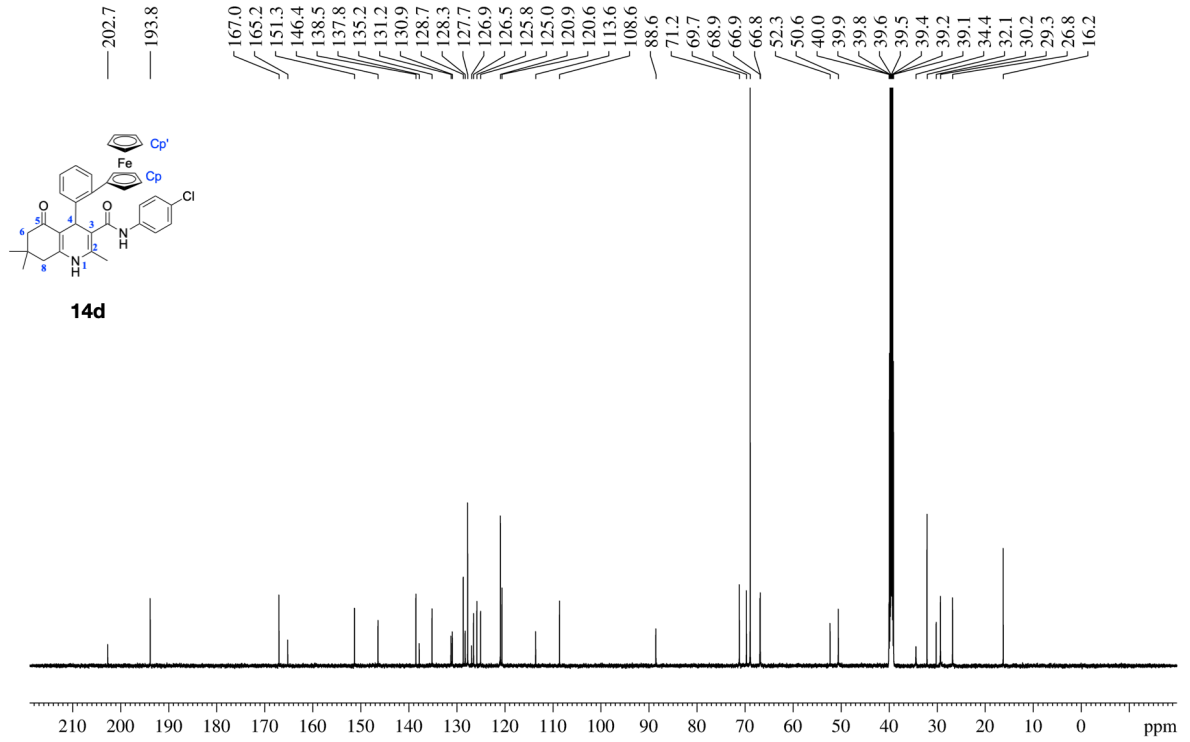

Figure S26. $^{13}C\{^{1}H\}$ NMR spectrum of **14d** in DMSO-d_6

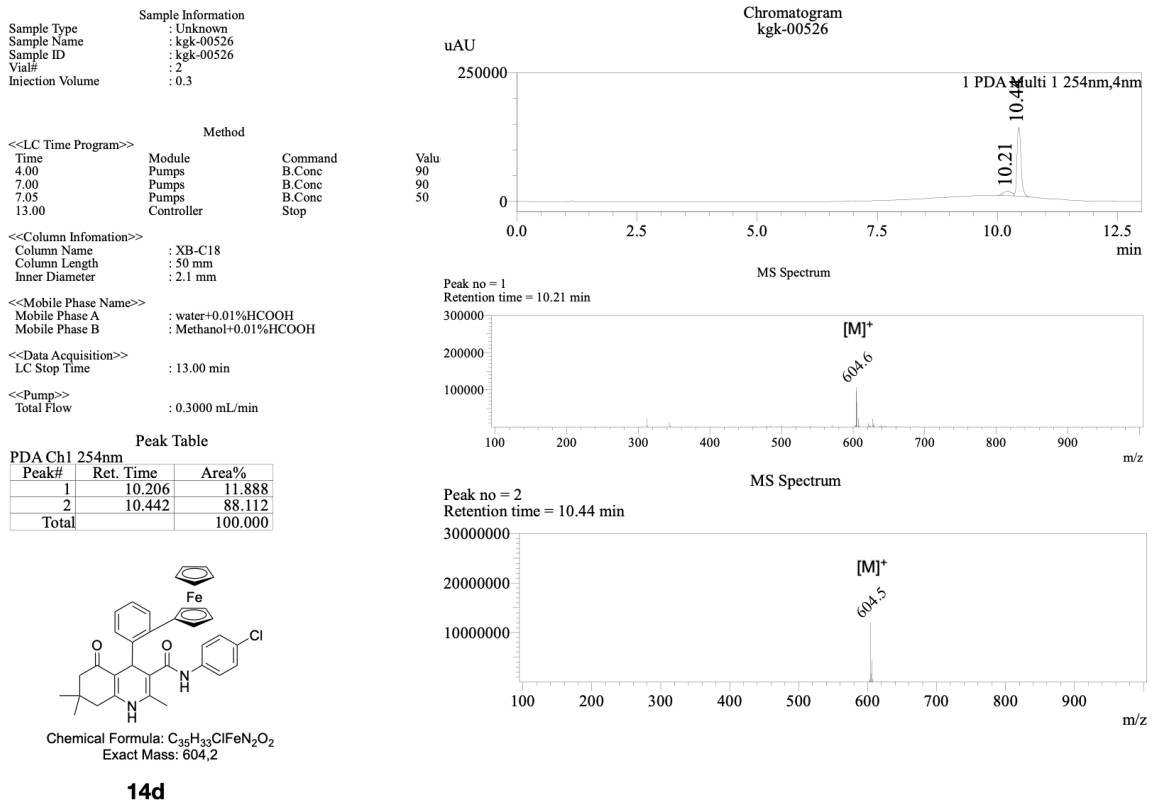

14d

Figure S27. $^{13}C\{^{1}H\}$ NMR spectrum of **14d** in DMSO-d_6

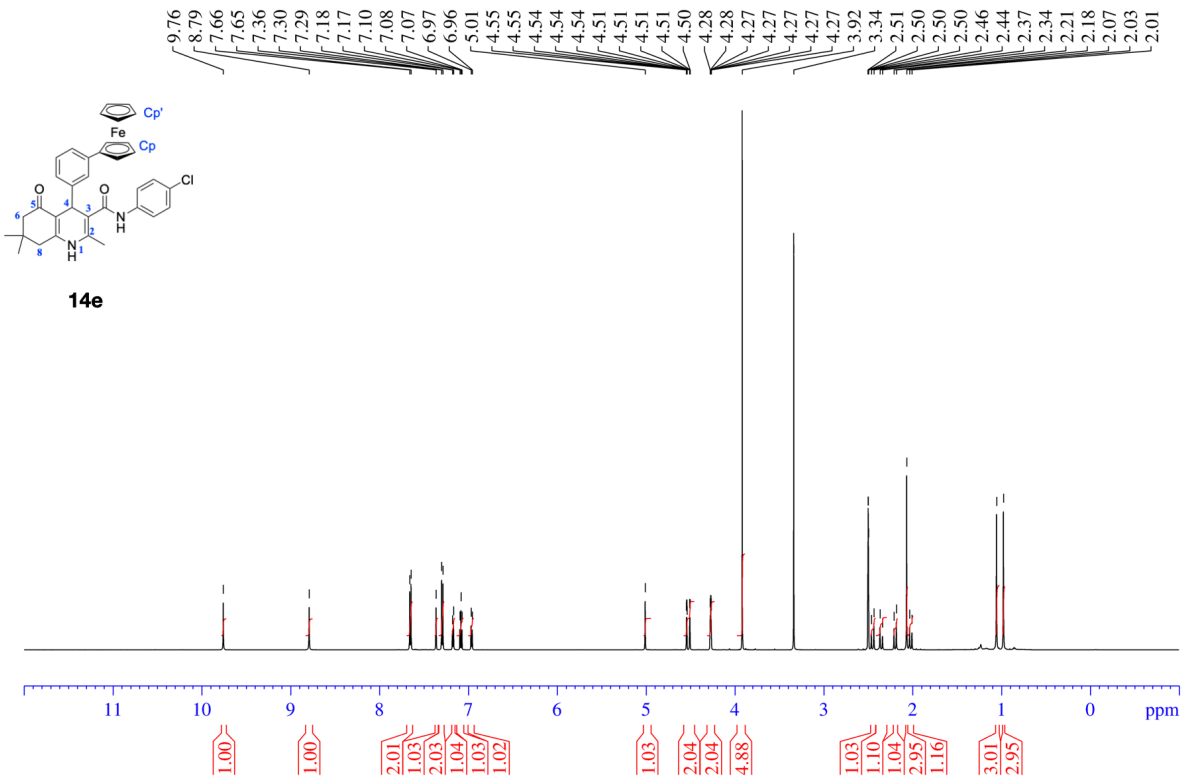

14e

Figure S28. $^{13}C\{^{1}H\}$ NMR spectrum of **14e** in DMSO-d_6

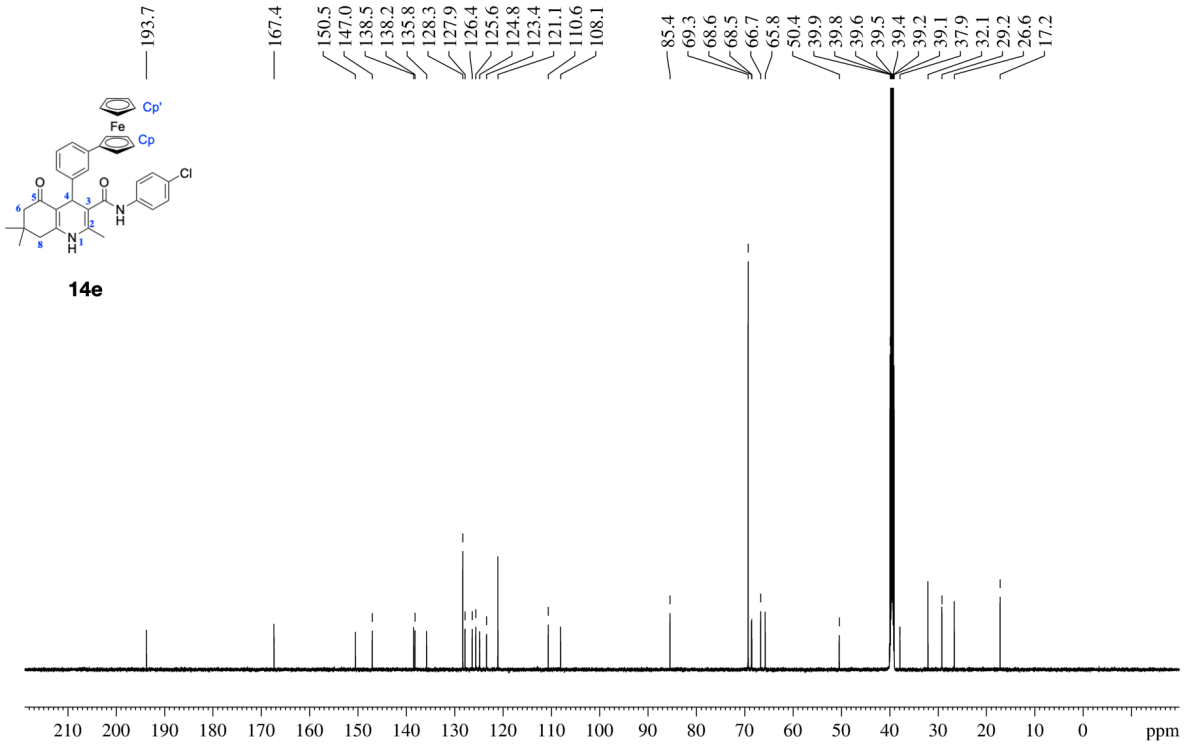

Figure S29. $^{13}C\{^{1}H\}$ NMR spectrum of **14e** in DMSO-d_6

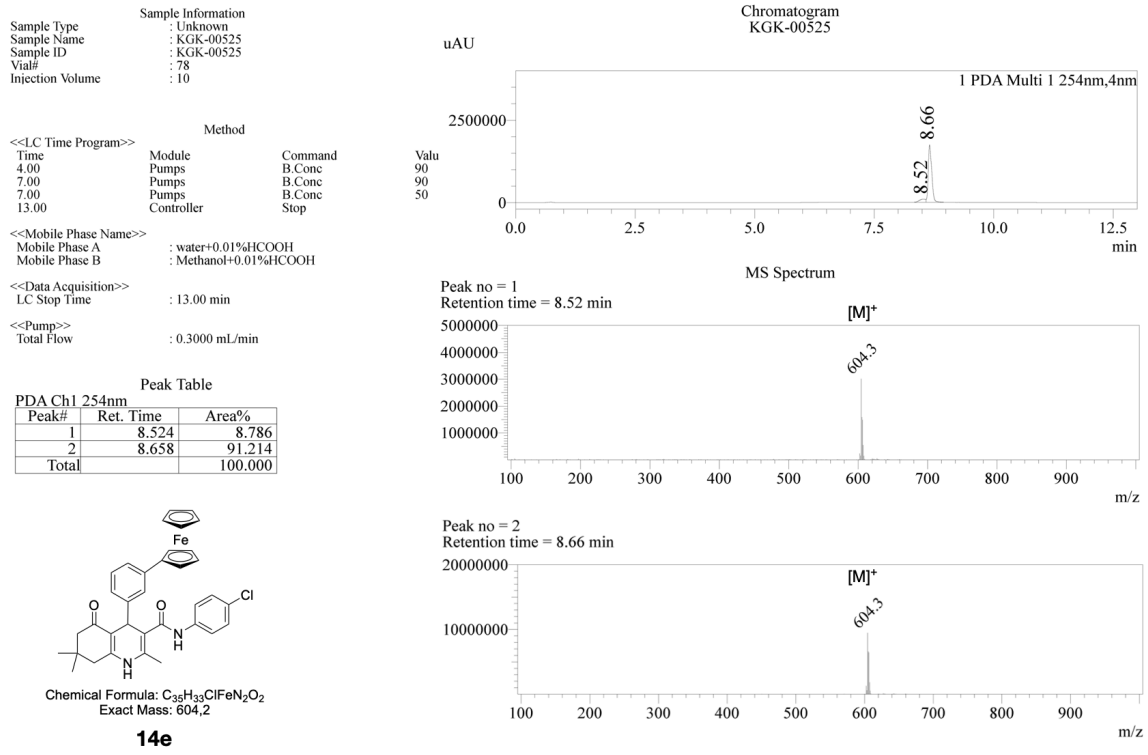

Figure S30. $^{13}C\{^{1}H\}$ NMR spectrum of **14e** in DMSO-d_6

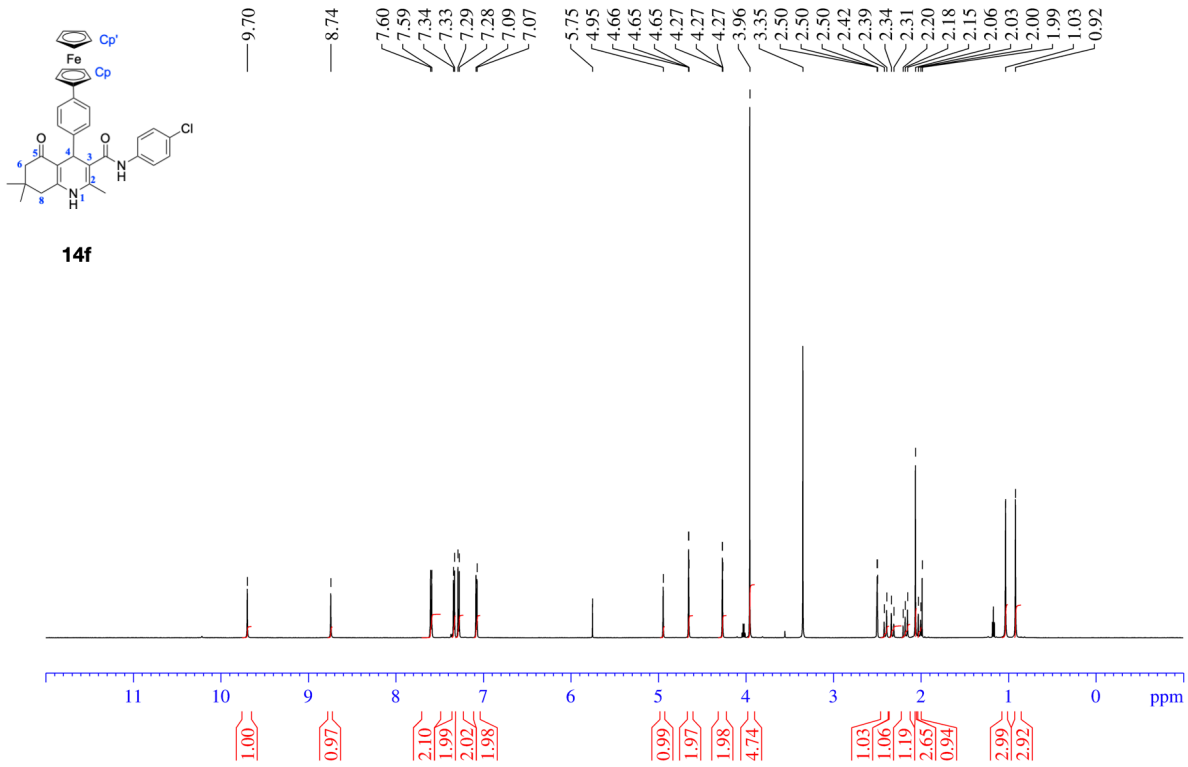

Figure S31. $^{13}C\{^{1}H\}$ NMR spectrum of **14f** in DMSO-d_6

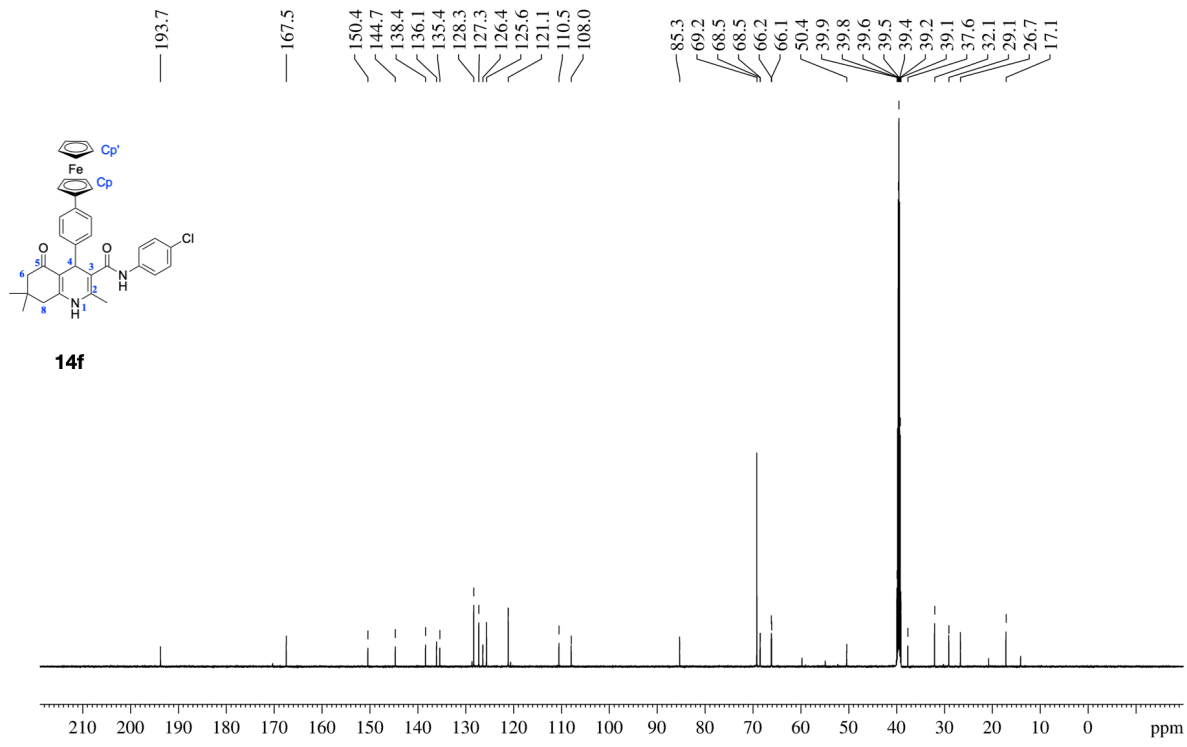

Figure S32. $^{13}C\{^{1}H\}$ NMR spectrum of **14f** in DMSO-d_6

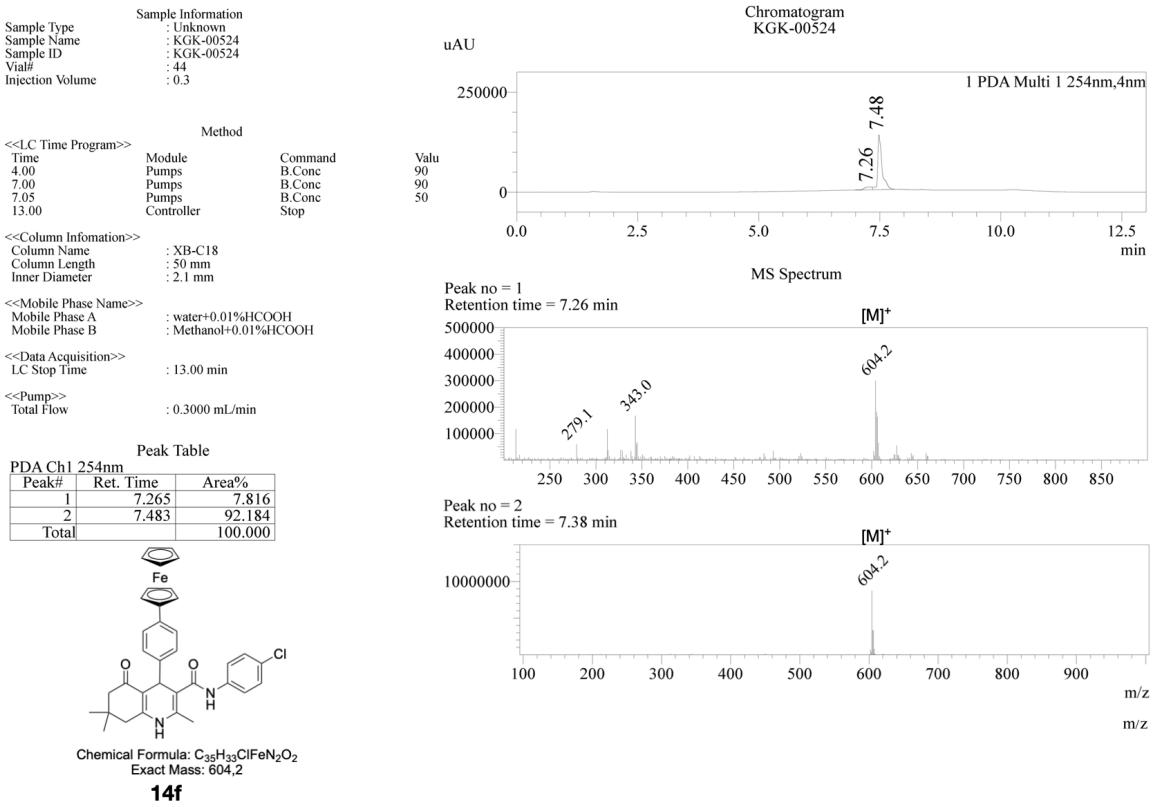

Figure S33. $^{13}C\{^{1}H\}$ NMR spectrum of **14f** in DMSO-d_6

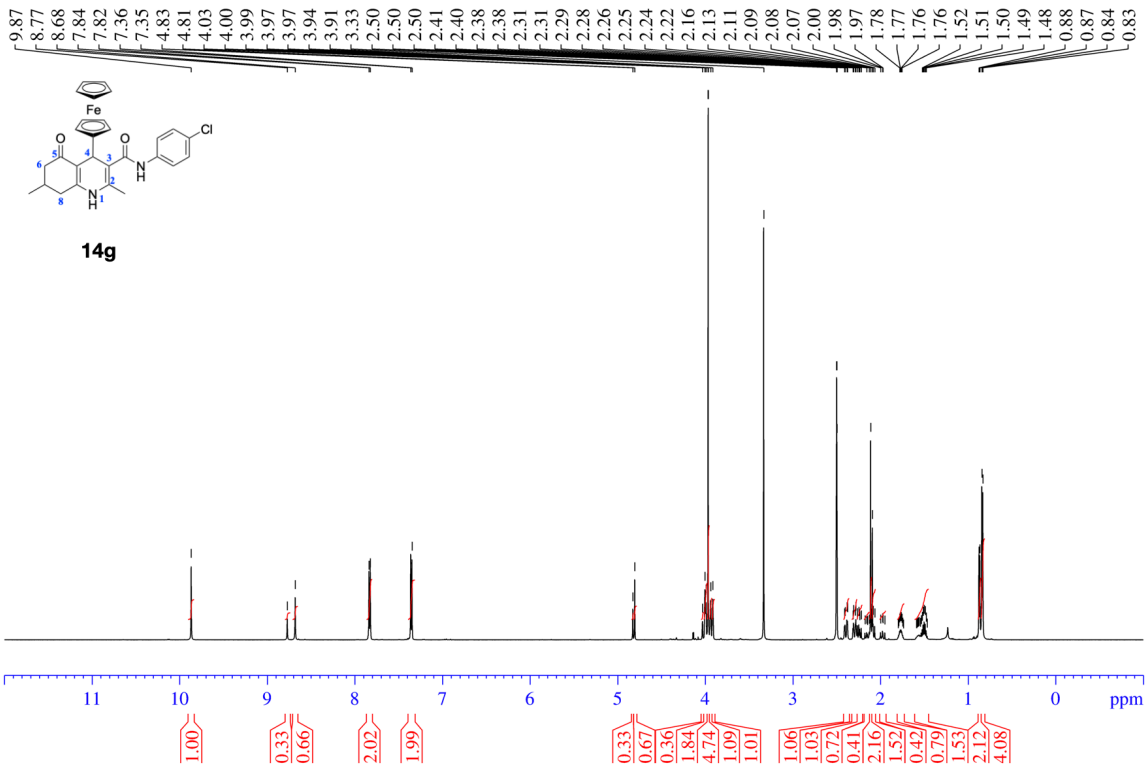

Figure S34. $^{13}C\{^{1}H\}$ NMR spectrum of **14g** in DMSO-d_6

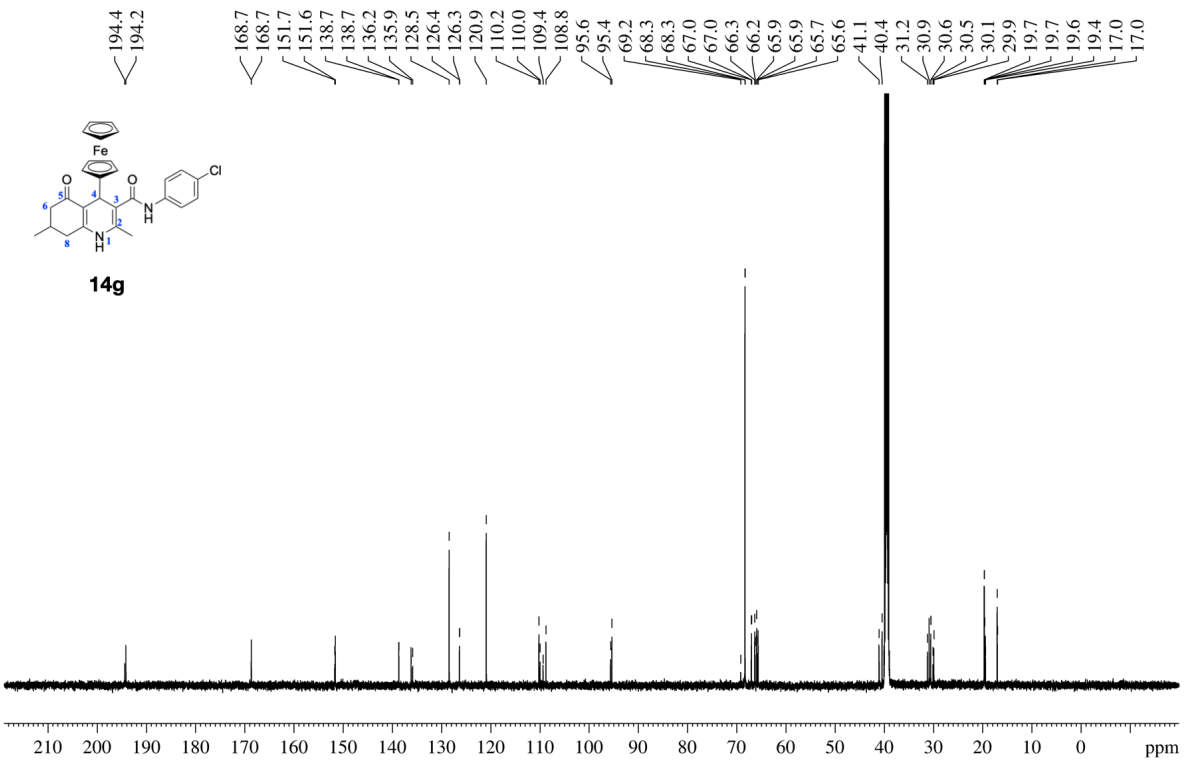

Figure S35. $^{13}C\{^{1}H\}$ NMR spectrum of **14g** in DMSO-d_6

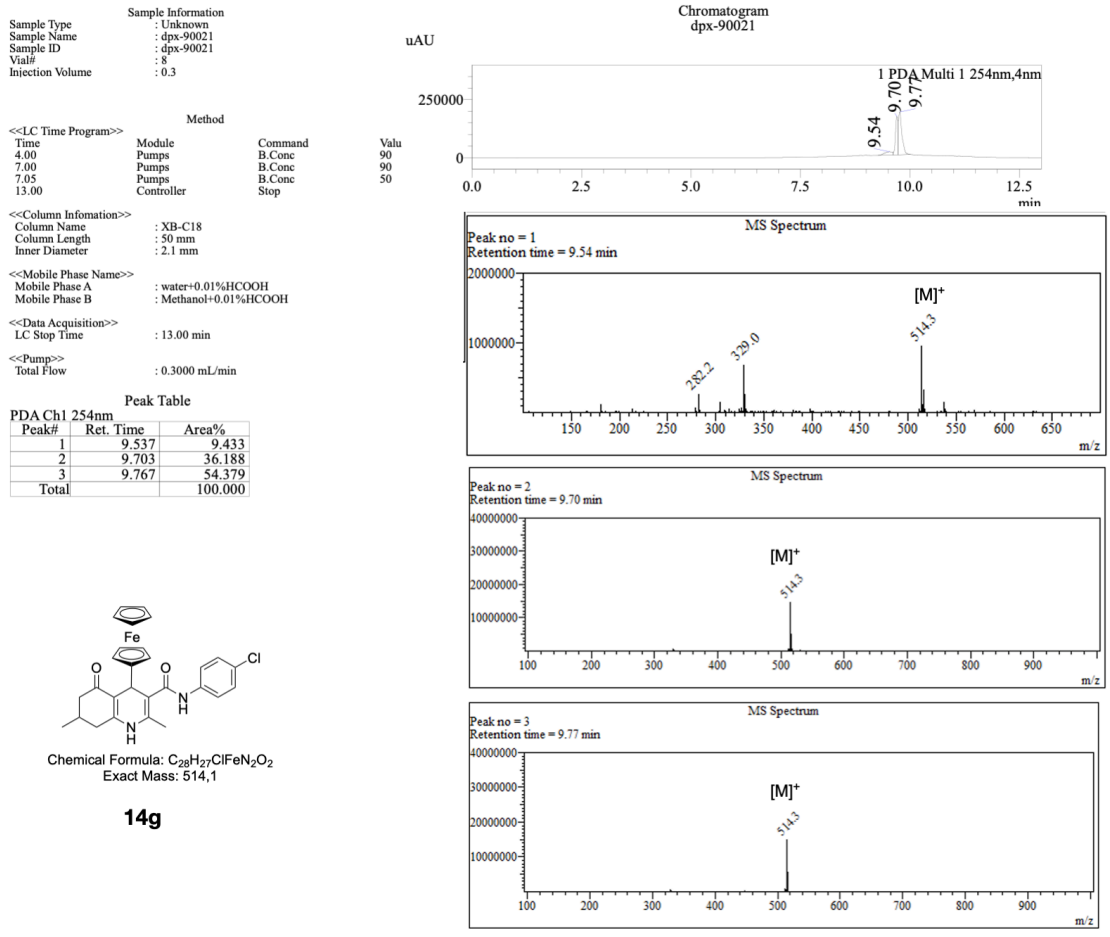

Figure S36. $^{13}C\{^{1}H\}$ NMR spectrum of **14g** in DMSO-d_6

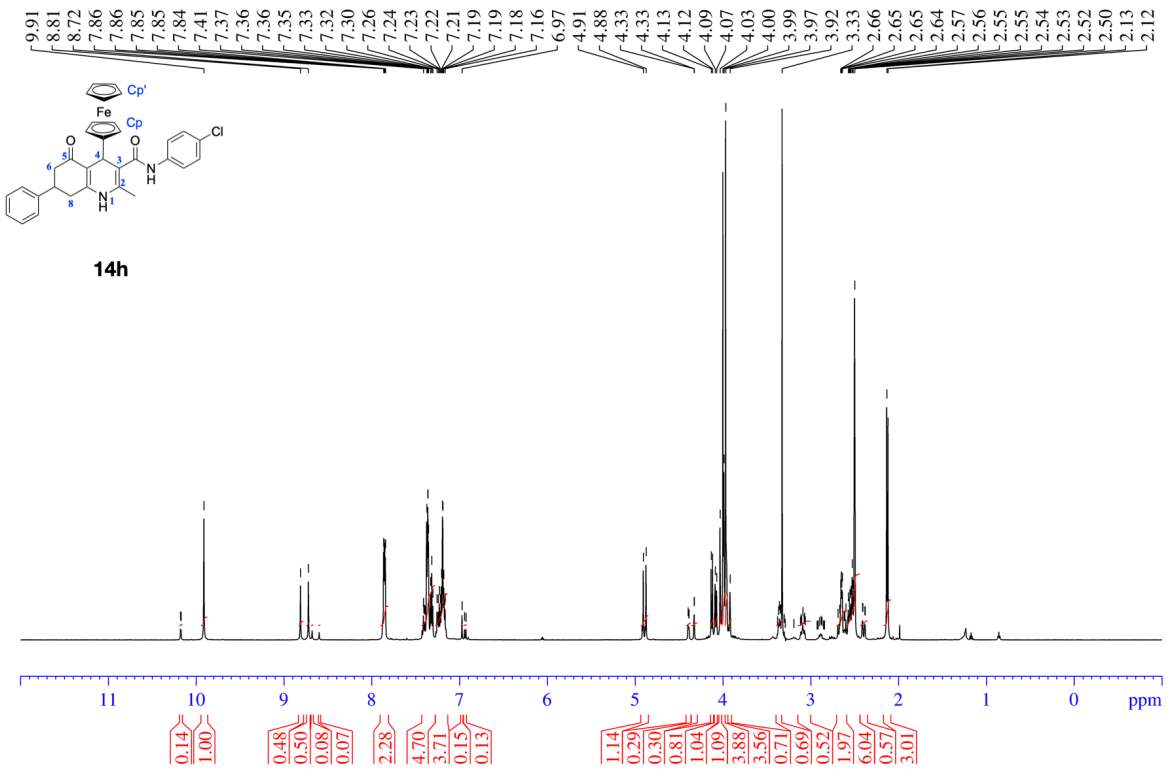

Figure S37. $^{13}C\{^{1}H\}$ NMR spectrum of **14h** in DMSO-d_6

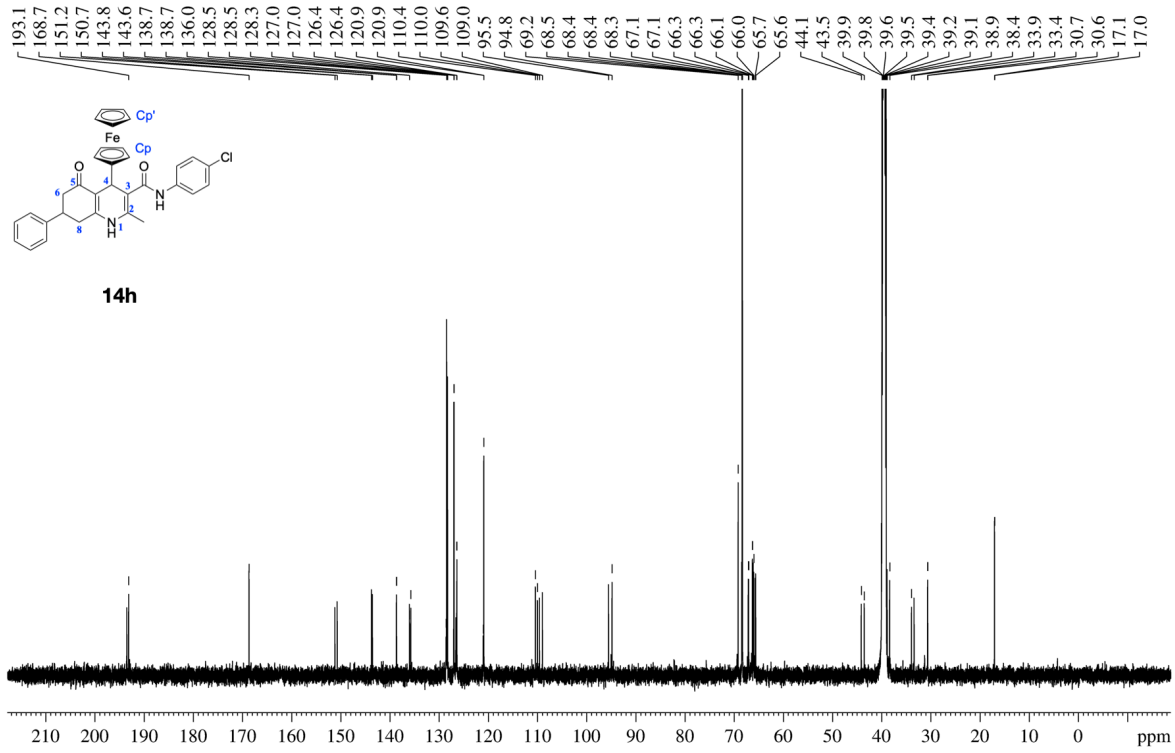

Figure S38. $^{13}C\{^{1}H\}$ NMR spectrum of **14h** in DMSO-d_6

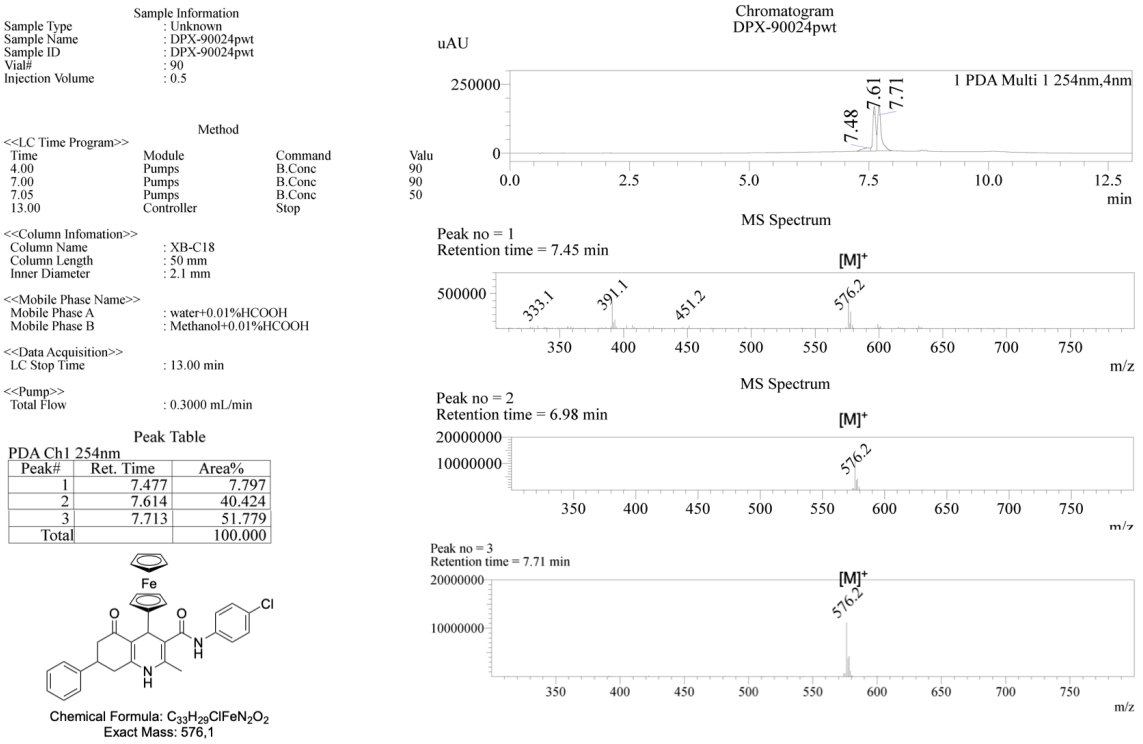

Figure S39. $^{13}C\{^{1}H\}$ NMR spectrum of **14h** in DMSO-d_6

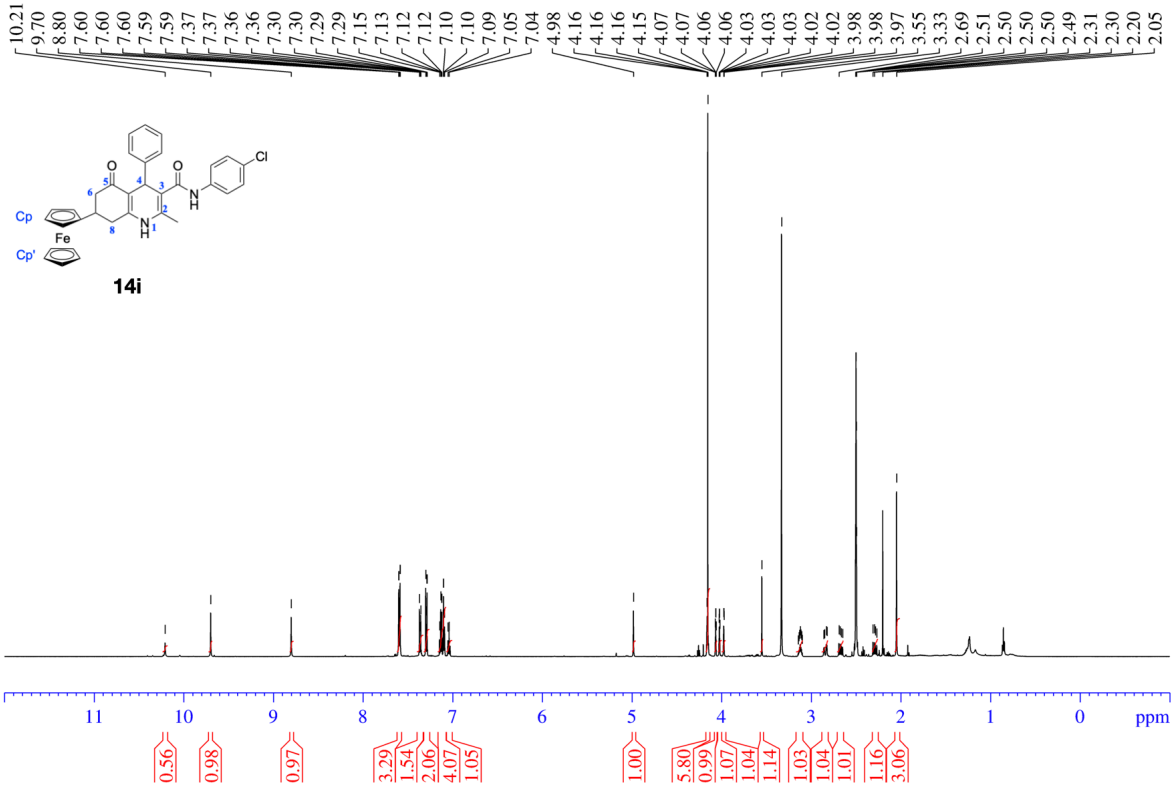

Figure S40. $^{13}C\{^{1}H\}$ NMR spectrum of **14i** in DMSO-d_6

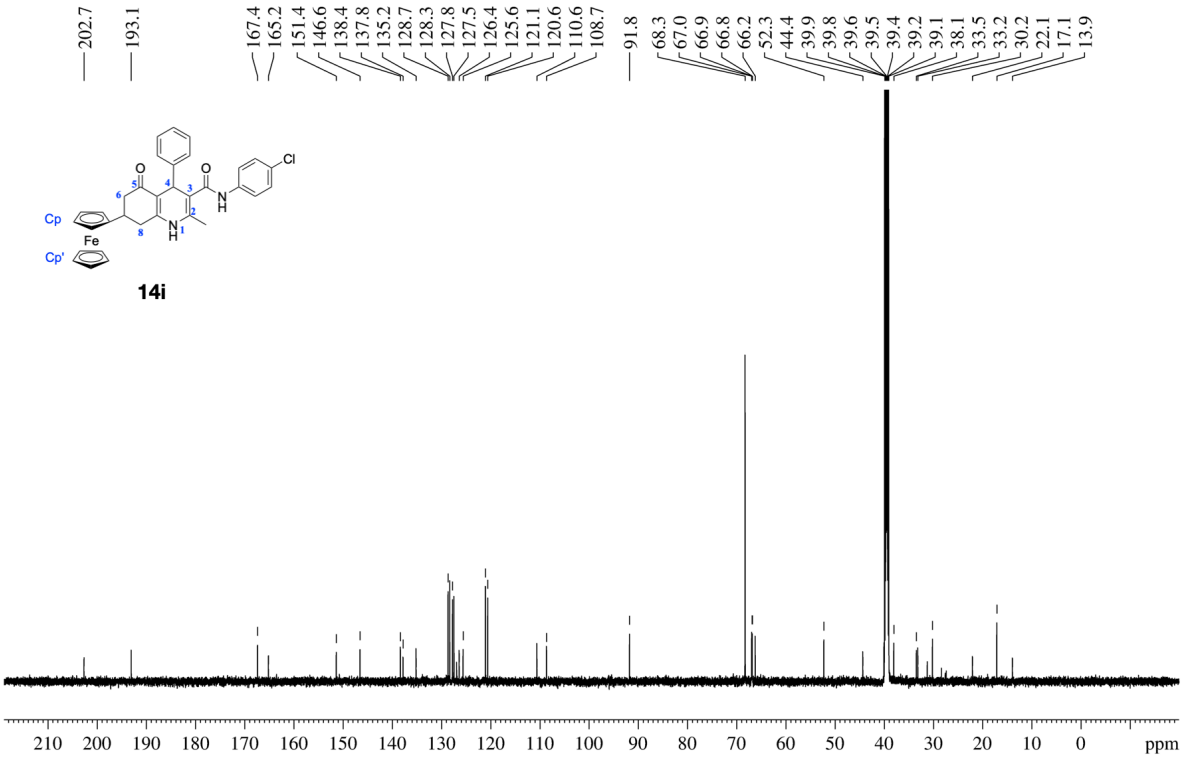

Figure S41. $^{13}C\{^{1}H\}$ NMR spectrum of **14i** in DMSO-d_6

Sample Information

Sample Type	: Unknown
Sample Name	: kgk-90026_MeOH_5-9-5
Sample ID	: kgk-90026_MeOH_5-9-5
Vial#	: 103
Injection Volume	: 0.5

Method

<<LC Time Program>>

Time	Module	Command	Valu
4.00	Pumps	B.Conc	90
7.00	Pumps	B.Conc	90
7.05	Pumps	B.Conc	50
13.00	Controller	Stop	

<<Mobile Phase Name>>

Mobile Phase A	: water+0.01%HCOOH
Mobile Phase B	: Methanol+0.01%HCOOH

<<Data Acquisition>>

LC Stop Time	: 13.00 min

<<Pump>>

Total Flow	: 0.3000 mL/min

Peak Table

PDA Ch1 254nm

Peak#	Ret. Time	Area%
1	7.911	100.000
Total		100.000

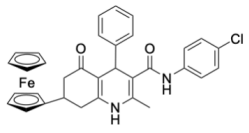

Chemical Formula: $C_{33}H_{29}ClFeN_2O_2$
Exact Mass: 576,1

14i

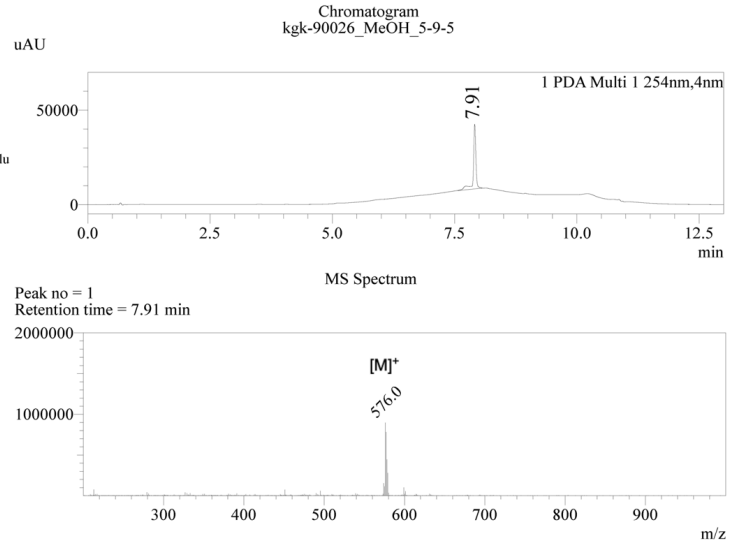

Figure S42. $^{13}C\{^{1}H\}$ NMR spectrum of **14i** in DMSO-d_6

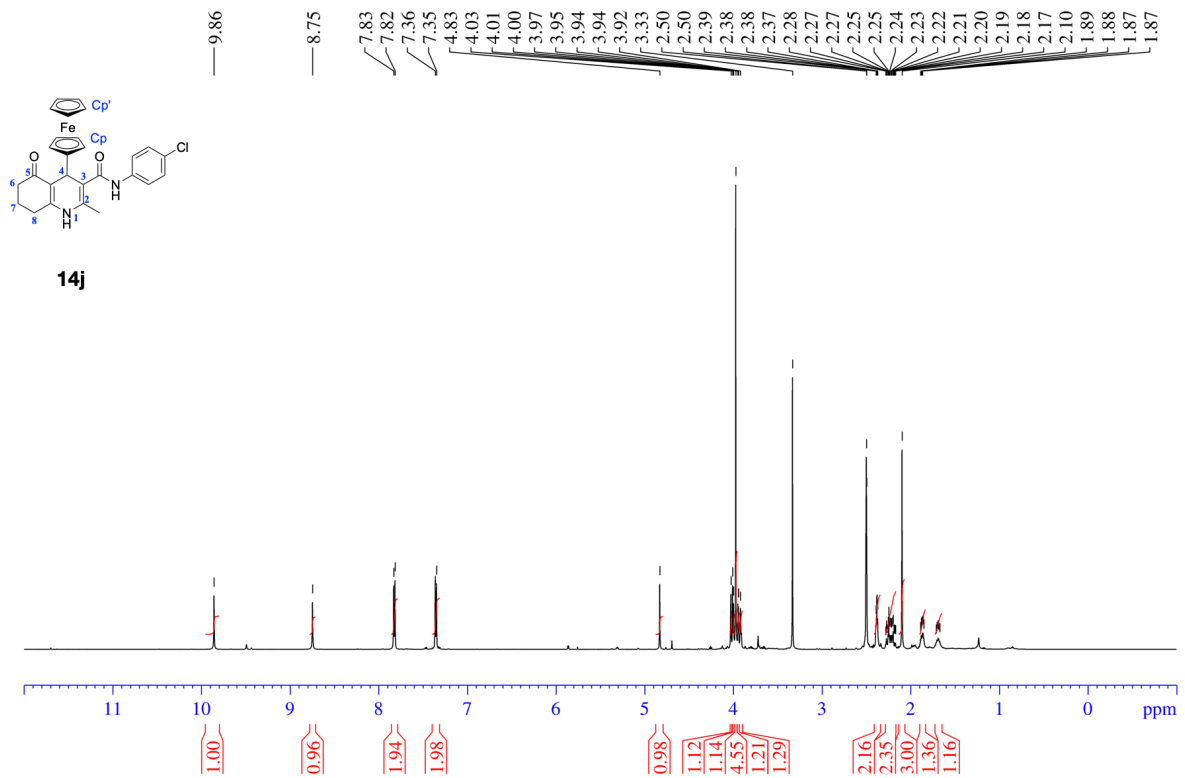

Figure S43. $^{13}C\{^{1}H\}$ NMR spectrum of **14j** in DMSO-d_6

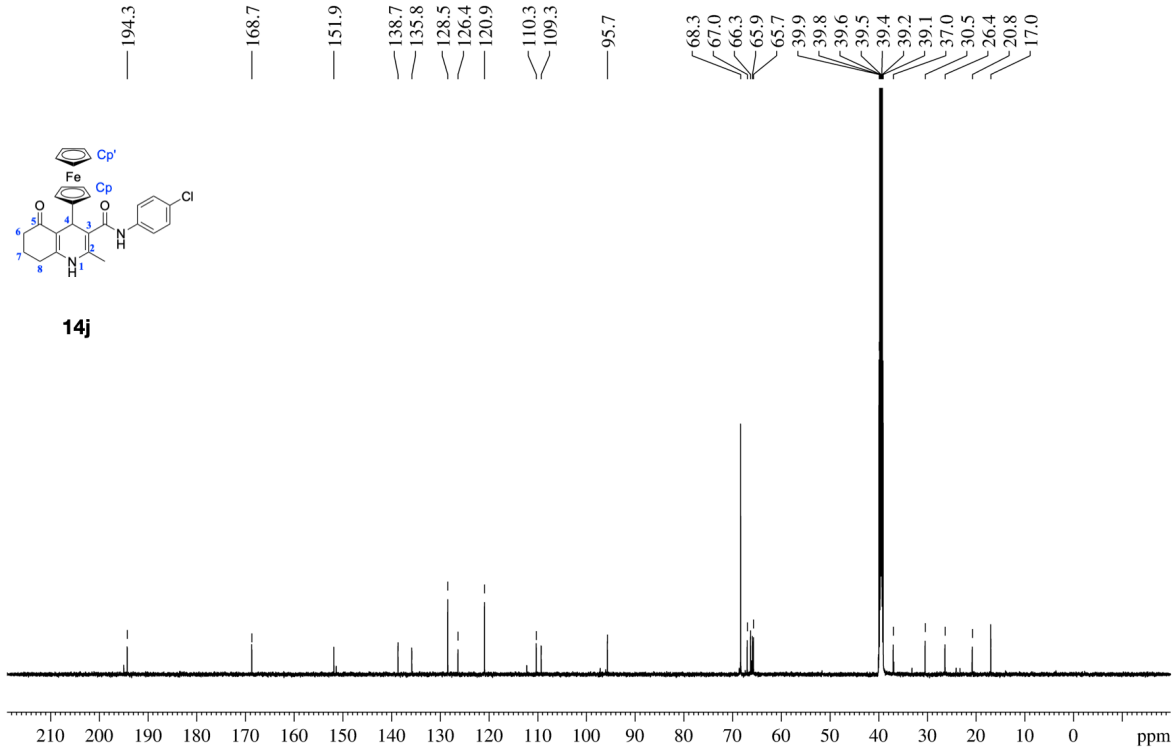

Figure S44. $^{13}C\{^{1}H\}$ NMR spectrum of **14j** in DMSO-d_6

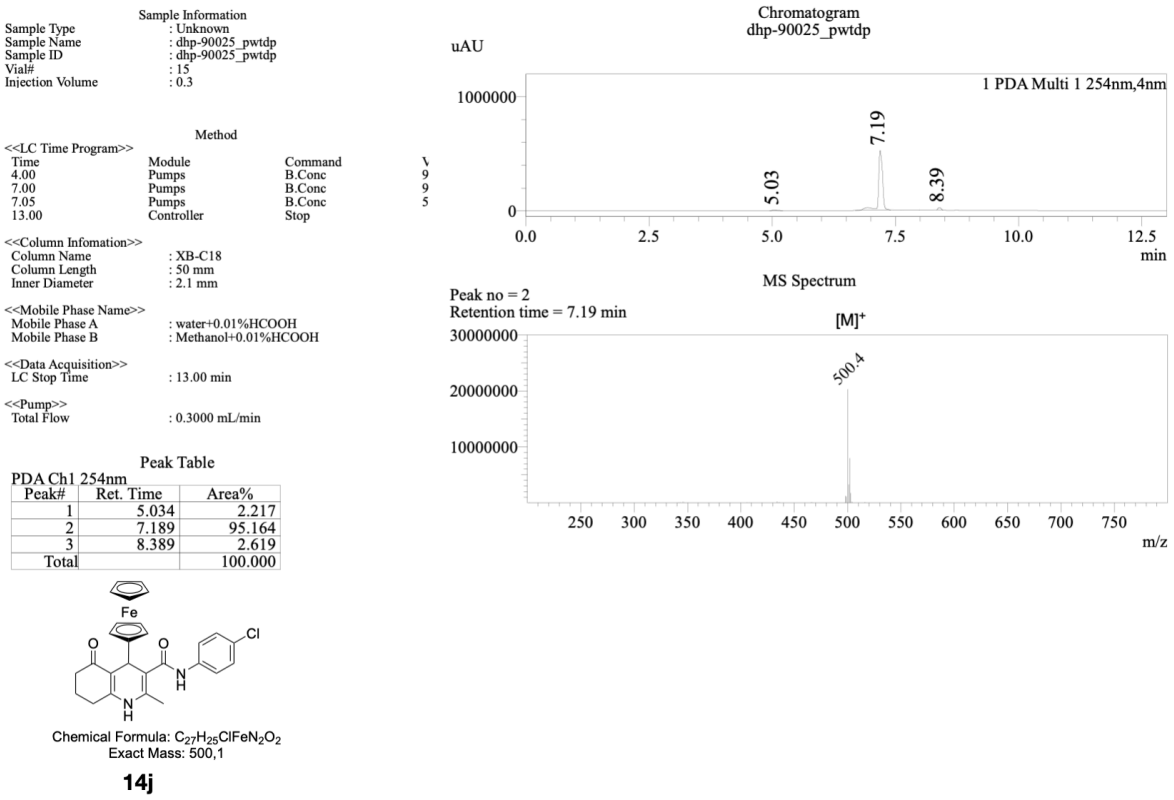

Figure S45. $^{13}C\{^{1}H\}$ NMR spectrum of **14j** in DMSO-d_6

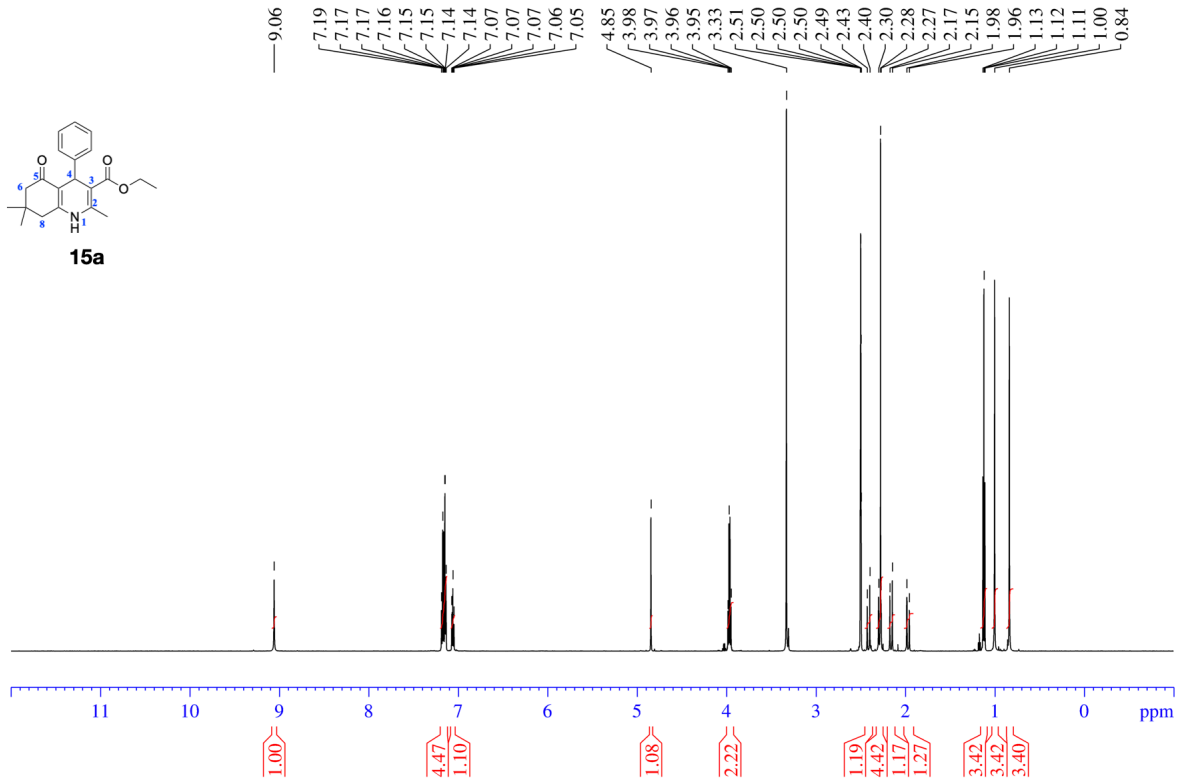

Figure S46. $^{13}C\{^{1}H\}$ NMR spectrum of **15a** in DMSO-d_6

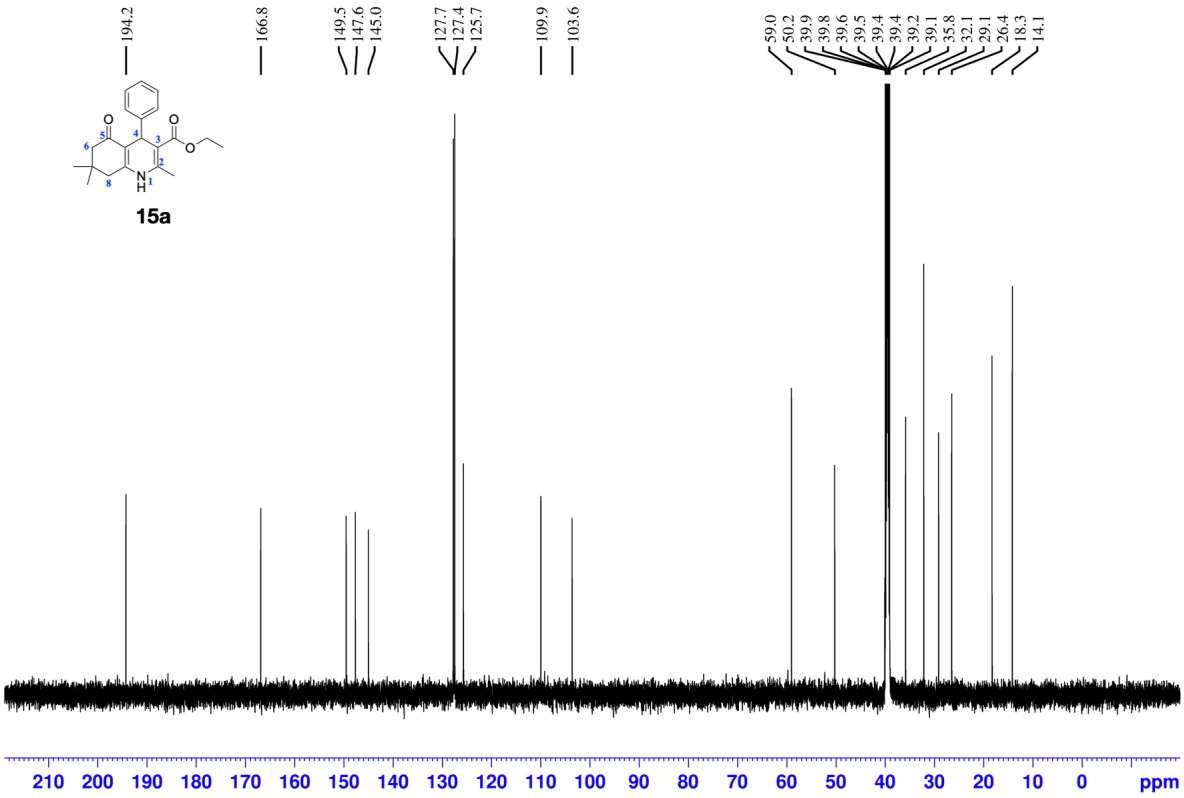

Figure S47. $^{13}C\{^{1}H\}$ NMR spectrum of **15a** in DMSO-d_6

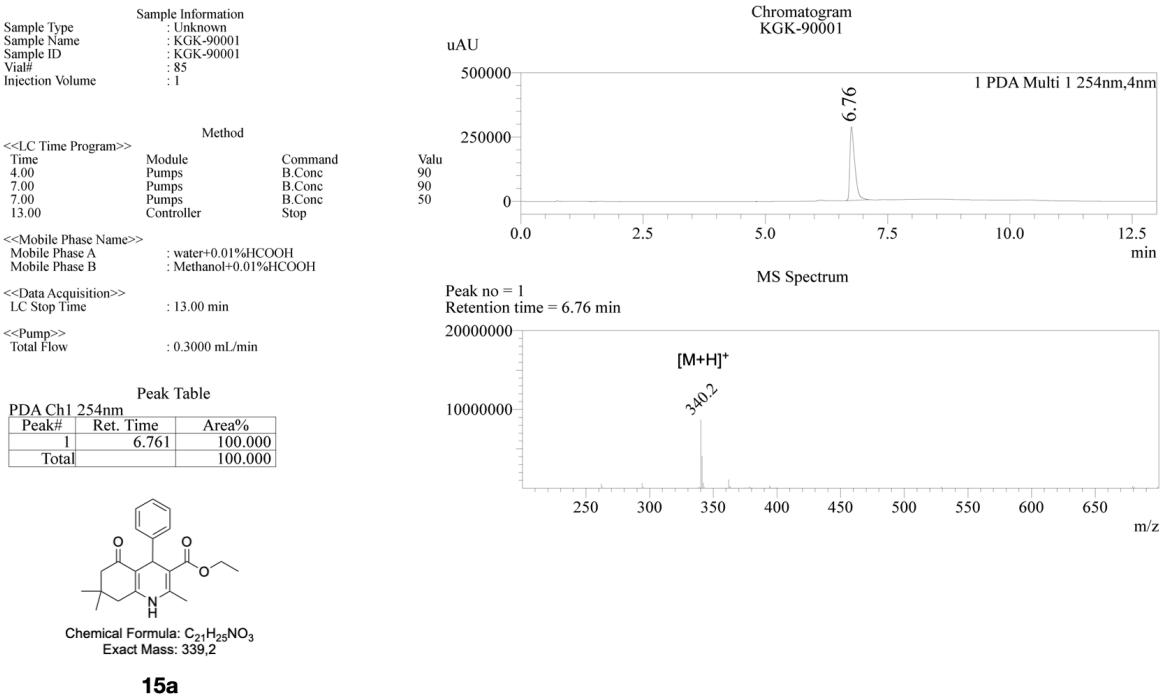

Figure S48. $^{13}C\{^{1}H\}$ NMR spectrum of **15a** in DMSO-d_6

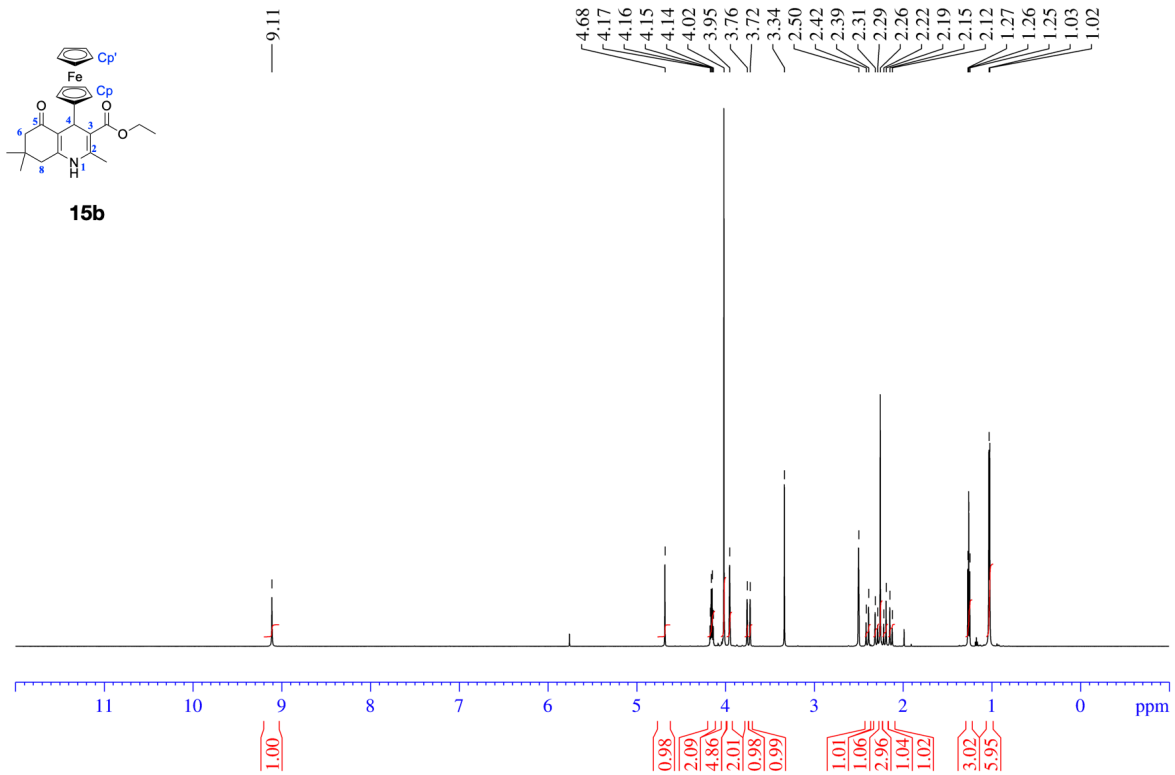

Figure S49. $^{13}C\{^{1}H\}$ NMR spectrum of **15b** in DMSO-d_6

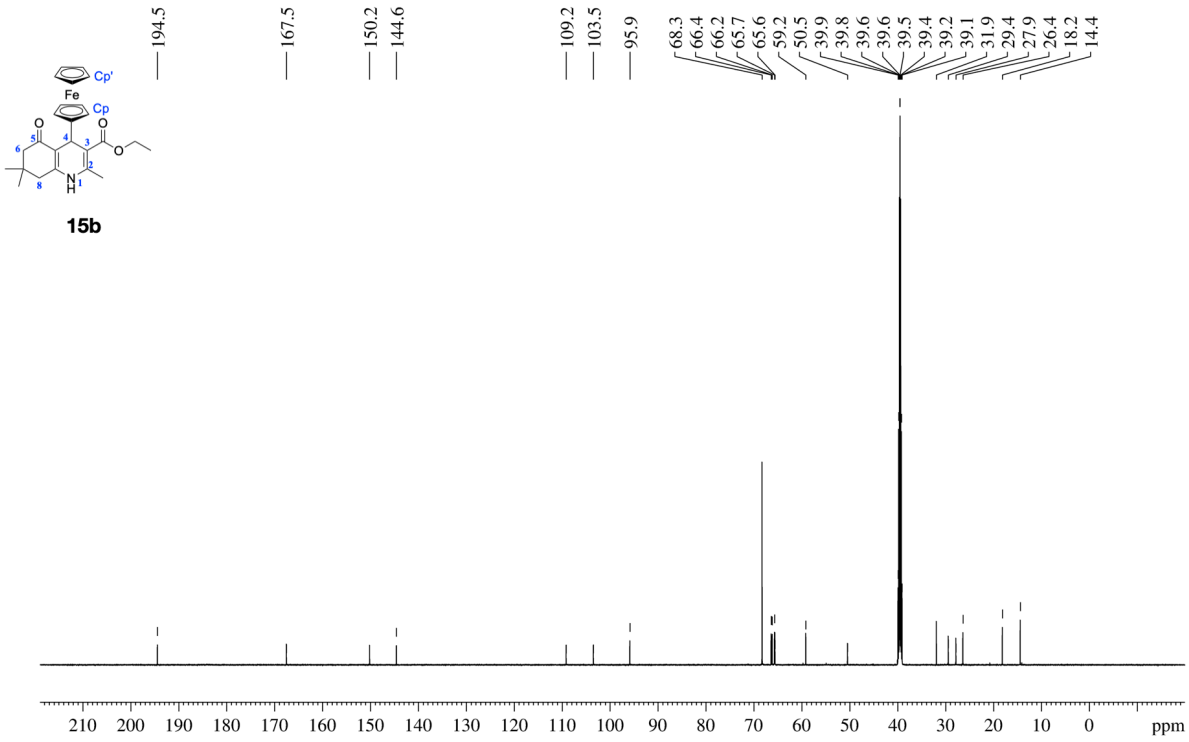

Figure S50. $^{13}C\{^{1}H\}$ NMR spectrum of **15b** in DMSO-d_6

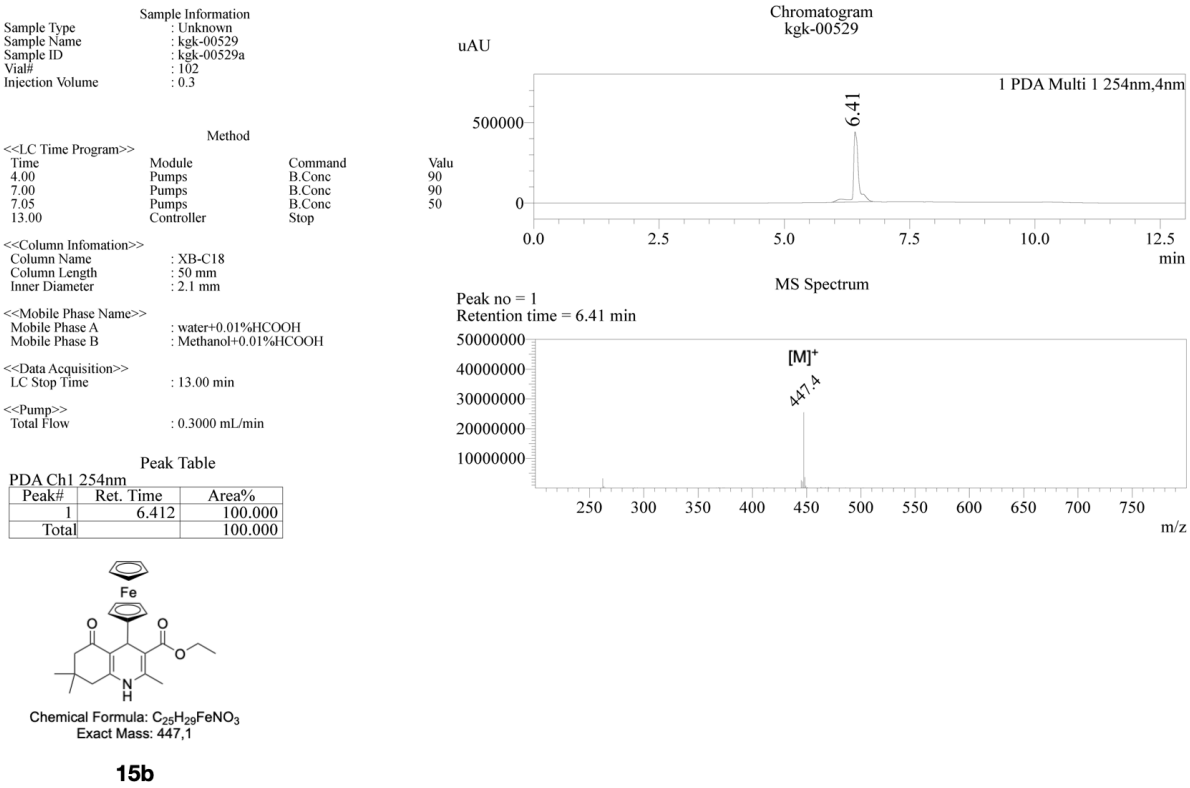

15b

Figure S51. $^{13}C\{^{1}H\}$ NMR spectrum of **15b** in DMSO-d_6

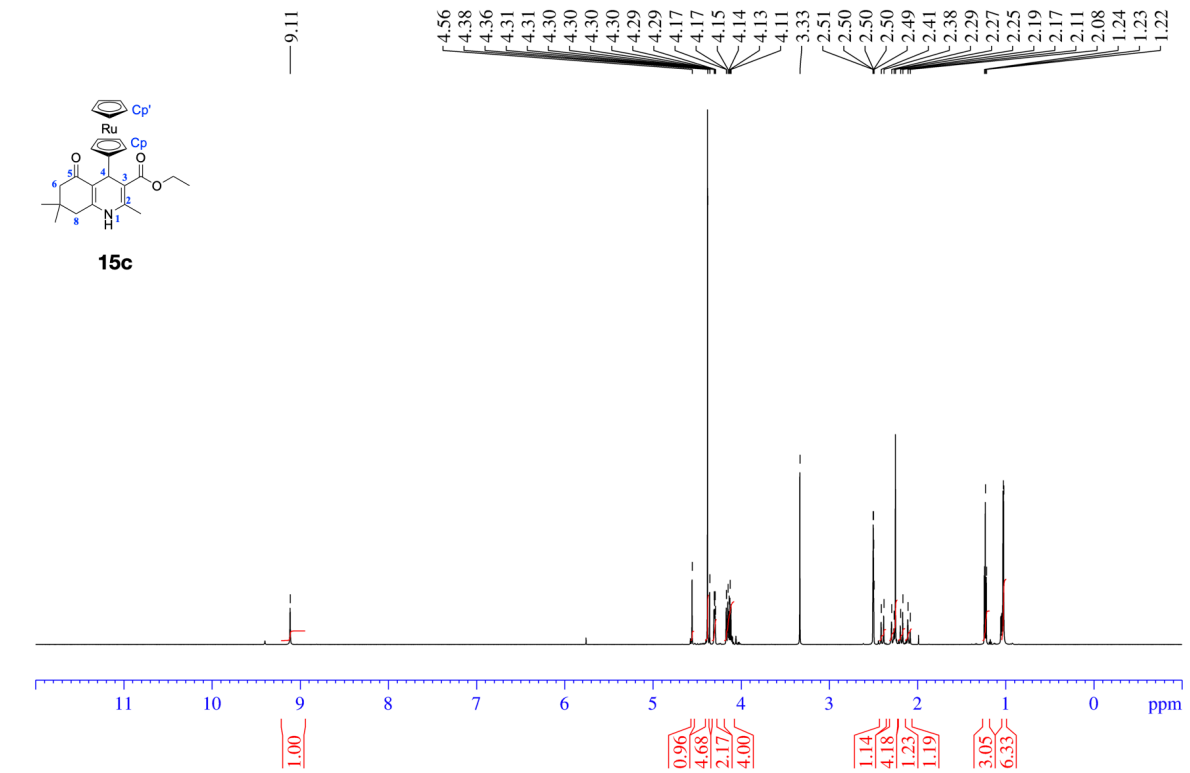

15c

Figure S52. $^{13}C\{^{1}H\}$ NMR spectrum of **15c** in DMSO-d_6

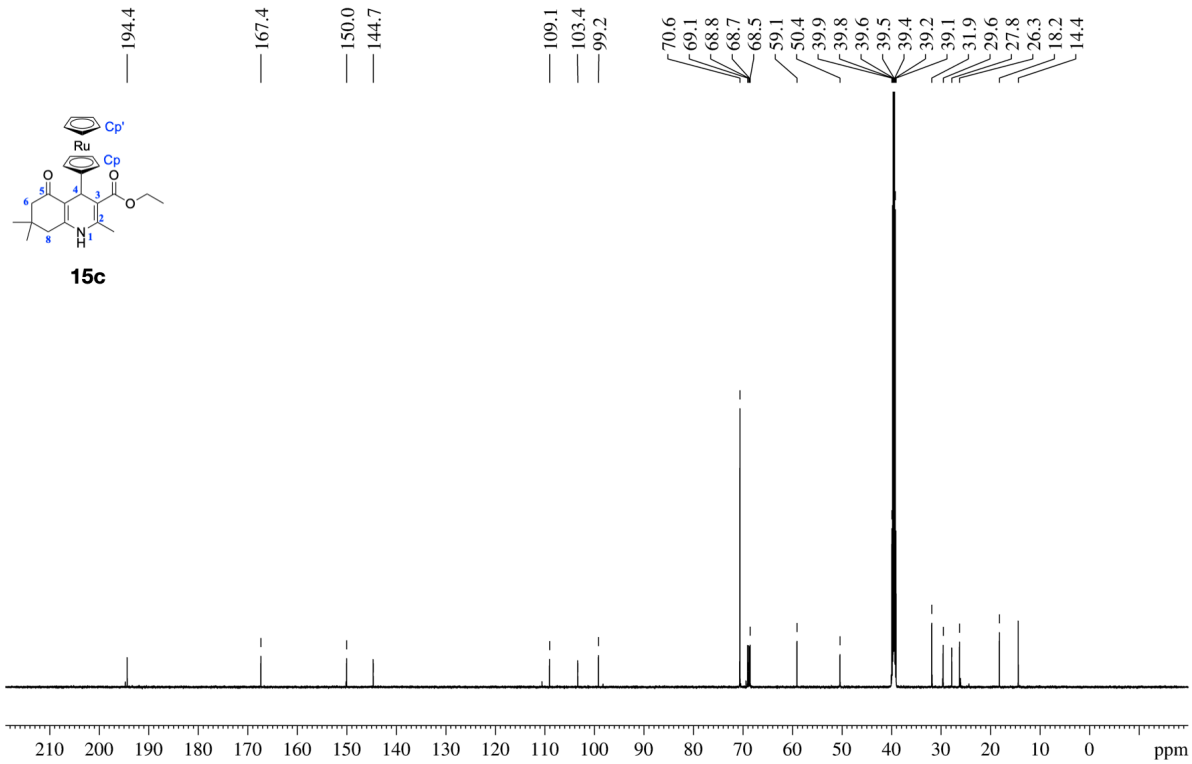

Figure S53. $^{13}C\{^{1}H\}$ NMR spectrum of **15c** in DMSO-d_6

Sample Information

Sample Type	: Unknown
Sample Name	: DPX-90032
Sample ID	: DPX-90032
Vial#	: 39
Injection Volume	: 0.3

Method

<<LC Time Program>>

Time	Module	Command	Valu
4.00	Pumps	B.Conc	90
7.00	Pumps	B.Conc	90
7.05	Pumps	B.Conc	50
13.00	Controller	Stop	

<<Column Infomation>>

Column Name	: XB-C18
Column Length	: 50 mm
Inner Diameter	: 2.1 mm

<<Mobile Phase Name>>

Mobile Phase A	: water+0.01%HCOOH
Mobile Phase B	: Methanol+0.01%HCOOH

<<Data Acquisition>>

LC Stop Time	: 13.00 min

<<Pump>>

Total Flow	: 0.3000 mL/min

Peak Table

PDA Ch1 254nm

Peak#	Ret. Time	Area%
1	6.211	9.644
2	6.356	90.356
Total		100.000

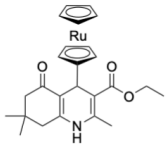

Chemical Formula: $C_{25}H_{29}NO_3Ru$
Exact Mass: 493,1

15c

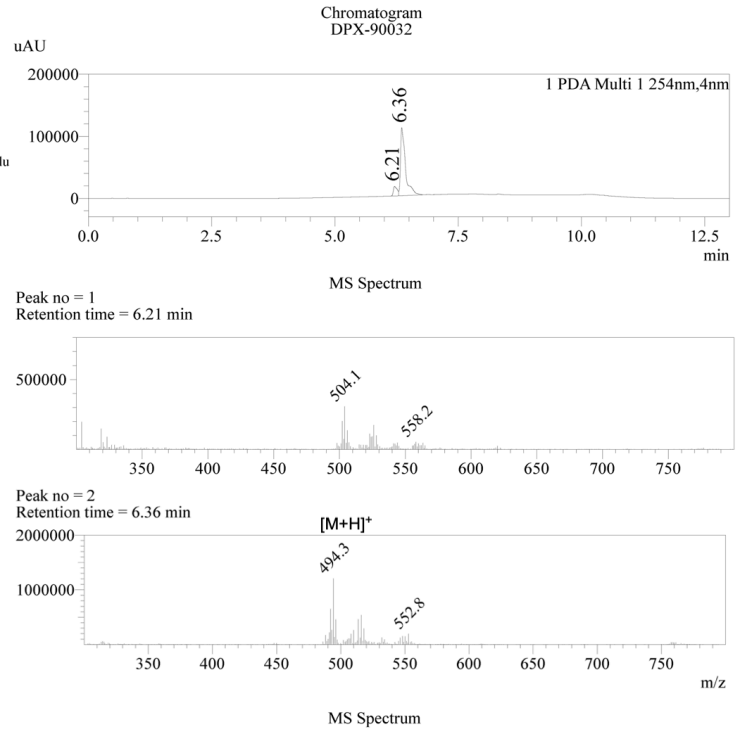

Figure S54. $^{13}C\{^{1}H\}$ NMR spectrum of **15c** in DMSO-d_6

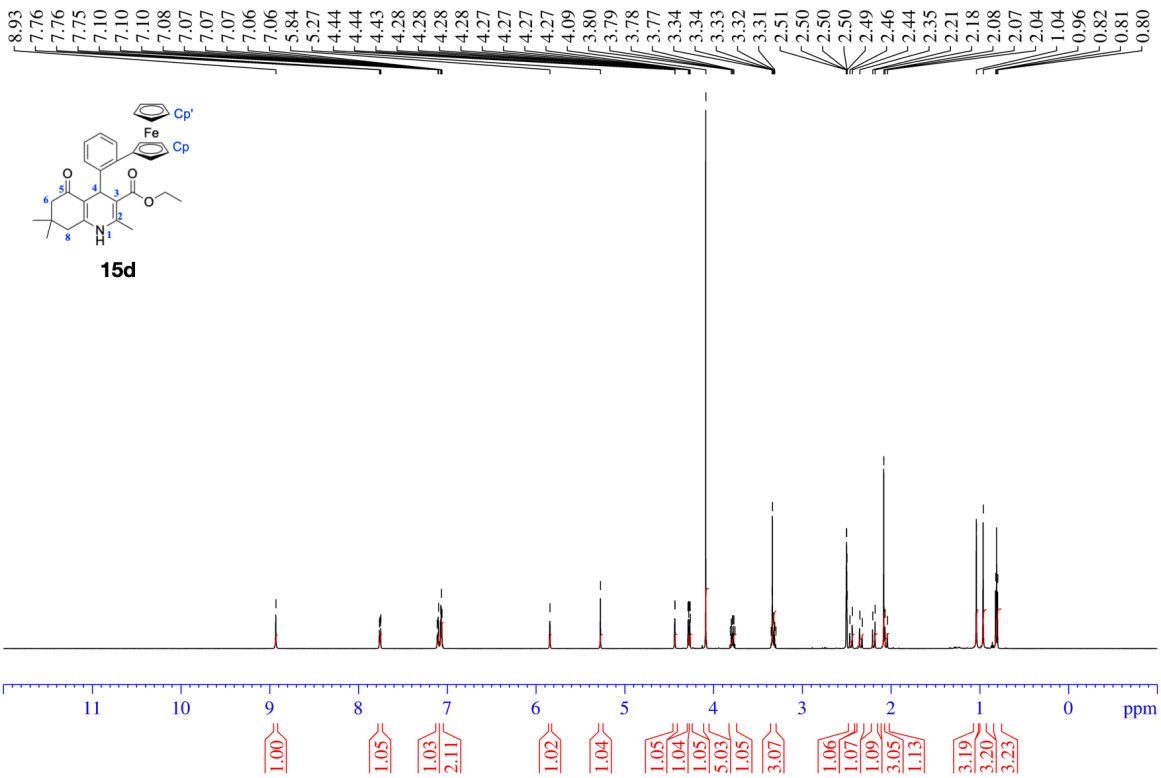

Figure S55. $^{13}C\{^{1}H\}$ NMR spectrum of **15d** in DMSO-d_6

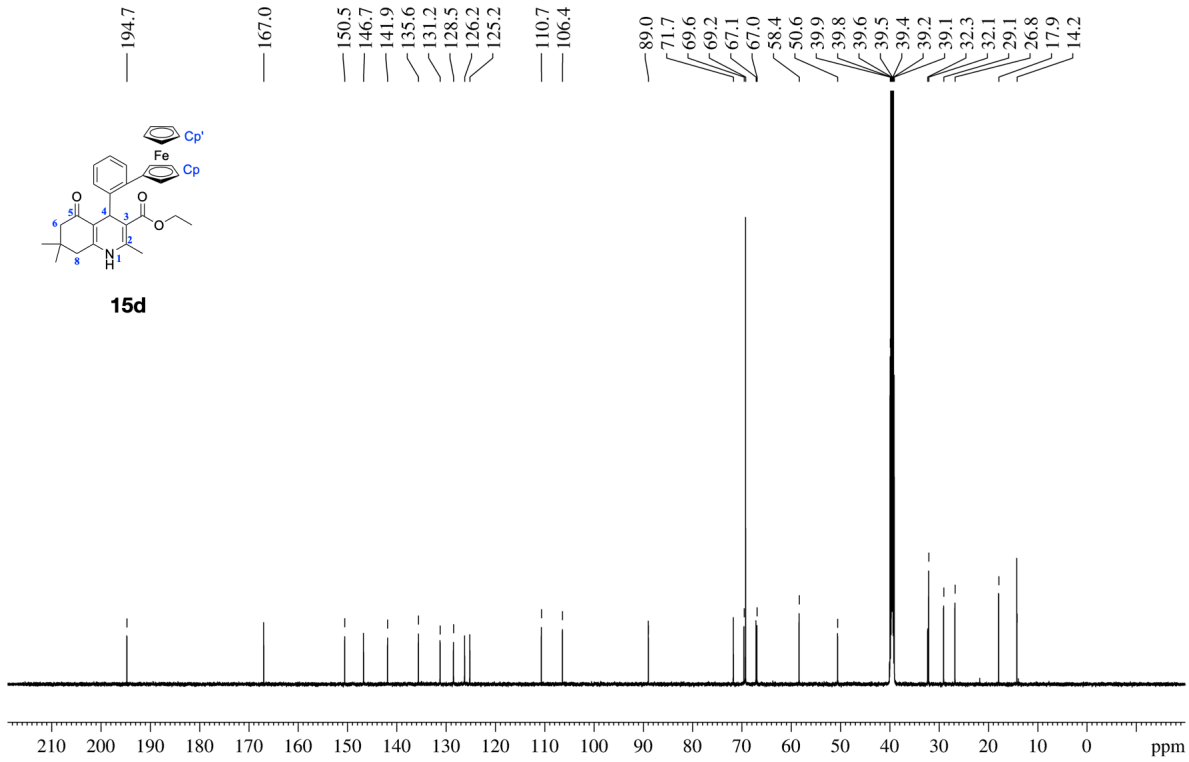

Figure S56. $^{13}C\{^{1}H\}$ NMR spectrum of **15d** in DMSO-d_6

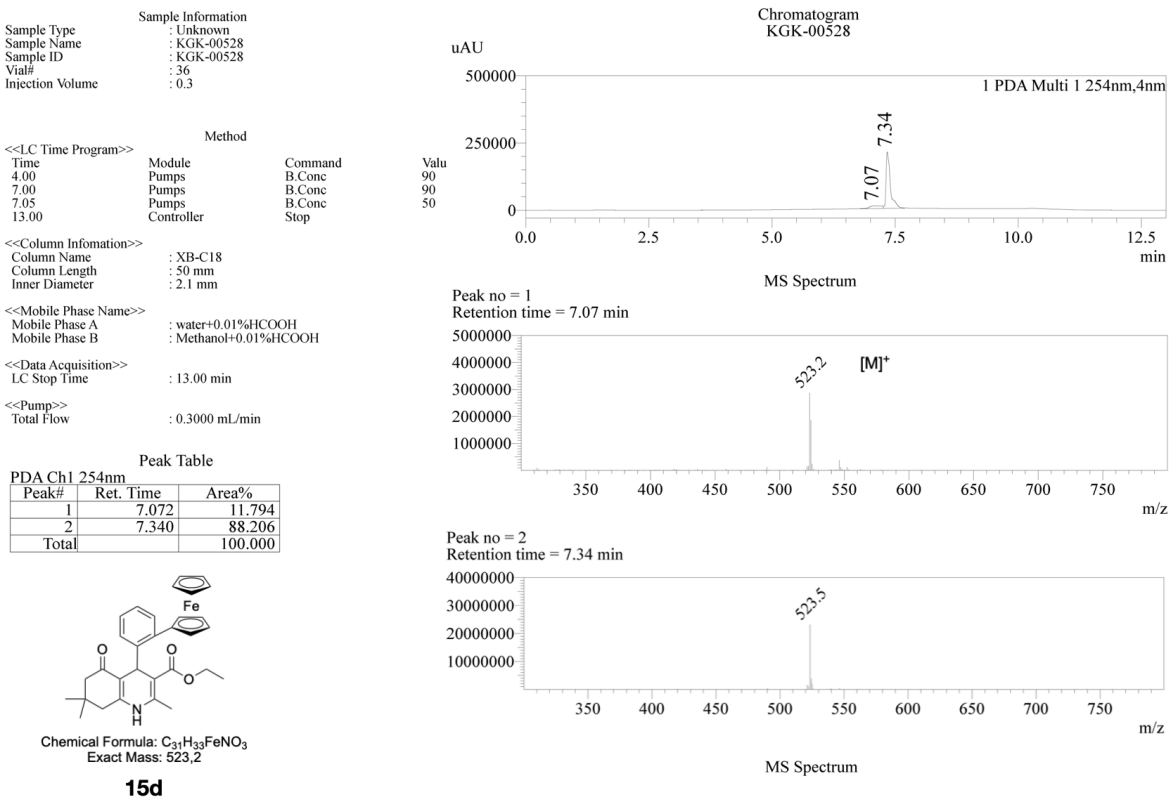

Figure S57. $^{13}C\{^{1}H\}$ NMR spectrum of **15d** in DMSO-d_6

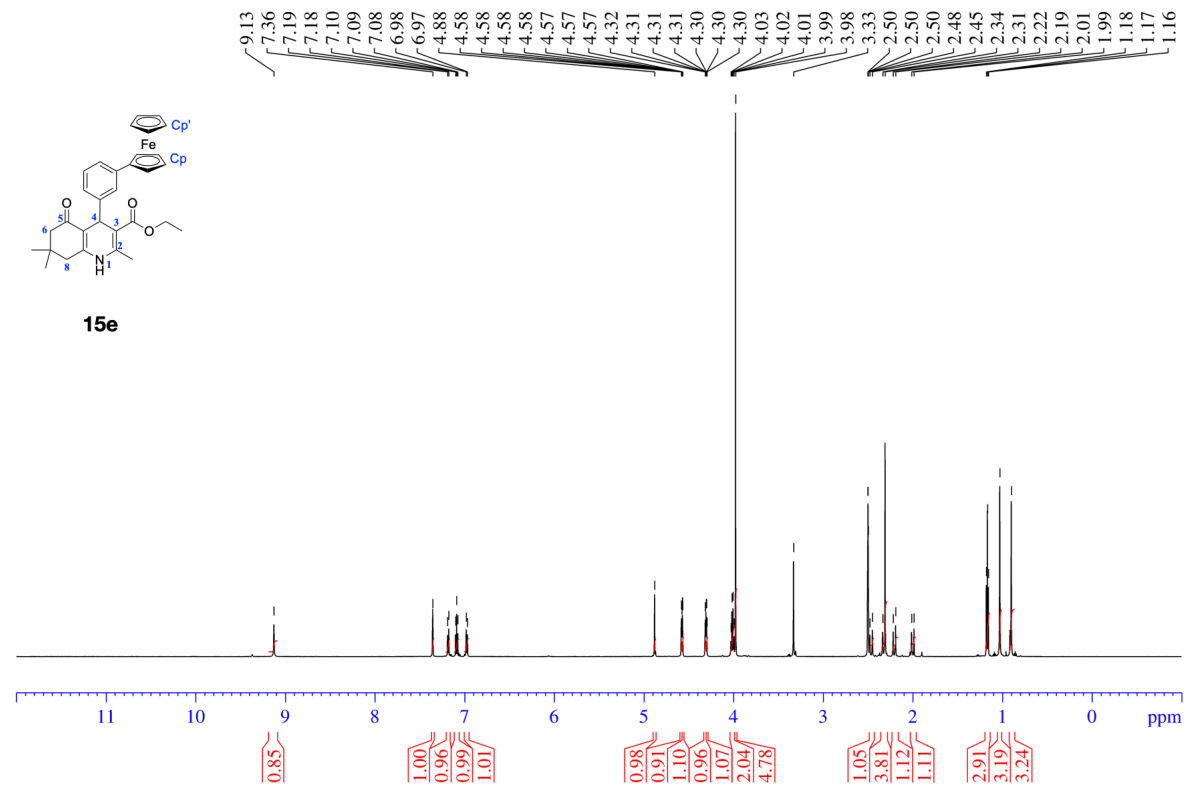

Figure S58. $^{13}C\{^{1}H\}$ NMR spectrum of **15e** in DMSO-d_6

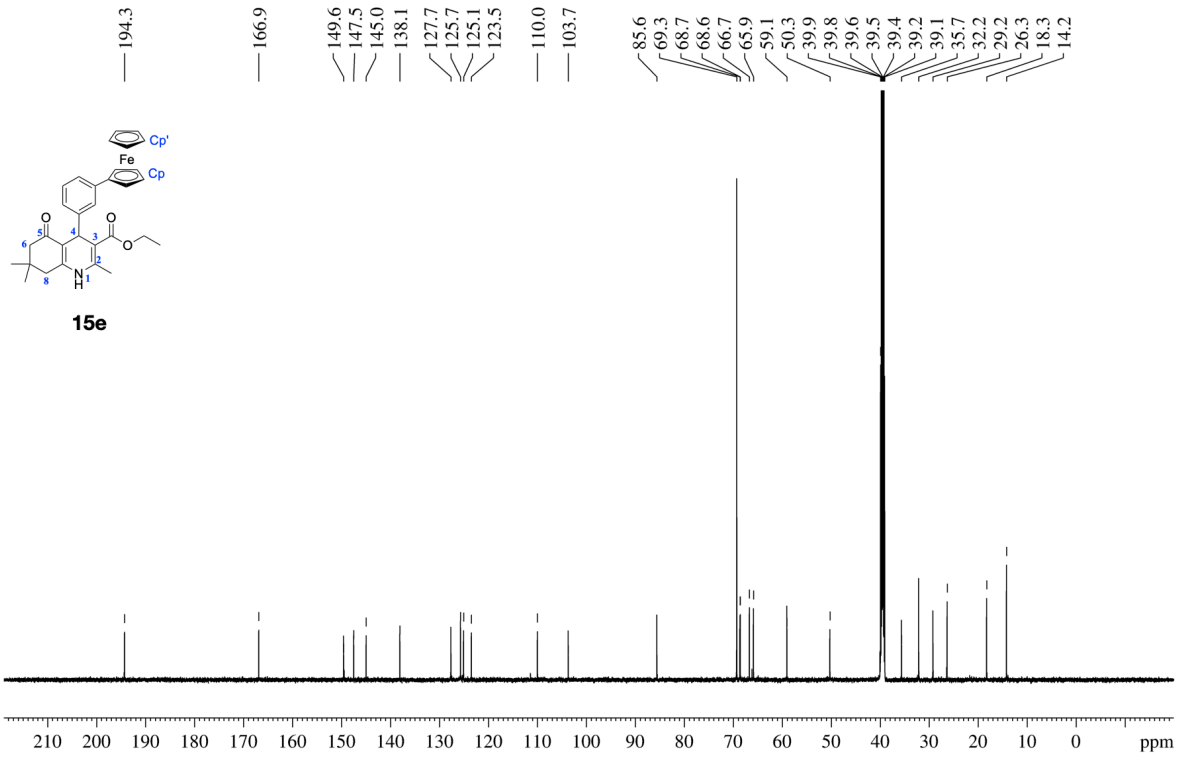

Figure S59. $^{13}C\{^{1}H\}$ NMR spectrum of **15e** in DMSO-d_6

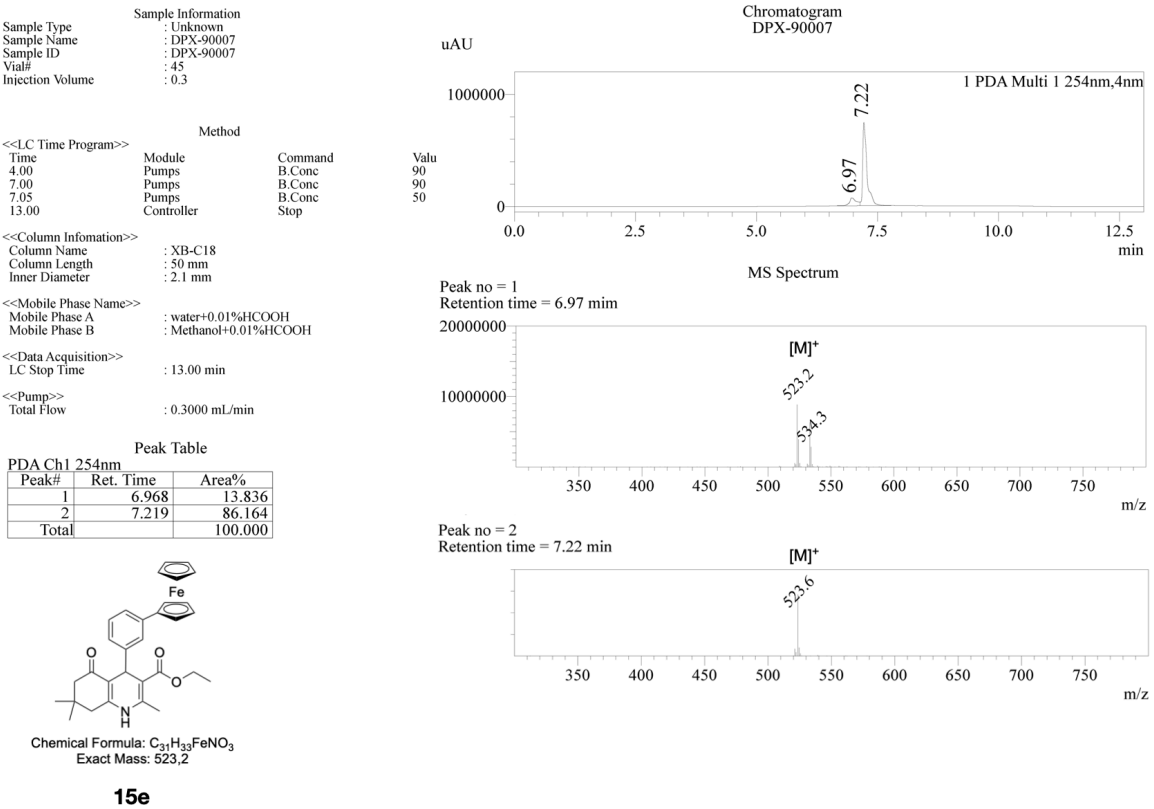

Figure S60. $^{13}C\{^{1}H\}$ NMR spectrum of **15e** in DMSO-d_6

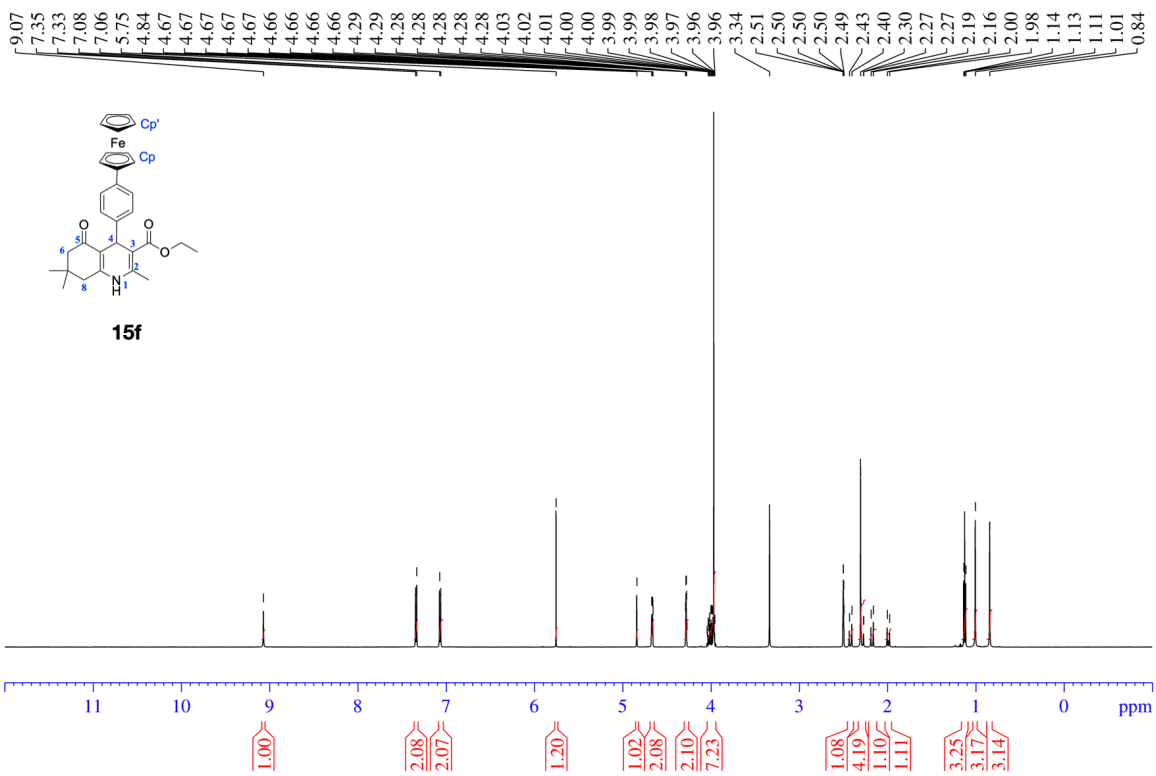

Figure S61. $^{13}C\{^{1}H\}$ NMR spectrum of **15f** in DMSO-d_6

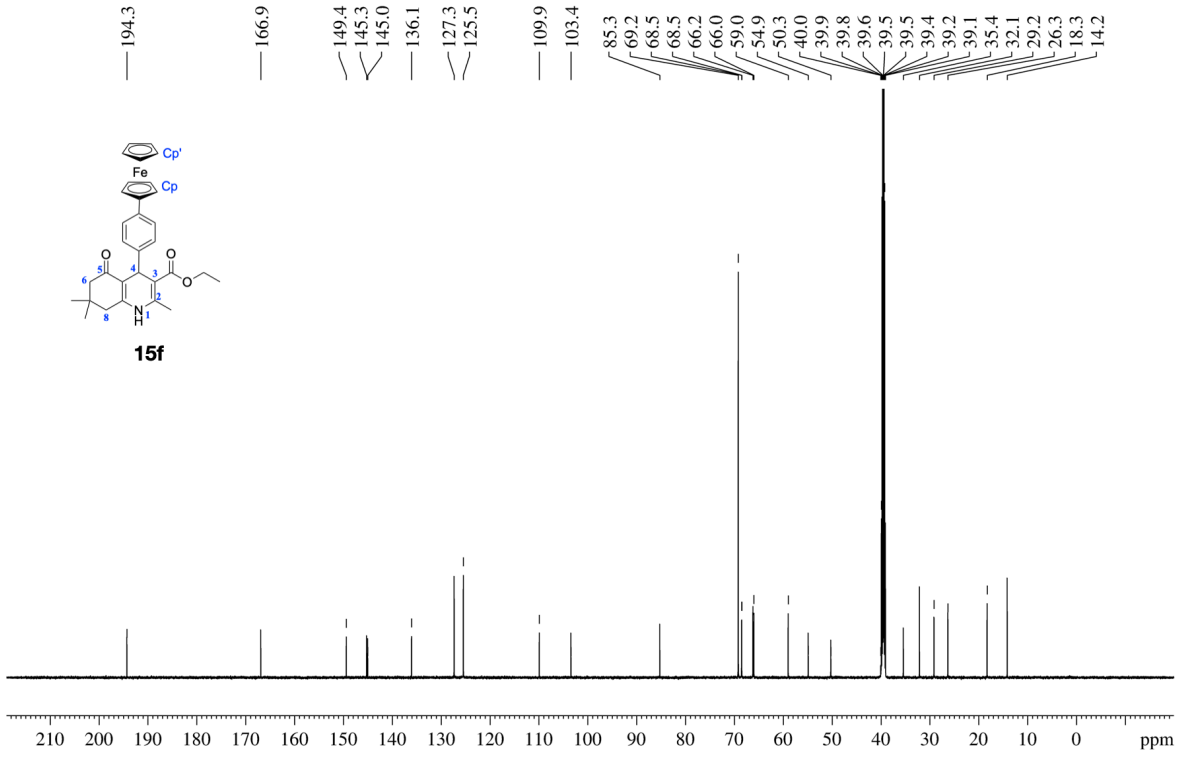

Figure S62. $^{13}C\{^{1}H\}$ NMR spectrum of **15f** in DMSO-d_6

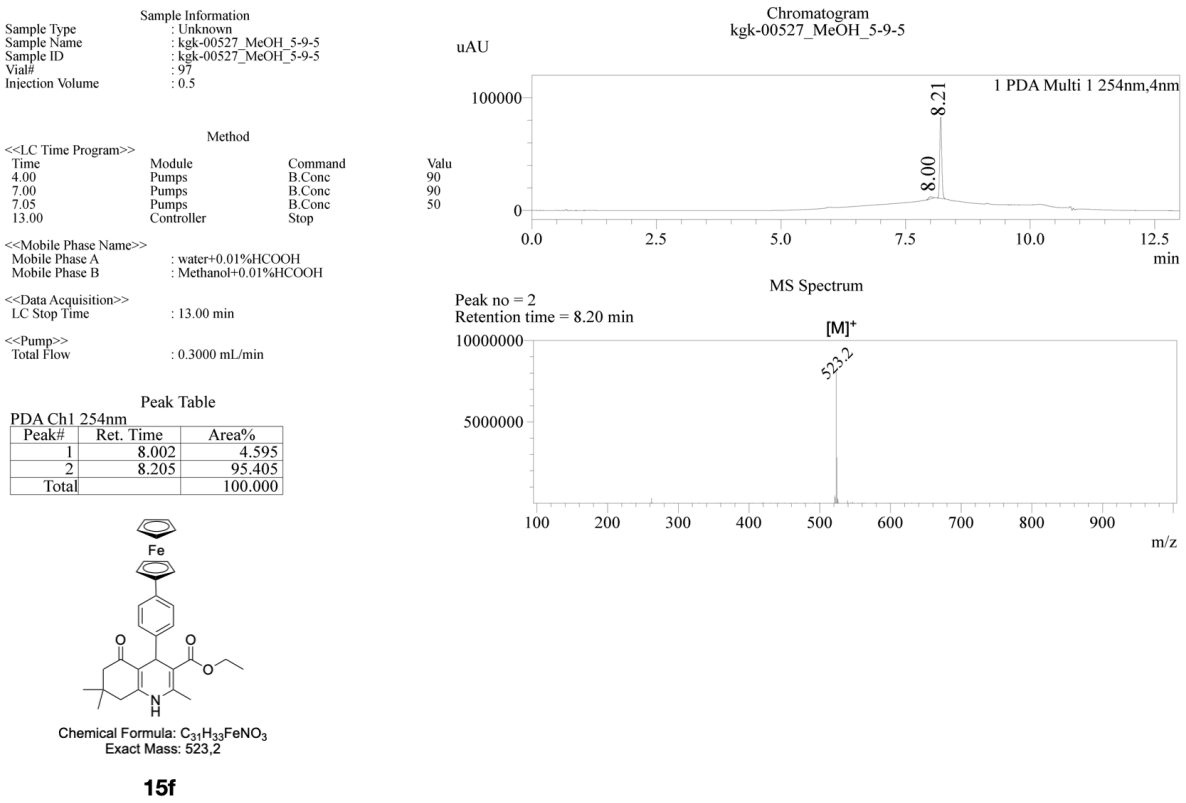

15f

Figure S63. $^{13}C\{^{1}H\}$ NMR spectrum of **15f** in DMSO-d_6

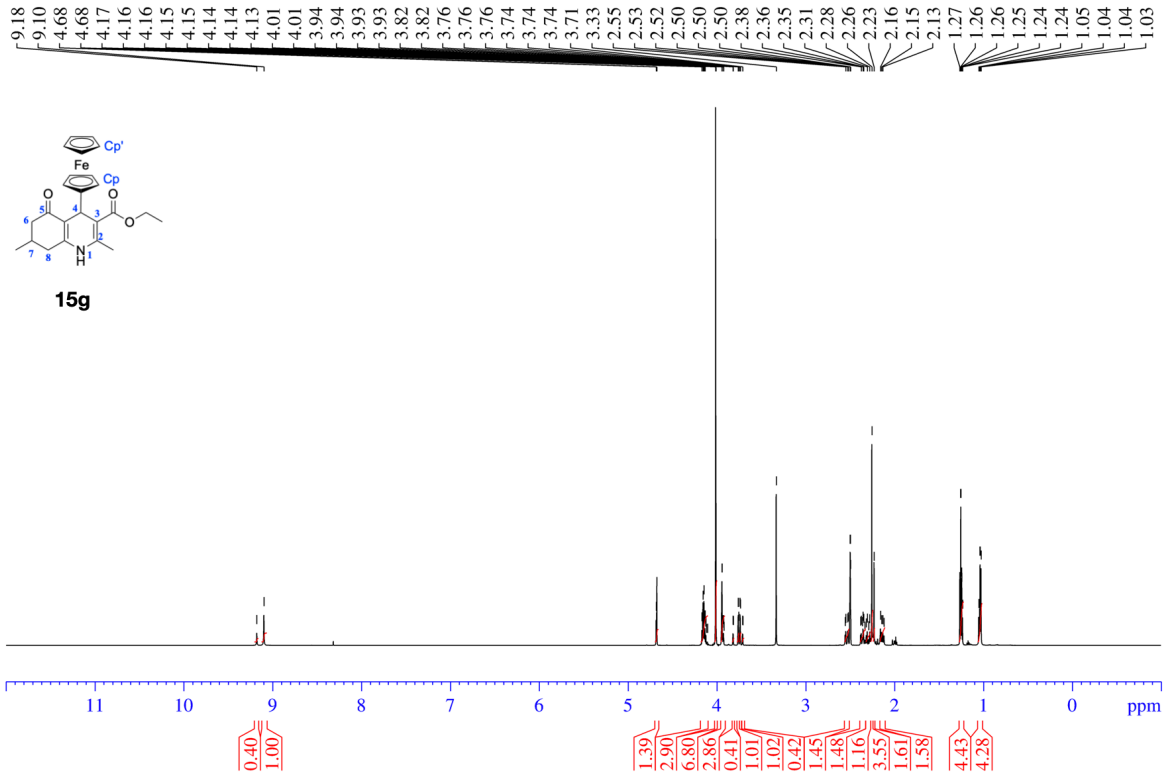

15g

Figure S64. $^{13}C\{^{1}H\}$ NMR spectrum of **15g** in DMSO-d_6

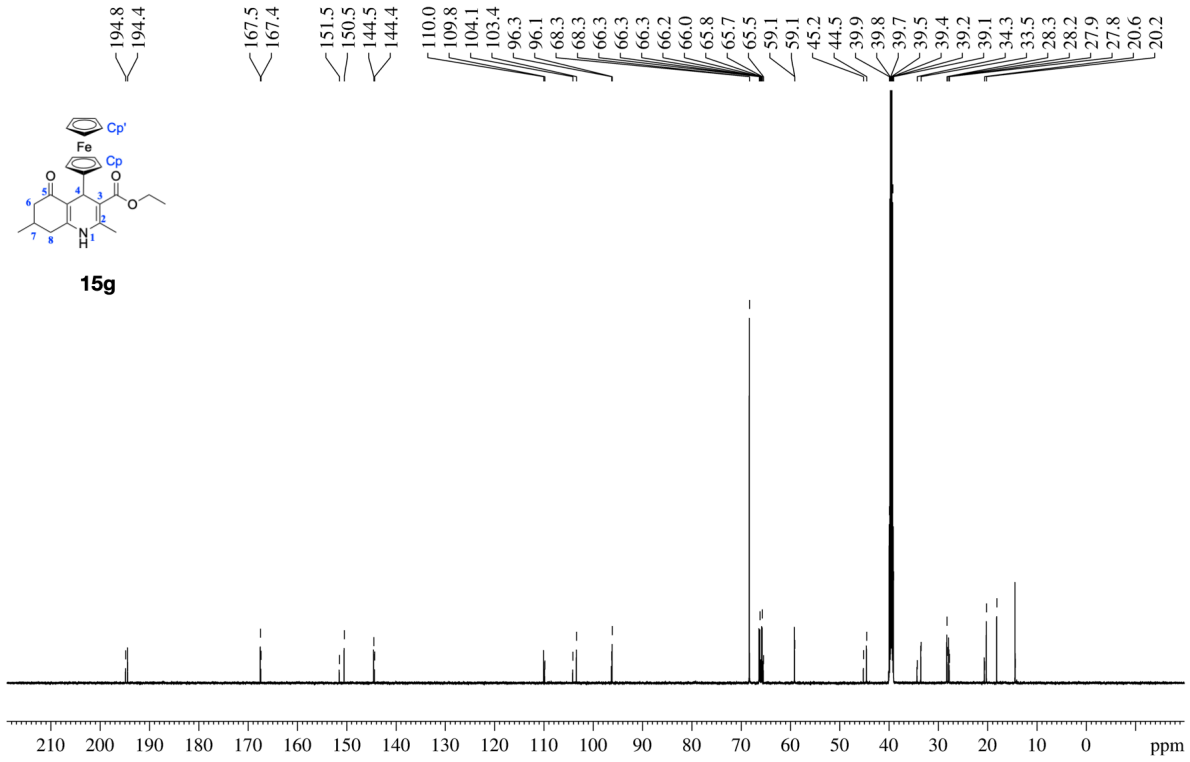

Figure S65. $^{13}C\{^{1}H\}$ NMR spectrum of **15g** in DMSO-d_6

Sample Information

Sample Type	: Unknown
Sample Name	: KGK-90018
Sample ID	: KGK-90018
Vial#	: 43
Injection Volume	: 0.3

Method

<<LC Time Program>>

Time	Module	Command	Valu
4.00	Pumps	B.Conc	90
7.00	Pumps	B.Conc	90
7.05	Pumps	B.Conc	50
13.00	Controller	Stop	

<<Column Infomation>>

Column Name	: XB-C18
Column Length	: 50 mm
Inner Diameter	: 2.1 mm

<<Mobile Phase Name>>

Mobile Phase A	: water+0.01%HCOOH
Mobile Phase B	: Methanol+0.01%HCOOH

<<Data Acquisition>>

LC Stop Time	: 13.00 min

<<Pump>>

Total Flow	: 0.3000 mL/min

Peak Table

PDA Ch1 254nm

Peak#	Ret. Time	Area%
1	5.846	8.843
2	6.097	91.157
Total		100.000

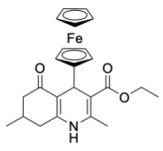

Chemical Formula: $C_{24}H_{27}FeNO_3$
Exact Mass: 433,1

15g

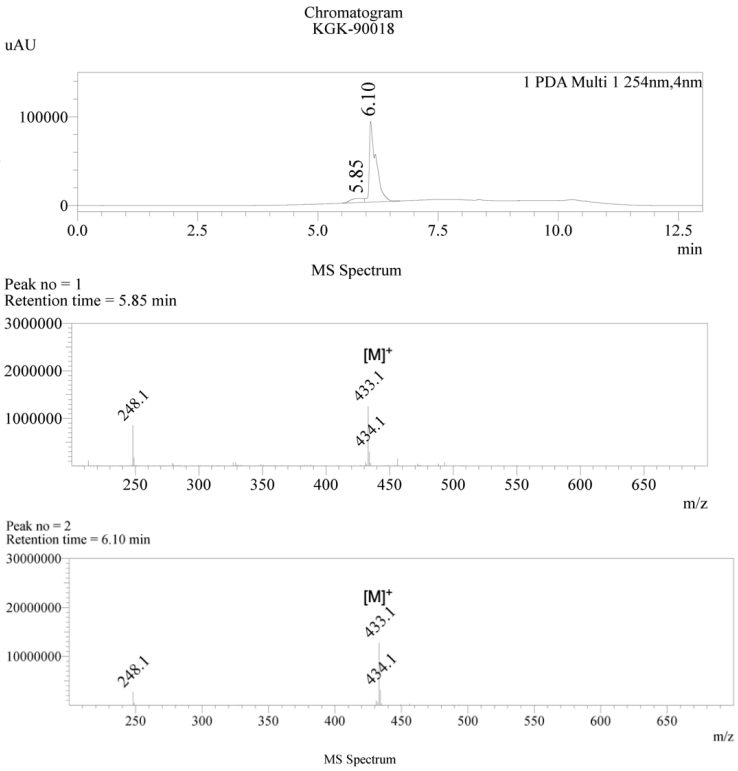

Figure S66. $^{13}C\{^{1}H\}$ NMR spectrum of **15g** in DMSO-d_6

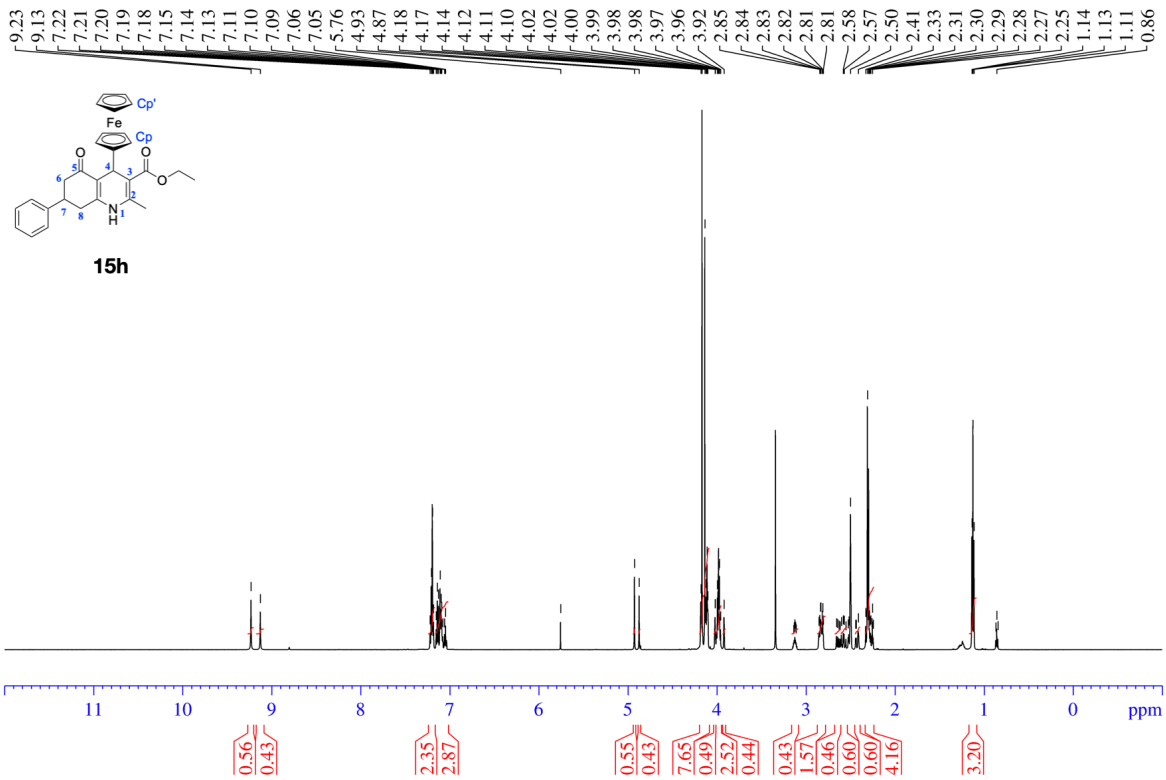

Figure S67. $^{13}C\{^{1}H\}$ NMR spectrum of **15h** in DMSO-d_6

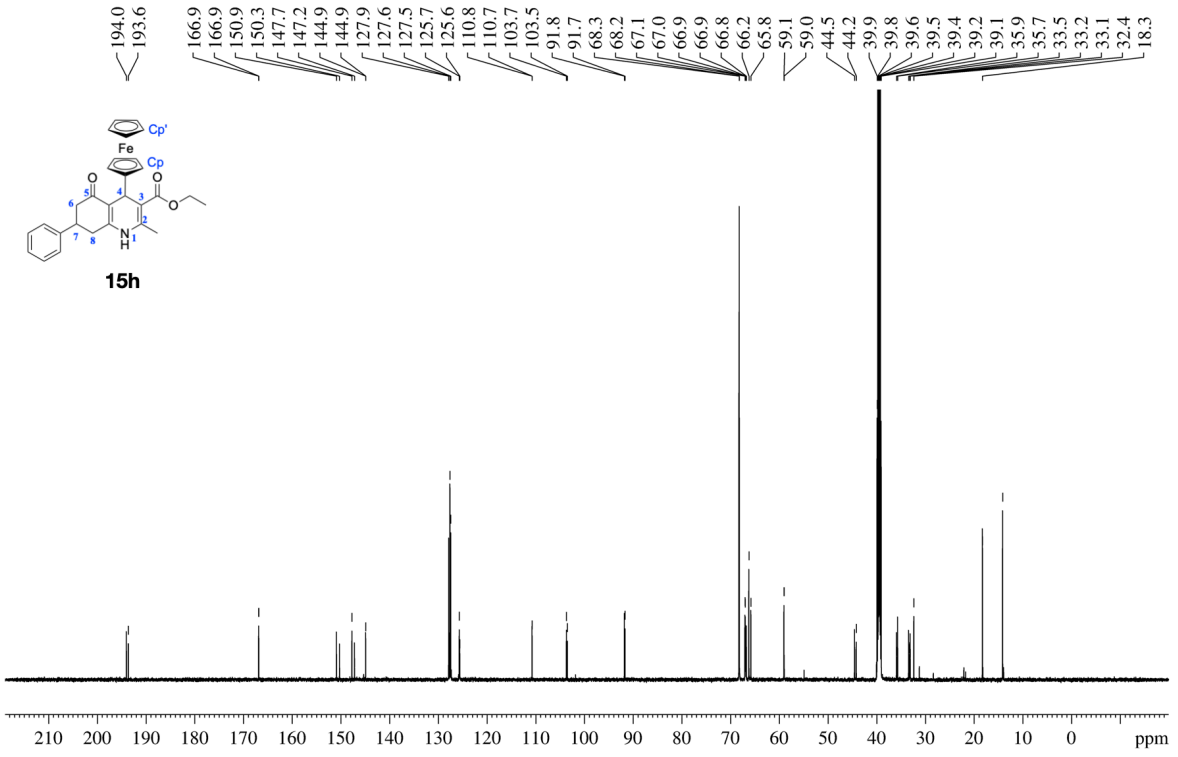

Figure S68. $^{13}C\{^{1}H\}$ NMR spectrum of **15h** in DMSO-d_6

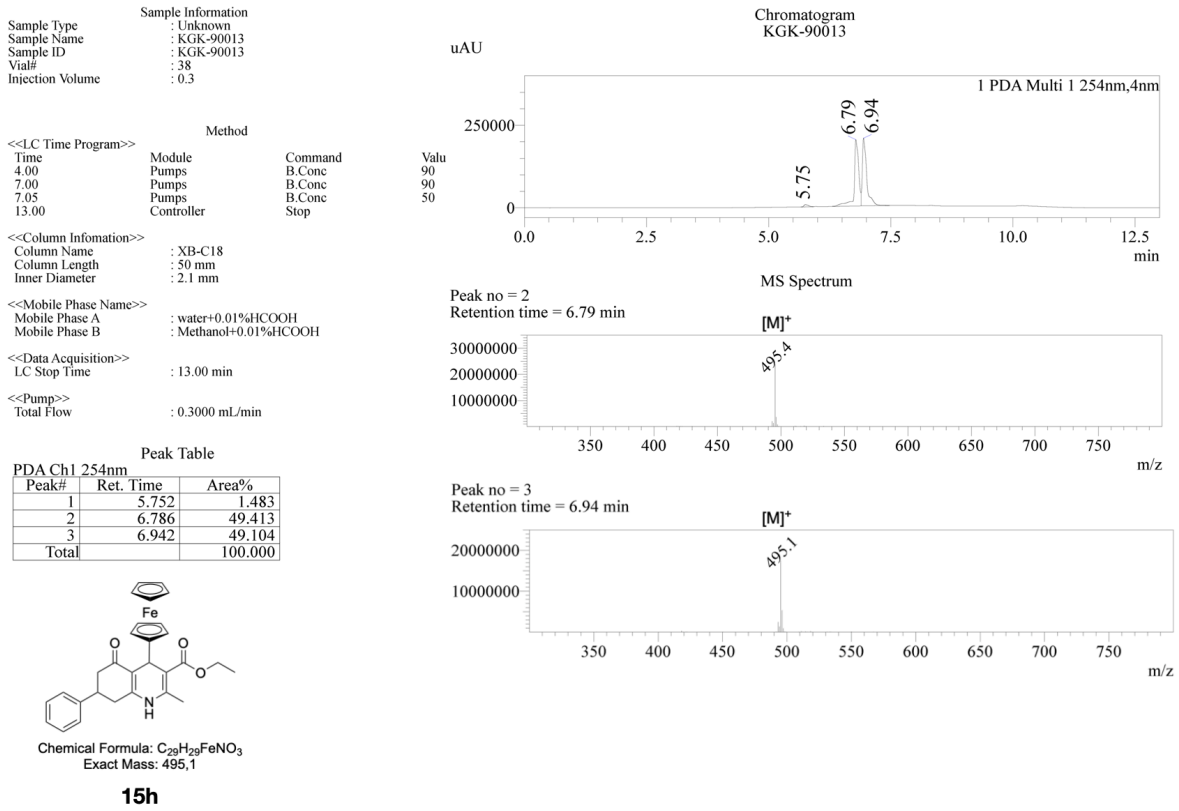

Figure S69. $^{13}C\{^{1}H\}$ NMR spectrum of **15h** in DMSO-d_6

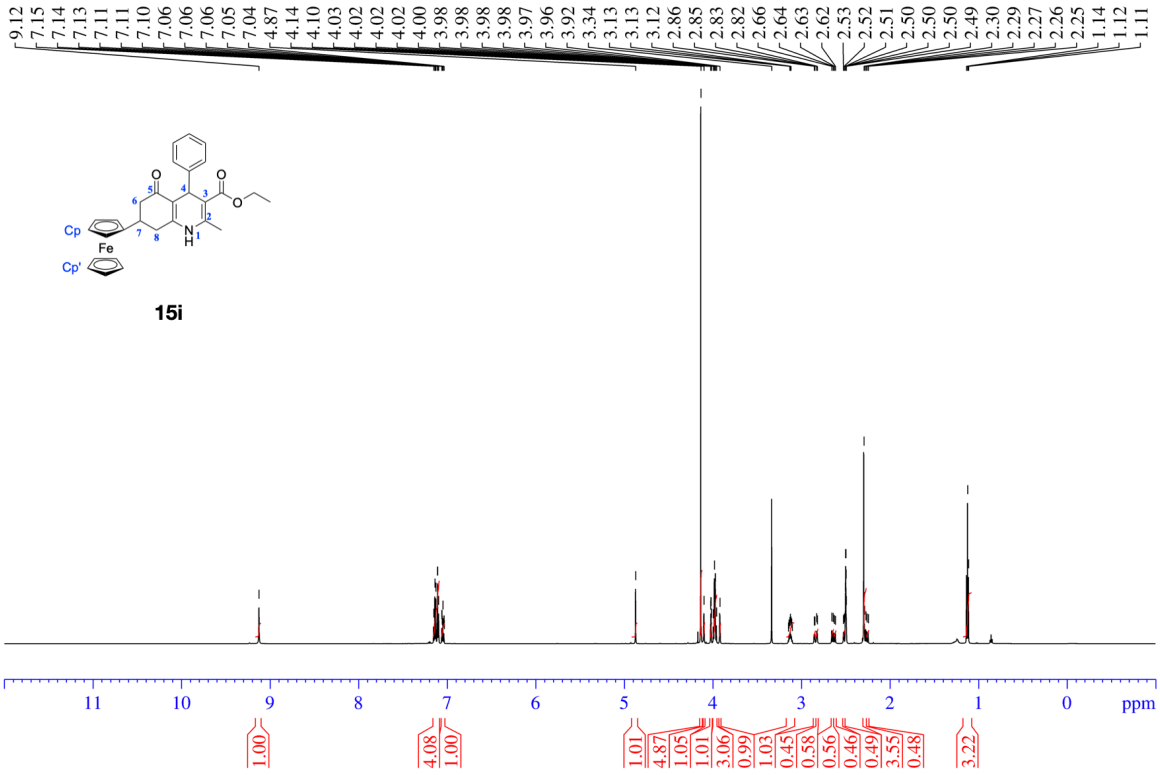

Figure S70. $^{13}C\{^{1}H\}$ NMR spectrum of **15i** in DMSO-d_6

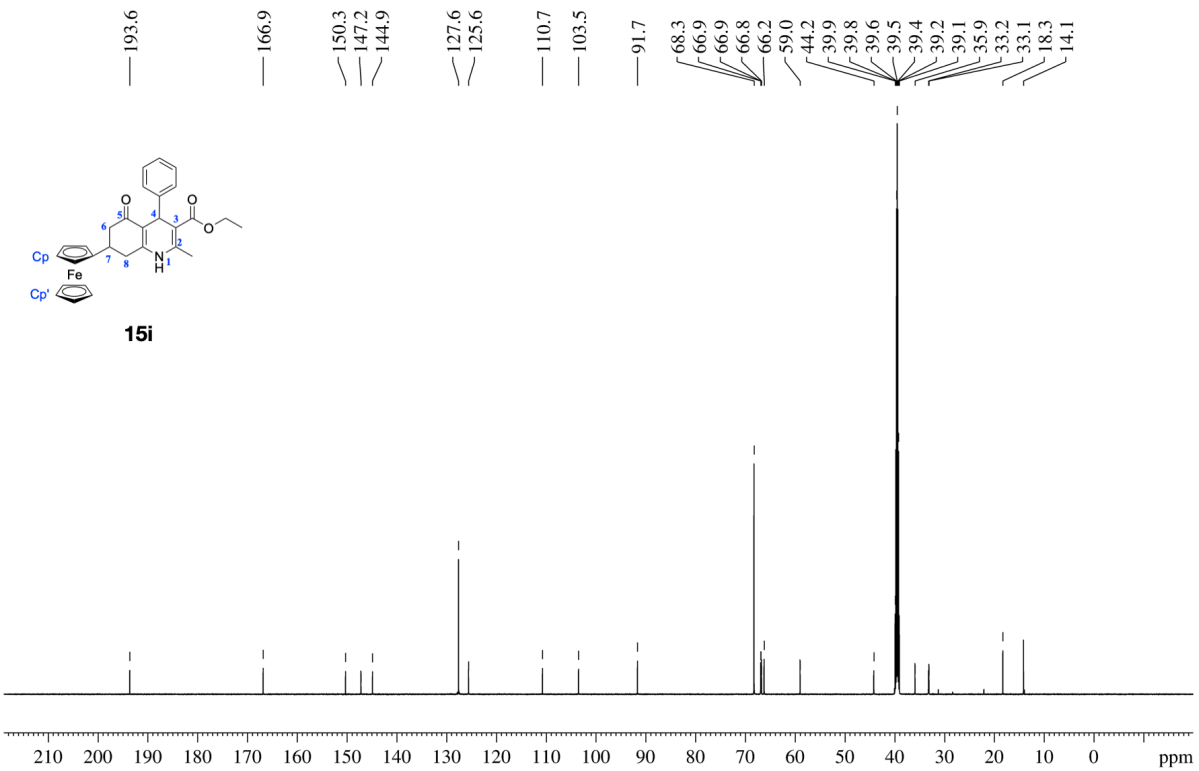

Figure S71. $^{13}C\{^{1}H\}$ NMR spectrum of **15i** in DMSO-d_6

Sample Information

Sample Type	: Unknown
Sample Name	: kgk-00545_MeOH_5-9-5
Sample ID	: kgk-00545_MeOH_5-9-5
Vial#	: 101
Injection Volume	: 0.5

Method

<<LC Time Program>>

Time	Module	Command	Valu
4.00	Pumps	B.Conc	90
7.00	Pumps	B.Conc	90
7.05	Pumps	B.Conc	50
13.00	Controller	Stop	

<<Mobile Phase Name>>

Mobile Phase A	: water+0.01%HCOOH
Mobile Phase B	: Methanol+0.01%HCOOH

<<Data Acquisition>>

LC Stop Time	: 13.00 min

<<Pump>>

Total Flow	: 0.3000 mL/min

Peak Table

PDA Ch1 254nm

Peak#	Ret. Time	Area%
1	7.770	100.000
Total		100.000

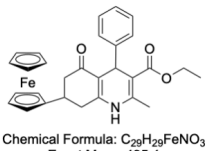

Chemical Formula: $C_{29}H_{29}FeNO_3$
Exact Mass: 495,1

15i

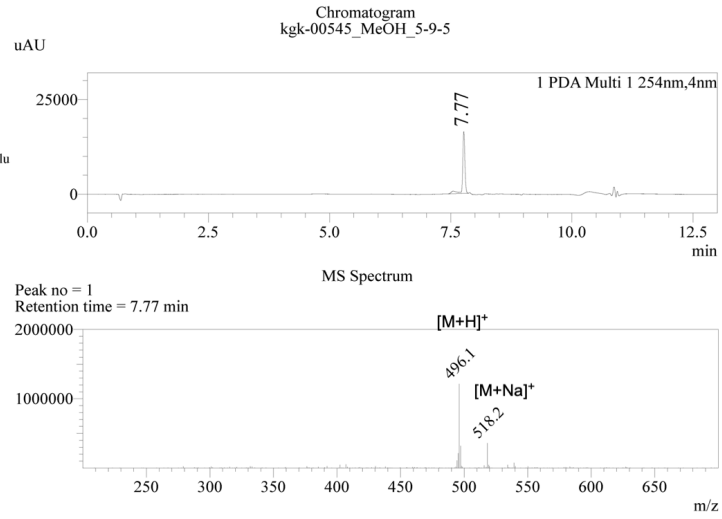

Figure S72. $^{13}C\{^{1}H\}$ NMR spectrum of **15i** in DMSO-d_6

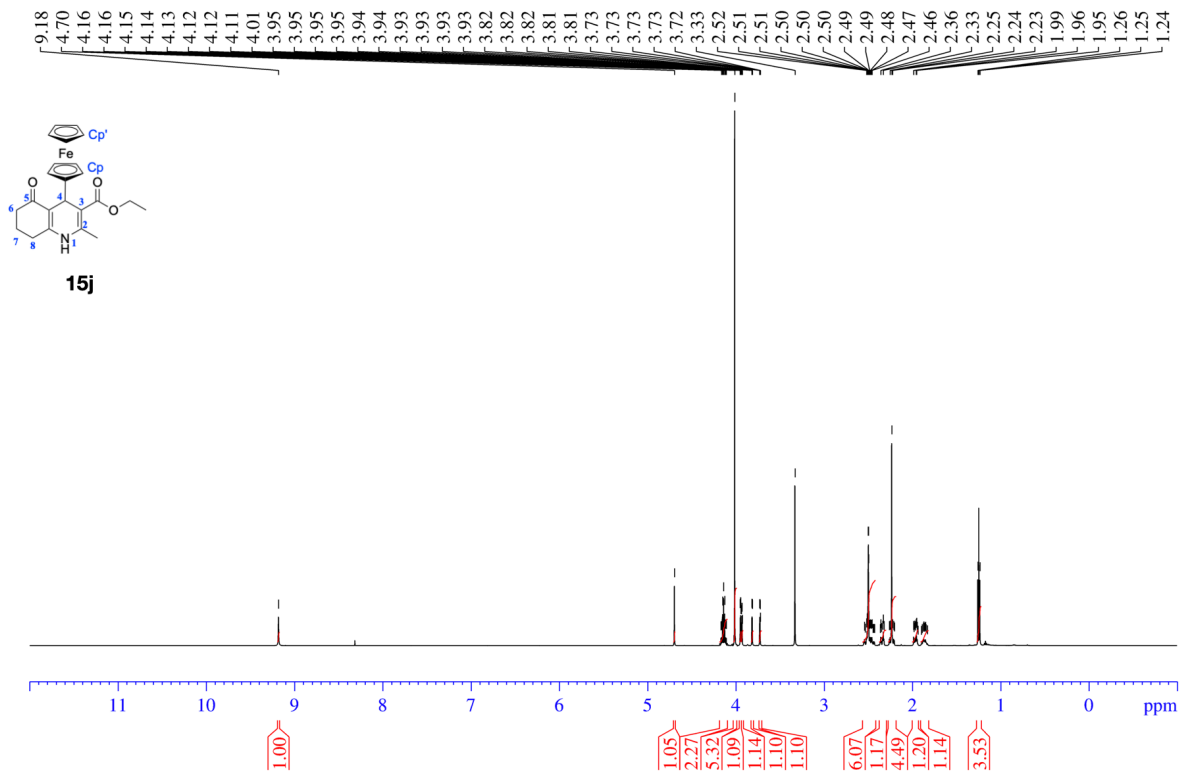

Figure S73. $^{13}C\{^{1}H\}$ NMR spectrum of **15i** in DMSO-d_6

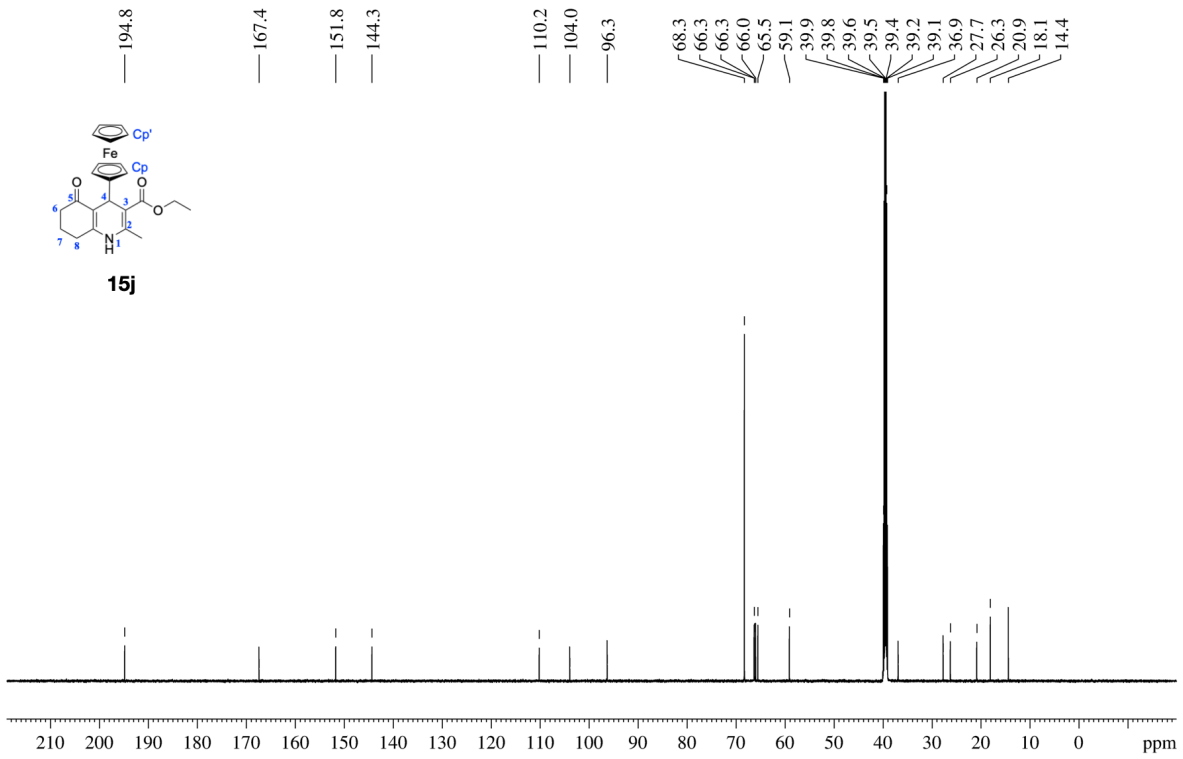

Figure S74. $^{13}C\{^{1}H\}$ NMR spectrum of **15j** in DMSO-d_6

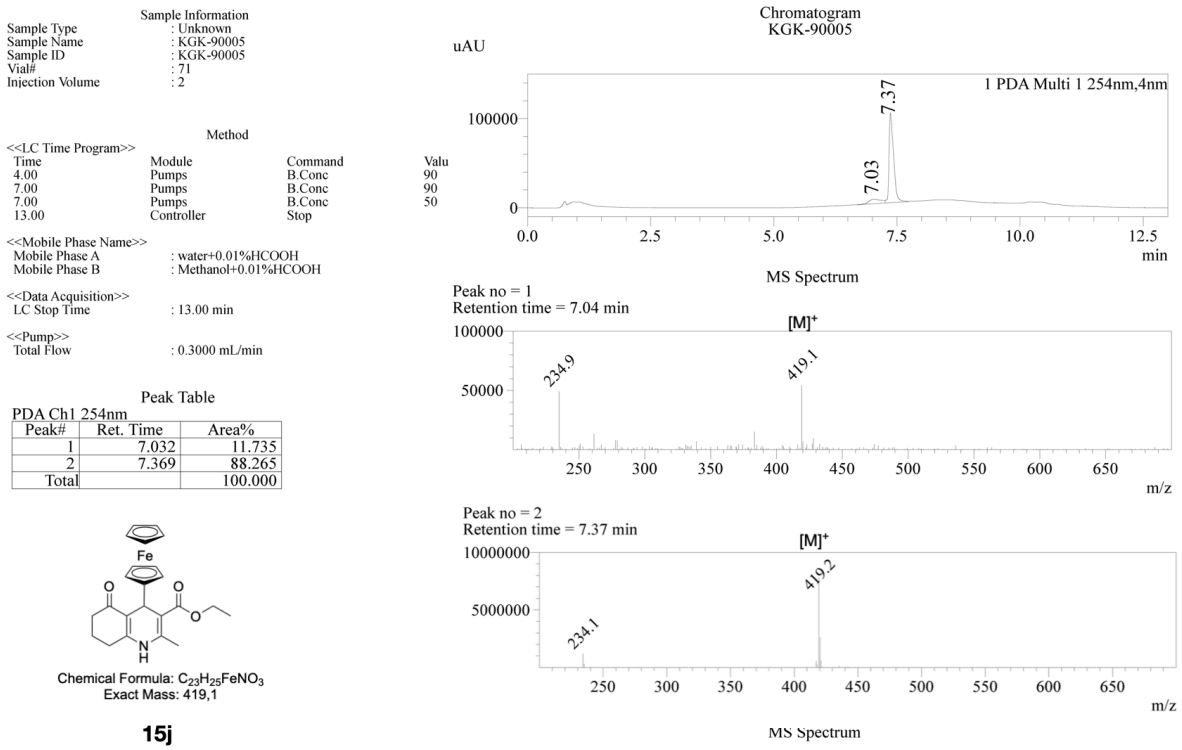

Figure S75. $^{13}C\{^{1}H\}$ NMR spectrum of **15j** in DMSO-d_6

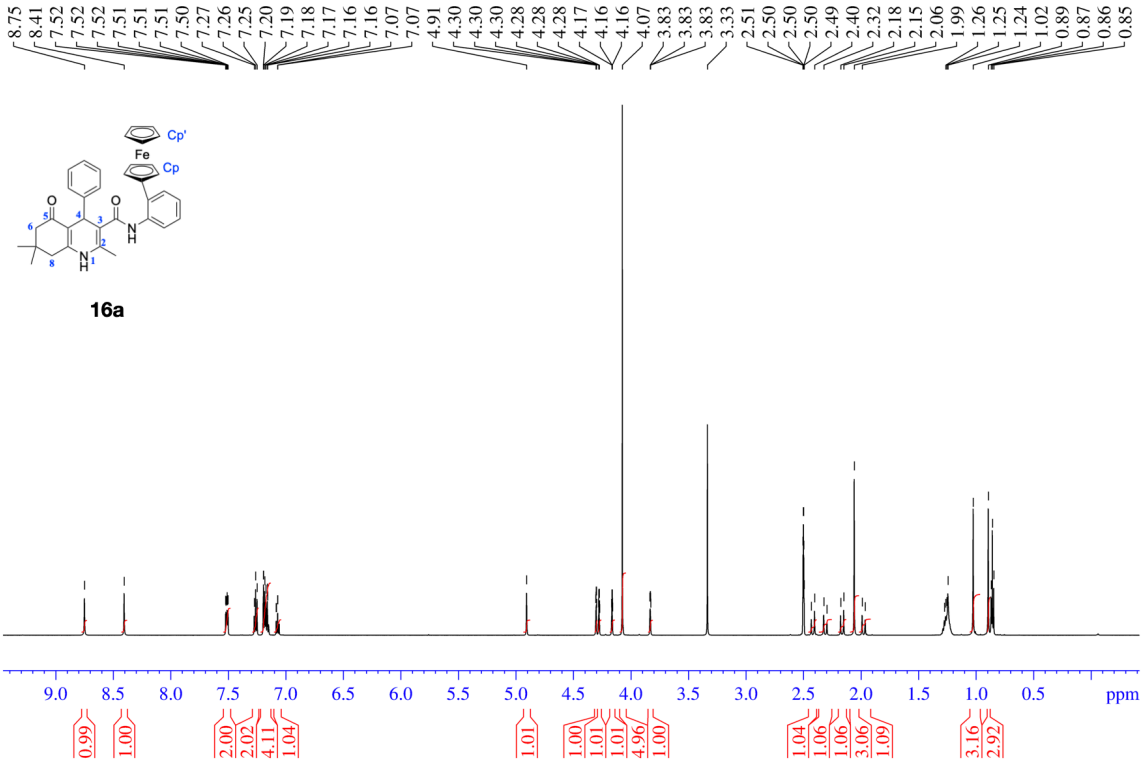

Figure S76. $^{13}C\{^{1}H\}$ NMR spectrum of **16a** in DMSO-d_6

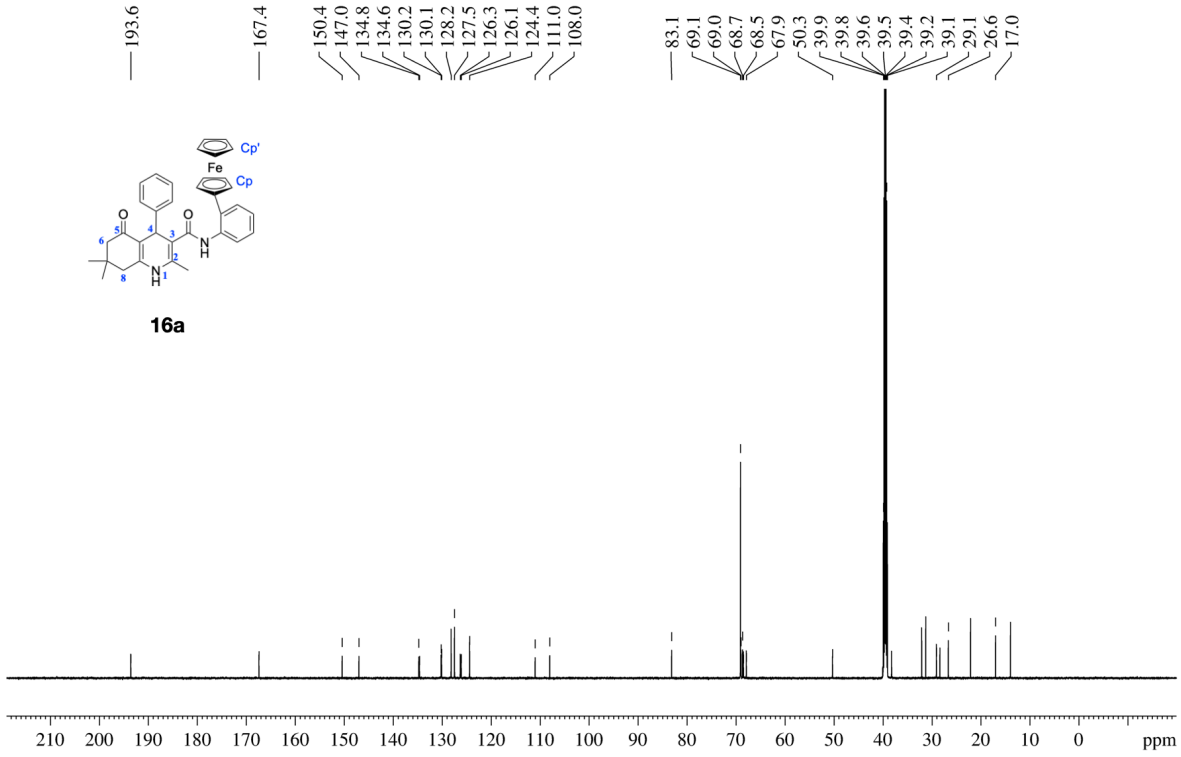

Figure S77. $^{13}C\{^{1}H\}$ NMR spectrum of **16a** in DMSO-d_6

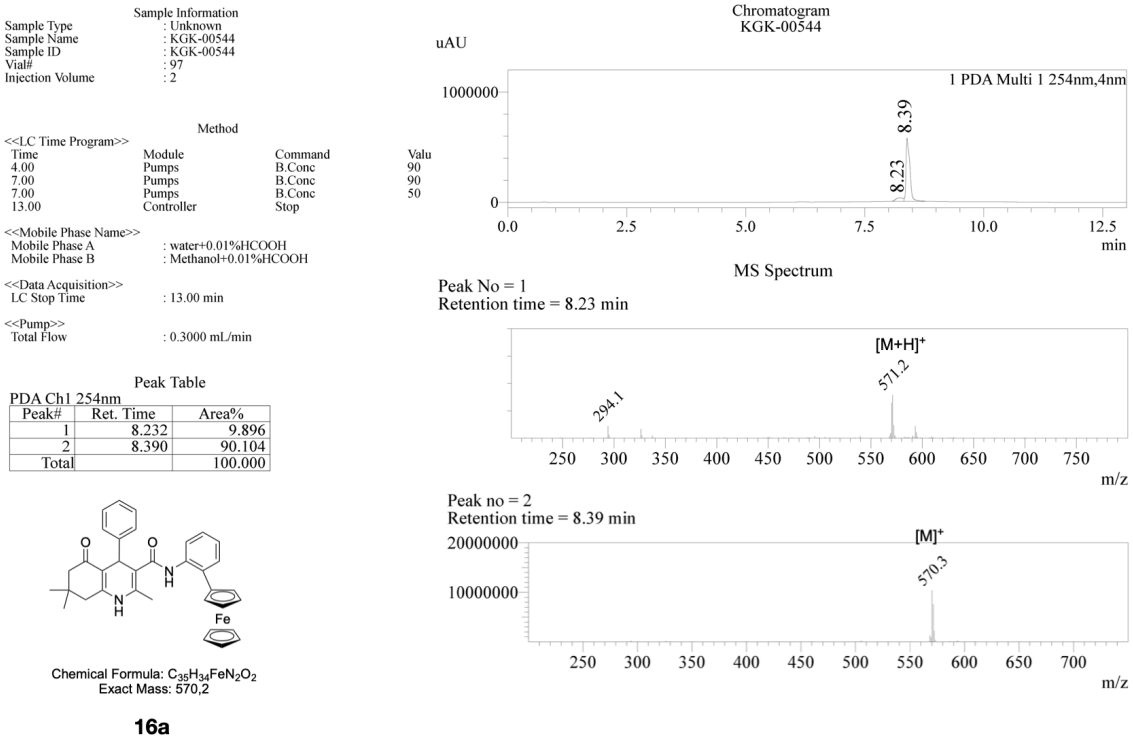

Figure S78. $^{13}C\{^{1}H\}$ NMR spectrum of **16a** in DMSO-d_6

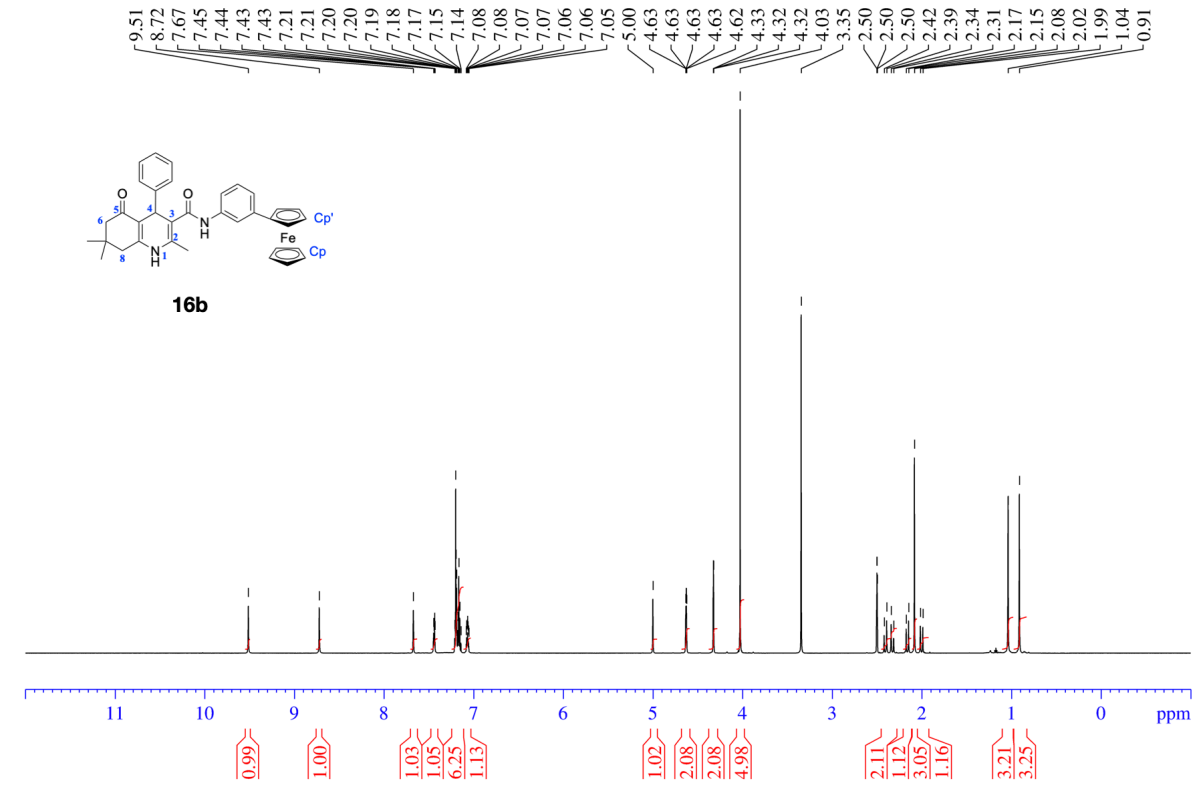

Figure S79. $^{13}C\{^{1}H\}$ NMR spectrum of **16b** in DMSO-d_6

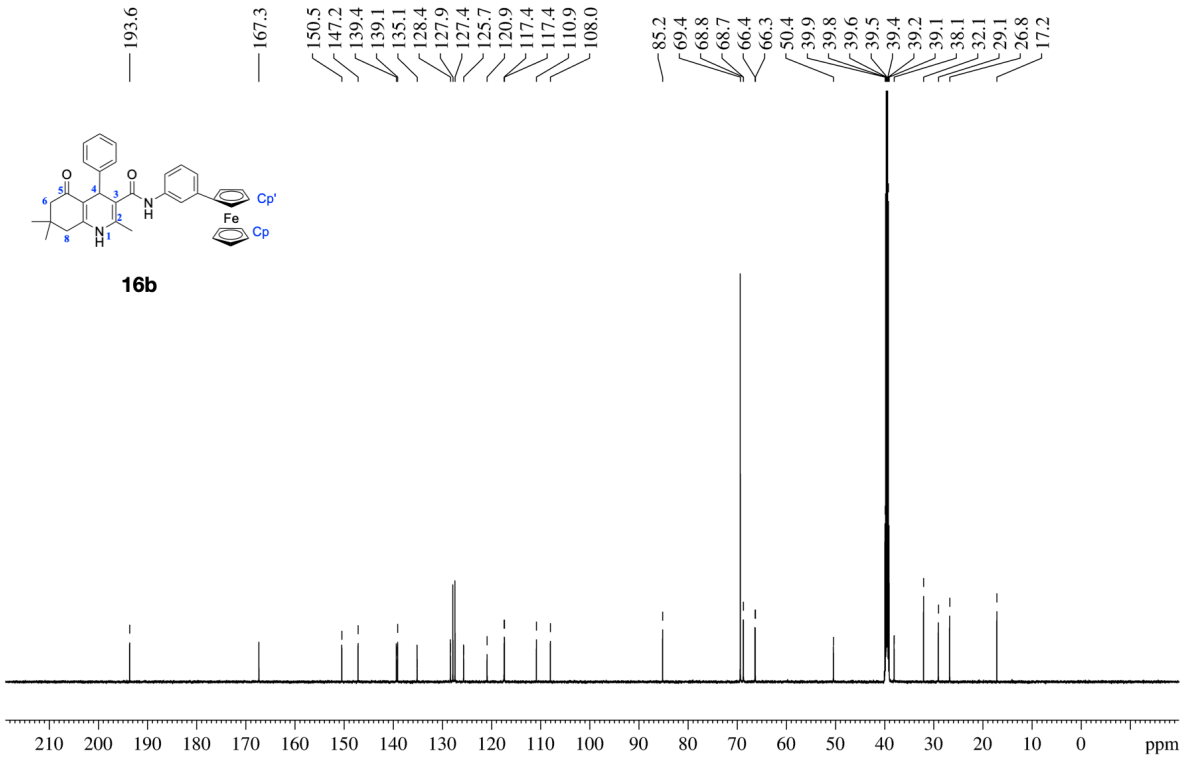

Figure S80. $^{13}C\{^{1}H\}$ NMR spectrum of **16b** in DMSO-d_6

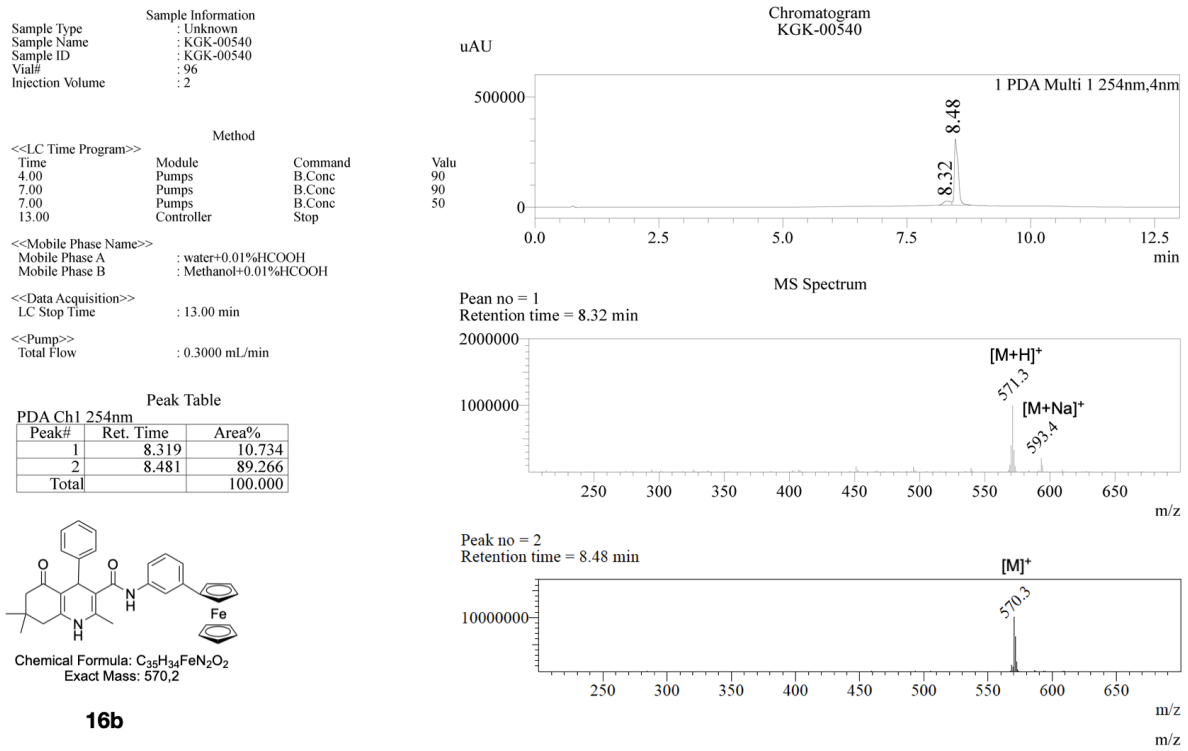

Figure S81. $^{13}C\{^{1}H\}$ NMR spectrum of **16b** in DMSO-d_6

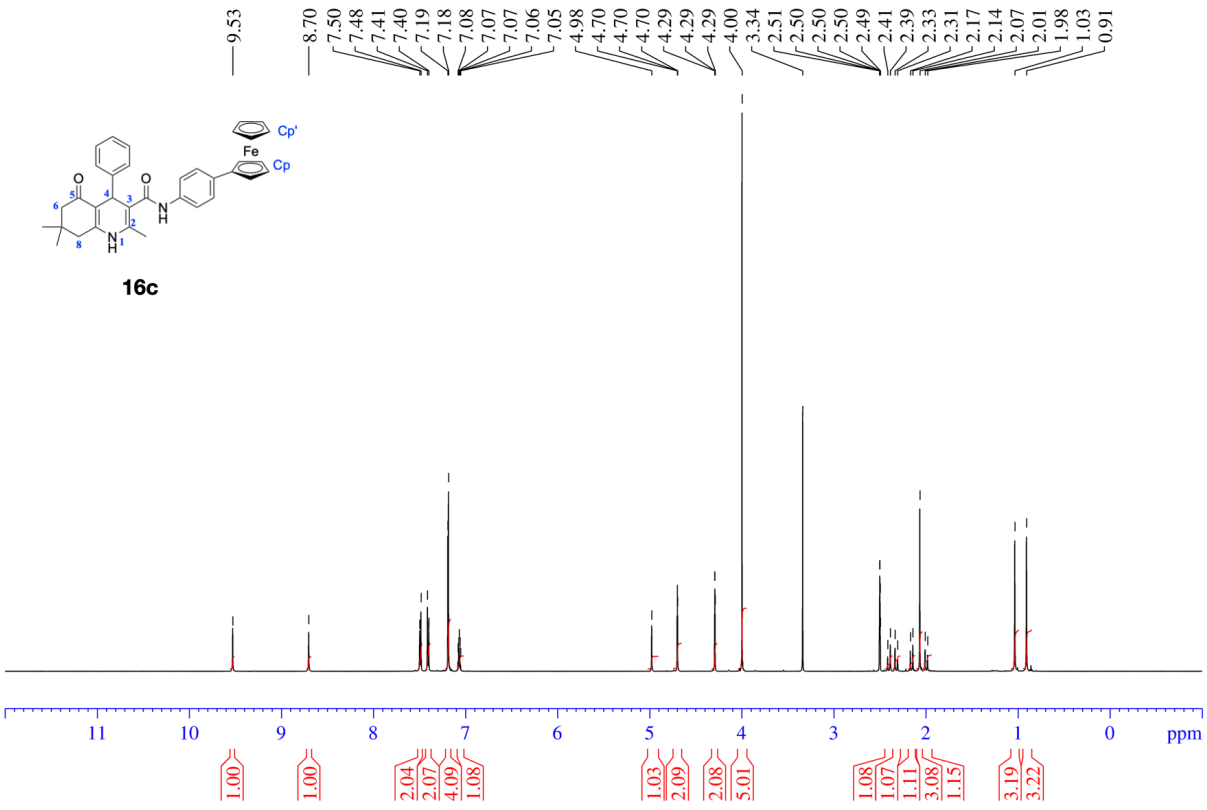

Figure S82. $^{13}C\{^{1}H\}$ NMR spectrum of **16c** in DMSO-d_6

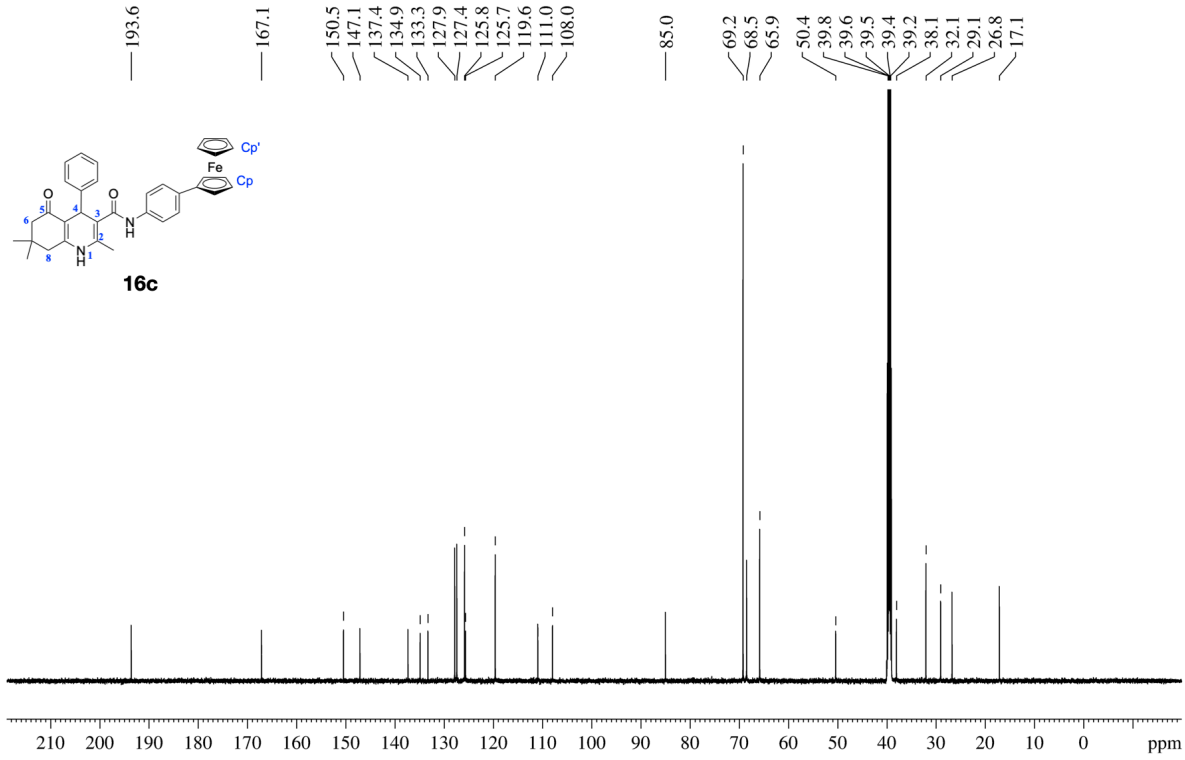

Figure S83. $^{13}C\{^{1}H\}$ NMR spectrum of **16c** in DMSO-d_6

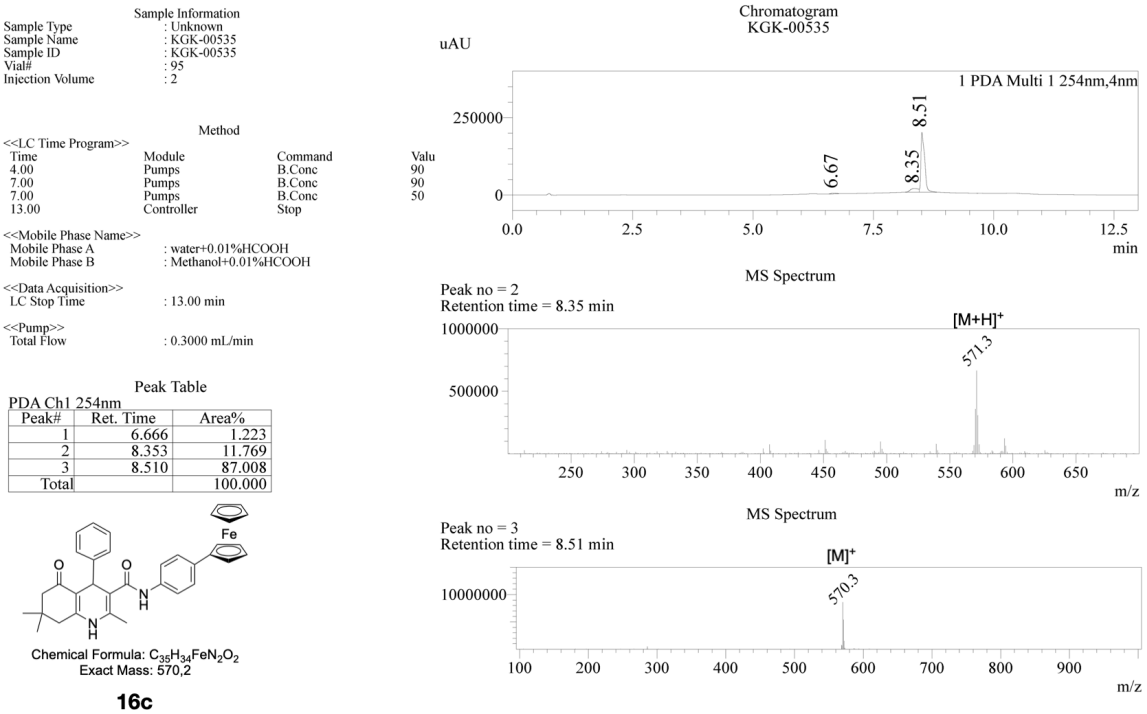

Figure S84. $^{13}C\{^{1}H\}$ NMR spectrum of **16c** in DMSO-d_6

Chemistry–A European Journal
Research Article
doi.org/10.1002/chem.202300813
Chemistry Europe
European Chemical Societies Publishing
www.chemeurj.org

Design, Synthesis, and Evaluation of Biological Activity of Ferrocene-Ispinesib Hybrids: Impact of a Ferrocenyl Group on the Antiproliferative and Kinesin Spindle Protein Inhibitory Activity

Karolina Kowalczyk,[a] Andrzej Błauż,[b] Daniel Moscoh Ayine-Tora,[c] Christian G. Hartinger,[d] Błażej Rychlik,[b] and Damian Plażuk*[a]

With the aim to combine more than one biologically-active component in a single molecule, derivatives of ispinesib and its (*S*) analogue were prepared that featured ferrocenyl moieties or bulky organic substituents. Inspired by the strong kinesin spindle protein (KSP) inhibitory activity of ispinesib, the compounds were investigated for their antiproliferative activity. Among these compounds, several derivatives demonstrated significantly higher antiproliferative activity than ispinesib with nanomolar IC_{50} values against cell lines. Further evaluation indicated that the antiproliferative activity is not directly correlated with their KSP inhibitory activity while docking suggested that several of the derivatives may bind in a manner similar to ispinesib. In order to investigate the mode of action further, cell cycle analysis and reactive oxygen species formation were investigated. The improved antiproliferative activity of the most active compounds may be assigned to synergic effects of various factors such as KSP inhibitory activity due to the ispinesib core and ability to generate ROS and induce mitotic arrest.

Introduction

Antimitotic agents are widely used for cancer chemotherapy.[1] The most important of them are taxanes and *Vinca* alkaloids, disrupting the normal dynamics of microtubules – structures playing a crucial role in mitosis – and consequently leading to cell death.[2] Due to the critical role of microtubules in many processes, also in non-dividing cells, the treatment with microtubule poisons is associated with many undesirable side effects. Therefore, compounds capable of affecting cancer cell division that will specifically inhibit the activity of other key players in mitosis are highly sought after.[3] Among various mitotic proteins, the motor proteins – kinesins – have attracted particular interest, with kinesine spindle protein (KSP, also known as Eg5 and KIF11) being a particularly promising target.[4] KSP plays a crucial role in forming the bipolar spindle in dividing cells and is virtually absent in non-dividing cells. KSP is required for transition from prophase to prometaphase and, therefore, its inhibition disrupts mitosis leading to mitotic arrest and apoptosis.[4a] The discovery of the first low-molecular-weight KSP inhibitors, such as *S*-trityl-L-cysteine[5] and monastrol,[6] initiated an extensive search for other Eg5 inhibitors.[7] KSP modulators with a variety of structures, for example, ispinesib, SB-743921,[8] MK-0731,[9] ARY-520,[10] K858[11] and others, have been reported.[12] Ispinesib is a small-molecule inhibitor of KSP ATPase activity, exhibiting high selectivity for KSP over other kinesins.[13] Ispinesib has been extensively studied in 16 phase I/II clinical trials, both as monotherapy and in combination therapies.[12a] Although none of the kinesin inhibitors has been approved for clinical use yet, searching for new, selective and effective antimitotic compounds is an important area of research.

One method of developing new drug candidates involves the structural modification of known active compounds which can improve or alter their biological activities. The incorporation of an organometallic scaffold to tune the bioactivity of known drugs is often more beneficial than use of purely organic substituents.[14] The introduction of an organometallic motif into an organic molecule allows, for example, to utilize unusual geometries and/or reactivity of the metal center. An example of this approach involves coupling a biologically active molecule to an organometallic group, particularly a sandwich[14c,i,l,15] or a half-sandwich complex.[14f,h,16] Previous studies have shown that introducing a ferrocenyl substituent into an antimitotic molecule increases the antitumor activity of the obtained conjugates.[14e,17] Moreover, in the case of ferrocenyl analogues of paclitaxel, a significantly increased ability to induce tubulin

[a] *K. Kowalczyk, Prof. D. Plażuk*
Laboratory of Molecular Spectroscopy, Department of Organic Chemistry
Faculty of Chemistry, University of Lodz
ul. Tamka 12, 91-403 Łódź (Poland)
E-mail: damian.plazuk@chemia.uni.lodz.pl

[b] *Dr. A. Błauż, Dr. B. Rychlik*
Cytometry Lab, Department of Oncobiology and Epigenetics
Faculty of Biology and Environmental Protection, University of Lodz
ul. Pomorska 141/143, 90-236 Łódź (Poland)

[c] *Dr. D. Moscoh Ayine-Tora*
Department of Chemistry
University of Ghana, LG 56, Legon-Accra (Ghana)

[d] *Prof. C. G. Hartinger*
School of Chemical Sciences
The University of Auckland, Private Bag 92019, Auckland 1142 (New Zealand)

Supporting information for this article is available on the WWW under https://doi.org/10.1002/chem.202300813

polymerization was observed compared to the parent compound.[18] The presence of an organometallic group in podophyllotoxin aminoconjugates was responsible for revealing dual inhibitory properties affecting both tubulin polymerization and topoisomerase II activity.[19] Furthermore, replacing a phenyl group in cytotoxic plinabulin with a ferrocenyl moiety led to compounds capable of circumventing multidrug resistance caused by overexpression of ABCB1 and ABCG2 proteins.[20] We have shown that conjugating a ferrocenyl substituent to monastrol resulted in higher antiproliferative and KSP inhibitory activity.[21] We also found that half-sandwich complexes of Ru, Rh, Ir and Os featuring a 2-(1-amino-2-methylpropyl)-3-benzyl-7-chloroquinazolin-4(3H)-one ligand showed high cytotoxicity and the ability to inhibit KSP activity.[22]

These results encouraged us to investigate the effect of a ferrocenyl organometallic group on the antiproliferative activity of ispinesib and its (*S*)-enantiomer in comparison to related organic derivatives (Figure 1). We report structure-activity relationship (SAR) studies based on antiproliferative activity, impact on cell cycle, induction of reactive-oxygen species formation, molecular docking and KSP inhibitory activity.

Results and Discussion

Three types of ispinesib analogues, i.e., (*S*)- and (*R*)-**2a**–**f**, **3a**–**e** and **4a**–**f** (Figure 1) were synthesized starting from enantiomerically pure (*S*)- and (*R*)-**5**[23] or (*S*)- and (*R*)-**1**.[23] The precursors *o*-, *m*- and *p*-ferrocenylbenzaldehyde (**6b**–**d**) were obtained by oxidation of the readily available benzyl alcohols with MnO_2,[18a] while the 1-adamantanecarboxaldehyde **6f** was prepared by oxidation of 1-adamantylmethanol with pyridine chlorochromate.[24] The type I compounds (*S*)- and (*R*)-**2a**–**f** were synthesized in a reaction of amines (*S*)- or (*R*)-**5** with the corresponding aldehydes **6a**–**f** and sodium triacetoxyborohydride in 1,2-dichloroethane. We found that the reductive amination conducted at room temperature for 24 h (Procedure A) or under microwave conditions with two cycles at 120 °C for 15 min (Procedure B) led to the desired products with comparable yields (Table S1). Unfortunately, partial racemization occurred (see Figure S1 for an example of chiral HPLC analysis) when conducting the reaction in the microwave. Therefore, all compounds of type I were synthesized according to procedure A, which prevented racemization (Figure S1).

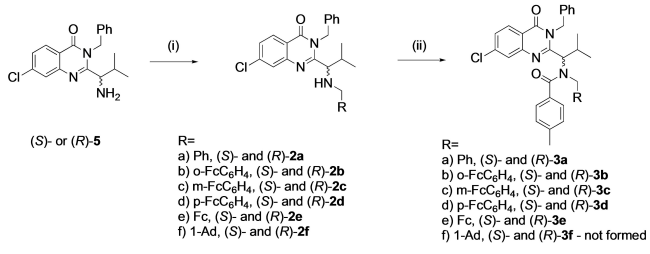

Figure 1. Three types of ispinesib analogues (**2a**–**f**, **3a**–**e** and **4a**–**f**) were designed to investigate the impact of different substituents and chirality on the biological activity.

Compounds **2a**–**f** were *N*-acylated in a reaction with *p*-toluoyl chloride in dichloromethane and DIPEA and afforded the compounds of type II, i.e., (*S*)- and (*R*)-**3a**–**e** in 20–99% yield (Scheme 1). However, the adamantyl analogues (*S*)- and (*R*)-**3f** were not formed, presumably due to the bulkiness of the adamantyl moiety.

The type III compounds (*S*)- and (*R*)-**4a**–**f** were prepared in two steps from enantiomerically pure ispinesib (*R*)-**1** and its (*S*)-enantiomer (*S*)-**1**[23] by reductive amination with aldehydes **6a**–**f** in 1,2-dichloroethane (Condition B) at 120 °C in the microwave for 15 min. This reaction was followed by treatment with sodium triacetoxyborohydride at 120 °C for another 15 min in the microwave (Scheme 2). The obtained products were fully characterized by 1D and 2D NMR, MS and elemental and HPLC-MS analysis and no racemization was observed.

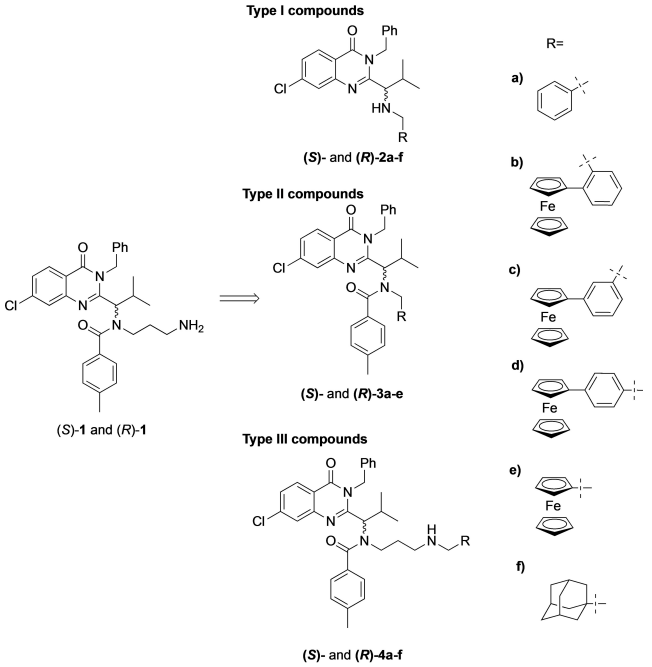

Scheme 1. Synthesis of ispinesisb analogues type I (**2a**–**f**) and type II (**3a**–**e**). Reagents and conditions: (i) 1.12 equiv RCHO (**6a**–**f**), 1.44 equiv $NaBH(OAc)_3$, 1,2-dichloroethane, RT, 24 h; (ii) 1.40 equiv *p*-toluoyl chloride, 1.2 equiv DIPEA, DCM, RT, 24 h.

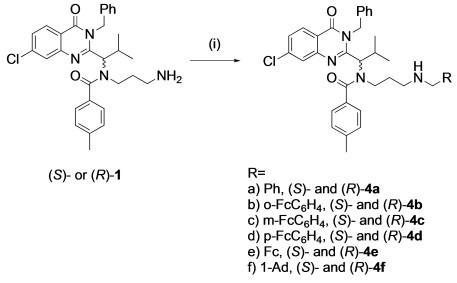

Scheme 2. Synthesis of ispinesib analogues type III (**4a**–**f**). Reagents and conditions: (i) 1.12 equiv RCHO (**6a**–**f**), 1.44 equiv $NaBH(OAc)_3$, 1,2-dichloroethane, MW, 120 °C, 15 min;

Cytotoxic activity

Using a two-step approach described previously,[19] we evaluated the antiproliferative activity of both the (*R*)- and (*S*)-enantiomers at a fixed concentration, i.e., equal to the IC_{50} value for ispinesib (*R*)-**1** and (*S*)-**1** for the respective cell lines (Figure 2).

To focus on a general pattern of activity for the investigated compounds and to avoid bias resulting from using a single cell line of specific background and often unusual biology, we decided to employ a panel of cell lines originating from different human tumors: lung carcinoma – A549, hepatocellular carcinoma – Hep G2, breast carcinoma – MCF7, and colorectal carcinoma cell lines of different staging: HCT116 (Dukes' A), SW620 (Dukes' C) and Colo 205 (Dukes' D).

Of the (*R*)-enantiomers of the type I compounds, only (*R*)-**2c** containing a *m*-ferrocenylbenzyl group demonstrated in the case of A549 and Colo 205 cells the same survival rate, a higher survival rate of about 44% in case of Hep G2 cells, or a significantly higher survival rate in the range of 18–30% for HCT116, MCF7 and SW620 cell lines compared to ispinesib. Further *N*-acylation of type I compounds (*R*)-**2a-e** led to the formation of type II molecules (*R*)-**3a**–**e** and they either showed reduced or slightly increased activity. Notably, only (*R*)-**3a** exhibited a significantly higher cytotoxicity compared to the analogous amine (*R*)-**2a**, whereas the transformation in the case of (*R*)-**3c** practically abolished its antiproliferative activity. It should be noted that all type II compounds bearing *o*-, *m*- or *p*-ferrocenylbenzyl substituents only exhibited activity comparable to that of ispinesib with survival rates in the range of 48.2-49.7% against SW620 cells. Further modification of the terminal amino group of ispinesib (*R*)-**1** (Type III compounds (*R*)-**4a**–**f**) resulted in substantially increased cytotoxicity in all cases, with kill rates exceeding 99%.

The (*S*)-enantiomers were significantly less bioactive than their (*R*) counterparts, with a few exceptions such as (*S*)-**3b** and (*S*)-**4e** in some cell lines (Figure 2). Some of the type III (*S*)-enantiomers demonstrated significantly higher activity than (*S*)-**1**, with (*S*)-**4a**, (*S*)-**4e**, and (*S*)-**4f** being the most active.

Based on the screening phase data, we selected the most active compounds, i.e., (*R*)-**2c**, (*R*)-**3c**, (*R*)-**4a-4f**, (*S*)-**4a**, (*S*)-**4e**, and (*S*)-**4f** for more detailed studies in which we determined their IC_{50} values towards a set of colon cancer cell lines, i.e., Colo 205, HCT116 and SW620, extended with a multidrug resistant (MDR), ABCB1-overexpressing variant of the latter – SW620E[25] (Table 1). The overall resistance of the cell lines towards the investigated ispinesib analogues followed the pattern Colo 205 < SW620 < HCT116 ≪ SW620E. Except for (*R*)-**3c**, all compounds exhibited higher antiproliferative activity than the corresponding ispinesib enantiomer toward non-MDR cancer cell lines. The response of the cells to the modifications of the parent compound was diverse. For example, the replacement of the 3-aminopropyl and *p*-tolyl substituents in ispinesib (*R*)-**1** with a *m*-ferrocenylbenzyl moiety in (*R*)-**2c** resulted in a 4.4-fold increased cytotoxicity (IC_{50} = 177 nM) towards HCT116 cells compared to (*R*)-**1** (IC_{50} = 848 nM) while the modification did not affect its activity in the other cell lines. However, *N*-acylation of (*R*)-**2c**, which led to (*R*)-**3c**, resulted in loss of activity towards Colo 205 and HCT116 cells while the compound remained cytotoxic towards SW620 cells (IC_{50} = 162 nM). All type III compounds derived from (*R*)-**1** were more active than the parent compound with the *p*-ferrocenylbenzyl analogue (*R*)-**4d** being the most potent derivative followed by *m*-ferrocenylbenzyl analogue (*R*)-**4c**. The antiproliferative potency of the *o*-ferrocenylbenzyl ((*R*)-**4b**), ferrocenyl ((*R*)-**4e**) and benzyl ((*R*)-**4a**) derivatives was similar. The introduction of an adamantylmethyl moiety as a bulky organic group in (*R*)-**4f** increased the cytotoxic activity compared to ispinesib, however, the effect was less pronounced than for the ferrocenyl

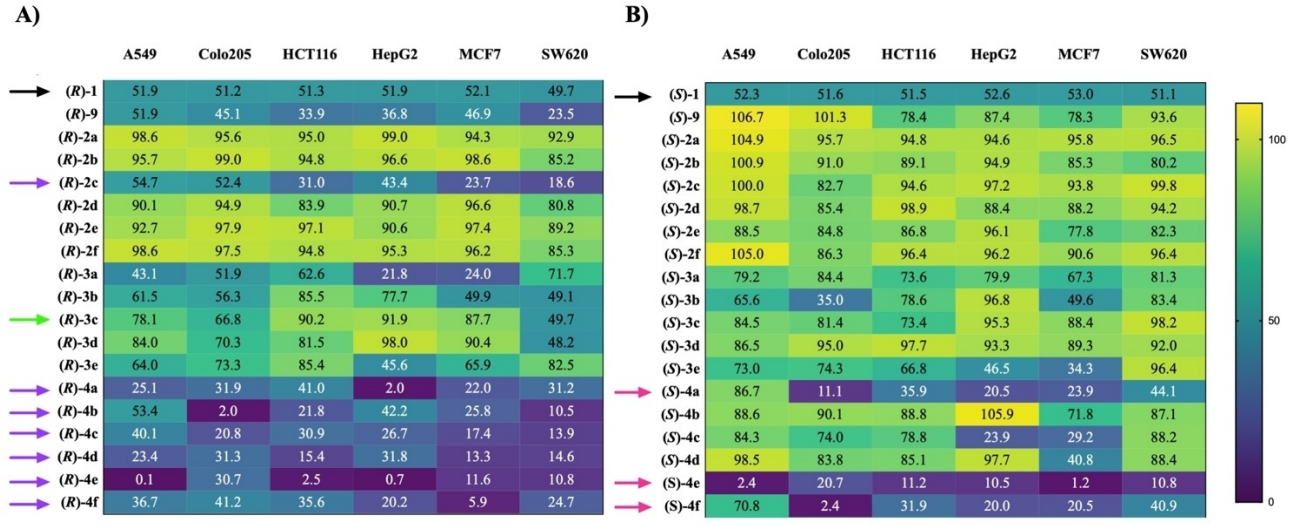

Figure 2. Averaged viability of cancer cells treated with the investigated compounds at concentrations equal to the IC_{50} values for (*R*)-**1** or (*S*)-**1**, respectively (0.20/0.76 μM for A549, 0.12/0.30 for Colo 205, 0.85/0.77 for HCT116, 0.17/0.25 for Hep G2, 0.21/0.42 for MCF7 and 0.18/0.36 for SW620), n = 3. Dispersion measures were omitted for the clarity of presentation. A) Data for (*R*)-isomers and B) for (*S*)-isomers.

Table 1. Activity (nM) of (*R*)- and (*S*)-**1** and their organic and organometallic analogues in human colorectal cancer cell lines (Exposure time 72 h; IC_{50} values and corresponding 95% confidence intervals in parentheses).

Compound	Colo 205	HCT116	SW620	SW620E
(*R*)-**1**	121	848	185	1,562
	(106–137)	(729–986)	(146–235)	(1,412–1,728)
(*R*)-**2c**	122	177	189	1,254
	(102–148)	(154–202)	(149–242)	(1,090–1,445)
(*R*)-**3c**	14,380	75,710	163	12,930
	(11,940–17,460)	(67,560–84,460)	(121–219)	(9,371–18,910)
(*R*)-**4a**	47	135	111	1,597
	(40–54)	(116–157)	(88–139)	(1,273–2,007)
(*R*)-**4b**	43	54	103	6,864
	(38–48)	(39–75)	(75–145)	(5,113–9,333)
(*R*)-**4c**	84	108	44	11,200
	(58–121)	(77–156)	(37–54)	(8,719–14,550)
(*R*)-**4d**	49	139	23	2,170
	(39–60)	(86–234)	(15–34)	(1,852–2,543)
(*R*)-**4e**	43	73	132	1,472
	(37–51)	(61–88)	(109–159)	(1,260–1,720)
(*R*)-**4f**	76	240	136	17,260
	(57–102)	(163–356)	(100–185)	(15,080–19,860)
(*S*)-**1**	305	774	355	2,734
	(251–370)	(637–943)	(317–397)	(2,269–3,311)
(*S*)-**4a**	200	691	292	918
	(164–246)	(630–759)	(260–328)	(779–1,085)
(*S*)-**4e**	122	671	127	2,084
	(103–144)	(529–857)	(108–148)	(1,806–2,406)
(*S*)-**4f**	164	704	662	7,495
	(128–212)	(564–882)	(450–985)	(6,442–8,738)

analogues. The positive effect of *N*-benzylation of ispinesib was also observed in the series of the (*S*)-enantiomers, however the impact of introducing phenyl, ferrocenyl or adamantyl substituents was lower than observed for their (*R*)-counterparts.

Unfortunately, none of the novel compounds was able to overcome the multidrug resistance of SW620E cells. The resistance index (RI, ratio of IC_{50} for SW620E to IC_{50} for SW620 for a selected compound) was usually higher for the investigated compounds than for ispinesib and its (*S*)-enantiomer (RI for (*R*)-**1** was 8.45 while it was 7.70 for (*S*)-**1**). A notable exception was the type III benzyl analogue (*S*)-**4a**, which exhibited marked activity towards the MDR cancer cell line (IC_{50} = 918 nM for (*S*)-**4a** compared to 2,734 nM for (*S*)-**1**, RI of 3.15).

Impact on the cell cycle

We investigated the compounds for their effects on the cell cycle as a coarse measure of their mechanisms of action (Figures 3 and S2 and Table 2). It was reported that ispinesib induces G_2/M arrest in cancer cells.[26] All investigated (*S*)-enantiomers exhibited a similar pattern in cell cycle distribution as (*S*)-**1** and ispinesib (*R*)-**1**. However, for the (*R*)-series of compounds, i.e. (*R*)-**3c**,**4c-f**, we observed a significantly higher reduction of the G_1 (up to 40%) and increased G_2/M (up to 46%) fractions of SW620 cells compared to ispinesib (*R*)-**1**. These results can be correlated with the elevated antiproliferative potential of the studied compounds toward SW620 cells, for example, the most antiproliferative active (*R*)-**4c–e** also induced G_2/M arrest. As expected, this effect was not observed in etoposide-resistance SW620E cells, which are significantly less sensitive toward the studied compounds, all of which caused a similar pattern of cell cycle phase distribution in SW620E cancer cells.

KSP inhibitory activity

The primary mechanism of biological activity of ispinesib is associated with its ability to inhibit KSP. Therefore, we evaluated the ability of the synthesized compounds to inhibit the KSP activity at 10 μM (Figure 4). Neither (*S*)-**1** nor its analogues demonstrated inhibitory activity at that concentration, while

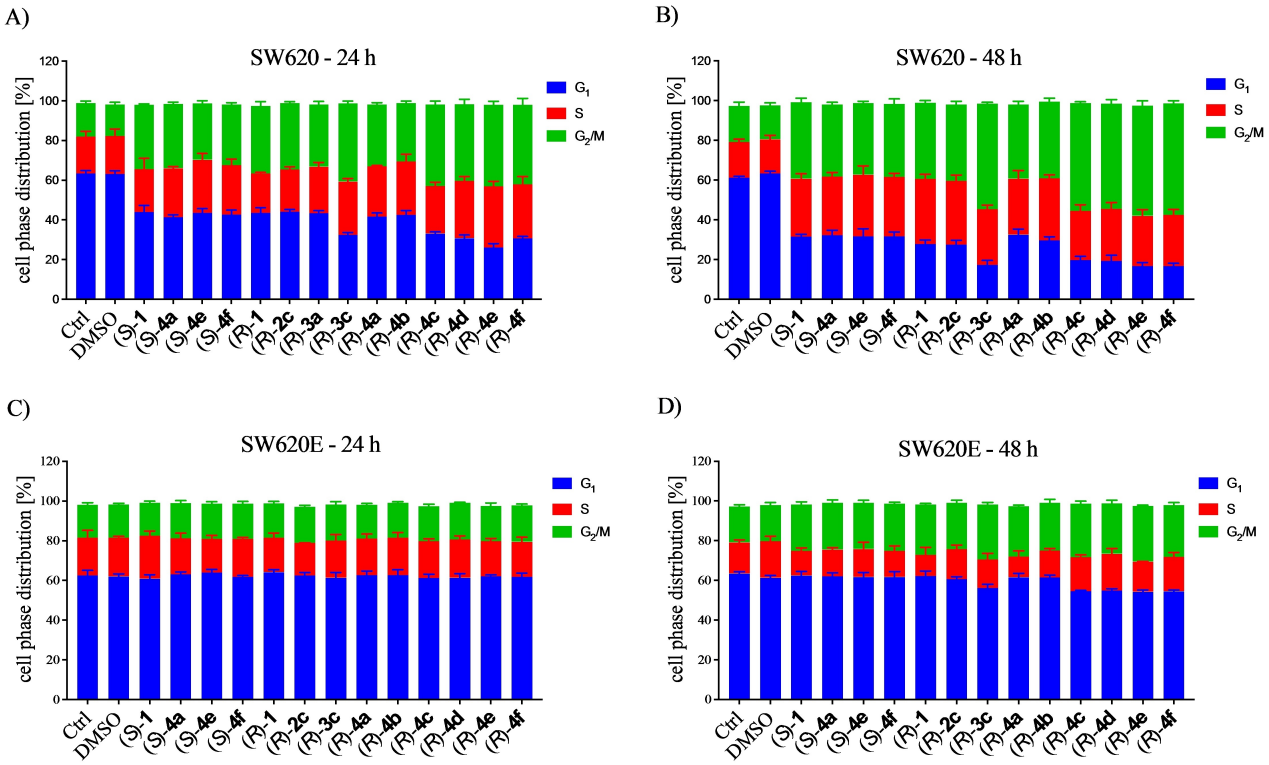

Figure 3. Cell cycle phase distribution in SW620 cells (A and B) and SW620E (C and D) exposed to (*S*)-**1** or ispinesib (*R*)-**1** and their analogues at concentrations equal to the IC_{75} values for 24 h (A and C) and 48 h (B and D). Data are presented as mean ± SEM, n = 3.

Table 2. Cell cycle phase distribution in SW620 cells exposed to (*S*)-**1** or ispinesib (*R*)-**1** and their analogues at concentrations equal to the IC_{75} values for 24 h and 48 h. Data are presented as mean ± SEM, n = 3.

Compound	24 h			48 h		
	G_1	S	G_2/M	G1	S	G_2/M
Ctrl	63.4 ± 1.5	18.6 ± 2.6	16.9 ± 0.9	61.2 ± 0.8	18.1 ± 1.4	18.2 ± 1.8
DMSO	63.2 ± 1.6	19.1 ± 3.5	15.9 ± 1.0	63.3 ± 1.2	17.2 ± 2.0	17.1 ± 1.2
(*S*)-**1**	44.0 ± 3.2	21.6 ± 5.4	32.4 ± 0.9	31.5 ± 1.2	29.2 ± 2.4	38.5 ± 2.0
(*S*)-**4a**	41.4 ± 1.2	24.7 ± 0.7	32.3 ± 0.9	32.2 ± 2.5	29.5 ± 2.0	36.3 ± 1.2
(*S*)-**4e**	43.6 ± 2.0	26.7 ± 3.2	28.4 ± 1.3	31.8 ± 3.7	30.9 ± 4.5	36.1 ± 0.9
(*S*)-**4f**	42.6 ± 2.3	25.0 ± 3.0	30.6 ± 0.9	31.7 ± 2.1	29.9 ± 1.7	36.6 ± 2.6
(*R*)-**1**	43.6 ± 2.5	19.8 ± 0.5	34.1 ± 2.1	27.8 ± 2.0	32.8 ± 2.3	38.3 ± 1.1
(*R*)-**2c**	44.1 ± 1.2	21.3 ± 1.3	33.4 ± 0.7	27.6 ± 2.2	32.1 ± 2.8	38.5 ± 1.5
(*R*)-**3c**	32.4 ± 1.2	26.9 ± 1.5	39.5 ± 1.0	17.3 ± 2.3	28.1 ± 2.0	53.1 ± 0.7
(*R*)-**4a**	41.7 ± 1.7	25.4 ± 0.3	31.1 ± 0.9	32.5 ± 2.7	28.3 ± 4.1	37.4 ± 1.6
(*R*)-**4b**	42.5 ± 2.2	26.9 ± 3.7	29.5 ± 1.0	29.7 ± 1.7	31.2 ± 1.8	38.6 ± 1.7
(*R*)-**4c**	33.1 ± 0.9	24.0 ± 1.8	41.2 ± 1.6	19.8 ± 1.8	24.7 ± 3.1	54.3 ± 0.6
(*R*)-**4d**	30.9 ± 1.5	28.8 ± 2.0	38.6 ± 2.5	19.3 ± 2.8	26.2 ± 3.1	52.9 ± 2.0
(*R*)-**4e**	26.1 ± 1.9	30.9 ± 2.5	41.1 ± 1.8	16.7 ± 1.8	25.2 ± 3.2	55.6 ± 2.4
(*R*)-**4f**	30.7 ± 1.0	27.3 ± 3.7	39.9 ± 3.3	16.7 ± 1.4	25.8 ± 2.7	56.1 ± 1.3

(*R*)-**1** exhibited high inhibitory potency. Interestingly, among the (*R*)-enantiomers, (*R*)-**2c**, (*R*)-**3a** and (*R*)-**3c** did not affect KSP activity, while (*R*)-**4b**, (*R*)-**4c** and (*R*)-**4d** demonstrated some minor effects. They reduced the KSP activity to 75–84% which was surprising in view of their high antiproliferative potential. The benzyl ((*R*)-**4a**), ferrocenylmethyl ((*R*)-**4e**), and 1-adamantymethyl ((*R*)-**4f**) ispinesib derivatives retained the ability to inhibit KSP significantly, while *o*-, m- or *p*-ferrocenyl-benzyl ((*R*)-**4b**–**d**) were significantly less potent KSP inhibitors than ispinesib.

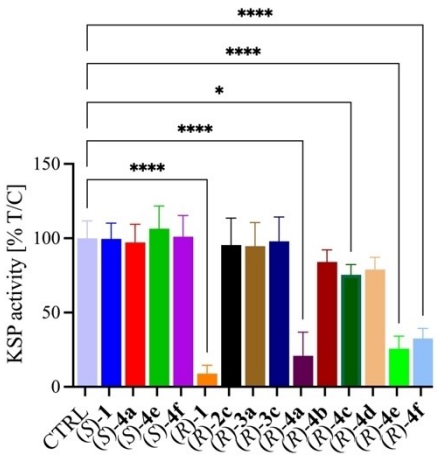

Figure 4. KSP inhibitory activity of (*S*)- and (*R*)-**1** and their analogues (10 μM). Data are presented as mean ± SEM, n = 3.

To further analyze the effects of the (*R*)-enantiomers of the type III compounds on kinesin activity, we examined their specificity towards a set of kinesins and kinesin-like proteins (Figure 5). Similarly to the parent compound, (*R*)-**4a**, (*R*)-**4e** and (*R*)-**4f** were highly specific for KSP while none of the investigated compounds affected the ATPase activity of other motor proteins.

For the most active compounds from the screening at 10 μM, we determined the KSP inhibitory activity expressed as the IC_{50} values, i.e., the concentration required to inhibit the KSP activity by 50% (Table 3). Compared to (*R*)-**1**, the investigated conjugates were 2–4 times less potent as KSP inhibitors, with the organometallic hybrid (*R*)-**4e** bearing the ferrocenylmethyl moiety exhibiting the highest KSP inhibitory activity.

All three compounds were among the most active in terms of antiproliferative potential, therefore one can infer that KSP inhibition is their dominant mode of action. However, other mechanisms are also of importance for the biological activity of these ispinesib analogues, as some poor KSP inhibitors were also highly cytotoxic.

Molecular docking

Molecules that showed promising biological activity were docked into the ispinesib binding site of KSP and compared to the results for ispinesib (*R*)-**1** and its (*S*)-enantiomer (*S*)-**1**. The docking was validated by comparing the configurations of ispinesib with the co-crystallized molecule in the crystal structures using GoldScore (GS),[27] ChemScore (CS),[28] ChemPLP,[29] and Astex statistical potential (ASP)[30] scoring

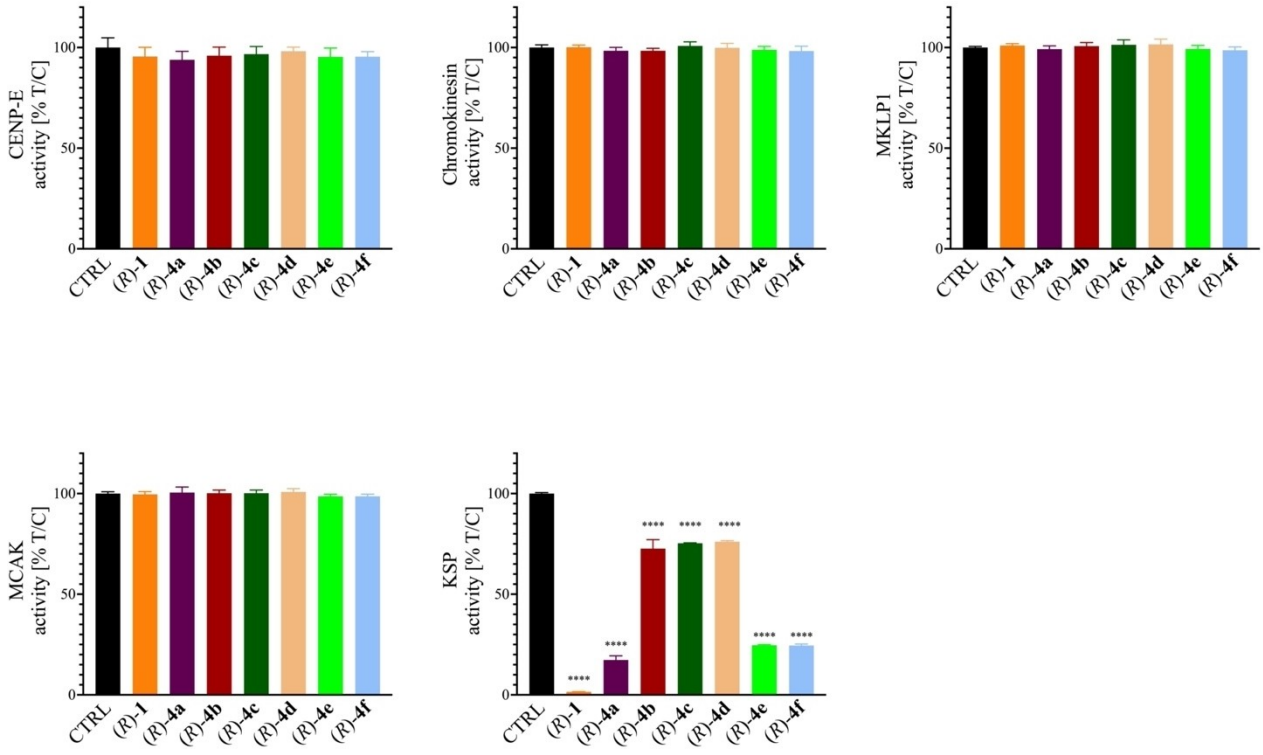

Figure 5. Inhibitory activity of (*S*)- and (*R*)-**1** and (*R*)-**4a-f** (10 μM) of kinesins and kinesin-like proteins. Data are presented as mean ± SEM, n = 3

Table 3. IC_{50} values for the most active KSP inhibitors (*R*)-**1**, (*R*)-**4a**, (*R*)-**4e** and (*R*)-**4f**. Data presented as mean and 95% confidence interval.

Compound	(*R*)-**1**	(*R*)-**4a**	(*R*)-**4e**	(*R*)-**4f**
IC_{50} [μM]	0.44	1.53	0.85	1.84
	(0.33–0.60)	(0.91–2.65)	(0.54–1.37)	(1.22–2.95)

functions (Table S2). The modelling showed that the molecules can bind in a variety of manners into the pocket depending on the chirality of the ispinesib backbone and the substituents introduced synthetically. For the (*R*)-enantiomers derived from (*R*)-**1** and in consequence of (*R*)-**4a**, configurations were among the highest-scoring poses that showed overlaps with the ispinesib core structure in an inner hydrophobic region in the binding pocket whilst the various substituents occupied a peripheral, more hydrophilic region. In general, the highest scores for all the docking functions were found for molecules derived from (*R*)-**4a** (Table S3). For example, the binding mode of (*R*)-**4e** is shown in Figure 5 and features hydrogen bonds of the carbonyl group of the benzamide moiety with the side chain amine moiety of Arg119 and the hydroxyl group of Tyr211. The benzyl group of the organometallic moiety also formed π-stacking interactions with the side chain indene of Trp127 and the phenolic group of Tyr211 (Figure 6). Compared to ispinesib, its (*S*)-enantiomer (*S*)-**1** gave lower values for 3 of the 4 scoring functions, and only GoldScore (GS) resulted in a higher result than ispinesib. However, GS scored ispinesib among the lowest structures upon docking and with all the other methods, the (*S*)-enantiomers gave lower scores than the equivalent (*R*)-enantiomers. These results reflect to some extent the studies on the KSP inhibitory activity of the compounds and the cytotoxicity of the compounds. It appears as the inhibition of KSP may not be the only mode of action relevant to the biological activity of the compounds.

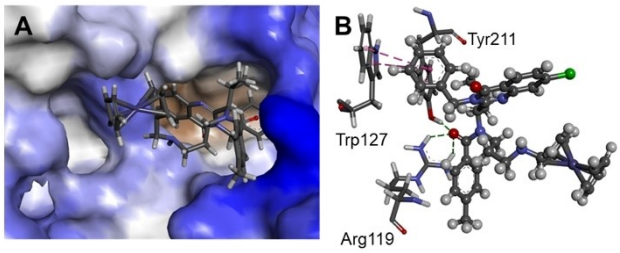

Figure 6. The highest scoring configuration of (*R*)-**4e** docked into the ispinesib binding site of KSP as predicted by ChemScore. (A) The molecule occupies the same binding pocket as ispinesib with the backbone largely overlapping with that of co-crystallized ispinesib. The protein surface is rendered where blue depicts a hydrophilic region on the surface, brown a hydrophobic region and grey shows neutral areas. (B) Hydrogen bonds are shown as green dotted lines between (*R*)-**4e** and the amino acids Tyr211 and Arg119. π-Stacking interactions are shown as purple doted lines between (*R*)-**4e** and the amino acids Trp127 and Tyr211

ROS generation

To explain the high antiproliferative activity of the ferrocenylbenzyl moiety-substituted compounds, which was not reflected in the KSP inhibition data, we investigated the induction of reactive oxygen species (ROS) formation in SW620 cells after exposure to the ispinesib analogues with the dihydrorhodamine 123 (DHR123) oxidation assay (Table 4). Neither ispinesib nor its (*S*)-enantiomer affected the ROS level in cells and neither did their benzyl analogues (*S*)-**4a** and (*R*)-**4a**. However, upon exposure to all the other compounds, the ROS generation increased by 15–29%. Despite a lack of significant correlation between the antiproliferative potential and ROS generation, the data suggests that the presence of a ferrocenyl moiety may induce oxidative stress within the cell. Interestingly, a similar effect was observed for the adamantyl-functionalized (*S*)-**4f** and (*R*)-**4f**, suggesting that the bulkiness of the conjugate may be more important than the ferrocenyl moiety for inducing oxidative stress within the cell. However, the observed level of ROS generation is comparatively small and its contribution to the antiproliferative potential of the compounds needs further investigation.

Conclusions

We have designed organometallic and organic analogues of ispinesib, resulting in a series of highly antiproliferative ferrocenyl ispinesib counterparts, which allowed to derive structure-activity relationships. The obtained analogues can be categorized in three types of compounds – those that lack the toluoyl moiety of ispinesib (type I), those that are functionalized on their tertiary amine group (type II) and the third group that was obtained by derivatization of its primary amine (type III). The cytotoxicity of the synthesized compounds was strongly dependent on their structure, however, was not found to be clearly correlated to the ability to inhibit KSP activity. Only the type I compound (*R*)-**2c** exhibited cytotoxic activity comparable to that of ispinesib with IC_{50} values in the nM range but it was not a KSP inhibitor, while it was able to induce more ROS formation than ispinesib. Among the type III compounds, the *N*-alkylated ispinesib derivatives exhibited similar or higher cytotoxicity than ispinesib with the most active being (*R*)-**4b-e**. However, only (*R*)-**4a**, (*R*)-**4e** and (*R*)-**4f** inhibited KSP activity in the sub- to low-μM concentration range. Interestingly, these were also the compounds that scored highly in many of the docking experiments relative to ispinesib. Although the con-

Table 4. ROS generation in SW620 cells exposed to the ispinesib analogues (1 μM) for 4 h. Data are presented as mean ± SEM, n = 3. Verapamil (10 μM) was added to all samples to inhibit any residual activity of the ABCB1 protein which eliminates rhodamine 123 from the cells. Data presented as mean ± SEM, n = 3.

Compound	Verapamil	(*S*)-**1**	(*S*)-**4a**	(*S*)-**4f**	(*R*)-**1**	(*R*)-**2c**	(*R*)-**3c**
ROS [%] vs control	103.7 ± 1.6	103.7 ± 1.9	103.7 ± 2.7	128.1 ± 3.8	102.1 ± 1.1	129.1 ± 2.0	116.7 ± 1.3
Compound	Verapamil	(*R*)-**4a**	(*R*)-**4b**	(*R*)-**4c**	(*R*)-**4d**	(*R*)-**4e**	(*R*)-**4f**
ROS [%] vs control	103.7 ± 1.6	102.5 ± 1.2	115.2 ± 1.4	125.9 ± 5.6	128.2 ± 3.1	120.8 ± 2.5	129.5 ± 4.0

jugation of a ferrocenylbenzyl moiety to ispinesib decreased the KSP inhibitory activity of the investigated conjugates, the presence of the ferrocenyl group but also of a bulky adamantyl moiety significantly increased the level of G_2/M fraction of cells. Also, the presence of either a ferrocenyl or adamantyl moiety increased ROS production in cancer cells. As the latter effects are small, oxidative stress will unlikely play an important role in their mode of action which warrants further investigation given the potent biological activity of many of the compounds.

Experimental Section

All reactions were carried out under Ar atmosphere. Commercially available chemicals and solvents were used as received unless stated otherwise. 1,2-Dichloroethane (1,2-DCE) and dichloromethane (DCM) for reactions were dried by distillation from calcium hydride prior to use. Column chromatography was performed on silica gel (Silicycle, 0.040–0.063 mm, 230–400 mesh). Thin-layer chromatography was performed on aluminum sheets precoated with silica (Silicycle). The purity of the synthesized compounds was determined by HPLC-MS analysis performed on a Phenomenex XB-C18 column (50×2.1 mm, 1.7 μm) with a mobile phase flow of 0.3 mL min^{-1} using a Shimadzu Nexera XR system equipped with SPD–M40 and LCMS-2020 detectors (see Supporting Information for details). The enantiomer ratios for (*S*)- and (*R*)-**2 a–f** were determined on a Lux Cellulose-2 column (250×4.6 mm) using IPA–n-heptane 1:9 as the mobile phase with a flow rate of 1 mL·min^{-1} using a Shimadzu HPLC system equipped with a PDA detector. ^{1}H and ^{13}C{^{1}H} NMR spectra were recorded on a Bruker ARX 600 MHz spectrometer (600.3 MHz for ^{1}H and 150.0 MHz for ^{13}C) at 294 K. Chemical shifts were calibrated on the residual solvent signals: [D_6]DMSO 2.51 ppm for ^{1}H and 39.5 ppm for ^{13}C. Synthesis of compounds along with atom numbering for the NMR assignment is presented in the Supporting Information.

General procedure A. Reductive amination at RT. Synthesis of amines (*S*)- and (*R*)-2 a–f

1.12 equiv of aldehyde was added to a solution of (*S*)- or (*R*)-**5** in 1,2-DCE (c = 0.1 M) and the resulting mixture was stirred at RT for 15 min. 1.44 equiv of sodium triacetoxyborohydride was added and the obtained mixture was stirred at RT for 24 h. After completion, the reaction mixture was diluted with DCM, washed with sodium bicarbonate and brine. The organic solution was dried over sodium sulfate and evaporated to dryness. The products were isolated by chromatography on silica gel using cyclohexane-ethyl acetate 7:3 as the eluent. If required, additional purification on silica gel using DCM or DCM-ethyl acetate 9:1 was performed. Synthesis of all reagents and target compounds and atom numbering for NMR assignment is presented in Supporting Information.

(*S*)-3-benzyl-2-(1-(benzylamino)-2-methylpropyl)-7-chloroquinazolin-4(3H)-one (*S*)-2 a: This compound was obtained in 56% yield using General procedure A starting from 200 mg of (*S*)-**5**, and 70 mg of benzaldehyde **6 a**. ^{1}H NMR (600 MHz, [D_6]DMSO) δ 8.18 (d, J = 8.6 Hz, 1H, H-5), 7.77 (d, J = 2.0 Hz, 1H, H-8), 7.59 (dd, J = 2.1, 8.6 Hz, 1H, H-6), 7.31 (t, J = 7.4 Hz, 2H, Ph-2), 7.26 (t, J = 7.3 Hz, 1H, Ph-2), 7.20 (t, J = 7.3 Hz, 2H, Ph-2), 7.16-7.11 (m, 5H, Ph-1), 5.48 (d, J = 16.4 Hz, 1H, CH_2), 5.19 (d, J = 16.1 Hz, 1H, CH_2), 3.55 (s, 1H), 3.51 (m, 2H, CH_2 and H-1′), 3.11 (d, J = 12.8 Hz, 1H, CH_2) 2.64 (br s., 1H, NH), 1.97-1.91 (m, 1H, H-2′), 0.88 (d, J = 6.7 Hz, 3H, H-3′), 0.73 (d, J = 6.4 Hz, 3H, H-3′). ^{13}C{^{1}H} NMR (151 MHz, [D_6]DMSO) δ 161.2, 161.1, 147.7, 140.3, 139.3, 136.5, 128.7 (CH), 128.7 (CH), 128.0 (CH), 127.7 (CH), 127.4 (CH), 127.1 (CH), 126.5 (CH), 126.4 (CH), 126.2 (CH), 118.8, 50.5 (CH_2), 45.3 (CH_2), 31.7 (CH), 20.1 (CH), 17.1 (CH); Elemental analysis calculated for $C_{26}H_{26}ClN_3O$ C 72.29, H 6.07, N 9.73, found C 72.21, H 5.98, N 9.94; HPLC-MS (see Supporting Information) analysis, R_f (HPLC) τ = 2.53 min, m/z calculated for $C_{26}H_{27}{}^{35}ClN_3O$ $[M+H]^+$ 432.2 found 432.4 $[M+H]^+$.

General procedure B. Reductive amination in a microwave reactor. Synthesis of (*S*)- and (*R*)-4 a–f

A mixture of 1.12 equiv of aldehyde and 1.0 equiv of (*S*)- or (*R*)-**1** in 1,2-DCE (c = 0.1 M) were placed in a reaction vessel, and the resulting mixture was stirred under MW at 120 °C for 15 min. After cooling to RT, 1.44 equiv of sodium triacetoxyborohydride was added and stirred for an additional 15 min at 120 °C under MW. The reaction mixture was diluted with DCM, washed with sodium bicarbonate and brine. The organic solution was dried over sodium sulfate and evaporated to dryness. The products were isolated by chromatography on silica gel using cyclohexane-ethyl acetate 7:3 as the eluent.

(*S*)-N-(1-(3-benzyl-7-chloro-4-oxo-3,4-dihydroquinazolin-2-yl)-2-methylpropyl)-N-(3-(benzylamino)propyl)-4-methylbenzamide (*S*)-4 a: This compound was obtained in 59% yield using General procedure B starting from 100 mg of (*S*)-**1** and 23 mg of **6 a**. ^{1}H NMR (600 MHz, [D_6]DMSO) δ 8.24 (d, J = 8.6 Hz, 1H, H-5), 7.76 (d, J = 2.0 Hz, 1H, H-8), 7.66 (dd, J = 2.0, 8.6 Hz, 1H, H-6), 7.36 (t, J = 7.5 Hz, 2H, CH_{Ar}), 7.30 (t, J = 7.3 Hz, 1H, CH_{Ar}), 7.27–7.21 (m, 8H, CH_{Ar}), 7.16 (t, J = 7.3 Hz, 1H, CH_{Ar}), 6.99 (d, J = 7.2 Hz, 2H, CH_{Ar}), 5.89 (d, J = 16.3 Hz, 1H, C$\underline{H}_2$Ph), 5.52 (d, J = 10.5 Hz, 1H, H-1′), 5.07 (d, J = 16.3 Hz, 1H, C$\underline{H}_2$Ph), 3.30 (t, J = 8.1 Hz, 2H, H-1″), 3.15 (s, 2H), 2.77-2.73 (m, 1H, H-2′), 2.29 (s, 3H, C$\underline{H}_3$C$_6$H$_4$CO), 1.93-1.85 (m, 2H), 1.23-1.20 (m, 1H), 0.90 (d, J = 6.8 Hz, 3H, H-3′), 0.90-0.68 (m, 1H), 0.48 (d, J = 6.4 Hz, 3H, H-3′). ^{13}C{^{1}H} (151 MHz, [D_6]DMSO) δ 171.9, 161.1, 155.4, 147.2, 140.6, 139.5, 138.6, 136.7, 133.9, 128.8 (CH), 128.7 (CH), 128.6 (CH), 128.1 (CH), 127.9 (CH), 127.5 (CH), 127.4 (CH), 126.5 (CH), 126.4 (CH), 126.3 (CH), 125.9 (CH), 119.1, 58.9 (CH), 51.9 (CH_2), 45.6 (CH_2), 45.1 (CH_2), 42.4 (CH_2), 29.5 (CH_2), 28.0 (CH), 20.8 (CH), 19.4 (CH), 18.1 (CH). Elemental analysis calculated for $C_{37}H_{39}ClN_4O_2$ C 73.19, H 6.47, N 9.23, found C 73.31, H 6.59, N 9.00. HPLC-MS (see Supporting Information) analysis, R_f (HPLC) τ = 2.06 min, m/z calculated for $C_{37}H_{40}{}^{35}ClN_4O_2$ $[M+H]^+$ 607.3 found 607.7 $[M+H]^+$.

General procedure C. Synthesis of compounds (*S*)- and (*R*)-3 a–e

1.4 equiv of p-toluoyl chloride was added to a solution of 1.0 equiv of amine (*S*)- or (*R*)-**2 a-f** and 1.2 equiv of diisopropylethylamine in anhydrous DCM (10 mL per 1 mmol of **2**). The resulting mixture was stirred at RT for 24 h, quenched by adding sodium bicarbonate and the product was extracted with DCM. The organic phase was washed with brine, dried over sodium sulfate and evaporated. The product was isolated by chromatography on silica using DCM-ethyl acetate 9:1 with 0.1% of ammonia.

(*S*)-N-benzyl-N-(1-(3-benzyl-7-chloro-4-oxo-3,4-dihydroquinazolin-2-yl)-2-methylpropyl)-4-methylbenzamide (*S*)-3 a: This compound was obtained in 20% yield using General procedure C starting from 200 mg of (*S*)-**2 a**. ^{1}H NMR (600 MHz, [D_6]DMSO) δ 7.88 (d, J = 8.3 Hz, 1H, H-5), 7.48-7.47 (m, 2H, CH_{Ar}), 7.41 (d, J = 7.9 Hz, 2H, CH_{Ar}), 7.38 (t, J = 7.6 Hz, 2H, CH_{Ar}), 7.32 (d, J = 7.1 Hz, 1H, CH_{Ar}), 7.29 (d, J = 7.7 Hz, 2H, CH_{Ar}), 7.21 (d, J = 7.9 Hz, 2H, CH_{Ar}), 6.77–6.75 (m, 4H, CH_{Ar}), 6.77-6.66 (m, 1H, CH_{Ar}), 5.92 (d, J = 16.2 Hz, 1H, C$\underline{H}_2$Ph), 5.66 (d, J = 10.4 Hz, 1H, H-1′), 5.17 (d, J = 16.2 Hz, 1H, C$\underline{H}_2$Ph), 4.72 (d, J = 17.2 Hz, 1H, C$\underline{H}_2$Ph), 4.54 (d, J = 17.2 Hz, 1H, C$\underline{H}_2$Ph), 2.95-2.91 (m, 1H, H-2′), 2.28 (s, 3H, C$\underline{H}_3$C$_6$H$_4$CO), 0.98 (d, J = 6.8 Hz, 3H, H-3′), 0.45 (d, J = 6.4 Hz, 3H, H-3′). ^{13}C{^{1}H} (151 MHz, [D_6]DMSO) δ 172.6,

160.1, 154.1, 146.8, 139.1, 138.6, 137.2, 136.8, 133.1, 128.9 (CH), 128.7 (CH), 128.0 (CH), 127.5 (CH), 127.4 (CH), 127.3 (CH), 126.5 (CH), 126.3 (CH), 126.2 (CH), 125.7 (CH), 124.8 (CH), 118.5, 58.9 (CH), 47.6 (CH_2), 44.8 (CH_2), 27.3 (CH), 20.8 (CH), 19.3 (CH), 17.9 (CH). Elemental analysis calculated for $C_{34}H_{32}ClN_3O$ C 74.24, H 5.86, N 7.64, found C 74.02, H 5.97, N 7.76. HPLC-MS (see Supporting Information) analysis, R_f (HPLC) $\tau = 2.40$ min, m/z calculated for $C_{34}H_{33}{}^{35}ClN_3O_2$ $[M+H]^+$ 550.2 found 550.4 $[M+H]^+$.

Cell viability assay – uptake of neutral red

10,000 cells were seeded per well of 96-well plate and left for 24 h to attach to the substrate. The test compounds were dissolved in DMSO, diluted in a complete culture medium and added to the cells in a 1:1 volume ratio. DMSO concentrations were kept to the same level and did not exceed 0.1%. After 70 h, neutral red was added to yield a final concentration of 0.033%, and kept in 37 °C for 2 h. Afterwards, the medium was discarded, the cells were washed two times with ice-cold PBS (138 mM NaCl, 5 mM KCl, 7.5 mM phosphate buffer, pH 7.4), and the incorporated dye was solubilized using 1% acetic acid in 50% ethanol for 10 min at an orbital platform shaker. The absorbance of the solution was measured 540 nm using an EnVision plate reader. All values were calculated as a percentage of control. IC_{50} values were calculated using GraphPad Prism Software ver. 9.

Cell cycle

100,000 cells per well were seeded in 6-well plates, and left for 24 h to attach to the substrate. The test compounds were added at the IC_{75} concentrations of (*S*)-**1** or (*R*)-**1** calculated from viability curves for the SW620 cell line. After 24 h and 48 h, the cells were trypsinized, washed once with ice cold PBS and fixed using 70% cold ethanol. The cells were then rehydrated with PBS and stained with 75 μM propidium iodide and 50 Kunitz units/mL of RNAse A in PBS for 30 min at 37 °C. The samples were analyzed on an LSRII (Becton Dickinson) instrument (excitation 488 nm, emission 575/26 nm) and the cell cycle phase distribution was determined with FlowJo 7.6.1 software (FlowJo, LLC) using a built-in cell cycle analysis module (Watson pragmatic algorithm).

ROS generation

100,000 cells per well were seeded in-6 well plates for 24 h. The cells were treated with the test compounds (1 μM), dihydrorhodamine 123 (1 μM) and verapamil (10 μM) for 4 h. The cells were then harvested and suspended in a complete medium. The samples were then collected on an LSRII (Becton Dickinson) instrument and median fluorescence (excitation 488 nm, emission 530/30 nm) was analyzed. Results were calculated as a percentage of control.

Kinesin ATPase inhibition assay

The kinesin modulatory activity was determined using Kinesin ATPase Endpoint Biochem Kit (Cytoskeleton Inc) according to the manufacturer's protocol. Phosphate release was measured at 650 nm (EnVision Plate Reader – Perkin Elmer, USA). The DMSO concentration in the samples was 0.1%.

Molecular Modelling

The compounds were docked to the crystal structure of human kinesin KSP (PDB ID: 4AP0, resolution 2.59 Å)[31] which was obtained from the Protein Data Bank (PDB).[32] Scigress version FJ 2.6[33] was used to prepare the crystal structure for docking, i.e., hydrogen atoms were added and co-crystallized ispinesib and adenosine-5′-diphosphate (ADP) were removed. The center of the binding pocket was defined as the nitrogen in the ring close to the carbonyl group. ($x = 41.663$, $y = 0.113$, $z = 11.931$) with a radius of 10 Å. The GoldScore (GS),[27] ChemScore (CS),[28] ChemPLP,[29] and Astex statistical potential (ASP)[30] scoring functions were implemented to validate the predicted binding modes and relative energies of the ligands using the GOLD v5.4 software suite. The co-crystallized ligand ispinesib was first docked and root mean square deviation (RMSD) values were calculated for the heavy atoms. ASP obtained average RMSDs of 0.9255, PLP of 0.7299, CS of 0.7265 and for GS a value of 0.8090 was found which show the strong prediction power of the scoring functions. The RMSD values and binding scores are given in Tables S1 and S2 in the Supporting Information.

Acknowledgements

This study was financially supported by the National Science Centre Poland (NCN) based on decision UMO-2015/17/B/ST5/02331. The authors wish to acknowledge the use of New Zealand eScience Infrastructure (NeSI) high performance computing facilities as part of this research funded jointly by the collaborating institutions and through the Ministry of Business, Innovation & Employment Research Infrastructure program. http://www.nesi.org.nz

Conflict of Interests

The authors declare no conflict of interest.

Data Availability Statement

The data that support the findings of this study are available from the corresponding author upon reasonable request.

Keywords: antiproliferative agents · enzyme inhibitors · ferrocene · ispinesib · organometallic compounds

[1] a) R. J. van Vuuren, M. H. Visagie, A. E. Theron, A. M. Joubert, *Cancer Chemother. Pharmacol.* **2015**, *76*, 1101–1112; b) C. Dumontet, M. A. Jordan, *Nat. Rev. Drug Discovery* **2010**, *9*, 790–803.
[2] E. Mukhtar, V. M. Adhami, H. Mukhtar, *Mol. Cancer Ther.* **2014**, *13*, 275–284.
[3] I. Marzo, J. Naval, *Biochem. Pharmacol.* **2013**, *86*, 703–710.
[4] a) O. Rath, F. Kozielski, *Nat. Rev. Cancer* **2012**, *12*, 527–539; b) H. Miki, Y. Okada, N. Hirokawa, *Trends Cell Biol.* **2005**, *15*, 467–476; c) N. Hirokawa, Y. Noda, Y. Tanaka, S. Niwa, *Nat. Rev. Mol. Cell Biol.* **2009**, *10*, 682–696; d) R. Chamariya, V. Suvarna, *Anti-Cancer Agents Med. Chem.* **2022**, *22*, 2517–2538; e) Y. Shi, X. Cui, T. Jiang, Y. Pan, Y. Lin, X. Feng, Z. Ding, C. Yang, Y. Tan, H. Wang, L. Dong, *Cell Death Dis.* **2022**, *13*, 799; f) K. Hansson, K. Radke, K. Aaltonen, J. Saarela, A. Mañas, J. Sjölund, E. M. Smith, K. Pietras, S. Påhlman, K. Wennerberg, D. Gisselsson, D. Bexell, *Sci. Transl. Med.* **2020**, *12*, eaba4434.
[5] S. DeBonis, D. A. Skoufias, L. Lebeau, R. Lopez, G. Robin, R. L. Margolis, R. H. Wade, F. Kozielski, *Mol. Cancer Ther.* **2004**, *3*, 1079–1090.
[6] T. U. Mayer, T. M. Kapoor, S. J. Haggarty, R. W. King, S. L. Schreiber, T. J. Mitchison, *Science* **1999**, *286*, 971–974.
[7] H. B. El-Nassan, *Eur. J. Med. Chem.* **2013**, *62*, 614–631.

[8] D. Bongero, L. Paoluzzi, E. Marchi, K. M. Zullo, R. Neisa, Y. Mao, R. Escandon, K. Wood, O. A. O'Connor, *Leuk. Lymphoma.* **2015**, *56*, 2945–2952.
[9] K. Holen, R. DiPaola, G. Liu, A. R. Tan, G. Wilding, K. Hsu, N. Agrawal, C. Chen, L. Xue, E. Rosenberg, M. Stein, *Invest. New Drugs* **2012**, *30*, 1088–1095.
[10] P. M. LoRusso, P. H. Goncalves, L. Casetta, J. A. Carter, K. Litwiler, D. Roseberry, S. Rush, J. Schreiber, H. M. Simmons, M. Ptaszynski, E. A. Sausville, *Invest. New Drugs* **2015**, *33*, 440–449.
[11] R. Nakai, S.-i. Iida, T. Takahashi, T. Tsujita, S. Okamoto, C. Takada, K. Akasaka, S. Ichikawa, H. Ishida, H. Kusaka, S. Akinaga, C. Murakata, S. Honda, M. Nitta, H. Saya, Y. Yamashita, *Cancer Res.* **2009**, *69*, 3901–3909.
[12] a) R. Shahin, S. Aljamal, *Future Sci. OA* **2022**, *8*, FSO778; b) I. Garcia-Saez, D. A. Skoufias, *Biochem. Pharmacol.* **2021**, *184*, 114364.
[13] L. Lad, L. Luo, J. D. Carson, K. W. Wood, J. J. Hartman, R. A. Copeland, R. Sakowicz, *Biochemistry* **2008**, *47*, 3576–3585.
[14] a) S. Top, A. Vessieres, G. Leclercq, J. Quivy, J. Tang, J. Vaissermann, M. Huche, G. Jaouen, *Chem. Eur. J.* **2003**, *9*, 5223–5236; b) C. Biot, F. Nosten, L. Fraisse, D. Ter-Minassian, J. Khalife, D. Dive, *Parasite* **2011**, *18*, 207–214; c) M. Patra, G. Gasser, *Nat. Chem. Rev.* **2017**, *1*, 0066; d) T. Hirao, T. Moriuchi, *Advances in Bioorganometallic Chemistry*, Elsevier, **2018**; e) P. Chellan, P. J. Sadler, *Chem. Eur. J.* **2020**, *26*, 8676–8688; f) W. D. J. Tremlett, D. M. Goodman, T. R. Steel, S. Kumar, A. Wieczorek-Blauz, F. P. Walsh, M. P. Sullivan, M. Hanif, C. G. Hartinger, *Coordin Chem. Rev.* **2021**, *445*, 213950; g) G. Jaouen, A. Vessières, S. Top, *Chem. Soc. Rev.* **2015**, *44*, 8802–8817; h) T. R. Steel, F. Walsh, A. Wieczorek-Blauz, M. Hanif, C. G. Hartinger, *Coordin Chem. Rev.* **2021**, *439*, 213890; i) B. Sharma, V. Kumar, *J. Med. Chem.* **2021**, *64*, 16865–16921; j) M. Rana, A. Perotti, L. M. Bisset, J. D. Smith, E. Lamden, Z. Khan, M. K. Ismail, K. Ellis, K. A. Armstrong, S. L. Hodder, C. Bertoli, L. Meneguello, R. A. M. de Bruin, J. R. Morris, I. Romero-Canelon, J. H. R. Tucker, N. J. Hodges, *Metallomics* **2022**, *14, mfac041*; k) B. S. Ludwig, J. D. G. Correia, F. E. Kühn, *Coordin Chem. Rev.* **2019**, *396*, 22–48; l) R. Wang, H. Chen, W. Yan, M. Zheng, T. Zhang, Y. Zhang, *Eur. J. Med. Chem.* **2020**, *190*, 112109.
[15] a) K. Kowalczyk, A. Blauz, W. M. Ciszewski, A. Wieczorek, B. Rychlik, D. Plazuk, *Dalton Trans.* **2017**, *46*, 17041–17052; b) N. Nicolaus, J. Zapke, P. Riesterer, J. M. Neudorfl, A. Prokop, H. Oschkinat, H. G. Schmalz, *ChemMedChem* **2010**, *5*, 661–665; c) D. Plazuk, A. Vessieres, E. A. Hillard, O. Buriez, E. Labbe, P. Pigeon, M. A. Plamont, C. Amatore, J. Zakrzewski, G. Jaouen, *J. Med. Chem.* **2009**, *52*, 4964–4967; d) M. Beauperin, S. Top, M. A. Richard, D. Plazuk, P. Pigeon, S. Toma, V. Polackova, G. Jaouen, *Dalton Trans.* **2016**, *45*, 13126–13134; e) E. Hillard, A. Vessieres, F. Le Bideau, D. Plazuk, D. Spera, M. Huche, G. Jaouen, *ChemMedChem* **2006**, *1*, 551–559; f) A. Vessieres, Y. Wang, M. J. McGlinchey, G. Jaouen, *Coord. Chem. Rev.* **2021**, *430*, 213658; g) Y. Wang, P. Pigeon, W. Li, J. Yan, P. M. Dansette, M. Othman, M. J. McGlinchey, G. Jaouen, *Eur. J. Med. Chem.* **2022**, *234*, 114202;
[16] a) T.-S. Kang, W. Wang, H.-J. Zhong, Z.-Z. Dong, Q. Huang, S. W. F. Mok, C.-H. Leung, V. K. W. Wong, D.-L. Ma, *Cancer Lett.* **2017**, *396*, 76–84; b) G. Li, H. Liu, R. Feng, T.-S. Kang, W. Wang, C.-N. Ko, C.-Y. Wong, M. Ye, D.-L. Ma, J.-B. Wan, *Redox Rep.* **2021**, *48*, 102129; c) W. Chen, X. Cai, Q. Sun, X. Guo, C. Liang, H. Tang, H. Huang, H. Luo, L. Chen, J. Chen, *Eur. J. Med. Chem.* **2022**, *236*, 114335; d) K. Vellaisamy, G. Li, W. Wang, C.-H. Leung, D.-L. Ma, *Chem. Sci.* **2018**, *9*, 8171–8177; e) L. Biancalana, H. Kostrhunova, L. K. Batchelor, M. Hadiji, I. Degano, G. Pampaloni, S. Zacchini, P. J. Dyson, V. Brabec, F. Marchetti, *Inorg. Chem.* **2021**, *60*, 9529–9541; f) Z. Feng, P. Tao, L. Zou, P. Gao, Y. Liu, X. Liu, H. Wang, S. Liu, Q. Dong, J. Li, *ACS Appl. Mater. Interfaces* **2017**, *9*, 28319–28330.
[17] P. Pigeon, Y. Wang, S. Top, F. Najlaoui, M. C. Garcia Alvarez, J. Bignon, M. J. McGlinchey, G. Jaouen, *J. Med. Chem.* **2017**, *60*, 8358–8368.
[18] a) D. Plazuk, A. Wieczorek, W. M. Ciszewski, K. Kowalczyk, A. Blauz, S. Pawledzio, A. Makal, C. Eurtivong, H. J. Arabshahi, J. Reynisson, C. G. Hartinger, B. Rychlik, *ChemMedChem* **2017**, *12*, 1882–1892; b) A. Wieczorek, A. Blauz, A. Zal, H. J. Arabshahi, J. Reynisson, C. G. Hartinger, B. Rychlik, D. Plazuk, *Chem. Eur. J.* **2016**, *22*, 11413–11421.
[19] K. Chrabaszcz, A. Blauz, M. Gruchala, M. Wachulec, B. Rychlik, D. Plazuk, *Chem. Eur. J.* **2021**, *27*, 6254–6262.
[20] A. Wieczorek, A. Blauz, J. Zakrzewski, B. Rychlik, D. Plazuk, *ACS Med. Chem. Lett.* **2016**, *7*, 612–617.
[21] A. Wieczorek-Blauz, K. Kowalczyk, A. Blauz, A. Makal, S. Pawledzio, C. Eurtivong, H. J. Arabshahi, J. Reynisson, C. G. Hartinger, B. Rychlik, D. Plazuk, *Dalton Trans.* **2022**, *51*, 491–508.
[22] M. Lomzik, M. Hanif, A. Budniok, A. Blauz, A. Makal, D. M. Tchon, B. Lesniewska, K. K. H. Tong, S. Movassaghi, T. Sohnel, S. M. F. Jamieson, A. Zafar, J. Reynisson, B. Rychlik, C. G. Hartinger, D. Plazuk, *Inorg. Chem.* **2020**, *59*, 14879–14890.
[23] J. P. Holland, M. W. Jones, S. Cohrs, R. Schibli, E. Fischer, *Bioorg. Med. Chem.* **2013**, *21*, 496–507.
[24] W. C. Vincek, C. S. Aldrich, R. T. Borchardt, G. L. Grunewald, *J. Med. Chem.* **1981**, *24*, 7–12.
[25] A. Blauz, B. Rychlik, *J. Pharmacol. Toxicol. Methods* **2017**, *84*, 57–65.
[26] a) Y. Murase, H. Ono, K. Ogawa, R. Yoshioka, Y. Ishikawa, H. Ueda, K. Akahoshi, D. Ban, A. Kudo, S. Tanaka, M. Tanabe, *Cancer Sci.* **2021**, *112*, 4641–4654; b) J. W. Purcell, J. Davis, M. Reddy, S. Martin, K. Samayoa, H. Vo, K. Thomsen, P. Bean, W. L. Kuo, S. Ziyad, J. Billig, H. S. Feiler, J. W. Gray, K. W. Wood, S. Cases, *Clin. Cancer Res.* **2010**, *16*, 566–576.
[27] G. Jones, P. Willett, R. C. Glen, A. R. Leach, R. Taylor, *J. Mol. Biol.* **1997**, *267*, 727–748.
[28] a) M. D. Eldridge, C. W. Murray, T. R. Auton, G. V. Paolini, R. P. Mee, *J. Comput.-Aided Mol. Des.* **1997**, *11*, 425–445; b) M. L. Verdonk, J. C. Cole, M. J. Hartshorn, C. W. Murray, R. D. Taylor, *Proteins* **2003**, *52*, 609–623.
[29] O. Korb, T. Stutzle, T. E. Exner, *J. Chem. Inf. Model.* **2009**, *49*, 84–96.
[30] W. T. Mooij, M. L. Verdonk, *Proteins* **2005**, *61*, 272–287.
[31] J. Lowe, H. Li, K. H. Downing, E. Nogales, *J. Mol. Biol.* **2001**, *313*, 1045–1057.
[32] a) H. M. Berman, J. Westbrook, Z. Feng, G. Gilliland, T. Bhat, H. Weissig, I. N. Shindyalov, P. E. Bourne, *Nucleic Acids Res.* **2000**, *28*, 235–242; b) H. Berman, K. Henrick, H. Nakamura, *Nat. Struct. Biol.* **2003**, *10*, 980.
[33] *Scigress: Version FJ 2.6 (EU 3.1.7) Fujitsu Limited 2008–2016*.

Manuscript received: March 13, 2023
Accepted manuscript online: June 18, 2023
Version of record online: July 31, 2023

Chemistry–A European Journal

Supporting Information

Design, Synthesis, and Evaluation of Biological Activity of Ferrocene-Ispinesib Hybrids: Impact of a Ferrocenyl Group on the Antiproliferative and Kinesin Spindle Protein Inhibitory Activity

Karolina Kowalczyk, Andrzej Błauż, Daniel Moscoh Ayine-Tora, Christian G. Hartinger, Błażej Rychlik, and Damian Plażuk*

Table of Contents

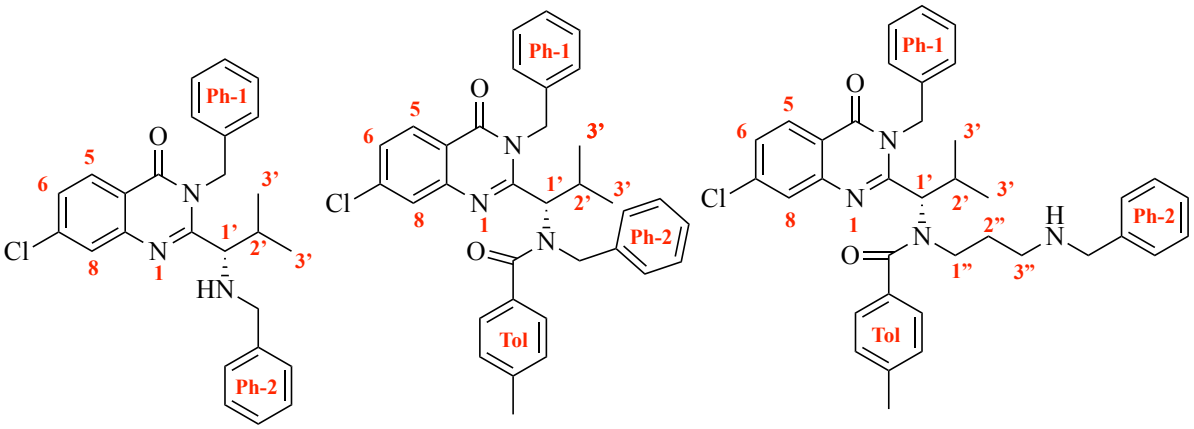

Atom numbering scheme for NMR assignment

(*R*)-3-benzyl-2-(1-(benzylamino)-2-methylpropyl)-7-chloroquinazolin-4(3H)-one (*R*)-2a. This compound was obtained in 55% yield according to General procedure A starting from 200 mg of (*R*)-**5**, and 70 mg of **6a**. ^{1}H and ^{13}C{^{1}H} NMR spectra were identical with those of (*S*)-**2a**. Elemental analysis calculated for $C_{26}H_{26}ClN_3O$ C 72.29, H 6.07, N 9.73, found C 72.27, H 6.03, N 9.84. HPLC-MS (SI) analysis, R_f (HPLC) τ = 2.50 min, m/z calculated for $C_{26}H_{27}{}^{35}ClN_3O$ $[M+H]^+$ 432.2 found 432.4 $[M+H]^+$.

(*S*)-3-benzyl-2-(1-((2-ferrocenylbenzyl)amino)-2-methylpropyl)-7-chloroquinazolin-4(3H)-one (*S*)-2b. This compound was obtained in 65% yield according to General procedure A starting from 100 mg of (*S*)-**5**, and 94 mg of 2-ferrocenylbenzaldehyde **6b**. ^{1}H NMR (600 MHz, DMSO) δ 8.23 (d, *J* = 8.5 Hz, 1H, H-5), 7.80 (d, *J* = 2.0 Hz, 1H, H-8), 7.63 (dd, *J* = 8.5, 2.0 Hz, 1H, H-6), 7.61 (dd, *J* = 9.0, 2.0 Hz, 1H, *o*-$C_6\underline{H}_4$Fc), 7.32 (t, *J* = 7.5 Hz, 2H, *o*-$C_6\underline{H}_4$Fc), 7.26 (t, *J* = 7.3 Hz, 1H, *o*-$C_6\underline{H}_4$Fc), 7.23-7.16 (m, 5H, $CH_2\underline{Ph}$), 5.61 (d, *J* = 16.1 Hz, 1H, $C\underline{H}_2$Ph), 5.23 (d, *J* = 16.2 Hz, 1H, $C\underline{H}_2$Ph), 4.47 (br s., 1H, Cp), 4.38 (br s., 1H, Cp), 4.14 (br s., 1H, Cp), 4.04 (br s., 1H, Cp), 3.94 (s, 5H, Cp'), 3.63 (dd, *J* = 6.0, 9.7 Hz, 1H, H-1'), 3.51 (d, *J* = 11.6 Hz, 1H, $C\underline{H}_2$NH), 3.25 (br s, 1H, $C\underline{H}_2$NH), 2.44 (t, *J* = 8.4 Hz, 1H, $CH_2N\underline{H}$), 2.05 (m, *J* = 6.5 Hz, 1H, H-2'), 0.92 (d, *J* = 6.7 Hz, 3H, H-3'), 0.83 (d, *J* = 6.2 Hz, 3H, H-3'). ^{13}C{^{1}H} (151 MHz, DMSO) δ 161.2, 160.8, 147.6, 139.3, 137.3, 137.0, 136.6, 130.2 (CH), 129.5 (CH), 128.8 (CH), 128.7 (CH), 127.5 (CH), 127.2 (CH), 126.5 (CH), 126.4 (CH), 126.3 (CH), 126.1 (CH), 118.8, 85.8 (Cp_{ipso}), 69.3 (Cp), 69.1 (Cp'), 68.9 (Cp), 67.8 (Cp), 63.7 (CH), 48.3 (CH_2) 45.2 (CH_2), 31.2 (CH), 20.3 (CH), 17.2 (CH). Elemental analysis calculated for $C_{36}H_{34}ClFeN_3O$ C 70.20, H 5.56, N 6.82, found C 70.14, H 5.52, N 7.16.

HPLC-MS analysis, R_f (HPLC) τ = 4.51 min, m/z calculated for $C_{36}H_{35}{}^{35}ClFeN_3O$ $[M+H]^+$ 616.3 found 616.3 $[M+H]^+$.

(*R*)-3-benzyl-2-(1-((2-ferrocenylbenzyl)amino)-2-methylpropyl)-7-chloroquinazolin-4(3H)-one (*R*)-2b. This compound was obtained in 55% yield according to General procedure A starting from 100 mg of (*R*)-**5**, and 94 mg **6b**. ^1H and $^{13}C\{^1H\}$ NMR spectra were identical with those of (*S*)-**2b**. Elemental analysis calculated for $C_{36}H_{34}ClFeN_3O$ C 70.20, H 5.56, N 6.82, found C 70.34, H 5.54, N 7.07. HPLC-MS analysis, R_f (HPLC) τ = 4.52 min, m/z calculated for $C_{36}H_{35}{}^{35}ClFeN_3O$ $[M+H]^+$ 616.2 found 616.2 $[M+H]^+$.

(*S*)-3-benzyl-2-(1-((3-ferrocenylbenzyl)amino)-2-methylpropyl)-7-chloroquinazolin-4(3H)-one (*S*)-2c. This compound was obtained in 59% yield according to General procedure A starting from 200 mg of (*S*)-**5**, and 184 mg of 3-ferrocenylbenzaldehyde **6c**. ^1H NMR (600 MHz, DMSO) δ 8.20 (d, *J* = 8.5 Hz, 1H, H-5), 7.79 (d, *J* = 2.0 Hz, 1H, H-8), 7.60 (dd, *J* = 8.5, 2.1 Hz, 1H, H-6), 7.38 (br s, 1H, CH_{Ar}), 7.36 (d, *J* = 7.8 Hz, 1H, CH_{Ar}), 7.30 (t, *J* = 7.5 Hz, 1H, CH_{Ar}), 7.24 (t, *J* = 7.3 Hz, 1H, CH_{Ar}), 7.16 (t, *J*= 7.6 Hz, 1H, CH_{Ar}), 7.12 (s, 1H, CH_{Ar}), 7.11 (s, 1H, CH_{Ar}), 6.96 (d, *J* = 7.5 Hz, 1H, CH_{Ar}), 5.41 (d, *J* = 16.0 Hz, 1H, C$\underline{H}_2$Ph), 5.29 (d, *J* = 15.6 Hz, 1H, C$\underline{H}_2$Ph), 4.69-4-67 (m, 2H, Cp), 4.32 (t, *J* = 1.8 Hz, 2H, Cp), 3.99 (s, 5H, Cp'), 3.62 (d, *J* = 13.7 Hz, 1H, C$\underline{H}_2$NH), 3.58 (br s, 1H, H-1'), 3.23 (d, *J* = 13.2 Hz, 1H, C$\underline{H}_2$NH), 2.72 (br s, $CH_2N\underline{H}$), 1.99-1.93 (m, 1H, H-2'), 0.93 (d, *J* = 6.7 Hz, 3H, H-3'), 0.72 (d, *J* = 6.2 Hz, 3H, H-3'). $^{13}C\{^1H\}$ (151 MHz, DMSO) δ 161.4, 161.2, 147.7, 140.4, 139.3, 138.6, 136.5, 128.7 (CH), 128.0 (CH), 127.4 (CH), 127.1 (CH), 126.5 (CH), 126.2 (CH), 125.3 (CH), 125.2 (CH), 124.4 (CH), 118.8, 85.0 (Cp_{ipso}), 69.3 (Cp'), 68.7 (Cp), 66.3 (Cp), 66.1 (Cp), 63.2 (CH), 50.3 (CH_2), 45.4 (CH_2), 31.7 (CH), 20.1 (CH), 17.3 (CH). Elemental analysis calculated for $C_{36}H_{34}ClFeN_3O$ C 70.20, H 5.56, N 6.82, found C 70.07, H 5.66, N 7.08. HPLC-MS analysis, R_f (HPLC) τ = 2.76 min, m/z calculated for $C_{36}H_{35}{}^{35}ClFeN_3O$ $[M+H]^+$ 616.2 found 616.3 $[M+H]^+$.

(*R*)-3-benzyl-2-(1-((3-ferrocenylbenzyl)amino)-2-methylpropyl)-7-chloroquinazolin-4(3H)-one (*R*)-2c. This compound was obtained in 61% yield according to General procedure A starting from 200 mg of (*R*)-**5**, and 184 mg of **6c**. ^1H and $^{13}C\{^1H\}$ NMR spectra were identical with those of (*S*)-**2c**. Elemental analysis calculated for $C_{36}H_{34}ClFeN_3O$ C 70.20, H 5.56, N 6.82, found C 70.01, H 5.59, N 6.92.

HPLC-MS analysis, R_f (HPLC) τ = 2.75 min, m/z calculated for $C_{36}H_{35}{}^{35}ClFeN_3O$ $[M+H]^+$ 616.2 found 616.3 $[M+H]^+$.

(*S*)-3-benzyl-2-(1-((4-ferrocenylbenzyl)amino)-2-methylpropyl)-7-chloroquinazolin-4(3H)-one (*S*)-2d. This compound was obtained in 81% yield according to General procedure A starting from 100 mg of (*S*)-**5**, and 94 mg of 4-ferrocenylbenzaldehyde **6d**. ^{1}H NMR (600 MHz, DMSO) δ 8.20 (d, *J* = 8.5 Hz, 1H, H-5), 7.80 (d, *J* = 2.0 Hz, 1H, H-8), 7.60 (dd, *J* = 8.5, 2.1 Hz, 1H, H-6), 7.39 (d, *J* = 8.2 Hz, 2H, $CH_2\underline{Ph}$), 7.34 (t, *J* = 7.3 Hz, 2H, $CH_2\underline{Ph}$), 7.30 (d, *J* = 7.2 Hz, 1H, $CH_2\underline{Ph}$), 7.13 (d, *J* = 7.3 Hz, 2H, *p*-$C_6\underline{H}_4Fc$), 7.07 (d, *J* = 8.1 Hz, 2H, *p*-$C_6\underline{H}_4Fc$), 5.45 (d, *J* = 16.0 Hz, 1H, $C\underline{H}_2Ph$), 5.25 (d, *J* = 16.4 Hz, 1H, $C\underline{H}_2Ph$), 4.72 (t, *J* = 1.4 Hz, 2H, Cp), 4.32 (t, *J* = 1.8 Hz, 2H, Cp), 3.98 (s, 5H, Cp'), 3.55 (br s, 1H, H-1') overlapped with 3.54 (d, *J* = 13.0 Hz, 1H, $C\underline{H}_2NH$), 3.14 (d, *J* = 13.0 Hz, 1H, $C\underline{H}_2NH$), 2.62 (br s, 1H, $CH_2N\underline{H}$), 1.97-1.93 (m, 1H, H-2'), 0.90 (d, *J* = 6.7 Hz, 3H, H-3'), 0.72 (d, *J* = 6.3 Hz, 3H, H-3'). $^{13}C\{^1H\}$ (151 MHz, DMSO) δ 161.24, 161.20, 147.7, 139.3, 137.8, 137.1, 136.5, 128.73 (CH), 128.68 (CH), 127.8 (CH), 127.5 (CH), 127.1 (CH), 126.5 (CH), 126.2 (CH), 125.5 (CH), 118.8, 84.8 (Cp_{ipso}), 69.3 (Cp'), 68.7 (Cp), 66.1 (Cp), 63.2 (CH), 50.3 (CH_2), 45.4 (CH_2), 31.7 (CH), 20.1 (CH), 17.2 (CH). Elemental analysis calculated for $C_{36}H_{34}ClFeN_3O$ C 70.20, H 5.56, N 6.82, found C 70.31, H 5.67, N 7.08. HPLC-MS analysis, R_f (HPLC) τ = 2.23 min, m/z calculated for $C_{36}H_{35}{}^{35}ClFeN_3O$ $[M+H]^+$ 616.2 found 616.2 $[M+H]^+$.

(*R*)-3-benzyl-2-(1-((4-ferrocenylbenzyl)amino)-2-methylpropyl)-7-chloroquinazolin-4(3H)-one (*R*)-2d. This compound was obtained in 78% yield according to General procedure A starting from 100 mg of (*R*)-**5**, and 94 mg of **6d**. ^{1}H and $^{13}C\{^1H\}$ NMR spectra were identical with those of (*S*)-**2d**. Elemental analysis calculated for $C_{36}H_{34}ClFeN_3O$ C 70.20, H 5.56, N 6.82, found C 70.48, H 5.57, N 7.05. HPLC-MS analysis, R_f (HPLC) τ = 2.26 min, m/z calculated for $C_{36}H_{35}{}^{35}ClFeN_3O$ $[M+H]^+$ 616.2 found 616.3 $[M+H]^+$.

(*S*)-3-benzyl-2-(1-(ferrocenylmethylamino)-2-methylpropyl)-7-chloroquinazolin-4(3H)-one (*S*)-2e. This compound was obtained in 80% yield according to General procedure A starting from 100 mg of (*S*)-**5**, and 70 mg of **6e**. ^{1}H NMR (600 MHz, DMSO) δ 8.23 (d, *J* = 8.5 Hz, 1H, H-5), 7.73 (d, *J* = 2.0 Hz, 1H, H-8), 7.62 (dd, *J* = 2.0, 8.6 Hz, 1H, H-6), 7.38 (t, *J* = 7.5 Hz, 2H, $CH_2\underline{Ph}$), 7.31 (t, *J* = 7.3 Hz, 1H, $CH_2\underline{Ph}$), 7.26 (d, *J* = 7.4 Hz, 2H, $CH_2\underline{Ph}$), 5.75 (d, *J* = 17.0 Hz, 1H, $C\underline{H}_2Ph$), 5.14 (d, *J* = 16.1 Hz, 1H, $C\underline{H}_2Ph$), 4.14-4.12 (s, 6H, Cp' and Cp), 4.02 (br s, 1H, Cp), 4.01

(br s, 1H, Cp), 3.91 (br s, 1H, Cp), 3.62 (s, 1H, H-1'), 3.00 (d, *J* = 12.6 Hz, 1H, C<u>H</u>$_2$NH), 2.62 (br s, 1H, C<u>H</u>$_2$NH), 2.39 (br s, 1H, CH$_2$N<u>H</u>), 1.93-1.88 (m, 1H, H-2'), 0.93 (d, *J* = 6.7 Hz, 3H, H-3'), 0.85 (d, *J* = 6.5 Hz, 3H, H-3'). ^{13}C{^{1}H} (151 MHz, DMSO) δ 161.7, 161.2, 147.7, 139.4, 136.6, 128.9 (CH), 128.8 (CH), 127.5 (CH), 127.1 (CH), 126.6 (CH), 125.8 (CH), 118.8, 87.3 (Cp$_{ipso}$), 68.1 (Cp'), 67.6 (Cp), 67.1 (Cp), 67.0 (Cp), 66.8 (Cp), 63.4 (CH), 45.9 (CH$_2$), 45.3 (CH$_2$), 32.3 (CH), 20.1 (CH), 17.0 (CH). Elemental analysis calculated for $C_{30}H_{30}ClFeN_3O$ C 66.74, H 5.60, N 7.78, found C 66.73, H 5.63, N 7.54. HPLC-MS analysis, R$_f$ (HPLC) τ = 3.56 min, m/z calculated for $C_{30}H_{31}{}^{35}ClFeN_3O$ $[M+H]^+$ 540.2 found 540.2 $[M+H]^+$.

(*R*)-3-benzyl-2-(1-(ferrocenylmethylamino)-2-methylpropyl)-7-chloroquinazolin-4(3H)-one (*R*)-2e. This compound was obtained in 85% yield according to General procedure A starting from 200 mg of (*R*)-**5**, and 140 mg of **6e**. ^{1}H and ^{13}C{^{1}H} NMR spectra were identical with those of (*S*)-**2e**. Elemental analysis calculated for $C_{30}H_{30}ClFeN_3O$ C 66.74, H 5.60, N 7.78, found C 66.94, H 5.71, N 7.77. HPLC-MS analysis, R$_f$ (HPLC) τ = 3.46 min, m/z calculated for $C_{30}H_{31}{}^{35}ClFeN_3O$ $[M+H]^+$ 540.2 found 540.2 $[M+H]^+$.

(*S*)-2-(1-((adamantan-1-ylmethyl)amino)-2-methylpropyl)-3-benzyl-7-chloroquinazolin-4(3H)-one (*S*)-2f. This compound was obtained in 70% yield according to General procedure A starting from 200 mg of (*S*)-**5**, and 108 mg of **6f**. ^{1}H NMR (600 MHz, DMSO) δ 8.20 (d, *J* = 8.5 Hz, 1H, H-5), 7.73 (d, *J* = 2.0 Hz, 1H, H-8), 7.59 (dd, *J* = 8.5, 2.0 Hz, 1H, H-6), 7.35 (t, *J* = 7.5 Hz, 2H, CH$_2$<u>Ph</u>), 7.29 (t, *J* = 7.3 Hz, 1H, CH$_2$<u>Ph</u>), 7.20 (d, *J* = 7.4 Hz, 2H, CH$_2$<u>Ph</u>), 5.79 (d, *J* = 16.4 Hz, 1H, C<u>H</u>$_2$Ph), 5.08 (d, *J* = 16.4 Hz, 1H) , C<u>H</u>$_2$Ph, 3.41 (dd, *J* = 10.4, 6.1 Hz, 1H, H-1'), 2.00-1.91 (m, 2H, CH$_2$N<u>H</u> and H-2'), 1.87 (dd, *J* = 11.6, 3.3 Hz, 1H, C<u>H</u>$_2$NH), 1.83 (br s, 3H, CH$_{(Ad)}$), 1.61-1.59 (m, 3H, CH$_{2(Ad)}$), 1.50-1.49 (m, 3H, CH$_{2(Ad)}$), 1.28-1.26 (m, 4H, CH$_{2(Ad)}$), 1.19-1.17 (m, 3H, CH$_{2(Ad)}$ and C<u>H</u>$_2$NH), 0.91 (d, *J* = 6.7 Hz, 3H, H-3'), 0.86 (d, *J* = 6.6 Hz, 3H, H-3'). ^{13}C{^{1}H} (151 MHz, DMSO) δ 161.7, 161.1, 147.7, 139.7, 139.3, 136.6, 128.7 (CH), 128.6 (CH), 127.3 (CH), 127.0 (CH), 126.4 (CH), 126.0 (CH), 118.6, 64.8 (CH$_{(Ad)}$), 59.1 (CH$_2$), 45.0 (CH$_2$), 39.9 (CH$_{2(Ad)}$) overlapped with DMSO residual peak, 36.6 (CH$_{2(Ad)}$), 33.1 (CH), 32.7, 27.7 (CH), 20.0 (CH), 17.3 (CH). Elemental analysis calculated for $C_{30}H_{36}ClN_3O$ C 73.52, H 7.40, N 8.57, found C 73.22, H 7.42, N 8.81. HPLC-MS analysis, R$_f$ (HPLC) τ = 2.10 min, m/z calculated for $C_{30}H_{37}{}^{35}ClN_3O$ $[M+H]^+$ 490.3 found 490.5 $[M+H]^+$.

(*R*)-2-(1-((adamantan-1-ylmethyl)amino)-2-methylpropyl)-3-benzyl-7-chloroquinazolin-4(3H)-one (*R*)-2f. This compound was obtained in 63% yield according to General procedure A starting from 200 mg of (*R*)-**5**, and 108 mg of **6f**. ^{1}H and ^{13}C{^{1}H} NMR spectra were identical with those of (*S*)-**2f**. Elemental analysis calculated for $C_{30}H_{36}ClN_3O$ C 73.52, H 7.40, N 8.57, found C 73.65, H 7.44, N 8.55. HPLC-MS analysis, R_f (HPLC) τ = 2.16 min, m/z calculated for $C_{30}H_{37}{}^{35}ClN_3O$ $[M+H]^+$ 490.3 found 490.5 $[M+H]^+$.

(*R*)-N-benzyl-N-(1-(3-benzyl-7-chloro-4-oxo-3,4-dihydroquinazolin-2-yl)-2-methylpropyl)-4-methylbenzamide (*R*)-3a. This compound was obtained in 27% yield according to General procedure C starting from 200 mg of (*R*)-**2a**. ^{1}H and ^{13}C{^{1}H} NMR spectra were identical with those of (S)-**3a**. Elemental analysis calculated for $C_{34}H_{32}ClN_3O$ C 74.24, H 5.86, N 7.64, found C 74.34, H 5.80, N 7.72. HPLC-MS analysis, R_f (HPLC) τ = 2.39 min, m/z calculated for $C_{34}H_{33}{}^{35}ClN_3O_2$ $[M+H]^+$ 550.2 found 550.4 $[M+H]^+$.

(*S*)-N-(2-ferrocenylbenzyl)-N-(1-(3-benzyl-7-chloro-4-oxo-3,4-dihydroquinazolin-2-yl)-2-methylpropyl)-4-methylbenzamide (*S*)-3b. This compound was obtained in 65% yield according to General procedure C starting from 50 mg of (*S*)-**2b**.^{1}H NMR (600 MHz, DMSO) δ 7.92 (d, *J* = 8.5 Hz, 1H, H-5), 7.49 (dd, *J* = 8.6, 2.0 Hz, 1H, H-6), 7.43 (d, *J* = 8.0 Hz, 1H, CH_{Ar}), 7.37 (t, *J* = 7.6 Hz, 1H, CH_{Ar}), 7.29 (m, *J* = 6.1 Hz, 1H, CH_{Ar}), 7.21 (d, *J* = 8.0 Hz, 1H, CH_{Ar}), 7.15 (d, *J* = 7.6 Hz, 1H, CH_{Ar}), 6.85 (t, *J* = 7.4 Hz, 1H, CH_{Ar}), 6.82 (d, *J* = 7.4 Hz, 1H, CH_{Ar}), 6.69 (t, *J* = 7.3 Hz, 1H, CH_{Ar}), 6.00 (d, *J* = 16.2 Hz, 1H, C$\underline{H}_2$Ph), 5.65 (d, *J* = 10.4 Hz, 1H, H-1'), 5.22 (d, *J* = 16.2 Hz, 1H, C$\underline{H}_2$Ph), 4.71 (d, *J* = 17.5 Hz, 1H, C$\underline{H}_2C_6H_4Fc$), 4.56 (d, *J* = 17.5 Hz, 1H, C$\underline{H}_2C_6H_4Fc$), 4.40 (br s, 1H, Cp), 4.36 (br s, 1H, Cp), 4.27 (br s, 1H, Cp), 4.19 (br s, 1H, Cp), 4.07 (s, 5H, Cp'), 2.70-2.63 (m, 1H, H-2'), 2.29 (s, 3H, C$\underline{H}_3C_6H_4CO$), 0.93 (d, *J* = 6.8 Hz, 3H, H-3'), 0.36 (d, *J* = 6.4 Hz, 3H, H-3'). ^{13}C{^{1}H} (151 MHz, DMSO) δ 172.8, 160.6, 153.9, 146.2, 139.1, 138.3, 136.8, 134.8, 134.4, 133.0, 130.4 (CH), 129.0 (CH), 128.7 (CH), 128.0 (CH), 127.5 (CH), 127.4 (CH), 126.6 (CH), 126.5 (CH), 126.2 (CH), 125.3 (CH), 125.2 (CH), 123.1 (CH), 118.5, 85.7 (Cp_{ipso}), 69.9 (Cp), 69.2 (Cp'), 69.1 (Cp), 68.0 (Cp), 67.7 (Cp), 58.8 (CH), 45.5 (CH_2), 44.8 (CH_2), 27.5 (CH), 20.8 (CH), 19.1 (CH), 17.8 (CH). Elemental analysis calculated for $C_{26}H_{26}ClN_3O$ C 71.99, H 5.49, N 5.72, found C 72.09, H 5.57, N 5.83. HPLC-MS

analysis, R_f (HPLC) τ = 2.16 min, m/z calculated for $C_{44}H_{40}{}^{35}ClFeN_3O_2$ $[M]^+$ 733.2 found 733.3 $[M]^+$.

(*R*)-N-(2-ferrocenylbenzyl)-N-(1-(3-benzyl-7-chloro-4-oxo-3,4-dihydroquinazolin-2-yl)-2-methylpropyl)-4-methylbenzamide (*R*)-3b. This compound was obtained in 61% yield according to General procedure C starting from 50 mg of (*R*)-**2b**. ^1H and $^{13}C\{^1H\}$ NMR spectra were identical with those of (S)-**3b**. Elemental analysis calculated for $C_{44}H_{40}ClFeN_3O_2$ C 71.99, H 5.49, N 5.72, found C 71.98, H 5.57, N 5.86. HPLC-MS analysis, R_f (HPLC) τ = 2.12 min, m/z calculated for $C_{44}H_{40}{}^{35}ClFeN_3O_2$ $[M]^+$ 733.2 found 733.4 $[M]^+$.

(*S*)-N-(3-ferrocenylbenzyl)-N-(1-(3-benzyl-7-chloro-4-oxo-3,4-dihydroquinazolin-2-yl)-2-methylpropyl)-4-methylbenzamide (*S*)-3c. This compound was obtained in 93% yield according to General procedure C starting from 70 mg of (*S*)-**2c**. ^1H NMR (600 MHz, DMSO) δ 7.88 (d, *J* = 8.5 Hz, 1H, H-5), 7.49 (d, *J* = 2.0 Hz, 1H, H-8), 7.41-7.37 (m, 1H, 5H, CH_{Ar}), 7.31-7.29 (m, 3H, CH_{Ar}), 7.21 (d, *J* = 8.0 Hz, 2H, CH_{Ar}), 6.92 (d, *J* = 7.7 Hz, 1H, CH_{Ar}), 6.79-6.75 (m, 1H, CH_{Ar}), 6.75 (s, 1H, CH_{Ar}), 6.59 (d, *J* = 7.6 Hz, 1H, CH), 5.91 (d, *J* = 16.1 Hz, 1H, C$\underline{H}_2$Ph), 5.66 (d, *J* = 10.5 Hz, 1H, H-1'), 5.22 (d, *J* = 16.1 Hz, 1H, C$\underline{H}_2$Ph), 4.74 (d, *J* = 17.0 Hz, 1H, C$\underline{H}_2C_6H_4Fc$), 4.60 (d, *J* = 17.0 Hz, 1H, *m*-C$\underline{H}_2C_6H_4Fc$), 4.41 (t, *J* = 1.7 Hz, 1H, Cp), 4.40 (t, *J* = 1.7 Hz, 1H, Cp), 4.26 (br s, 2H, Cp), 3.86 (s, 5H, Cp'), 2.95-2.88 (m, 1H, H-2'), 2.27 (s, 3H, C$\underline{H}_3C_6H_4CO$), 0.98 (d, *J* = 6.8 Hz, 3H, H-3'), 0.44 (d, *J* = 6.4 Hz, 3H, H-3'). $^{13}C\{^1H\}$ (151 MHz, DMSO) δ 172.5, 160.6, 154.2, 146.8, 139.2, 139.0, 138.5, 137.4, 136.8, 133.2, 128.9 (CH), 128.7 (CH), 128.1 (CH), 127.6 (CH), 127.5 (CH), 127.4 (CH), 126.6 (CH), 126.4 (CH), 126.3 (CH), 123.9 (CH), 122.6 (CH), 122.5 (CH), 118.5, 84.0 (Cp_{ipso}), 69.1 (Cp'), 68.7 (Cp), 66.3 (Cp), 65.6 (Cp), 59.1 (CH), 47.5 (CH_2), 44.8 (CH_2), 27.8 (CH), 20.8 (CH), 19.3 (CH), 18.0 (CH). Elemental analysis calculated for $C_{44}H_{40}ClFeN_3O_2$C 71.99, H 5.49, N 5.72, found C 71.90, H 5.52, N 5.82. HPLC-MS analysis, R_f (HPLC) τ = 2.40 min, m/z calculated for $C_{44}H_{40}{}^{35}ClFeN_3O_2$ $[M]^+$ 733.2 found 733.4 $[M]^+$.

(*R*)-N-(3-ferrocenylbenzyl)-N-(1-(3-benzyl-7-chloro-4-oxo-3,4-dihydroquinazolin-2-yl)-2-methylpropyl)-4-methylbenzamide (*R*)-3c. This compound was obtained in 93% yield according to General procedure C starting from 70 mg of (*R*)-**2c**. ^1H and $^{13}C\{^1H\}$ NMR spectra were identical with those of (S)-**3c**. Elemental analysis calculated for $C_{44}H_{40}ClFeN_3O_2$ C 71.99, H 5.49, N 5.72, found C

71.87, H 5.49, N 5.87. HPLC-MS analysis, R_f (HPLC) τ = 2.39 min, m/z calculated for $C_{44}H_{40}{}^{35}ClFeN_3O_2$ $[M]^+$ 733.2 found 733.4 $[M]^+$.

(*S*)-N-(4-ferrocenylbenzyl)-N-(1-(3-benzyl-7-chloro-4-oxo-3,4-dihydroquinazolin-2-yl)-2-methylpropyl)-4-methylbenzamide (*S*)-3d. This compound was obtained in 65% yield according to General procedure C starting from 50 mg of (*S*)-**2d**. ^{1}H NMR (600 MHz, DMSO) δ 7.90 (d, *J* = 8.5 Hz, 1H, H-5), 7.57 (d, *J* = 2.0 Hz, 1H, H-8), 7.45 (dd, *J* = 8.5, 2.0 Hz, 1H, H-6), 7.41-7.37 (m, 4H, CH_{Ar}), 7.33-7.30 (m, 3H, CH_{Ar}), 7.21 (d, *J* = 8.0 Hz, 2H, CH_{Ar}), 6.95 (d, *J* = 8.2 Hz, 2H, CH_{Ar}), 6.68 (d, *J* = 8.1 Hz, 2H, CH_{Ar}), 5.95 (d, *J* = 16.2 Hz, 1H, C$\underline{H}_2$Ph), 5.67 (d, *J* = 10.5 Hz, 1H, H-1'), 5.22 (d, *J* = 16.2 Hz, 1H, C$\underline{H}_2$Ph), 4.68 (d, *J* = 17.2 Hz, 1H, *p*-C$\underline{H}_2C_6H_4Fc$), 4.57 (d, *J* = 17.2 Hz, 1H, *p*-C$\underline{H}_2C_6H_4Fc$), 4.42 (br s, 1H, Cp), 4.40 (br s, 1H, Cp), 4.24 (br s, 1H, Cp), 4.23 (br s, 1H, Cp), 3.87 (s, 5H, Cp'), 2.96-2.91 (m, 1H, H-2'), 2.28 (s, 3H, C$\underline{H}_3C_6H_4CO$), 0.99 (d, *J* = 6.8 Hz, 3H, H-3'), 0.46 (d, *J* = 6.4 Hz, 3H, H-3'). ^{13}C{^{1}H} (151 MHz, DMSO) δ 172.5, 160.7, 154.3, 146.9, 139.0, 138.8, 136.8, 134.9, 133.2, 128.9 (CH), 128.7 (CH), 128.2 (CH), 127.6 (CH), 127.5 (CH), 126.6 (CH), 126.3 (CH), 125.2 (CH), 124.9 (CH), 118.6, 84.5 (Cp_{ipso}), 69.2 (Cp'), 68.52 (Cp), 68.46 (Cp), 66.4 (Cp), 65.7 (Cp), 59.0 (CH), 47.3 (CH_2), 44.9 (CH_2), 27.7 (CH), 20.8 (CH), 19.3 (CH), 17.9 (CH). Elemental analysis calculated for $C_{44}H_{40}ClFeN_3O_2$ C 71.99, H 5.49, N 5.72, found C 71.94, H 5.61, N 5.76. HPLC-MS analysis, R_f (HPLC) τ = 2.81 min, m/z calculated for $C_{44}H_{40}{}^{35}ClFeN_3O_2$ $[M]^+$ 733.2 found 733.4 $[M]^+$.

(*R*)-N-(4-ferrocenylbenzyl)-N-(1-(3-benzyl-7-chloro-4-oxo-3,4-dihydroquinazolin-2-yl)-2-methylpropyl)-4-methylbenzamide (*R*)-3d. This compound was obtained in 74% yield according to General procedure C starting from 50 mg of (*R*)-**2d**. ^{1}H and ^{13}C{^{1}H} NMR spectra were identical with those of (*S*)-**3d**. Elemental analysis calculated for $C_{44}H_{40}ClFeN_3O_2$ C 71.99, H 5.49, N 5.72, found C 71.94, H 5.61, N 5.76. HPLC-MS analysis, R_f (HPLC) τ = 2.61 min, m/z calculated for $C_{44}H_{40}{}^{35}ClFeN_3O_2$ $[M]^+$ 733.2 found 733.4 $[M]^+$.

(*S*)-N-ferrocenylmethyl-N-(1-(3-benzyl-7-chloro-4-oxo-3,4-dihydroquinazolin-2-yl)-2-methylpropyl)-4-methylbenzamide (*S*)-3e. This compound was obtained in 47% yield according to General procedure C starting from 70 mg of (*R*)-**2e**. ^{1}H NMR (600 MHz, DMSO) δ 8.09 (d, *J* = 8.6 Hz, 1H, H-5), 7.83 (d, *J* = 2.0 Hz, 1H, H-8), 7.62 (dd, *J* = 2.0, 8.5 Hz, 1H, H-6), 7.41 (d, *J* = 8.0 Hz, 2H, $CH_3C_6\underline{H}_4CO$), 7.35-7.33 (m, 3H, $CH_2\underline{Ph}$), 7.28 (t, *J* = 7.3 Hz, 2H, $CH_2\underline{Ph}$), 7.21 (d, *J* = 7.6 Hz, 2H, $CH_3C_6\underline{H}_4CO$), 5.69

(d, *J* = 16.3 Hz, 1H, C$\underline{H}_2$Ph), 5.45 (d, *J* = 10.5 Hz, 1H, H-1'), 4.95 (d, *J* = 16.3 Hz, 1H, C$\underline{H}_2$Ph), 4.75 (d, *J* = 16.1 Hz, 1H, C$\underline{H}_2$Fc), 4.29 (d, *J* = 16.2 Hz, 1H, C$\underline{H}_2$Fc), 3.70 (s, 2H, Cp), 3.63 (s, 5H, Cp'), 3.39-3.38 (m, 1H, Cp), 3.12 (s, 1H, Cp), 2.90-2.83 (m, 1H, H-2'), 2.38 (s, 3H, C$\underline{H}_3$C$_6$H$_4$CO), 0.91 (d, *J* = 6.8 Hz, 3H, H-3'), 0.55 (d, *J* = 6.4 Hz, 3H, H-3'). ^{13}C{^{1}H} (151 MHz, DMSO) δ 171.7, 160.7, 154.7, 147.2, 139.14, 139.06, 136.7, 133.5, 128.8 (CH), 128.6 (CH), 128.4 (CH), 127.7 (CH), 127.3 (CH), 126.9 (CH), 126.6 (CH), 126.3 (CH), 119.3, 83.7 (Cp$_{ipso}$), 68.3 (Cp' and Cp), 67.5 (Cp), 66.8 (Cp), 66.3 (Cp), 58.9 (CH), 44.7 (CH$_2$), 43.4 (CH$_2$), 27.7 (CH), 20.9 (CH), 19.7 (CH), 18.0 (CH). Elemental analysis calculated for $C_{38}H_{36}ClFeN_3O_2$ C 69.36, H 5.51, N 6.39, found C 69.33, H 5.41, N 6.33. HPLC-MS analysis, R_f (HPLC) τ = 3.84 min, m/z calculated for $C_{38}H_{36}{}^{35}ClFeN_3O_2$ $[M]^+$ 657.2 found 657.2 $[M]^+$.

(*R*)-N-ferrocenylmethyl-N-(1-(3-benzyl-7-chloro-4-oxo-3,4-dihydroquinazolin-2-yl)-2-methylpropyl)-4-methylbenzamide (*R*)-3e. This compound was obtained in 53% yield according to General procedure C starting from 100 mg of (*R*)-**2e**. ^{1}H and ^{13}C{^{1}H} NMR spectra were identical with those of (*S*)-**3e**. Elemental analysis calculated for $C_{38}H_{36}ClFeN_3O_2$ C 69.36, H 5.51, N 6.39, found C 69.29, H 5.66, N 6.68. HPLC-MS analysis, R_f (HPLC) τ = 3.78 min, m/z calculated for $C_{38}H_{36}{}^{35}ClFeN_3O_2$ $[M]^+$ 657.2 found 657.2 $[M]^+$.

(*R*)-N-(1-(3-benzyl-7-chloro-4-oxo-3,4-dihydroquinazolin-2-yl)-2-methylpropyl)-N-(3-(benzylamino)propyl)-4-methylbenzamide (*R*)-4a. This compound was obtained in 59% yield according to General procedure B starting from 100 mg of (*R*)-**1** and 23 mg of **6a**. ^{1}H and ^{13}C{^{1}H} NMR spectra were identical with those of (*S*)-**4a**. Elemental analysis calculated for $C_{37}H_{39}ClN_4O_2$ C 73.19, H 6.47, N 9.23, found C 72.99, H 6.64, N 9.25. HPLC-MS analysis, R_f (HPLC) τ = 2.12 min, m/z calculated for $C_{37}H_{40}{}^{35}ClN_4O_2$ $[M+H]^+$ 607.3 found 607.7 $[M+H]^+$.

(*S*)-N-(1-(3-benzyl-7-chloro-4-oxo-3,4-dihydroquinazolin-2-yl)-2-methylpropyl)-N-(3-(2-ferrocenylbenzylamino)propyl)-4-methylbenzamide (*S*)-4b. This compound was obtained in 59% yield according to General procedure B starting from 100 mg of (*S*)-**1** and 63 mg of **6b**. ^{1}H NMR (600 MHz, DMSO) δ 8.23 (d, *J* = 8.6 Hz, 1H, H-5), 7.72 (d, *J* = 2.0 Hz, 1H, H-8), 7.67 (dd, *J* = 7.7, 1.0 Hz, 1H, CH$_{Ar}$), 7.65 (dd, *J* = 8.6, 2.1 Hz, 1H, H-6), 7.36 (d, *J* = 7.6 Hz, 1H, CH$_{Ar}$), 7.31 (t, *J* = 7.3 Hz, 1H, CH$_{Ar}$), 7.27-7.19 (m, 7H, CH$_{Ar}$), 7.13-7.11 (m, 1H, CH$_{Ar}$), 7.01 (d, *J* = 7.2 Hz, 1H, CH$_{Ar}$), 5.90 (d, *J* = 16.3 Hz, 1H, C$\underline{H}_2$Ph), 5.53 (d, *J* = 10.5 Hz, 1H, H-1'), 5.10 (d, *J* = 16.3 Hz,

1H, C$\underline{H}_2$Ph), 4.50 (br s, 1H, Cp), 4.43 (br s, 1H, Cp), 4.28-4.27 (m, 2H, Cp), 4.08 (s, 5H, Cp'), 3.33-3.30 (m, 2H, CH_2), 3.27 (br s, 2H, o-C$\underline{H}_2C_6H_4Fc$), 2.81-2.74 (m, 1H, H-2'), 2.28 (s, 3H, C$\underline{H}_3C_6H_4CO$), 1.95-1.86 (m, 1H, 2H, CH_2), 1.25-1.17 (m, 2H, CH_2 and NH), 0.91 (d, *J* = 6.8 Hz, 3H, H-3'), 0.76-0.72 (m, 1H, CH_2), 0.49 (d, *J* = 6.4 Hz, 3H, H-3'). $^{13}C\{^1H\}$ (151 MHz, DMSO) δ 171.9, 161.1, 155.3, 147.2, 139.5, 138.6, 137.7, 136.9, 136.7, 133.9, 130.4 (CH), 128.84 (CH), 128.78 (CH), 128.73 (CH), 128.66 (CH), 128.0 (CH), 127.4 (CH), 126.5 (CH), 126.4 (CH), 126.2 (CH), 125.9 (CH), 125.8 (CH), 119.1, 86.4 (Cp_{ipso}), 69.4 (Cp), 69.3 (Cp), 69.2 (Cp'), 67.80 (Cp), 67.78 (Cp), 59.0 (CH), 50.6 (CH_2), 46.3 (CH_2), 45.1 (CH_2), 42.4 (CH_2), 29.8 (CH_2), 28.1 (CH), 20.9 (CH), 19.5 (CH), 18.1 (CH). Elemental analysis calculated for $C_{47}H_{47}ClFeN_4O_2$ C 71.35, H 5.99, N 7.08, found C 71.32, H 6.09, N 7.35. HPLC-MS analysis, R_f (HPLC) τ = 1.97 min, m/z calculated for $C_{47}H_{48}{}^{35}ClFeN_4O_2$ $[M+H]^+$ 791.3 found 791.3 $[M+H]^+$.

(*R*)-N-(1-(3-benzyl-7-chloro-4-oxo-3,4-dihydroquinazolin-2-yl)-2-methylpropyl)-N-(3-(2-ferrocenylbenzylamino)propyl)-4-methylbenzamide (*R*)-4b. This compound was obtained in 65% yield according to General procedure B starting from 100 mg of (*R*)-**1** and 63 mg of **6b**. ^1H and $^{13}C\{^1H\}$ NMR spectra were identical with those of (*S*)-**4b**. Elemental analysis calculated for $C_{47}H_{47}ClFeN_4O_2$ C 71.35, H 5.99, N 7.08, found C 71.41, H 5.97, N 7.21. HPLC-MS analysis, R_f (HPLC) τ = 1.99 min, m/z calculated for $C_{47}H_{48}{}^{35}ClFeN_4O_2$ $[M+H]^+$ 791.3 found 791.4 $[M+H]^+$.

(*S*)-N-(1-(3-benzyl-7-chloro-4-oxo-3,4-dihydroquinazolin-2-yl)-2-methylpropyl)-N-(3-(3-ferrocenylbenzylamino)propyl)-4-methylbenzamide (*S*)-4c. This compound was obtained in 52% yield according to General procedure B starting from 100 mg of (*S*)-**1** and 63 mg of **6c**. ^1H NMR (600 MHz, DMSO) δ 8.25 (d, *J* = 8.6 Hz, 1H, H-5), 7.75 (d, *J* = 1.9 Hz, 1H, H-8), 7.66 (dd, *J* = 8.6, 2.0 Hz, 1H, H-6), 7.38-7.36 (m, 3H, CH_{Ar}), 7.31 (d, *J* = 7.3 Hz, 1H, CH_{Ar}), 7.28-7.20 (m, 7H, CH_{Ar}), 7.17 (t, *J* = 7.6 Hz, 1H, CH_{Ar}), 6.82 (d, *J* = 7.5 Hz, 1H, CH_{Ar}), 5.90 (d, *J* = 16.3 Hz, 1H, C$\underline{H}_2$Ph), 5.54 (d, *J* = 10.6 Hz, 1H, H-1'), 5.09 (d, *J* = 16.3 Hz, 1H, C$\underline{H}_2$Ph), 4.72 (br s, 1H, Cp), 4.7- (br s, 1H, Cp), 4.34 (br s, 2H, Cp), 3.98 (s, 5H, Cp'), 3.38-3.32 (m, 1H, 2H, CH_2), 3.21-3.16 (m, 2H, CH_2), 2.82-2.76 (m, 1H, H-2'), 2.28 (s, 3H, C$\underline{H}_3C_6H_4CO$), 1.99-1.95 (m, 1H, CH_2), 1.93-1.89 (m, 1H, CH_2), 1.27-1.22 (m, 1H, CH_2), 0.91 (d, *J* = 6.7 Hz, 3H, H-3'), 0.75 (m, *J* = 5.8 Hz, 1H, CH_2), 0.49 (d, *J* = 6.3 Hz, 3H, H-3'). $^{13}C\{^1H\}$ (151 MHz, DMSO) δ 171.9, 161.1, 155.4, 147.2, 140.5, 139.5, 138.6, 138.5, 136.7, 133.9, 128.83 (CH), 128.75 (CH), 128.7 (CH), 128.00 (CH), 127.96 (CH), 127.90 (CH), 127.4 (CH),

126.5 (CH), 126.4 (CH), 125.9 (CH), 125.2 (CH), 125.0 (CH), 124.1 (CH), 119.1, 85.0 (Cp_{ipso}), 69.3 (Cp'), 68.7 (Cp), 66.22 (Cp), 66.18 (Cp), 58.9 (CH), 51.9 (CH_2), 45.6 (CH_2), 45.1 (CH_2), 42.4 (CH_2), 29.5 (CH_2), 28.1 (CH), 20.8 (CH), 19.4 (CH), 18.1 (CH). Elemental analysis calculated for $C_{47}H_{47}ClFeN_4O_2$ C 71.35, H 5.99, N 7.08, found C 71.42, H 5.98, N 7.21. HPLC-MS analysis, R_f (HPLC) τ = 1.88 min, m/z calculated for $C_{47}H_{48}{}^{35}ClFeN_4O_2$ $[M+H]^+$ 791.3 found 791.3 $[M+H]^+$.

(*R*)-N-(1-(3-benzyl-7-chloro-4-oxo-3,4-dihydroquinazolin-2-yl)-2-methylpropyl)-N-(3-(3-ferrocenylbenzylamino)propyl)-4-methylbenzamide (*R*)-4c. This compound was obtained in 59% yield according to General procedure B starting from 100 mg of (*R*)-**1** and 63 mg of **6c**. ^1H and $^{13}C\{^1H\}$ NMR spectra were identical with those of (*S*)-**4c**. Elemental analysis calculated for $C_{47}H_{47}ClFeN_4O_2$ C 71.35, H 5.99, N 7.08, found C 71.47, H 6.04, N 7.25. HPLC-MS analysis, R_f (HPLC) τ = 1.94 min, m/z calculated for $C_{47}H_{48}{}^{35}ClFeN_4O_2$ $[M+H]^+$ 791.3 found 791.5 $[M+H]^+$.

(*S*)-N-(1-(3-benzyl-7-chloro-4-oxo-3,4-dihydroquinazolin-2-yl)-2-methylpropyl)-N-(3-(4-ferrocenylbenzylamino)propyl)-4-methylbenzamide (*S*)-4d. This compound was obtained in 23% yield according to General procedure B starting from 100 mg of (*S*)-**1** and 63 mg of **6d**. ^1H NMR (600 MHz, DMSO) δ 8.26 (d, *J* = 8.6 Hz, 1H, H-5), 7.78 (d, *J* = 2.0 Hz, 1H, H-8), 7.68 (dd, *J* = 8.6, 2.1 Hz, 1H, H-6), 7.41 (d, *J* = 8.1 Hz, 2H, CH_{Ar}), 7.37 (t, *J* = 7.5 Hz, 2H, CH_{Ar}), 7.31 (t, *J* = 7.3 Hz, 1H, CH_{Ar}), 7.28-7.23 (m, 6H, CH_{Ar}), 6.94 (d, *J* = 8.1 Hz, 2H, CH_{Ar}), 5.91 (d, *J* = 16.2 Hz, 1H, C$\underline{H}_2$Ph), 5.53 (d, *J* = 10.5 Hz, 1H, H-1'), 5.08 (d, *J* = 16.3 Hz, 1H, C$\underline{H}_2$Ph), 4.74 (t, *J* = 1.8 Hz, 2H, Cp), 4.33 (t, *J* = 1.8 Hz, 2H, Cp), 4.00 (s, 5H, Cp'), 3.34-3.32 (m, 2H, H-1''), 3.16-3.11 (m, 2H, p-C$\underline{H}_2C_6H_4$Fc), 2.80-2.74 (m, 1H, H-2'), 2.31 (s, 3H, C$\underline{H}_3C_6H_4$CO), 1.95-1.90 (m, 2H, H-3''), 1.29-1.24 (m, 2H, CH_2 and NH), 0.91 (d, *J* = 6.8 Hz, 3H, H-3'), 0.75-0.70 (m, 1H, CH_2), 0.49 (d, *J* = 6.4 Hz, 3H, H-3'). $^{13}C\{^1H\}$ (151 MHz, DMSO) δ 171.9, 161.1, 155.4, 147.2, 139.5, 138.6, 138.2, 136.8, 136.7, 133.9, 128.9 (CH), 128.8 (CH), 128.7 (CH), 128.1 (CH), 127.6 (CH), 127.4 (CH), 126.6 (CH), 126.4 (CH), 125.9 (CH), 125.5 (CH), 119.1, 84.9 (Cp_{ipso}), 66.2 (Cp'), 68.7 (Cp), 66.1 (Cp), 58.9 (CH), 51.8 (CH_2), 45.6 (CH_2), 45.1 (CH_2), 42.4 (CH_2), 29.5 (CH_2), 28.1 (CH), 20.9 (CH), 19.4 (CH), 18.1 (CH). Elemental analysis calculated for $C_{47}H_{47}ClFeN_4O_2$ C 72.29, H 6.07, N 9.73, found C 72.21, H 5.98, N 9.94. HPLC-MS analysis, R_f (HPLC) τ = 1.37 min, m/z calculated for $C_{47}H_{48}{}^{35}ClFeN_4O_2$ $[M+H]^+$ 791.3 found 791.3 $[M+H]^+$.

(*R*)-N-(1-(3-benzyl-7-chloro-4-oxo-3,4-dihydroquinazolin-2-yl)-2-methylpropyl)-N-(3-(4-ferrocenylbenzylamino)propyl)-4-methylbenzamide (*R*)-4d. This compound was obtained in 33% yield according to General procedure B starting from 100 mg of (*R*)-**1** and 63 mg of **6d**. ^{1}H and ^{13}C{^{1}H} NMR spectra were identical with those of (*S*)-**4d**. Elemental analysis calculated for $C_{47}H_{47}ClFeN_4O_2$ C 71.35, H 5.99, N 7.08, found C 71.38, H 5.99, N 7.26. HPLC-MS analysis, R_f (HPLC) τ = 1.39 min, m/z calculated for $C_{47}H_{48}{}^{35}ClFeN_4O_2$ $[M+H]^+$ 791.3 found 791.3 $[M+H]^+$.

(*S*)-N-(1-(3-benzyl-7-chloro-4-oxo-3,4-dihydroquinazolin-2-yl)-2-methylpropyl)-N-(3-(ferrocenylmethylamino)propyl)-4-methylbenzamide (*S*)-4e. This compound was obtained in 47% yield according to General procedure B starting from 100 mg of (*S*)-**1** and 47 mg of **6e**. ^{1}H NMR (600 MHz, DMSO) δ 8.26 (d, *J* = 8.6 Hz, 1H, H-5), 7.82 (d, *J* = 2.0 Hz, 1H, H-8), 7.70 (dd, *J* = 8.6, 2.1 Hz, 1H, H-6), 7.38 (t, *J* = 7.5 Hz, 2H, CH_{Ar}), 7.31 (t, *J* = 7.3 Hz, 1H, CH_{Ar}), 7.33-7.25 (m, 6H, CH_{Ar}), 5.92 (d, *J* = 16.2 Hz, 1H, C$\underline{H}_2$Ph), 5.54 (d, *J* = 10.5 Hz, 1H, H-1'), 5.10 (d, *J* = 16.3 Hz, 1H, C$\underline{H}_2$Ph), 4.02 (s, 5H, Cp'), 4.01 (t, *J* = 1.8 Hz, 2H, Cp), 3.89 (br s, 1H, Cp), 3.88 (br s, 1H, Cp), 3.32 (t, *J* = 8.2 Hz, 2H, H-1''), 2.88-2.85 (m, 2H, C$\underline{H}_2$Fc), 2.79-2.75 (m, 1H, H-2'), 2.34 (s, 3H, C$\underline{H}_3C_6H_4CO$), 1.98-1.82 (m, 2H, H-3''), 1.24-1.17 (m, 2H, H-2'' and NH), 0.91 (d, *J* = 6.8 Hz, 3H, H-3'), 0.70-0.67 (m, 1H, H-2''), 0.49 (d, *J* = 6.4 Hz, 3H, H-3'). ^{13}C{^{1}H} (151 MHz, DMSO) δ 171.9, 161.1, 155.4, 147.3, 139.6, 138.6, 136.7, 133.9, 128.9 (CH), 128.8 (CH), 128.7 (CH), 128.1 (CH), 127.4 (CH), 126.6 (CH), 126.4 (CH), 125.9 (CH), 119.1, 87.1 (Cp_{ipso}), 68.1 (Cp'), 67.7 (Cp), 67.6 (Cp), 67.0 (Cp), 58.9 (CH), 47.1 (CH_2), 45.8 (CH_2), 45.1 (CH_2), 42.3 (CH_2), 29.6 (CH_2), 28.1 (CH), 20.9 (CH), 19.4 (CH), 18.1 (CH). Elemental analysis calculated for $C_{41}H_{43}ClFeN_4O_2$ C 68.86, H 6.06, N 7.83, found C 69.02, H 5.99, N 8.05. HPLC-MS analysis, R_f (HPLC) τ = 3.84 min, m/z calculated for $C_{41}H_{44}{}^{35}ClFeN_4O_2$ $[M+H]^+$ 715.3 found 715.1 $[M+H]^+$.

(*R*)-N-(1-(3-benzyl-7-chloro-4-oxo-3,4-dihydroquinazolin-2-yl)-2-methylpropyl)-N-(3-(ferrocenylmethylamino)propyl)-4-methylbenzamide (*R*)-4e. This compound was obtained in 47% yield according to General procedure B starting from 100 mg of (*R*)-**1** and 47 mg of **6e**. ^{1}H and ^{13}C{^{1}H} NMR spectra were identical with those of (*S*)-**4e**. Elemental analysis calculated for $C_{41}H_{43}ClFeN_4O_2$ C 68.86, H 6.06, N 7.83, found C 69.02, H 6.20, N 8.09. HPLC-MS analysis, R_f (HPLC) τ = 3.80 min, m/z calculated for $C_{41}H_{44}{}^{35}ClFeN_4O_2$ $[M+H]^+$ 715.3 found 715.5 $[M+H]^+$.

(*S*)-N-(3-((adamantan-1-ylmethyl)amino)propyl)-N-(1-(3-benzyl-7-chloro-4-oxo-3,4-dihydroquinazolin-2-yl)-2-methylpropyl)-4-methylbenzamide (*S*)-4f. This compound was obtained in 31% yield according to General procedure B starting from 100 mg of (*S*)-**1** and 35 mg of **6f**. ^{1}H NMR (600 MHz, DMSO) δ 8.24 (d, *J* = 8.6 Hz, 1H, H-5), 7.80 (d, *J* = 2.0 Hz, 1H, H-8), 7.67 (dd, *J* = 8.6, 2.0 Hz, 1H, H-6), 7.37 (t, *J* = 7.5 Hz, 2H, CH_{Ar}), 7.31 (t, *J* = 7.3 Hz, 1H, CH_{Ar}), 7.27-7.25 (m, 6H, CH_{Ar}), 5.91 (d, *J* = 16.3 Hz, 1H, C$\underline{H}_2$Ph), 5.53 (d, *J* = 10.5 Hz, 1H, H-1'), 5.08 (d, *J* = 16.3 Hz, 1H, C$\underline{H}_2$Ph), 3.26 (t, *J* = 8.1 Hz, 2H, H-1''), 2.80-2.74 (m, 1H, H-2'), 1.99-1.83 (m, 1H, H'-3''), 1.89-1.83 (m, 1H, H-3''), 1.83 (br s, 3H, CH_{Ad}), 1.63-1.51 (m, 3H, $CH_{2(Ad)}$), 1.53-1.49 (m, 3H, $CH_{2(Ad)}$), 1.24-1.15 (m, 2H, H-2'' and NH), 1.15 (br s, 6H, $CH_{2(Ad)}$) 0.90 (d, *J* = 6.8 Hz, 3H, H-3'), 0.68-0.63 (m, 1H, H-2''), 0.49 (d, *J* = 6.3 Hz, 3H, H-3'). ^{13}C{^{1}H} (151 MHz, DMSO) δ 171.9, 161.1, 155.4, 147.3, 139.6, 138.5, 136.7, 134.0, 128.9 (CH), 128.8 (CH), 128.7 (CH), 128.1 (CH), 127.4 (CH), 126.6 (CH), 126.4 (CH), 125.9 (CH), 119.1, 61.1 (CH_2), 58.8 (CH), 47.4 (CH_2), 45.1 (CH_2), 42.5 (CH_2), 40.1 (CH_2), 36.8 (CH_2), 32.7, 29.6 (CH_2), 28.0 (CH), 27.8 (CH), 20.9 (CH), 19.5 (CH), 18.0 (CH). Elemental analysis calculated for $C_{41}H_{49}ClN_4O_2$ C 74.02, H 7.42, N 8.42, found C 73.80, H 7.40, N 8.61. HPLC-MS (SI) analysis, R_f (HPLC) τ = 2.40 min, m/z calculated for $C_{41}H_{50}{}^{35}ClN_4O_2$ $[M+H]^+$ 665.4 found 665.4 $[M+H]^+$.

(*R*)-N-(3-((adamantan-1-ylmethyl)amino)propyl)-N-(1-(3-benzyl-7-chloro-4-oxo-3,4-dihydroquinazolin-2-yl)-2-methylpropyl)-4-methylbenzamide (*R*)-4f. This compound was obtained in 50% yield according to General procedure B starting from 100 mg of (*R*)-**1** and 35 mg of **6f**. ^{1}H and ^{13}C{^{1}H} NMR spectra were identical with those of (*S*)-**4f**. Elemental analysis calculated for $C_{41}H_{49}ClN_4O_2$ C 74.02, H 7.42, N 8.42, found C 73.83, H 7.31, N 8.54. HPLC-MS analysis, R_f (HPLC) τ = 2.41 min, m/z calculated for $C_{41}H_{50}{}^{35}ClN_4O_2$ $[M+H]^+$ 665.4 found 665.7 $[M+H]^+$.

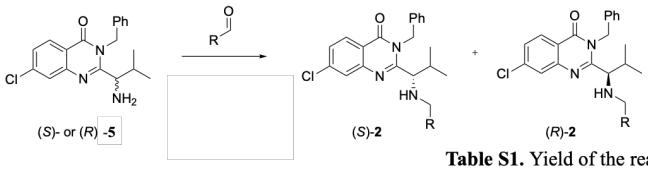

Procedure:
A: 1,2-DCE, NaBH(OAc)3, RT, 24h
B: 1,2-DCE, MW, 120 ºC, 15 min;
then NaBH(OAc)3, 1,2-DCE, MW, 120 ºC, 15 min

Table S1. Yield of the reaction of (*S*)- and (*R*)-**9** with aldehydes under procedure **A** and **B**

Aldehyde RCHO	Procedure A* Yield	Procedure A* Yield	Procedure B** Yield	Procedure B** Yield
R	Substrate (*S*)-**5**	Substrate (*R*)-**5**	Substrate (*S*)-**5**	Substrate (*R*)-**5**
Ph	56%	55%	51%	61%
o-C_6H_4Fc	65%	55%	61%	61%
m-C_6H_4Fc	59%	61%	61%	55%
p-C_6H_4Fc	81%	78%	77%	72%
Fc	80%	85%	82%	88%
Ad	70%	63%	71%	66%

* - no racemization observed; **- partial racemization occur

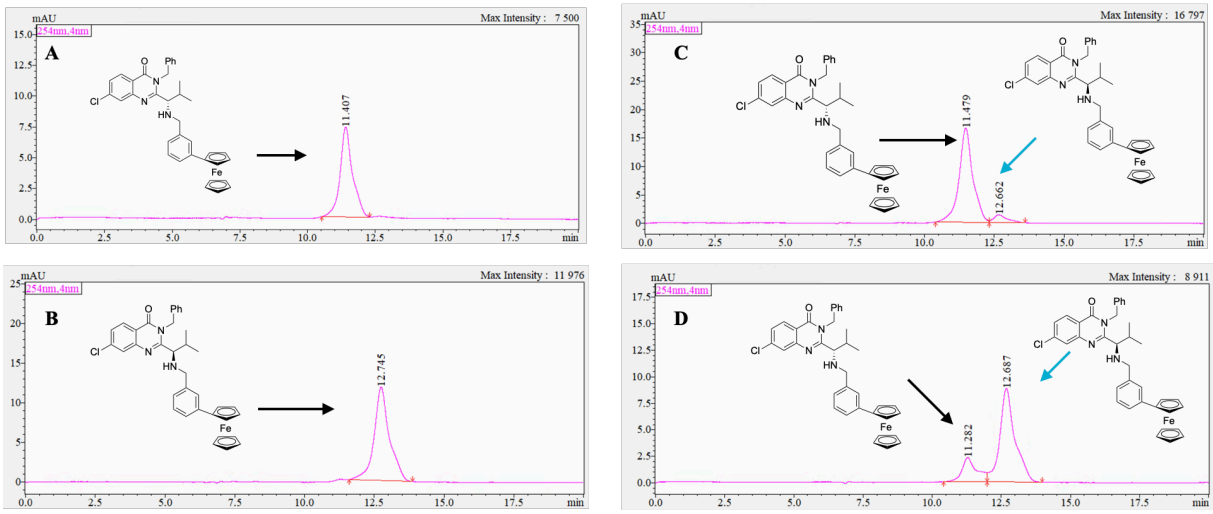

Figure S1. Chiral HPLC analysis of **2c** obtained under various conditions. A) HPLC chromatogram of the product obtained from (*S*)-**5** and **6c** under condition A; B) Analysis of the product obtained from (*R*)-**5** and **6c** under condition A; C) HPLC chromatogram of the product obtained from (*S*)-**5** and **6c** under condition B; D) Analysis of the product obtained from (*R*)-**5** and **6c** under condition B;

A)

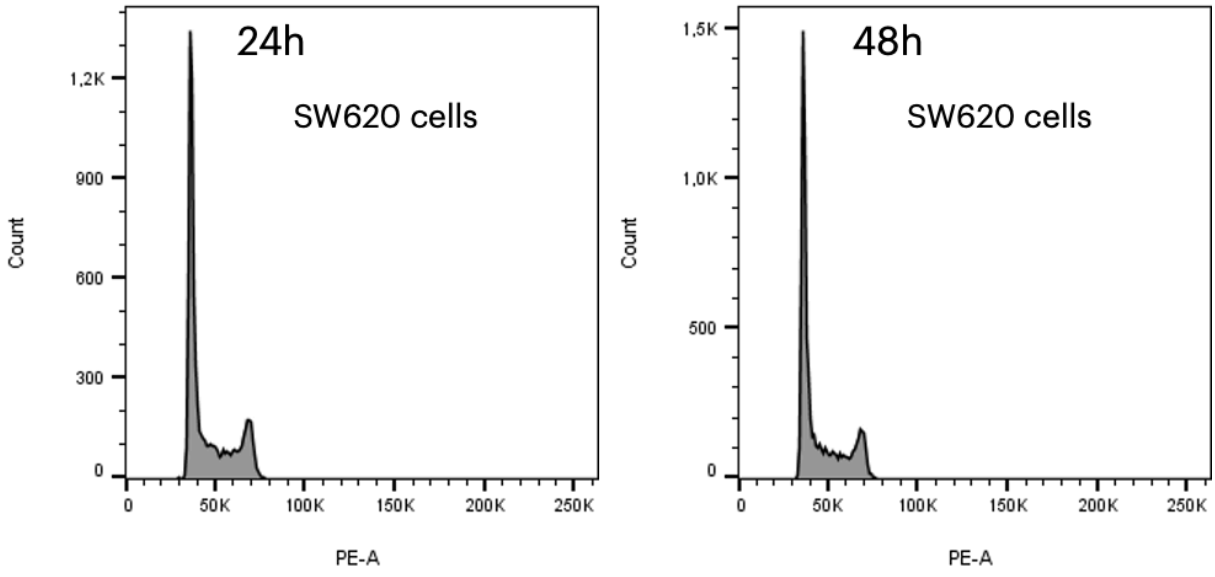

SW620_SW620_24h.fcs
Single Cells
8231

SW620_SW620_48.fcs
Single Cells
8162

B)

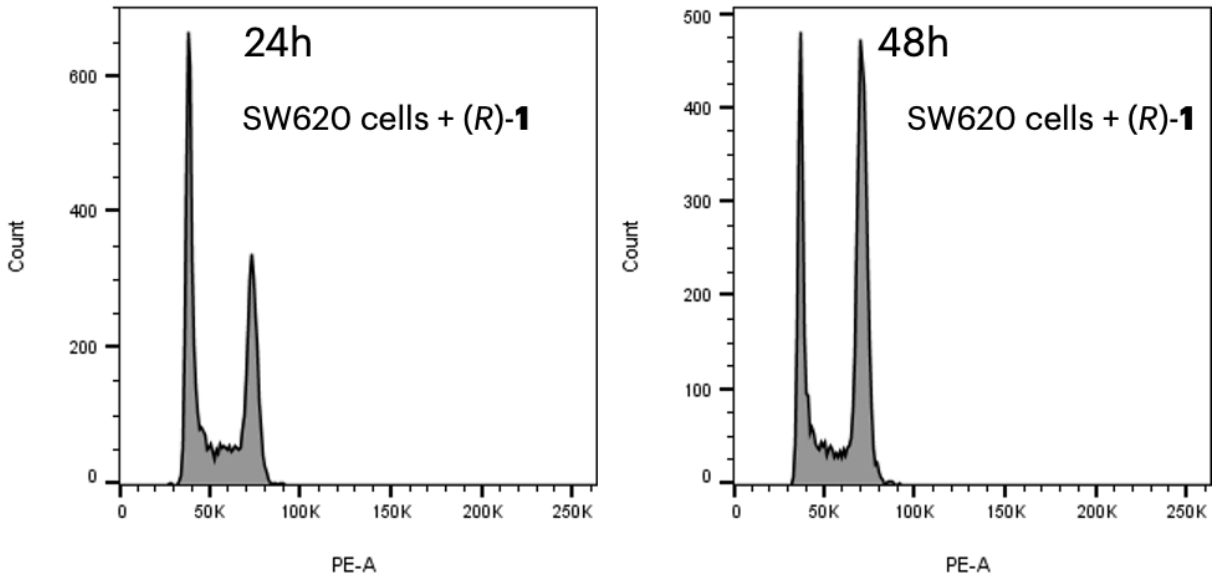

SW620_SW620_24_r1.fcs
Single Cells
6893

SW620_SW620_48_r1.fcs
Single Cells
6195

C)

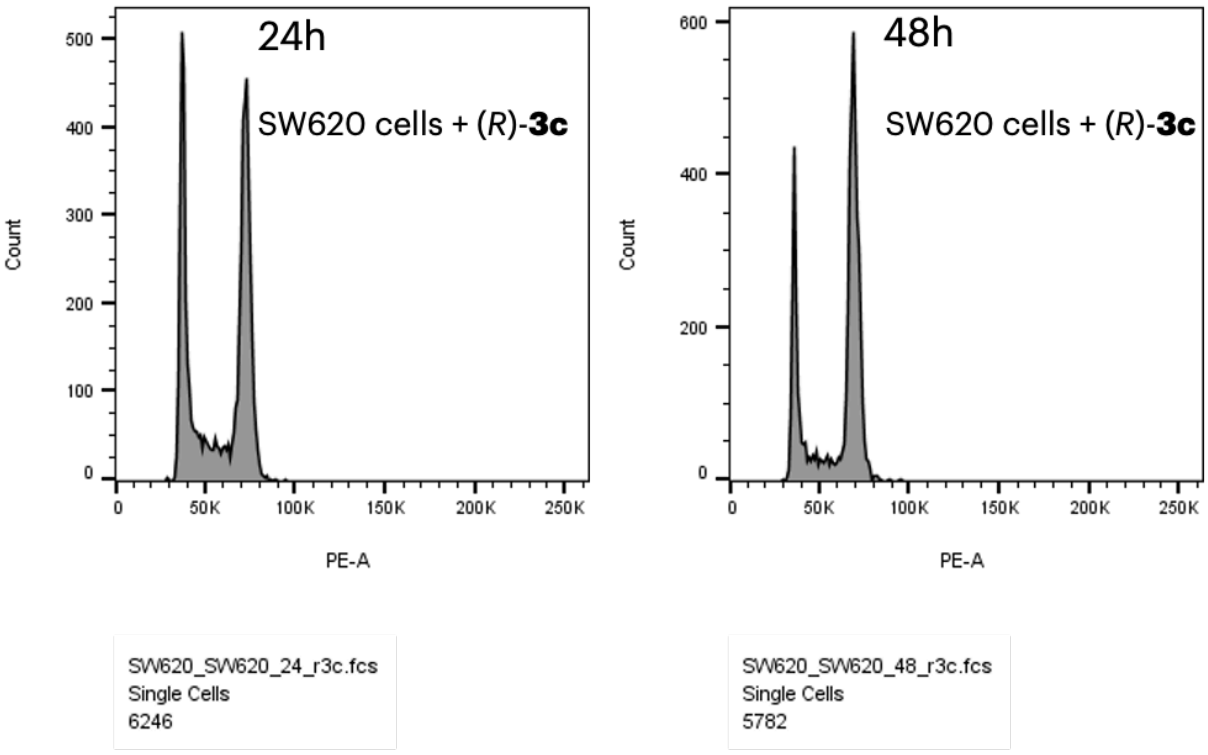
24h
SW620 cells + (R)-3c
Count
PE-A
SW620_SW620_24_r3c.fcs
Single Cells
6246
48h
SW620 cells + (R)-3c
Count
PE-A
SW620_SW620_48_r3c.fcs
Single Cells
5782

D)

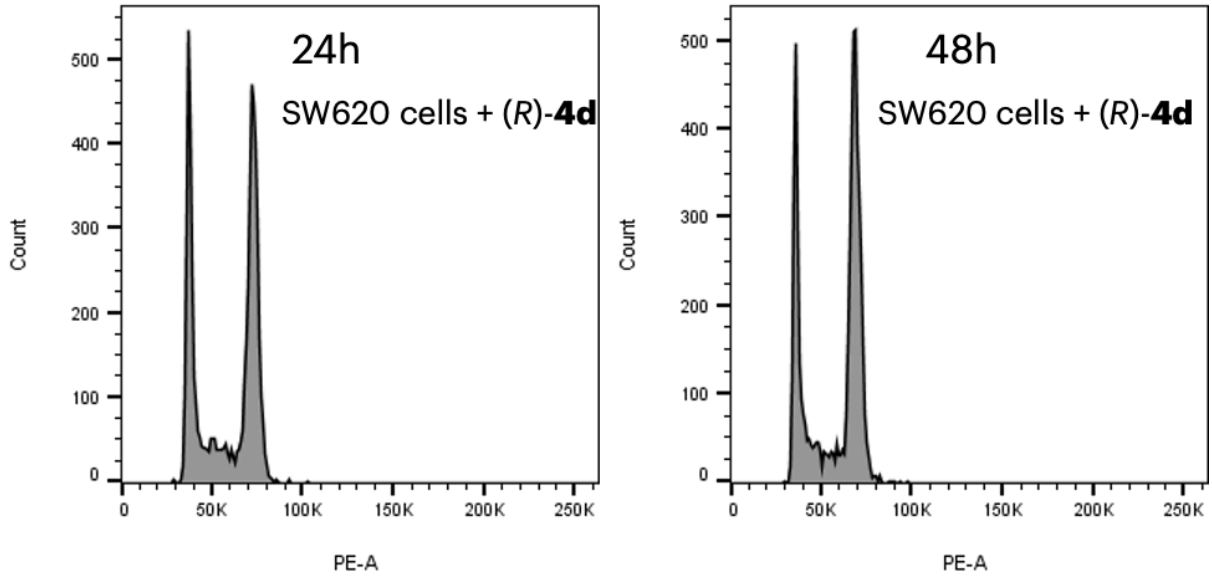

SW620_SW620_24_r4d.fcs
Single Cells
6269

SW620_SW620_48_r4d.fcs
Single Cells
6109

E)

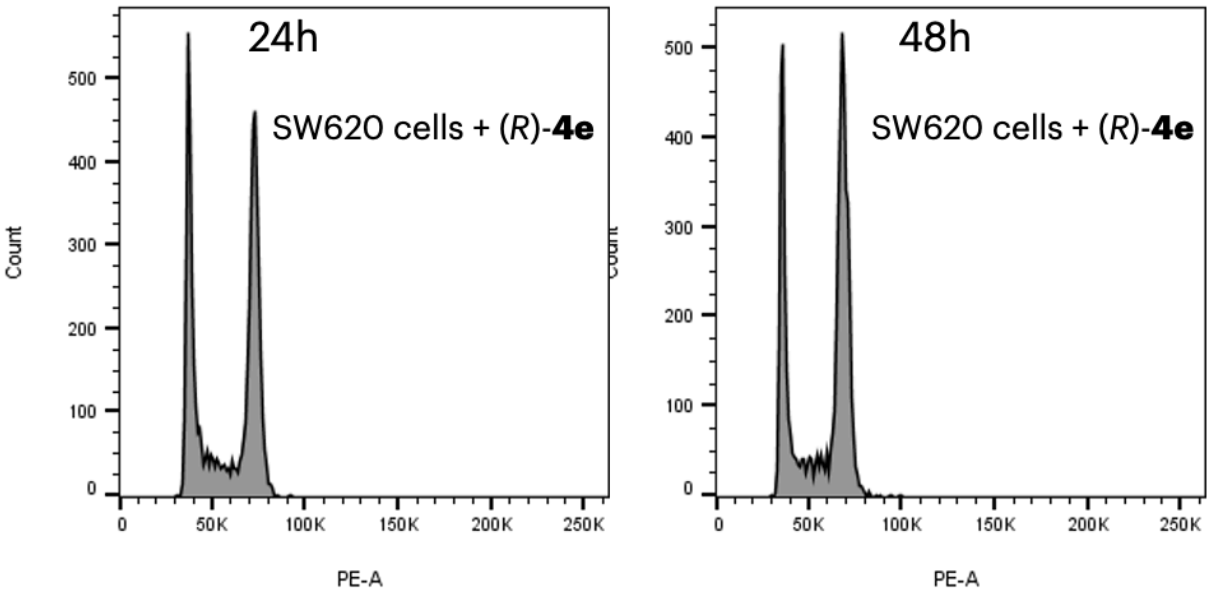

SW620_SW620_24_r4e.fcs
Single Cells
6228

SW620_SW620_48_r4e.fcs
Single Cells
6232

F)

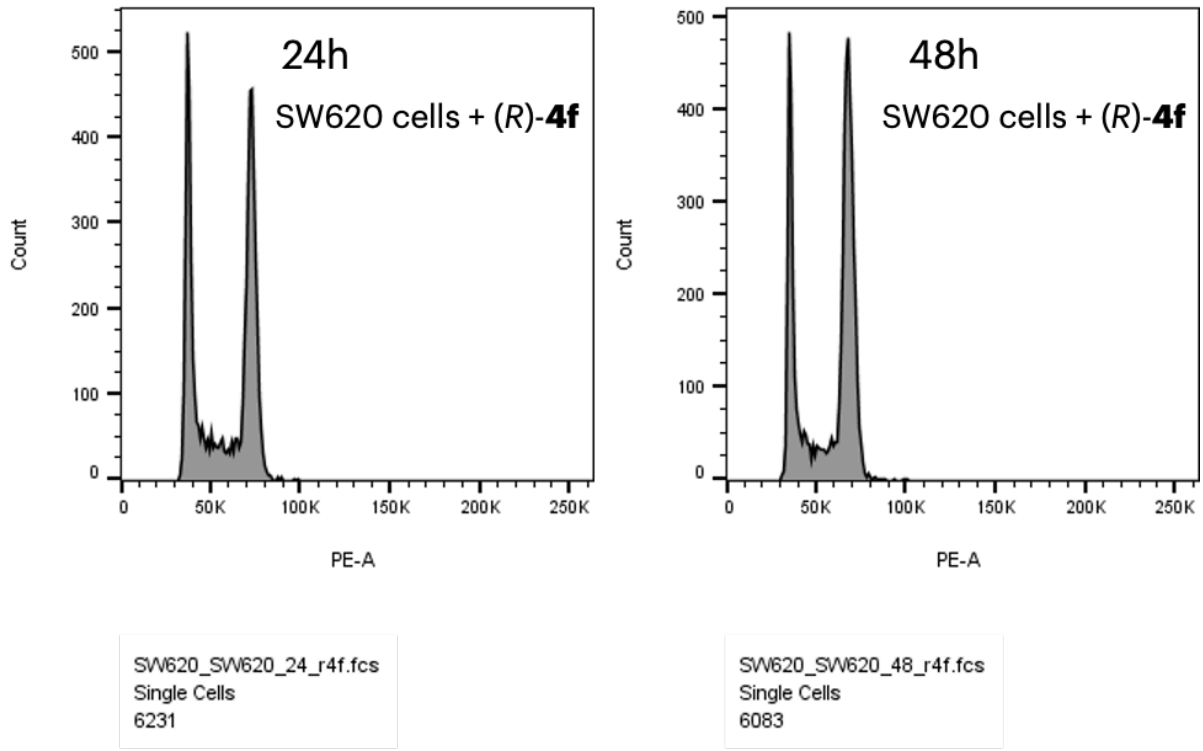

Figure S2. of the (*R*)-**1** and its analogues (*R*)-**3c**, (*R*)-**4c**, (*R*)-**4e** and (*R*)-**4f** on the SW620 cell cycle measured after 24- and 48-hour exposure. Note the increased G2/M fraction of the cells clearly visible at approx. 75 KU

Table S2. RMSD values for the heavy atoms when comparing co-crystallized ispinesib (*R*)-**1** with the docked molecule.

Pose	ASP	ChemPLP	CS	GS
1	0.9569	0.5933	0.6412	1.0677
2	0.8536	0.8291	0.6083	0.4090
3	0.9660	0.7674	0.9299	0.9503
Mean	0.9255	0.7299	0.7265	0.8090

Table S3. Results for the different scoring functions for ispinesib (*R*)-**1** and its derivatives.

Compound	ASP	ChemPLP	ChemScore	GoldScore
(*R*)-**1** (ispinesib)	48.7	109.6	42.6	83.4
(*R*)-**2c**	45.4	103.8	40.4	82.1
(*R*)-**3c**	49.2	120.0	47.5	95.8
(*R*)-**4a**	53.4	120.2	45.7	121.1
(*R*)-**4b**	54.7	123.2	45.3	124.6
(*R*)-**4c**	50.7	121.2	44.1	124.1
(*R*)-**4d**	52.8	120.9	45.1	114.3
(*R*)-**4e**	49.5	120.1	46.7	120.7
(*R*)-**4f**	52.0	113.7	43.4	80.1
(*S*)-**1**	43.7	99.3	36.2	93.8
(*S*)-**4a**	46.1	107.3	40.9	105.8
(*S*)-**4e**	45.4	110.4	39.5	102.4
(*S*)-**4f**	45.2	105.2	38.6	86.4

NMR spectra

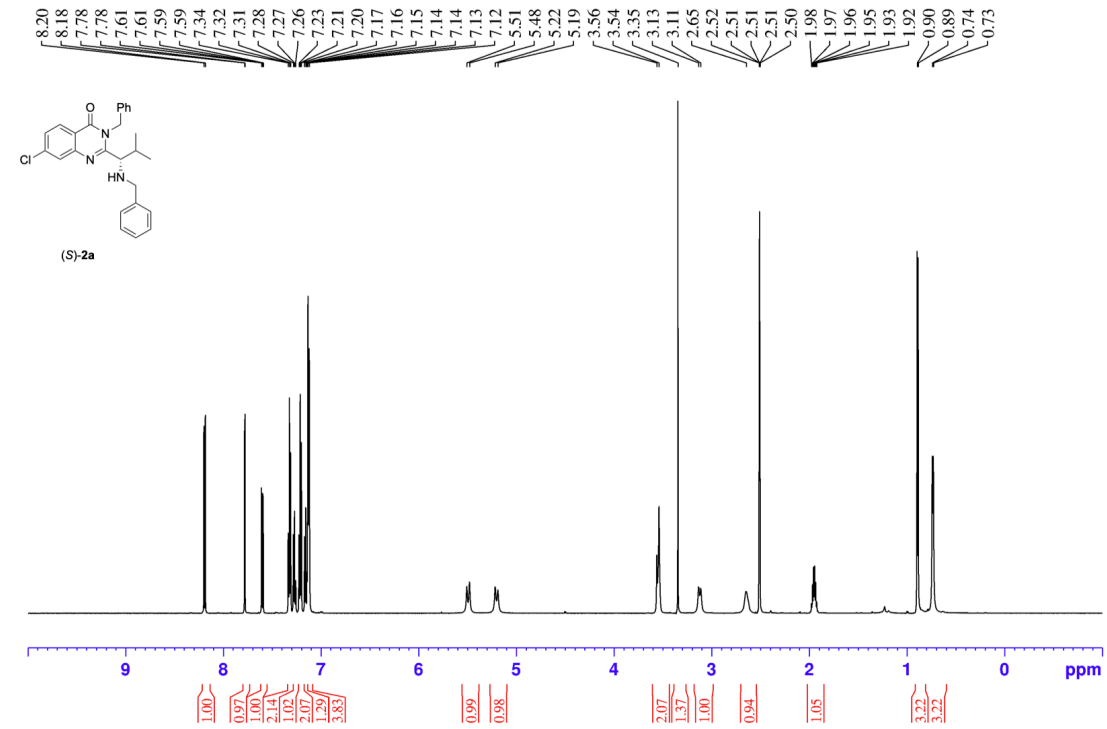

Figure S3. ^{1}H NMR of (*S*)-2a in DMSO-d$_6$

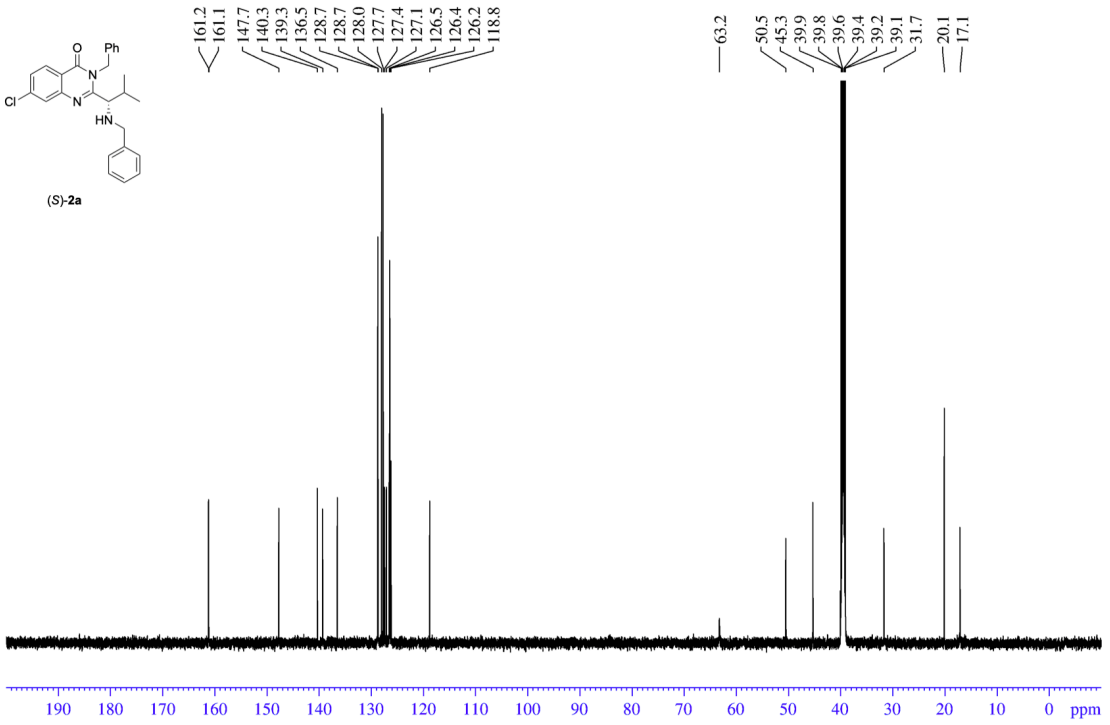

Figure S4. ^{13}C{^{1}H} NMR of (*S*)-2a in DMSO-d$_6$

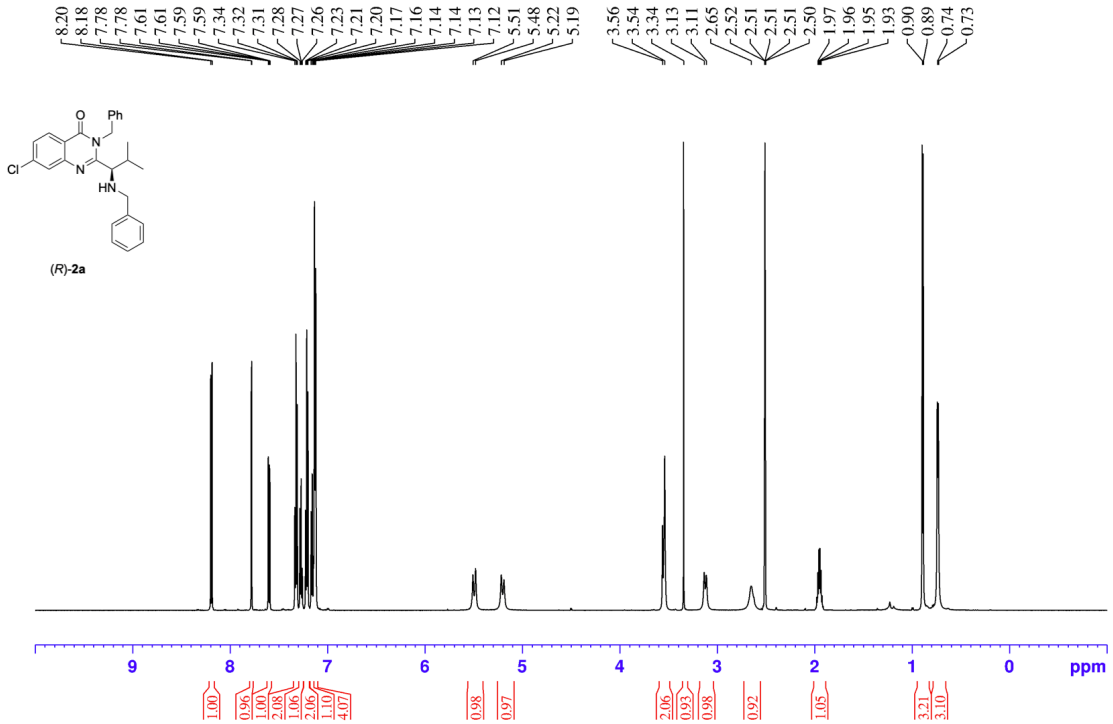

Figure S5. ^{1}H NMR of (*R*)-2a in DMSO-d$_6$

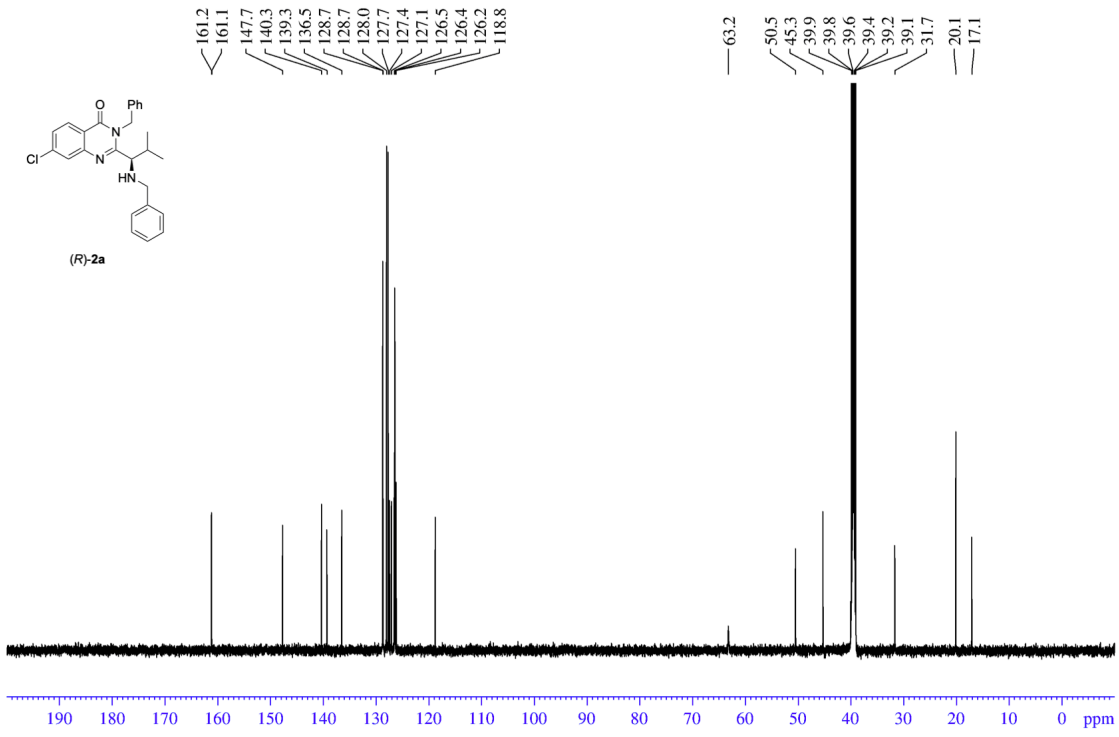

Figure S6. ^{13}C{^{1}H} NMR of (*R*)-2a in DMSO-d$_6$

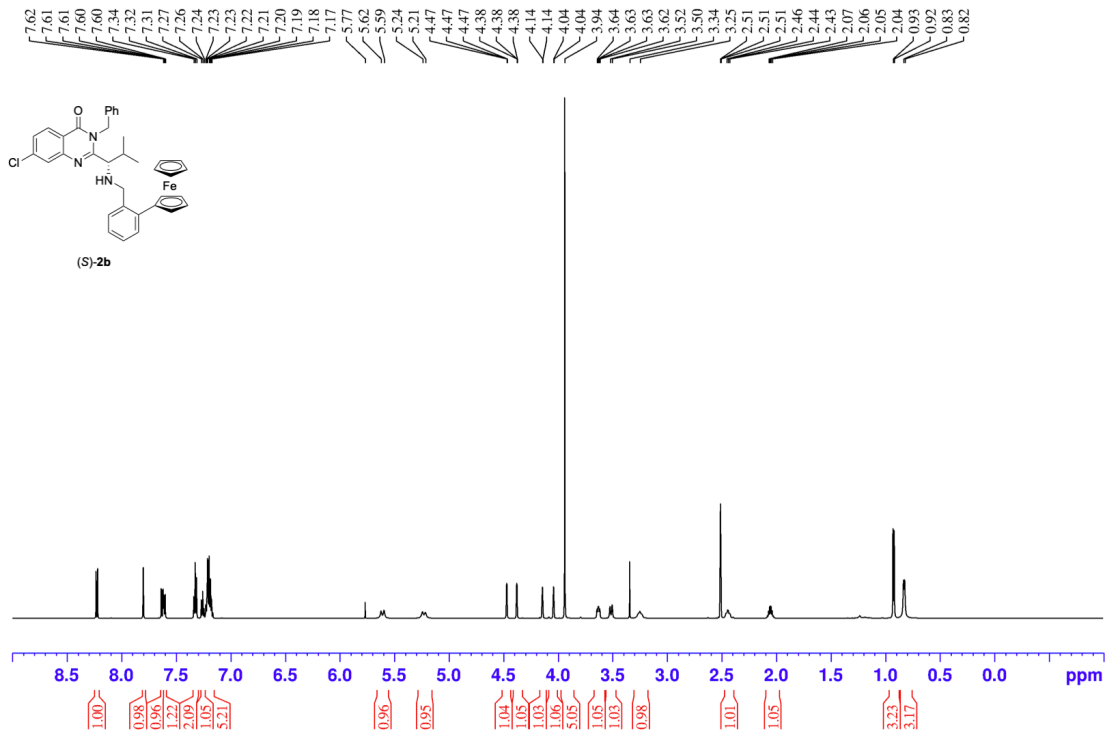

Figure S7. ^{1}H NMR of (*S*)-2b in DMSO-d$_6$

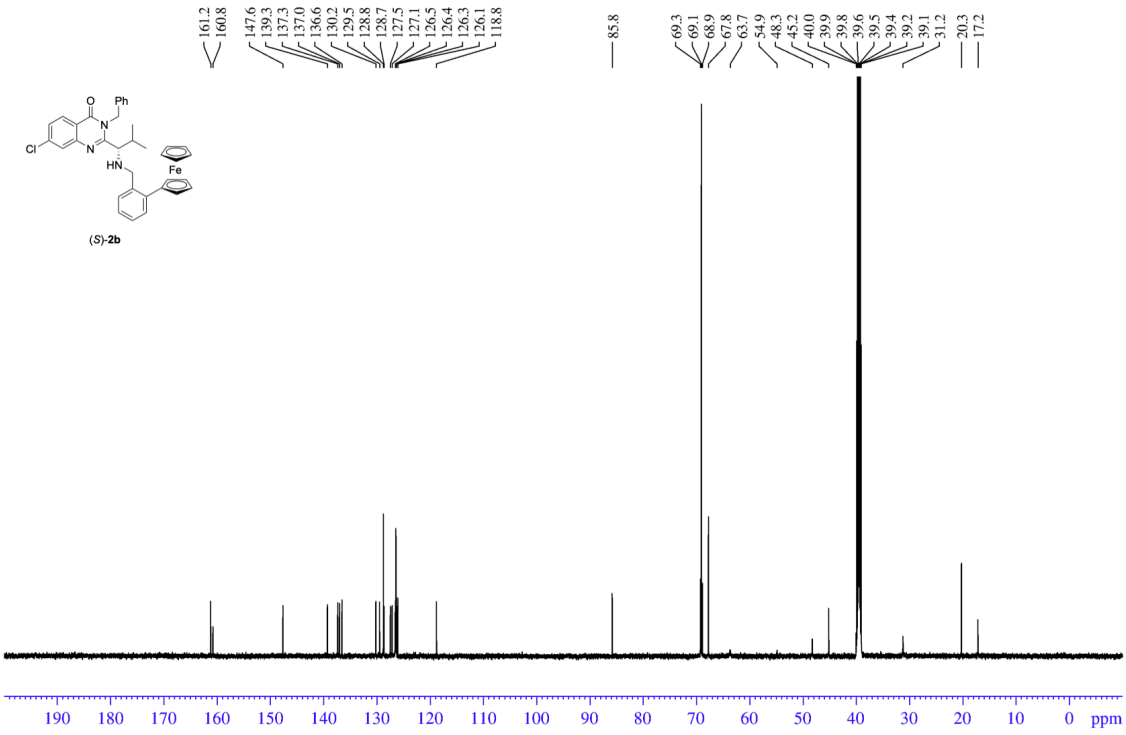

Figure S8. ^{13}C{^{1}H} NMR of (*S*)-2b in DMSO-d$_6$

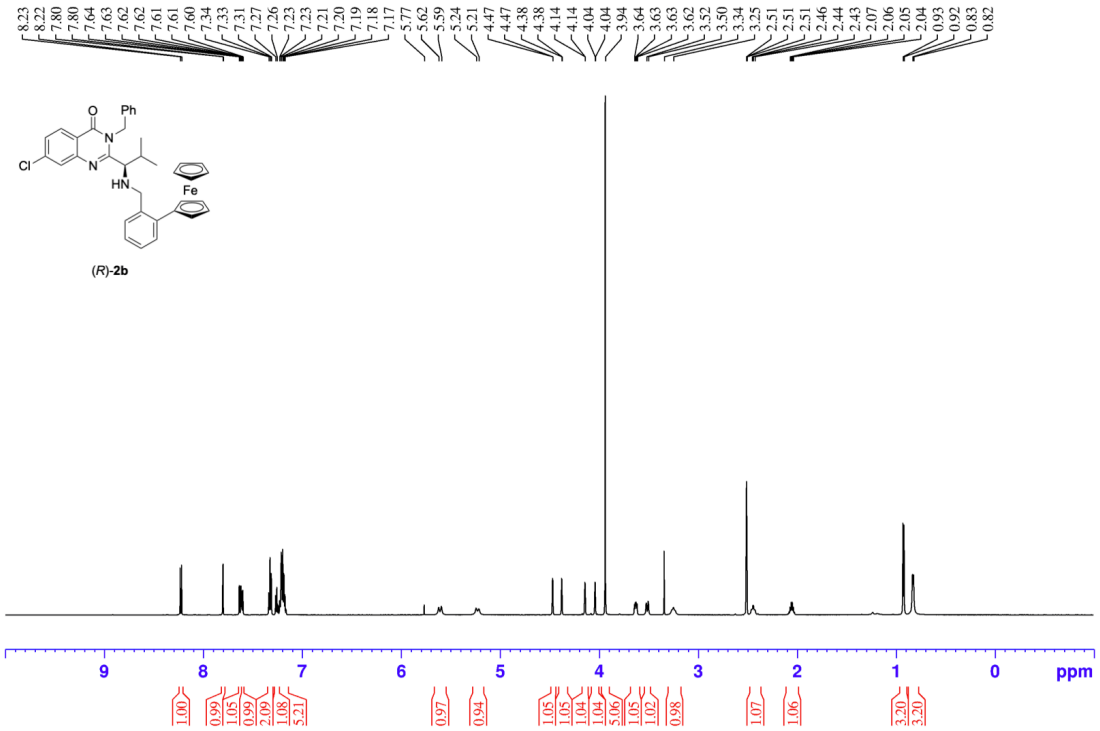

Figure S9. ^{1}H NMR of (*R*)-2b in DMSO-d$_6$

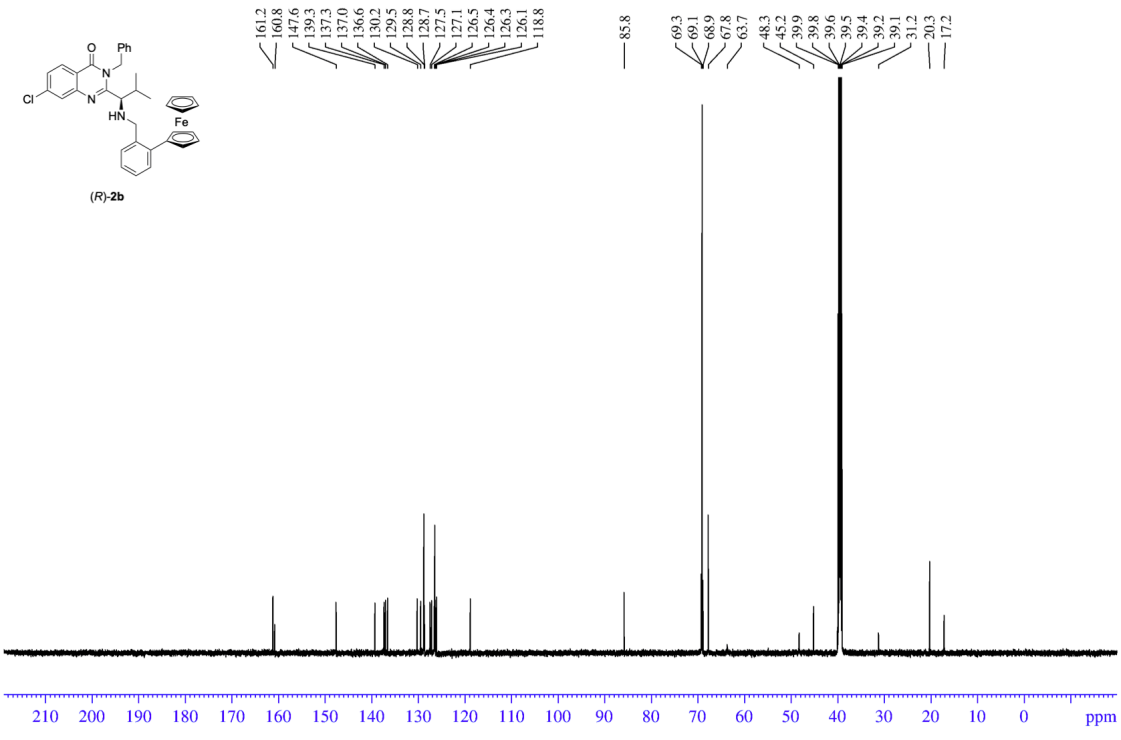

Figure S10. ^{13}C{^{1}H} NMR of (*R*)-2b in DMSO-d$_6$

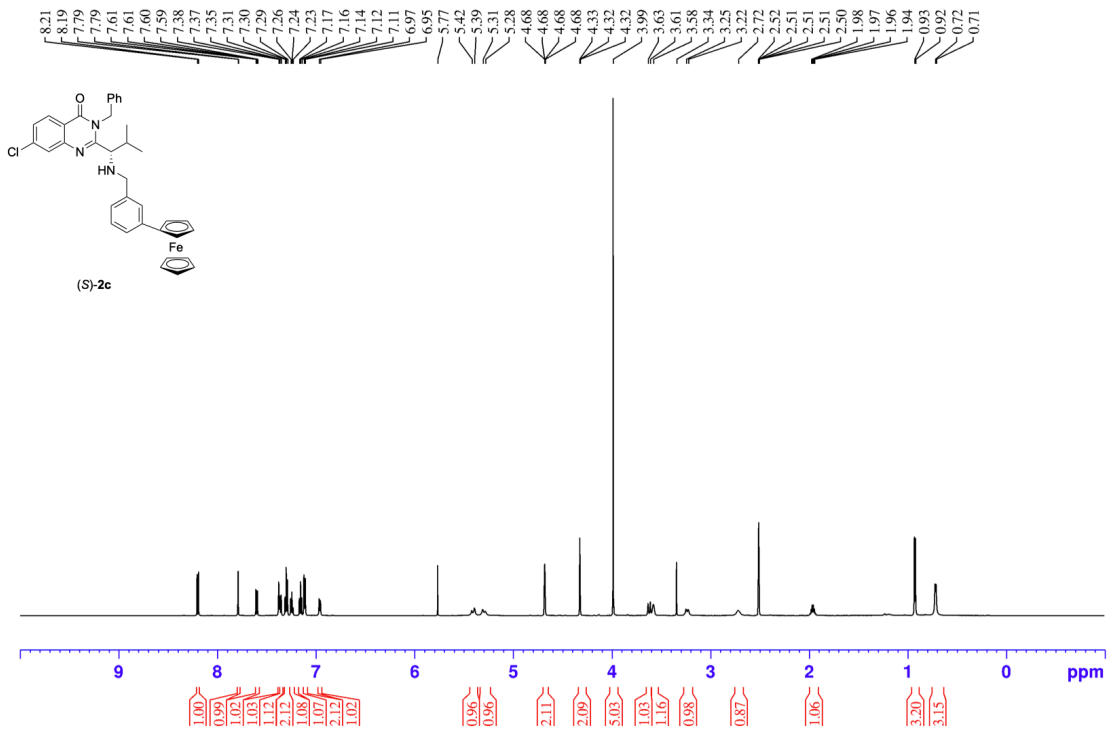

Figure S11. ^{1}H NMR of (*S*)-2c in DMSO-d$_6$

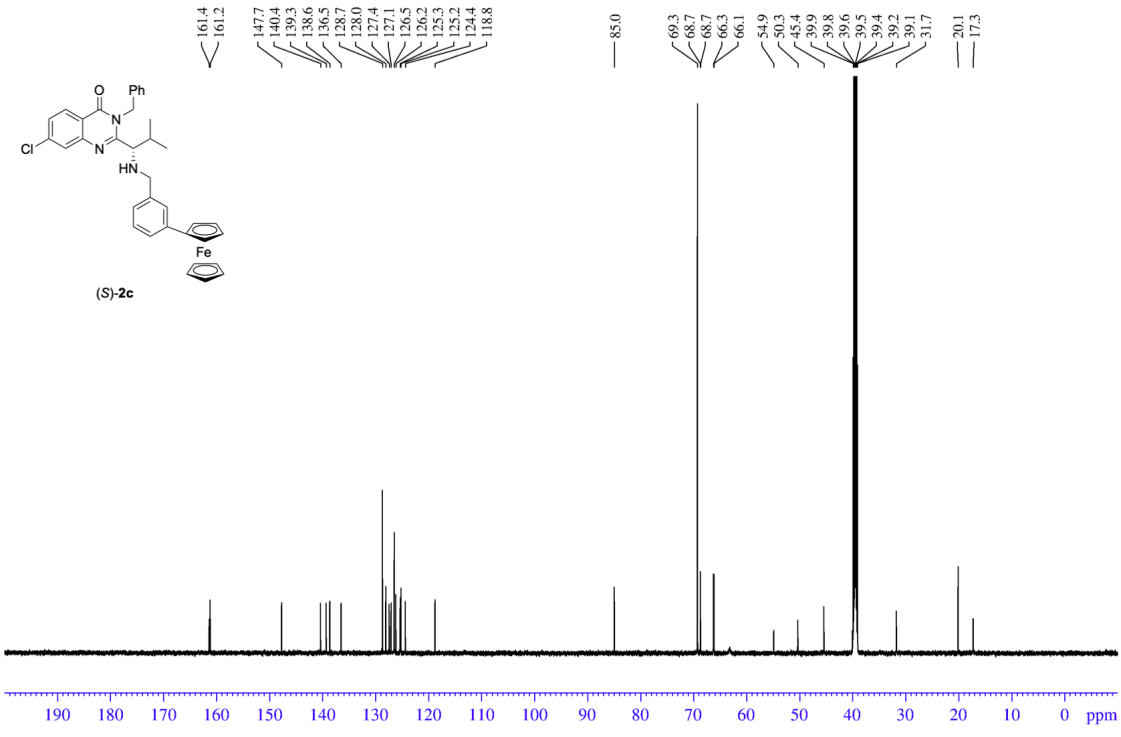

Figure S12. ^{13}C{^{1}H} NMR of (*S*)-2c in DMSO-d$_6$

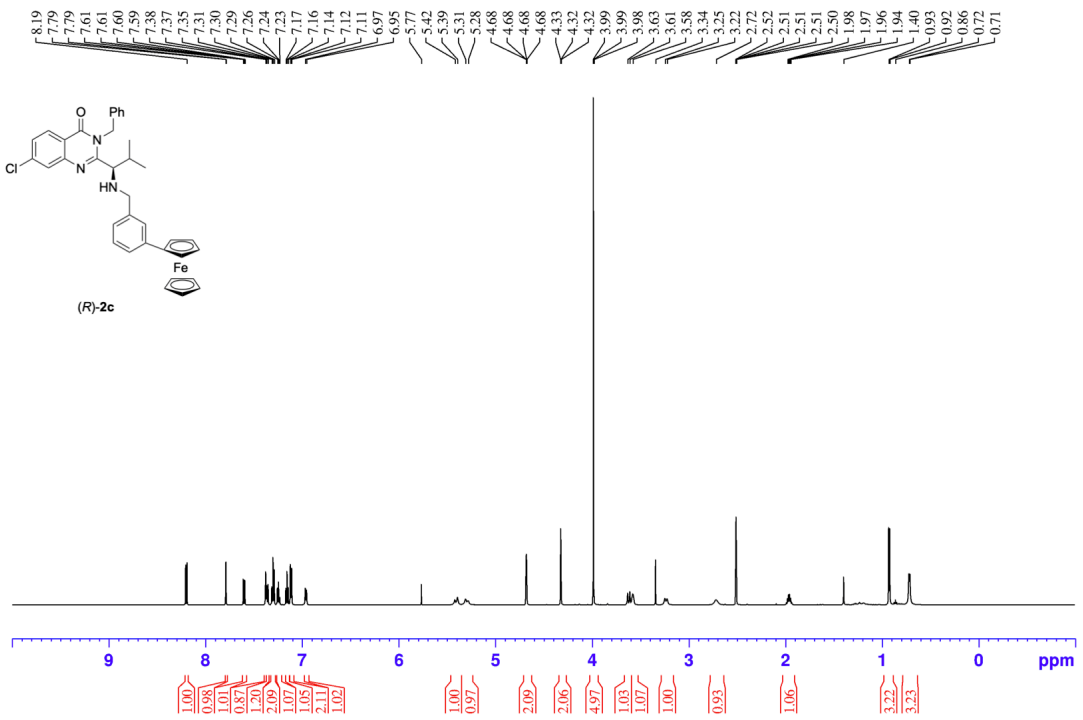

Figure S13. ^{1}H NMR of (*R*)-2c in DMSO-d$_6$

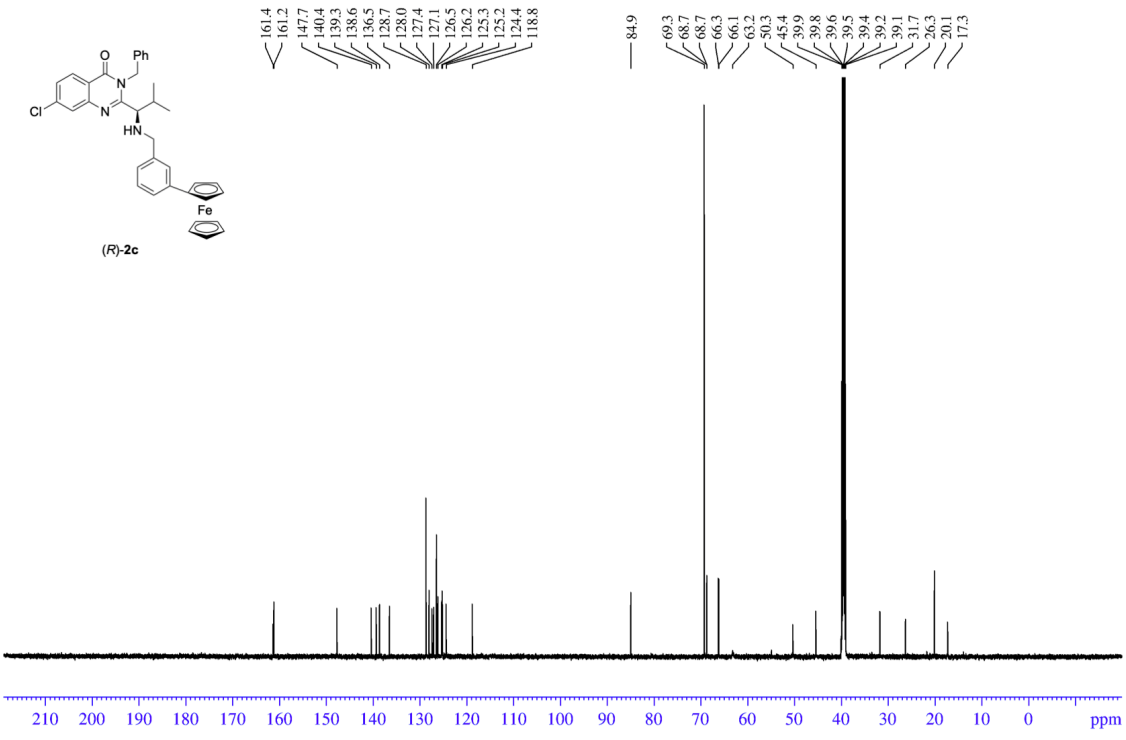

Figure S14. ^{13}C{^{1}H} NMR of (*R*)-2c in DMSO-d$_6$

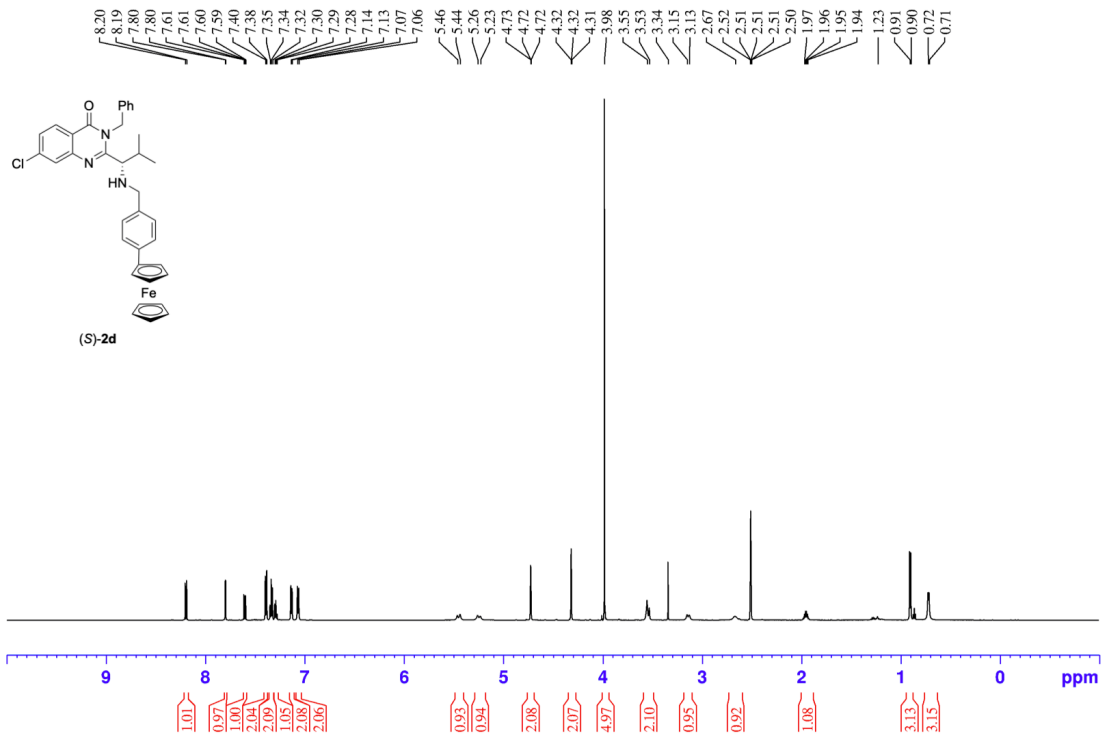

Figure S15. ^{1}H NMR of (*S*)-2d in DMSO-d$_6$

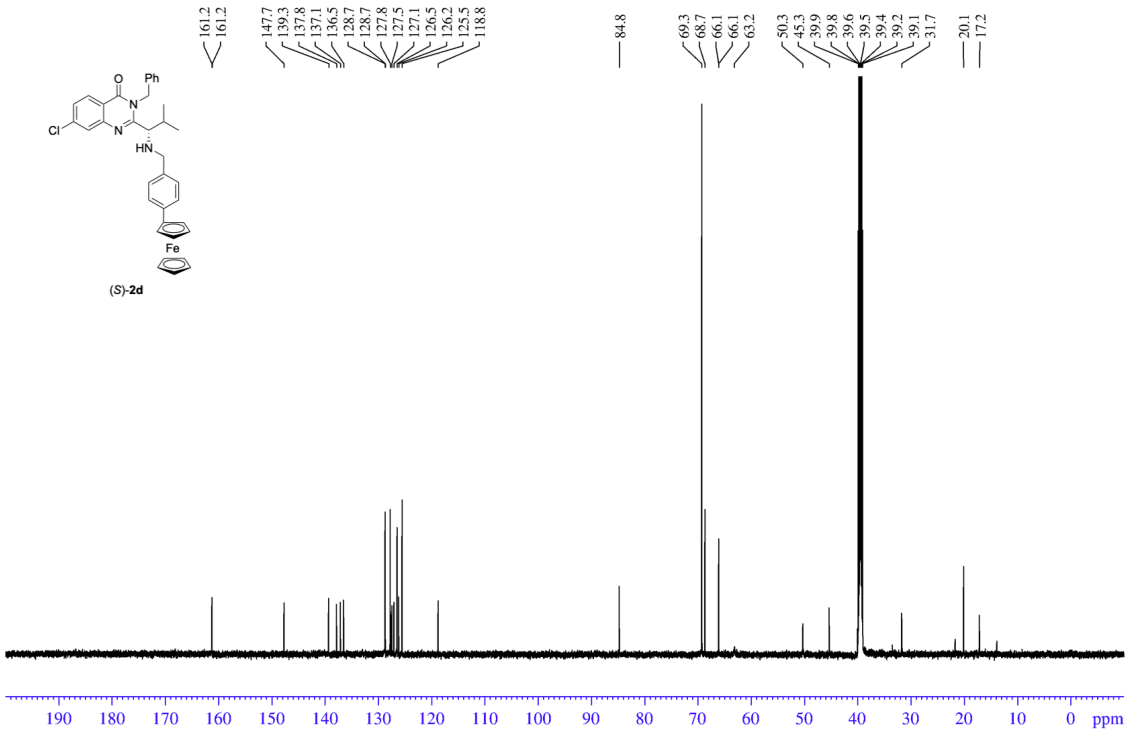

Figure S16. ^{13}C{^{1}H} NMR of (*S*)-2d in DMSO-d$_6$

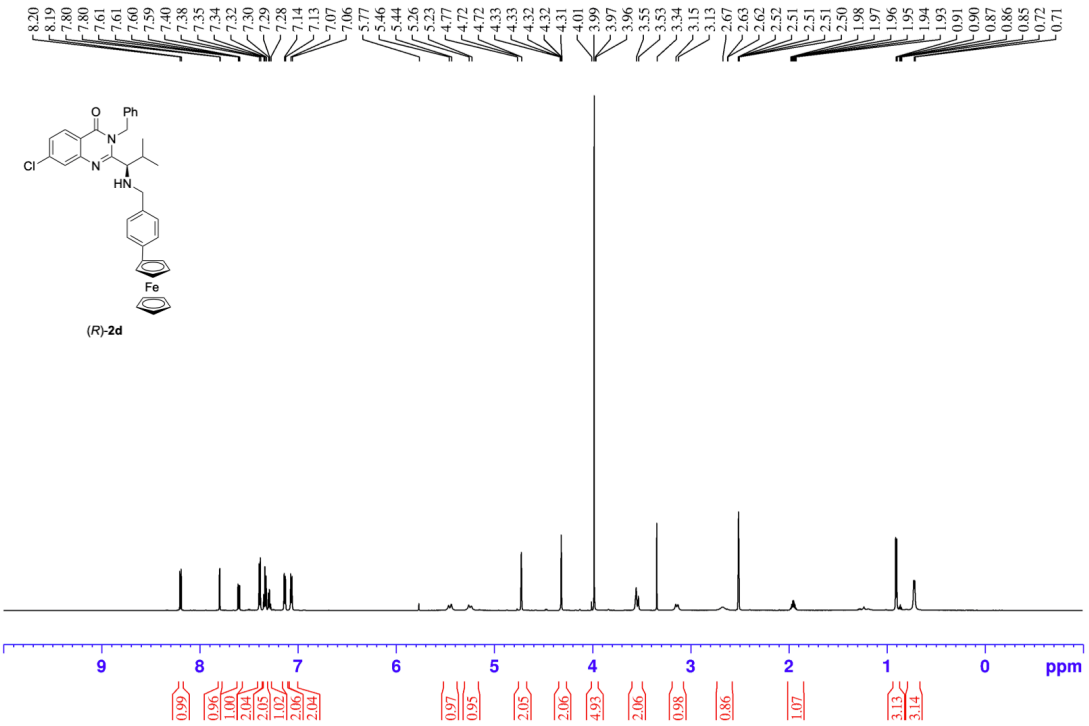

Figure S17. ^{1}H NMR of (*R*)-2d in DMSO-d$_6$

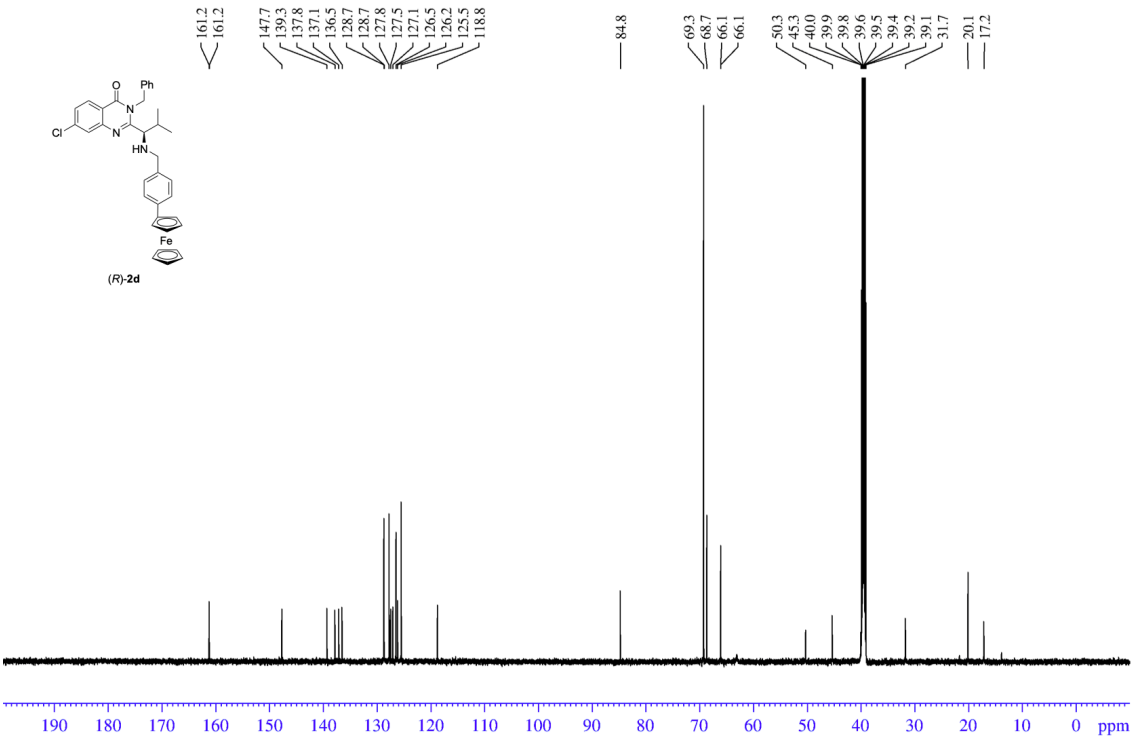

Figure S18. ^{13}C{^{1}H} NMR of (*R*)-2d in DMSO-d$_6$

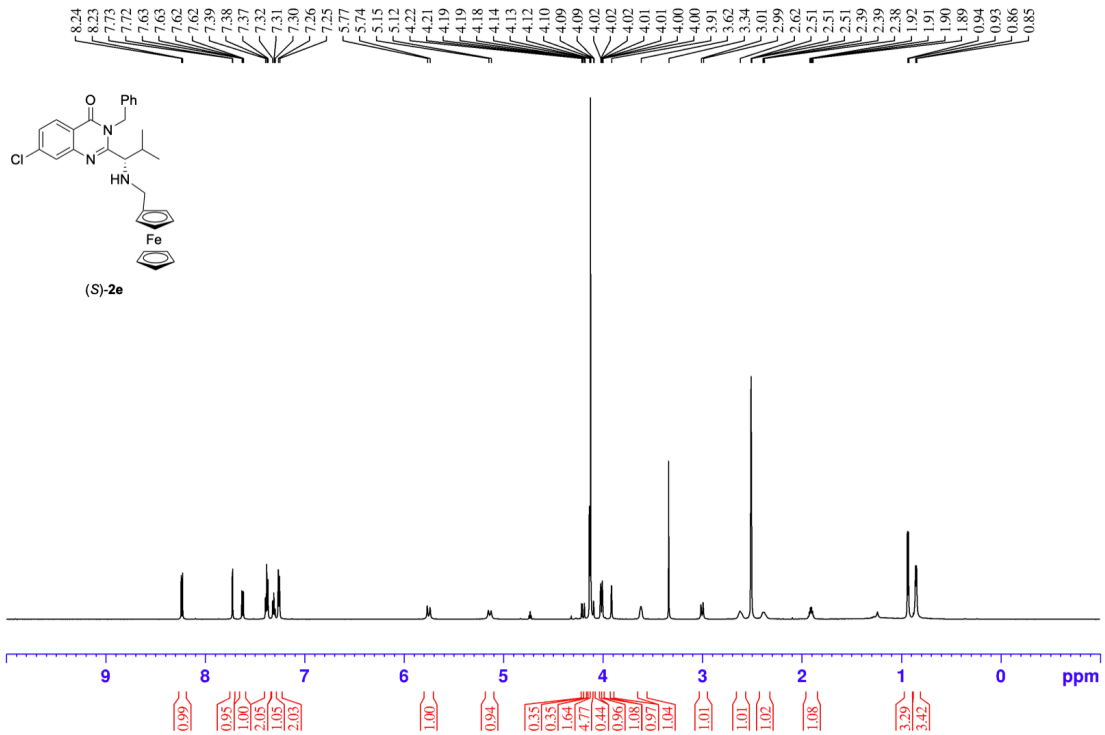

Figure S19. ^{1}H NMR of (*S*)-2e in DMSO-d$_6$

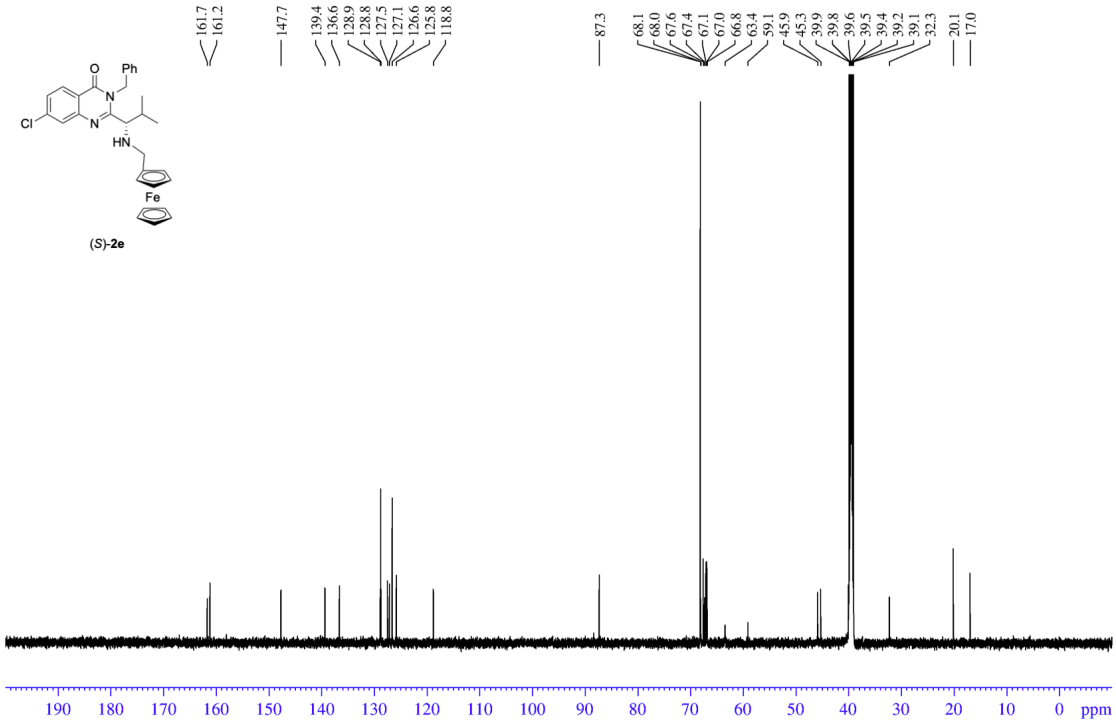

Figure S20. ^{13}C{^{1}H} NMR of (*S*)-2e in DMSO-d$_6$

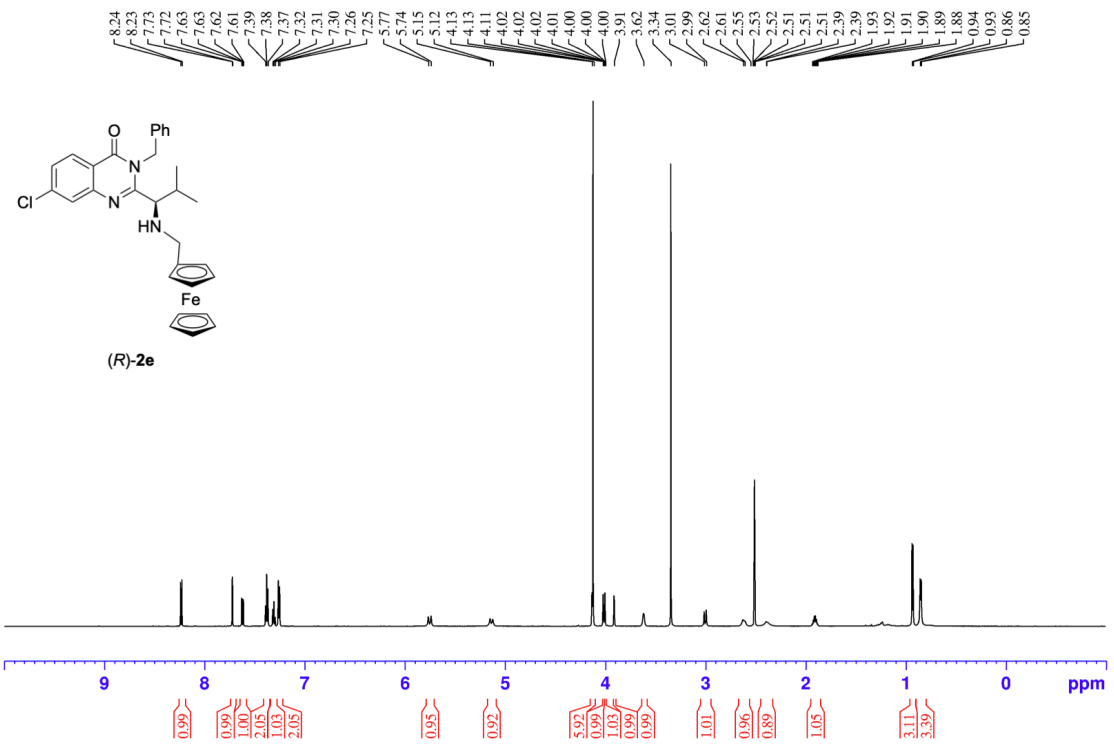

Figure S21. ^{1}H NMR of (*R*)-2e in DMSO-d$_6$

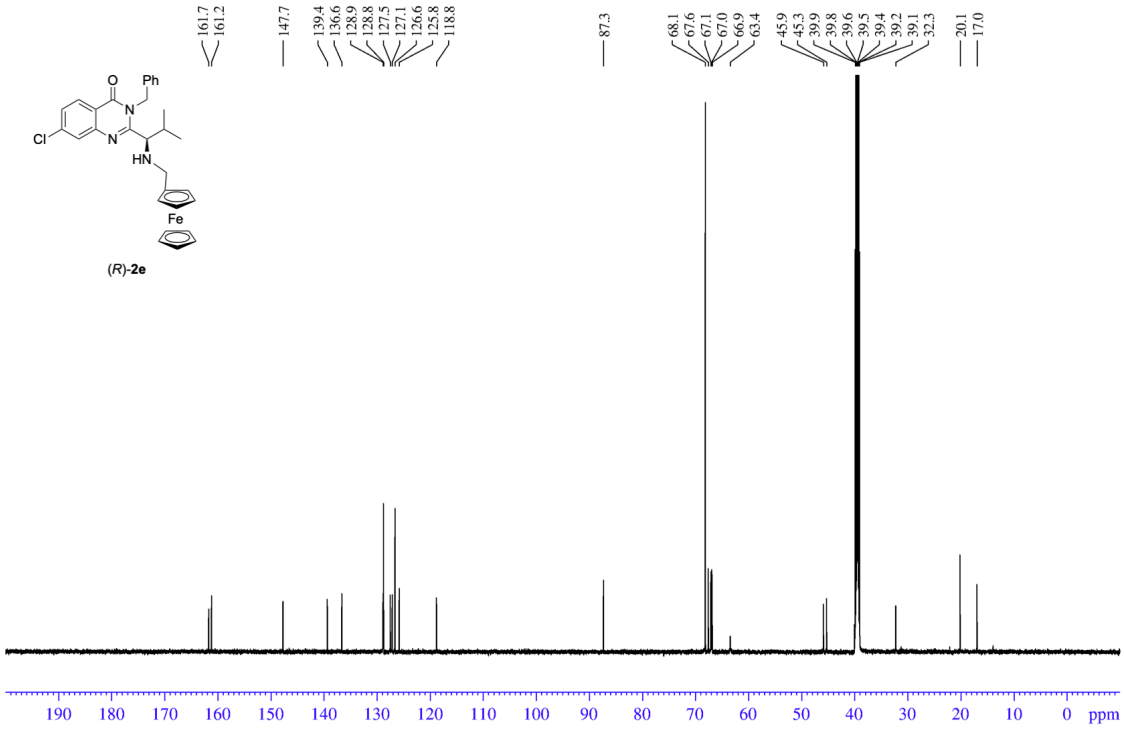

Figure S22. ^{13}C{^{1}H} NMR of (*R*)-2e in DMSO-d$_6$

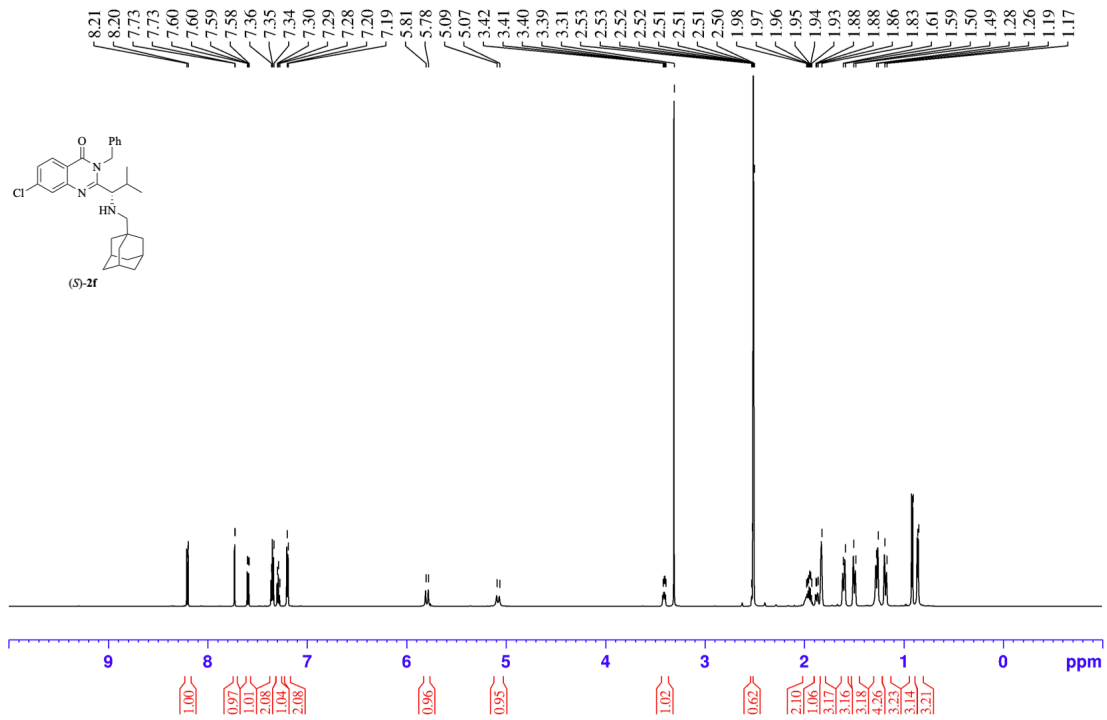

Figure S23. ^{1}H NMR of (*S*)-2f in DMSO-d$_6$

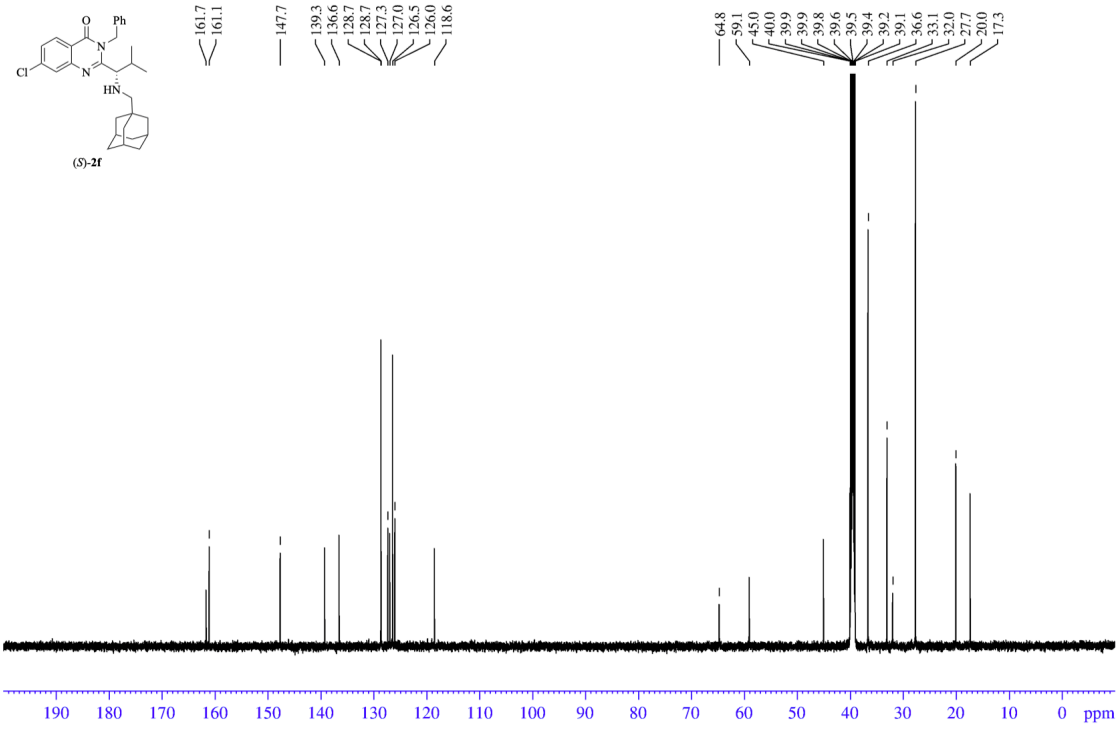

Figure S24. ^{13}C{^{1}H} NMR of (*S*)-2f in DMSO-d$_6$

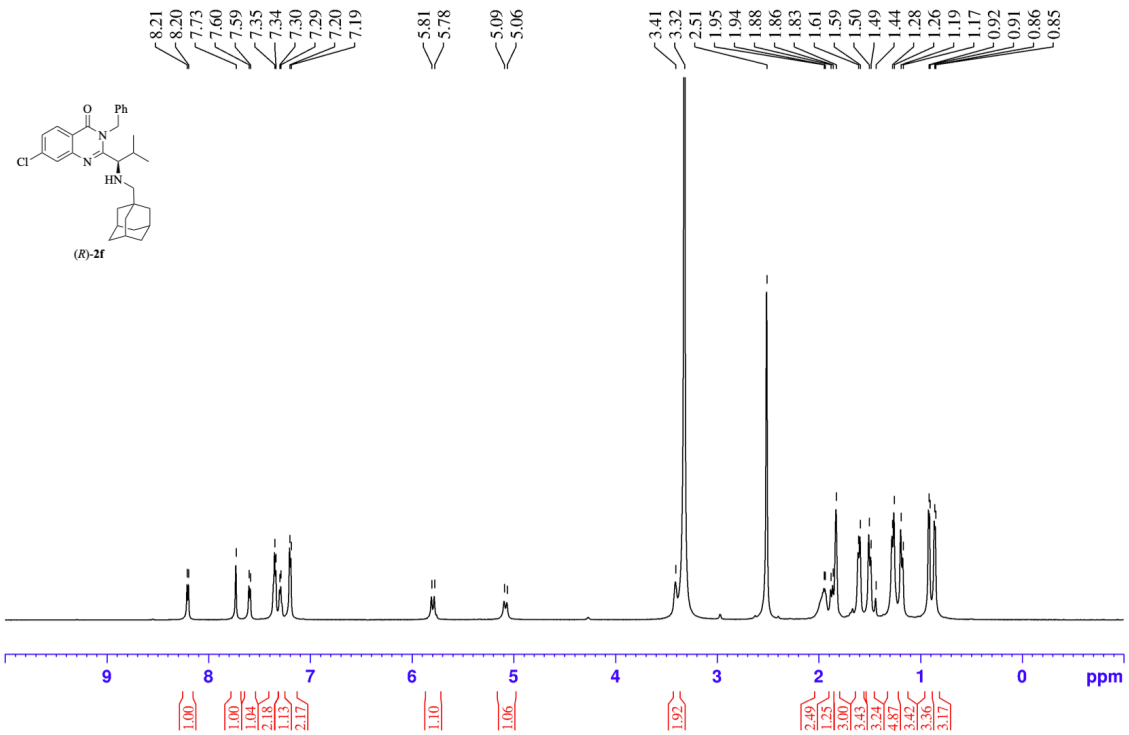

Figure S25. ^{1}H NMR of (*R*)-2f in DMSO-d$_6$

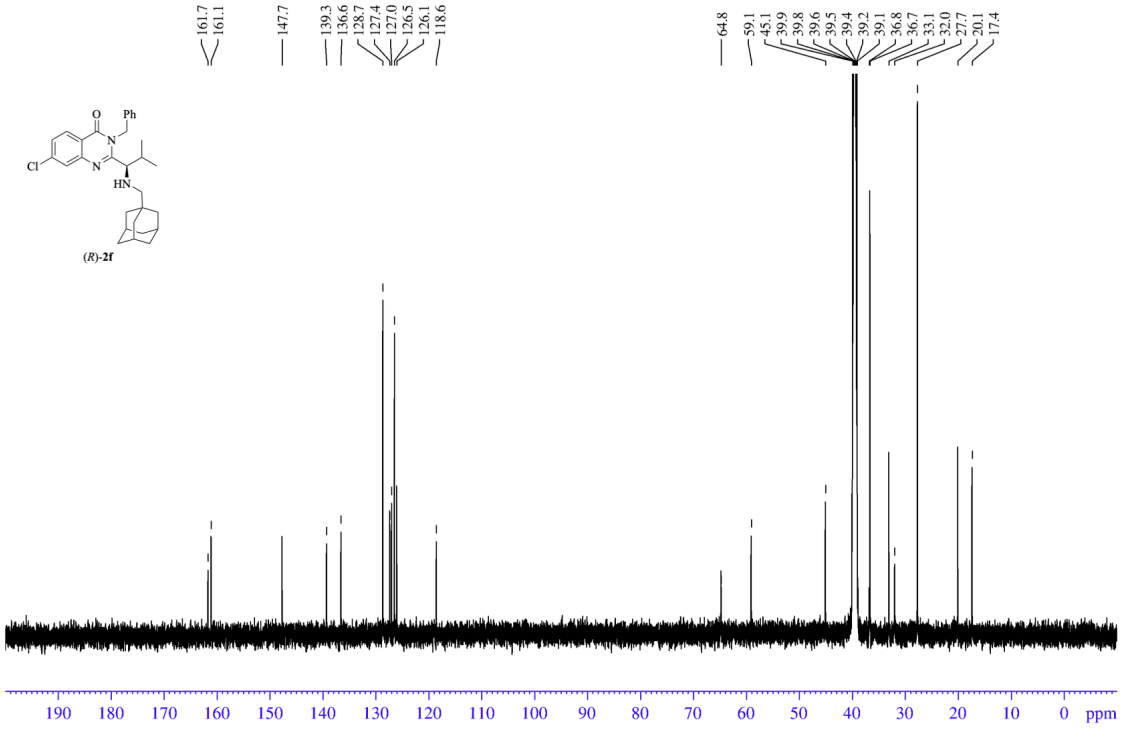

Figure S26. ^{13}C{^{1}H} NMR of (*R*)-2f in DMSO-d$_6$

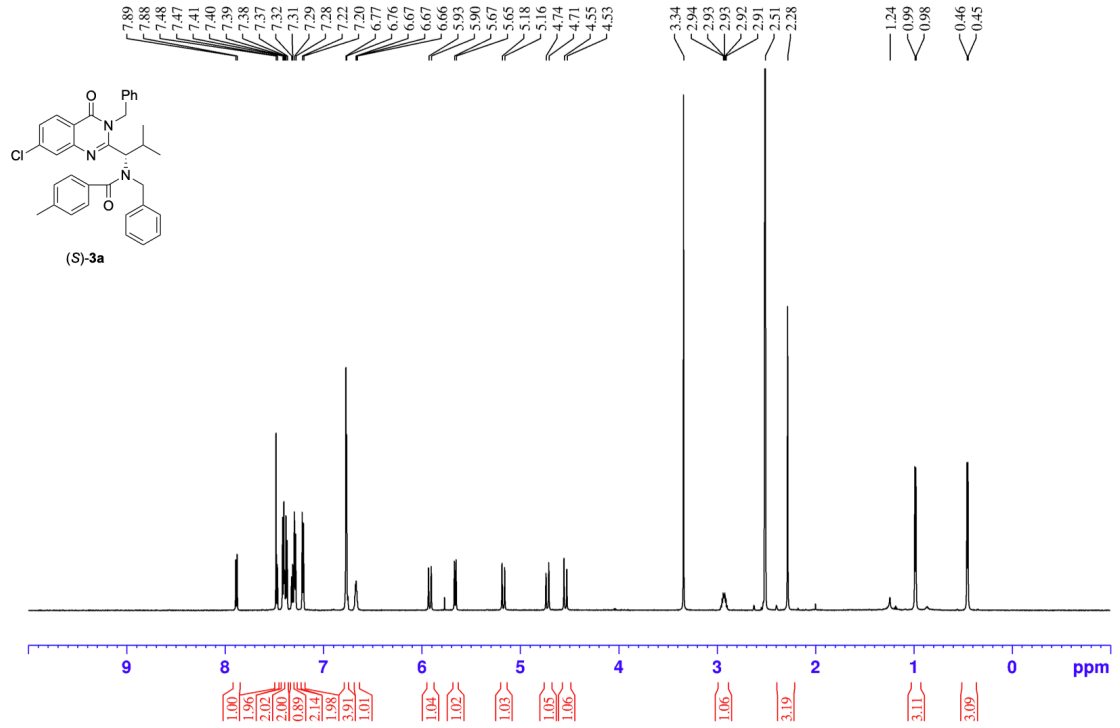

Figure S27. ^{1}H NMR of (*S*)-3a in DMSO-d$_6$

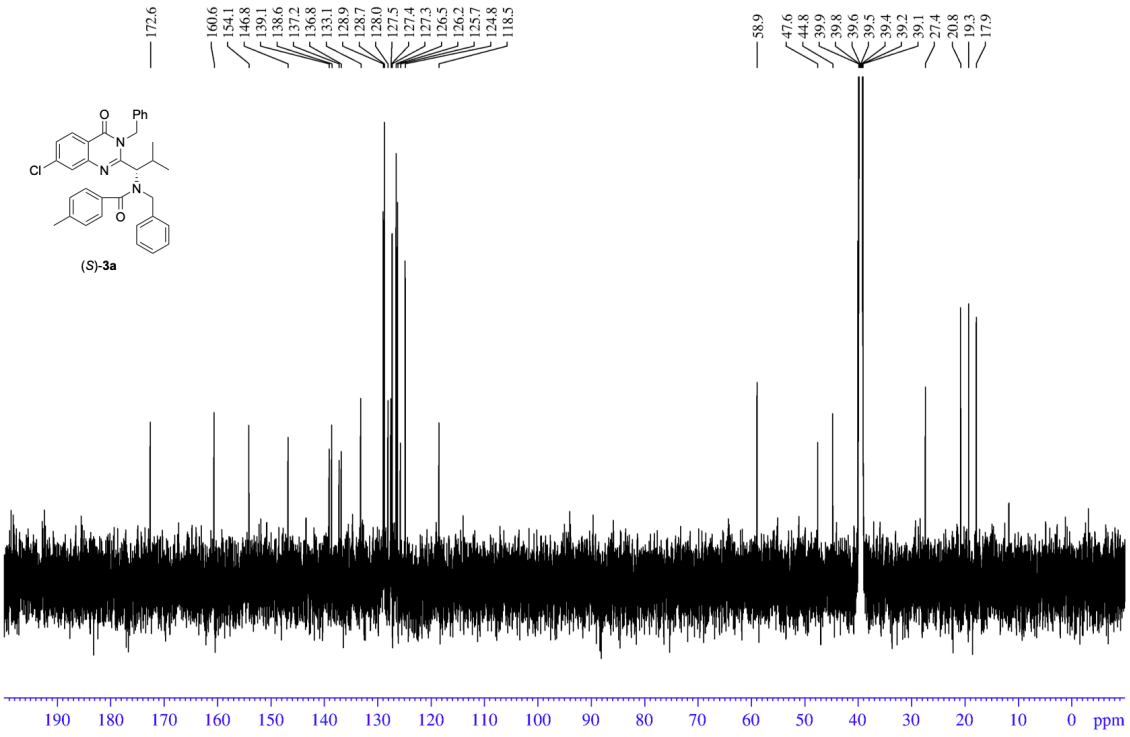

Figure S28. ^{13}C{^{1}H} NMR of (*S*)-3a in DMSO-d$_6$

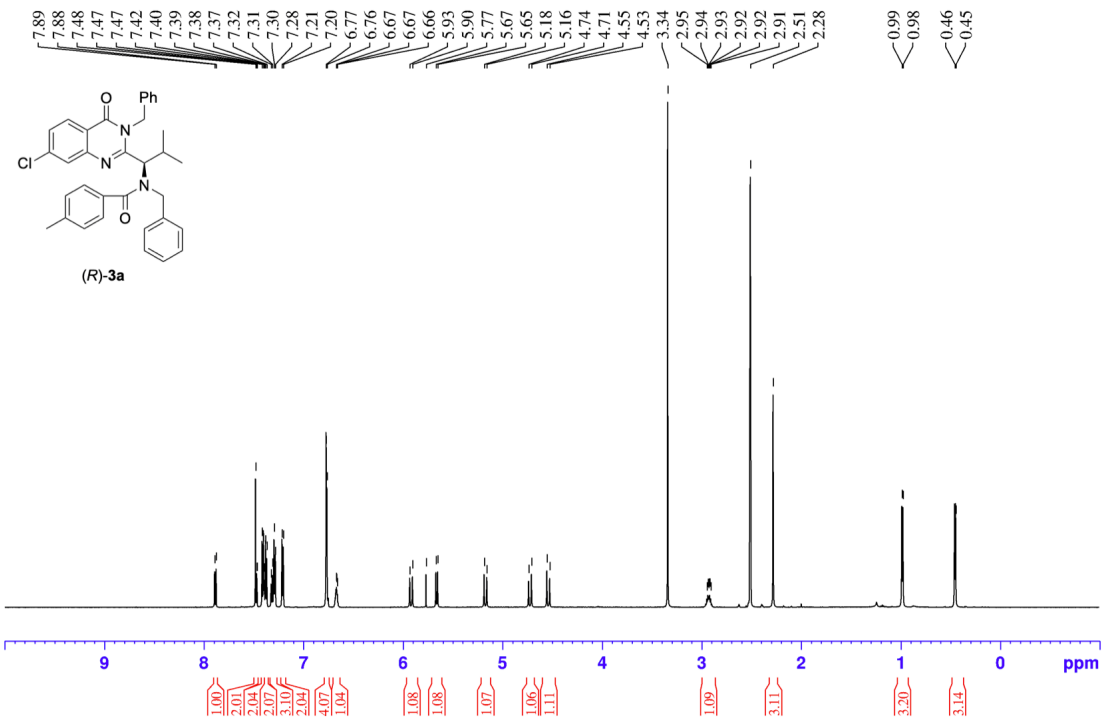

Figure S29. ^{1}H NMR of (*R*)-3a in DMSO-d$_6$

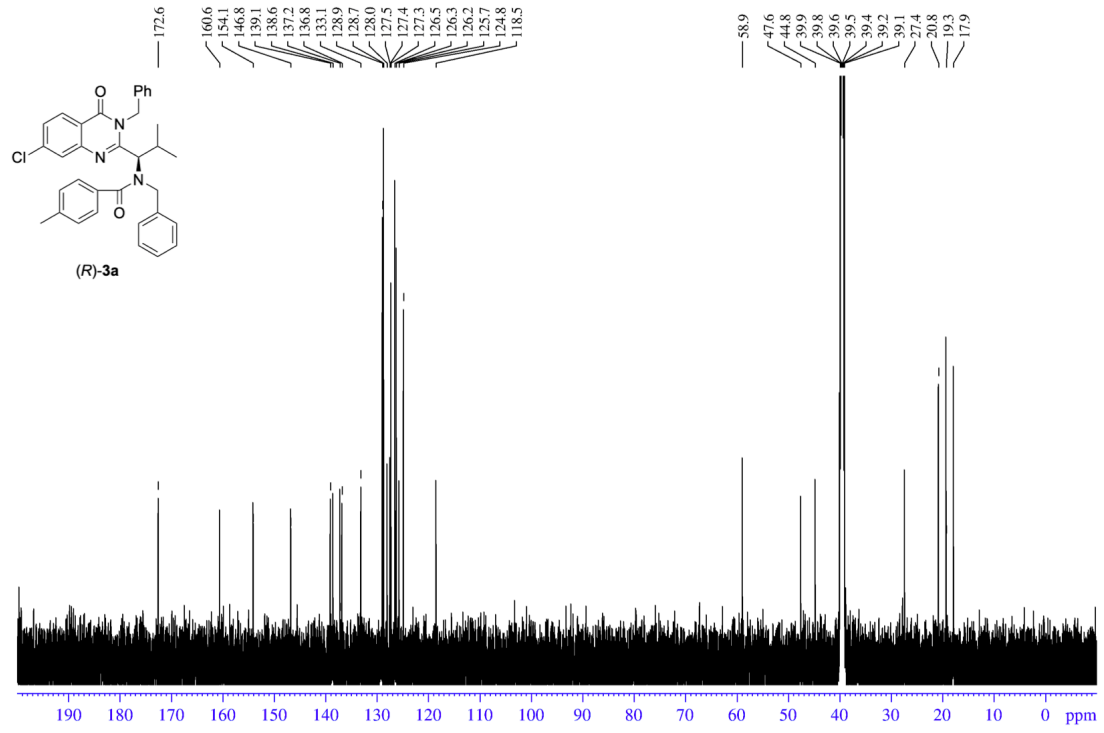

Figure S30. ^{13}C{^{1}H} NMR of (*R*)-3a in DMSO-d$_6$

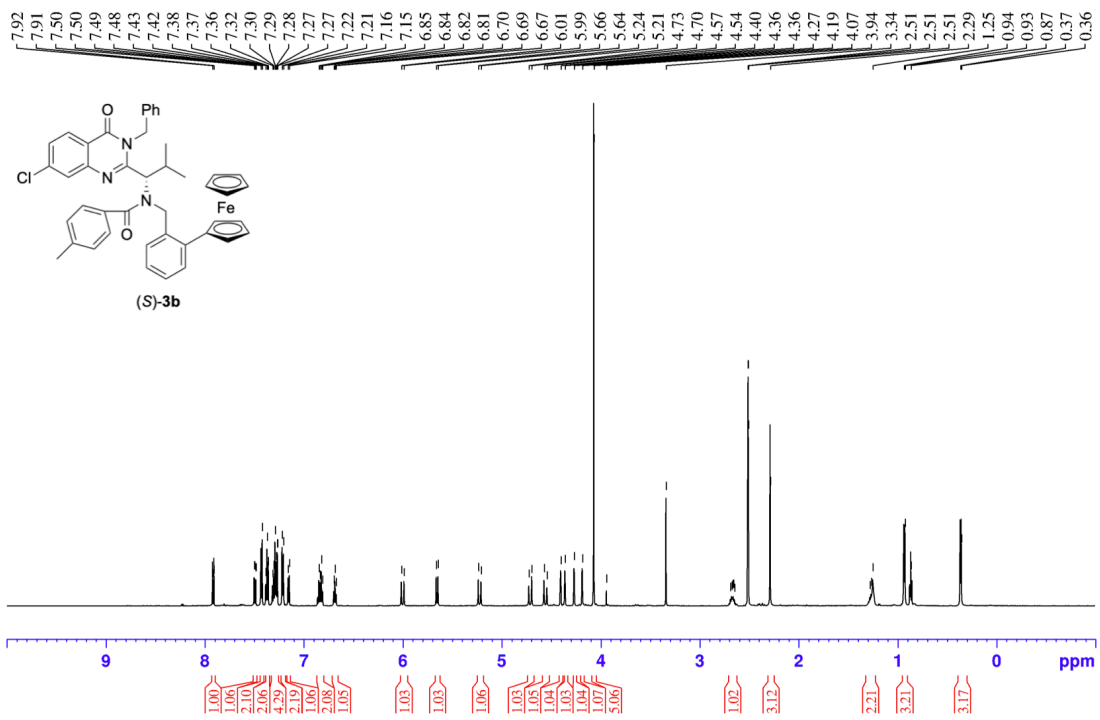

Figure S31. ^{1}H NMR of (*S*)-3b in DMSO-d$_6$

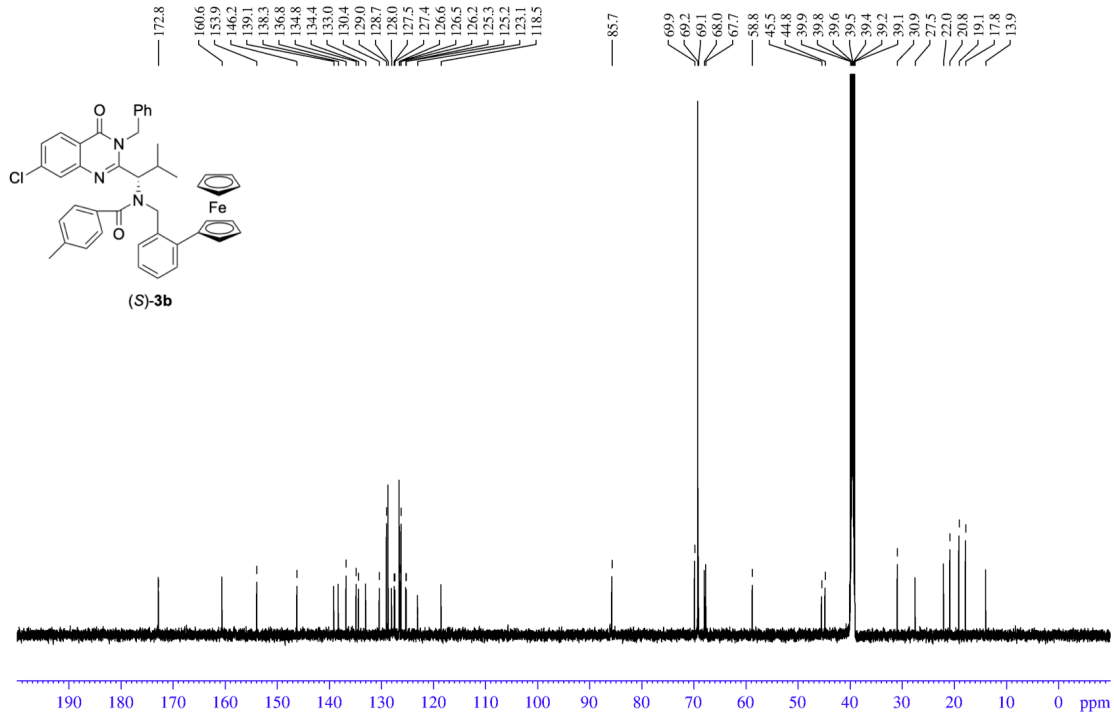

Figure S32. ^{13}C{^{1}H} NMR of (*S*)-3b in DMSO-d$_6$

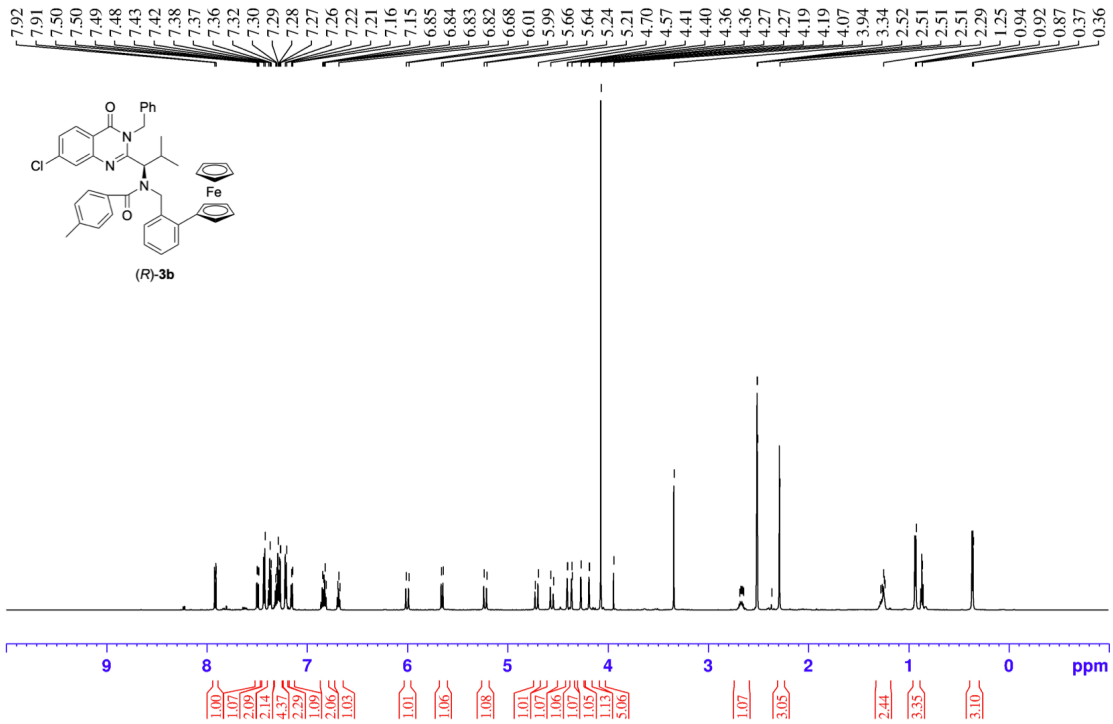

Figure S33. ^{1}H NMR of (*R*)-3b in DMSO-d$_6$

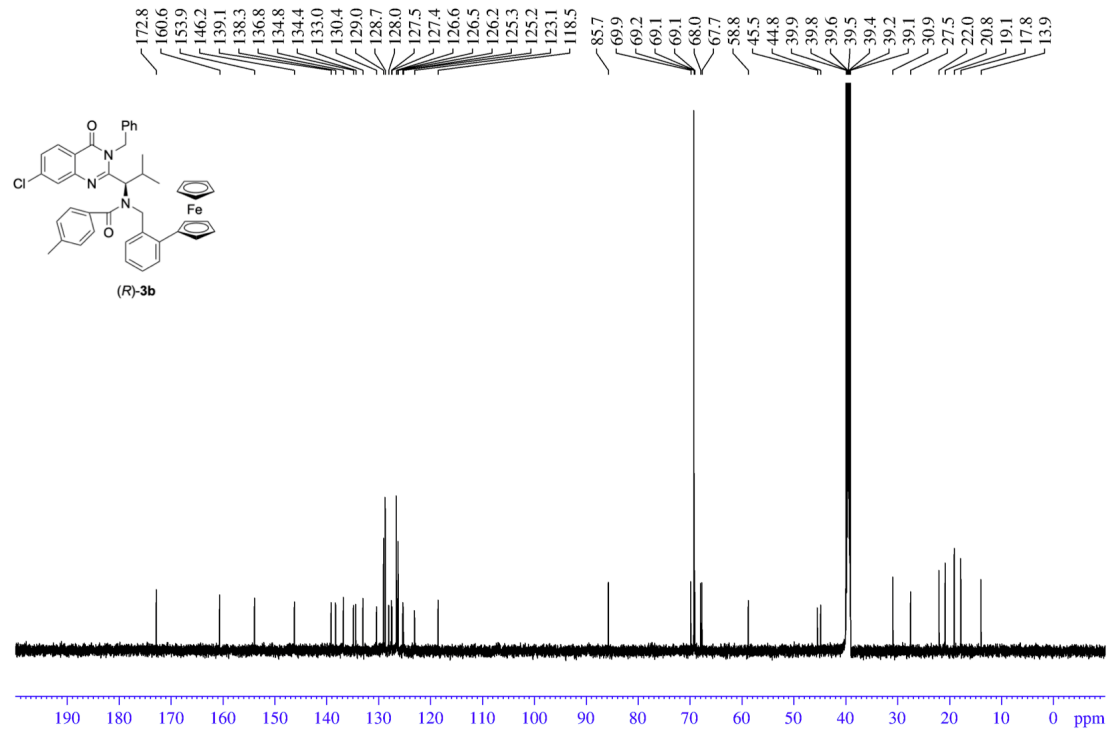

Figure S34. ^{13}C{^{1}H} NMR of (*R*)-3b in DMSO-d$_6$

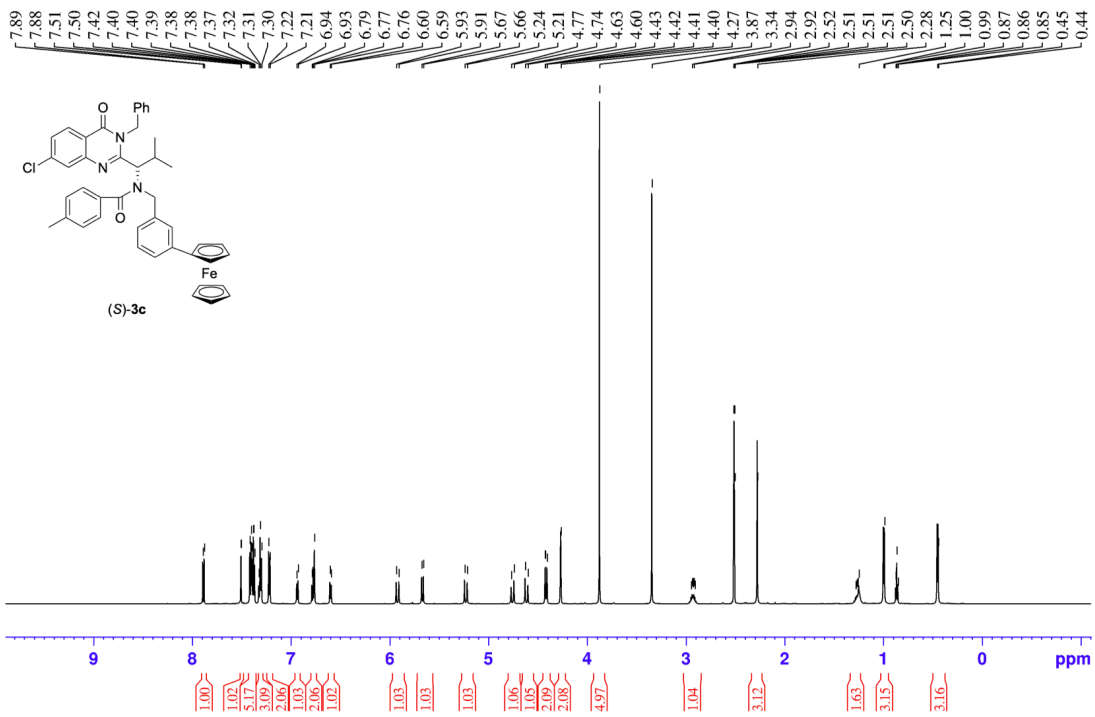

Figure S35. ^{1}H NMR of (*S*)-3c in DMSO-d$_6$

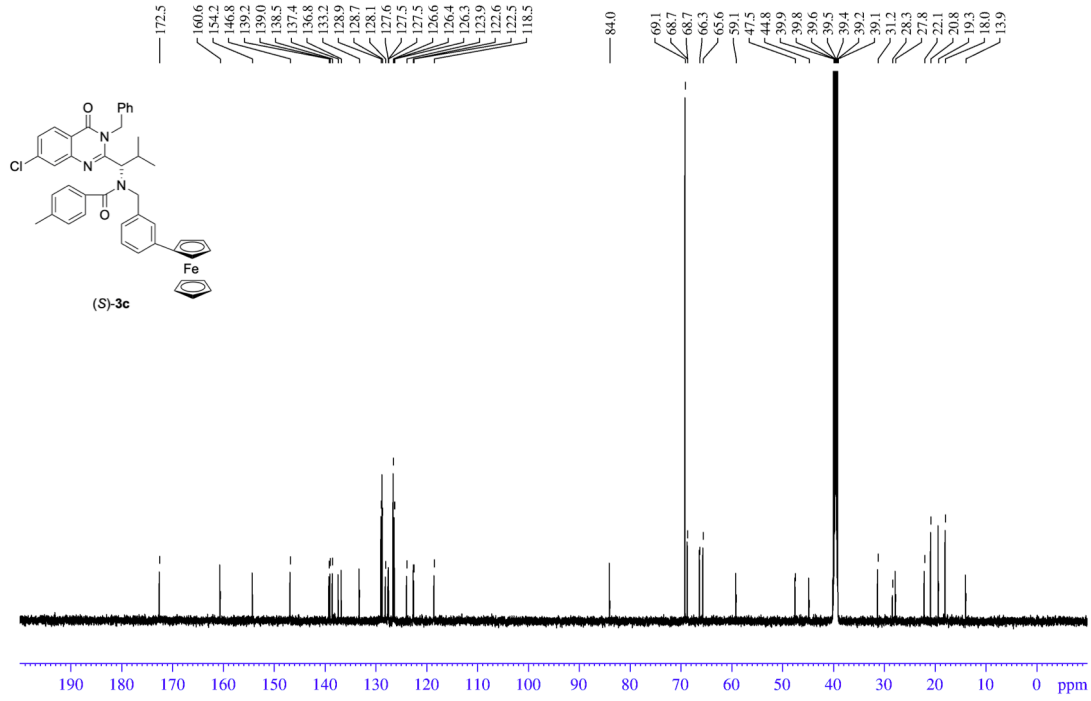

Figure S36. ^{13}C{^{1}H} NMR of (*S*)-3c in DMSO-d$_6$

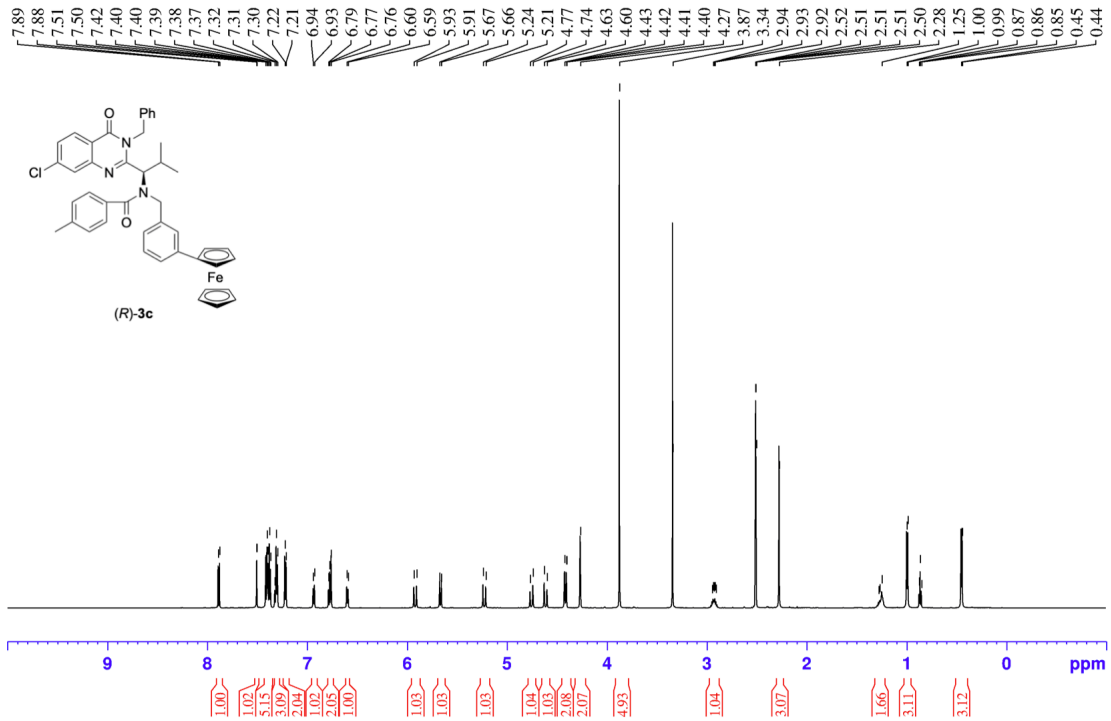

Figure S37. ^{1}H NMR of (*R*)-3c in DMSO-d$_6$

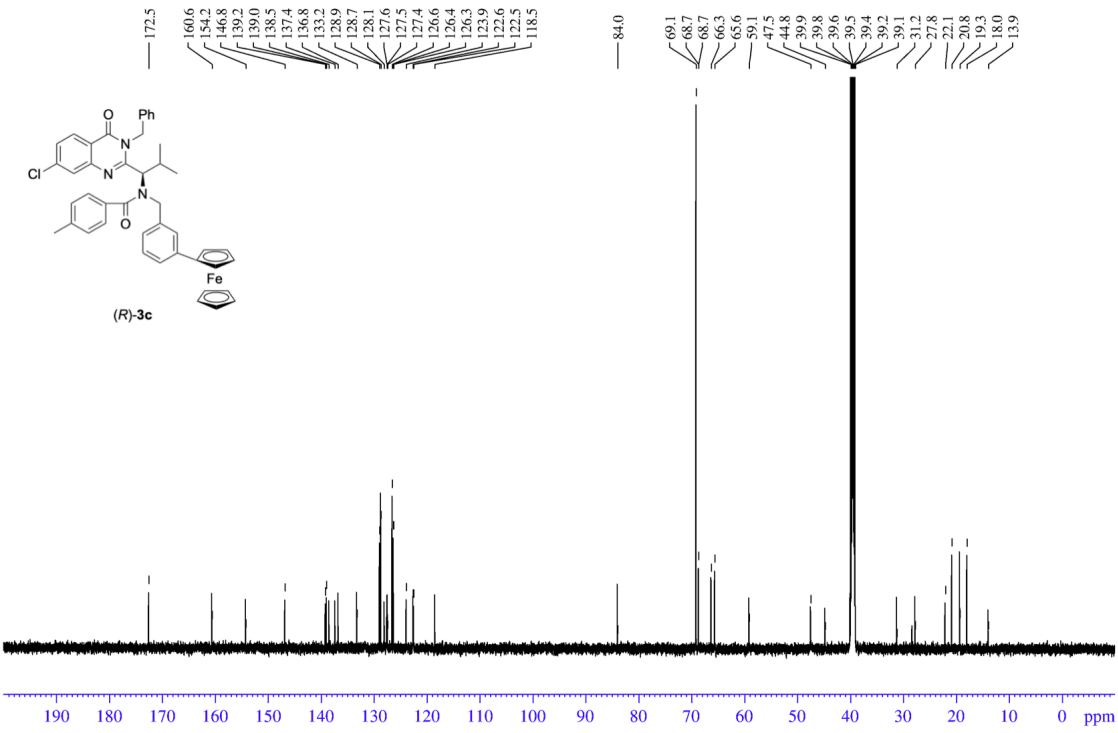

Figure S38. ^{13}C{^{1}H} NMR of (*R*)-3c in DMSO-d$_6$

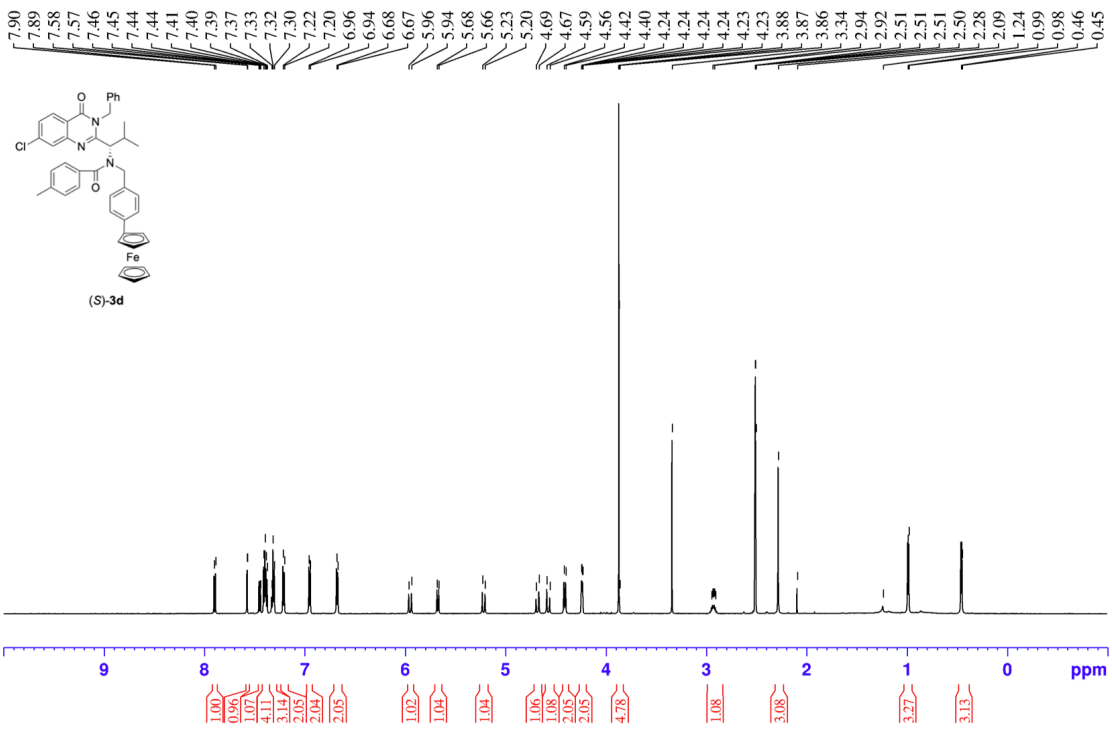

Figure S39. ^{1}H NMR of (*S*)-3d in DMSO-d$_6$

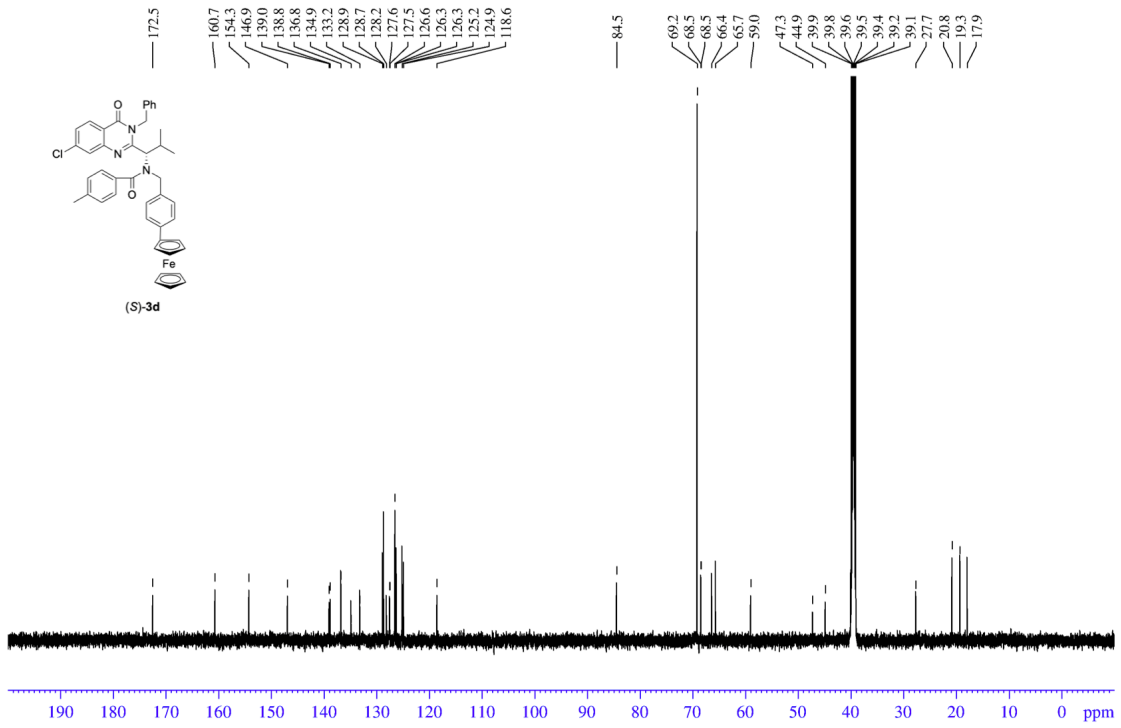

Figure S40. ^{13}C{^{1}H} NMR of (*S*)-3d in DMSO-d$_6$

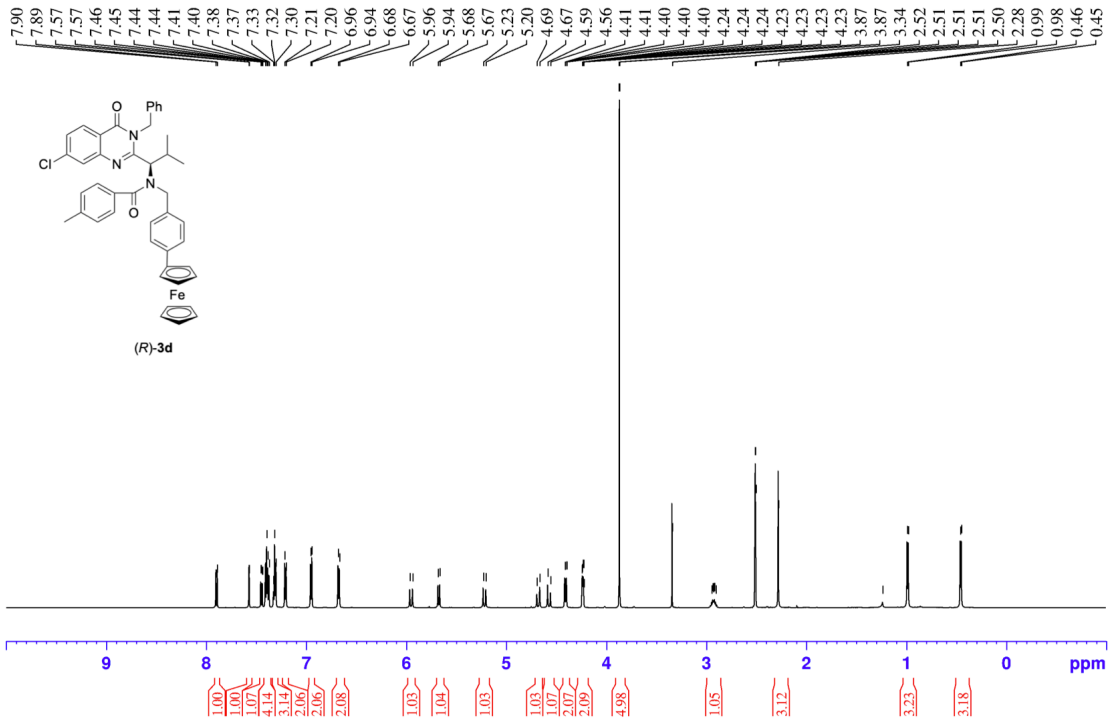

Figure S41. ^{1}H NMR of (*R*)-3d in DMSO-d$_6$

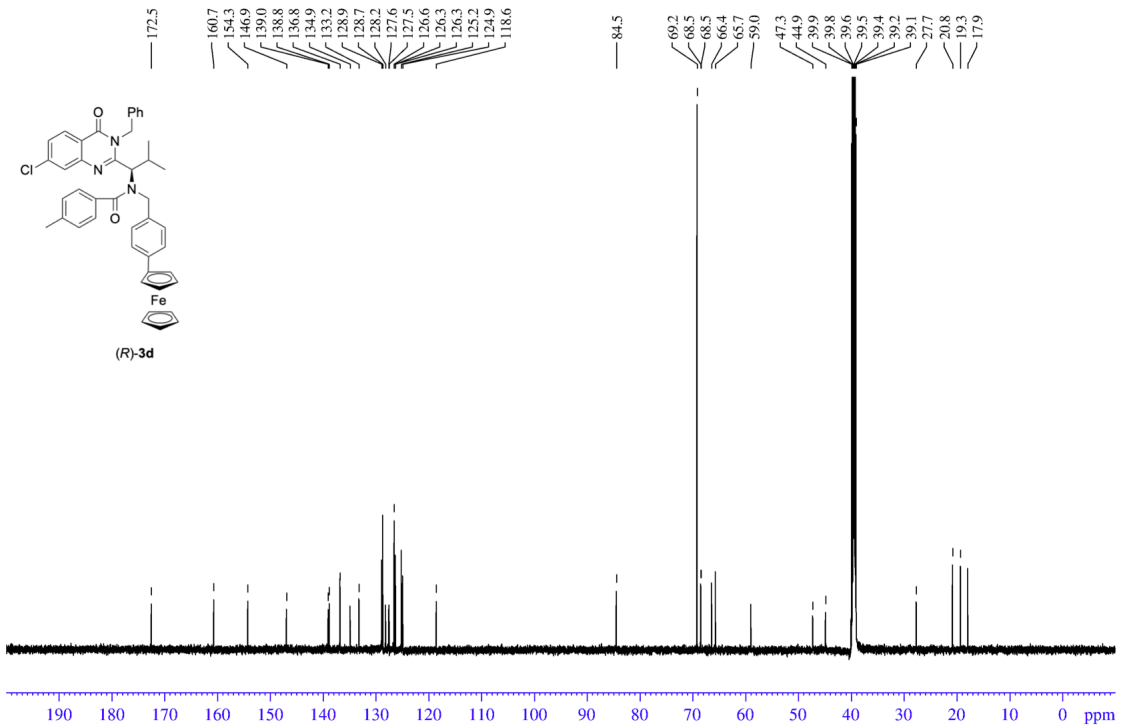

Figure S42. ^{13}C{^{1}H} NMR of (*R*)-3d in DMSO-d$_6$

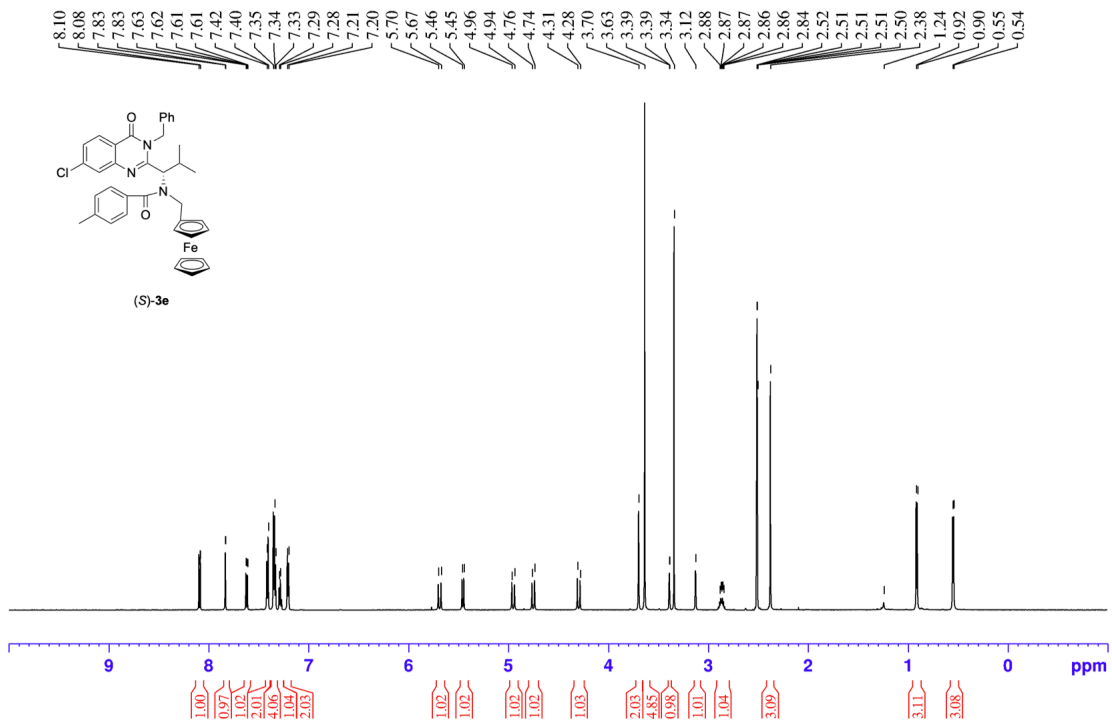

Figure S43. ^{1}H NMR of (*S*)-3e in DMSO-d$_6$

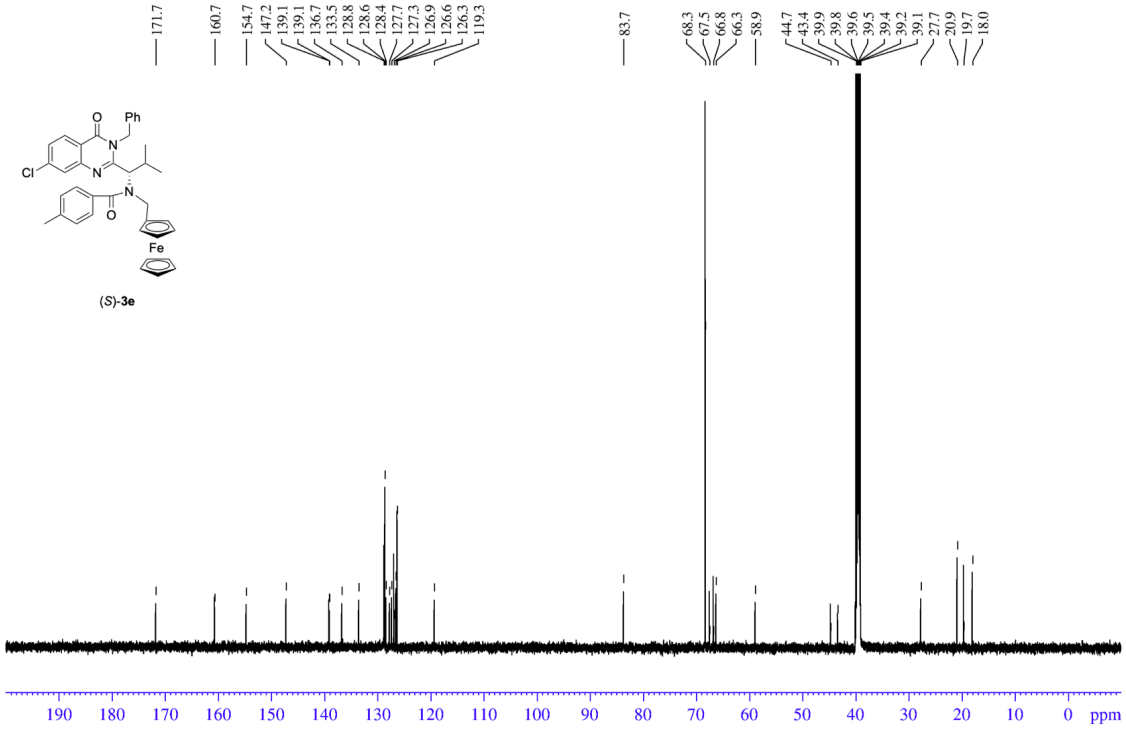

Figure S44. ^{13}C{^{1}H} NMR of (*S*)-3e in DMSO-d$_6$

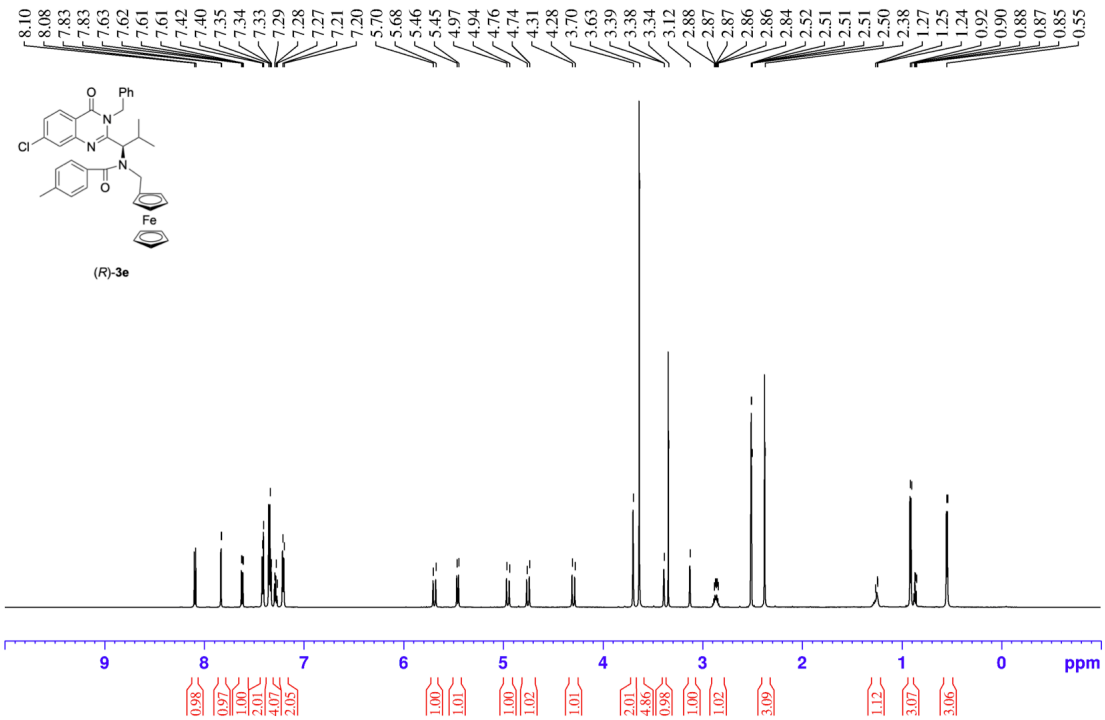

Figure S45. ^{1}H NMR of (*R*)-3e in DMSO-d$_6$

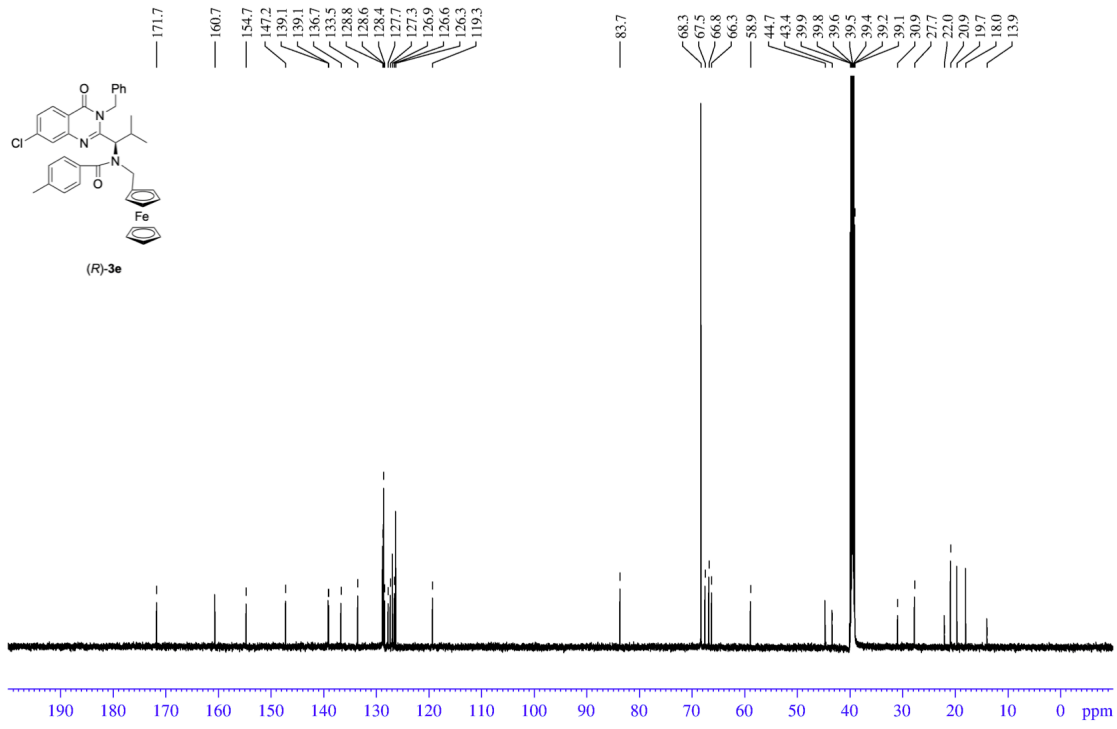

Figure S46. ^{13}C{^{1}H} NMR of (*R*)-3e in DMSO-d$_6$

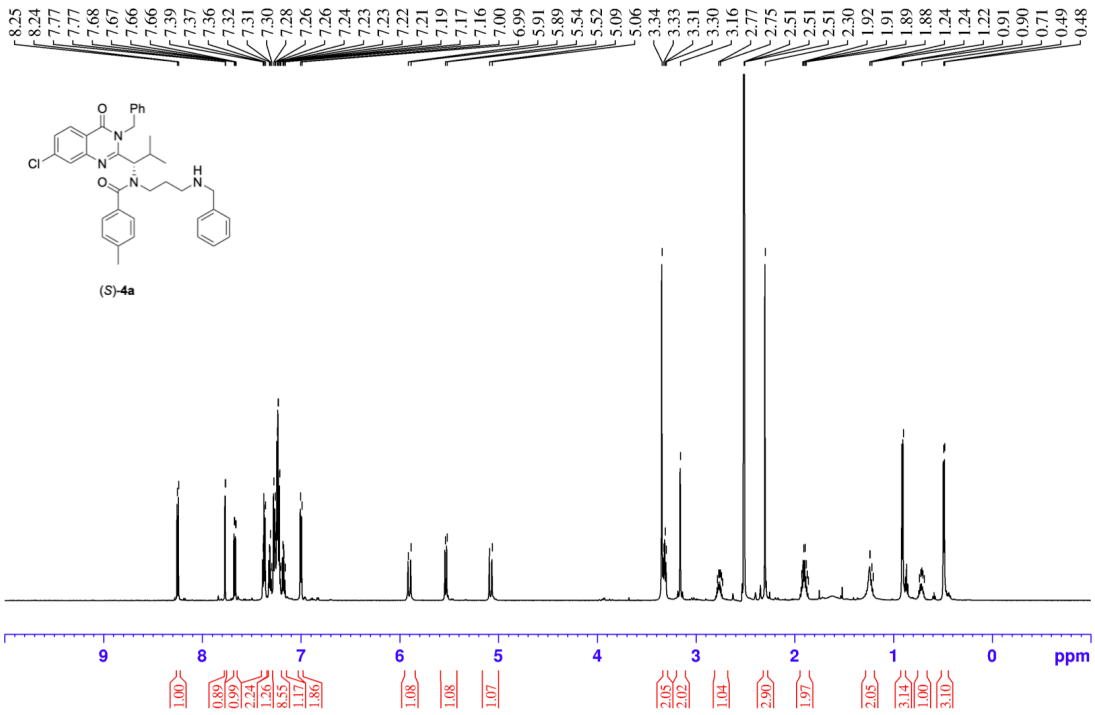

Figure S47. ^{1}H NMR of (*S*)-4a in DMSO-d$_6$

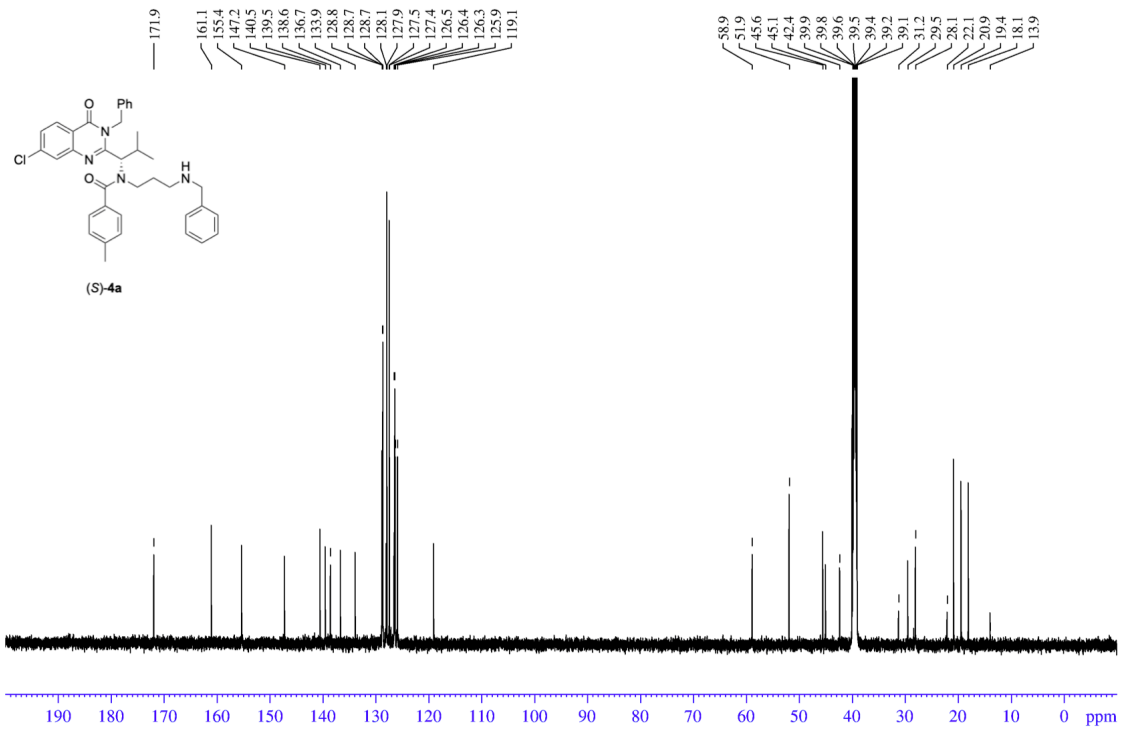

Figure S48. ^{13}C{^{1}H} NMR of (*S*)-4a in DMSO-d$_6$

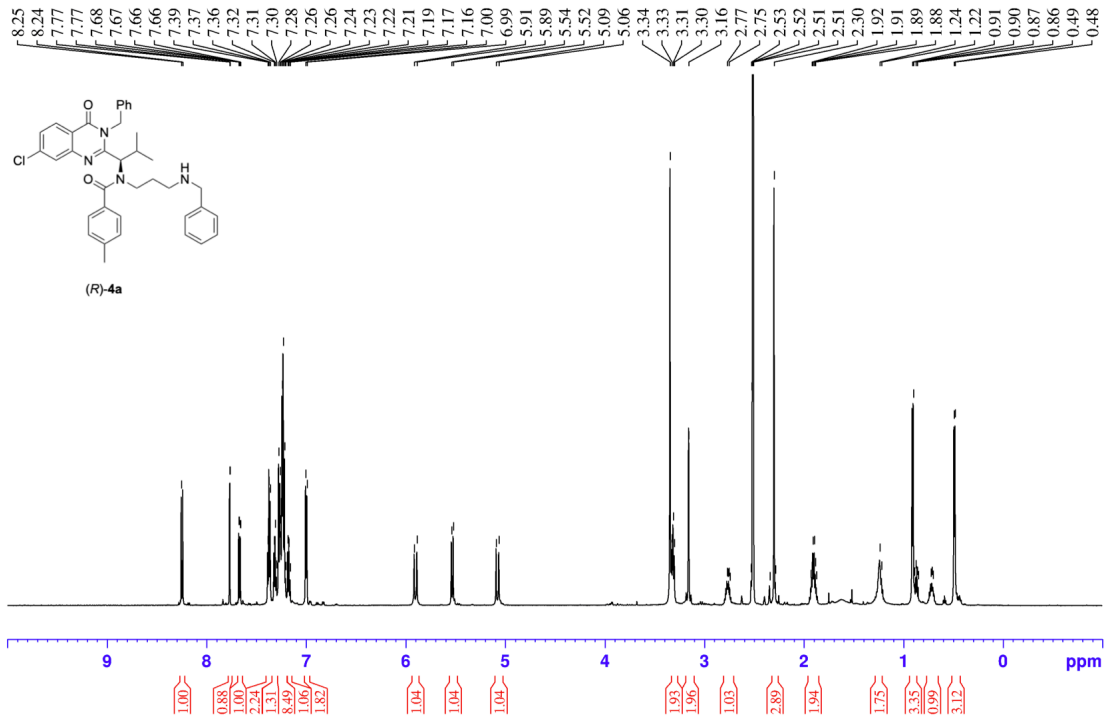

Figure S49. ^{1}H NMR of (*R*)-4a in DMSO-d$_6$

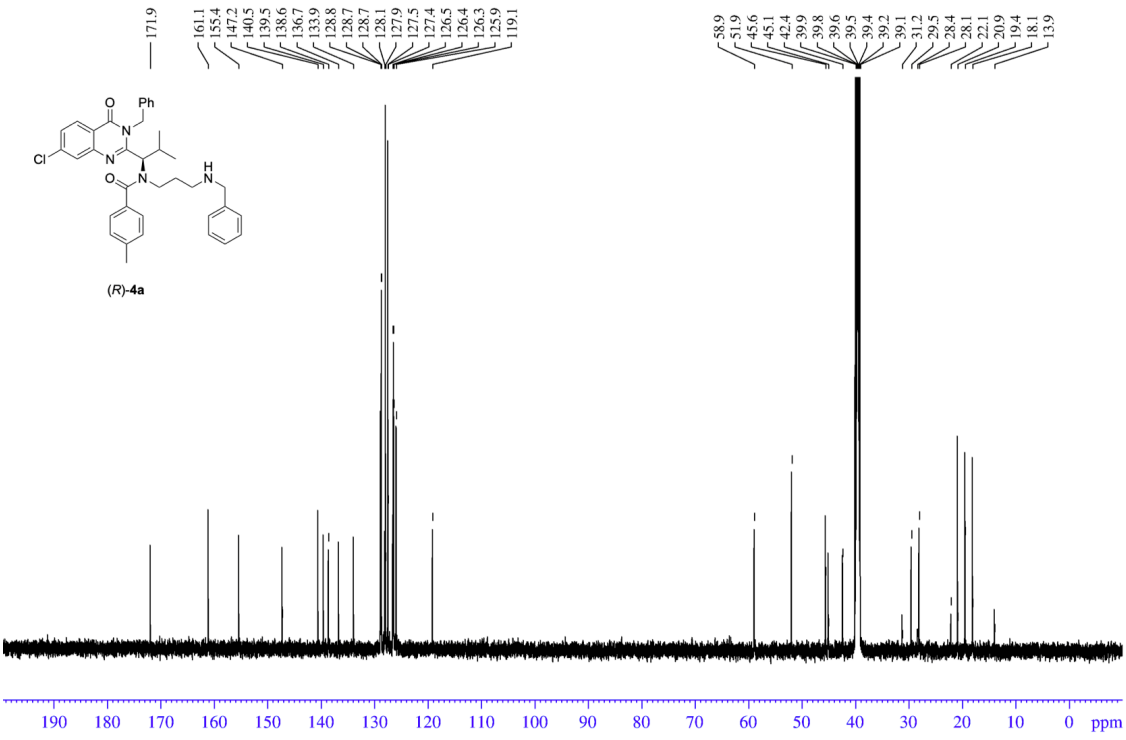

Figure S50. ^{13}C{^{1}H} NMR of (*R*)-4a in DMSO-d$_6$

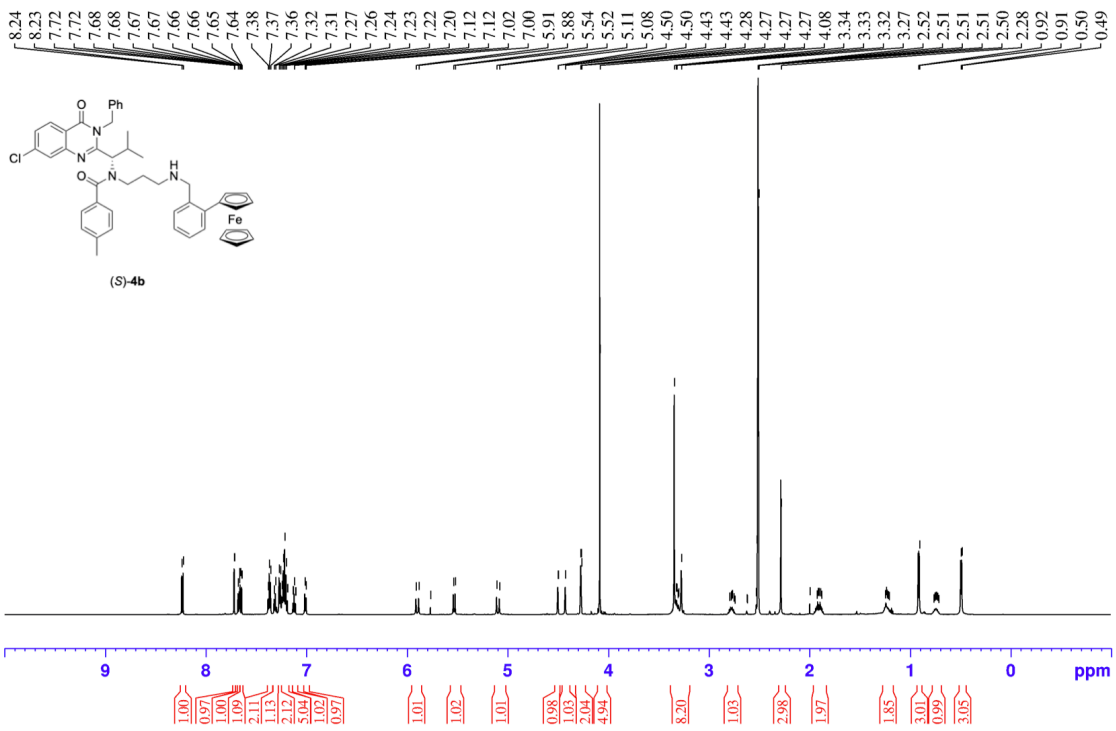

Figure S51. ^{1}H NMR of (*S*)-4b in DMSO-d$_6$

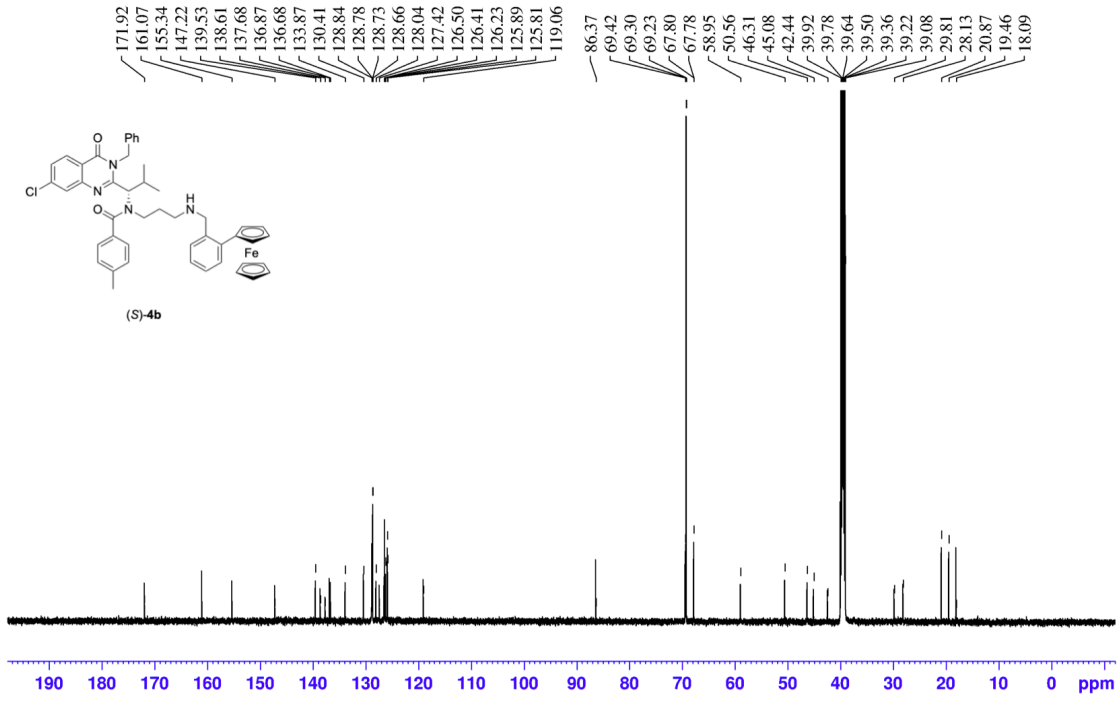

Figure S52. ^{13}C{^{1}H} NMR of (*S*)-4b in DMSO-d$_6$

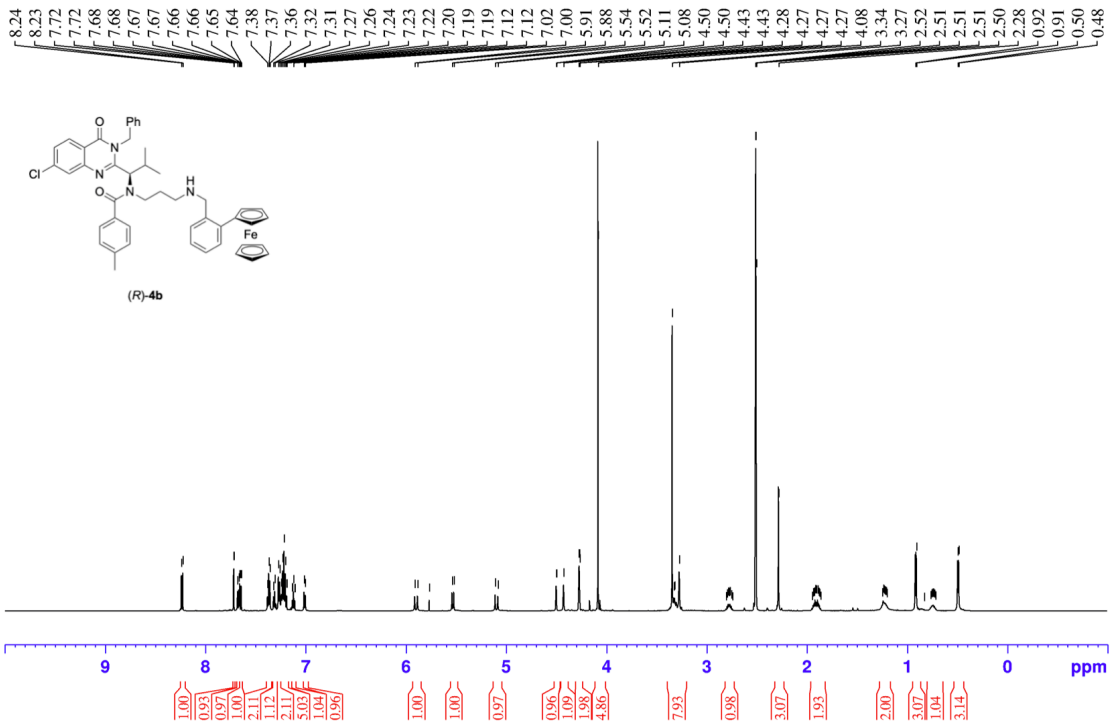

Figure S53. ^{1}H NMR of (*R*)-4b in DMSO-d$_6$

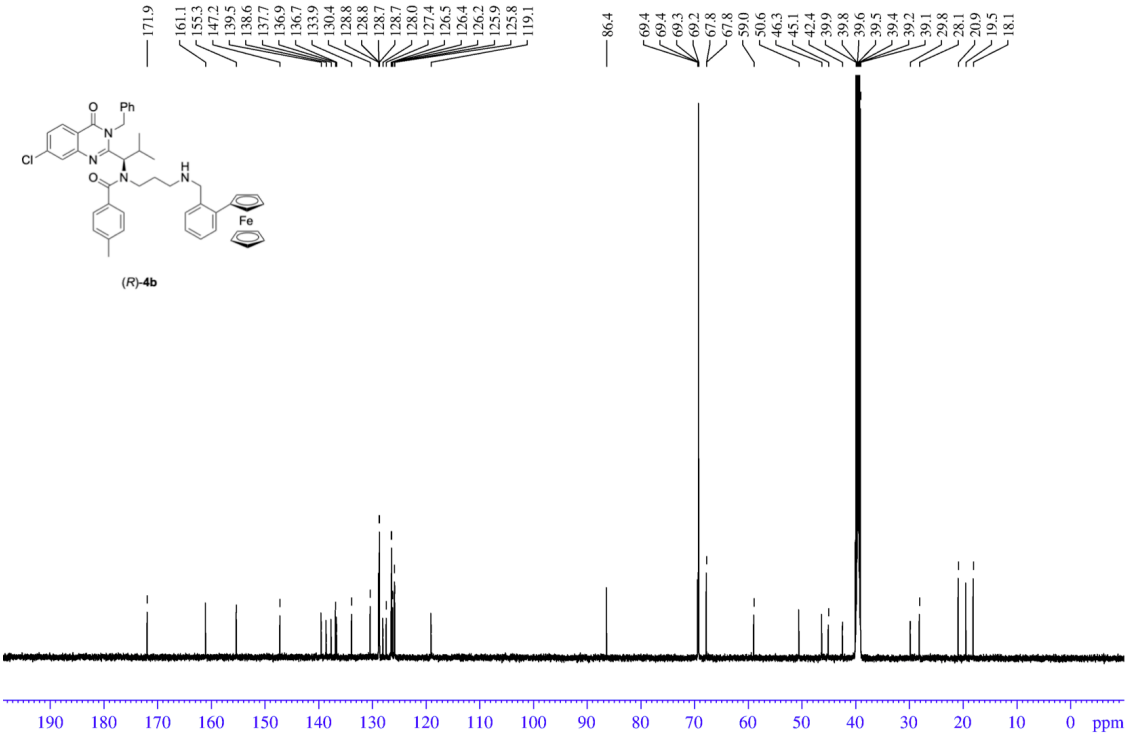

Figure S54. ^{13}C{^{1}H} NMR of (*R*)-4b in DMSO-d$_6$

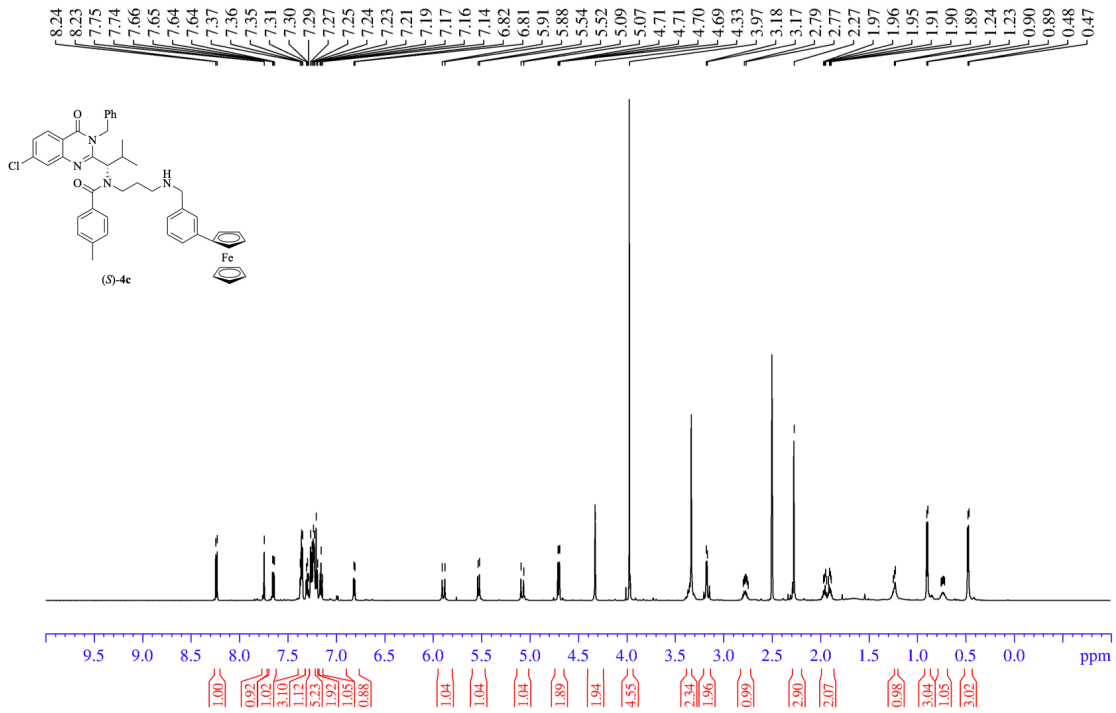

Figure S55. ^{1}H NMR of (*S*)-4c in DMSO-d$_6$

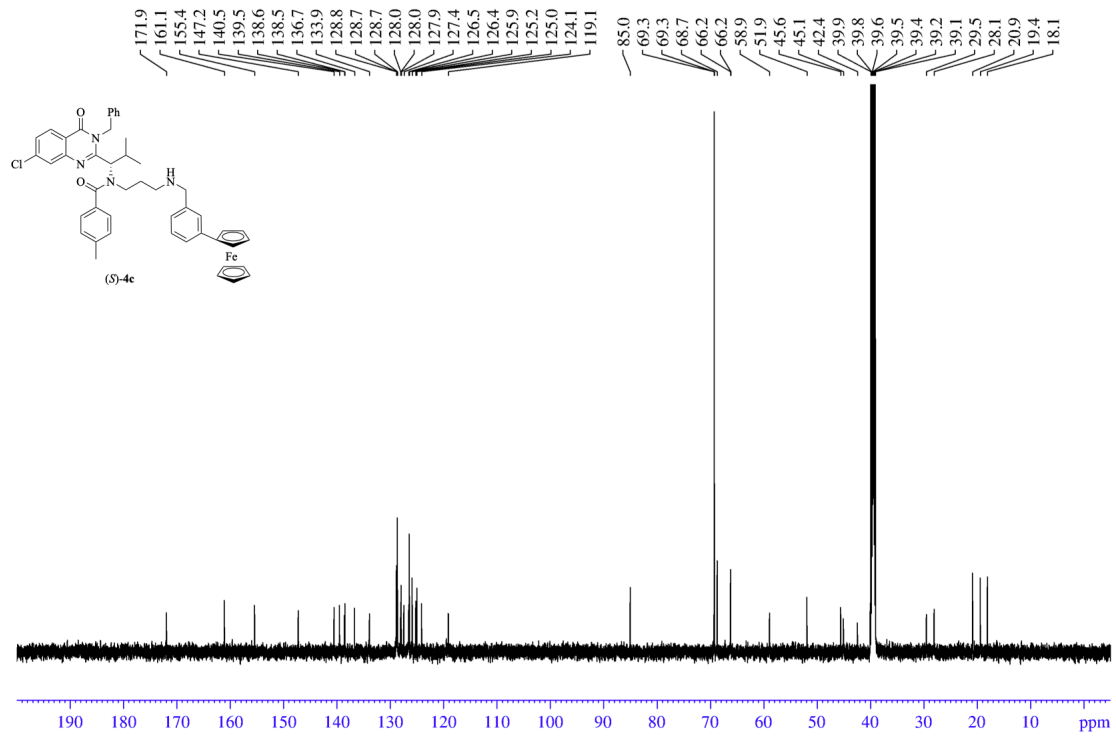

Figure S56. ^{13}C{^{1}H} NMR of (*S*)-4c in DMSO-d$_6$

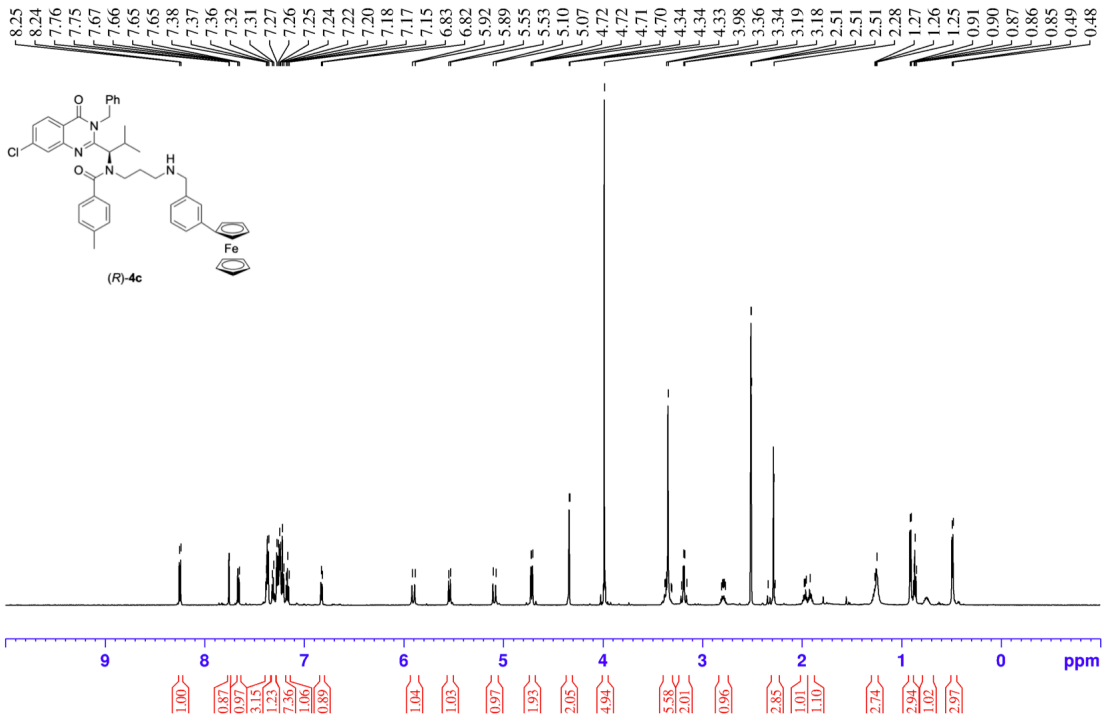

Figure S57. ^{1}H NMR of (*R*)-4c in DMSO-d$_6$

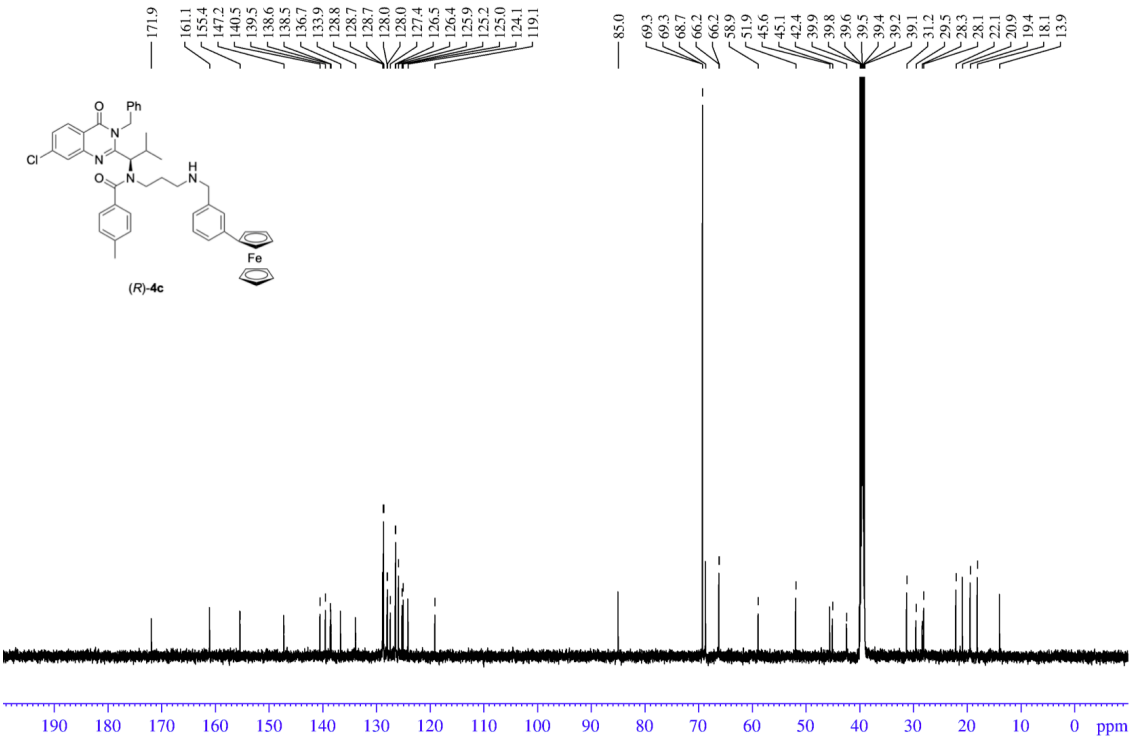

Figure S58. ^{13}C{^{1}H} NMR of (*R*)-4c in DMSO-d$_6$

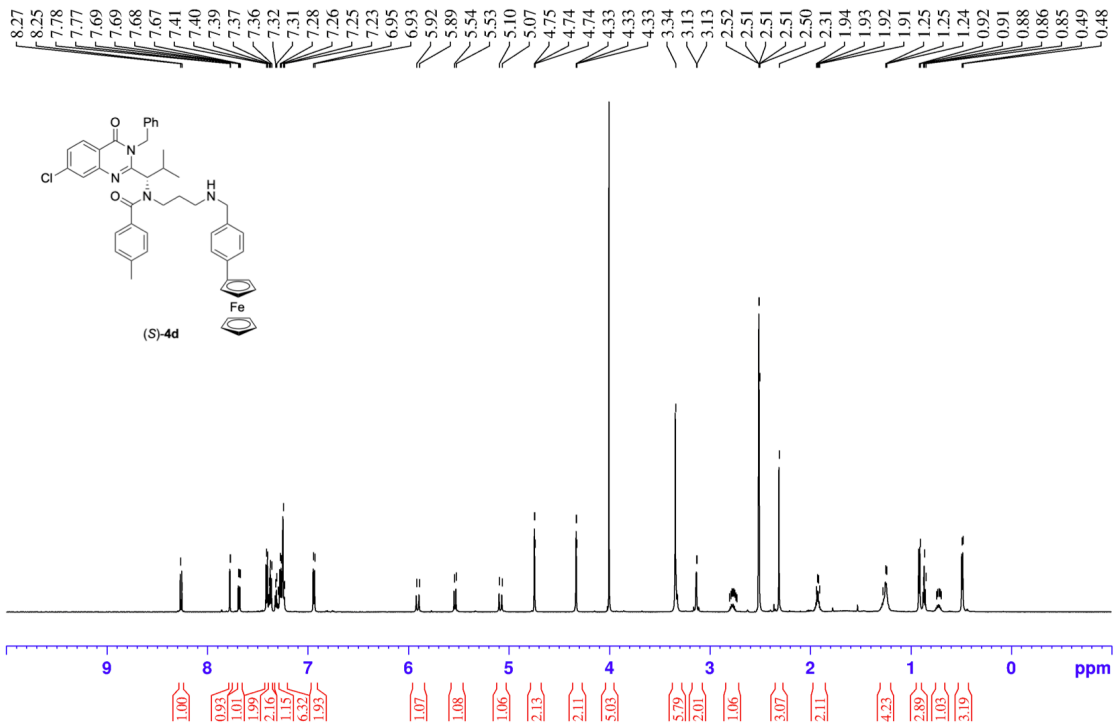

Figure S59. ^{1}H NMR of (*S*)-4d in DMSO-d$_6$

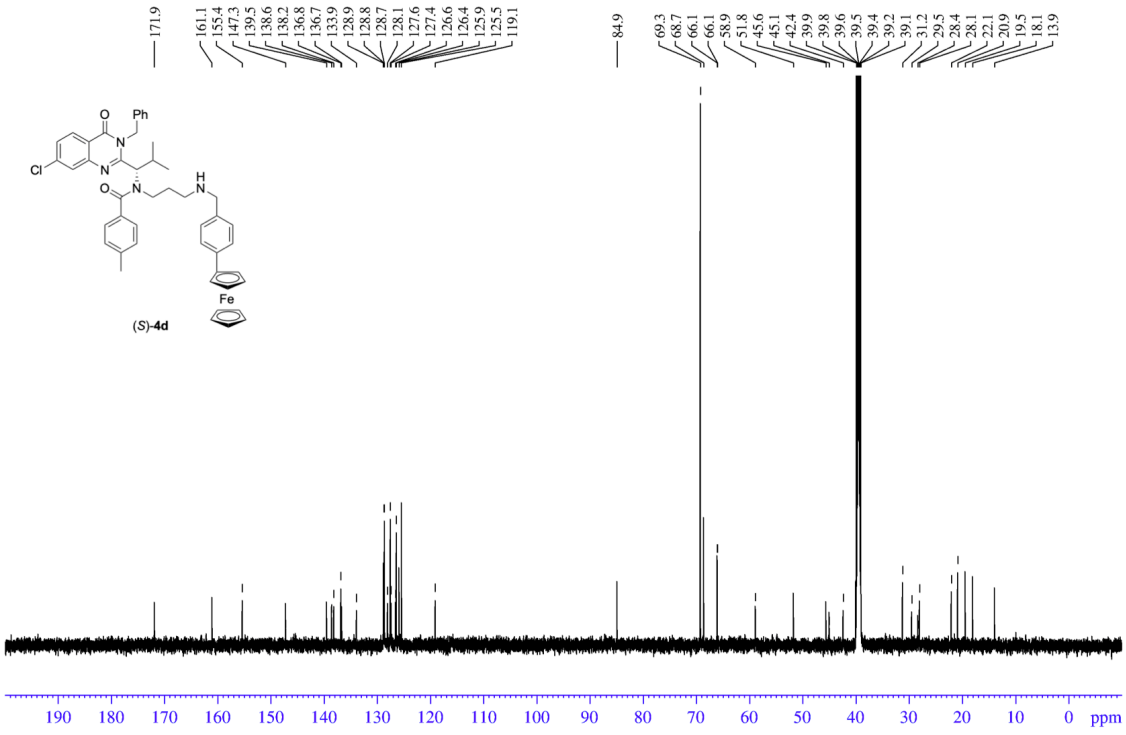

Figure S60. ^{13}C{^{1}H} NMR of (*S*)-4d in DMSO-d$_6$

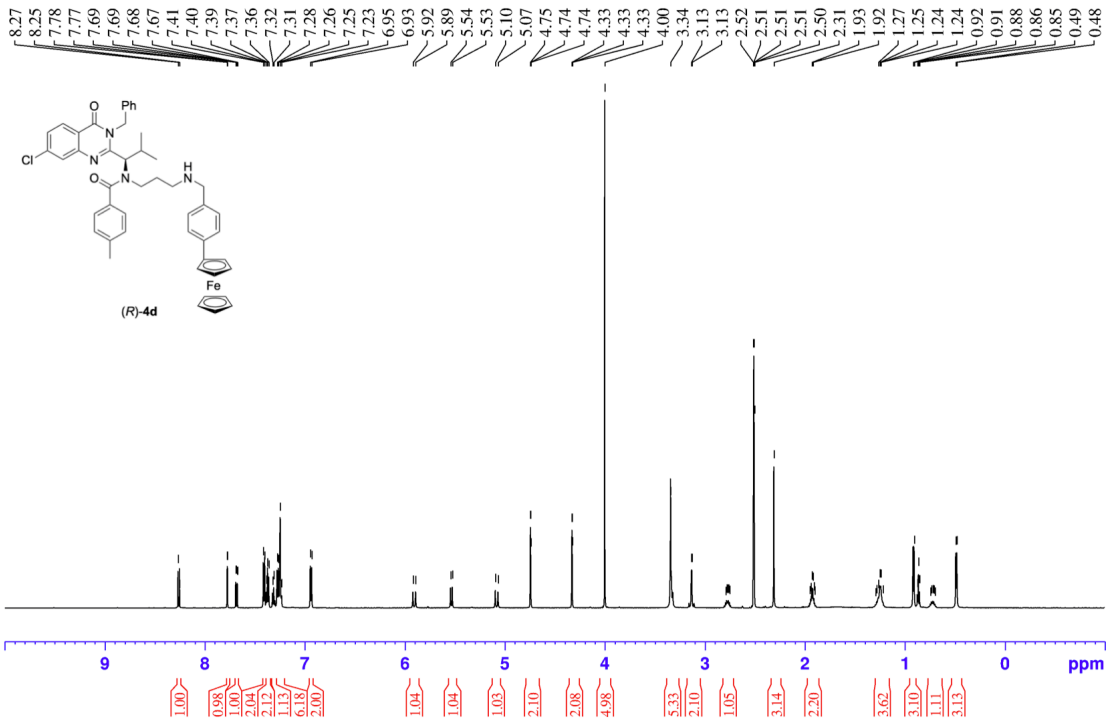

Figure S61. ^{1}H NMR of (*R*)-4d in DMSO-d$_6$

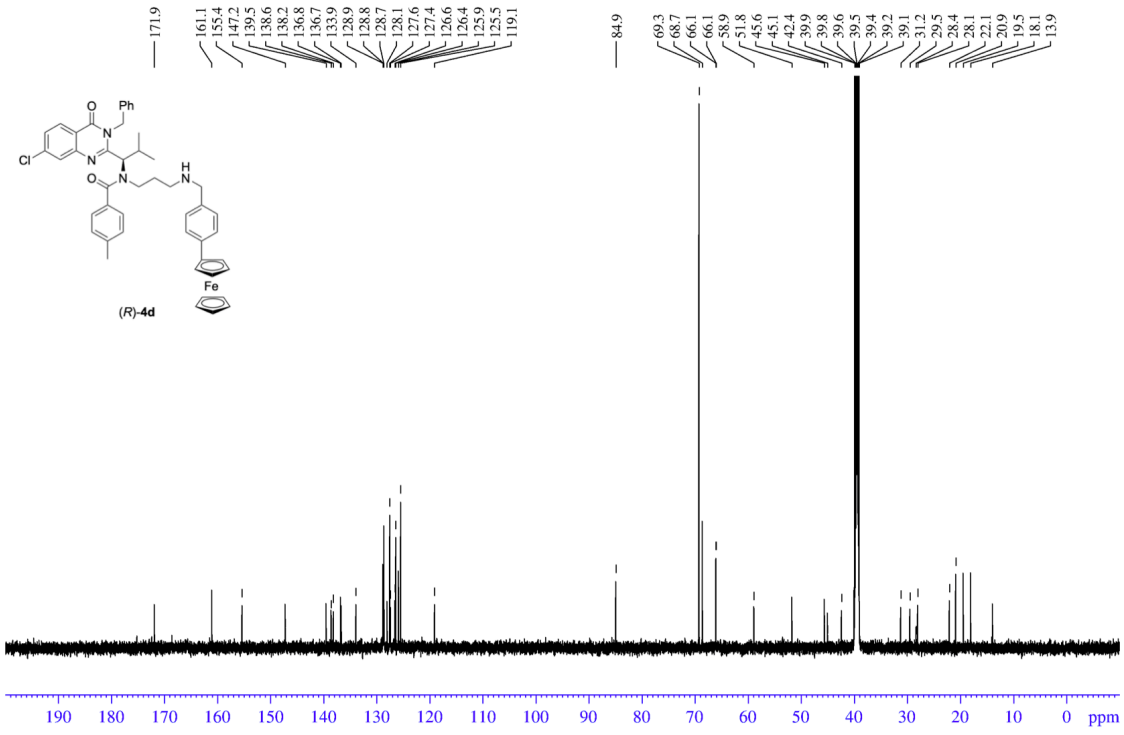

Figure S62. ^{13}C{^{1}H} NMR of (*R*)-4d in DMSO-d$_6$

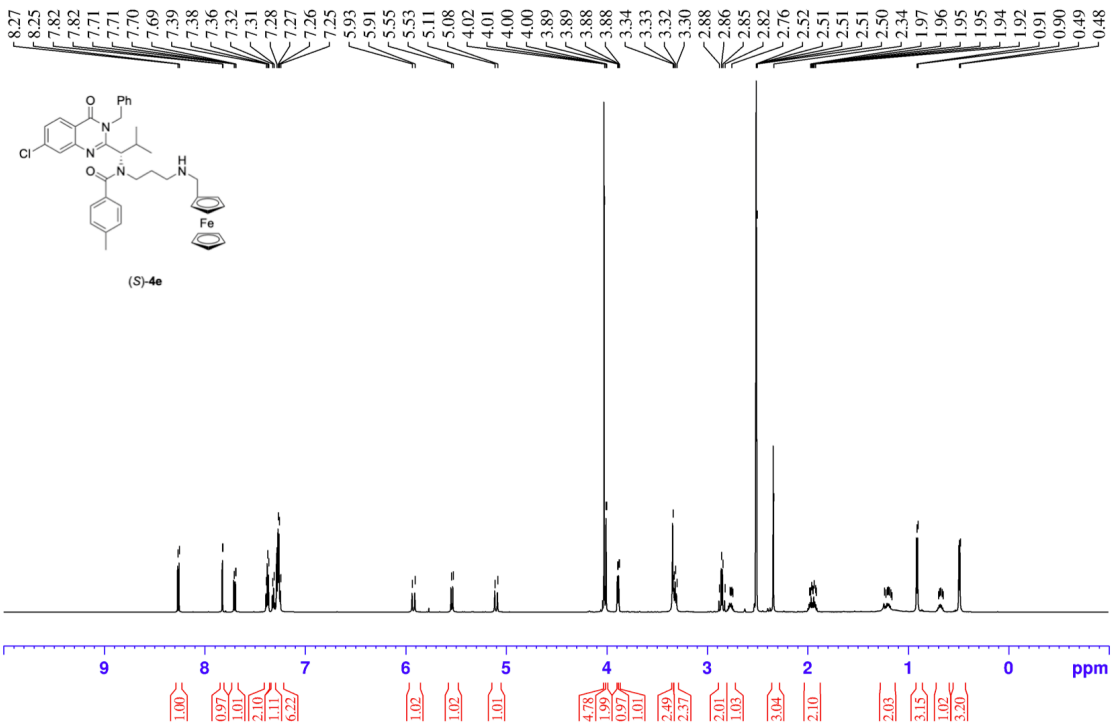

Figure S63. ^{1}H NMR of (*S*)-4e in DMSO-d$_6$

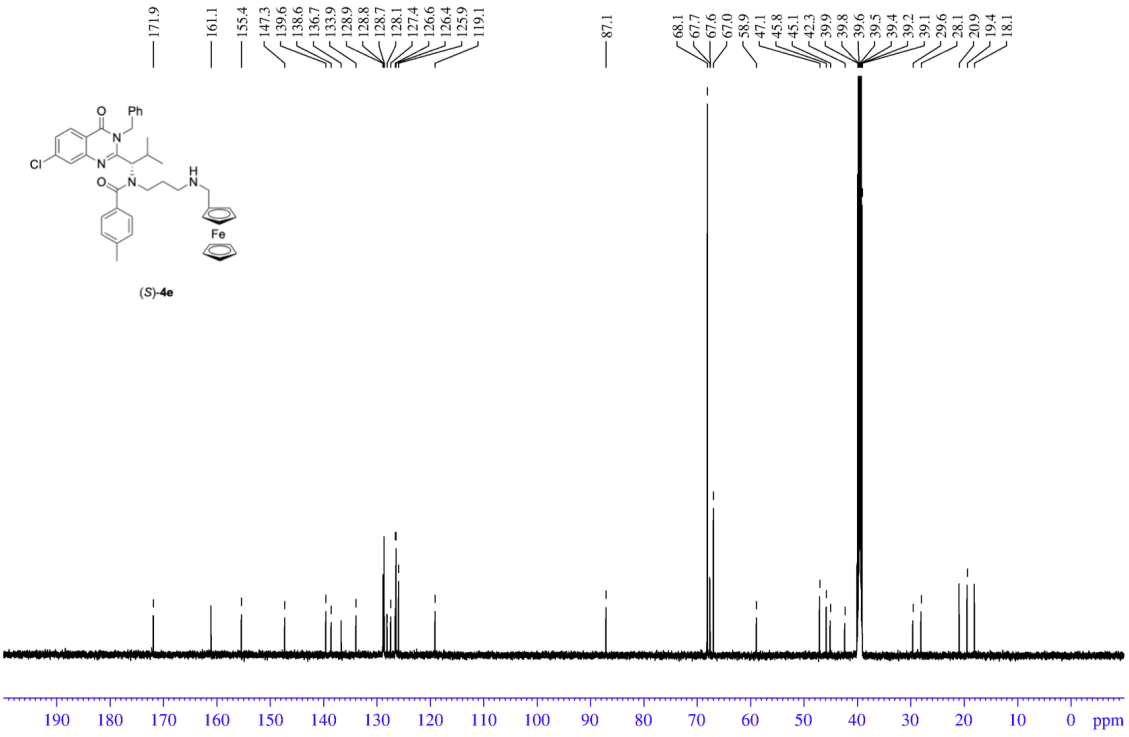

Figure S64. ^{13}C{^{1}H} NMR of (*S*)-4e in DMSO-d$_6$

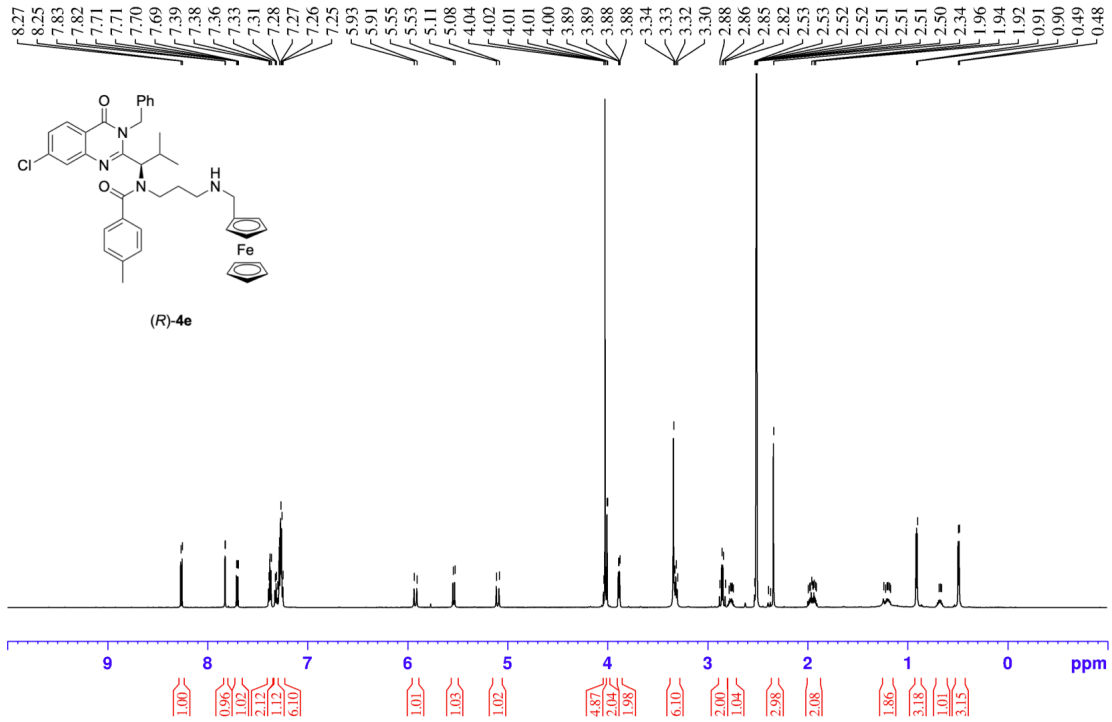

Figure S65. ^{1}H NMR of (*R*)-4e in DMSO-d$_6$

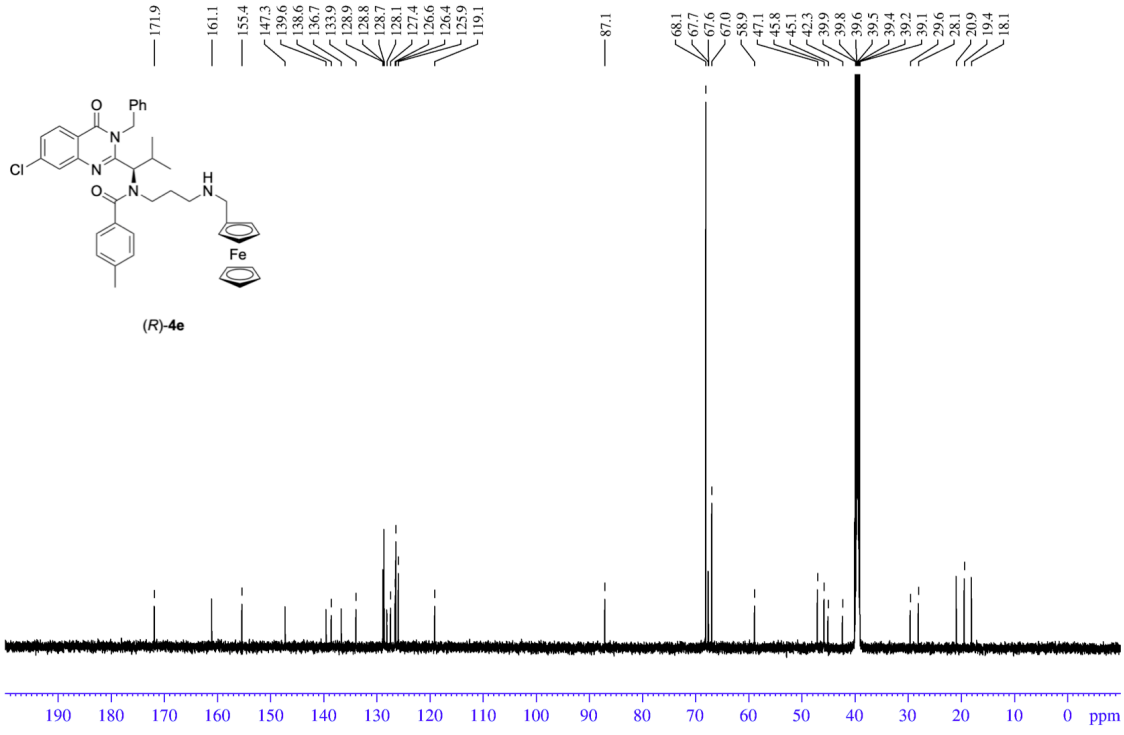

Figure S66. ^{13}C{^{1}H} NMR of (*R*)-4e in DMSO-d$_6$

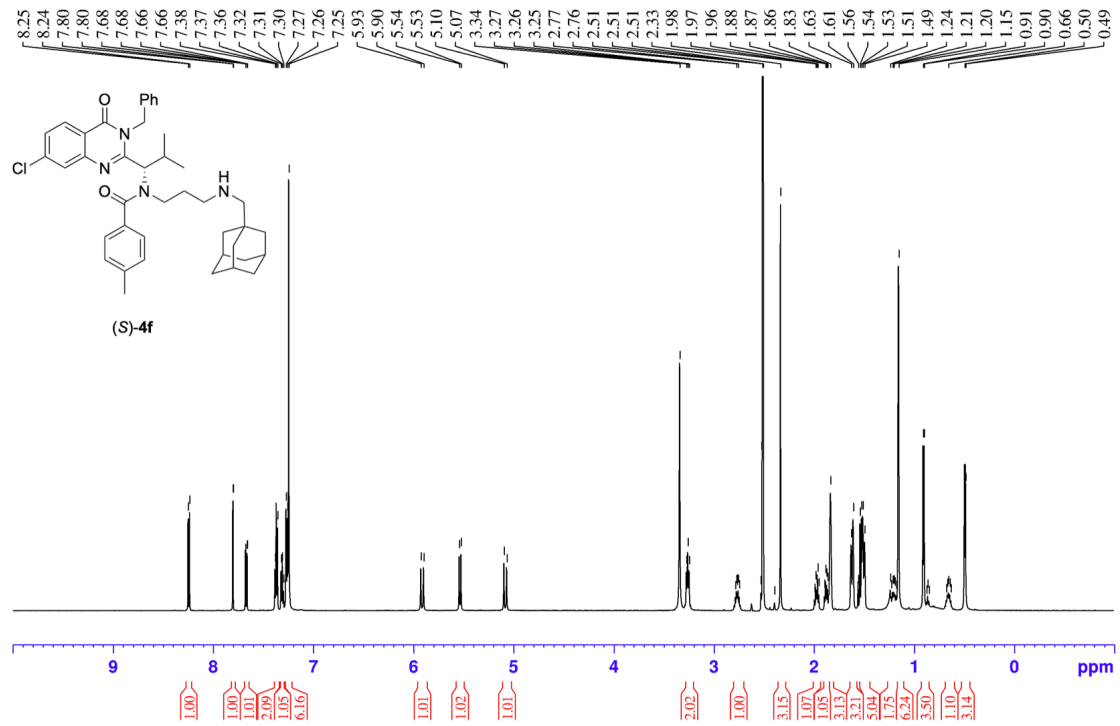

Figure S67. ^{1}H NMR of (*S*)-4f in DMSO-d$_6$

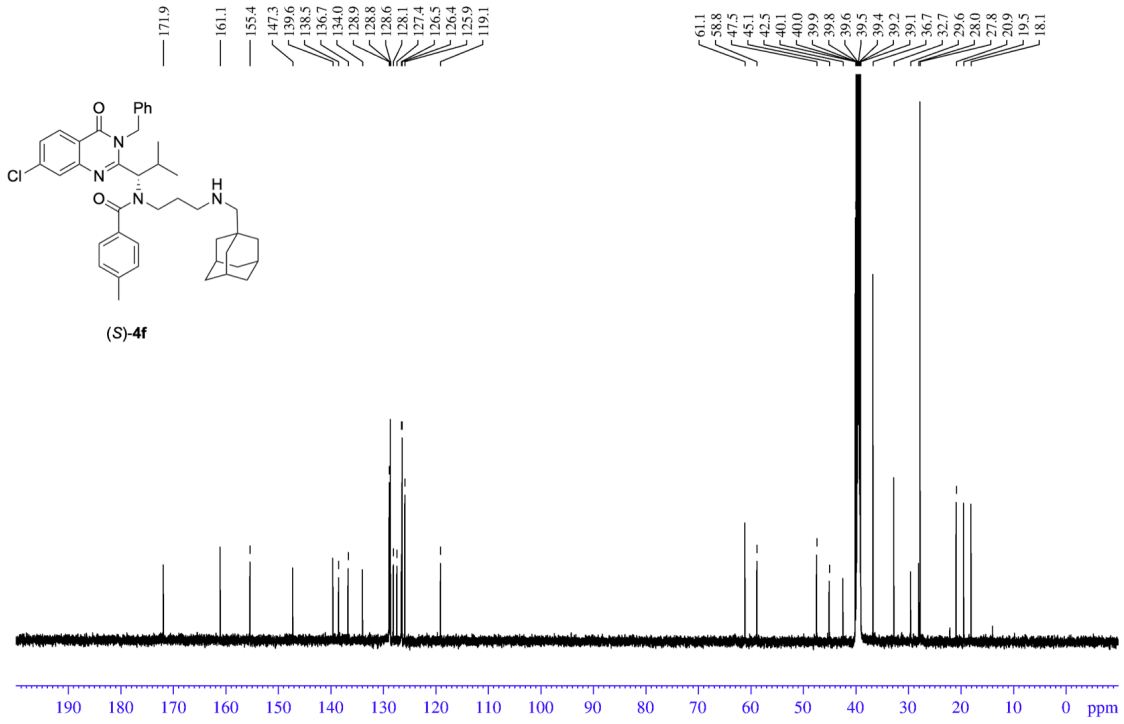

Figure S68. ^{13}C{^{1}H} NMR of (*S*)-4f in DMSO-d$_6$

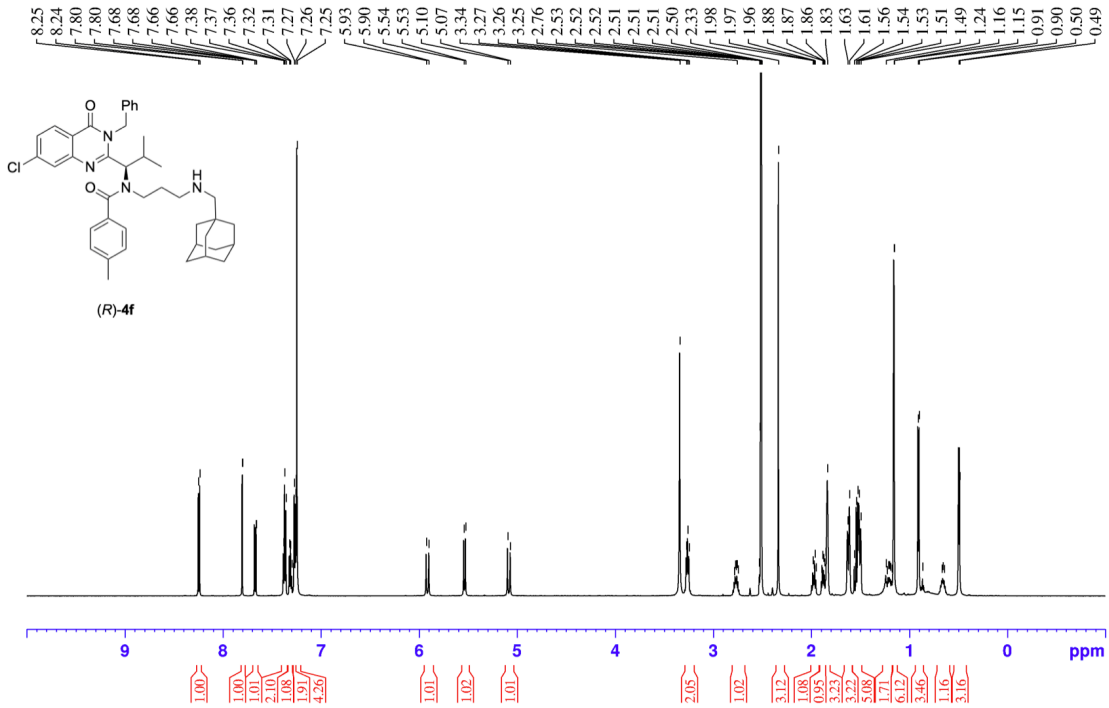

Figure S69. ^{1}H NMR of (*R*)-4f in DMSO-d$_6$

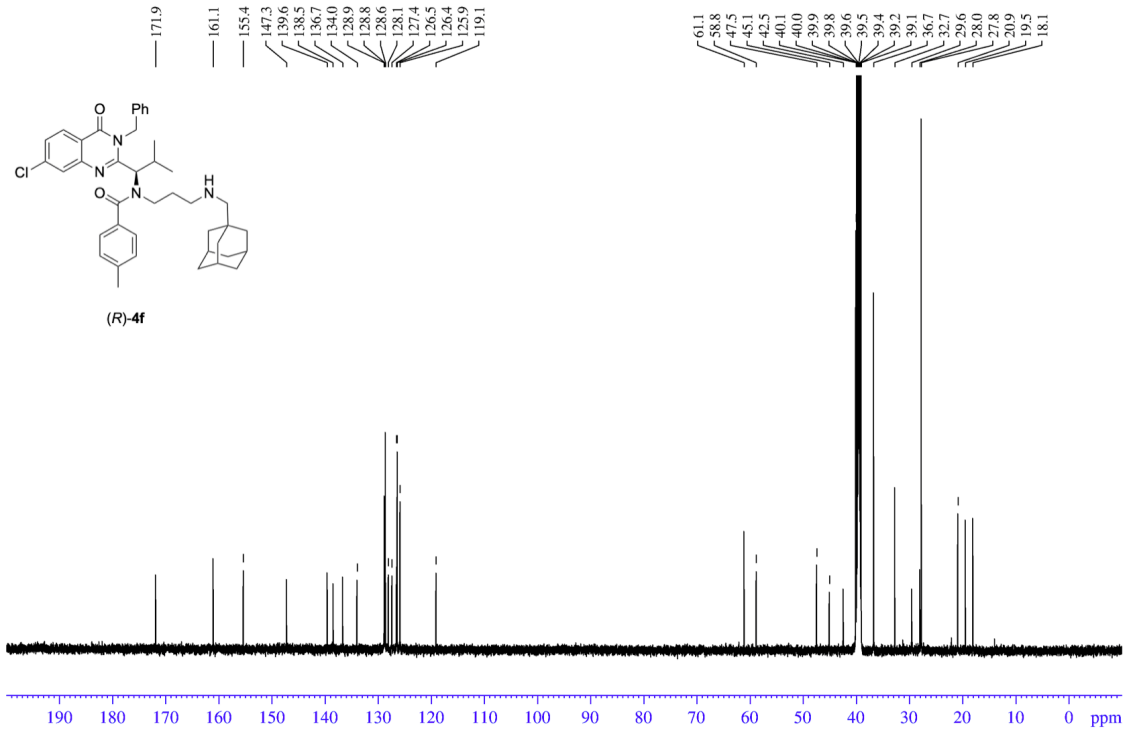

Figure S70. ^{13}C{^{1}H} NMR of (*R*)-4f in DMSO-d$_6$

HPLC-MS analysis

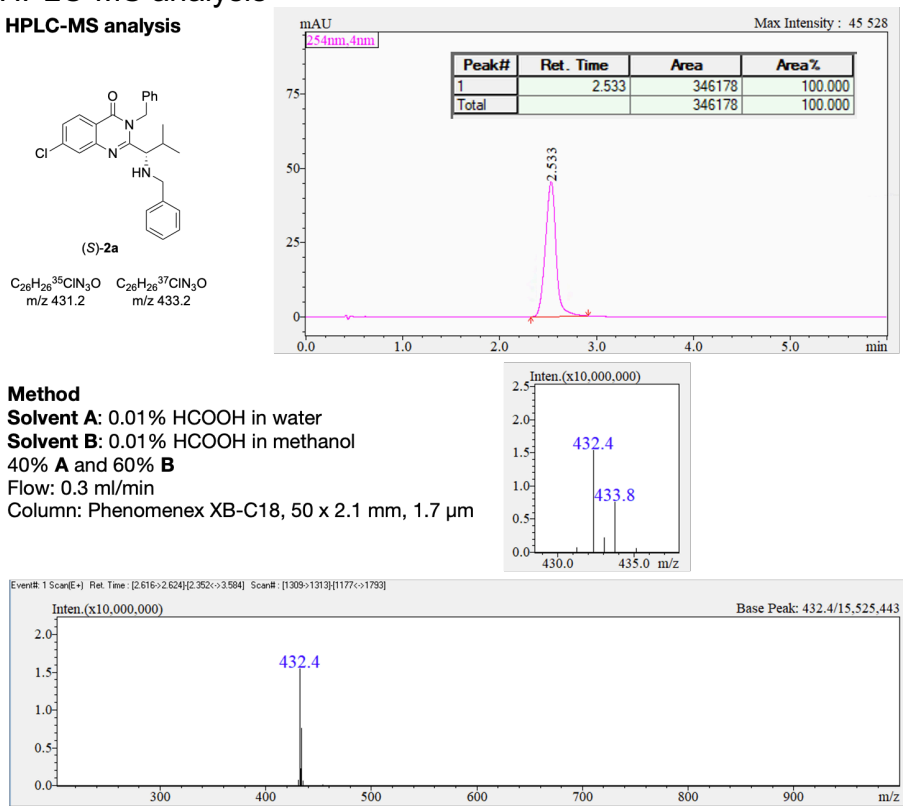

Figure S71. HPLC-MS analysis of (*S*)-2a

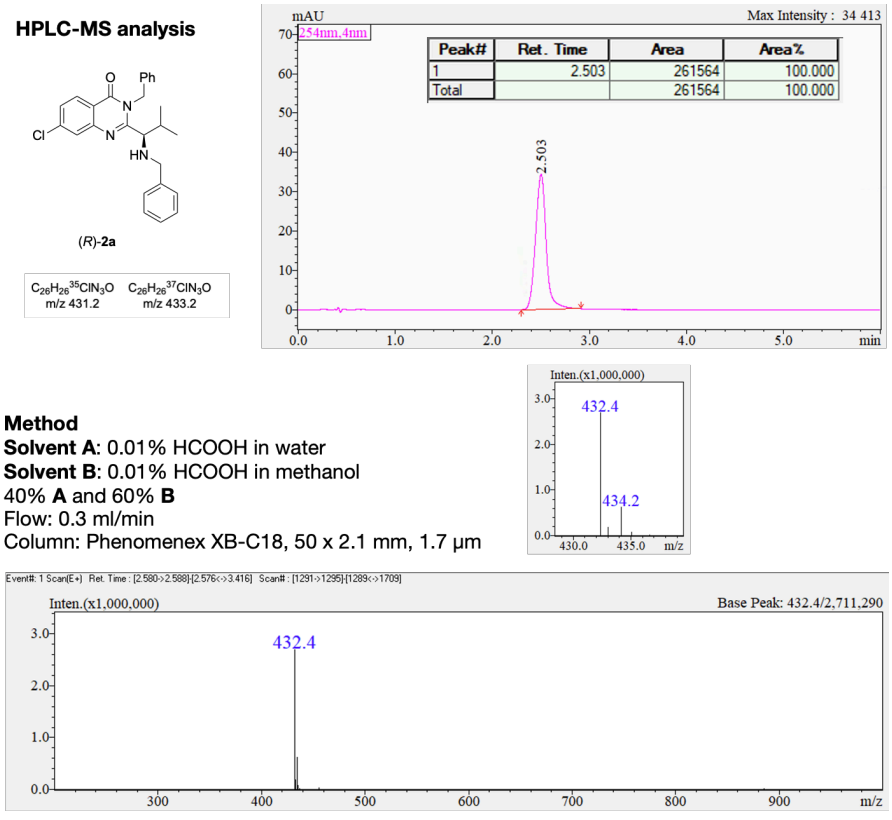

Figure S72. HPLC-MS analysis of (*R*)-2a

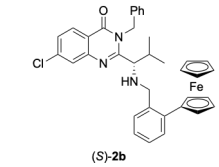

(*S*)-**2b**

$C_{36}H_{34}{}^{35}ClFeN_3O$ m/z 615.2 $C_{36}H_{34}{}^{37}ClFeN_3O$ m/z 617.2

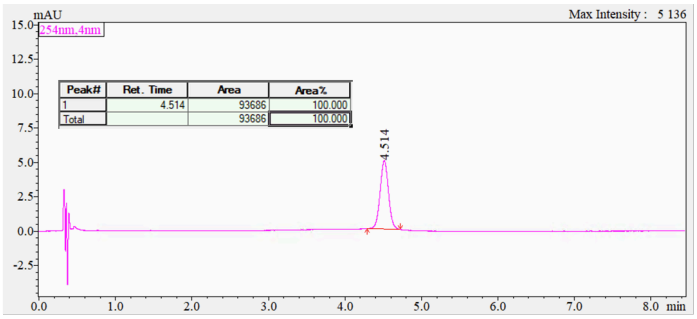

Method
Solvent A: 0.01% HCOOH in water
Solvent B: 0.01% HCOOH in methanol
20% **A** and 80% **B**
Flow: 0.3 ml/min
Column: Phenomenex XB-C18, 50 x 2.1 mm, 1.7 µm

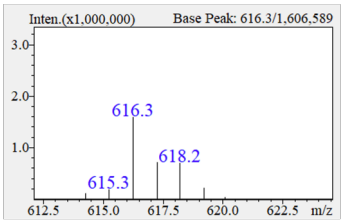

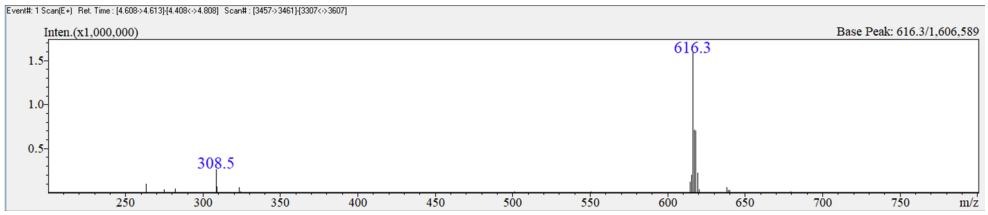

Figure S73. HPLC-MS analysis of (*S*)-2b

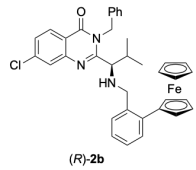

(*R*)-**2b**

$C_{36}H_{34}{}^{35}ClFeN_3O$ m/z 615.2 $C_{36}H_{34}{}^{37}ClFeN_3O$ m/z 617.2

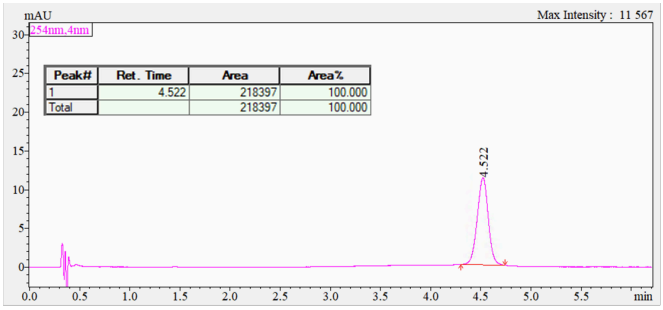

Method
Solvent A: 0.01% HCOOH in water
Solvent B: 0.01% HCOOH in methanol
20% **A** and 80% **B**
Flow: 0.3 ml/min
Column: Phenomenex XB-C18, 50 x 2.1 mm, 1.7 µm

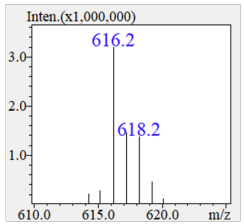

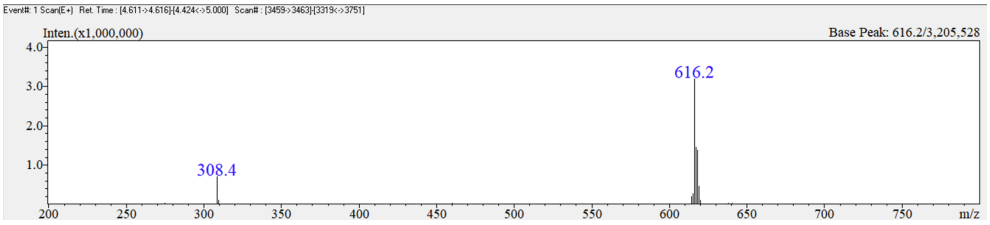

Figure S74. HPLC-MS analysis of (*R*)-2b

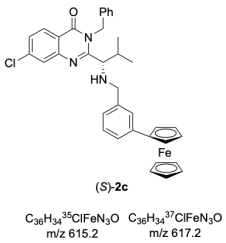

(*S*)-**2c**

$C_{36}H_{34}{}^{35}ClFeN_3O$ m/z 615.2 $C_{36}H_{34}{}^{37}ClFeN_3O$ m/z 617.2

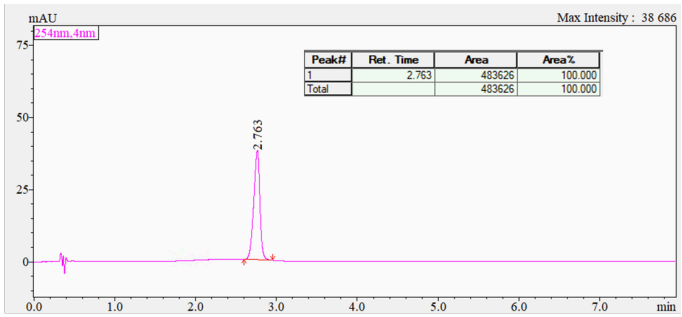

Method
Solvent A: 0.01% HCOOH in water
Solvent B: 0.01% HCOOH in methanol
20% **A** and 80% **B**
Flow: 0.3 ml/min
Column: Phenomenex XB-C18, 50 x 2.1 mm, 1.7 µm

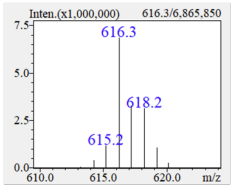

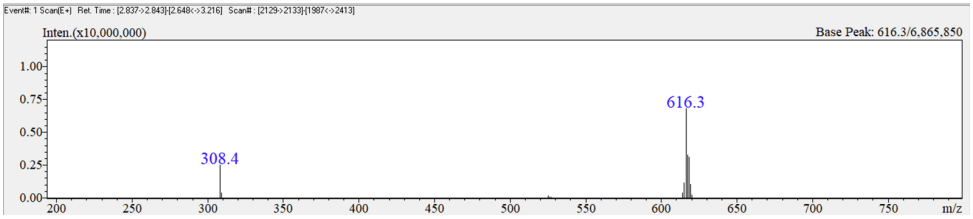

Figure S75. HPLC-MS analysis of (*S*)-2c

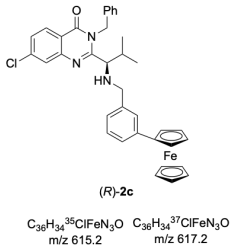

(*R*)-**2c**

$C_{36}H_{34}{}^{35}ClFeN_3O$ m/z 615.2 $C_{36}H_{34}{}^{37}ClFeN_3O$ m/z 617.2

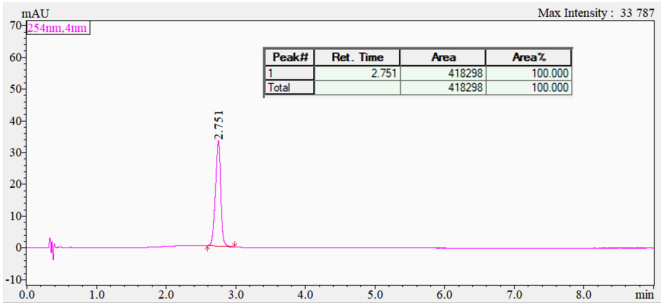

Method
Solvent A: 0.01% HCOOH in water
Solvent B: 0.01% HCOOH in methanol
20% **A** and 80% **B**
Flow: 0.3 ml/min
Column: Phenomenex XB-C18, 50 x 2.1 mm, 1.7 µm

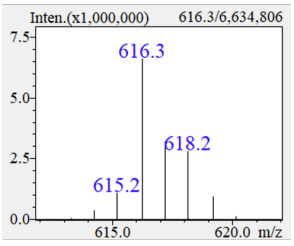

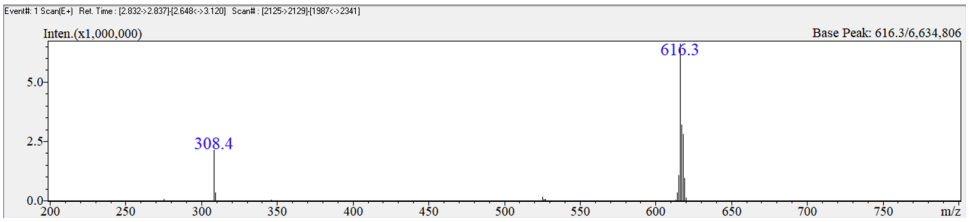

Figure S76. HPLC-MS analysis of (*R*)-2c

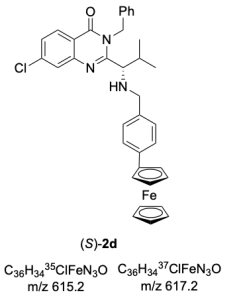

(*S*)-**2d**

$C_{36}H_{34}{}^{35}ClFeN_3O$ m/z 615.2 $C_{36}H_{34}{}^{37}ClFeN_3O$ m/z 617.2

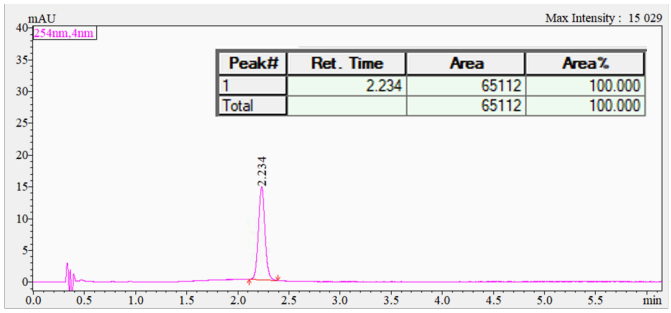

Method
Solvent A: 0.01% HCOOH in water
Solvent B: 0.01% HCOOH in methanol
Solvent C: 0.01% HCOOH in acetonitrile
30% **A**, 35% **B** and 35% **C**
Flow: 0.3 ml/min
Column: Phenomenex XB-C18, 50 x 2.1 mm, 1.7 µm

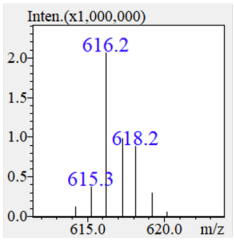

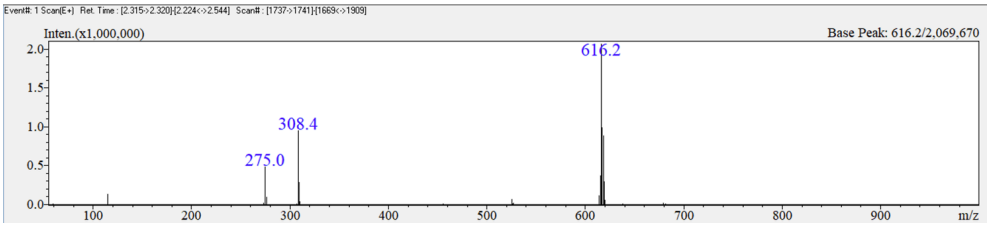

Figure S77. HPLC-MS analysis of (*S*)-2d

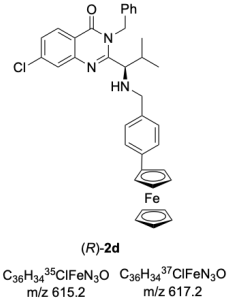

(*R*)-**2d**

$C_{36}H_{34}{}^{35}ClFeN_3O$ m/z 615.2 $C_{36}H_{34}{}^{37}ClFeN_3O$ m/z 617.2

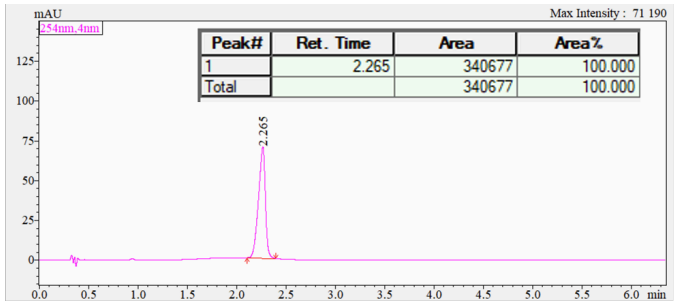

Method
Solvent A: 0.01% HCOOH in water
Solvent B: 0.01% HCOOH in methanol
Solvent C: 0.01% HCOOH in acetonitrile
30% **A**, 35% **B** and 35% **C**
Flow: 0.3 ml/min
Column: Phenomenex XB-C18, 50 x 2.1 mm, 1.7 µm

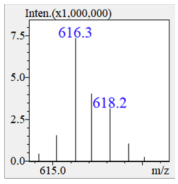

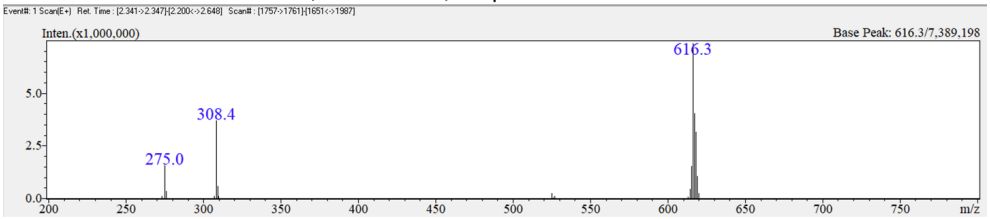

Figure S78. HPLC-MS analysis of (*R*)-2d

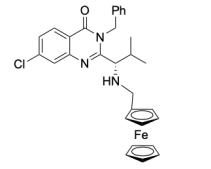

(*S*)-**2e**

$C_{30}H_{30}{}^{35}ClFeN_3O$ m/z 539.1 $C_{30}H_{30}{}^{37}ClFeN_3O$ m/z 541.1

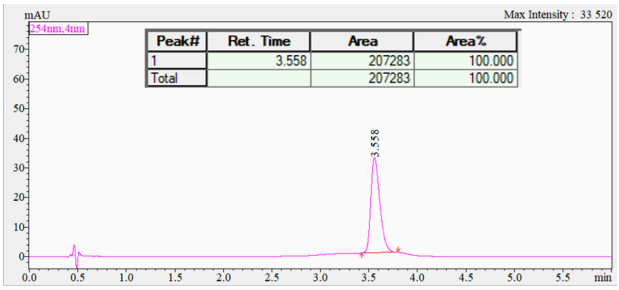

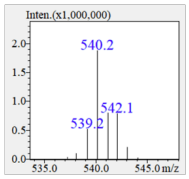

Method
Solvent A: 0.01% HCOOH in water
Solvent B: 0.01% HCOOH in methanol
Solvent C: 0.01% HCOOH in acetonitrile
50% **A**, 25% **B** and 25% **C**
Flow: 0.3 ml/min
Column: Phenomenex XB-C18, 50 x 2.1 mm, 1.7 µm

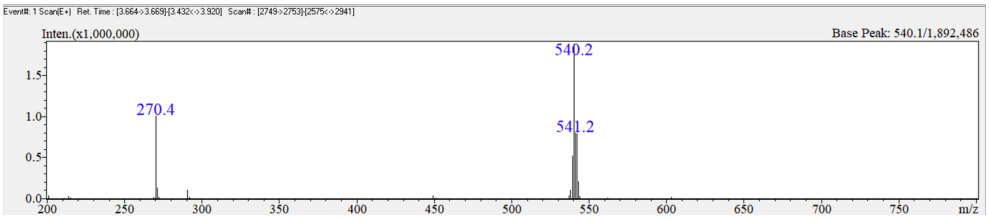

Figure S79. HPLC-MS analysis of (*S*)-2e

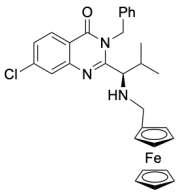

(*R*)-**2e**

$C_{30}H_{30}{}^{35}ClFeN_3O$ m/z 539.1 $C_{30}H_{30}{}^{37}ClFeN_3O$ m/z 541.1

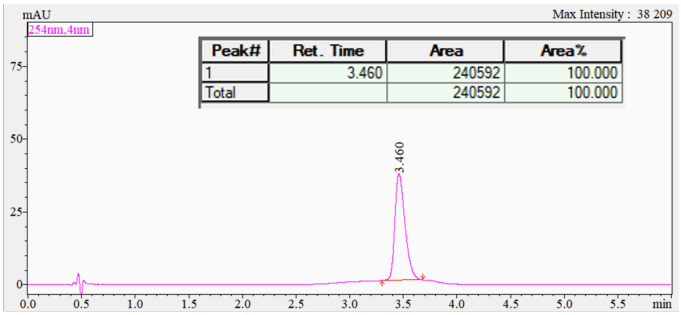

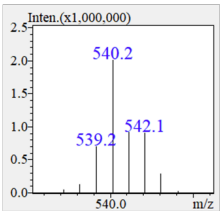

Method
Solvent A: 0.01% HCOOH in water
Solvent B: 0.01% HCOOH in methanol
Solvent C: 0.01% HCOOH in acetonitrile
50% **A**, 25% **B** and 25% **C**
Flow: 0.3 ml/min
Column: Phenomenex XB-C18, 50 x 2.1 mm, 1.7 µm

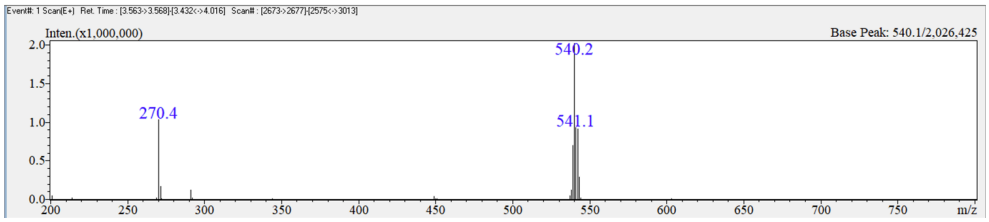

Figure S80. HPLC-MS analysis of (*R*)-2e

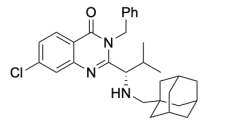

(*S*)-**2f**

$C_{30}H_{36}{}^{35}ClN_3O$ m/z 489.3 $C_{30}H_{36}{}^{37}ClN_3O$ m/z 491.3

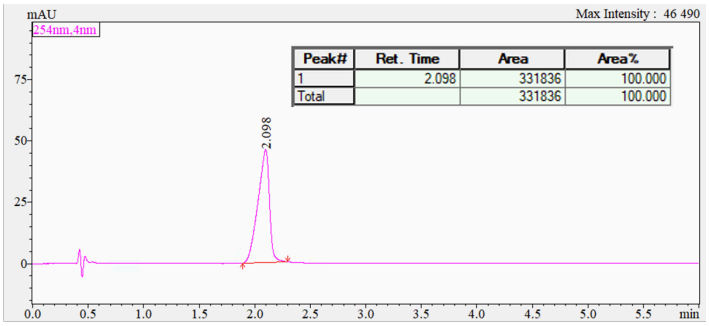

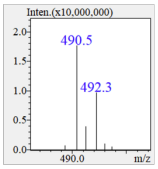

Method
Solvent A: 0.01% HCOOH in water
Solvent B: 0.01% HCOOH in methanol
20% **A** and 80% **B**
Flow: 0.3 ml/min
Column: Phenomenex XB-C18, 50 x 2.1 mm, 1.7 µm

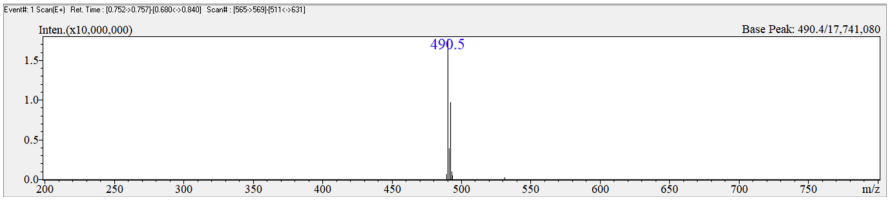

Figure S81. HPLC-MS analysis of (*S*)-2f

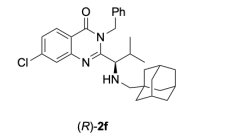

(*R*)-**2f**

$C_{30}H_{36}{}^{35}ClN_3O$ m/z 489.3 $C_{30}H_{36}{}^{37}ClN_3O$ m/z 491.3

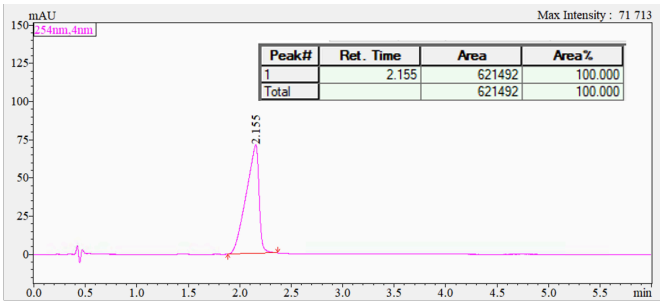

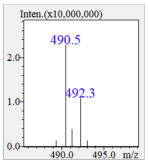

Method
Solvent A: 0.01% HCOOH in water
Solvent B: 0.01% HCOOH in methanol
20% **A** and 80% **B**
Flow: 0.3 ml/min
Column: Phenomenex XB-C18, 50 x 2.1 mm, 1.7 µm

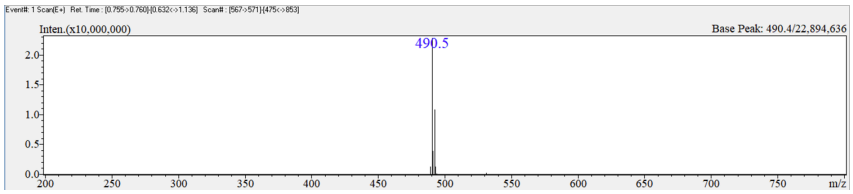

Figure S82. HPLC-MS analysis of (*R*)-2f

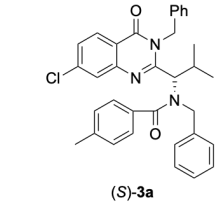

(*S*)-**3a**

$C_{34}H_{32}{}^{35}ClN_3O_2$ m/z 549.2 $C_{34}H_{32}{}^{37}ClN_3O_2$ m/z 551.2

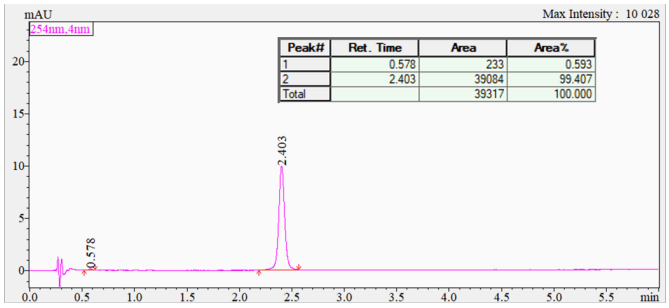

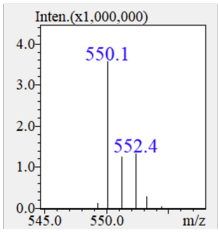

Method
Solvent A: 0.01% HCOOH in water
Solvent B: 0.01% HCOOH in acetonitrile
20% **A** and 80% **B**
Flow: 0.3 ml/min
Column: Phenomenex XB-C18, 50 x 2.1 mm, 1.7 μm

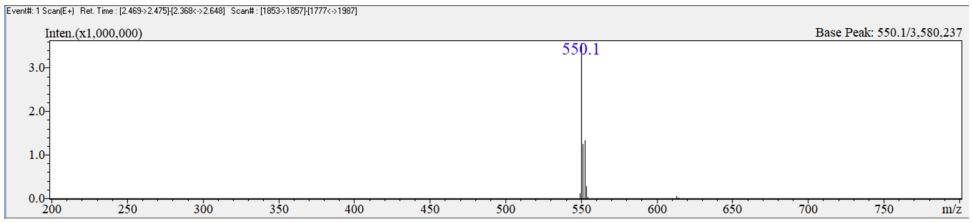

Figure S83. HPLC-MS analysis of (*S*)-3a

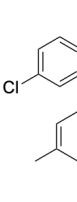

(*R*)-**3a**

$C_{34}H_{32}{}^{35}ClN_3O_2$ m/z 549.2 $C_{34}H_{32}{}^{37}ClN_3O_2$ m/z 551.2

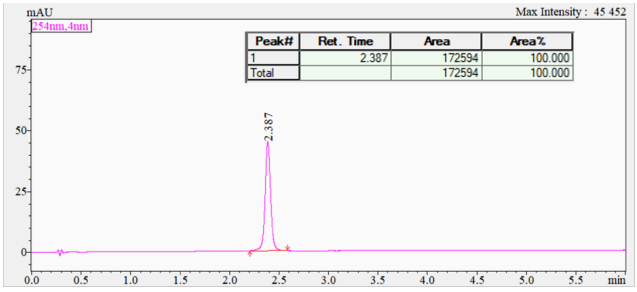

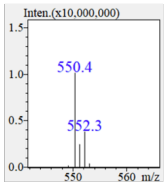

Method
Solvent A: 0.01% HCOOH in water
Solvent B: 0.01% HCOOH in acetonitrile
20% **A** and 80% **B**
Flow: 0.3 ml/min
Column: Phenomenex XB-C18, 50 x 2.1 mm, 1.7 μm

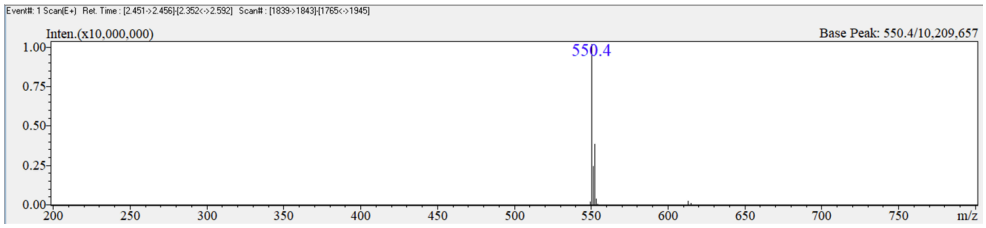

Figure S84. HPLC-MS analysis of (*R*)-3a

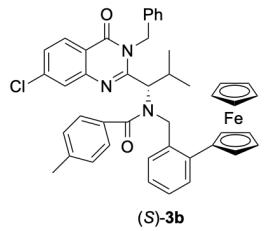

(*S*)-**3b**

$C_{44}H_{40}{}^{35}ClFeN_3O_2$ m/z 733.2

$C_{44}H_{40}{}^{37}ClFeN_3O_2$ m/z 735.2

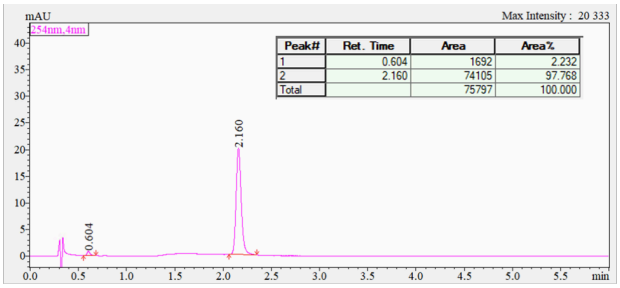

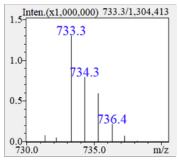

Method
Solvent A: 0.01% HCOOH in water
Solvent B: 0.01% HCOOH in methanol
Solvent C: 0.01% HCOOH in acetonitrile
10% **A**, 45% **B** and 45% **C**
Flow: 0.3 ml/min
Column: Phenomenex XB-C18, 50 x 2.1 mm, 1.7 µm

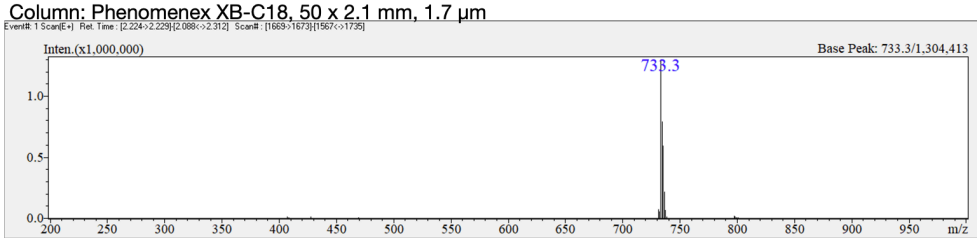

Figure S85. HPLC-MS analysis of (*S*)-3b

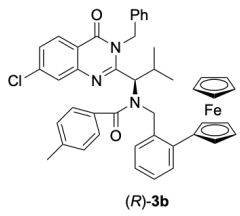

(*R*)-**3b**

$C_{44}H_{40}{}^{35}ClFeN_3O_2$ m/z 733.2

$C_{44}H_{40}{}^{37}ClFeN_3O_2$ m/z 735.2

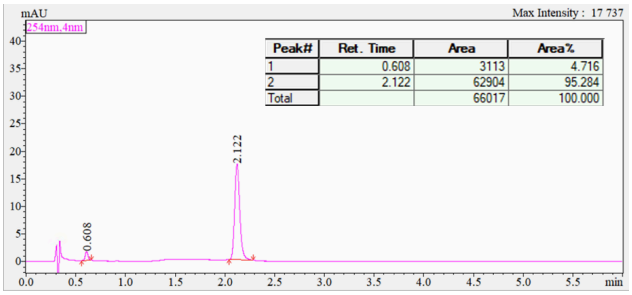

Method
Solvent A: 0.01% HCOOH in water
Solvent B: 0.01% HCOOH in methanol
Solvent C: 0.01% HCOOH in acetonitrile
10% **A**, 45% **B** and 45% **C**
Flow: 0.3 ml/min
Column: Phenomenex XB-C18, 50 x 2.1 mm, 1.7 µm

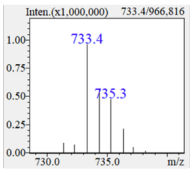

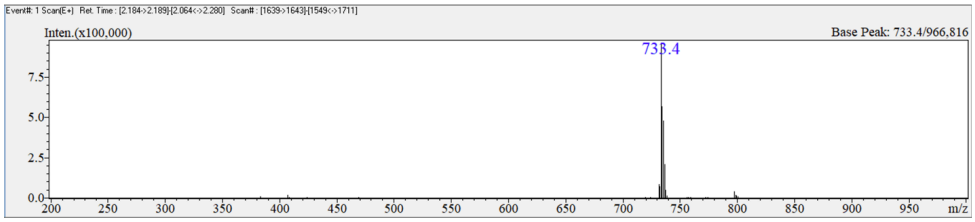

Figure S86. HPLC-MS analysis of (*R*)-3b

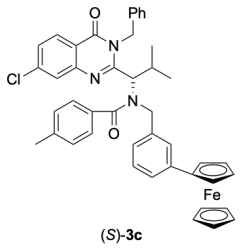

(*S*)-**3c**

$C_{44}H_{40}{}^{35}ClFeN_3O_2$ m/z 733.2 $C_{44}H_{40}{}^{37}ClFeN_3O_2$ m/z 735.2

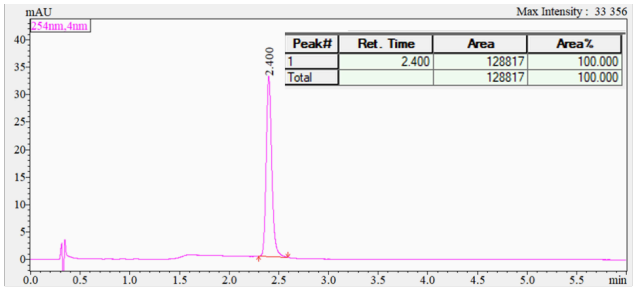

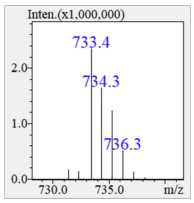

Method
Solvent A: 0.01% HCOOH in water
Solvent B: 0.01% HCOOH in methanol
Solvent C: 0.01% HCOOH in acetonitrile
10% **A**, 45% **B** and 45% **C**
Flow: 0.3 ml/min
Column: Phenomenex XB-C18, 50 x 2.1 mm, 1.7 µm

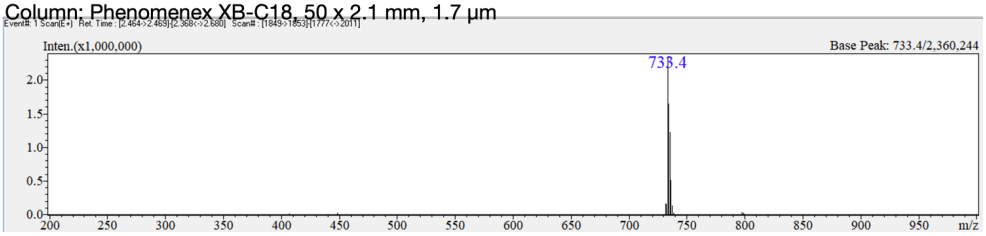

Figure S87. HPLC-MS analysis of (*S*)-3c

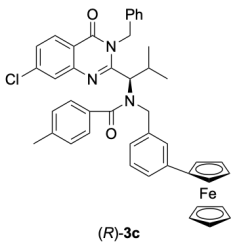

(*R*)-**3c**

$C_{44}H_{40}{}^{35}ClFeN_3O_2$ m/z 733.2 $C_{44}H_{40}{}^{37}ClFeN_3O_2$ m/z 735.2

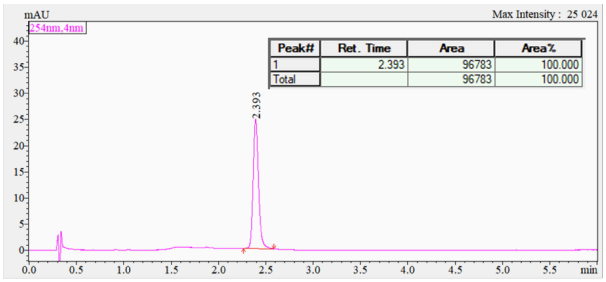

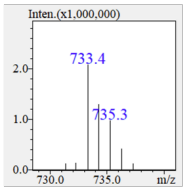

Method
Solvent A: 0.01% HCOOH in water
Solvent B: 0.01% HCOOH in methanol
Solvent C: 0.01% HCOOH in acetonitrile
10% **A**, 45% **B** and 45% **C**
Flow: 0.3 ml/min
Column: Phenomenex XB-C18, 50 x 2.1 mm, 1.7 µm

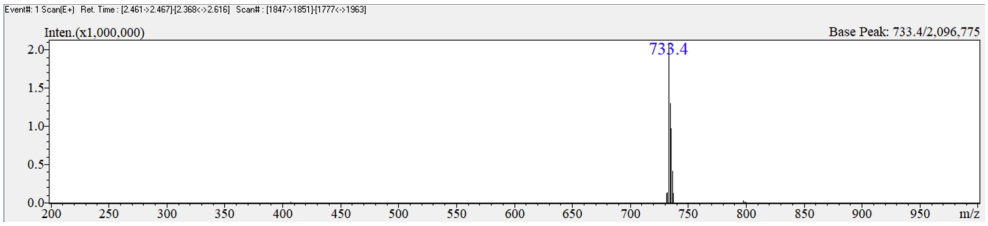

Figure S88. HPLC-MS analysis of (*R*)-3c

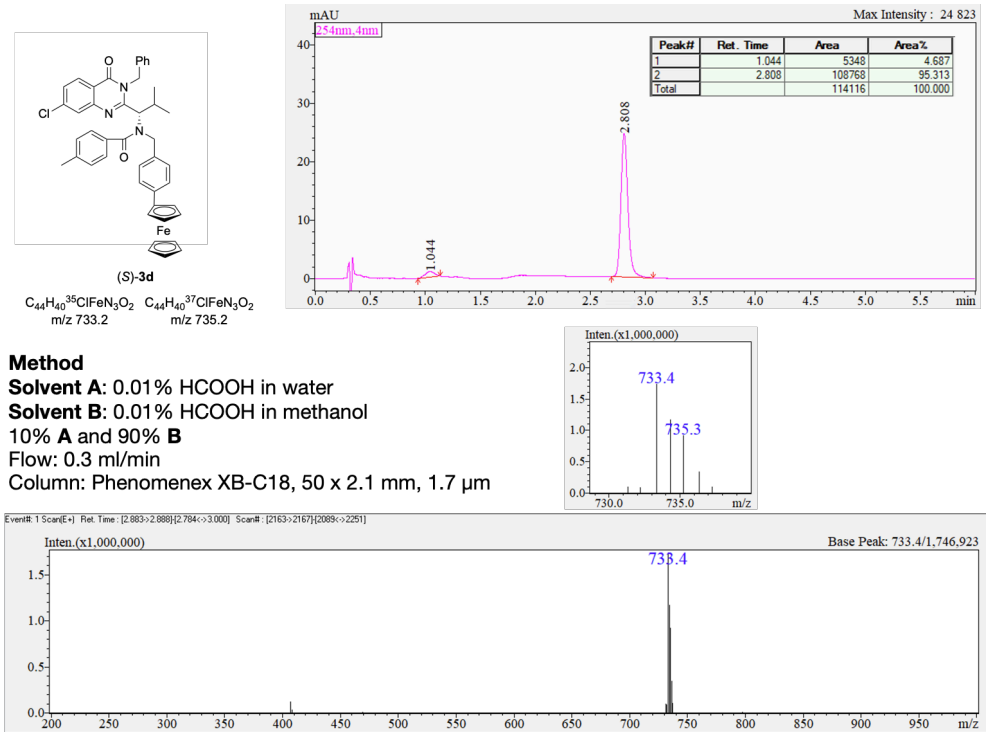

Figure S89. HPLC-MS analysis of (*S*)-3d

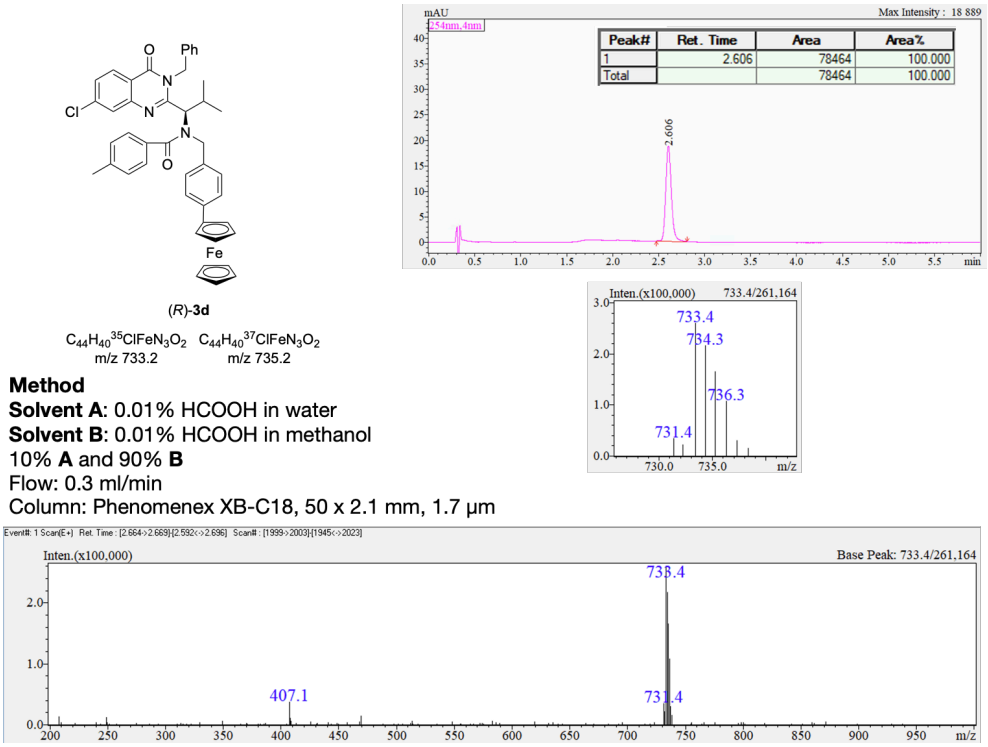

Figure S90. HPLC-MS analysis of (*R*)-3d

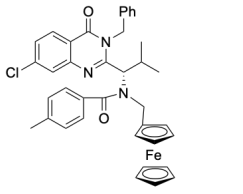

(*S*)-**3e**

$C_{38}H_{36}{}^{35}ClFeN_3O_2$ m/z 657.2 $C_{38}H_{36}{}^{37}ClFeN_3O_2$ m/z 659.2

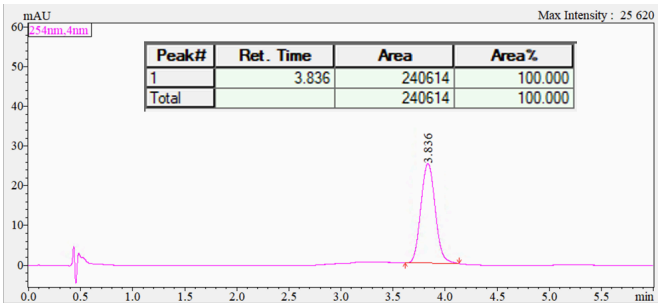

Method
Solvent A: 0.01% HCOOH in water
Solvent B: 0.01% HCOOH in methanol
15% **A** and 85% **B**
Flow: 0.3 ml/min
Column: Phenomenex XB-C18, 50 x 2.1 mm, 1.7 µm

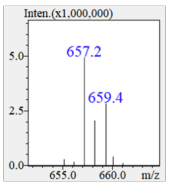

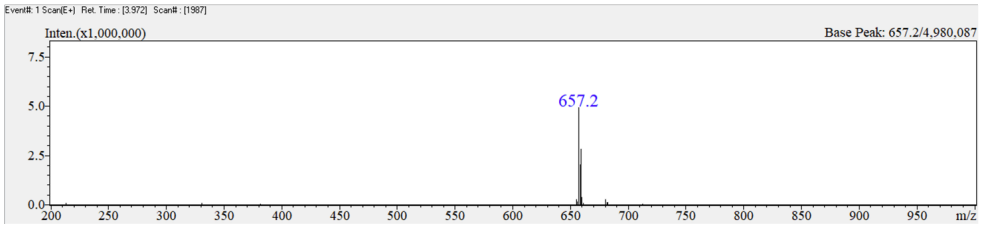

Figure S91. HPLC-MS analysis of (*S*)-3e

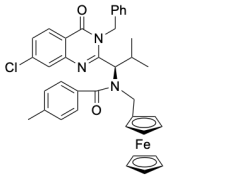

(*R*)-**3e**

$C_{38}H_{36}{}^{35}ClFeN_3O_2$ m/z 657.2 $C_{38}H_{36}{}^{37}ClFeN_3O_2$ m/z 659.2

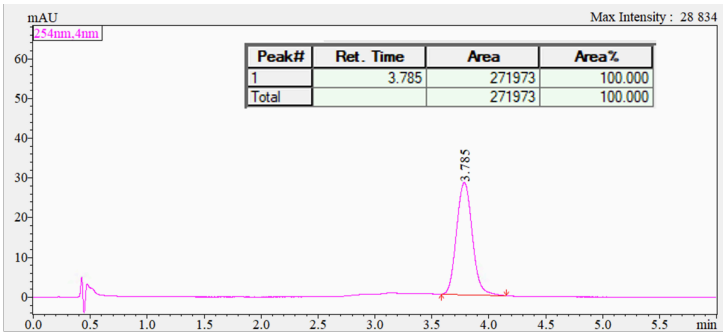

Method
Solvent A: 0.01% HCOOH in water
Solvent B: 0.01% HCOOH in methanol
25% **A** and 85% **B**
Flow: 0.3 ml/min
Column: Phenomenex XB-C18, 50 x 2.1 mm, 1.7 µm

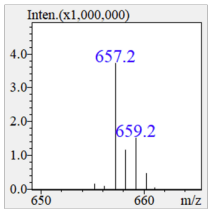

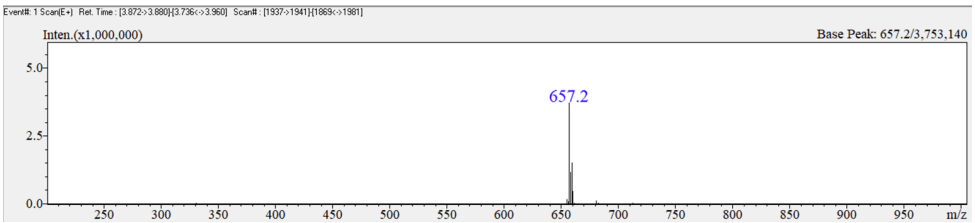

Figure S92. HPLC-MS analysis of (*R*)-3e

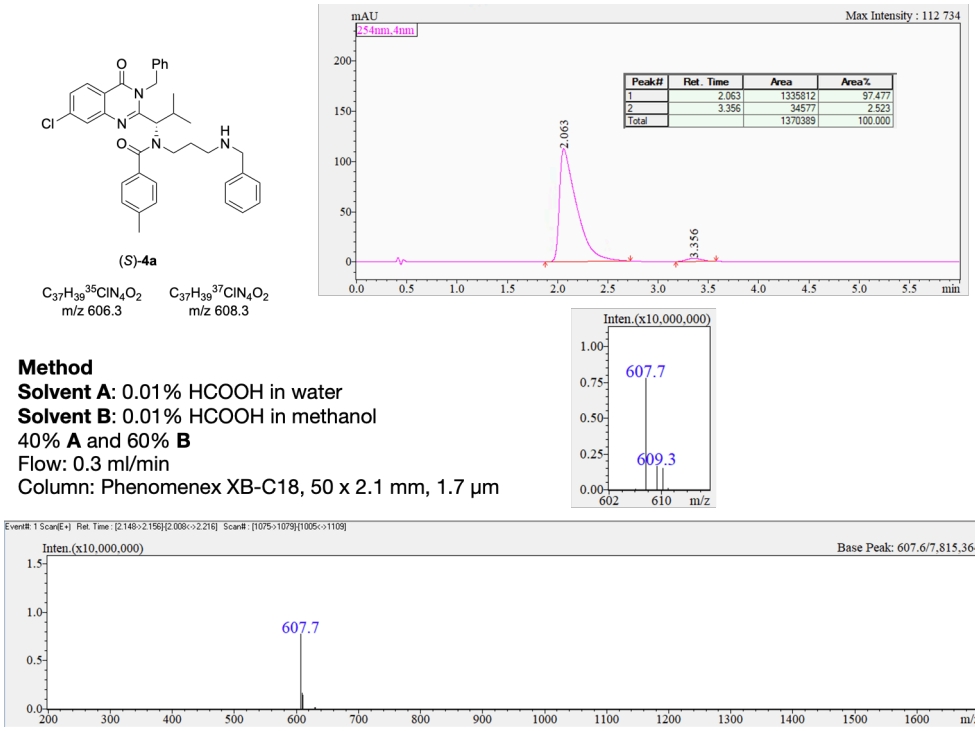

Figure S93. HPLC-MS analysis of (*S*)-4a

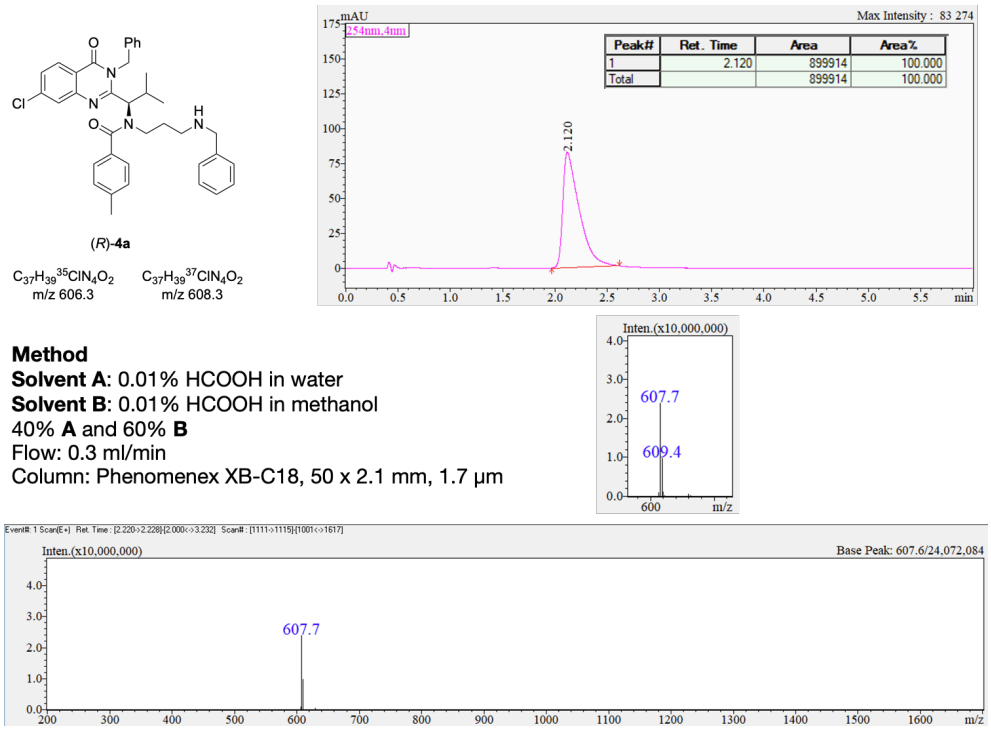

Figure S94. HPLC-MS analysis of (*R*)-4a

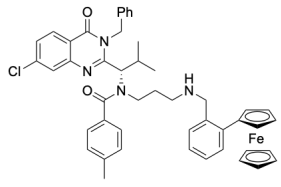

(*S*)-**4b**

$C_{47}H_{47}{}^{35}ClFeN_4O_2$ m/z 790.3 $C_{47}H_{47}{}^{37}ClFeN_4O_2$ m/z 792.3

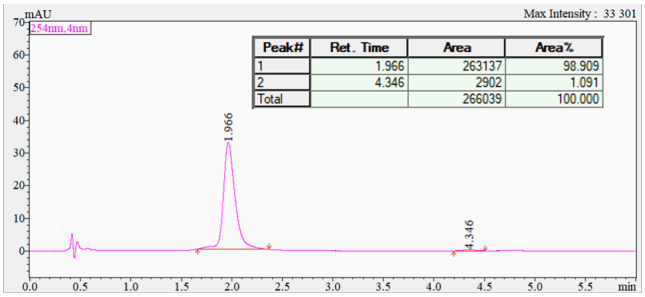

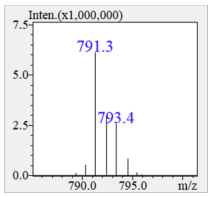

Method
Solvent A: 0.01% HCOOH in water
Solvent B: 0.01% HCOOH in methanol
30% **A** and 70% **B**
Flow: 0.3 ml/min
Column: Phenomenex XB-C18, 50 x 2.1 mm, 1.7 µm

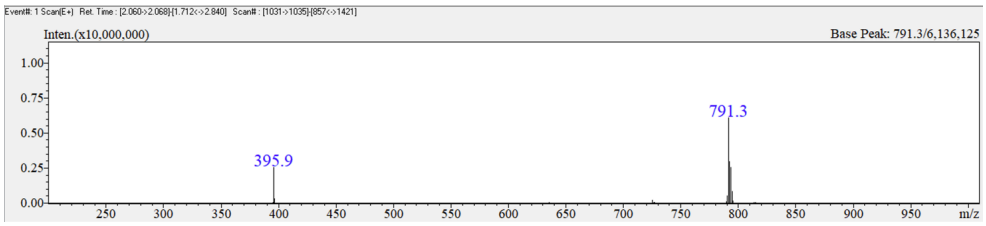

Figure S95. HPLC-MS analysis of (*S*)-4b

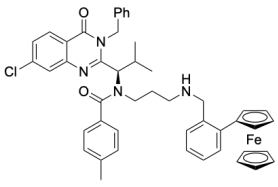

(*R*)-**4b**

$C_{47}H_{47}{}^{35}ClFeN_4O_2$ m/z 790.3 $C_{47}H_{47}{}^{37}ClFeN_4O_2$ m/z 792.3

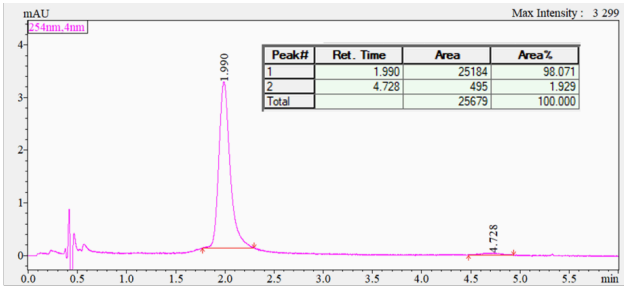

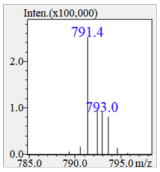

Method
Solvent A: 0.01% HCOOH in water
Solvent B: 0.01% HCOOH in methanol
30% **A** and 70% **B**
Flow: 0.3 ml/min
Column: Phenomenex XB-C18, 50 x 2.1 mm, 1.7 µm

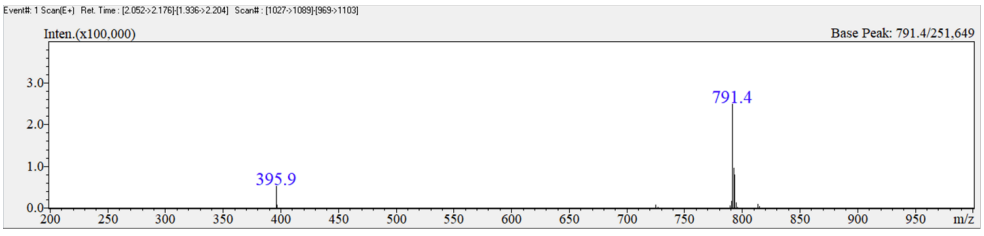

Figure S96. HPLC-MS analysis of (*R*)-4b

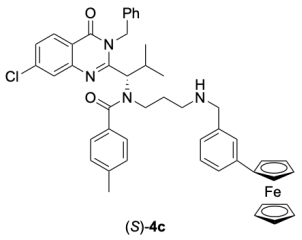

(*S*)-**4c**

$C_{47}H_{47}{}^{35}ClFeN_4O_2$ m/z 790.3 $C_{47}H_{47}{}^{37}ClFeN_4O_2$ m/z 792.3

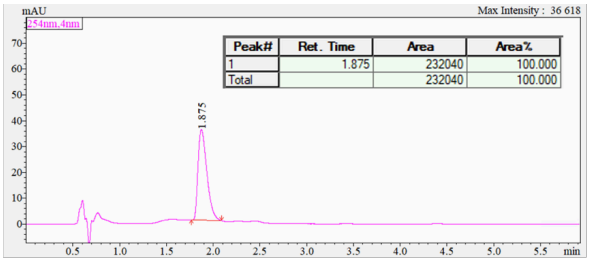

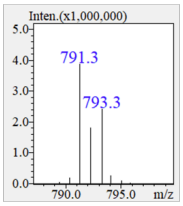

Method
Solvent A: 0.01% HCOOH in water
Solvent B: 0.01% HCOOH in methanol
Solvent C: 0.01% HCOOH in acetonitrile
30% **A**, 35% **B** and 35% **C**
Flow: 0.3 ml/min
Column: Phenomenex XB-C18, 50 x 2.1 mm, 1.7 μm

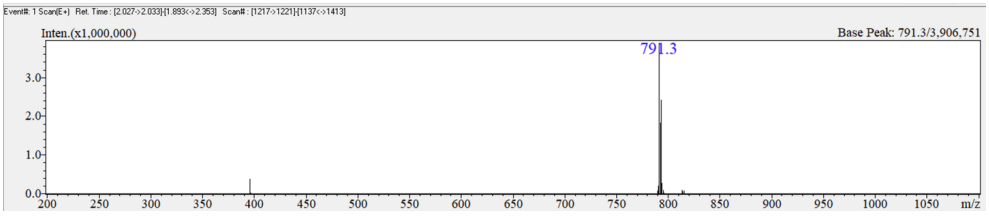

Figure S97. HPLC-MS analysis of (*S*)-4c

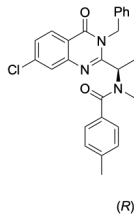

(*R*)-**4c**

$C_{47}H_{47}{}^{35}ClFeN_4O_2$ m/z 790.3 $C_{47}H_{47}{}^{37}ClFeN_4O_2$ m/z 792.3

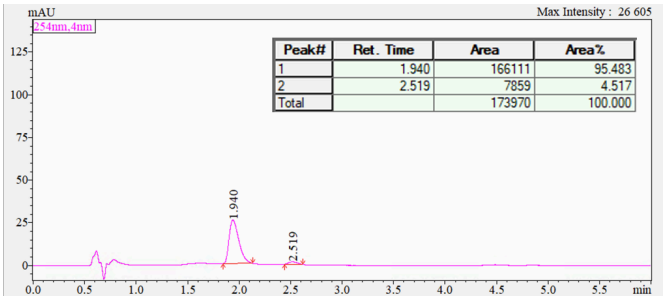

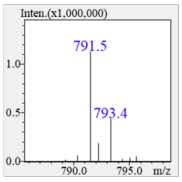

Method
Solvent A: 0.01% HCOOH in water
Solvent B: 0.01% HCOOH in methanol
Solvent C: 0.01% HCOOH in acetonitrile
30% **A**, 35% **B** and 35% **C**
Flow: 0.3 ml/min
Column: Phenomenex XB-C18, 50 x 2.1 mm, 1.7 μm

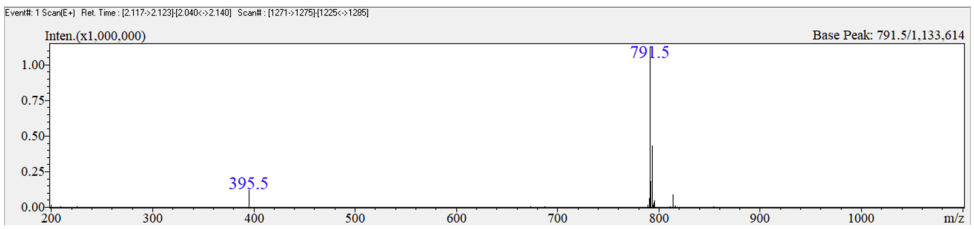

Figure S98. HPLC-MS analysis of (*R*)-4c

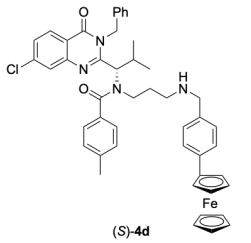

(*S*)-**4d**

$C_{47}H_{47}{}^{35}ClFeN_4O_2$ m/z 790.3 $C_{47}H_{47}{}^{37}ClFeN_4O_2$ m/z 792.3

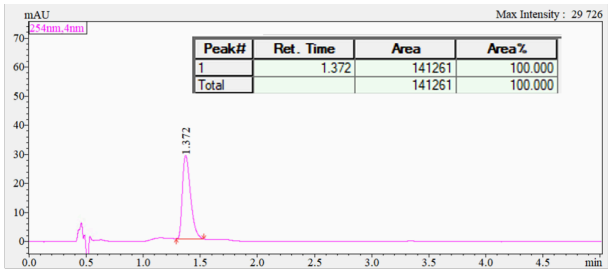

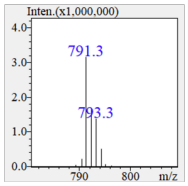

Method
Solvent A: 0.01% HCOOH in water
Solvent B: 0.01% HCOOH in methanol
Solvent C: 0.01% HCOOH in acetonitrile
30% **A**, 35% **B** and 35% **C**
Flow: 0.3 ml/min
Column: Phenomenex XB-C18, 50 x 2.1 mm, 1.7 µm

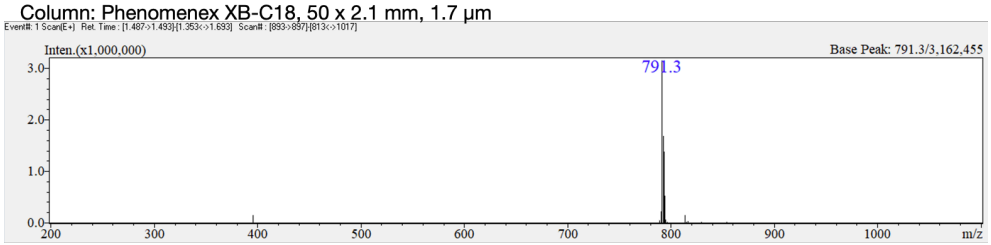

Figure S99. HPLC-MS analysis of (*S*)-4d

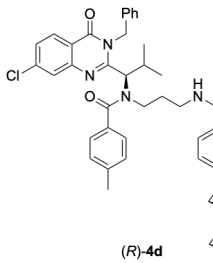

(*R*)-**4d**

$C_{47}H_{47}{}^{35}ClFeN_4O_2$ m/z 790.3 $C_{47}H_{47}{}^{37}ClFeN_4O_2$ m/z 792.3

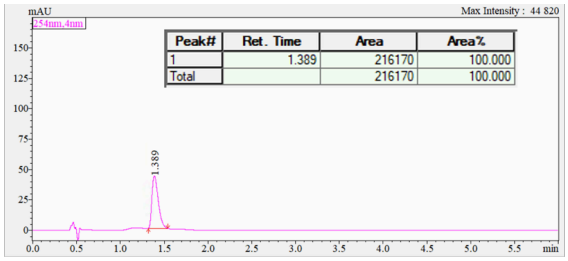

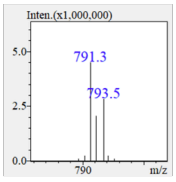

Method
Solvent A: 0.01% HCOOH in water
Solvent B: 0.01% HCOOH in methanol
Solvent C: 0.01% HCOOH in acetonitrile
30% **A**, 35% **B** and 35% **C**
Flow: 0.3 ml/min
Column: Phenomenex XB-C18, 50 x 2.1 mm, 1.7 µm

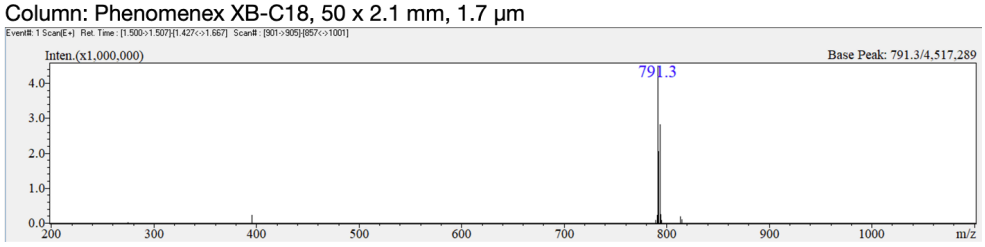

Figure S100. HPLC-MS analysis of (*R*)-4d

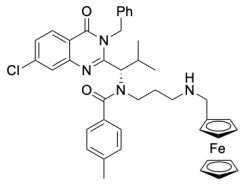

(*S*)-**4e**

$C_{41}H_{43}{}^{35}ClFeN_4O_2$ m/z 714.2 $C_{47}H_{43}{}^{37}ClFeN_4O_2$ m/z 716.2

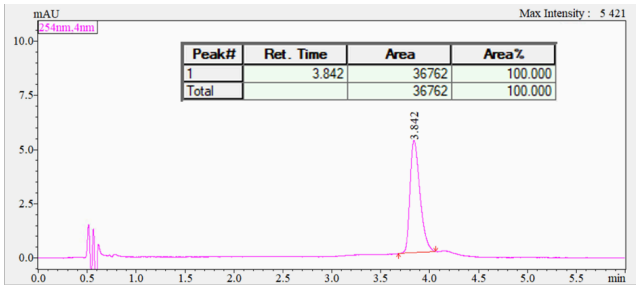

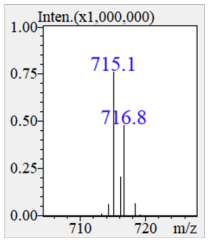

Method
Solvent A: 0.01% HCOOH in water
Solvent B: 0.01% HCOOH in methanol
Solvent C: 0.01% HCOOH in acetonitrile
40% **A**, 30% **B** and 30% **C**
Flow: 0.3 ml/min
Column: Phenomenex XB-C18, 50 x 2.1 mm, 1.7 µm

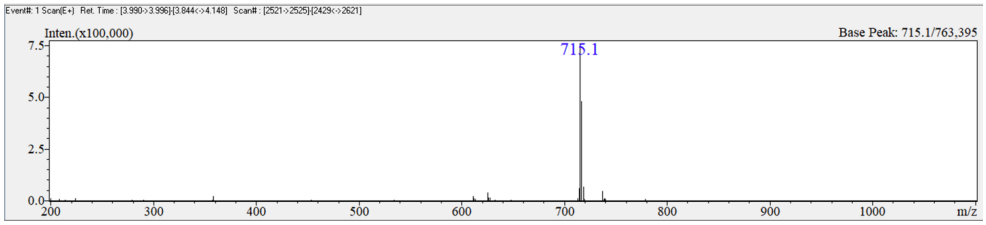

Figure S101. HPLC-MS analysis of (*S*)-4e

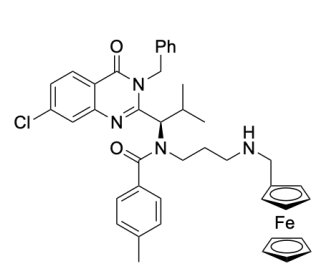

(*R*)-**4e**

$C_{41}H_{43}{}^{35}ClFeN_4O_2$ m/z 714.2 $C_{47}H_{43}{}^{37}ClFeN_4O_2$ m/z 716.2

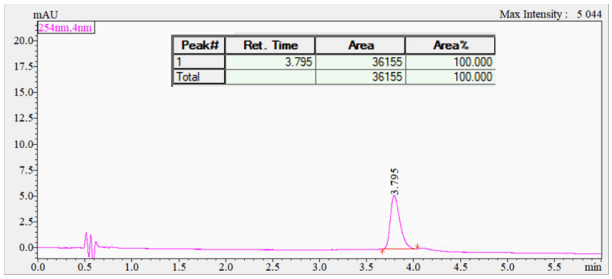

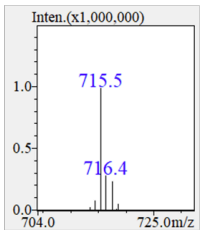

Method
Solvent A: 0.01% HCOOH in water
Solvent B: 0.01% HCOOH in methanol
Solvent C: 0.01% HCOOH in acetonitrile
40% **A**, 30% **B** and 30% **C**
Flow: 0.3 ml/min
Column: Phenomenex XB-C18, 50 x 2.1 mm, 1.7 µm

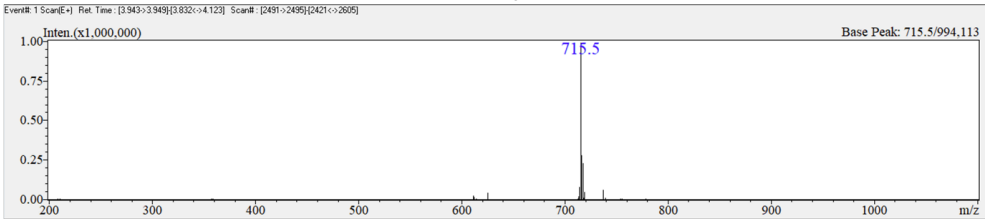

Figure S102. HPLC-MS analysis of (*R*)-4e

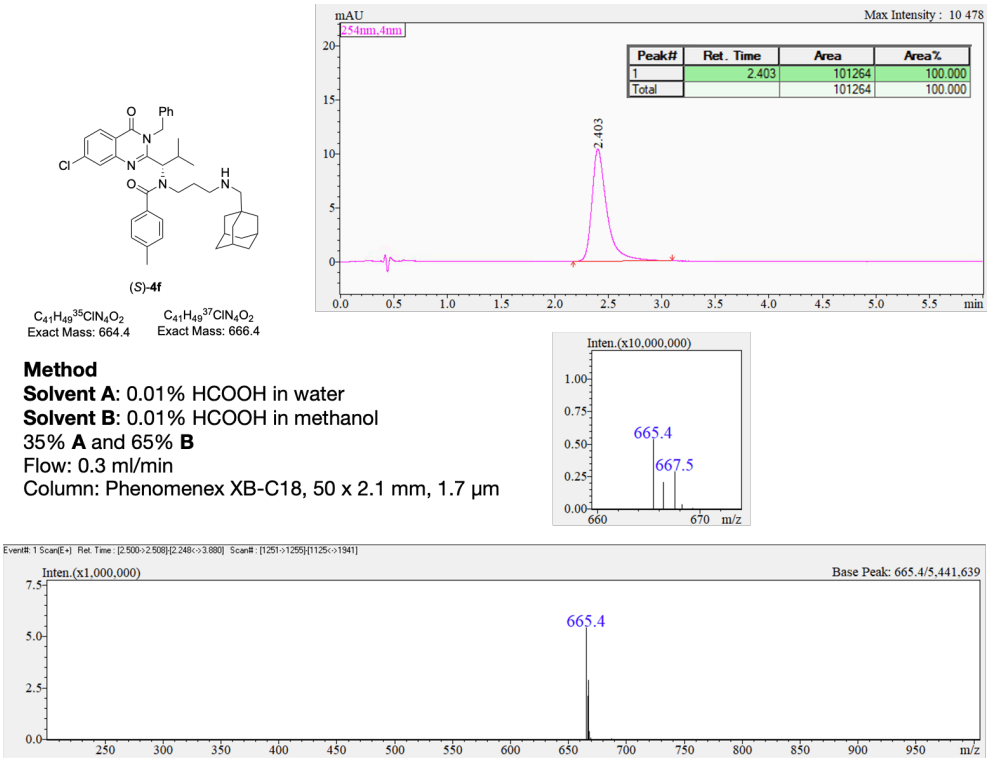

Figure S103. HPLC-MS analysis of (*S*)-4f

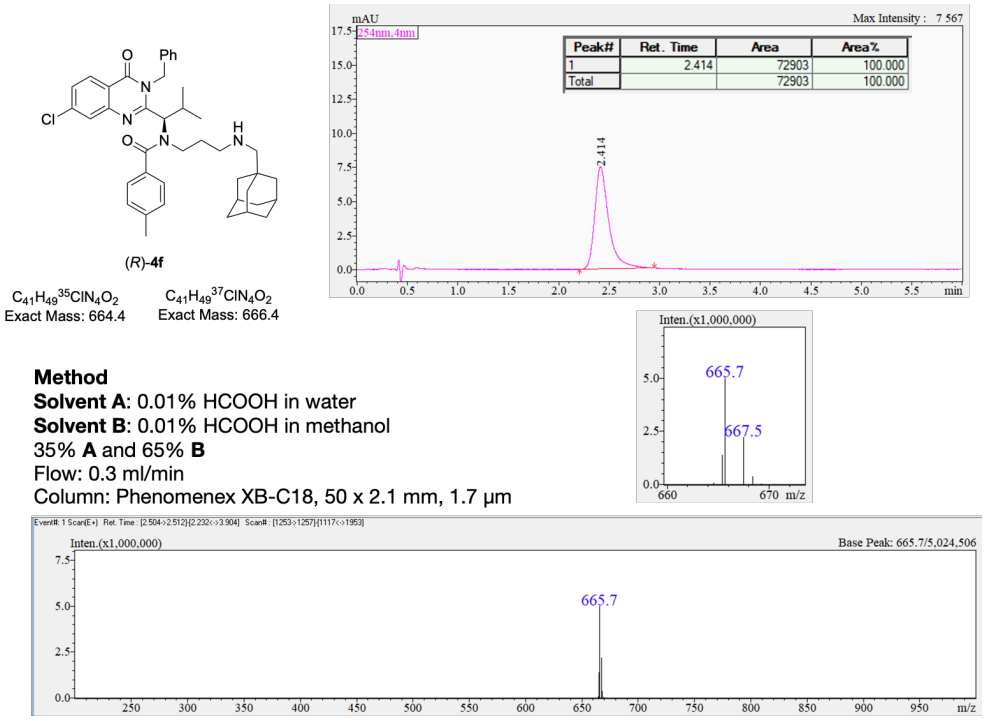

Figure S104. HPLC-MS analysis of (*R*)-4f

Dr hab. Damian Plażuk, prof. UŁ

Pracownia Spektroskopii Molekularnej

Katedra Chemii Organicznej

Wydział Chemii UŁ

Łódź, 18.09.2024

Oświadczenie

Niniejszym oświadczam, iż mój udział w publikacji:

1. Anna Wieczorek-Błauż, Karolina Kowalczyk, Andrzej Błauż, Anna Makal, Sylwia Pawlędzio, Chatchakorn Eurtivong, Homayon J. Arabshahi, Jóhannes Reynisson, Christian G. Hartinger, Błażej Rychlik, Damian Plażuk* „Impact of the ferrocenyl group on cytotoxicity and KSP inhibitory activity of ferrocenyl monastrol conjugates" *Dalton Trans.*, **2022**, 51, 491

   polegał na opracowaniu koncepcji badań i ich zaplanowaniu. Zebraniu, analizie i opracowaniu wyników badań. Przygotowaniu manuskryptu publikacji. Korespondencji z edytorem. Pozyskaniu finansowania.

2. Karolina Kowalczyk, Andrzej Błauż, Daniel Moscoh Ayine -Tora, Christian G. Hartinger, Błażej Rychlik, Damian Plażuk* „Design, Synthesis, and Evaluation of Biological Activity of Ferrocene-Ispinesib Hybrids: Impact of a Ferrocenyl Group on the Antiproliferative and Kinesin Spindle Protein Inhibitory Activity" *Chem.Eur. J.*, **2023**, 29

   polegał na opracowaniu koncepcji badań i ich zaplanowanie. Zebraniu, analizie i opracowaniu wyników badań. Przygotowaniu manuskryptu publikacji. Korespondencji z edytorem. Pozyskaniu finansowania.

3. Karolina Kowalczyk, Andrzej Błauż, Krzysztof Krawczyk, Błażej Rychlik, Damian Plażuk* „Design and Synthesis of Ferrocenyl 1,4-Dihydropyridines and Their Evaluation as Kinesin-5 Inhibitors" Dalton Trans., **2024** DOI: 10.1039/D4DT01853B

WYDZIAŁ
CHEMII
Uniwersytet Łódzki

UNIC

polegał na opracowaniu koncepcji badań i ich zaplanowaniu. Przeprowadzeniu syntez niektórych związków. Zebraniu, analizie i opracowaniu wyników badań. Przygotowaniu manuskryptu publikacji. Korespondencji z edytorem. Pozyskaniu finansowania.

Damian Plażuk

Łódź, 18.09.2024

Dane:

dr Andrzej Błauż

Pracownia Cytometrii

Katedra Biologii Nowotworów i Epigentyki

Wydział Biologii i Ochrony Środowiska

Uniwersytet Łódzki

Oświadczenie

Niniejszym oświadczam, iż mój udział w publikacji:

1. Anna Wieczorek-Błauż, Karolina Kowalczyk, Andrzej Błauż, Anna Makal, Sylwia Pawlędzio, Chatchakorn Eurtivong, Homayon J. Arabshahi, Jóhannes Reynisson, Christian G. Hartinger, Błażej Rychlik, Damian Plażuk* „Impact of the ferrocenyl group on cytotoxicity and KSP inhibitory activity of ferrocenyl monastrol conjugates" *Dalton Trans*., **2022**, 51, 491

   polegał na przeprowadzeniu badan mających określić cytotoksyczność badanych związków, ich zdolność do wpływu na generowanie reaktywnych form tlenu oraz oceny potencjalnego wpływu tych związków na cykl komórkowy i aktywność KSP. Dodatkowo zaangażowany byłem w proces przygotowania manuskryptu.

2. Karolina Kowalczyk, Andrzej Błauż, Daniel Moscoh Ayine -Tora, Christian G. Hartinger, Błażej Rychlik, Damian Plażuk* „Design, Synthesis, and Evaluation of Biological Activity of Ferrocene-Ispinesib Hybrids: Impact of a Ferrocenyl Group on the Antiproliferative and Kinesin Spindle Protein Inhibitory Activity" *Chem.Eur. J.*, **2023**, 29

   polegał na przeprowadzeniu badan mających określić cytotoksyczność badanych związków, ich zdolność do wpływu na generowanie reaktywnych form tlenu oraz oceny potencjalnego wpływu tych związków na cykl komórkowy i aktywność KSP. Dodatkowo zaangażowany byłem w proces przygotowania manuskryptu.

3. Karolina Kowalczyk, Andrzej Błauż, Krzysztof Krawczyk, Błażej Rychlik, Damian Plażuk* „Design and Synthesis of Ferrocenyl 1,4-Dihydropyridines and Their Evaluation as Kinesin-5 Inhibitors" Dalton Trans., **2024** DOI: 10.1039/D4DT01853B

polegał na przeprowadzeniu badan mających określić cytotoksyczność badanych związków, ich zdolność do wpływu na generowanie reaktywnych form tlenu oraz oceny potencjalnego wpływu tych związków na cykl komórkowy i aktywność KSP. Dodatkowo zaangażowany byłem w proces przygotowania manuskryptu.

podpis

Warszawa, 13.09.2024

Dane:

Oświadczenie

Niniejszym oświadczam, iż mój udział w publikacji:

Anna Wieczorek-Błauż, Karolina Kowalczyk, Andrzej Błauż, Anna Makal, Sylwia Pawlędzio, Chatchakorn Eurtivong, Homayon J. Arabshahi, Jóhannes Reynisson, Christian G. Hartinger, Błażej Rychlik, Damian Plażuk* „Impact of the ferrocenyl group on cytotoxicity and KSP inhibitory activity of ferrocenyl monastrol conjugates" *Dalton Trans*., **2022**, 51, 491

polegał na pomiarach XRD oraz analizie strukturalnej badanych związków.

Sylwia Pawlędzio

podpis

SCHOOL OF CHEMICAL SCIENCES
Faculty of Science

Professor Christian Hartinger

THE UNIVERSITY OF AUCKLAND
Te Whare Wānanga o Tāmaki Makaurau
NEW ZEALAND

Science Centre Building No 302
Room 10-1021, 23 Symonds Street
Auckland 1010, NZ

Telephone 64 9 373 7599 ext 83220
Facsimile 64 9 373 7422
email: c.hartinger@auckland.ac.nz
web: http://hartinger.auckland.ac.nz

University of Auckland
Private Bag 92019
Auckland 1142, NZ

Auckland, 14.09.2024

Statement

I hereby declare that my participation in the publication:

1. Anna Wieczorek-Błauż, Karolina Kowalczyk, Andrzej Błauż, Anna Makal, Sylwia Pawlędzio, Chatchakorn Eurtivong, Homayon J. Arabshahi, Jóhannes Reynisson, Christian G. Hartinger, Błażej Rychlik, Damian Plażuk* „Impact of the ferrocenyl group on cytotoxicity and KSP inhibitory activity of ferrocenyl monastrol conjugates" *Dalton Trans*., **2022**, 51, 491

consisted of supervising the docking studies and drafting the respective parts in the manuscript.

2. Karolina Kowalczyk, Andrzej Błauż, Daniel Moscoh Ayine -Tora, Christian G. Hartinger, Błażej Rychlik, Damian Plażuk* „Design, Synthesis, and Evaluation of Biological Activity of Ferrocene-Ispinesib Hybrids: Impact of a Ferrocenyl Group on the Antiproliferative and Kinesin Spindle Protein Inhibitory Activity" *Chem.Eur. J*., **2023**, 29

consisted of supervising the docking studies and drafting the respective parts in the manuscript.

Best regards,

Prof. Christian Hartinger

SCHOOL OF CHEMICAL SCIENCES
Faculty of Science

Professor Christian Hartinger

Science Centre Building No 302
Room 10-1021, 23 Symonds Street
Auckland 1010, NZ

Telephone 64 9 373 7599 ext 83220
Facsimile 64 9 373 7422
email: c.hartinger@auckland.ac.nz
web: http://hartinger.auckland.ac.nz

University of Auckland
Private Bag 92019
Auckland 1142, NZ

Auckland, 22.09.2024

Statement

I hereby declare that John Arabshahi participation in the publication:

1. Anna Wieczorek-Błauż, Karolina Kowalczyk, Andrzej Błauż, Anna Makal, Sylwia Pawlędzio, Chatchakorn Eurtivong, Homayon J. Arabshahi, Jóhannes Reynisson, Christian G. Hartinger, Błażej Rychlik, Damian Plażuk* „Impact of the ferrocenyl group on cytotoxicity and KSP inhibitory activity of ferrocenyl monastrol conjugates" *Dalton Trans*., **2022**, 51, 491

consisted of docking studies.

Best regards,

Prof. Christian Hartinger

WYDZIAŁ BIOLOGII
i OCHRONY
ŚRODOWISKA
Uniwersytet Łódzki

UNIC

Łódź, dnia 20 września 2024 r.

Dr Błażej Rychlik
Pracownia Cytometrii
Katedra Epigenetyki i Biologii Nowotworów
Wydział Biologii i Ochrony Środowiska Uniwersytetu Łódzkiego

Oświadczenie

Niniejszym oświadczam, iż mój udział w publikacji:

1. Anna Wieczorek-Błauż, Karolina Kowalczyk, Andrzej Błauż, Anna Makal, Sylwia Pawlędzio, Chatchakorn Eurtivong, Homayon J. Arabshahi, Jóhannes Reynisson, Christian G. Hartinger, Błażej Rychlik, Damian Plażuk* „Impact of the ferrocenyl group on cytotoxicity and KSP inhibitory activity of ferrocenyl monastrol conjugates" *Dalton Trans*., **2022**, 51, 491

polegał na zaplanowaniu i nadzorze nad wykonaniem eksperymentów biologicznych, wykonaniu części oznaczeń aktywności Eg-5 i innych kinezyn, analizie wyników i współpracy w przygotowaniu manuskryptu.

2. Karolina Kowalczyk, Andrzej Błauż, Daniel Moscoh Ayine -Tora, Christian G. Hartinger, Błażej Rychlik, Damian Plażuk* „Design, Synthesis, and Evaluation of Biological Activity of Ferrocene-Ispinesib Hybrids: Impact of a Ferrocenyl Group on the Antiproliferative and Kinesin Spindle Protein Inhibitory Activity" *Chem.Eur. J*., **2023**, 29

polegał na zaplanowaniu i nadzorze nad wykonaniem eksperymentów biologicznych, wykonaniu części oznaczeń aktywności Eg-5 i innych kinezyn, analizie wyników i współpracy w przygotowaniu manuskryptu.

3. Karolina Kowalczyk, Andrzej Błauż, Krzysztof Krawczyk, Błażej Rychlik, Damian Plażuk* „Design and Synthesis of Ferrocenyl 1,4-Dihydropyridines and Their Evaluation as Kinesin-5 Inhibitors" Dalton Trans., **2024** DOI: 10.1039/D4DT01853B

polegał na zaplanowaniu i nadzorze nad wykonaniem eksperymentów biologicznych, wykonaniu części oznaczeń aktywności Eg-5, analizie wyników i współpracy w przygotowaniu manuskryptu.

(48) 42 635 41 00
Pomorska 141/143, 90-236 Łódź
blazej.rychlik@biol.uni.lodz.pl

biol.uni.lodz.pl

Łódź, 22.09.2024

Dane: Krzysztof Krawczyk

Oświadczenie

Niniejszym oświadczam, iż mój udział w publikacji:

1. Karolina Kowalczyk, Andrzej Błauż, Krzysztof Krawczyk, Błażej Rychlik, Damian Plażuk* „Design and Synthesis of Ferrocenyl 1,4-Dihydropyridines and Their Evaluation as Kinesin-5 Inhibitors" Dalton Trans., 2024 DOI: 10.1039/D4DT01853B

   polegał na wykonaniu testów proliferacji i analizie uzyskanych wyników z użyciem programu GraphPad Prism 10.2.1, jak również testów do analizy cyklu komórkowego oraz generacji reaktywnych form tlenu wraz z pomiarem na cytometrze przepływowym Symphony A1 (Becton Dickinson)

podpis

K. Krawczyk

dr hab. Anna Makal, prof. UW
Pracownia Krystalochemii
Wydział Chemii UW
ul. Żwirki i Wigury 101
02-089 Warszawa

Warszawa, 19 września 2024

OŚWIADCZENIE

Oświadczam, że w pracy:

Anna Wieczorek-Błauż, Karolina Kowalczyk, Andrzej Błauż, Anna Makal, Sylwia Pawlędzio, Chatchakorn Eurtivong, Homayon J. Arabshahi, Jóhannes Reynisson, Christian G. Hartinger, Błażej Rychlik, Damian Plażuk
„Impact of the ferrocenyl group on cytotoxicity and KSP inhibitory activity of ferrocenyl monastrol conjugates" Dalton Trans., 2022, 51, 491

mój udział polegał na wykonaniu rentgenowskich pomiarów strukturalnych dla związku **3a** oraz superwizji pomiarów strukturalnych dla związku **6a** oraz na wykonaniu rentgenowskiej analizy strukturalnej dla tych związków (paragraf „Single crystal X-ray diffraction analysis").

Z poważaniem,

Anna Makal

Łódź, 23.09.2024

Oświadczenie

Niniejszym oświadczam, iż mój udział w publikacji:

1. Anna Wieczorek-Błauż, Karolina Kowalczyk, Andrzej Błauż, Anna Makal, Sylwia Pawlędzio, Chatchakorn Eurtivong, Homayon J. Arabshahi, Jóhannes Reynisson, Christian G. Hartinger, Błażej Rychlik, Damian Plażuk* „Impact of the ferrocenyl group on cytotoxicity and KSP inhibitory activity of ferrocenyl monastrol conjugates” *Dalton Trans*., **2022**, 51, 491

   polegał na: opracowaniu warunków reakcji i zsyntezowaniu ferrocenylowych pochodnych monastrolu, zaplanowaniu syntezy i zsyntezowaniu ferrocenylowych pochodnych *β*-ketoestrów, badaniach LC-MS przebiegu reakcji, analizach widm NMR, pracy nad końcową wersją manuskryptu.

podpis

Dr Jóhannes Reynisson FRSC
Lecturer in drug discovery

School of Pharmacy and Bioengineering
T: +44(0)1782 733985
email: j.reynisson@keele.ac.uk

Keele UNIVERSITY

16th September 2024

Dr Jóhannes Reynisson FRSC
School of Pharmacy and Bioengineering
Keele University
Newcastle-under-Lyme
Staffordshire ST5 5BG UK

Re: Letter for Ms. Karolina Kowalczyk regarding my participation the below publication

I hereby declare that my participation in the below publication was the supervision of the molecular modelling work, the write-up of this work and overall contribution in writing and finalizing the paper.

Anna Wieczorek-Błauż, Karolina Kowalczyk, Andrzej Błauż, Anna Makal, Sylwia Pawlędzio, Chatchakorn Eurtivong, Homayon J. Arabshahi, Jóhannes Reynisson, Christian G. Hartinger, Błażej Rychlik, Damian Plażuk* „Impact of the ferrocenyl group on cytotoxicity and KSP inhibitory activity of ferrocenyl monastrol conjugates" *Dalton Trans*., **2022**, 51, 491

If you have any further questions, do not hesitate to contact me.

Jóhannes Reynisson

Dr Jóhannes Reynisson FRSC

Keele University
Staffordshire
ST5 5BG UK

T: +44(0)1782 732000
keele.ac.uk

Place and date

22/09/2024

Your data

Daniel Moscoh Ayine-Tora

University of Ghana

Department of Chemistry

Legon-Accra

Statement

I hereby declare that my participation in the publication:

Karolina Kowalczyk, Andrzej Błauż, Daniel Moscoh Ayine -Tora, Christian G. Hartinger, Błażej Rychlik, Damian Plażuk* „Design, Synthesis, and Evaluation of Biological Activity of Ferrocene-Ispinesib Hybrids: Impact of a Ferrocenyl Group on the Antiproliferative and Kinesin Spindle Protein Inhibitory Activity" *Chem.Eur. J.*, **2023**, 29

consisted of the molecular docking and modelling of the compounds.

Signature